THE JOURNAL OF

PHYSICAL

CHEMISTRY

Volume 67

JULY—DECEMBER, 1963

PAGES 1399—2918

THE JOURNAL OF
PHYSICAL CHEMISTRY

NOTES

COMMUNICATIONS TO THE EDITOR

AUTHOR INDEX

RADIATION CHEMISTRY OF LIQUID ETHANE[1]

BY HUGH A. GILLIS[2]

Radiation Research Laboratories, Mellon Institute, Pittsburgh, Pa.

Received August 20, 1962

Product yields of the radiolysis of liquid ethane at $-78°$ with X-rays have been determined to be: $G(H_2) = 3.60$, $G(n\text{-}C_4H_{10}) = 2.54$, $G(C_2H_4) = 0.73$, $G(C_3H_8) = 0.65$, $G(CH_4) = 0.56$, and $G(C_2H_2) = 0.11$. From these results it is calculated that $G(CH_3\cdot)/G(C_2H_5\cdot) \leq 0.10$. This result is approximately as expected from the e.s.r. experiments of Fessenden and Schuler on liquid ethane in which the ratio of steady-state concentrations of methyl and ethyl radicals was estimated to be 0.04.

The recent e.s.r. experiments of Fessenden and Schuler on liquid ethane have shown that the predominant radical species present during irradiation are ethyl, methyl, and vinyl radicals.[3,4] Hydrogen atoms were not observed in these experiments. From intensity measurements the steady-state concentrations of the methyl and vinyl radicals were estimated to be, respectively, 4 and 3% of that of the ethyl radical. The present study was undertaken in order to compare the relative radical yields from chemical experiments with these e.s.r. observations. Further, a measure of the radical yields provides the basis for a quantitative estimate of the rate of production of ethyl radicals in the e.s.r. experiments. From this and the observed steady-state concentration of radicals, the lifetime and absolute rate constant for the second-order reaction of the ethyl radicals can be calculated. It was also hoped that this study of liquid ethane, because of the relative simplicity of the molecule involved, would provide one of the least complicated examples of the radiation chemistry of an organic system.

Experimental

The ethane used in all experiments was Phillips research grade and was stated to be 99.9% pure. In an effort to further purify it, especially from ethylene, the sample was distilled into a trap containing high activity silica gel at $-120°$, then subjected to a trap-to-trap distillation with only the middle half being retained. The purified ethane showed none of the irradiation products as impurities when the normal analytical procedure was followed. An examination was made for impurities boiling higher than ethane by means of high sensitivity (β-ionization detector) gas chromatography. None were found. Vacuum line techniques were used to handle the samples which had a liquid volume of 1.0 ± 0.1 cc. Irradiation vessels were spherical Pyrex bulbs having diameters of the order of 1 cm. and attached break seals. Less than 1% of the sample was in the vapor phase.

(1) Presented before the Division of Physical Chemistry at the 139th National Meeting of the American Chemical Society, St. Louis, Mo., March, 1961. Supported, in part, by the U. S. Atomic Energy Commission.

(2) Chemistry Department, Western Reserve University, Cleveland, Ohio.

(3) R. W. Fessenden and R. H. Schuler, *J. Chem. Phys.*, **33**, 935 (1960).

(4) R. W. Fessenden and R. H. Schuler, private communication.

Two types of irradiation were used in this work: Co^{60} γ-rays and 3 mev. X-rays (or more accurately bremsstrahlung) produced by the bombardment of a tungsten target with electrons from a Van de Graaff accelerator. The absorbed dose rate was determined by the Fricke dosimeter with appropriate corrections being made for electron density. In the γ-ray work the dose rate was 1.79×10^{19} e.v. g. $^{-1}$ hr. $^{-1}$, and in the X-ray experiments it was about five times greater.

After irradiation, samples were transferred to a vacuum line and product gases volatile at $-196°$ were collected and analyzed mass spectrometrically. High boiling products were determined by gas chromatographic analysis on a silica gel column. A thermal conductivity detector was employed in these measurements. Under the conditions used, acetylene and propane came off the column as a single fraction. This fraction was collected in several experiments and shown by mass spectrometric analysis to consist of 85% propane and 15% acetylene.

Results and Discussion

The results obtained from the irradiation of pure liquid ethane at $-78°$ with X-rays are shown in Fig. 1. Data for methane are not included in the figure since they overlap the propane points. The methane production was, however, also found to be proportional to dose. Similar linear production of products was observed with Co^{60} γ-rays in a series of seven experiments analogous to those reported in Fig. 1. Higher boiling saturated products were looked for and not found.

Yields for irradiations at $-78°$ with X-rays and γ-rays and at $-120°$ with X-rays are summarized in Table I along with the results of a single experiment in which HI was added as a scavenger. The yields for the γ-ray irradiations at $-78°$ are about 15% lower than those for the X-ray experiments at the same temperature; this difference is greater than the estimated error.

The carbon to hydrogen ratio of the total products is calculated to be 1:3.07 from the γ-ray results, 1:3.01 from the X-ray results at $-78°$, and 1:3.07 from X-ray results at $-120°$. The material balance is thus seen to be unusually good and there does not appear to be any major undetected product.

The products found in the present work were qualitatively the same as those reported for the radiolysis of

Fig. 1.—Yields in the radiolysis of 1.0 ± 0.1 cc. of liquid ethane at $-78°$ with X-rays: H_2, △; n-C_4H_{10}, □; C_2H_4, ○; C_3H_8, ●.

ethane in the gas phase at very low conversions.[5] In the latter work the material balance is calculated to be C:H = 1:3.43. This seems to be outside the experimental error of the analysis so that higher boiling undetected products may have been produced. The principal quantitative differences in the measured products are the higher yields of hydrogen (8.8 vs. 3.6) and of ethylene ($\sim$2 vs. 0.7) in the gas phase radiolysis.

Reactions of Hydrogen Atoms.—Proposed reactions of hydrogen atoms must accommodate the fact that they could not be detected in the e.s.r. experiments at $-138°$. This places an upper limit on their concentration of approximately 1% of the measured ethyl radical concentration, or 10^{-9} M at a dose rate of 6×10^{21} e.v. g.$^{-1}$ hr.$^{-1}$. There are three fates of hydrogen atoms which may be considered: diffusion controlled reaction with other radicals (principally ethyl since they were present at higher concentration)

$$H\cdot + C_2H_5\cdot \longrightarrow C_2H_6 \qquad (1a)$$

$$H\cdot + C_2H_5\cdot \longrightarrow H_2 + C_2H_4 \qquad (1b)$$
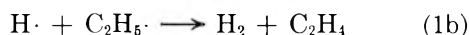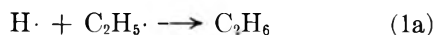
abstraction from ethane

$$H\cdot + C_2H_6 \longrightarrow H_2 + C_2H_5\cdot \qquad (2)$$
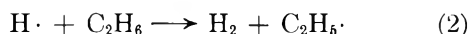
or reaction with ethylene, a radiation product

$$H\cdot + C_2H_4 \longrightarrow C_2H_5\cdot \qquad (3)$$

Reactions 1a and 1b seem improbable because they would imply a diffusion coefficient of a hydrogen atom approximately 100 times that of an ethyl radical.

Either reaction 2 or 3 must predominate over the range of energy absorbed in these experiments; if there

(5) K. Yang and P. L. Gant, J. Phys. Chem., **65**, 1861 (1961).

were an effective competition the yields of H_2 and C_2H_4 would not be linear with dose as indicated in Fig. 1. In the radiolysis of liquid n-pentane, n-hexane, and n-heptane at $-70°$, it has been concluded that the reaction analogous to 2 is not important for ethylene concentrations greater than 0.01 M.[6] Hydrogen atoms add to ethylene even at low temperatures as is evidenced by the fact that in the e.s.r. experiments[4] irradiation of C_2H_6 containing C_2D_4 at $-138°$ produced $C_2D_4H\cdot$ at a concentration of 50–100% that of $C_2H_5\cdot$. In order to estimate the concentration of ethylene required for reaction 3 to compete with reaction 2, a choice of Arrhenius parameters for both reactions is required. These are not available but an order of magnitude may be arrived at by using Hardwick's data for the reaction of hydrogen atoms with CH_3 groups[7] and α-olefins[8] in the liquid phase at room temperature. If it is assumed that these reactions have equal pre-exponential factors, then $E_2 - E_3 = 4.3$ kcal. A calculation based on this difference of activation energies indicates that reaction 3 must be important even at the lowest ethylene concentration indicated in Fig. 1 (about 2×10^{17} molecules cc.$^{-1}$). Reaction 2 must be important at very low concentrations, and therefore the curve for ethylene in Fig. 1 should show a small positive intercept. However the analyses were not precise enough to make this detectable. Therefore for all irradiations the observed ethylene yield is essentially equal to the true initial yield less the yield of hydrogen atoms. It follows that none of the observed hydrogen yield results from the reaction of thermalized, non-spur hydrogen atoms since these preferentially add to the ethylene rather than abstract from the solvent.

It is also concluded that hydrogen atoms were not seen in the e.s.r. experiments at $-138°$ because reaction 2 is already very fast at the considerable (1×10^{19} molecules cc.$^{-1}$) concentration of ethylene that would have been built up before the spectrum could have been examined.

Reaction of Methyl and Ethyl Radicals.—Fessenden and Schuler[3] observed that the concentration of ethyl radicals was proportional to the one-half power of the absorbed dose rate. Ethyl radicals must be consumed by radical–radical reactions which are in the main

$$C_2H_5\cdot + C_2H_5\cdot \longrightarrow C_4H_{10} \qquad (4a)$$

$$\longrightarrow C_2H_4 + C_2H_6 \qquad (4b)$$

$$CH_3\cdot + C_2H_5\cdot \longrightarrow C_3H_8 \qquad (5a)$$

$$\longrightarrow C_2H_4 + CH_4 \qquad (5b)$$

$$C_2H_3\cdot + C_2H_5\cdot \longrightarrow C_4H_8 \qquad (6)$$
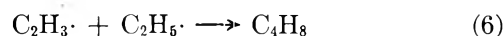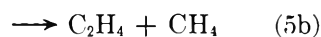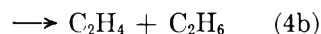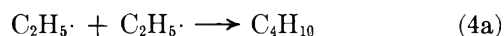
In the gas phase k_{4b}/k_{4a} has been reported to be 0.12 between 100 and 250°.[9] However in a more recent study it has been concluded that the ratio increases with decrease in temperature in both liquid and gas phases[10]; values of 0.162 at $-65°$ in the gas phase, 0.208 at $-78°$ in isoöctane, and 0.265 at $-65°$ in isopropyl alcohol were found. The value 0.208 is perhaps most appropriate for liquid ethane at $-78°$;

(6) R. A. Holroyd and G. W. Klein, J. Am. Chem. Soc., **84**, 4000 (1962).
(7) T. J. Hardwick, J. Phys. Chem., **65**, 101 (1961).
(8) T. J. Hardwick, ibid., **66**, 291 (1962).
(9) R. K. Brinton and E. W. R. Steacie, Can. J. Chem., **33**, 1840 (1955).
(10) M. Matsuoka, P. S. Dixon, A. P. Stefani, and M. Szwarc, Proc. Chem. Soc., 304 (1962).

Radiation	Temp., °C.	Dose rate, e.v. g.$^{-1}$ hr.$^{-1}$ × 10^{-19}	H_2	CH_4	C_2H_4	C_2H_2	C_3H_8	n-C_4H_{10}
Co^{60} γ-rays	− 78	1.79	3.26	0.49	0.63	0.09	0.50	2.14
3 mev. X-rays	− 78	9.0	3.60	.56	.73	.11	.65	2.54
3 mev. X-rays	−120	9.0	3.74	.59	.97	.11	.58	2.19
3 mev. X-rays	−120^a	9.0	5.12	.50	2.12	.05	.34	0.47

^{a} Sample contained 0.10 mole % HI.

a calculation based on it, and the assumption that all of the butane results from reaction 4a, indicates that about 72% of the observed ethylene yield results from disproportionation of ethyl radicals. The remainder, plus the ethylene used up in reaction 3, presumably results from non-radical processes.

Hardwick[8] found that at room temperature hydrogen abstraction is an important reaction of hydrogen atoms with α-olefins from C_5 to C_{10}. The e.s.r. results indicate that this is not an important reaction with ethylene at low temperatures if the proposed mechanism is correct. Similarly Holroyd and Klein[6] did not report evidence for the abstraction reaction in the radiolysis of hydrocarbon solutions of ethylene.

In the gas phase $k_{5b}/k_{5a} = 0.06$.[11] If this result applies also in the liquid phase at low temperatures, reaction 5b may be regarded as negligible in the present work.

This work was carried out prior to the identification of vinyl radicals in the e.s.r. experiments and no attempt was made to examine the butane fraction for the very small amount of butene-1 expected.

Methane probably results from the abstraction of an atom of hydrogen from ethane by a hot methyl radical, or from a molecular elimination reaction, as in the direct photolysis of gaseous ethane.[12] Hydrogen abstraction by a thermalized methyl radical, for which the gas phase activation energy is 10.4 kcal.,[13] should not be important at the temperature and dose rates of the present experiments.

Effect of Hydrogen Iodide.—Hydrogen iodide is expected to be a good radical scavenger even at low temperatures. A single experiment was carried out

with hydrogen iodide as a solute and is reported in Table I. In this experiment the HI was present at such a low concentration that electron capture by it is considered unlikely.[14] A calculation shows that a high percentage of the hydrogen iodide was consumed during the reaction, to eventually produce molecular iodine, so that some of the radical scavenging was probably done by the latter species. The hydrogen iodide presumably reacted with hydrogen atoms to give an increased yield of hydrogen gas, a decreased yield for 3 and as a result a higher yield for ethylene. It is worthy of note that the increase in the hydrogen yield is very nearly equivalent to the increase in ethylene, in agreement with the proposed mechanism. The hydrogen iodide also reacted with methyl and ethyl radicals to markedly decrease the yields of butane and propane. The residual yields of these products could represent spur or non-radical yields or could be due to incomplete scavenging.

Radical Yields.—If all of the butane and propane result from reactions 4a and 5a, if $k_{4b}/k_{4a} = 0.21$ and $k_{5b}/k_{5a} = 0.06$, then for the irradiations with X-rays at −120°, $G(C_2H_5 \cdot) = 5.91$, $G(CH_3 \cdot) = 0.61$, and $G(CH_3 \cdot)/G(C_2H_5 \cdot) = 0.10$. On the same basis $G(CH_3 \cdot)/G(C_3H_5 \cdot)$ is 0.10 and 0.09 for the irradiations with X-rays and γ-rays at −78°, respectively. However if the yields of propane and butane determined in the experiment with added hydrogen iodide are truly molecular, then $G(CH_3 \cdot)/G(C_2H_5 \cdot) = 0.06$. The ratio of steady-state concentrations would be expected to be slightly lower than these numbers because of the higher diffusion rate of the smaller methyl radical. Therefore the agreement with the e.s.r. ratio of 0.04 may be considered quite good.

(11) C. A. Heller, J. Chem. Phys., 28, 1255 (1958).

(12) H. Okabe and J. R. McNesby, ibid., 34, 668 (1961).

(13) A. F. Trotman-Dickenson, Quart. Rev. (London), 7, 198 (1953).

(14) L. J. Forrestal and W. H. Hamill, J. Am. Chem. Soc., 83, 1535 (1961).

DEVELOPMENT OF A METHOD FOR MEASURING IONIC SELF-DIFFUSION

By Guy F. Allen,[1] Helmut Schurig,[2] Laird Slade, and Henry C. Thomas[3]

Department of Chemistry, University of North Carolina, Chapel Hill, N. C.

Self-diffusion coefficients of ions traceable by γ-ray emitters can be deduced from determinations of the total activity of a "short rod" of the material from which the diffusion takes place through a thin membrane into a rapidly stirred bath at zero activity. Earlier work with this method was inadequate both theoretically and experimentally. Mathematical and experimental developments are described which enable an assessment of the accuracy of the results for self-diffusion in gels. Results for sodium, cesium, and cobalt(II) (as chlorides) at various concentrations are reported.

In two earlier papers[4,5] describing the principle and an application of the method, here to be further discussed, the authors were overly optimistic as to the adequacy of the numerical treatment of their data as well as to the reliability of the diffusion cell used in the work. We now describe further analysis and development of this method for the measurement of self-diffusion coefficients of ions and report results for sodium, cesium, and cobalt chlorides in 2% agar gels at several concentrations.

The experiment is designed for the measurement of the diffusion of ions which can be followed by the aid of γ-emitting isotopic tracers. The method has thus far been demonstrated only for ionic diffusion in gels essentially in equilibrium with aqueous solutions of the ion. The experiment depends upon a series of measurements of the decreasing total amount of activity in a "short rod" of gel as diffusion takes place through a thin permeable membrane into the equilibrium solution at zero radioactivity.

Mathematical Treatment

In order to discuss more easily the nature and effect of the principal approximation utilized in the analysis of the diffusion problem, we write the exact statement. The earlier work[4,5] with this method must be considered unreliable because of a lack of appreciation of the effects of this approximation. The experimental arrangement may be represented as

D	D_m	$c = c_1$
c	c_m	$\theta = 0$
θ	θ_m	
Gel	Membrane	Rapidly stirred bath

| 0 | a | $a + b$ |

$$-x\rightarrow$$

Here we write θ, θ_m for a quantity proportional to the fraction of the ions radioactive. The actual value of θ depends on the geometry and efficiency of the counter used in the measurement. Since, however, all significant experimental quantities appear as ratios of $\theta(t)$ to $\theta(0) \equiv \theta_0$, that is, as activities relative to values at initial times, it is necessary only to ensure that the response of the counter is made independent of the distribution of the radioactivity within it. This is done as described below. The usual assumption is made that

(1) The greater part of the experimental material here reported has been taken from work done by Guy F. Allen toward the degree of Doctor of Philosophy at the University of North Carolina.

(2) Max-Planck-Institut für Metallforschung, Stuttgart, Germany.

(3) To whom any communications may be directed.

(4) H. C. Thomas, *Proc. Natl. Acad. Sci.*, **42**, 909 (1956).

(5) T. Fujii and H. C. Thomas, *J. Phys. Chem.*, **62**, 1566 (1958).

the stoichiometrically negligible trace of tagged ion is chemically identical with the bulk of the ion of interest. If the experiment is performed so that all the concentrations, c, are constant in time in their appropriate regions, and if we assume instantaneous isotopic equilibrium at the interfaces, the diffusion problem is

$$D \frac{\partial^2\theta}{\partial x^2} = \frac{\partial\theta}{\partial t} \qquad 0 < x < a \qquad (1)$$

$$\frac{\partial\theta}{\partial x} = 0 \qquad x = 0 \qquad (2)$$

$$\theta = \theta_m \qquad x = a \qquad (3)$$

$$\zeta \frac{\partial\theta}{\partial x} = \frac{\partial\theta_m}{\partial x} \qquad x = a \qquad (4)$$

where $\qquad \zeta = Dc/D_m c_m \qquad (5)$

$$D_m \frac{\partial^2\theta_m}{\partial x^2} = \frac{\partial\theta_m}{\partial t} \qquad a < x < a + b \qquad (6)$$

$$\theta_m = 0 \qquad x = a + b \qquad (7)$$

$$\theta = \theta_m = \theta_0 \qquad t = 0, \ 0 \le x \le a + b \qquad (8)$$

The quantity actually measured may be written

$$Q = Ac \int_0^a \theta dx + Ac \int_a^{a+b} \theta_m dx \qquad (9)$$

that is, a quantity proportional to the total amount of radioactivity in the region 0 to $a + b$, the constant A being proportional to the cross section of the diffusion cell and to the efficiency of the counter. The portion of the cell containing the diffusing system is mounted in the well of a scintillating crystal and this total activity Q is measured periodically as the diffusion progresses. We need a solution of the problem for Q/Q_0 from which the value of D can be determined, where Q_0 is the initial count.

The depth of the cell proper, *i.e.*, the length of the "short rod," a, is carefully measured. It is impossible, however, to measure accurately either the thickness, b, of the wet membrane or the bulk concentration, c_m. As here stated we have a four parameter problem, with D, D_m, ζ, and b as adjustable constants. Aside from the fact that such a problem is effectively intractable as regards computation, one could scarcely expect any reliability in a determination of D by such a means.

The problem therefore is reduced by using very thin membranes and assuming, subject to justification, that the membrane is sufficiently thin that we have a linear gradient of θ within it at all times after the start of the experiment. We examine this important point later.

Equations 4, 5, and 6 therefore are to be replaced by

$$cD \frac{\partial \theta}{\partial x} = -c_m D_m \frac{\theta}{b} \quad x = a$$

or

$$\xi \frac{\partial \theta}{\partial x} = -\theta \quad x = a \quad (10)$$

with

$$\xi = b \frac{Dc}{D_m c_m} \quad (11)$$

We now have a problem with only two parameters, D, the quantity we seek, and ξ, the effective thickness of the membrane.

A further simplification, which for a thin membrane introduces the need for a small correction, described below, is to consider that the contribution of the membrane to the total measured activity is negligible after the start of the experiment, so that we may write

$$\frac{Q}{Q_0} = \int_0^a \frac{\theta}{\theta_0} \, \mathrm{d}(x/a) \quad (12)$$

As has been shown,[4] the solution of this simplified problem can be written

$$\frac{Q}{Q_0} = 1 - \frac{1}{\pi i} \frac{1}{a} \int_L \frac{e^{\lambda^2 Dt} \mathrm{d}\lambda}{\lambda^2} \times$$

$$\frac{e^{a\lambda} - a^{-a\lambda}}{(\lambda\xi + 1)e^{a\lambda} - (\lambda\xi - 1)e^{-a\lambda}} \quad (13)$$

where L refers to the Bromwich path in the complex plane of λ, the infinite vertical to the right of all the singularities of the integrand.

The earlier series representations[4] of (13) are most useful for obtaining a qualitative idea of the nature of the results. They have not proved to be adaptable to a computation which does justice to the precision obtainable in the experiment. A single experiment may produce from thirty to a hundred or more values of Q/Q_0 and t. We require a method for selecting by the method of least squares the values of D and ξ which best represent the data. As is shown in the Appendix, expression 13 can be evaluated by a contour integration with the result

$$\frac{Q}{Q_0} = 2 \sum_{n=1}^{\infty} \frac{e^{-\alpha_n^2 Dt/a^2}}{\alpha_n^2} \frac{1}{\omega^2 \alpha_n^2 + \omega + 1} \quad (14)$$

in which $\omega = \xi/a$ and the α_n are the positive roots of

$$\omega \alpha \tan \alpha = 1$$

The α_n increase with n by increments of approximately π, and hence the series in (14) converges very rapidly for any but extremely small values of t. In order to use a minimum of computer time we apply the method of least squares in the following manner. Writing $f_i = f(D, \xi, t_i)$ for the value of Q/Q_0 computed from (14) for specified D, ξ, at time t_i, we need, for an experiment in which m measurements are made, solutions for D and ξ of

$$\sum_{i=1}^{m} \left\{ \left(\frac{Q}{Q_0} \right)_i - f_i \right\} \frac{\partial f_i}{\partial D} = 0$$

$$\quad (15)$$

$$\sum_{i=1}^{m} \left\{ \left(\frac{Q}{Q_0} \right)_i - f_i \right\} \frac{\partial f_i}{\partial \xi} = 0$$

The derivatives in (15) are quite complicated and it is impractical to search directly for solutions of these transcendental equations. Hence, experimental values, $(Q/Q_0)_i$, are plotted against the square root of the average elapsed time for the measurement, $\sqrt{t_i}$. As has been shown[4] the slope and intercept of the straight line through the central portion of this curve give approximate values of D and ξ through the relation

$$\frac{Q}{Q_0} \simeq 1 + \frac{\xi}{a} - \frac{2}{a} \sqrt{\frac{Dt}{\pi}} \quad (16)$$

(In the earlier work it was considered possible to draw this line so as to give a sufficiently accurate value for D. This is illusory, unless one is content with an uncertainty in D of as much as 10%.) Using these approximate values of D and ξ as a guide, a set of values D_j and ξ_k are selected so as to enclose the values which minimize the deviations of the data for a particular experiment with respect to the curve (14) computed from these values. (A preliminary trial may be necessary in order to accomplish this.) We then cause to be computed the quantities ϵ_D and ϵ_ξ defined by the relations

$$\epsilon_D = 2 \sum_{i=1}^{m} \left\{ \left(\frac{Q}{Q_0} \right)_i - f(D_j, \xi_k, t_i) \right\} \frac{\partial f(D_j, \xi_k, t_i)}{\partial D}$$

$$\quad (17)$$

$$\epsilon_\xi = 2 \sum_{i=1}^{m} \left\{ \left(\frac{Q}{Q_0} \right)_i - f(D_j, \xi_k, t_i) \right\} \frac{\partial f(D_j, \xi_k, t_i)}{\partial \xi}$$

for all the pairs D_j, ξ_k. The ranges for both D and ξ are small; hence we find that a plot, say, of the values of ϵ_D for a fixed ξ against the D_j gives a nearly straight line and determines a value of ξ for which ϵ_D vanishes. We thus determine a set of pairs D_0, ξ_0 which causes ϵ_D to vanish and similarly another set which causes ϵ_ξ to vanish. Plots of D_0 vs. ξ_0 give two intersecting straight lines (if the ranges have been properly chosen); the intersection of these lines produces the pair, D, ξ, which satisfies (15).[6] A poor guess as to the required ranges of D and ξ will give lines which fail to intersect. An example of this computation is given in Fig. 1a–c. In an actual case it is unnecessary to make the plots indicated; linear interpolations suffice. The most noticeable feature of the lines in Fig. 1c is the small angle between them. This angle is an inverse measure of the difficulty of the experiment. In early and abortive experiments we had cases in which no intersection at all could be obtained; the lines osculated over a wide range. It seems probable that an analysis of the significance of the experiment could be given in terms of the intersection of these lines. This, however, we have not attempted.

Before discussing the effect of assuming a linear gradient in the membrane, it will be convenient to describe the actual experiment in some detail.

Experimental

The Diffusion Cell.—The success of the experiment depends principally on two things: the confinement of the gel in the form of a short rod of accurately known length and the use of a very thin membrane. The membrane must be stretched tautly
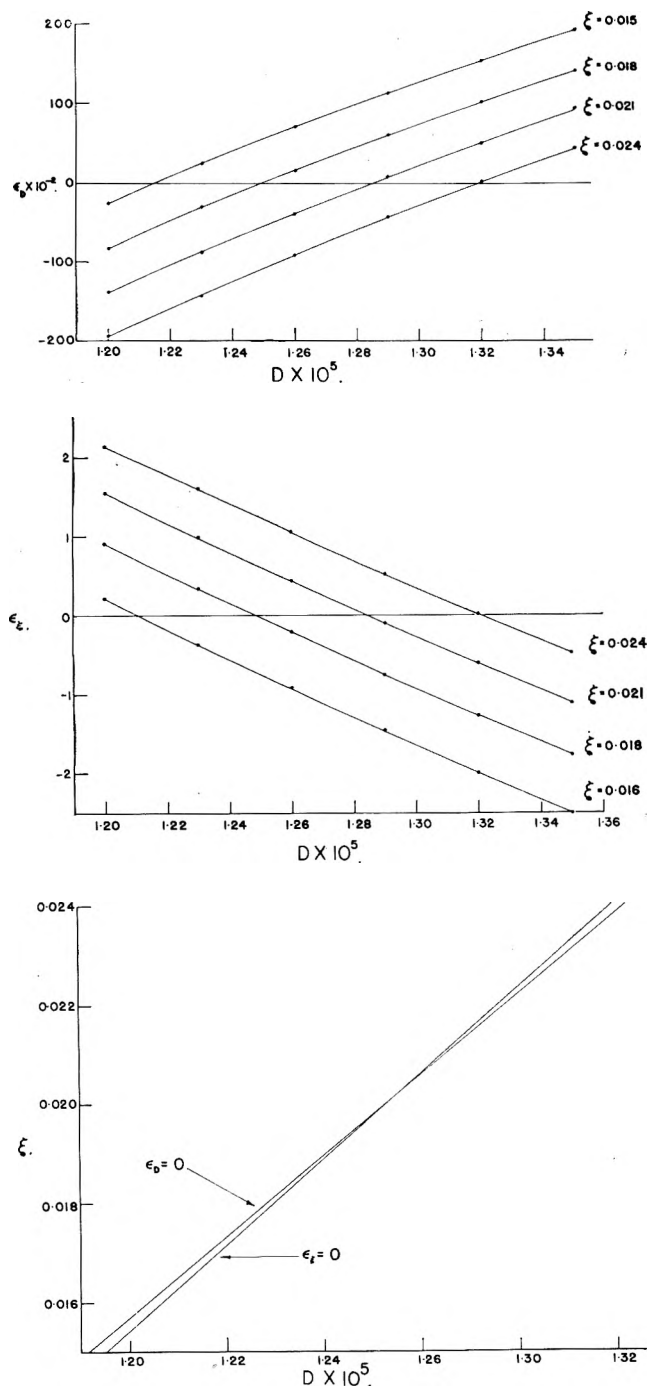
Fig. 1.—(a), (b) The quantities ϵ_D and ϵ_ξ of eq. 17; (c) the determination of the "best" values of D and ξ according to the least squares procedure.

Fig. 2.—The diffusion cell.

over and in perfect contact with the surface of the gel so that it withstands without distortion the effects of a rapidly moving stream of solution. These requirements, as we believe we can show, are accomplished to an ascertainable degree by the apparatus shown in Fig. 2.

The gel is confined in a stainless steel cavity between the membrane and a glass plate as shown in Fig. 2, detail. In actual use the sequence of steps is as follows. The central section is first fixed into place. During an experiment the solution, constituting the "rapidly stirred bath at zero activity" passes down the annular space between the middle and inner parts of the cell, across the surface of the membrane, and then out of the cell through the central hole. The character of the flow of the solution across the membrane is controlled by the speed of the pump, which produces a flow rate of 700 ml./min., and by the height of the inner section above the membrane, which is adjusted before the membrane is put into place. Leakage is prevented by appropriate O-rings. Three nibs equally spaced
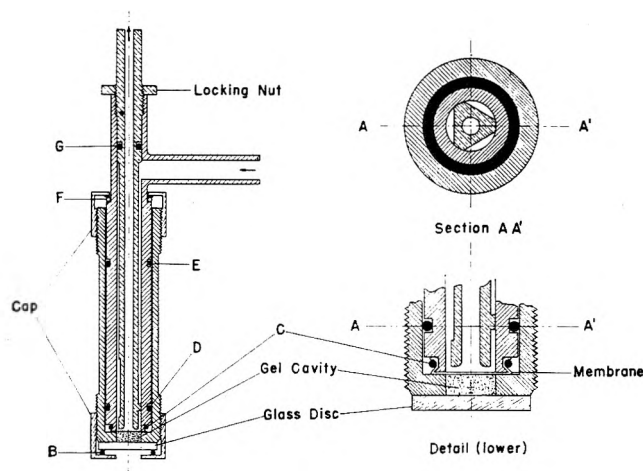
around the bottom of this inner section hold it concentric with the middle section. Large changes in the rate of flow of the solution have been shown not to affect the results.

The membrane consists of unwater-proofed cellophane.[7] A piece of the material is soaked for 4 hr. or more in the solution intended for an experiment. The bit of cellophane, blotted to remove excess solution (an essential point), is carefully positioned on the lower end of the middle section of the cell, held in an inverted position, and the neoprene O-ring B is put in place. When the membrane is taut and free of wrinkles, the extra cellophane is trimmed from around the O-ring. The middle section is now inserted into the outer shell and the upper cap tightened, thus clamping the membrane across the empty gel cavity. Great care is here necessary to avoid damaging the delicate membrane. Rotation of the middle section is prevented by the Teflon O-ring E and brass washer; no shear is produced in the membrane on tightening the upper aluminum cap.

The lower end of the cell is now screwed into a plate of steel, the upper surface of which has been ground flat, smooth, and perpendicular to the gel cavity. With the whole clamped in the inverted position, a warm solution of agar is placed on the cellophane, over-filling the cavity to allow for contraction. When gelation is complete, the semisolid stands above the cavity in a "meniscus" some 3 mm. high. With an ordinary straight razor sliding over the steel plate, the meniscus of the gel is removed a bit at a time. After carefully aligning the bottom of the cell cavity with the top of the steel plate, a final slice trims the short rod to the length determined by the depth of the cavity. A glass plate is then dropped over the gel and fastened firmly into place with the gasket and lower cap.

We have in use two cells, the gel cavities of which measure 0.3264 and 0.6828 cm. in depth. The uncertainty in the measurement of these depths is about 0.0008 cm. The corresponding uncertainties in D are about 0.5 and 0.25% (twice the fractional uncertainty in the length, a, of the short rod). Actually, of course, because of distortions in the surface of the gel, we cannot hope for better than an approach to this accuracy. The deeper cell was available only during the latter part of the work.

Preparation of the Gel.—A weighed quantity of agar[8] is placed in a 10-ml. volumetric flask together with an appropriate quantity of a solution of the salt under study along with enough radioactive tracer to give the desired concentration and counting rate after dilution. The flask is filled to the mark; its contents are mixed and placed loosely stoppered in boiling water until the agar dissolves. This solution is divided, in 1-ml. portions, between several small test tubes, which are stoppered and retained for the diffusion experiment. For each diffusion experiment, one of these tubes is held for about a minute in boiling water to melt the gel, which is then quickly transferred to the cell by an ordinary medicine dropper.

The Detector.—A well type scintillation detector using a thallium-activated sodium iodide crystal is used to measure the

radiation from the gel cavity. The cell fits snugly into the well of the crystal. The usual photomultiplier, linear amplifier, high speed scaler, and electronic timer are used. The elapsed time of an experiment is measured by a continuously running stopwatch, elapsed times being taken to the middle of the one minute counting intervals. When the initial counting rate is maintained below 300,000/min. counting losses are negligible with our equipment. The reservoir into which the diffusion takes place contains 3 l. of solution. The volume of this solution actually within the active volume of the crystal is about 1 ml. The maximum activity of this solution, at the end of an experiment, is approximately one tenth of the background count and is therefore entirely negligible.

To obtain the data necessary to ensure that the results are independent of the distribution of activity in the cell, we have proceeded as follows. A thin radioactive source was prepared by placing a circle of filter paper in a glass cylinder, just fitting the well of the crystal, the bottom of which had been ground flat. The paper was moistened with a drop of solution containing Co^{60} and covered with a glass plate. This plate was held firmly in place by a glass rod sealed to the upper part of the cylinder. This contrivance was placed in the well of the crystal and careful measurements of the counting rate were determined at various distances from the bottom, as measured by a cathetometer. A nearly linear decrease in counting rate was observed as the source was moved upward. This result was confirmed as to the slope of the line giving rate vs. depth in well by clamping a similar source between glass plates in the bottom of the diffusion cell. With respect to the center of the cell these results correspond to a relative efficiency of our crystal given by

$$\epsilon = 1 - 0.0285 \left(\frac{x}{a} - 0.5 \right) \text{ for the shallow cell}$$

and

$$\epsilon = 1 - 0.046 \left(\frac{x}{a} - 0.5 \right) \text{ for the deeper cell}$$

The value of Q/Q_0 actually observed is, therefore

$$\int_0^a \frac{\theta}{\theta_0} \epsilon \, d(x/a)$$

rather than the quantity given by eq. 12. The relative values of these quantities were obtained by graphical integrations of the profiles for θ/θ_0 vs. x/a (for the case of $\xi = 0$ given by Crank.[9] Since the variation in counting rate with cell depth is linear, we obtain zero correction for Q_0, i.e., for the case in which $\theta =$ constant. At later stages of the experiment the observed values of Q/Q_0 must be corrected downward because of the higher efficiency near the well bottom.

To make the data correspond more exactly to the simplification implied by eq. 12, i.e., to arrange the omission of the contribution to the measured value of Q due to the ion content of the membrane, another small correction is strictly necessary. After the initial stage of the experiment, when the gradient in the membrane has nearly reached linearity, the count due to the membrane is to be deducted from the total count. We estimate the magnitude of this correction as follows.

It is to be noted first that in filling the cell with the radioactive gel we necessarily introduce that volume of gel which corresponds to the value of Q_0 used in the mathematical development, the value which corresponds to an "empty" membrane. It is, of course, impossible to prevent the membrane from taking up a portion of this activity during the filling process, thereby producing a disturbance in the simple boundary conditions assumed for the experiment. Because the diffusion coefficients are small and because we get little mixing of the gel in the filling process, this maldistribution of activity may reasonably be supposed to occur only in the immediate neighborhood of the membrane. The disturbance is, in any case, relatively small as will be shown. We may expect then that shortly after the start of the diffusion into the solution the distribution of activity near the membrane will approach that assumed in the theory. Unfortunately, it does not seem to be possible to check this point directly. We are forced to rely on the following indirect evidence. In a long experiment the computations have been carried out in three

(9) J. Crank, "Mathematics of Diffusion," Oxford, 1956, p. 46.

ways: (a) the first half of the measurements were omitted, (b) the second half were omitted, and (c) every other measurement over the whole course of the experiment was omitted. The results obtained from these three computations are

	$D \times 10^5$	ξ
(a)	1.223	0.0191
(b)	1.222	.0190
(c)	1.220	.0184

There thus seems to be no evidence that the initial disturbance of the boundary conditions affects our values of D by a significant amount.

To assess the necessity of deducting the activity residing in the membrane during an experiment direct measurements have been made of the initial amount of this activity. The cell was filled as usual and counted. The gel was then removed, the membrane wiped, and the metal parts of the cell carefully cleaned. After reassembling the cell the membrane alone was counted. These measurements have been made for all the gels studied. The fraction of the activity taken up by the membrane, which we denote by q_0/Q_0, is found to depend both on the nature and the concentration of the ion under study. As it should be, q_0/Q_0 is found to be inversely proportional to the depth of the cell. Fortunately this ratio is small even for our shallower cell. Representative values, including the largest found, are given in Table I.

TABLE I[a]

SELECTED VALUES OF FRACTIONAL ACTIVITY OF MEMBRANES
(q_0/Q_0)

Cell depth, cm.	Concn., moles/ l.	Wt. % agar	CsCl	q_0/Q_0 NaCl	CoCl₂
0.3264	0.010	1	....	0.018(0.026)	....
		2	0.015(0.034)	.012	0.014(0.025)
		4	....	.010(0.024)	....
0.6828	0.010	1	....	0.010	....
		2	....	.007	....
		4	....	.006	....

[a] The numbers in parentheses are for 300 gage cellophane; the others are for the thinnest cellophane.

For a linear gradient in the membrane the correction to be applied to Q/Q_0 because of the activity in the membrane is

$$- \frac{1}{2} \frac{\theta(a,t)}{\theta_0} \frac{q_0}{Q_0}$$

We assume that the appropriate initial count of the membrane, q_0, is close to the value determined in the separate experiment just described. Noting that the flux through the membrane, as given through the boundary condition (10), is just $-dQ/dt$, we may evaluate $-\frac{1}{2}[\theta(a,t)/\theta_0]q_0/Q_0$ in terms of $d(Q/Q_0)/dt$ and find for the correction to be subtracted

$$\frac{a\xi}{240D} \frac{1}{\sqrt{t'}} \left| \frac{d(Q/Q_0)}{d\sqrt{t'}} \right| \frac{q_0}{Q_0}$$

where t' is in minutes and the derivative is taken for convenient application to the plot of the data vs. $\sqrt{t}$, in which the slope is nearly constant over wide ranges. For typical experiments with the thin cellophane this correction decreases from 0.00042 to 0.00009; for the thicker cellophane, from 0.00097 to 0.00021. It is thus nearly negligible and has been disregarded in the results reported in this paper. Certainly this correction should be taken into account in work striving for greater accuracy.

The agreement between the observations and the curve computed for the least square values of D and ξ may be illustrated by data from the experiment mentioned above in which the computations were carried out over different portions of the run. In each of these a total of sixty pairs of values of Q/Q_0 and t was used. For the three cases the following values of $\sqrt{\Sigma\delta^2/60}$ were obtained: (a) 0.0019, (b) 0.0018, (c) 0.0018. These deviations were computed for the whole course of the experiment regardless of the portion used in determining the values of D and ξ. In this experiment $Q_0 = 250,000$, and the computations variously extended from $Q/Q_0 = 0.94$ to $Q/Q_0 = 0.14$. Thus the agreement near the beginning of the experiment $(1/460)$ corresponds closely to the counting error $(1/475)$. Toward the

end of the experiment the agreement is somewhat less satisfactory ($1/_{70}$ as compared with $1/_{100}$ for the counting error).

Results

We report here self-diffusion coefficient of Na^+, Cs^+, and Co^{++} in chloride solutions in 2% agar gels at 25°. The gels have been prepared with solutions of several different concentrations. The tracers employed were Na^{22}, Cs^{134}, and Co^{60}. The results are given in Tables II, III, and IV, together with the computed values of ξ; here each value of D is the outcome of an independent experiment. All of the results in Tables II, III, and IV were obtained with the thinnest cellophane membrane. In order to assess the accuracy of the principal approximation of the theory of the experiment, that of a linear gradient in the membrane, additional experiments have been made with a thicker cellophane, denoted 300 gage. For purposes of comparison average diffusion coefficients from all experiments using different membrane thicknesses are assembled in Table V. The dry thickness of the cellophane is immaterial, and we cannot measure its true thickness under experimental conditions. An appropriate measure of the "effective thickness" is supplied by the values of ξ given in this table. It is there seen that to within our estimate of accuracy the thickness of the confining membrane is without influence on the results.

TABLE II

SELF-DIFFUSION COEFFICIENTS OF Cs^+ IN CsCl FOR 2% AGAR GEL AT 25° (THINNEST CELLOPHANE)

Concn. of CsCl, moles/l.		$D \times 10^5$, cm.²/sec.	ξ, cm.
0.001		1.90	0.0025
		1.89	.0021
	Av.	1.90	
.010		1.88	.0092
		1.90	.0086
	Av.	1.89	
.050		1.91	.0181
		1.91	.0190
		1.94	.0187
	Av.	1.92	
.100		1.92	.0211
		1.92	.0210
	Av.	1.92	
.250		1.91	.0204
		1.90	.0229
	Av.	1.90	

TABLE III

SELF-DIFFUSION COEFFICIENTS OF Na^+ IN NaCl FOR 2% AGAR GEL AT 25° (THINNEST CELLOPHANE)

Concn. of NaCl, moles/l.		$D \times 10^5$, cm.²/sec.	ξ, cm.
0.001		1.224	0.0054
		1.221	.0046
		1.204	.0048
		1.239	.0058
	Av.	1.222	
.010		1.266	.0086
		1.257	.0105
		1.277	.0104
	Av.	1.267	
.050		1.293	.0185
		1.298	.0194
		1.260	.0166
		1.273	.0157
		1.258	.0176
	Av.	1.276	
.500		1.242	.0241
		1.228	.0233
	Av.	1.235	
1.000		1.179	.0202
		1.172	.0212
	Av.	1.176	

TABLE IV

SELF-DIFFUSION COEFFICIENTS OF Co^{++} IN CoCl₂ FOR 2% AGAR GEL AT 25° (THINNEST CELLOPHANE)

Concn. of CoCl₂, moles/l.		$D \times 10^5$, cm.²/sec.	ξ, cm.
0.001		0.421	0.0040
		.441	.0053
	Av.	.431	
.010		.575	.0228
		.576	.0208
		.573	.0200
		.580	.0200
		.574	.0238
	Av.	.576	
.050		.627	.0272
		.625	.0300
	Av.	.626	
.250		.601	.0263
		.601	.0286
	Av.	.601	

Discussion

In a pure non-reactive solvent self-diffusion coefficients of ions at low concentration should theoretically obey a limiting equation of the form

$$\frac{D}{\Lambda_0/|z|} = \frac{RT}{F^2} - S\sqrt{c}$$

in which Λ_0 is the limiting ionic conductance, $|z|$ the charge number of the ion, and S a complicated function of limiting ionic mobilities.[10] In Fig. 3 are given plots of our values of D vs. $\sqrt{c}$. The most salient feature of these is the sharp drop in D near $c = 0.001$ M for sodium

and for cobalt. Agar contains acidic groups which in the 2% gel are near 0.001 M in concentration. Freise[11] has discussed diffusion in gels of this character and has made similar observations for the bulk diffusion of salts. The effect is similar to that obtained by Richman and Thomas[12] in a resinous ion exchanger. It is interesting that in the case of cesium the effect is nearly absent. One concludes that this ion is bound much less tightly by the fixed groups of the gel.

Figure 3 includes a plot of Mills'[13] self-diffusion data for the sodium ion in aqueous solution. The values for the agar gel are seen to be consistently lower at the inter-

(10) See, e.g., H. S. Harned and B. B. Owen, "The Physical Chemistry of Electrolytic Solutions," 3rd Ed., Reinhold Publ. Corp., New York, N. Y., 1958, p. 245.

(11) V. Freise, Z. physik. Chem. (Frankfurt), 4, 129 (1955).
(12) D. Richman and H. C. Thomas, J. Phys. Chem., 60, 273 (1956).
(13) R. Mills, J. Am. Chem. Soc., 77, 6116 (1955).

TABLE V

DIFFUSION COEFFICIENTS OBTAINED USING MEMBRANES OF DIFFERENT THICKNESSES

Concn., moles/l.	Cell depth, cm.	Wt. % agar	$D \times 10^5$, cm.²/sec., thinnest cellophane	ξ, cm.	$D \times 10^5$, cm.²/sec., 300 gage cellophane	ξ, cm.
			CsCl			
0.010	0.3264	2.0	1.89	0.008$_8$	1.84	0.012$_5$
.050	.3264	2.0	1.92	.018$_6$	1.91	.038$_0$
			NaCl			
0.010	0.3264	1.0	1.29$_0$	0.007$_2$	1.292	0.015$_0$
.010	.6828	1.0	1.273	.009$_8$	1.27$_0$	.017$_9$
.010	.3264	2.0	1.267	.009$_8$	1.27$_0$	.014$_8$
.010	.3264	4.0	1.19$_5$	.008$_9$	1.182	.014$_9$
.010	.6828	4.0	1.174	.011$_6$	1.174	.020$_2$
.050	.3264	2.0	1.276	.017$_6$	1.27$_3$	.038
			CoCl₂			
0.010	0.3264	2.0	0.576	0.022$_0$	0.567	0.043$_2$
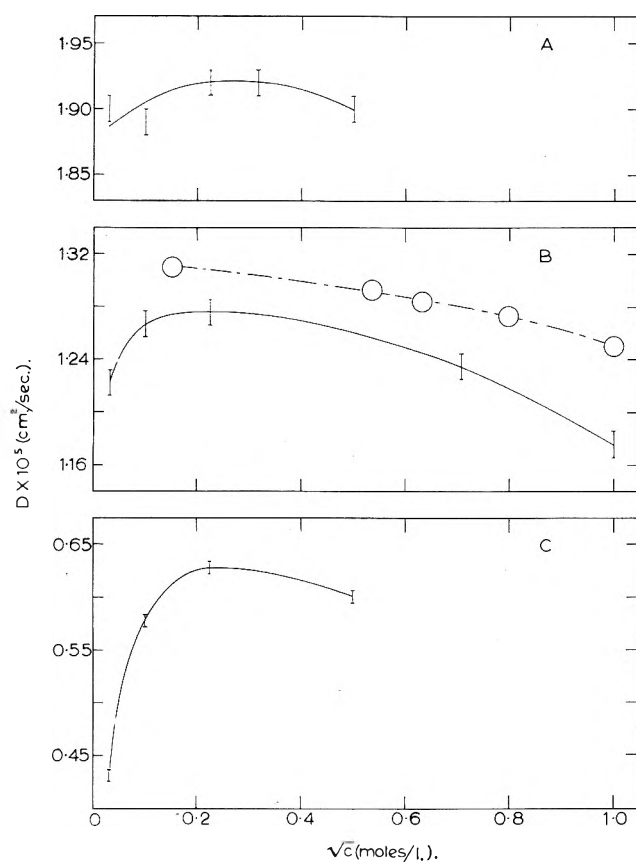
Fig. 3.—Concentration dependence of self-diffusion coefficients in 2% agar gels: (A), Cs in CsCl; (B), Na in NaCl (the circles are Mills'[13] data for aqueous solutions); (C), Co in CoCl₂ at 25°.

mediate concentrations where the fixed acidic groups are of no consequence. This is to be expected; our solutions are only 98% water and there must be tortuosity in the diffusion path due to the agar network. Without a detailed theory of the complications in the gel at low concentration, it is not possible to give a convincing comparison of our results with the requirements of the Nernst limiting law.

Appendix

The Contour Integration for Q/Q_0.—We have to find the singularities of the integrand in expression 13. Since $e^{a\lambda} - e^{-a\lambda} = 2a\lambda(1 + a^2\lambda^2/6 + \ldots)$ and since $\lambda = 0$ is not a zero of $(\lambda\xi + 1)e^{a\lambda} - (\lambda\xi - 1)e^{-a\lambda}$, the integrand has a simple pole at the origin. If we put this last expression in the form

$$a\lambda \tanh a\lambda = -a/\xi = -1/\omega$$

the remaining singularities are poles at the roots of

$$\omega z \tanh z = -1 \qquad (A)$$

in which $\omega = \xi/a$ is real and positive. There are therefore poles along the imaginary axis at the roots of

$$\omega y \tan y = 1$$

These are the only roots of (A), as the following consideration shows
$z \tanh z =$

$$\frac{[x \tanh x(1 + \tan^2 y) - y \tan y(1 - \tanh^2 x)] + i[y \tanh x(1 + \tan^2 y) + x \tan y(1 - \tanh^2 x)]}{1 + \tanh^2 x \tan^2 y}$$

Since for $|x| > 0$, $\tanh^2 x < 1$, and since x and $\tanh x$ have the same sign, the imaginary part of this expression can vanish only if y and $\tan y$ have opposite signs. But in this case the real part is necessarily positive, hence $z \tanh z$ cannot be real negative xcept for $x = 0$. Along the exceptional lines $y = (2n + 1)\pi/2$, $z \tanh z = [x + i(2n + 1)\pi/2]\coth x$, and there are no roots of (A).

The integrand in (13) is odd; thus, because of the exponential factor, the circuit around the imaginary axis gives us twice the integral we seek. Evaluating the residues and grouping them in pairs at $\pm i\alpha_n$ we find (14).

For ω small, a thin membrane, the roots of $\omega\alpha \tan \alpha = 1$ are nearly odd multiples of $\pi/2$. Successive terms of the series are approximately in the ratio $\exp\{-2(n + 1)\pi^2 Dt/a^2\}$, making for rapid convergence.

THE DISCRETE-ION EFFECT AND COLLOID STABILITY THEORY
TWO PARALLEL PLATES IN A SYMMETRICAL ELECTROLYTE[1]

By S. Levine and G. M. Bell

Department of Mathematics, University of Manchester, and Department of Mathematics, Chelsea College of Science and Technology, London, S.W.3, England

A general expression based on Grahame's double layer model is derived for the interaction energy of the electric double layers of two parallel colloidal plates immersed in an aqueous binary symmetrical electrolyte. The results constitute a further development of the stability theory of Derjaguin and Landau and Verwey and Overbeek. The specific character of the adsorbed counterions in the Stern layer is taken into account through the specific (chemical) adsorption energy, the distance of the adsorption (inner Helmholtz) plane from the colloidal wall, and the number of absorption sites occupied by each counterion. Any variation of the dielectric constant of the "inner region" with surface potential is, however, ignored and the Gouy–Chapman theory is applied to the diffuse layer. Two types of discrete-ion effect relating to the adsorbed counterions are considered. One is the entropy correction due to the ion size and the other (which is the more important) is the difference between the actual electric potential at an adsorbed counterion and the average potential on the adsorption plane. This difference, termed the "discreteness-of-charge" effect, adds a new negative term, very nearly proportional to the density of adsorbed counterions, to the adsorption energy. In consequence, as the potential-determining ion concentration and hence the interfacial potential vary, the potential at the limit of the diffuse layer (the outer Helmholtz plane) at the critical coagulation condition passes through a maximum. A corresponding maximum is found in the concentration of coagulating electrolyte. A convenient method of calculating the interaction energy for moderately large outer Helmholtz plane potentials is developed and the linear superposition approximation is also used. By comparison and by considering correction terms the two methods are shown to be reasonably accurate. The conclusion is that none of the simple formulas previously proposed for the variation of coagulating electrolyte concentration with valency can be generally valid and that the Schulze–Hardy rule must describe a range of ratios of coagulating concentration dependent on the specific adsorption characteristics of the counterion. The theoretical results are compared with experiment particularly for the silver halide sols.

1. Introduction

In two recent papers[2,3] (called I and II) the authors incorporate the so-called discreteness-of-charge effect (or discrete-ion effect) into the stability theory of lyophobic colloids of Derjaguin and Landau[4] and Verwey and Overbeek[5] (D.L.V.O. theory). In view of the complexity of the problem the model of two parallel plate-like particles of infinite thickness, immersed in a large volume of aqueous, binary, symmetrical flocculating electrolyte, is chosen. The concentration in the dispersion medium of the potential-determining anions, responsible for the negative plate charge, is assumed negligibly small. The Stern–Grahame picture of the electric double layer (Fig. 1), originally applied to the mercury–electrolyte interface, is modified to correct for the discrete character of the adsorbed counterions and is assumed to apply to the surfaces of the colloidal plates. In a recent communication[6] (III), the authors show that this discrete-ion effect can be interpreted in terms of a "self-atmosphere" potential at an adsorbed counterion. An important consequence of this innovation is that the electrostatic potential at the outer Helmholtz plane (O.H.P.), the boundary between the Stern "inner region" and the diffuse layer, exhibits a maximum as the potential across the interface varies at constant electrolyte concentration. This is in accord with experiment for the mercury system[7] and a maximum at other interfaces is suggested by the

observation of a maximum in the ζ potential of silver bromide sols,[8,9] glass–electrolyte interface,[10] and O/W emulsions stabilized by surface active ions.[11,12] The inner region is treated as a homogeneous uniform medium with both dielectric constant and width fixed, independent of surface charge densities. Colloid stability theory should include dielectric saturation and electrostriction in the inner region but for brevity these will not be discussed here. However an entropy term in the adsorption isotherm due to the size of the partially hydrated ions will be introduced. The Gouy–Chapman theory is applied to the diffuse layer.

According to the conventional D.L.V.O. theory the electrolyte concentration required for flocculation increases with the surface potential of the colloidal particles. In contrast, our theory predicts that the flocculating concentration increases with this potential when it is small but then attains a maximum and decreases. With univalent coagulating ions this maximum is found at high potentials, which are seldom attainable in coagulating hydrophobic sols but the maximum is reached with polyvalent coagulating ions. This is a consequence of the maximum in the potential at the O.H.P. and therefore will not occur if the "self-atmosphere" effect for an adsorbed ion is ignored. Qualitative agreement is obtained between our theory and the experimental work on the dependence of flocculating electrolyte concentration on surface potential, most of which has been done with silver halide sols in *"statu nascendi"* by Tezak, Matijević, Mirnik,

(1) Part of this paper was presented at the Unilever Research Symposium, held at Noordwijk, Netherlands, from September 19th to 22nd, 1961.

(2) S. Levine, G. M. Bell, and D. Calvert, *Nature*, **191**, 699 (1961).

(3) S. Levine and G. M. Bell, *J. Colloid Sci.*, **17**, 838 (1962).

(4) B. V. Derjaguin and L. Landau, *Acta Physicochim. URSS*, **14**, 633 (1941).

(5) E. J. W. Verwey and J. Th. G. Overbeek, "Theory of the Stability of Lyophobic Colloids," Elsevier, Amsterdam, 1948.

(6) S. Levine, G. M. Bell, and D. Calvert, *Can. J. Chem.*, **40**, 518 (1962); see also G. M. Bell, S. Levine, and B. Pethica, *Trans. Faraday Soc.*, **58**, 904 (1962).

(7) D. C. Grahame, *Chem. Rev.*, **41**, 441 (1947); *Z. Elektrochem.*, **62**, 264 (1958); D. C. Grahame and B. A. Soderberg, *J. Chem. Phys.*, **22**, 449 (1954).

(8) K. N. Davies and A. K. Holliday, *Trans. Faraday Soc.*, **48**, 1066 (1952).

(9) R. H. Ottewill and R. F. Woodbridge, to be published.

(10) S. A. Greenberg, T. N. Chang, and R. Jarnutowski, *J. Polymer Sci.*, **58**, 147 (1962).

(11) P. J. Anderson, *Trans. Faraday Soc.*, **55**, 1421 (1959).

(12) D. A. Haydon, *Proc. Roy. Soc.* (London), **A258**, 319 (1960).

and their schools[13-15] but there is one difference for AgI sols. In I and II a simple approximation to the electric double layer interaction was obtained by linear superposition (L.S.) of the potential distributions of the interpenetrating diffuse layers. A noticeable drop in the coagulating concentration on each side of the maximum was found whereas, according to Mirnik, et al.,[15,16] the coagulating concentration in AgI systems is almost independent of the plate potential. In the present paper, a general expression will be obtained for the electrochemical free energy of interaction per unit area of the plates, based on the electric double layer model described above. A practicable method of calculating this energy for large potentials at the O.H.P. is developed by employing an expansion due to Derjaguin and Landau[4] and Hoskin and Levine.[17] It is found that over a large range of surface potential the variation in the coagulating electrolyte concentration is reduced by choosing large potentials at the O.H.P. Comparison is made with linear superposition and a method of improving upon the latter is also given. The different formulations of the Schulze–Hardy rule, as suggested by Tezak[13-15,18] and by the D.L.V.O. theory are also discussed.

2. Notation and Preliminary Relations

$2h$ separation of the two plates

d thickness of the inner region

$h' = h - d$ distance between the median plane and O.H.P.

β distance between the wall and the plane of centers of adsorbed counterions (inner Helmholtz plane or I.H.P.)

$\gamma = d - \beta$ distance between the I.H.P. and O.H.P.

ϵ, ϵ_1 dielectric constant of the (aqueous) dispersion medium and inner region

$K = \epsilon_1/4\pi d$ capacity per unit area of the inner region

e, k, T electronic charge, Boltzmann's constant, absolute temperature

ψ_0 potential at the colloidal wall, independent of h

$\psi_d = \psi_d(h), \psi_\beta = \psi_\beta(h), \psi_m = \psi_m(h)$ potentials at the O.H.P., I.H.P., and median plane

$\eta_d = e\psi_0/kT, \eta_d = \eta_d(h) = e\psi_d(h)/kT, \eta_m = \eta_m(h) = e\psi_m(h)/kT$ dimensionless quantities

$\Psi_d = \psi_d(\infty), H_d = \eta_d(\infty)$ values of ψ_d and η_d at infinite plate separation

$\Delta\psi_d = \psi_d(h) - \Psi_d, \Delta\eta_d = \eta_d(h) - H_d$

$k = \mathrm{sech}\ ^1/_2 \eta_m(h), v = \mathrm{sech}\ ^1/_2 zH_d$

z_β, z_s valencies of coagulating cation and potential-determining anion

$z - z$ valency type of coagulating electrolyte. For negative plates $z = z_\beta$

n number per unit volume of z-z electrolyte (dissociated) molecules in dispersion medium

n_0 number per unit volume of solvent (water) molecules

κ Debye–Hückel parameter, defined by $\kappa^2 = 8\pi n z^2 e^2/\epsilon kT$

$\theta = \kappa h', X = \kappa e/4\pi K$ dimensionless quantities

$\nu_\beta = \nu_\beta(h)$ number of adsorbed cations per unit area of I.H.P.

$\sigma_\beta = z_\beta e\nu_\beta = \sigma_\beta(h)$ charge per unit area of adsorbed cations on the I.H.P.

$\sigma_d = \sigma_d(h)$ net charge contained in a column of diffuse layer, of unit cross-section and contained between the O.H.P. and median plane. From the Gouy–Chapman theory of the diffuse layer the value of σ_d at infinite plate separation is given by eq. 2.1

(13) B. Tezak, E. Matijević, and K. F. Schulz, J. Phys. Chem., 55, 1567 (1951); 59, 769 (1955).

(14) J. P. Kratohvil, M. Orhanović, and E. Matijević, ibid., 64, 1216 (1960).

(15) M. Mirnik, F. Flajsman, K. F. Schulz, and B. Tezak, ibid., 60, 1473 (1956); M. Mirnik, F. Flajsman, and B. Tezak, Kolloid Z., 185, 138 (1962).

(16) M. Mirnik, J. Phys. Chem., 65, 1635 (1961).

(17) N. E. Hoskin and S. Levine, Phil. Trans. Roy. Soc. (London), 248, 449 (1956).

(18) E. Matijević, D. Broadhurst, and M. Kerker, J. Phys. Chem., 63, 1552 (1959).
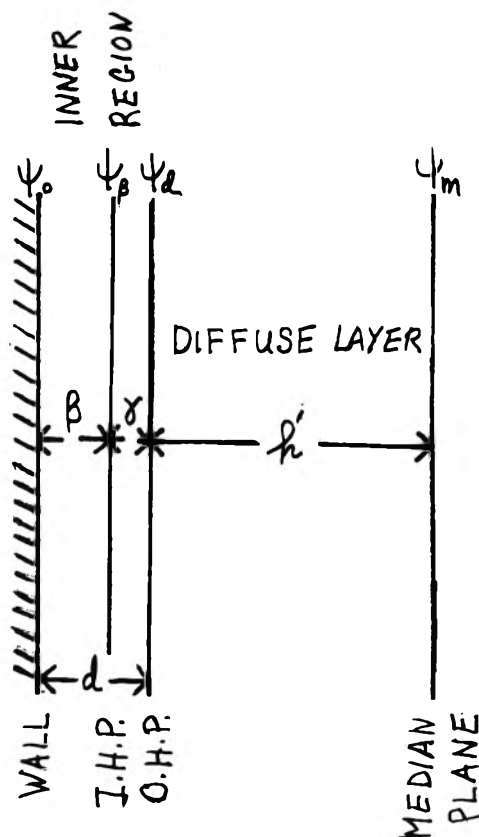
Fig. 1.—Grahame model of electric double layer, applied to two parallel plates at separation $2h$.

$$\Sigma_d = \sigma_d(\infty) = -\frac{4nze}{\kappa}\sinh\ ^1/_2 zH_d \qquad (2.1)$$

$\nu_s = \nu_s(h), \sigma_v = z_s e\nu_s = \sigma_0(h)$ number of potential-determining ions and charge per unit area on plate wall

$N_\beta = \nu_\beta(\infty), \Sigma_\beta = \sigma_\beta(\infty), N_s = \nu_s(\infty)$ values of ν_β, σ_β, and ν_s at infinite plate separation

$\Delta\sigma_\beta = \sigma_\beta(h) - \Sigma_\beta, \Delta\sigma_d = \sigma_d(h) - \Sigma_d$

$\Psi_0 = \psi_0 - \chi'$ where χ' is the potential across inner region when $\sigma_0 = \sigma_\beta = 0$, due to the Lange χ potential

N_a number of adsorption sites per unit area of plate

$Q = kTd^2K/e\beta\gamma$ quantity having dimensions of charge per unit area

$\sigma_\beta^0 = Q/z_\beta g$ surface charge density which is approximately equal to the value of Σ_β at which $|\Psi_d|$ is a maximum. In this paper, the maximum refers to the magnitude of the potential, irrespective of sign.

$r = \Sigma_\beta/\sigma_\beta^0$ dimensionless parameter measuring the density of adsorbed cations

$\phi_\beta = -\dfrac{\beta\gamma g\sigma_\beta}{d^2K} = -\dfrac{kTg\sigma_\beta}{eQ}$ self-atmosphere potential at an adsorbed cation, caused by its disturbing influence on neighboring adsorbed ions. This is defined as the potential at the center of a circular area in the I.H.P. of radius r_0 where $\pi r_0^2\sigma_\beta = z_\beta e$, due to a charge density $-\sigma_\beta$ uniformly distributed over this area. (From above definition $z_\beta e\phi_\beta kT = -r$.)

g factor occurring in the "self-atmosphere" potential of an adsorbed ion. It depends on the dielectric constants of particle, inner region, and diffuse layer, on the electrolyte concentration, and decreases somewhat with surface density of adsorbed ions.[6] For the silver halide systems it probably has a value in the vicinity of d/β. We assume g independent of r_0 and also $\epsilon \gg \epsilon_1$.

$$\mu_\beta = \xi_\beta + z_\beta e\psi_\beta + \Phi_\beta' + z_\beta e\phi_\beta +$$
$$kT \ln\ [\nu_\beta/(N_a - p\nu_\beta)^p] \qquad (2.2)$$

chemical potential of adsorbed cation (counterion) with center on the I.H.P. ξ_β is the chemical (short-range) energy of adsorption, and Φ_β' is due to the electrostatic image potential of the ion. The last term is due to the entropy of distribution

of the ions on the adsorption sites of the I.H.P. This includes a "co-area" term, which is obtained by adapting the volume fraction statistics of Flory[19] and Huggins[20] to the hydrated cations each occupying p adsorption sites and thus allows for the size of the adsorbed ions

$$R(r) = r - \ln r + p \ln (1 - pbr),$$
$$b = \sigma_\beta{}^0/N_a z_\beta e \quad (2.3)$$

$\mu_s = \xi_s + z_s e \psi_0$ chemical potential of potential-determining ion on plate wall

$\mu_{\beta 0} = \xi_{\beta 0} + kT \ln (n/n_0)$ chemical potential of counterion in solution, where activity coefficient is equated to unity

μ_{s0} chemical potential of potential determining ion in the solution, having a form similar to $\mu_{\beta 0}$. The volume of electrolyte is so large that $\mu_{\beta 0}$ and μ_{s0} are independent of any variation in ν_β and ν_s. On equating μ_s to μ_{s0}, the surface potential ψ_0 and hence η_0, are constant in the equilibrium state, being independent of h and n.

$\Phi_\beta = \xi_{\beta 0} - \xi_\beta + \Phi_\beta{}'$ specific absorption potential energy of cation in the I.H.P.

$\mu_\beta{}^* = \mu_\beta - z_\beta e \psi_d$, $\mu_s{}^* = \mu_s - z_s e \psi_d$ quantities which may be described as the contributions of the inner layer to μ_β and μ_s, respectively.

$$\bar{\mu}_\beta = \mu_\beta - \mu_{\beta 0} = z_\beta e \psi_d + \mu_\beta{}^* - \mu_{\beta 0}, \quad \bar{\mu}_s = \mu_s - \mu_{s0} =$$
$$z_s e \psi_d + \mu_s{}^* - \mu_{s0} \quad (2.4)$$

These two quantities vanish at thermodynamic equilibrium. If the plate separation $2h$ is varied under equilibrium, it follows that

$$\frac{d\mu_\beta{}^*}{dh} + z_\beta e \frac{d\psi_d}{dh} = 0, \quad \frac{d\mu_s{}^*}{dh} + z_s e \frac{d\psi_d}{dh} = 0 \quad (2.5)$$

$F(h)$ electrochemical free energy to be associated with the double layers per unit area of the two plates

$I(h) = F(h) - F(\infty)$ interaction energy of the double layers per unit area of the two plates

$I^*(h)$ interaction energy defined as follows: Suppose that there is no inner region and that the plates are separated by a distance $2(h - d) = 2h'$ and have a constant potential due to potential-determining ions only on the plate walls. Although assumed independent of h, this potential is assigned the value $\psi_d = \psi_d(h)$. According to the D.L.V.O. theory

$$I^*(h) = 2 \int_0^{\psi_d} \sigma_d d\psi_d + \frac{16nkT}{\kappa} (\cosh \tfrac{1}{2} z\eta_d - 1) \quad (2.6)$$

The second term is simply $-F(\infty)$ for a plate potential ψ_d, by the D.L.V.O. theory

$$p_e(h) = -\frac{1}{2} \frac{dI(h)}{dh} = 4nkT \left(\frac{1}{k^2} - 1 \right) \quad (2.7)$$

double layer force of repulsion between plates per unit area. The right-hand expression is well known for the Gouy–Chapman model, in which potential-determining ions constitute the whole surface charge and the diffuse layers extend right up to the plate walls. This is simply the ideal (osmotic) pressure due to the thermal motion of ions at the medium plane, a result originally due to Frumkin and Gorodetskaja[21] and Langmuir.[22]

A constant in the van der Waals energy of attraction per unit area

$$U(h) = I(h) - A/48\pi h'^2 \quad (2.8)$$

total interaction energy per unit area of plates. For simplicity we assume the van der Waals constant for the medium of the inner region is equal to that of the plate medium and the plates are infinitely thick.

(19) P. J. Flory, *J. Chem. Phys.*, **10**, 51 (1942).

(20) M. L. Huggins, *J. Phys. Chem.*, **46**, 151 (1942); *Ann. N. Y. Acad. Sci.*, **43**, 1 (1942).

(21) A. Frumkin and A. Gorodetskaja, *Acta Physicochim. URSS.*, **9**, 327 (1939).

(22) I. Langmuir, *J. Chem. Phys.*, **6**, 893 (1938).

$K(k), E(k)$ complete elliptic integrals of the first and second kinds, respectively

$$G(k) = \{2E(k) - 2k - (1 - k^2)K(k)\}/k$$

$$H(k) = 3(1 - k^2)K(k) + 4k - 4E(k)$$

$$\omega = \frac{6}{\pi} \frac{\epsilon^2}{KA} \left(\frac{kT}{ze} \right)^2 \text{ dimensionless quantity}$$

$$t = \tanh \tfrac{1}{4} z\eta_d(h), \quad t_0 = \tanh \tfrac{1}{4} z H_d$$

$$C_1 = 4\theta - 3 + \frac{4 \cosh \tfrac{1}{2} z\eta_d(h)}{\sinh^2 \tfrac{1}{2} z\eta_d(h)}$$

3. The Free Energy

As a preliminary we state the electrostatic equations derived from the model of Grahame[7] and Devanathan[23] for the inner region of the double layer, namely

$$\psi_0 - \psi_\beta = \frac{\beta \sigma_0}{Kd} + \frac{\beta}{d} \chi', \quad \psi_\beta - \psi_d =$$

$$\frac{\gamma(\sigma_0 + \sigma_\beta)}{Kd} + \frac{\gamma}{d} \chi', \quad \sigma_0 + \sigma_\beta + \sigma_d = 0 \quad (3.1)$$

We define $F(h)$ as the difference in free energy per unit area between the actual state of the two plates at separation $2h$ and a state in which the plates are uncharged and all ions are dissolved in the electrolyte (i.e., $\nu_\beta = \nu_s = 0$. By imagining that potential-determining anions and coagulating cations are transferred from the dispersion medium to the plate walls, we have on integrating by parts

$$F(h) = 2 \int_{\nu_\beta{}' = \nu_s{}' = 0}^{\nu_\beta{}' = \nu_\beta, \, \nu_s{}' = \nu_s} \bar{\mu}_\beta d\nu_\beta{}' + \bar{\mu}_s d\nu_s{}' = 2(\bar{\mu}_\beta \nu_\beta +$$

$$\bar{\mu}_s \nu_s) - 2 \int_{\nu_\beta{}' = \nu_s{}' = 0}^{\nu_\beta{}' = \nu_\beta, \, \nu_s{}' = \nu_s} \nu_\beta{}' d\bar{\mu}_\beta + \nu_s{}' d\bar{\mu}_s$$

$$= 2(\bar{\mu}_\beta \nu_\beta + \bar{\mu}_s \nu_s) + 2 \int_0^{\psi_d} \sigma_d d\psi_d{}' -$$

$$2 \int_{\nu_\beta{}' = \nu_s{}' = 0}^{\nu_\beta{}' = \nu_\beta, \, \nu_s{}' = \nu_s} \nu_\beta{}' d\mu_\beta{}^* + \nu_s{}' d\mu_s{}^* \quad (3.2)$$

The two integrals in the right-hand member are obtained by using (2.4), the last relation of (3.1) in the form $\sigma_d = -(z_\beta e \nu_\beta + z_s e \nu_s)$, and the fact that $\mu_{\beta 0}$ and μ_{s0} remain constant while ν_β and ν_s vary. If complete equilibrium is maintained as h varies then $\bar{\mu}_\beta = \bar{\mu}_s = 0$ when $\nu_\beta{}' = \nu_\beta$, $\nu_s{}' = \nu_s$ and the first term is zero. Using (2.2) and (3.1)

$$\mu_\beta{}^* = \xi_\beta + \Phi_\beta{}' + z_\beta e \frac{\gamma}{d} \chi' + z_\beta e \frac{\gamma(\sigma_0 + \sigma_\beta)}{Kd} -$$

$$kT z_\beta e \frac{g\sigma_\beta}{eQ} + kT \ln [\nu_\beta/(N_a - p\nu_\beta)^p] \quad (3.3)$$

and

$$\mu_s{}^* = \xi_s + z_s e \chi' + \frac{z_s e \sigma_0}{K} + z_s e \frac{\gamma \sigma_\beta}{Kd} \quad (3.4)$$

It follows that if K is assumed constant independent of ν_β and ν_s, g is independent of ν_s, and $\mu_\beta{}^*$ and $\mu_s{}^*$ are regarded as functions of ν_β, ν_s, pressure, and temperature, then

$$\frac{\partial \mu_\beta{}^*}{\partial \nu_s} = \frac{\partial \mu_s{}^*}{\partial \nu_\beta} = \frac{\gamma}{d} \frac{z_\beta z_s e^2}{K} \quad (3.5)$$

(23) M. A. V. Devanathan, *Trans. Faraday Soc.*, **50**, 373 (1954).

Also since the Gouy–Chapman theory is applied to the diffuse layer, ψ_d is a function of σ_d, h, and n only and thus $z_\beta e(\partial \psi_d / \partial \nu_s) = z_s e(\partial \psi_d / \partial \nu_\beta)$. It follows that the self-consistency condition

$$\partial \mu_\beta / \partial \nu_s = \partial \mu_s / \partial \nu_\beta \tag{3.6}$$

is satisfied. From (3.5) we may conclude that the last integral on the right of (3.2) is independent of the path of integration between given limits. The simplest way to evaluate this integral is to put $\nu_\beta' = \lambda \nu_\beta$, $\nu_s' = \lambda \nu_s$, and to vary λ from 0 to 1. Then replacing ν_β, ν_s, σ_β, and σ_s in (3.3) and (3.4) by $\lambda \nu_\beta$, $\lambda \nu_s$, $\lambda \sigma_\beta$, and $\lambda \sigma_s$, respectively, and assuming the equilibrium state where $\bar\mu_\beta = \bar\mu_s = 0$, (3.2) becomes

$$F(h) = 2 \int_0^{\psi_d} \sigma_d d\psi_d' - \frac{\gamma(\sigma_\beta{}^2 + 2\sigma_0\sigma_\beta)}{Kd} - \frac{\sigma_0{}^2}{K} +$$

$$\mathbf{k}T \frac{g\sigma_\beta{}^2}{eQ} + 2\mathbf{k}T(p-1)\frac{\sigma_\beta}{z_\beta e} -$$

$$2N_a\mathbf{k}T \ln[N_s z_\beta e / (N_a z_\beta e - p\sigma_\beta)] \tag{3.7}$$

This generalizes the expression for $F(h)$ based on the Stern picture of the double layer, which was obtained by one of the authors in an earlier paper.[24] In the special case where the inner region contains no counterions (3.7) reduces to a result derived by Mackor.[25] The formula (3.7) can also be obtained by applying the Debye–Hückel charging process to all the ions in the electric double layers under the conditions of fixed densities ν_β and ν_s, a method already employed for simpler surface conditions.[26]

Although (3.7) clearly displays the various contributions to the free energy an alternative form is more convenient for computation and is also applicable when equilibrium is not maintained as h varies. We assume, however, that the surface ions are in equilibrium with the dispersion medium at infinite separation so that, since the Gouy–Chapman theory is applied to the diffuse layer, (3.2) becomes

$$F(\infty) = -\frac{16n\mathbf{k}T}{\kappa}(\cosh \tfrac{1}{2}zH_d - 1) -$$

$$2 \int_{\nu_\beta' = 0, \, \nu_s' = 0}^{\nu_\beta' = N_\beta, \, \nu_s' = N_s} \nu_\beta' d\mu_\beta{}^* + \nu_s' d\mu_s{}^* \tag{3.8}$$

Subtracting (3.8) from (3.2), we have

$$I(h) = 2(\bar\mu_\beta \nu_\beta + \bar\mu_s \nu_s) + 2\int_0^{\psi_d} \sigma_d d\psi_d' +$$

$$\frac{16n\mathbf{k}T}{\kappa}(\cosh \tfrac{1}{2}zH_d - 1) -$$

$$2 \int_{\nu_\beta' = N_\beta, \, \nu_s' = N_s}^{\nu_\beta' = \nu_\beta, \, \nu_s' = \nu_s} \nu_\beta' d\mu_\beta{}^* + \nu_s' d\mu_s{}^* \tag{3.9}$$

In the last integral on the right of (3.9) any path of integration between the fixed limits is permissible and it will be supposed that ν_β' and ν_s' traverse their actual values as the plate separation diminishes from ∞ to $2h$. Then making use of (2.1) and (2.3) and noting that $\mu_{\beta 0}$ and μ_{s0} remain constant, this integral becomes

(24) S. Levine, *J. Colloid Sci.*, **6**, 1 (1951).

(25) E. L. Mackor, *Rec. trav. chim. Pays-Bas*, **70**, 841 (1951).

(26) Y. Ikeda, *J. Phys. Soc. Japan*, **8**, 49 (1953); R. A. Marcus, *J. Chem. Phys.*, **6**, 1057 (1955); G. M. Bell and S. Levine, *Trans. Faraday Soc.*, **53**, 143 (1957); S. A. Rice and M. Nagasawa, "Polyelectrolyte Solutions," Academic Press, New York, N. Y., 1961.

$$-2 \int_{\nu_\beta' = N_\beta, \, \nu_s' = N_s}^{\nu_\beta' = \nu_\beta, \, \nu_s' = \nu_s} \nu_\beta' d\bar\mu_\beta + \nu_s' d\bar\mu_s - 2\int_{\Psi_d}^{\psi_d} \sigma_d d\psi_d' =$$

$$-2 \int_{\nu_\beta' = N_\beta, \, \nu_s' = N_s}^{\nu_\beta' = \nu_\beta, \, \nu_s' = \nu_s} \nu_\beta' d\bar\mu_\beta + \nu_s' d\bar\mu_s +$$

$$\frac{8nze}{\kappa} \Delta\psi_d \sinh \tfrac{1}{2}zH_d - 2\int_0^{\Delta\psi_d} \Delta\sigma_d d(\Delta\psi_d) \tag{3.10}$$

It is now convenient to subtract (2.6) from (3.9) and to substitute (3.10) to obtain

$$I(h) - I^*(h) = 2 \int_{\nu_\beta' = N_\beta, \, \nu_s' = N_s}^{\nu_\beta' = \nu_\beta, \, \nu_s' = \nu_s} \bar\mu_\beta d\nu_\beta + \bar\mu_s d\nu_s -$$

$$\frac{2\mathbf{k}T}{e} \int_0^{\Delta\eta_d} \Delta\sigma_d d(\Delta\eta_d) + \frac{4n\mathbf{k}T}{\kappa}[-8\cosh \tfrac{1}{2}zH_d \times$$

$$\sinh^2 \tfrac{1}{4}z\Delta\eta_d - 4\sinh \tfrac{1}{2}zH_d \{\sinh \tfrac{1}{2}z\Delta\eta_d - \tfrac{1}{2}z\Delta\eta_d\}] \tag{3.11}$$

Mackor[25] suggested working with this difference when the inner region is free of counterions but did not express it in the form given here. There are two important cases: (a) surface ion equilibrium, when $\bar\mu_\beta = \bar\mu_s = 0$ as the separation varies from ∞ to $2h$; (b) the potential determining ions unable to diffuse quickly enough to change ν_s appreciably as h varies. This may occur when such ions have a very low density in the dispersion medium and also when there is a very high energy barrier between the plane of potential-determining ions in the plate and the O.H.P., as in the case of clays. Instead of the condition $\bar\mu_s = 0$ we would have $d\nu_s = 0$. Thus in both cases (a) and (b) the first term on the right-hand side of (3.11) vanishes. It will be shown that only small values of $\Delta\eta_d$ need be considered when investigating conditions for stability. If we consider case (a), (2.5) is integrated from $h = \infty$ to $h = h$ and the changes in $\mu_\beta{}^*$ and $\mu_s{}^*$ are denoted by $\Delta\mu_\beta{}^*$ and $\Delta\mu_s{}^*$, respectively. Then $\Delta\mu_\beta{}^* + z_\beta\mathbf{k}T\Delta\eta_d = 0$, $\Delta\mu_s{}^* + z_s\mathbf{k}T\Delta\eta_d = 0$ where $\Delta\mu_\beta{}^*$ and $\Delta\mu_s{}^*$ are functions of ν_β and ν_s. It follows that $\Delta\nu_\beta$ and $\Delta\nu_s$ are both proportional to $\Delta\eta_d$ for small enough $\Delta\eta_d$ and provided the factor of proportionality q remains finite

$$\Delta\sigma_d = -e(z_s\Delta\nu_s + z_\beta\Delta\nu_\beta) = qz\Delta\eta_d \tag{3.12}$$

Thus, retaining terms up to $(\Delta\eta_d)^2$ it follows from (3.11) and (3.12) that

$$I(h) - I^*(h) = -\frac{z\mathbf{k}T}{e}\left[q + \frac{2nze}{\kappa}\cosh \tfrac{1}{2}zH_d\right](\Delta\eta_d)^2 \tag{3.13}$$

For case (b) we have the conditions $\Delta\mu_\beta{}^* + z_\beta\mathbf{k}T\Delta\eta_d = 0$ and $\Delta\nu_s = 0$. Hence $\Delta\nu_\beta$ is again proportional to $\Delta\eta_d$ and (3.12) and (3.13) are still applicable but of course the constant q is different. It should be stressed that the structure of the inner region, which governs the form of q, has not been introduced in the derivation of this compact relation (3.13), which is valid for the important case of small $\Delta\eta_d$. However the Gouy–Chapman theory has been assumed for the diffuse layer.

To determine q for the case (a) we employ the relations III (4.7) and III (4.8),[6] which are obtained from (3.1) and the equilibrium conditions for the adsorbed counterions and which are written here as

$$\eta_d = \frac{d}{\beta}\left[\frac{1}{z_\beta}\ln\frac{n}{n_0} + \frac{1}{z_\beta}\ln\left\{\frac{(N_a z_\beta e - p\sigma_\beta)^p}{(N_a z_\beta e)^{p-1}\sigma_\beta}\right\} - \right.$$
$$\left. \frac{\gamma}{d}\eta_0 - \frac{(g-1)}{Q}\sigma_\beta + \frac{\Phi_\beta}{z_\beta kT} + \frac{e}{kT}\frac{\gamma}{d}\chi'\right] \quad (3.14)$$

$$\eta_0 = \eta_d - \frac{d^2}{\beta\gamma}\frac{\sigma_d}{Q} - \frac{d}{\gamma}\frac{\sigma_\beta}{Q} + \frac{e\chi'}{kT} \quad (3.15)$$

If we regard these equations as pertaining to separation $2h$ and subtract the corresponding relations for a single plate ($h = \infty$), then on expanding in a Taylor series, it follows that

$$\Delta\eta_d = -\frac{d}{\beta z_\beta \Sigma_\beta}\left[1 - \frac{z_\beta(g-1)\Sigma_\beta}{Q} + \right.$$
$$\left. \frac{p^2\Sigma_\beta}{N_a z_\beta e - p\Sigma_\beta}\right]\Delta\sigma_\beta - \frac{1}{2}\frac{d}{\beta z_\beta}\left[\frac{p^3}{(N_a z_\beta e - p\Sigma_\beta)^2} - \right.$$
$$\left. \frac{1}{\Sigma_\beta^2}\right](\Delta\sigma_\beta)^2 + \cdots$$

$$= \frac{d^2}{\beta\gamma}\frac{\Delta\sigma_d}{Q} + \frac{d}{\gamma}\frac{\Delta\sigma_\beta}{Q} \quad (3.16)$$

Retaining only the linear term in $\Delta\sigma_\beta$ and eliminating $\Delta\sigma_\beta$, we obtain (3.12) where

$$q = \frac{kT}{ze}K[1 + S(r)], \quad S(r) = \frac{\beta}{\gamma}\frac{r}{g}\bigg/\left[1 - \right.$$
$$\left. \left(1 - \frac{1}{g}\right)r + \frac{p^2 rb}{1 - prb}\right] \quad (3.17)$$

Alternatively, we can start with (3.7), subtract the corresponding expression for $F(\infty)$, and by employing (3.1) derive

$$I(h) - I^*(h) = J(h) + 2N_a kT\left[\ln\left(1 - \right.\right.$$
$$\left.\frac{p\Delta\sigma_\beta}{N_a z_\beta e - p\Sigma_\beta}\right) + \frac{p\Delta\sigma_\beta}{N_a z_\beta e - p\Sigma_\beta}\right] - \frac{2kT}{e}\frac{\beta}{d}\Sigma_\beta\left[\Delta\eta_d + \right.$$
$$\left. \frac{d}{\beta z_\beta \Sigma_\beta}\left(1 - \frac{z_\beta(g-1)\Sigma_\beta}{Q} + \frac{p^2\Sigma_\beta}{N_a z_\beta e - p\Sigma_\beta}\right)\Delta\sigma_\beta\right] - $$
$$K\left(\frac{kT}{e}\right)^2(\Delta\eta_d)^2 + \frac{(g-1)}{Kd^2}\beta\gamma(\Delta\sigma_\beta)^2 \quad (3.18)$$

where $J(h)$ is the last term (with the brackets) on the right-hand side of (3.11). By expanding the logarithmic term and using (3.16) to eliminate $\Delta\sigma_\beta$ the formula (3.13) with q given by (3.17) is readily verified. If $g > 1$, the coefficient of $\Delta\sigma_\beta$ in the second member of (3.16) will vanish at $r = r_1$, defined by

$$\left(1 - \frac{1}{g}\right)r_1 = 1 + \frac{p^2 br_1}{1 - pbr_1} \quad (3.19)$$

Since $S(r_1) = \infty$, $q = \infty$, $d\eta_d/d\sigma_\beta = 0$ and it can be shown that $d\psi_d/dh = 0$. Expanding in powers of $\Delta\sigma_d$ rather than $\Delta\eta_d$, from (3.16) and (3.19) $\Delta\eta_d$ is of order $(\Delta\sigma_d)^2$ at $r = r_1$ and hence from (3.11) $I(h) - I^*(h)$ is of order $(\Delta\sigma_d)^3$, but we shall not require its explicit form. In case (b), by substituting (3.15) and the last equation in (3.1), we can express (3.14) as

$$\eta_d = \frac{1}{z_\beta}\ln\frac{n}{n_0} + \frac{1}{z_\beta}\ln\left\{\frac{(N_a z_\beta e - p\sigma_\beta)^p}{(N_a z_\beta e)^{p-1}\sigma_\beta}\right\} + $$
$$\frac{(g - d/\beta)}{Q}\sigma_\beta - \frac{d}{\beta}\frac{\sigma_0}{Q} + \frac{\Phi_\beta}{z_\beta kT} \quad (3.20)$$

Putting $\sigma_0 = z_s e\nu_s = $ constant and using a development similar to that of (3.16), since $\Delta\sigma_d = = \Delta\sigma_\beta$ we have

$$q = \frac{kT}{ze}KS'(r), \quad S'(r) = \frac{d^2 r}{\beta\gamma g}\bigg/$$
$$\left[1 - \left(1 - \frac{d}{\beta g}\right)r + \frac{p^2 br}{1 - pbr}\right] \quad (3.21)$$

An alternative method for obtaining $I(h)$ is to determine the force between the plates and then to integrate this with respect to the separation. It will be shown that the double layer force per unit area is still given by (2.7) provided that (i) the median plane is embedded in the diffuse layers to which the Gouy–Chapman theory is applied, (ii) the surface conditions do not depend explicitly on h, and (iii) each type of surface ion either remains in equilibrium with the dispersion medium as h varies or its number remains constant. If we differentiate the last expression of (3.2)

$$p_e(h) = -\frac{1}{2}\frac{dF(h)}{dh} = \int_0^{\psi_d}\left(\frac{\partial(-\sigma_d)}{\partial h}\right)_{\psi_d'}d\psi_d' - $$
$$\sigma_d\frac{d\psi_d}{dh} + \nu_\beta\frac{d}{dh}(\mu_\beta^* - \bar{\mu}_\beta) + $$
$$\nu_s\frac{d}{dh}(\mu_s^* - \bar{\mu}_s) - \bar{\mu}_\beta\frac{d\nu_\beta}{dh} - \bar{\mu}_s\frac{d\nu_s}{dh} \quad (3.22)$$

Now, making use of (2.4) and remembering that $\mu_{\beta 0}$ and $\mu_{s 0}$ do not vary with h, the second term on the right-hand side of (3.22) cancels with the third and fourth terms. If then either $\bar{\mu}_\beta = 0$ or $d\nu_\beta/dh = 0$ and either $\bar{\mu}_s = 0$ or $d\nu_s/dh = 0$

$$p_e(h) = \int_0^{\psi_d}\left(\frac{\partial(-\sigma_d)}{\partial h}\right)_{\psi_d'}d\psi_d' \quad (3.23)$$

This is now in a form depending on the diffuse layer alone and becomes identical with the force expression derived by Verwey and Overbeek[5] on the Gouy–Chapman model, when $-\sigma_d$ and ψ_d are replaced by σ_0 and ψ_0. The validity of (2.7) follows immediately. We have also verified (2.7) directly by differentiating (3.7) and making use of (2.4) and (3.1).

For small concentrations of potential-determining ions the potential ψ_0 might not have time to adjust itself completely during the momentary approach of two colloidal particles and the double layer interaction will be intermediate between the two extreme cases (a) and (b). However, this only affects the form of the quantity q and it will be seen in the following sections that this introduces a small correction to the interaction energy. Hence, in the rest of the paper we shall be concerned entirely with case (a).

4. Flocculation Criteria at Large ψ_d

An appropriate expression for σ_d, necessary to determine $\Delta\eta_d$, is provided by a first integral of the Poisson–Boltzmann equation, namely

$$\sigma_d = \pm \frac{4nze}{\kappa} [\sinh^2 {}^1/_2 z\eta_d - \sinh^2 {}^1/_2 z\eta_m]^{1/2} =$$

$$- \frac{4nze}{\kappa} \sinh {}^1/_2 z\eta_d \left[1 - \frac{k^{-2} - 1}{2 \sinh^2 {}^1/_2 z\eta_d} + \dots \right] \quad (4.1)$$

where the first two terms of the above expansion can be used as an approximation if either the potential ψ_d (and thus $\sinh {}^1/_2 z\eta_d$) is large or if the separation is large enough for k to be nearly equal to 1. If we subtract (2.1) from (4.1), expand $\Delta\sigma_d$ in powers of $\Delta\eta_d$, and then make use of (3.12) and (3.17) to eliminate $\Delta\sigma_d$, it is readily verified that

$$z\Delta\eta_d = \frac{X(k^{-2} - 1)}{\sinh {}^1/_2 zH_d[1 + X \cosh {}^1/_2 zH_d + S(r)]} \quad (4.2)$$

if $\Delta\eta_d$ is small. This expresses the variation of the potential at the O.H.P., ψ_d, with separation $2h$, in terms of the potential at the median plane ψ_m. It can be seen at once that $\Delta\eta_d$ will be small if either the potential or the separation are large, which is consistent with the conditions assumed in expanding $\Delta\sigma_d$. To the approximation (4.2), $\Delta\eta_d = 0$ when $S(r) = \infty$ at $r = r_1$.

An expansion for $I^*(h)$ which is suitable at large potential ψ_d is obtained from the work of Derjaguin and Landau[4] and Hoskin and Levine.[17] The solution of the Poisson–Boltzmann equation leads to the following relation which does not involve explicitly the surface conditions

$$\kappa h' = kK(k) = \operatorname{sech} {}^1/_2 z\eta_d -$$
$$\qquad {}^1/_6(k^{-2} + 1) \operatorname{sech}^3 {}^1/_2 z\eta_d + \dots \quad (4.3)$$

The interaction energy $I^*(h)$ is so defined that η_d is regarded as independent of h and therefore of k. Since $\psi_m = 0$ and therefore $k = 1$ at $h = \infty$, and $h' = h - d$ where d is assumed constant, it follows that

$$I^*(h) = 2 \int_{h'}^{\infty} p_e(h) dh = \frac{8nkT}{\kappa} \times$$

$$\int_k^1 \left(\frac{1}{k^2} - 1 \right) \frac{d(h'\kappa)}{dk} dk = \frac{8nkT}{\kappa} [G(k) +$$

$$\qquad {}^1/_{12}(1 - k^{-2}) \operatorname{sech}^3 {}^1/_2 z\eta_d + \dots] \quad (4.4)$$

The first term only in each of the series (4.3) and (4.4) does not vanish at infinite potential at the O.H.P., a result obtained by Derjaguin and Landau.[4] If we retain terms up to order v^3, then η_d can be replaced by H_d in the second term in the series (4.4). Substituting (3.17), (4.2), and (4.4) into (3.13)

$$I(h) = \frac{8nkT}{\kappa} \left[G(k) - \frac{X(k^{-2} - 1)^2 v^2}{4\left[1 + \frac{X}{v} + S(r) \right]} + \right.$$

$$\left. \qquad {}^1/_2(k^{-2} - 1)^2 v^3 + \dots \right] \quad (4.5)$$

correct to order v^3. This result can also be obtained by integrating the force formula (2.6). By expanding $\operatorname{sech} {}^1/_2 z\eta_d$ in powers of $\Delta\eta_d$ and substituting (4.2) the series (4.3) becomes

$$\kappa h' = kK(k) - r + \frac{X(k^{-2} + 1)v^2}{2\left[1 + \frac{X}{v} + S(r) \right]} -$$

$$\qquad {}^1/_6(k^{-2} + 1)v^3 + \dots \quad (4.6)$$

The integral formula in (4.4) now yields the series (4.6) for $I(h)$ if it is borne in mind that v and r, both of which refer to the state at $h = \infty$, are constants independent of r.

The conditions of flocculation are assumed to be

$$U(h) = 0, \quad dU(h)/dh = 0 \quad (4.7)$$

These represent the disappearance of the potential energy barrier whereas the experimental threshold of coagulation may correspond to a small barrier, but this approximation probably overestimates the coagulating concentration in a systematic manner and is therefore acceptable. Making use of (2.7) and (2.8), these lead to the relations

$$h' p_e(h) = I(h), \quad p_e(h) = A/48\pi h'^2 \quad (4.8)$$

The first relation in (4.8) yields

$$v = \frac{kH(k)}{1 - k^2} + \frac{X(k^{-2} - 1)v^2}{1 + \frac{X}{v} + S(r)} - \frac{v^3}{3k^2} + \dots \quad (4.9)$$

and it is convenient to express the second relation in the form

$$X = \omega(h'\kappa)^3(k^{-2} - 1) \quad (4.10)$$

At infinite plate separation $\eta_m = 0$, and making use of (2.1), equation (3.15) becomes

$$\eta_0 = H_d + 2\frac{X}{z} \sinh {}^1/_2 zH_d - \frac{dr}{\gamma g z_\beta} + \frac{e\chi'}{kT} \quad (4.11)$$

at $h = \infty$. Hence, substituting (4.11), (3.14) may be written as

$$R(r) = B(z) + z_\beta H_d + 2X \frac{\gamma z_\beta}{dz} \sinh {}^1/_2 zH_d - 2 \ln X$$

$$\qquad (4.12)$$

where $R(r)$ is defined in (2.3) and $B(z)$ is constant for each z. Also

$$\ln n = 2 \ln (XK) + \ln \left(\frac{2\pi kT}{\epsilon(ze)^2} \right) \quad (4.13)$$

If (4.6) is substituted into (4.10), the flocculation conditions are expressed in terms of the four equations (4.9)–(4.12) from which we can in principle eliminate k and H_d and so arrive at two equations involving X, r, and η_0. If now r is regarded as a parameter, these represent a relation between X and η_0 and therefore, by (4.13), the variation of flocculating electrolyte concentration n with the plate potential ψ_0.

In the limiting case of infinite potential at the O.H.P. $|H_d| = \infty$, $v = 0$ and hence by (4.9) $H(k) = 0$ with solution $k = 0.543$ and by (4.6) $\kappa h' = 0.929$. The equation (4.10) reduces to a result derived by Derjaguin and Landau[4]

$$\kappa = \frac{46.1}{A} \epsilon \left(\frac{kT}{ze} \right)^2 \quad \text{or} \quad n = \frac{84.4}{A^2} \frac{\epsilon^3(kT)^5}{(ze)^6} \quad (4.14)$$

representing the inverse sixth-power valency law (the z^{-6} law) which is the simplest version of the Schulze–Hardy rule in the D.L.V.O. stability theory. As k increases from its smallest value 0.543, v increases and therefore $|\Psi_d|$ decreases, $\kappa h'$ increases slowly but X decreases and hence the flocculating concentration cannot exceed the value defined by (4.14). The function $R(r)$ has a minimum at $r = r_m$ defined by

$$\frac{dR}{dr} = 1 - \frac{1}{r_m} - \frac{bp^2}{1 - pbr_m} = 0 \quad (4.15)$$

but if the "self-atmosphere" effect is ignored, the term r in the function $R(r)$ is absent and no such minimum exists. We may regard X as a function of Ψ_d and therefore from (4.12) $d\Psi_d/dr = 0$ at $r = r_m$; also $d\Psi_d/d\psi_0 = 0$ since $|\psi_0|$ is found to increase steadily with r. The coagulating concentration n diminishes steadily with decrease in $|\Psi_d|$ and so the stability conditions derived above lead to the relation

$$(dn/d\psi_0)_{r = r_m} = 0 \quad (4.16)$$

A plot of the flocculating electrolyte concentration $vs.$ the plate potential thus exhibits a maximum at $r = r_m$. The numerical solution of the simultaneous equations (4.6) and (4.9)–(4.13) defining the flocculation conditions is not tedious if terms of order v^3 are omitted and this is a very good approximation for $k < 0.70$ ($|z\Psi_d| > 100$ mv.) and is still reasonable for $k < 0.80$ ($|z\Psi_d| > 60$ mv.). It will be designated as the H.P. (high-potential) approximation and most of the calculations in section 6 have been performed with this approximation. A value of k is chosen and the remaining relevant quantities are expressed in terms of k, namely, v by (4.9), $\kappa h'$ by (4.6), X by (4.10), r by (4.12), ψ_0 by (4.11), and n by (4.13).

In the original D.L.V.O. theory the double layer interaction per unit area of plates at separation $2h'$ is given by $I^*(h)$ provided ψ_d is replaced by ψ_0. Thus v becomes $v_0 = \mathrm{sech} \, \frac{1}{2} z\eta_0$ and the terms involving X are absent on the right-hand sides of (4.6) and (4.9). Making use of the expansion by Hoskin and Levine[17] of $I^*(h)$ up to terms in v_0^5, the latter two relations on the D.L.V.O. theory read

$$\kappa h' = kK(k) - v_0 - \frac{1}{6k^2}(1 + k^2)v_0^3 -$$

$$\frac{1}{40k^4}(3 + 2k^2 + 3k^4)v_0^5 + \ldots \quad (4.17)$$

and

$$v_0 = \frac{kH(k)}{1 - k^2} - \frac{v_0^3}{3k^2} - \frac{1}{40k^4}(7 + 2k^2 - k^4)v_0^5 + \ldots$$

$$(4.18)$$

and these determine ψ_0 and $\kappa h'$ as functions of the parameter k at the flocculating conditions. The dependence of the flocculating electrolyte concentration on k and therefore on ψ_0 is obtained from (4.10) and (4.13). It is observed that $\ln n$ does not involve the capacity K, since K does not occur in the D.L.V.O. theory.

5. Large Separation Approximation

In papers I and II the three relations (4.10)–(4.12) were expressed rather differently in terms of the L.S.

approximation, which is valid at large plate separations. It is possible to improve upon this approximation by employing an expansion developed by Levine and Suddaby[27] for the Gouy–Chapman model. This yields for the force per unit area

$$p_e(h) = -\frac{1}{2}\left[\frac{\partial I^*(h)}{\partial h'}\right]_{\eta_d} =$$

$$64nkTe^{-2\theta} t^2[1 - 2t^2e^{-2\theta}(C_1 - 1) + \ldots] \quad (5.1)$$

Also we need to substitute $k^{-2} - 1 = 16 t_0^2 e^{-2\theta}$ into the expression (4.2) for $z\Delta\eta_d$. If now (5.1) is expanded in powers of $\Delta\eta_d$ and (4.2) is substituted, then up to terms of order $e^{-2\theta}$, $p_e(h)$ proves to have the same form as (5.1) provided η_d is replaced by H_d and C_1 by

$$D_1 = 4\theta - 3 + \frac{4}{\sinh^2 \frac{1}{2}zH_d}\left[\cosh \frac{1}{2}zH_d - \frac{2X}{1 + S(r) + X \cosh \frac{1}{2}zH_d}\right] \quad (5.2)$$

$I(h)$ is now easily obtained by integrating $p_e(h)$ with respect to h at constant H_d and the first stability condition in (4.8) can be expressed as

$$t_0^4(2\theta - 1) + t_0^2(12\theta - 8\theta^2 - 3) - 2\theta + 1 +$$

$$(\theta - 1)e^{2\theta} = \frac{X}{1 + S(r)}\left[\left(\frac{1 + t_0^2}{1 - t_0^2}\right)(3 - 12\theta +$$

$$8\theta^2)t_0^2 - (\theta - 1)e^{2\theta} + (1 - 2\theta)(t_0^4 - 6t_0^2 + 1)\right]$$

$$(5.3)$$

Also (4.10) becomes

$$X = \frac{96e^{-2}}{\pi}\frac{\epsilon^2}{KA}\left(\frac{kT}{ze}\right)^2 t_0^2 L,$$

$$L = \theta^2 e^{-2(\theta - 1)}[1 - D_1 t_0^2 e^{-2\theta} + \ldots] \quad (5.4)$$

and (4.12) is

$$R(r) = z_\beta H_d + 2X\frac{\gamma^2\beta}{dz}\sinh \frac{1}{2}zH_d -$$

$$2 \ln (t_0^2 L) + D(z) \quad (5.5)$$

where $D(z) = B(z) + 4 - 2 \ln [(96/\pi)(kT/ze)^2(\epsilon^2/KA)]$. The linear approximation is obtained by putting $\theta = 1$ and $L = 1$ and then the constant $D(z)$ becomes identical with that introduced in II.[3] In this approximation (5.5) is solved for r as a function of H_d and then ψ_0 and n at coagulation can be found from (4.11), (5.4), and (4.13). In the D.L.V.O. theory we replace t_0 by $\tanh \frac{1}{4}z\eta_0$ and equate the left-hand side of (5.3) to zero. This yields θ as a function of ψ_0 and the flocculating concentration at specified ψ_0 is given by (5.4) and (4.13). In the theory presented here, the simultaneous equations (5.3)–(5.5) need only be solved (by an iteration process) for moderate values of Ψ_d, since the H.P. approximation is more accurate at high potentials.

6. Numerical Results and Comparison with Experiment

From the results of the previous sections we can plot the coagulating concentration of added electrolyte against the surface potential ψ_0 for given values of the

(27) S. Levine and A. Suddaby, $Proc. Phys. Soc.$ (London), **A64**, 287, 431 (1951).

relevant parameters. This coagulating concentration has been expressed by the dimensionless parameter X and at $T = 25°$ ($\epsilon = 78.54$) this may be converted to concentration in mole/l. by using the relation $\kappa = 0.3291 z \sqrt{c} \times 10^8$ to give

$$\log c = 2 \log KX/z - 16.6264 \qquad (6.1)$$

Experimentally it is not ψ_0 but the concentration or activity of the potential-determining ion which is measured; by the Nernst equation the natural logarithm of this activity contains the term $z_s e \psi_0/kT$. Accordingly, for a typical colloidal system, negative AgI sol, we transform from ψ_0 to pI (minus the common logarithm of the activity of the potential-determining I^- ion). From (5.4), (4.11), and (4.12), when $\Psi_d = 0$, $X = 0$, $r = 0$ and hence $\Sigma_\beta = 0$, $\psi_0 - \chi' = 0$, and by electrical neutrality $\sigma_0(\infty) = 0$. Since experimentally pI $= 10.6$ at the isoelectric point[28] for AgI we may write the Nernst equation as

$$\text{pI} = 10.6 + 0.4343 \Psi_0/25.71 \qquad (6.2)$$

where Ψ_0 is measured in millivolts. Since the isoelectric points for AgBr and AgCl are at pBr $= 6.9$ and pCl $= 5.7$,[28] we may change to pBr or pCl, respectively, instead of pI simply by shifting the log c–pI curves by 3.7 or 5.8 units to the left. Now Mirnik, et al.,[15] find pI $= 9.8$, pBr $= 6.0$, and pCl $= 3.3$ at their so-called negative stability limit, which we identify with the condition $\Psi_d = 0$. One reason for these differences is the dependence of the isoelectric point on the age and mode of preparation of the silver halide crystals. Several authors[28-30] find that the pBr increases with crystal size at the isoelectric point for freshly prepared AgBr sols. This may be related to the existence of a Schottky or Frenkel defect diffuse layer inside the crystal.[31]

In Fig. 2 and 3 we give log c–pI curves calculated for the D.L.V.O. theory at $A = 2 \times 10^{-12}$ erg cm.^{2}. The accuracy of the L.S. and H.P. approximations is illustrated by comparing the results they give with exact results derived by using various suitable expansions[27,32] referred to in previous sections. From Fig. 2 it can be seen that the L.S. approximation overestimates the coagulation concentration which however tends to a limiting value c_m, proportional to z^{-6}, on both the exact and L.S. curves at small pI (large Ψ_0). In Fig. 3 the exact curves for $z = 1$ and those given by the H.P. approximation, the L.S. approximation, and its extension described in section 5 are compared. The L.S. and H.P. curves cross at $k = 0.79$ ($|z\Psi_0| = 64$ mv.) and, as would be expected, the H.P. approximation is better at higher, and the L.S. at lower, potentials.

Typical log c–pI coagulation curves for the extension to the D.L.V.O. theory with the H.P. approximation (solid curves) and L.S. approximation (broken curves) are shown in Fig. 4, 5, and 6, the relevant parameters being given in Tables I and II. To reduce computation N_a has been chosen to give the same values of b as in some of the results of II.[3] The constants $B(z)$

(28) H. R. Kruyt, "Colloid Science," Vol. 1, Elsevier, Amsterdam, 1952.

(29) P. F. J. A. Julien, Thesis, Utrecht, 1933; G. H. Jonker, Thesis, Utrecht, 1943.

(30) J. Barr and H. O. Dickinson, J. Phot. Sci., 9, 222 (1961); see also reference 9.

(31) T. B. Grimley and N. F. Mott, Discussions Faraday Soc., 1, 3 (1947); T. B. Grimley, Proc. Roy. Soc. (London), A201, 40 (1950).

(32) S. Levine and G. M. Bell, Can. J. Chem., 38, 1346 (1960).

Fig. 2.—Logarithm of coagulating concentration against pI or plate potential for 1–1, 2–2, and 3–3 electrolytes in the D.L.V.O. theory. For each valency, the lower curve represents the exact calculation and the upper one the L.S. approximation. $A = 2 \times 10^{-12}$ erg cm.^{2} and $T = 25°$.
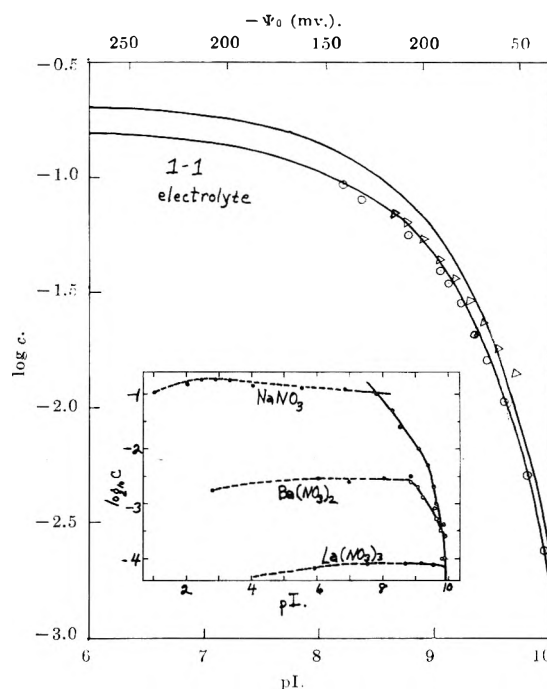
Fig. 3.—Logarithm of coagulating concentration against pI or plate potential for a 1–1 electrolyte in the D.L.V.O. theory. The lower curve is the exact result and the upper one the L.S. approximation. The points inside the triangles represent the H.P. approximation and those inside the circles are the extension to the L.S. approximation. Figure 3a (inset).—Experimental curves for AgI based on reference 16, Fig. 5.

for curves A, B, and C in Fig. 4 were determined by choosing convenient values for the parameter k at the maximum in $|\Psi_d|$.

The Tezak–Mirnik (henceforward T.M.) rule is that the flocculating value of log c is a linear function of z, making the log c–pI curves for $z = 1, 2$, and 3 equidistant. In the present theory the T.M. rule can be satisfied at one particular value of pI by proper choice of the parameters; for example, the constants $B(z)$. This value of pI is marked with arrows, further details

TABLE I

CHARACTERISTICS OF PLOTS BETWEEN ELECTROLYTE CONCENTRATION AND SURFACE POTENTIAL AT CRITICAL COAGULATION

K, μfarad./cm.^{2}; Ψ_0, Ψ_d, mv.; $\sigma_\beta{}^0$, μcoul./cm.^{2}; c, mole/l.; $\Sigma_\beta = r\sigma_\beta{}^0$; $A = 2 \times 10^{-12}$ erg cm.^{2}; $N_a = (3/8) \times 10^{15}$ cm.$^{-2}$; $T = 25°$; $\epsilon = 78.54$; $\gamma/d = 1/4$; $g = 4/3$

High potential approximation

	Curve	z	p	$B(z)$	K	$\sigma_\beta{}^0$	b	ω	r_1	Maximum k	r	$-\Psi_d$	$-\Psi_0$	$h'\kappa$
Fig. 4 (solid curves)	A	1	1	11.39	30	3.084	0.0514	1.601	...	0.67	1.057	115	669	1.004
	B	2	3	12.96	20	1.028	.00856	0.600	6.33	.60	1.086	82	419	0.967
	C	3	5	10.97	20	0.685	.00380	.267	7.16	.58	1.108	62	241	.954
	D	3	5	8.75	20	0.685	.00380	.267	7.16	.595	1.108	56	185	.964

Tezak-Mirnik form of Schulze-Hardy rule

	Curve	k	r	$-\Psi_d$	$-\Psi_0$	$-\log c$	Curve	k	r	$-\Psi_d$	$-\Psi_0$	$-\log c$
Fig. 4 (solid curves)	A	0.705	0.031	99	394	1.30	A	0.724	0.0090	91	319	1.37
	B	.603	0.83	78	394	2.76	B	.610	0.092	77	319	2.78
	C	.713	13.6	31	394	4.21	C	.710	10.6	32	319	4.18

Linear superposition approximation

$$D(z) = B(z) + 2 \ln Kz^2 - 9.29, \quad \log c = 2 \log (0.910 \times 10^{-12}/Az^2) + 4 \log t_0$$

	Broken curve	z	$D(z)$	Maximum r	$-\Psi_d$	$-\Psi_0$	Curve with same parameters	
Fig. 4	E	1	8.92	1.057	111	666	A	Parameters having same values are—
	F	2	12.44	1.086	79	417	B (Fig. 4)	p, K, b, $\sigma_\beta{}^0$, ω
	G	3	12.07	1.108	60	235	C	
Fig. 6	F	2	8.89	1.086	70	283	B (Fig. 6)	
	G	3	13.03	1.108	63	263	C	

TABLE II

CHARACTERISTICS OF PLOTS BETWEEN ELECTROLYTE CONCENTRATION AND SURFACE POTENTIAL AT CRITICAL COAGULATION

Same units as in Table I. $\gamma/d = 1/5$, $g = 5/4$ for curves H and I of Fig. 5
$\gamma/d = 1/4$, $g = 4/3$ for all other curves

High potential approximation

	Curve	$B(z)$	K	$\sigma_\beta{}^0$	b	ω	r_1	Maximum k	r	$-\Psi_d$	$-\Psi_0$	$h'\kappa$
Fig. 5	H	9.19	16	0.685	0.00380	0.334	14.7	0.595	1.108	56	219	0.964
($z = 3$)	I	5.46	16	0.685	.00380	.334	14.7	.651	1.108	42	124	.995
($p = 5$)	J	7.24	30	1.028	.00571	.178	...	.593	1.173	57	160	.963

Fig.	Curve	z	p	$B(z)$	K	$\sigma_\beta{}^0$	b	ω	r_1	Maximum k	r	$-\Psi_d$	$-\Psi_0$	$h'\kappa$	z^{-6} law k	r	$-\Psi_d$	$-\Psi_0$
	A						Same as for curve A in Table I (Fig. 4)								0.70	0.038	78	416
6	B	2	3	9.42	20	1.028	0.00856	0.600	6.33	0.628	1.086	70	283	0.983	.70	7.96	39	416
	C	3	5	11.93	20	0.685	.00380	.267	7.16	.576	1.108	65	266	.952	.70	14.2	26	416
	D	3	5	11.93	15	0.514	.00285	.356	5.81	.585	1.078	60	260	.957				

Tezak-Mirnik form of Schulze-Hardy rule

Fig.	Curve	k	r	$-\Psi_d$	$-\Psi_0$	$-\log c$	Curve	k	r	$-\Psi_d$	$-\Psi_0$	$-\log c$	Curve	k	r	$-\Psi_d$	$-\Psi_0$	$-\log c$
4	A	0.698	0.046	102	426	1.27	A	0.750	0.0015	80	241	1.49	A	0.724	0.0090	91	319	1.38
4	B	.601	1.42	81	426	2.75	B	.628	0.013	76	241	2.83	B	.610	0.092	76	319	2.78
5	H	.722	11.1	30	426	4.23	I	.710	5.53	32	241	4.18	J	.710	10.8	32	319	4.18

being given in Tables I and II. Curve D (for $z = 3$) in Fig. 4 was obtained by changing the constant $B(3)$ used for curve C in such a way that the T.M. rule holds for curves A, B, and D at $k = 0.71$. It is of interest to investigate whether the T.M. law can be satisfied near the maximum in $|\Psi_d|$ since it should then be valid over a larger range of pI. A typical calculation in Table III, in which some of the parameters have been so chosen that the maximum is confined to a narrow range of pI for all three valencies, demonstrates that this law can be approximately satisfied near the maximum. The quantities $\log c$, r, k, and Ψ_d are evaluated at a common pI = 6.11 where the maximum of curve C ($z = 3$) is located. The units and the parameters A, g, γ/d, p, and N_a are the same as for curves A, B, and C in Fig. 6. It is seen that for $z = 1$ and 2, r is reasonably near the value r_m at the maximum. In Tables I and II the constant differences $\Delta \log c$ expressing the T.M. law lie in the range 1.36–1.48 and in the two examples calculated in II,[3] $\Delta \log c = 1.56$ and 1.74. In Table III,

this difference is not quite constant, taking the values 1.14 and 0.96. The experimental results by the "*statu nascendi*" method quoted by Mirnik[33] for silver halide sols and given in Table IV also obey the T.M. law only approximately.

TABLE III

TEZAK-MIRNIK LAW NEAR MAXIMUM

z	$B(z)$	K	b	k	$-\Psi_d$	$-\Psi_0$	$-\log c$	r	r_m
1	4.50	30	0.0514	0.78	69	266	1.64	1.180	1.057
2	9.05	30	.00963	.61	76	266	2.78	0.834	1.137
3	11.93	20	.00380	.576	65	266	3.74	1.108	1.108

TABLE IV

VALUES OF $\Delta \log c$

	Mirnik AgI	AgBr	AgCl		Ghosh AgI		z^{-6} law
K–Ba	1.91	1.44	0.88	K–Ba	1.62		6 log 2 = 1.81
Ba–La	1.77	1.62	1.18	Ba–Al	1.11		6 log 1.5 = 1.06

(33) M. Mirnik, private communication.

TABLE V

CORRECTIONS TO HIGH POTENTIAL AND LINEAR SUPERPOSITION APPROXIMATIONS

(Corrections denoted by letter δ, Ψ_d in millivolts)

H.P. approximation

Curve	z	$\delta B(z)$	k	$-\Psi_d$	pI	$-\log c$	$\delta(pI)$	$\delta(-\log c)$
A (Fig. 4 and 6)	1	-0.08	0.67	115	-0.70	1.17	0.10	0.006
			.72	92	4.99	1.36	.17	.02
B (Fig. 4)	2	-0.05	.6	82	3.51	2.75	.04	.002
			.7	50	8.76	3.09	.02	.01
			.7	50	0.67	3.09	.12	- .01
C (Fig. 4)	3	-0.02	.58	62	6.54	3.75	.004	.002
			.82	18	10.24	4.73	- .06	.01
			.82	18	2.65	7.73	.22	- .04

L.S. approximation

Curve	z	$\delta D(z)$	H_d	$-\Psi_d$	pI	$-\log c$	$\delta(pI)$	$\delta(-\log c)$
E (Fig. 4 and 6)	1	-0.08	1.5	39	9.63	2.47	0.03	0.08
			4	103	2.39	1.16	1.08	.15
F (Fig. 4)	2	-0.05	1.0	26	10.0	3.83	0.04	.11
			2.5	64	7.06	2.78	.38	.15
			2.5	64	1.81	2.78	- .23	.15
G (Fig. 4)	3	-0.02	0.8	21	10.18	4.63	- .08	.13
			0.8	21	2.88	4.63	- .18	.15

Mirnik[16] claims that, as well as obeying the T.M. rule, the flocculating concentration is constant over a wide range of pI. (Experimental results of Mirnik, et al.,[15] are shown in Fig. 3a.) In our theory (see II[3]) the slope of the log c–pI curve on the low pI (high potential) side decreases with γ/d and thus a reduction in γ/d gives better agreement with Mirnik's condition. This is illustrated for $z = 3$ in Fig. 5 where for curves H and I the ratio γ/d has been reduced from $^1/_4$ to $^1/_5$. As $g = d/\beta$, this means that g has been reduced from $^4/_3$ to $^5/_4$. The capacity K is adjusted to keep b unaltered and the constants $B(z)$ are so chosen that the T.M. rule (marked by arrows) applies at assigned values of pI. The other parameters and conditions relating to the above rule are given in Table II. The result of correcting for the decrease in g with increase in r is similar. In the particular case where $\epsilon >> \epsilon_i$ and the dielectric constants of the inner region and particle medium are equal, it may be shown (III)[6] that

$$g = \frac{d}{\beta}\left[1 - 2\frac{\gamma}{r_0} + \ldots\right] = \frac{d}{\beta}\left[1 - 2\gamma\left(\frac{\pi r \sigma_\beta{}^0}{ze}\right)^{1/2} + \ldots\right]$$

$$= \frac{d}{\beta}\left[1 - 0.089 \ (r\sigma_\beta{}^0/z)^{1/2} + \ldots\right] \quad (6.3)$$

if $\gamma = 1$ Å. and $\sigma_\beta{}^0$ is measured in μcoul./cm. Such a decrease in g with increasing r will also increase the value r_1, defined by (3.19) at which, $d\psi_d/dh = 0$, and indeed this point may not be observed in practice.

To illustrate the effect of varying the capacity K, curve J in Fig. 5 which differs from curve D in Fig. 4 by an increase in K from 20 to 30 μfarad./cm.[2] has been drawn. The constant $B(3)$ in curve J has been so chosen that J intersects D at $k = 0.71$ (marked by an arrow) where the T.M. law is obeyed. Apart from a shift in the position of the maximum, it is observed that there is little change in the log c–pI plot.

The well known rule that the flocculating concentration is proportional to $z(z^{-6}$ law) is also only obeyed at isolated values of pI. From (4.6), (4.9), and (4.10), in the H.P. approximation XK has the functional form $z^{-2}f(k)$ and hence from (4.13) n has the form $z^{-6}g(k)$. If the z^{-6} law applies then k must have the same value for $z = 1, 2$, and 3 at a given η_0 or pI. This is illustrated in Fig. 6 where the parameters for curves A, B, and C are the same as for A, B, and C, respectively, of Fig. 4 except for the constants $B(2)$ and $B(3)$ which are fixed by as-
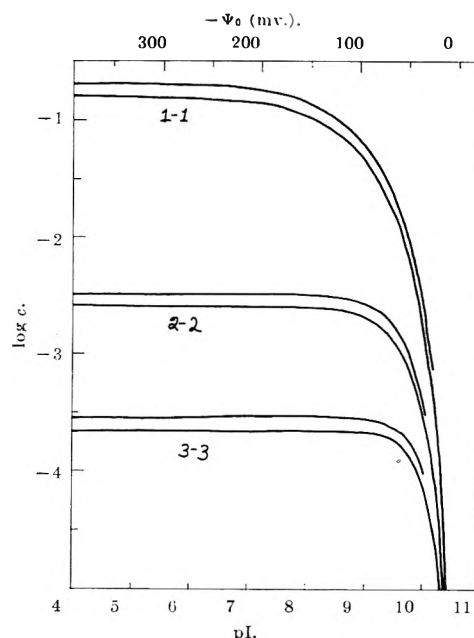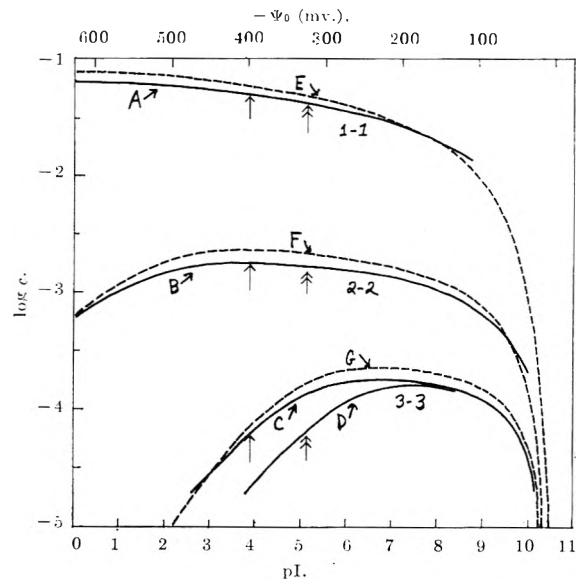

Fig. 4.—Logarithm of coagulating concentration against pI or plate potential for 1-1, 2-2, and 3-3 electrolytes in the present theory. Solid curves are the H.P. approximation and the broken curves are the L.S. approximation. On the solid curves (A, B, C and A, B, D) the Tezak–Mirnik formulation of the Schulze–Hardy rule is valid at the arrows. The L.S. approximation for curve D is not shown. Parameter values in Tables I and II.
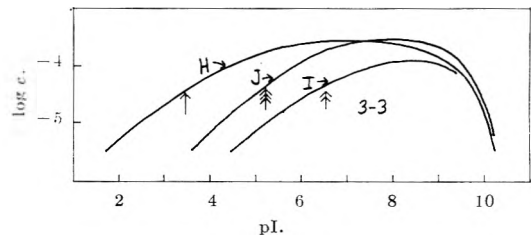
Fig. 5.—Logarithm of coagulating concentration against pI for a 3-3 electrolyte (H.P. approximation) in the present theory. The arrows mark the value of pI where the T.M. law is valid between each of the three curves and the curves A ($z = 1$) and B ($z = 2$) in Fig. 4. Parameter values in Tables I and II.
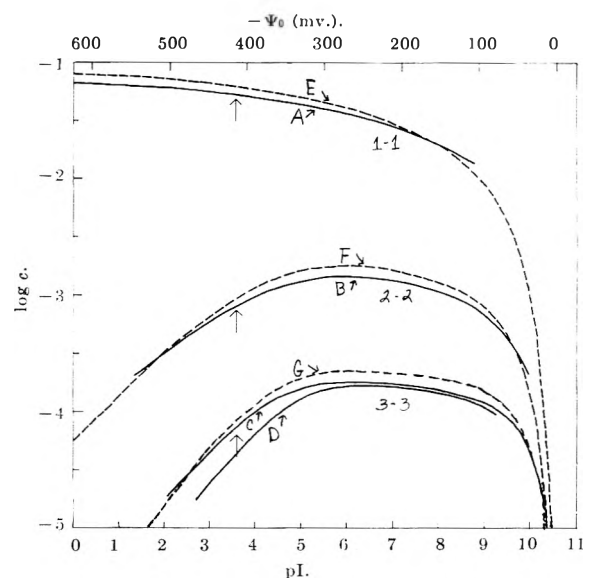
Fig. 6.—Similar plots to those in Fig. 4, with different parameters for 2-2 and 3-3 electrolytes. The curves A and E for the 1-1 electrolyte are identical with those in Fig. 4. The L.S. approximation for curve D is not shown. On the solid curves (A, B, C) the z^{-6} law is valid at the arrows. Parameter values in Tables I and II.

suming that the z^{-6} law holds at $k = 0.70$; further details are given in Table II. Curve D differs from C in
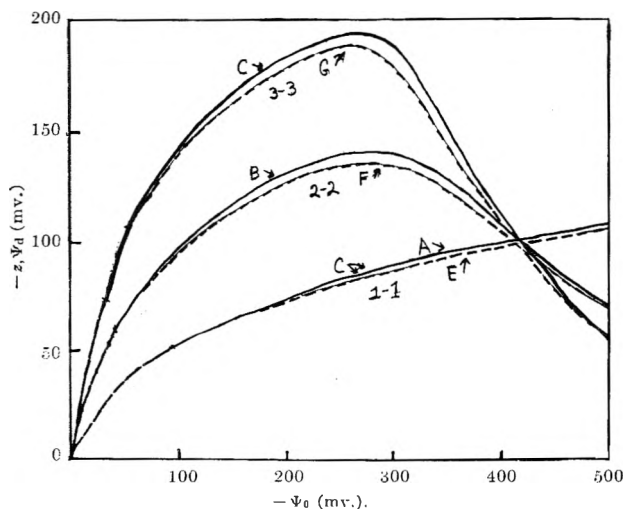
Fig. 7.—Variation of potential at the O.H.P. with plate potential at coagulation. Solid curves are a re-plot of A, B, C (H.P. approximation) and broken curves a re-plot of E, F, G (L.S. approximation) in Fig. 6. The common point of intersection marks the z^{-6} law.

Fig. 6 only in the change of the capacity K from 20 to 15 μfarad./cm.^{2}. There is no value of pI at which the z^{-6} law is obeyed exactly between the curves A, B, and C in Fig. 6. Finally, in Fig. 7, the three curves A, B, and C and the corresponding L.S. plots have been redrawn to show the variation of $z\Psi_d$ with Ψ_0. The z^{-6} law is obeyed at the point of common intersection.

By decreasing the van der Waals constant A all the curves can be displaced parallel to the log c axis with no change in shape and in the direction of increasing c, provided the capacity K and the density of adsorption sites N_a are simultaneously increased so that KA and K/N_a remain constant. From (4.6), (4.9), and (4.10) the product KX depends only on A and k and it follows from (4.13) that if k (or Ψ_d) is unaltered, a change in ln n and therefore log c depends only on a corresponding change in A. To ensure that n_0 and hence pI are unaffected in this operation, it is seen from (4.11) and (4.12) that, as well as Ψ_d, the quantities b, X, and γ/d must not vary and this is achieved by keeping KA and K/N_a fixed.

Figures 2 and 3 suggest that the maximum in the log c–pI plot becomes flatter as the potential Ψ_d increases. Indeed, for the smaller values of Ψ_d considered in II,[3] steeper maxima than those shown in Fig. 4, 5, and 6 were obtained, particularly on the low potential (large pI) side. Although the agreement with the experimental results for AgI (Fig. 3a) is improved by increasing Ψ_d our theory still predicts a larger slope in the (log c–pI) curve at small pI.

Since the corrections to the H.P. and L.S. approximations derived in Fig. 4 and 5 will be small it is sufficient to indicate their magnitudes with the aid of a few typical examples in Table V. The corrections are found to be consistent with those illustrated in Fig. 3 and with differences between the H.P. and L. S. curves in Fig. 4 and 6.

We have concentrated on the experiments of the "*statu nascendi*" schools and on their interpretations of the Schulze–Hardy rule for silver halide sols. However, the z^{-6} law is consistent with Ostwald's empirical "activity coefficient" rule[34] which seems to predict approximately the coagulating concentration in a number of

(34) W. Ostwald, *J. Phys. Chem.*, **42**, 981 (1938).

sols. Our theory indicates a range of flocculating concentrations, having a complicated dependence on a whole number of factors. One aspect of coagulation worthy of comment is the relation between the potential Ψ_d and the valency z. If the z^{-6} law is obeyed, then for both the H.P. and L. S. approximations, Ψ_d is proportional to z^{-1}. With the T.M. law Ψ_d is not simply related to z, although it does decrease with increasing valency. Now according to Ghosh and his school[35] coagulation occurs at a definite ζ-potential irrespective of the valency of the counterions. If the ζ-potential may be equated to Ψ_d this means that Ψ_d is independent of z at flocculation. This is approximately true in the calculations of Table III, but not in the other examples given here and in II.[3] Furthermore, the corresponding values for Δ log c obtained by Ghosh and shown in Table IV indicate that $|\Psi_d|$ should diminish with increase in z. The situation may be summed up by saying that from the theory presented in this paper none of the simple rules which have been proposed for the variation of coagulating concentration with valency can be generally valid. This applies to the T.M. law that Δ log c is independent of z and pI, to the z^{-6} law, and to the rule of Ghosh that the ζ-potential is independent of z.

7. Discussion

Our theoretical results agree better with the "*statu nascendi*" experiments on AgBr and AgCl (see II[3]) than on AgI in respect to the values of Δ log c, the maximum in log c, and the limited range of pBr and pCl over which the T.M. law holds. Mirnik[16] maintains that the interpretation of the "*statu nascendi*" flocculating experiments on AgBr and AgCl is uncertain because of other processes, such as recrystallization[36] competing with coagulation, but the difference between AgI and AgBr may be partly explained in another way. A maximum in the ζ-potential of AgBr sol under variation of pBr at constant ionic strength[8,9] implies a maximum in the (log c–pBr) coagulation curves. However, a maximum in the ζ-potential of AgI is not definitely established experimentally[9] although a very shallow maximum from the low pI side is indicated on the experimental coagulation curves in Fig. 3a,[36a] which is consistent with the results of Kruyt and Klompé.[37] Lijklema[38] has suggested that the Stern (univalent) ions may be located at some distance from the AgI surface so that γ/d would be small. Indeed our present form for ϕ_β vanishes when $\gamma/d = 0$ and for $p = 1$ the theory reduces to the classical Stern one, where the I.H.P. and O.H.P. coincide and the potential at the O.H.P. has no maximum. However, the expression for ϕ_β is only a first approximation (III[6])[39] and a more accurate treatment will yield ϕ_β small but different from zero at $\gamma/d = 0$. It should be noted that our theory predicts

(35) B. N. Ghosh, S. C. Rakshit, and D. K. Chattoraj, *Trans. Faraday Soc.*, **50**, 729 (1954); *Kolloid Z.*, **154**, 48 (1957).

(36) R. H. Ottewill and A. Watanabe, *ibid.*, **171**, 33 (1960).

(36a) Note Added in Proof.—Recently Lyklema (*Trans. Faraday Soc.*, **59**, 418 (1963)) has calculated a minimum in the surface excess of co-ions for the negative AgI–simple 1–1 electrolyte system when the pI is changed at constant ionic strength, particularly at 0.1 *M*. This indicates a maximum in the potential $|\Psi_d|$ at the O.H.P.

(37) H. R. Kruyt and M. A. M. Klompé, *Kolloid Beih.*, **54**, 484 (1943).

(38) J. Lijklema, *Kolloid Z.*, **175**, 129 (1961).

(39) Compare V. G. Levich, V. A. Kiryanov, and V. S. Krylov, *Dokl. Akad. Nauk S.S.S.R.*, **135**, 1425 (1960); V. G. Levich and V. S. Krylov, *ibid.*, **140**, 518 (1962).

that the maximum becomes more pronounced as the valency of the counterion increases.

A number of other factors ignored or inadequately treated in this paper need to be included in a more detailed comparison with experiment. For example, the function $R(r)$ would be affected by the non-uniform distribution of so-called active spots on which the potential-determining ions are adsorbed, and various corrections to the Gouy–Chapman theory of the diffuse layer should be considered. Apart from the inadequacies of our double-layer model, the theory has been developed for two parallel plates, whereas the "*statu nascendi*" experiments apply to particles with mean radius comparable with the double-layer thickness, particularly with polyvalent counterions. This should not affect the general shape of the (log c–pI) coagulation curves but there will be some relative displacement between the different valencies.[5]

CONTACT ANGLES AND INTERFACIAL TENSIONS IN THE MERCURY–WATER–BENZENE SYSTEM

By Edward B. Butler

Pan American Petroleum Corporation, Tulsa, Oklahoma

Received September 26, 1962

The interfacial tensions between mercury and benzene and between mercury and water were measured by the pendent drop method. The values did not change either with time or with temperature over the range 10 to 50°. The interfacial tension between mercury and water saturated with benzene changes with temperature as does the interfacial tension between mercury and benzene saturated with water and as does the interfacial tension between water and benzene. None of the interfacial tensions changed with time. The values for the contact angles (measured through the water phase) were calculated from the interfacial tension data. The contact angles were also measured. Although the experimental values tended to drift toward the calculated equilibrium values, the two never coincided. The structures at the mercury–benzene and at the mercury–water interfaces are inferred from the interfacial tension data. The extremely long times apparently required for the measured contact angles to reach the equilibrium values are then explained in terms of the structures at the interfaces.

Introduction

Contact angles are a measure of the degree to which a solid is wet by one liquid in preference to another. Such measurements find application in fields such as ore flotation, detergency, and lubrication. At Pan American contact angles are used to determine whether or not a reservoir rock is oil-wet. This information is applied in reservoir engineering to obtain more complete oil recovery from the porous rock in which the oil is stored.[1] Unfortunately the interpretation of wettability in terms of contact angles is not entirely certain, for the numerical value of the contact angle depends on the way it is formed. Further progress in the application of contact angles as a measure of wettability will be aided by a better understanding of the way contact angles approach equilibrium.

The purpose of the present work is to examine the reasons for the existence of an advancing contact angle which differs from the receding angle. The relationship between the contact angle θ, the solid–liquid interfacial tensions γ_{os} and γ_{ws}, and the liquid–liquid interfacial tension γ_{ow} is stated by Young's equation.[2,3]

$$\cos\theta = \frac{\gamma_{os} - \gamma_{ws}}{\gamma_{ow}} \qquad (1)$$

Since all of the quantities on the right-hand side of eq. 1 are thermodynamic free energies, their values are determined by the state of the system, consequently θ is uniquely defined. But a unique value of θ is not found when contact angles are actually measured. Almost every investigator has found two contact angles

—an advancing angle and a receding one. Moreover, the value of the angles in any particular system has varied with the investigator. Harkins[4] is one of the few workers to claim a single value for the experimentally measured contact angle.

A number of explanations have been advanced to account for this discrepancy between Young's equation and experiment. Among these are surface roughness, lack of surface cleanliness, and surface heterogeneity, but none has been adequate. An answer to the discrepancy between theory and experiment could be obtained if measured values for the interfacial tensions could be substituted in Young's equation so that θ could be calculated. Unfortunately, except for a few special cases, solid–liquid interfacial tensions cannot be measured. Experimental verification of Young's equation does not exist and Newman's triangle, which may be viewed as a generalized case of Young's equation, has been verified only once.[5] Another attempt at a verification of Newman's triangle was not entirely satisfactory.[6]

Since interfacial tensions cannot be measured between solids and liquids, a three-phase liquid system in which all the interfacial tensions could be measured was chosen for this investigation. This system was mercury, water, and benzene. The equilibrium contact angle in this system can be calculated from the measured interfacial tensions and compared with the experimental angle. Such a comparison will help differentiate among the many possible causes for the existence of an advancing angle different from the

(1) R. O. Leach, O. R. Wagner, H. W. Wood, and C. F. Harpke, *J. Petrol. Tech.*, **14**, 114 (1962).

(2) T. Young, *Phil. Trans.*, **54**, (1805); Works (Ed. Peacock), Vol. I, p. 432.

(3) A. Dupree, "Theorie Mechanique de la Chaleur," 1896, p. 393.

(4) W. D. Harkins, "Physical Chemistry of Surfaces," Reinhold Publ. Corp., New York, N. Y., 1952, pp. 278–281.

(5) C. A. Smolders, Doctoral Thesis, University of Utrecht, Netherlands, 1961.

(6) D. J. Donahue and F. E. Bartell, *J. Phys. Chem.*, **56**, 480 (1952).

receding angle. Verification of Young's equation should be another result of the work.

The pendent[7] drop method developed by Andreas, Hauser, and Tucker[8] and further developed as an absolute method by Mills[9] and Fordham[10] was chosen for the measurement of interfacial tensions between the liquids, because the interfacial tension of a single pendent drop could be measured over a period of many hours. Any change in interfacial tension with time could then be observed. If one of the interfacial tensions were to approach equilibrium slowly, then any hysteresis observed when the contact angles were measured could be explained in terms of the slow equilibrium. If the interfacial tensions were to reach equilibrium rapidly, then any contact angle hysteresis observed would require a different explanation.

Experimental

Purification of Mercury.—Air was bubbled through triple-distilled mercury. A fine spray of the metal was dropped through a column of 10% nitric acid and then through a column of distilled water. The treated mercury was put into a still connected to the manifold of a high-vacuum system by means of a mercury float valve. Float valves were used throughout the high vacuum apparatus to avoid any possible contamination of the system with grease. A liquid nitrogen trap between the vacuum pumps and the main manifold prevented the entry of contaminants from the pumps. The system was evacuated to 10^{-8} mm. pressure as indicated by a Philips ionization gage. The 250-cc. bulb in which the mercury was heated was connected by a short neck to another immediately above it. This upper bulb was connected to a water condenser and to an air condenser. The water condenser led back to the bulb containing the mercury through a U seal. The air condenser led to a second one which led to a manifold to which the sample bulbs were attached. The air condensers were of the cold finger type. The mercury vapor entered the bottom of the first condenser and left near the top. The vapor entered the second near the top and left at the bottom. The mercury in the 250-cc. bulb was heated by a flame. An electric heater was inserted into the finger of the second condenser to heat it and to prevent mercury distilling into the sample bulbs at this time. The whole apparatus was flamed. The mercury was then heated for 2 or 3 hr. above 200° and under total reflux. At the end of this time the first air condenser was heated with the electric heater and the mercury was distilled into the sample bulbs. One end of the sample tube was pulled down to form a seal-off where the tube was attached to the purification system. The other end was closed by a break-seal. The sample bulbs were sealed and pulled off the line when they contained 25 cc. of mercury. Five or six sample bulbs were prepared at one time. This method for the purification of mercury is similar to that used by Kemball.[11]

Purification of the Water.—A solution containing 5 g. of $KMnO_4$ and 8 g. of 85% phosphoric acid in 500 ml. of distilled water was boiled under total reflux at atmospheric pressure for 8 hr. or more to destroy any organic matter which might be present in the water.

The acid permanganate solution was put into the apparatus in which it was distilled and freed from air. This apparatus consisted of a 500-cc. flask which led to a baffle some 75 cm. long and 8 cm. in diameter. In the baffle water vapor rose up an inner tube 65 cm. long and 2.5 cm. in diameter, then came down an outer concentric tube which was closed at the top and which was 4 cm. in diameter. The vapor then rose through the outer jacket of the baffle and went to a condenser. The moisture which accumulated at the bottom of the baffle was returned to the 500-cc. flask through a U seal. The upper end of the baffle was also connected to the main manifold of the high vacuum system by means of a mercury float valve. The condenser led

(7) Spelling "Webster's Third New International Dictionary," G. and C. Merriam Company, Springfield, Mass., 1961.

(8) J. M. Andreas, E. A. Hauser, and W. B. Tucker, *J. Phys. Chem.*, **42**, 1001 (1936).

(9) O. S. Mills, *Brit. J. Appl. Phys.*, **4**, 247 (1953).

(10) S. Fordham, *Proc. Roy. Soc.* (London), **A194**, 1 (1948).

(11) C. Kemball, *Trans. Faraday Soc.*, **42**, 526 (1946).

to the center of a U. One side of the U led back to the 500-cc. flask through a spray trap. The other side of the U went to the bottom of the second 500-cc. flask somewhat higher in position than the first. This flask led to a baffle like the first. This baffle was also connected to the main manifold of the high vacuum system through a mercury float valve, and to a condenser. The condenser led to a conductivity cell, and the conductivity cell led to a 25-cc. sample bulb through a syphon arm. The sample bulb led to the second 500-cc. flask through another siphon arm and through another spray trap.

After the acid permanganate solution was put into the first 500-cc. bulb. The apparatus was evacuated through the two float valves for 30 min. or longer. The trap which served to keep water vapor out of the vacuum pump was immersed in liquid nitrogen during this time. The system was then isolated from the trap and the pump by means of the float valves. The magnetic stirrer and the heater under the first 500-cc. flask were turned on, and a flow of water was started through the condensers. After 50 to 100 ml. of water had accumulated in the second 500-cc. flask the heater under it and a heat lamp above it were turned on. The water was now distilled from the second flask into the conductivity cell. The conductivity cell periodically filled with water and emptied into the sample bulb. The water in the sample bulb periodically emptied into the second 500-cc. flask and siphoned back into the first at longer intervals. The whole system was pumped out several times (for 5 min. each) at intervals of 2 or 3 hr. to be sure that all air and CO_2 had been removed from the system.

The specific conductivity of the water in the conductivity cell was calculated from the potential across the cell, from the current through the cell, and from the cell constant. The cell constant was found by calibration of the cell with 0.001 M KCl solution. The specific conductivity of the water accepted for filling the sample bulb was not more than $9(10^{-8})$ mho at 30°. Ordinary conductivity or equilibrium water has a specific conductivity of 10^{-6} mho at 25°.

After the sample bulb was filled, it was sealed off from the water purification system. The sample bulb was then sealed into the apparatus in which the water was to be used and the break-off was opened when desired.

Purification of the Benzene.—Reagent grade benzene which, according to the manufacturer's label, contained less than 0.0005% thiophene was passed through a column of silica gel into a round bottom 500-cc. flask containing lumps of sodium. The benzene purification system consisted of three such 500-cc. flasks connected to each other through simple distillation columns. The benzene was frozen with liquid nitrogen and the system was pumped out through the high vacuum system described in the previous paragraph. The benzene system was shut off from the main vacuum system and the benzene was allowed to melt. This procedure was repeated five or six times during the three or four days the benzene stood in contact with the sodium metal. At the end of this time, the benzene was distilled from flask to flask and then into the sample bulbs. The sample bulbs were similar to those used for the water samples. The benzene in the 25-cc. sample bulbs was frozen with liquid nitrogen and pulled off the line.

The Pendent Drop Apparatus.—A collimated beam from a 100-w. concentrated arc with a flat end window passed through the pendent drop cell and fell on the lens of the camera. The 32 mm. micro-Tessar lens on the camera was mounted on a microscope tube that could be focused on the pendent drop. The image of the drop was focused on the ground glass screen in the Polaroid Land attachment. A series of pictures of a single pendent drop at a chosen temperature could then be taken over a period of time. The pendent drop cell was mounted on a short optical bench at right angles to, but completely separated from the optical bench which held the camera and the light source. This arrangement prevented jarring the pendent drop cell during the manipulation of the camera. The whole apparatus was placed in a basement room comparatively free from vibration.

A stainless steel pin of known diameter was used to obtain the enlargement factor necessary for the calculation of the drop size measurements. After a series of pictures were taken of a pendent drop at a given temperature, the insulated box holding the pendent drop cell was moved out of the way without altering the position of the camera in any manner. The steel pin was put in a carriage on the short optical bench in place of the insulated box. The pin was brought into focus by means of

a screw drive on the carriage and a picture was taken. The pin was refocused three more times by means of the screw drive on the carriage holding the pin and each time another picture was taken. The average value of the diameters of the images in the four photographs was the value used to calculate the enlargement factor.

Water from a thermostat holding 22 gal. was circulated through the insulated box holding the pendent drop cell. The temperature in the thermostat was controlled to ±0.01° to prevent changes in the drop size during measurement. Temperature control to ±0.001° was later found necessary for the contact angle measurements. The pendent drop cell was held in the insulated box in such a manner that the windows of the cell were exposed. Light entering and leaving the cell was thus undistorted by any other intervening glass.

The Pendent Drop Cells.—The pendent drop cell used to measure the interfacial tension between mercury and water, and mercury and benzene is illustrated in Fig. 1. The cell body was a commercial absorption cell 50 mm. long and 25 mm. in diameter. The windows were polished optically flat to reduce distortion of the photographed drop image. The two electrodes were sealed into the cell to prevent the accumulation of static charge on the drop during its formation.[11] These electrodes were connected together and to ground during a measurement. The 25-cc. bulb sealed into the 10-mm. tube near the seal-offs held any excess benzene, water, or mercury. The 5-cc. bulb with the electrode sealed into it was completely filled with mercury as was the capillary tube which connects the bulb and the cell body. The capillary tip at which the drop formed had a 1-mm. inside diameter. The cell was placed in the insulated box at a temperature 5° lower than the desired temperature. The temperature was rapidly raised 5° by means of water circulated through the box from the 22-gal. thermostat. A pendent drop formed at the tip and reached full size within one to three minutes. When data at a higher temperature were desired, the temperature of the thermostat was raised to within 5° of the desired temperature. The excess mercury fell off the tip a drop at a time and accumulated in the lower part of the cell. The temperature was then rapidly raised 5° to form a new drop.

The cell which was used to measure the interfacial tension between the water and the benzene was similar to the cell described in the previous paragraph. The bulb, which was now completely filled with water instead of mercury, had a 10-cc. volume and the dropper tip was a short piece of platinum tube with a 2-mm. inside diameter. A pendent water drop was formed in the cell in much the same manner as was the pendent mercury drop.

The interfacial tensions were calculated from the equations given by Andreas, Hauser, and Tucker[8] and from the tables given by Fordham[10] and Mills.[9] The values for the densities of benzene, water, and mercury were taken from the literature.[12,13]

The Contact Angle Cell.—The cell in which a contact angle between mercury, benzene, and water was formed is shown in Fig. 2. This cell was designed to bring a benzene drop into contact with a mercury surface which has been only in contact with water. The 3-cc. bulb was completely filled with benzene at 5°. The cell was placed in the thermostat at 5° and the temperature was slowly raised. A drop of benzene formed on the platinum dropper tip and approached the rounded surface on the mercury held in the 4-mm. tube coming up from the bottom of the cell. This tube had been previously filled by sloshing mercury into it. When the pendent drop of benzene had approached the mercury surface very closely but had not touched it, the thermostat regulation was checked and the temperature was raised very slowly until the drop touched the mercury. The instant at which the mercury and benzene touched was unmistakable, for the benzene appeared to jump when it touched the mercury surface. The temperature was immediately stabilized and a series of pictures of the contact angle were taken on Polaroid Land (No. 146 L) transparency film. When the contact angle was desired at a different temperature, the drop was removed by rocking the cell back and forth so that mercury sloshed from end to end. The mercury knocked the drop off and also renewed the mercury surface in the 4-mm. tube.

(12) "Lange's Handbook of Chemistry," 6th Edition, Handbook Publishers, Sandusky, Ohio, 1946, p. 1358.

(13) "International Critical Tables of Numerical Data," Vol. 6, McGraw-Hill Book Co., New York, N. Y., 1926-1933.
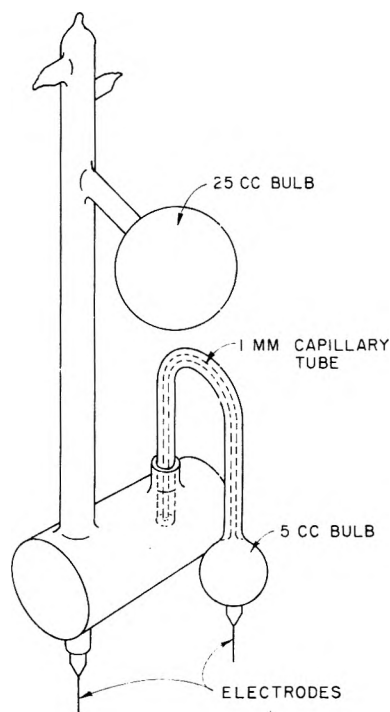
Fig. 1.—Pendent drop cell for interfacial tension measurements.
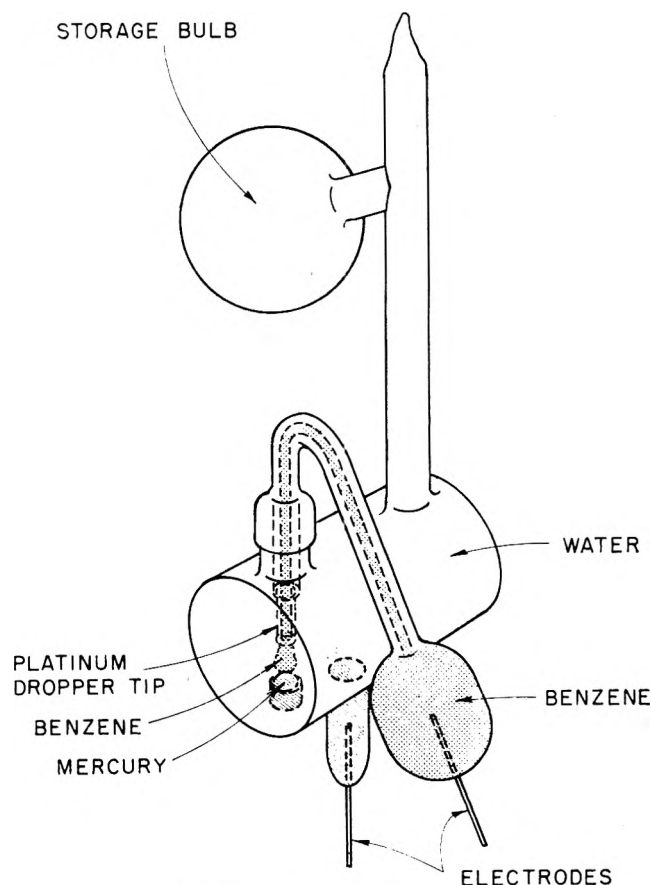
Fig. 2.—Cell for the contact angle measurements.

The Filling of the Cells.—The appropriate cell was sealed into the high vacuum system and pumped down to 10^{-8} mm. and heated at 300° overnight. The sample bulbs containing the mercury and the water or benzene had been sealed onto the cell before it was pumped out. The cell along with its attached sample bulbs was sealed and pulled off the vacuum line. After the cell had cooled, the break-seal was opened, the mercury entered the cell, and the mercury sample bulb was sealed and pulled off the cell. The cell was then tilted in such a manner that the capillary tip was submerged in mercury and the 5-cc.

bulb (Fig. 2) filled with mercury. The tilted position of the cell was maintained and the 5-cc. bulb was cooled with ice. The break-off on the benzene sample tube or water sample tube was then broken and the liquid allowed to enter the cell. The sample tube was sealed off and removed from the cell. The cell was then placed in the insulated box on the thermostat. The box was filled with enough ice to cover the 5-cc. bulb on the cell. A stream of dry nitrogen was blown across windows of the cell to keep them from fogging. The whole box was moved into position so that the camera could be focused on the drop. A stream of water from the thermostat was started through the box, the thermostat being at a higher temperature than the ice-water in the box. A drop would then grow on the capillary tip. The camera was focused on this drop.

When the cell used to measure the interfacial tension between water and benzene was filled, the bulb attached to the dropper tip was filled with water at about 4°, then the excess water was removed from the cell body proper by gently warming it. Were this not done, then the excess water tended to wet the cell windows and the light traveling through this layer produced a distorted image of the water drop. The cell body was allowed to cool, then the benzene was put into the cell. After the benzene had filled the cell body, the cell was tilted so that a small amount of water ran from the reservoir bulb into the cell body. This water saturated the benzene. The cell was then placed in the insulated box.

Measurement of the Contact Angle.—The Polaroid transparency pictures of the contact angles were placed in a slide holder and the picture was projected onto an 8.5 × 11 in. piece of white paper. A drafting triangle was used to draw tangents to the curves defining the contact angle. The angle between the tangent lines was then measured with a protractor. Although the protractor was capable of measuring to two minutes of arc, the precision of measurement was probably only ±2°. The contact angle measured was through the water phase.

Results

The interfacial tensions between mercury and pure water and between mercury and pure benzene are presented in Tables I and II, respectively. The interfacial tensions did not change with time during the 24-hr. period over which most of the measurements were made. The first data point which was taken within 3 min. after the drop had started to form was the same within the limits of error as the last data point which was taken some 1300 min. later. Tables I and II also show that the interfacial tensions have no temperature coefficient within limits of error in the measurements. The interfacial tensions between mercury and water saturated with benzene are given in Table III at a number of temperatures. Similar data for the interfacial tension between mercury and benzene saturated with water are given in Table IV. Again there was no variation of interfacial tension with time at any temperature. The first measurement, which was made within 3 min. after the mercury drop started to form, was the same within the limits of error as the last measurement which in one case was made as long as 5116 min. later.

TABLE I

INTERFACIAL TENSION BETWEEN MERCURY AND PURE WATER

Temp., °C.	No. of pictures taken of drop	Time over which drop was measured, min.	Interfacial tension, dynes/cm.	Std. dev.
15.6	10	1059	415.1	2.35
26.7	11	1338	415.8	1.92
38.4	11	1347	413.4	1.22
49.0	11	1365	412.5	1.86
		Av. of all values	414.2	2.29

Table V gives the interfacial tension between water and benzene at temperatures above 30°. Data below

TABLE II

INTERFACIAL TENSION BETWEEN MERCURY AND PURE BENZENE

Temp., °C.	No. of pictures taken of drop	Time over which drop was measured, min.	Interfacial tension, dynes/cm.	Std. dev.
10.6	11	1160	358.5	1.00
21.1	10	293	356.7	1.41
31.1	11	959	357.4	1.70
41.1	11	1359	359.3	2.66
		Av. of all values	358.1	2.10

TABLE III

INTERFACIAL TENSIONS BETWEEN MERCURY AND WATER SATURATED WITH BENZENE

Temp., °C.	No. of pictures taken of drop	Time over which drop was measured, min.	Interfacial tension, dynes/cm.	Std. dev.
10.2	13	997	403.6	1.75
16.4	11	1306	396.0	1.76
22.3	13	4196	396.3	0.75
27.8	12	1321	394.3	1.56
34.1	12	1316	390.5	1.80
36.7	15	226	391.9	1.62
39.3	12	1335	388.4	2.15
41.1	21	1313	388.9	1.47
49.2	22	5116	390.4	1.23
53.8	12	225	388.9	1.52

TABLE IV

INTERFACIAL TENSION BETWEEN MERCURY AND BENZENE SATURATED WITH WATER

Temp., °C.	No. of pictures taken of drop	Time over which drop was measured, min.	Interfacial tension, dynes/cm.	Std. dev.
11.8	23	4031	359.0	1.61
16.2	25	1331	358.8	2.35
20.7	28	1322	359.6	1.91
25.2	27	1314	359.3	1.30
28.5	3	7	357.9	2.32
37.7	4	25	359.1	2.80
42.1	19	968	358.3	2.20
50.0	24	1027	354.3	2.54
54.2	20	1142	355.3	2.10
58.7	19	1311	357.0	2.54
62.9	15	80	356.3	1.89

TABLE V

INTERFACIAL TENSION BETWEEN WATER AND BENZENE

Temp., °C.	No. of pictures taken of drop	Time over which drop was measured, min.	Interfacial tension, dynes/cm.	Std. dev.
30.0	14	327	33.0	0.47
37.0	12	137	33.8	.90
43.5	23	483	32.9	.38
50.4	30	693	31.9	.44
57.1	23	1405	31.6	.28
65.9	13	66	30.9	.42

30° were taken from the work of Harkins and Cheng.[14] The interfacial tension between water and benzene did not change with time.

The contact angle θ should be calculated from the interfacial tension data by means of the equation

$$\cos \theta = \frac{\gamma_{23}^2 - \gamma_{12}^2 - \gamma_{13}^2}{2\gamma_{12}\gamma_{13}} \quad (2)$$

where γ_{23} is the interfacial tension between mercury and benzene saturated with water, γ_{13} is the interfacial

(14) W. D. Harkins and Y. C. Cheng, *J. Am. Chem. Soc.*, **43**, 49 (1921).

tension between mercury and water saturated with benzene, and γ_{12} is the interfacial tension between water and benzene. Actually θ was calculated by means of Young's equation

$$\cos \theta = \frac{\gamma_{23} - \gamma_{13}}{\gamma_{12}} \qquad (3)$$

but it differs insignificantly from the θ calculated from eq. 2. The calculated θ is plotted against the temperature in Fig. 3. According to the calculation the benzene would spread on the mercury surface below 20° and above 45°. Between 20 and 45° the calculated contact angle falls to a minimum value of 154°. Figure 4 shows plots of measured contact angles against time at several temperatures. The calculated values and the measured values do not agree.

Discussion

The interfacial tensions between mercury and benzene and between mercury and water reported in this paper differ markedly from those reported by Bartell and Bard[15] and Bartell and Bjorklund.[16] In no case was any drift of the interfacial tensions with time observed over periods of 24 hr. or longer. The interfacial tension between mercury and water saturated with benzene was measured over a period of about 72 hr. at 49.2°, but no change in interfacial tension with time was detected. The value of the interfacial tension between mercury and pure water, 414.2 dynes/cm. is comparable with the 420 and 426 dynes/cm. reported in the literature.[5,17] The interfacial tension between mercury and pure benzene is 358 dynes/cm. This value is close to the value of 362 dynes/cm. reported by Harkins.[18]

Regardless of the source of the 1 to 2% difference between these values and the literature values, the important point is that the interfacial tensions all reached equilibrium in less than 3 min. The rapidity with which the interfacial tensions reached equilibrium led to the belief that contact angle equilibrium would also be rapid. The actual experiment in which a benzene drop was brought into contact with a mercury surface which had previously been covered with water showed that equilibrium was approached extremely slowly. In fact equilibrium was reached in only one case, and then only after a period of 60 hr. In that case the angle initially formed was very high. In other cases an angle which started at about 60° never got much greater than 110°, yet the calculated equilibrium value is 180°. These observations were made repeatedly at many temperatures and in at least three different contact angle cells.

The discrepancy between the equilibrium contact angle which was calculated from the interfacial tension data and the experimentally measured angle cannot be dismissed as being the result of surface roughness, impurities, or surface heterogeneity. The mercury-water-benzene system was chosen because such factors were eliminated. Freedom from impurities has been demonstrated by the stability of the interfacial tensions over times as long as 72 hr. Some property of the

(15) F. E. Bartell and R. J. Bard, *J. Phys. Chem.*, **56** 532 (1952).
(16) F. E. Bartell and C. W. Bjorklund, *ibid.*, **56**, 453 (1952).
(17) D. C. Henry and J. Jackson, *Nature*, **142**, 616 (1938).
(18) W. D. Harkins, "The Physical Chemistry of Surfaces," Reinhold Publ. Corp., New York, N. Y., 1952, p. 29.
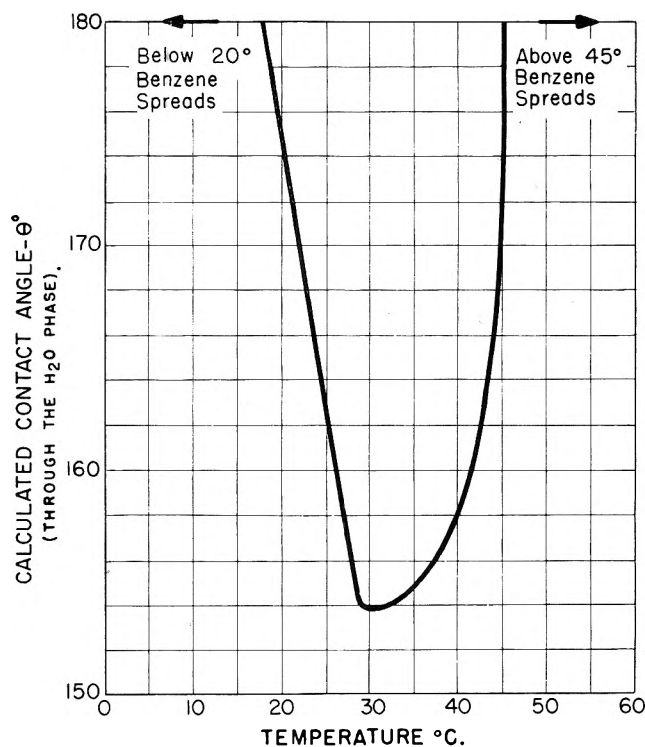
Fig. 3.—Contact angles calculated from the interfacial tension data by means of Young's equation and plotted against the temperature.
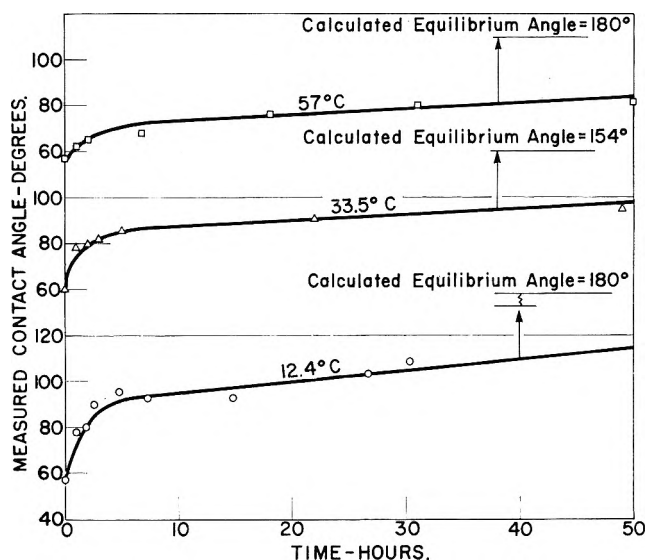
Fig. 4.—Experimentally measured contact angles plotted against time.

system must be responsible for the very slow approach to equilibrium shown by the contact angles.

The structure of the surface at the mercury–water and at the mercury–benzene interfaces can be inferred from the interfacial tension data and some insight into the behavior of the contact angle can be obtained from the surface structure. Inspection of Table I and Table II shows that the interfacial tensions between mercury and pure benzene and between mercury and pure water have no temperature coefficients. By contrast the interfacial tensions between mercury and benzene saturated with water and between mercury and water saturated with benzene do change with temperature. These facts must mean that the variations in the systems in which the water is saturated with benzene and *vice versa* are the result of a change of concentration of the

Fig. 5.—(A) Interfacial tension between mercury and water saturated with benzene plotted against the mole fraction of benzene in the water phase; (B) interfacial tension between mercury and benzene saturated with water plotted against the mole fraction of water in the benzene phase.

benzene dissolved in the water and of the water dissolved in the benzene rather than the result of the temperature change. In other words the variation of the interfacial tension is primarily a function of concentration. This is not to say that the temperature has absolutely no effect on the system, but rather that the overwhelming effect is the result of the concentration change.

In Fig. 5 the interfacial tensions between mercury and the solutions are plotted against the mole fraction of solute. The solubilities of benzene in water[19-21] and of water in benzene were taken from the literature.[22] Plotted in this way the shapes of the curves for the interfacial tension between mercury and water saturated with benzene and for the interfacial tension between mercury and benzene saturated with water are remarkably similar. These curves suggest that adsorption of the solute is occurring in the regions where the slopes are steep. The change in slope occurs between 10 and 35° for the case where mercury is in contact with water saturated with benzene, and between 40 and 50° for the case where mercury is in contact with benzene saturated with water. The Gibbs adsorption isotherm cannot be applied as such to obtain information about adsorption at the mercury surface, for any change in γ is the result of a change in both temperature and composition of the solution. However, an equation which provides a method for finding the composition at the mercury–water interface can be derived.

The interfacial tension γ_{Hg-H_2O} between mercury and water is a function of both the temperature T and the activity a of the benzene dissolved in the water. Therefore

$$d\gamma_{Hg-H_2O} = (\partial\gamma_{Hg-H_2O}/\partial \ln a)_T \, d \ln a +$$

$$(\partial\gamma_{Hg-H_2O}/\partial T)_a \, dT \quad (4)$$

$$\frac{d\gamma_{Hg-H_2O}}{d \ln a} = \left(\frac{\partial\gamma_{Hg-H_2O}}{\partial \ln a}\right)_T + \left(\frac{\partial\gamma_{Hg-H_2O}}{\partial T}\right)_a \frac{dT}{d \ln a} \quad (5)$$

According to the Gibbs adsorption isotherm

(19) D. M. Alexander, J. Phys. Chem., 63, 1021 (1959).
(20) R. L. Bohon and W. F. Claussen, J. Am. Chem. Soc., 73, 1571 (1951).
(21) D. S. Arnold, C. A. Planck, E. E. Erikson, and F. P. Pike, J. Chem. Eng. Data, 3, 253 (1958).
(22) A. Seidel, "Solubility of Organic Compounds," D. Van Nostrand Co., Inc., Princeton, N. J., 3rd Edition, 1941, p. 368.

$$\left(\frac{\partial\gamma_{Hg-H_2O}}{\partial \ln a}\right)_T = -RT\Gamma_2^1 \quad (6)$$

where Γ_2^1 is the surface excess and R is the gas constant.

Substitution of $RT\Gamma_2^1$ in eq. 5 followed by rearrangement gives

$$\Gamma_2^1 = -\frac{1}{RT}\frac{\partial\gamma_{Hg-H_2O}}{\partial \ln a} + \frac{1}{RT}\left(\frac{\partial\gamma_{Hg-H_2O}}{\partial T}\right)_a \frac{dT}{d \ln a} \quad (7)$$

The quantity $\ln a$ which appears in eq. 7 can be calculated. At each temperature at which γ_{Hg-H_2O} was measured the water phase is in equilibrium with the benzene phase. If the activity of the liquid benzene phase can be calculated for each temperature, then the activity of the benzene in the water phase is known at once. The problem now becomes that of calculating the activity of liquid benzene as a function of temperature. The effect of the dissolved water in the benzene phase on the activity of the liquid benzene is so small as to be negligible and is ignored in the calculation.

Let the standard state at which the activity is taken as unity be liquid benzene at 278°K. and consider the process in which the temperature of the liquid benzene is raised from 278 to T°K. The change in activity as a result of this process is given by the familiar equation.

$$\frac{d \ln a}{dT} = \frac{\Delta H}{RT^2} \quad (8)$$

The quantity ΔH is calculated from the relationship between ΔH, C_p, and T and from an empirical equation giving C_p as a function of T.[23,24] The integration of eq. 8 then gives an equation for $\ln a$ as a function of the temperature.

A plot of γ_{Hg-H_2O} against the calculated values for $\ln a$ at the corresponding temperatures varies linearly over the range 10–40° where adsorption is apparently occurring at the mercury–water interface. The slope of d $\gamma_{Hg-H_2O}/d \ln a$ in this region is -55.6. Substitution of this quantity in eq. 7 gives

$$\Gamma_2^1 = \frac{6.70 \, (10^{-7})}{T} + \frac{1}{RT}\left(\frac{\partial\gamma_{Hg-H_2O}}{\partial T}\right)_a \frac{dT}{d \ln a} \quad (9)$$

In eq. 9 the quantity $dT/d \ln a$ is positive for $\ln a$ increases as T increases. The entropy term, $(\partial\gamma_{Hg-H_2O}/\partial T)$ is also positive as is shown by the reasoning which follows. The plot of γ_{Hg-H_2O} against T when no benzene is present has a zero slope. The addition of benzene causes a decrease in γ_{Hg-H_2O}, a change indicative of adsorption of benzene at the mercury surface. Imagine a case in which the temperatures increase while the activity of the benzene in the water remains constant. Under these circumstances γ_{Hg-H_2O} would, if it did anything, tend to increase because the benzene adsorbed on the mercury surface would tend to desorb as the temperature increased. The entropy term would therefore be positive in sign. That this reasoning is correct is borne out by the data

(23) "Handbook of Chemistry and Physics," 40th Edition, Chemical Rubber Publishing Co., Cleveland, Ohio, 1958, p. 2278.
(24) The equation used for C_p was: $C_p = 3.31859 + 0.112684T - 0.000056646T^2$.

obtained by Kemball and Rideal[25] for the surface tension of mercury over a temperature range in the presence of a constant pressure of benzene. In this case $d\partial/dT$ is positive also. Since $dT/d \ln a$ and the entropy term are both positive in sign, their product is positive.

Since the last term on the right-hand side of eq. 9 is positive, the $\Gamma_2{}^1$ calculated without this last term will be a minimum value. The reciprocal of the product of $\Gamma_2{}^1$ and Avogadro's number gives an area for the benzene molecule of 6 to 7 Å.[2], an area which is a maximum for the area of the benzene molecule. These areas are much too small compared to the literature values.[26,27] A benzene molecule on edge has an area of 24 to 26 Å.[2], and a benzene molecule lying flat has an area of 40 Å.[2].

Up to this point the deductions which have been made are on an apparently sound basis. Unfortunately attempts to explain the behavior of the system in detail become more and more speculative. The small area found for the benzene molecule could be explained by multilayer adsorption of benzene. But multilayer adsorption seems unlikely, for in this case the mercury surface would be covered with a layer of benzene two to six molecules thick. A drop of benzene coming in contact with such a layer would certainly form a near-zero contact angle, for the outermost benzene molecules in the adsorbed layer would be expected to behave much like those in liquid benzene insofar as their attraction for other molecules is concerned.

Since the mercury surface at the mercury–water interface is covered with a layer of benzene as is the mercury at the benzene–mercury interface, why does not the benzene-advancing contact angle rapidly reach the calculated equilibrium value when a benzene drop is placed on a previously water-covered mercury sur-

face? Regardless of the particular way the benzene molecules are arranged on the mercury surface, a drop of benzene placed on such a benzene covered surface would be expected to wet the surface. In fact the benzene might always be expected to form a zero contact angle on such a surface. But it does not. The behavior of the system might be explained by a layer of water molecules attached to the adsorbed benzene by π-bonds. A drop of benzene approaching such a surface would come into contact with a layer of water molecules. Since the benzene could not wet the surface until the water left the interface, the slow approach to contact angle equilibrium would be explained by slow desorption of the adsorbed water.

In contrast to the mercury surface at the mercury–water interface, no adsorption of solute takes place at the mercury–benzene interface between 10 and 40°, for the slope of $\gamma_{Hg-benzene}$ against the log of the activity of the water in the benzene is zero. In this region the mercury surface must be covered with benzene packed much the same way as it is packed at the water–mercury interface. Since this surface is already covered with a layer of benzene, water coming into contact with such a surface might be expected to rapidly come to equilibrium with it. If this is the case, then a contact angle formed by water advancing over a previously benzene-covered mercury surface should reach equilibrium rapidly. Experimental difficulties have so far prevented this test.

One of the objectives of this work has been achieved. The existence of a water-advancing contact angle different from a water-receding angle has been explained in terms of molecular structures at the interfaces. Alternate explanations such as surface roughness, surface inhomogeneity, and impurities were eliminated in the system. Verification of Young's equation and substantiation of the proposed surface structures await further experimentation.

(25) C. Kemball and F. Rideal, *Proc. Roy. Soc.* (London), **A187**, 53 (1946).

(26) J. M. Robertson. *Chem. Rev.*, **16**, 417 (1951).

(27) N. K. Adam, "Physics and Chemistry of Surfaces." Oxford University Press, London. Third Edition, 1941, p. 50.

THE KINETICS OF THE REACTION BETWEEN PLUTONIUM(VI) AND IRON(II)[1]

By T. W. Newton and F. B. Baker

University of California, Los Alamos Scientific Laboratory, Los Alamos, New Mexico

The kinetics of the reaction Pu(VI) + Fe(II) = Pu(V) + Fe(III) have been studied in acid perchlorate solutions between 0 and 25°. The rate is given by $-d[Pu(VI)]/dt = [Pu(VI)][Fe(II)]\{A + (B + C[H^+])^{-1}\}$ from 0.05 to 2.0 M HClO$_4$ at $\mu = 2.0$. This rate law indicates the presence of a metastable binuclear intermediate, probably Pu(V)·Fe(III). Values of ΔH^* and ΔS^* have been computed for the formation of the three activated complexes required by the rate law. The effect of ionic strength between 0.05 and 2.0 M and the effect of 0.10 M Cl$^-$ were determined.

Introduction

This paper continues a series[2] in which the kinetics of various aqueous oxidation–reduction reactions of plutonium ions are described. The rate laws and the thermodynamic quantities of activation are of interest for sets of similar reactions in helping to learn about the factors which influence these rates. The kinetics

of the reduction of Pu(VI) by U(IV),[3] Pu(III),[4a] Ti(III),[4b] V(III),[4c] and Sn(II)[5] have been reported previously. Fe(II) is of interest in that it represents a divalent ion which is capable of reducing Pu(VI) at a measurable rate in the absence of a complexing agent such as chloride ion.

Fe(II) was chosen also to see whether evidence could

(3) T. W. Newton, *ibid.*, **62**, 943 (1958).

(4) S. W. Rabideau and R. J. Kline, (a) *ibid.*, **62**, 617 (1958); (b) *ibid.*, **63**, 1502 (1959); (c) *ibid.*, **62**, 414 (1958).

(5) S. W. Rabideau and B. J. Masters, *ibid.*, **65**, 1256 (1961).

be found for a complex such as Pu(V)·Fe(III) which is analogous to the Np(V)·Fe(III)[6] and U(V)·Cr(III)[7] complexes which have recently been reported.

Previous, fragmentary work on the reduction of Pu(VI) by Fe(II) is summarized by Connick,[8] who states that the reaction is rapid at room temperature.

Experimental

Reagents.—Stock solutions of plutonium were prepared by dissolving weighed amounts of the pure metal in 70% HClO₄ and diluting to 1 M in acid. Portions of these solutions were taken as needed and oxidized to Pu(VI) by fuming with additional HClO₄ and treatment with ozone. Excess ozone was removed by passing a stream of oxygen for several hours. These solutions were used within eight hours of preparation to minimize the effects of alpha particle self-reduction. The solutions were analyzed for Pu(VI) using a spectrophotometric titration in which the plutonium was reduced to Pu(IV) with standard Fe(II). The titration medium was 8 M H₂SO₄, and the indicator was ferrous phenanthroline. The HClO₄ in the Pu(VI) solutions was determined from the densities of the solutions using Brickwedde's data[9]; a small correction was applied for the PuO₂-(ClO₄)₂ which was present.

A stock solution of Fe(II) was prepared by dissolving a weighed amount of Mallinckrodt analytical reagent grade iron wire in enough standardized 3 M HClO₄ to make a final solution which was 0.1 M Fe(II) in 0.50 M HClO₄. This stock solution was found to contain about 2 × 10⁻³ M Cl⁻.[10] Further dilution of this solution was made to prepare the stock solutions for the rate runs. Aliquots of 100 or more ml. were titrated with standard Ce(IV) to the ferrous phenanthroline end point.

The HClO₄ solutions were prepared by diluting analytica reagent grade concentrated acid and were assayed by density determinations.[9] The concentrated acid had been freed of reducing impurities by boiling at atmospheric pressure and cooling in a stream of scrubbed argon.

Solutions of LiClO₄ and NaClO₄ were prepared by neutralizing the appropriate analytical reagent grade carbonate with HClO₄, boiling out the CO₂, and crystallizing from water, three times for the LiClO₄ and once for the NaClO₄. The salt solutions were analyzed by density determinations; the concentration vs. density functions were determined from previously analyzed solutions.[3]

The water used in the preparation of all the solutions was doubly distilled; the second distillation was from alkaline KMnO₄ in an all-Pyrex still.

The concentration units employed in this paper are moles per liter, M, at 23°. The actual volume concentrations will be slightly different at lower temperatures, for example 1% greater at 0°.

Catalytic Impurities.—The possibility that catalytic impurities were present in the various reagents was investigated. The rates of the reaction using specially purified reagents were compared with the corresponding rates using the ordinary reagent. In all cases the rate differences were within the experimental error, 3% or less. The iron was repurified by recrystallizing Fe(ClO₄)₃ from concentrated HClO₄ and reducing to Fe(II) electrolytically. The plutonium was purified by the use of a cation-exchange (Dowex 50) column; Pu(VI) was eluted using 1 M HCl, the middle fraction was converted to PuO₂(ClO₄)₂ by fuming with HClO₄. The HClO₄ was distilled at about 60° under low pressure. The salts, LiClO₄ and NaClO₄, were given an extra crystallization from water.

Apparatus.—Rate runs were made in specially shaped Pyrex absorption cells which were positioned in a small water-filled thermostat in the light beam of a Cary recording spectrophotometer, Model 14, No. 5. The cells were similar to small erlenmeyer flasks to which two 25 mm. o.d. tubes were sealed coaxially to provide a light path of about 10 cm. The ends of these tubes were left rounded since the water in the small thermo-

stat eliminated most of the focusing effect which otherwise would have been present. The contents of the cells were stirred from below by means of Teflon covered magnetic stirring bars. The spectrophotometer was operated in the infrared range with the cell compartment covers removed. The reaction was started by injecting one of the reactants into a solution of the other already in the cell. The injection was by means of a 5-ml. hypodermic syringe with a large stainless steel needle. The temperature of the mixture was determined to within 0.1° with a small thermometer about 1 min. after the mixing. With this apparatus 5 ml. from the syringe could be mixed into 60 ml. in the cell in less than 5 seconds.

In spite of the curvature of the cell windows, adherence to Beer's law was found to be satisfactory. Tests with CoSO₄ and Pr(ClO₄)₃ solutions showed that the total spread in apparent extinction coefficients up to an absorbance of 1.7 was 0.4 and 0.9%, respectively. Pr was used for this test since it has a very narrow absorption band similar to that of Pu(VI).

Procedure.—Sixty ml. of solution containing Pu(VI) and appropriate amounts of salt and acid were placed in the reaction cell and allowed to come to the desired temperature. The analyzed Fe(II) stock solution in 0.50 M acid was kept in a separate vessel at approximately the same temperature. Five ml. of this solution was injected into the stirred Pu(VI) solution at the time the spectrophotometer recorder strip chart was started. The course of the reaction was recorded as absorbance at 8300 Å. vs. time; chart speed was 8 in./min.

Calculations.—The initial reactant concentrations were determined from the concentrations of the analyzed stock solutions. The concentration of Pu(VI) vs. time was found from the absorbance at 8300 Å. where the extinction coefficient is about 550 M⁻¹ cm.⁻¹, which is much larger than that of any other species present. The amount of Pu(VI) consumed in the reaction was determined from the difference between the initial and final absorbance values. Apparent second-order rate constants were calculated from the data of the individual runs by a non-linear least-squares program for the IBM 7090 computer which minimized the sum of the squares of the differences between the observed and calculated absorbance values.[11] For comparison, thirteen of the rate runs were calculated graphically in the usual way, (log [Pu(VI)] − log [Fe(II)]) vs. time, as well as by least squares. No consistent difference in the results was found, although the mean difference was 0.9% and the maximum difference was 2.5%.

In the next section it is shown that under certain conditions the amount of Pu(VI) reduced does not correspond exactly to the amount of Fe(II) added. A correction was made for this lack of stoichiometry. For convenience it was assumed that the rates of any side reactions of Fe(II) are proportional to the rate of the main reaction. A sample calculation showed that if instead the rates of the side reactions are proportional to [Pu(V)][Fe(II)] rather than to [Pu(VI)][Fe(II)], the corrected k′ under this assumption is only 3.5% less than before for the extreme case of an 8% discrepancy in the stoichiometry.

Experimental Results

Stoichiometry.—The oxidation potentials in HClO₄ solutions[12] are such that a slight excess of Fe(II) is capable of reducing Pu(VI) all the way to Pu(III) according to the reactions

$$Pu(VI) + Fe(II) = Pu(V) + Fe(III) \quad (1)$$

$$Pu(V) + Fe(II) = Pu(IV) + Fe(III) \quad (2)$$

$$Pu(IV) + Fe(II) = Pu(III) + Fe(III) \quad (3)$$
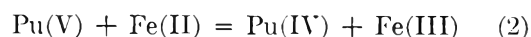
The equilibrium quotient for (1) in 1 M HClO₄ is 1 × 10³. This means that in the absence of (2) and (3) 99% of Fe(II) added to a 10% excess of Pu(VI) will be oxidized to Fe(III). Our experiments have shown that at concentrations near 10⁻⁴ M, reactions 2 and 3 are in-

(6) J. C. Sullivan, J. Am. Chem. Soc., **84**, 4256 (1962).

(7) T. W. Newton and F. B. Baker, Inorg. Chem., **1**, 368 (1962).

(8) R. E. Connick, in "The Actinide Elements;" edited by G. T. Seaborg and J. J. Katz, National Nuclear Energy Series, Division IV, Vol. 14A, McGraw-Hill Book Co., Inc., New York, N. Y., 1954, Chap. 8, p. 265.

(9) L. H. Brickwedde, J. Research Natl. Bur. Std., **42**, 309 (1949).

(10) It was later found that the amount of Cl⁻ produced could be greatly reduced if the iron were dissolved in 0.3 M HClO₄.

(11) We are indebted to R. H. Moore for writing this program. It is based on R. H. Moore and R. K. Ziegler, Los Alamos Scientific Laboratory Report, LA-2367, October 15, 1959. Available from the Office of Technical Services, U. S. Department of Commerce, Washington, D. C., $2.25.

(12) S. W. Rabideau, J. Am. Chem. Soc., **78**, 2705 (1956), for Pu potentials, and R. E. Connick and W. H. McVey, ibid., **73**, 1798 (1951), for Fe potentials

THE JOURNAL OF PHYSICAL CHEMISTRY

Please enter my subscription to
THE JOURNAL OF PHYSICAL CHEMISTRY for 1963 (12 issues).
Price for ACS members $12.00; price for nonmembers $24.00.
Postage per year: Foreign $1.20; PUAS $0.80; Canada $0.40

Please type or print

NAME_____

ADDRESS_____

CITY_____ZONE_____STATE/COUNTRY_____

SIGNED_____

☐ I AM AN ACS MEMBER.

☐ **CHECK ENCLOSED**
(payable to the American Chemical Society)

☐ **BILL ME LATER**

BUSINESS REPLY MAIL

No Postage Stamp Necessary if Mailed in The United States

POSTAGE WILL BE PAID BY —

AMERICAN CHEMICAL SOCIETY

1155 Sixteenth Street, N.W.

Washington 6, D. C.

ATTN. R. H. BELKNAP

deed relatively unimportant. The ratio [Pu(VI) reduced]/[Fe(II) oxidized] was determined and found to be only slightly less than unity as long as Pu(VI) was in excess; see Table I. The data show that the stoichiometry is influenced by the $HClO_4$ concentration; this means that the hydrogen ion dependences of the other reactions are not the same as for reaction 1.

TABLE I
EFFECT OF $HClO_4$ CONCENTRATION ON
THE STOICHIOMETRY AT 0.2°

Initial concentrations: $8 \times 10^{-5} M$ Pu(VI), $5 \times 10^{-5} M$ Fe(II),
and $\mu = 2.0$ (LiClO$_4$)

$(HClO_4)$, M	2.0	1.5	1.0	0.5	0.25	0.05
$\dfrac{\text{Pu(VI) reduced}}{\text{Fe(II) oxidized}}$	0.92	0.95	0.97	0.98	0.99	1.01

Preliminary experiments at 0° in 1 M $HClO_4$ indicate that reaction 2 is about 0.04 as fast as (1) under similar conditions. The value found for the apparent second-order rate constant was about 16 M^{-1} sec.$^{-1}$. This result is in reasonable agreement with the excess oxidation of Fe(II) shown in Table I. At higher reactant concentrations the situation is more complicated in that the rate constants for (1) and (2) are not sufficient to explain the results. Thus, Pu(VI) was injected into a vigorously stirred solution of Fe(II) at 0° such that the concentrations in the mixture were $1.94 \times 10^{-3} M$ and $7.52 \times 10^{-3} M$, respectively, in 1 M $HClO_4$. The spectrum was determined as a function of time and extrapolated to the time of mixing. At this time the concentration of Pu(IV) was estimated to be $1.4 \times 10^{-3} M$ and that of Pu(III) to be zero. According to the rate constant given above for reaction 2, only $0.54 \times 10^{-3} M$ Pu(IV) should have formed during the two-second time of mixing. This suggests that a reaction such as

$$Pu(VI) + 2Fe(II) = Pu(IV) + 2Fe(III) \quad (4)$$

has a rate which depends on the square (or higher) power of the Fe(II) concentration and thus is important at higher concentrations.

Pu(VI) and Fe(II) Dependences.—In the study of the kinetics of reaction 1 the concentration of Fe(II) was kept below $10^{-4} M$ and all of the rate runs were consistent with the assumption that the reaction is first power in each of the reactants, [Pu(VI)] and [Fe(II)], that is $-d[Pu(VI)]/dt = k'[Pu(VI)][Fe(II)]$. The least squares calculations described above give absorbance values in agreement with the experimental ones and the deviations show no systematic trends. A typical example is given in Table II. Additional evi-

TABLE II
TYPICAL RATE RUN

Initial concentrations: $4.47 \times 10^{-5} M$ Pu(VI), $3.82 \times 10^{-5} M$ Fe(II), 0.42 M $HClO_4$, and 1.58 M NaClO$_4$; 9.8°

Time, sec.	Absorbance (obsd.)	Absorbance (calcd.)	Time, sec.	Absorbance (obsd.)	Absorbance (calcd.)
0.0	0.249	...	22.5	0.136	0.135
5.0	.211	0.211	25.0	.129	.129
7.5	.195	.195	27.5	.122	.124
10.0	.180	.181	30.0	.118	.119
12.5	.170	.169	32.5	.113	.114
15.0	.160	.159	35.0	.110	.110
17.5	.150	.150	37.5	.107	.106
20.0	.143	.142	40.0	.103	.103
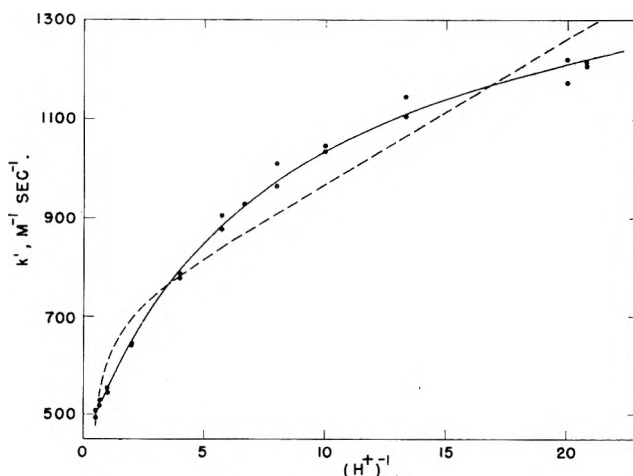
Fig. 1.—Apparent second-order rate constant, k', vs. $[H^+]^{-1}$: solid line, eq. 5; dashed line, eq. 6.

dence is provided by the results of a series of runs in which the initial concentrations of Pu(VI) and Fe(II) were varied by factors of 2 and 4, respectively. These data are shown in Table III.

TABLE III
APPARENT SECOND-ORDER RATE CONSTANT, k', AT DIFFERENT
INITIAL CONCENTRATIONS OF Pu(VI) AND Fe(II)
Conditions: 0.2° and 0.42 M $HClO_4$

Initial [Pu(VI)], $M \times 10^5$	Initial [Fe(II)], $M \times 10^5$	k', M^{-1} sec.$^{-1}$	Initial [Pu(VI)], $M \times 10^5$	Initial [Fe(II)], $M \times 10^5$	k', M^{-1} sec.$^{-1}$
15.7	7.25	270, 271	7.85	7.44	272
15.7	5.37	271	7.85	5.65	276
15.7	3.56	273, 268	7.85	3.77	266
15.7	1.75	281	7.85	1.85	274

The equilibrium quotient for (1) is such that large [Fe(III)]/[Fe(II)] ratios will make the back reaction important. An experiment in which the [Fe(III)]$_0$ was $5 \times 10^{-3} M$ and [Fe(II)]$_0$ was $5 \times 10^{-5} M$ indeed showed the presence of the back reaction, but gave no evidence for a Fe(III) effect on the forward rate.

Hydrogen Ion Dependence.—Series of rate determinations were made in which the hydrogen ion concentration was varied from 0.050 to 2.00 M at constant ionic strength and constant temperature. The hydrogen ion dependence was found to be quite complicated; the simplest function capable of reproducing the data satisfactorily contains three adjustable parameters. The function is

$$k' = A + \frac{1}{B + C(H^+)} \quad (5)$$

Figure 1 is a plot of k' vs. $(H^+)^{-1}$ in LiClO$_4$ solutions of ionic strength 2.0 at 0.1°, the solid line is calculated using (5) and the parameters listed in Table IV. These were calculated from the experimental data using a non-linear least-squares program[13] in which the sum of the squares of the per cent deviations between the observed and calculated k' values is minimized. The quality of the fit of the function is given by 100 $[(1/n)$ $\Sigma (k'_{obs} - k'_{calc})^2/(k'_{obs})^2]^{1/2}$ which may be called the root mean square per cent deviation (r.m.s. % dev.). For these data the value of this quantity is 1.57%. The fit of the data to the function can also be described by

(13) We thank R. K. Ziegler and the Statistical Section of this Laboratory for providing this program.

TABLE IVA

Apparent Second-Order Rate Constants at Various Temperatures and Hydrogen Ion Concentrations; $\mu = 2.00$

LiClO₄ solutions

HClO₄, M (0.1°)	k', M⁻¹ sec⁻¹ (0.1°)	HClO₄, M (9.8°)	k', M⁻¹ sec⁻¹ (9.8°)	HClO₄, M (25.0°)	k', M⁻¹ sec⁻¹ (25.0°)
0.048	1208	0.050	2141	0.294	2658, 2609
	1215		2039		2707, 2716
	1212		2021		2612, 2820
			2048		
.050	1175	.075	1882	.343	2476
	1221		1926	.537	1999, 2071
.075	1147	.100	1769		2096, 2166
	1108		1697		2148, 2044
.100	1048	.125	1637		2012, 2031
	1035		1728	1.025	1618, 1610
.125	1012	.150	1584		1689, 1623
	970		1589		1738, 1660
.150	932		1543		1610
	930	.175	1478	1.512	1450, 1480
.175	906		1574		1480, 1379
	877	.250	1347		1427, 1521
.250	787		1348		1469, 1550
	779	.500	1079	1.903	1372
.500	642		1078	2.000	1314, 1362
	645	1.00	881		1357, 1295
1.00	555	2.00	737		1376, 1301
	545		784		
1.50	529				
	517				
2.00	494				
	508				
	508				

NaClO₄ solutions

HClO₄, M (0.1°)	k', M⁻¹ sec⁻¹ (0.1°)	HClO₄, M (9.8°)	k', M⁻¹ sec⁻¹ (9.8°)	HClO₄, M (25.0°)	k', M⁻¹ sec⁻¹ (25.0°)
0.043	1051	0.050	1670	0.294	2409
	1048		1685		2566
			1681		2345
.050	1012		1667		2313
	1003				2448
.172	804	.172	1367		
	794		1365	0.537	2008
.375	653	.375	1079		2109
	633		1109		2093
.420	658	.419	1080		2038
	641		1073		2004
	667	.700	938	1.025	1589
.700	561		931		1599
	557	.975	834		1685
.975	565		851		1633
.982	534	1.025	866		1572
1.025	529		843		1555
	534	1.35	807	2.00	1314
1.35	503		802		1362
	515	1.70	766		1357
1.70	516		763		1376
	515	1.90	738		
1.91	490		789		
	538	2.00	729		
2.00	509		753		
	515				

TABLE IVB

Summary of Experimental Results

$$k' = A + [B + C\,(H^+)]^{-1} \text{ or } k' = D + E\,(H^+)^{-1} + F\,(H^+)$$

	LiClO₄ soln., μ = 2 (0.1°)	LiClO₄ soln., μ = 2 (9.8°)	LiClO₄ soln., μ = 2 (25.0°)	NaClO₄ soln., μ = 2 (0.1°)	NaClO₄ soln., μ = 2 (9.8°)	NaClO₄ soln., μ = 2 (25.0°)	0.1 M Cl⁻ in NaClO₄ soln., μ = 2 (0.1°)	0.1 M Cl⁻ in NaClO₄ soln., μ = 2 (9.8°)
1. No. of runs, n	26	22	37	25	24	26	23	23
2. A, M⁻¹ sec⁻¹	437 ± 5[a]	627 ± 17	1002 ± 42	455 ± 8	612 ± 10	950 ± 68	699 ± 10	1051 ± 30
3. B × 10⁴, M sec	9.17 ± 0.2	5.31 ± 0.14	2.09 ± 0.37	12.62 ± 0.55	7.69 ± 0.13	3.59 ± 0.37	8.36 ± 2.01	6.23 ± 0.99
4. C × 10³, sec	7.53 ± 0.32	3.43 ± 0.22	1.33 ± 0.15	10.08 ± 0.94	3.37 ± 0.18	1.09 ± 0.19	24.84 ± 4.46	8.32 ± 1.95
5. r.m.s. % dev.[b]	1.57	2.20	2.95	2.58	1.57	2.85	2.94	4.75
6. D, M⁻¹ sec⁻¹	695 ± 28	1202 ± 49	1425 ± 59	606 ± 17	1031 ± 31	1537 ± 80		
7. E, sec⁻¹	28.6 ± 2.5	49.2 ± 4.7	382 ± 21	20.6 ± 1.6	34.4 ± 3.0	282 ± 27		
8. -F, M⁻² sec⁻¹	116 ± 18	249 ± 33	141 ± 29	62.8 ± 12.3	167 ± 20	171 ± 41		
9. r.m.s. % dev.[b]	6.50	6.30	2.82	5.04	5.17	3.36		

[a] The uncertainties listed are the standard deviations computed by the least-squares program. [b] Root mean square deviation = $100[(1/n)\Sigma(k'_{obs} - k'_{calc})^2/(k'_{obs})^2]^{1/2}$.

stating: 1.3% mean deviation and 5.9% maximum deviation.

An alternative three-parameter function was tried, it is

$$k' = D + E/(H^+) + F(H^+) \qquad (6)$$

The best values for the parameters in this equation were found as before and the resulting function is shown in Fig. 1 as the dashed line. Using (6) and the values of the parameters listed in Table IVB, the experimental data are reproduced with an r.m.s. % dev. of 6.50.

Temperature Dependence.—The effect of hydrogen ion concentration on the rate was determined also at 9.8 and 25.0° in NaClO₄ solutions as well as in LiClO₄ solutions. The results of these determinations are listed in Table IVA. The sets of data were fitted to eq. 5 and to eq. 6. The results of these calculations are summarized in Table IVB.

The relative quality of the fit provided by the two functions is seen by comparing row 5 and row 9 (Table IVB) which give the r.m.s. % deviations for the two functions. Except for the sets at 25°, eq. 5 gives a much better fit of the data. At this temperature the rates are quite high; so acid concentrations below 0.29 M could not be used. The limited range of acid concentration accounts for the fact that the two functions are equally satisfactory for the 25° data. This result demonstrates the necessity for varying concentrations as widely as possible in order to distinguish between alternative functions.

Chloride Ion Dependence.—A short series of experiments was made in order to determine the magnitude of the effect of chloride on the reaction rate. As before, the rate was first power in each of the reactants and the hydrogen ion dependence was given by eq.

TABLE V

EFFECT OF IONIC STRENGTH ON THE APPARENT SECOND-ORDER RATE CONSTANT IN 0.05 M HClO$_4$ AT 0.1°

(Units are M^{-1} sec.$^{-1}$)

μ, M	0.05	0.25	0.65	1.20	2.0
k' (in NaClO$_4$)	159, 165	307	513, 525	696	1011, 987, 997
k' (in LiClO$_4$)	160, 159, 161	332	549, 552, 562	778	1228, 1199, 1220

5. The values determined for the parameters A, B, and C are given in the last two columns of Table IV.

Ionic Strength Dependence.—The effect of ionic strength on the apparent second-order rate constant was determined in 0.05 M HClO$_4$ solutions at 0.1°. Both LiClO$_4$ and NaClO$_4$ were used to vary the ionic strength between 0.05 and 2.0 M. The results of these experiments are summarized in Table V. The observed ionic strength dependence can be approximated by a Debye–Hückel expression for which the product of the charges on the reactant ions is +4 and the "mean distance of closest approach" is 6.5 Å. in NaClO$_4$ solutions and 6.0 Å. in the LiClO$_4$ solutions. For the NaClO$_4$ data the root mean square % deviation is 8 and for the LiClO$_4$ data it is 10. These deviations are outside the experimental error, but considering the complexity of the mechanism and the ionic strength range covered, approximate agreement is all that can be expected.

Interpretation and Discussion

Possible Medium Effects.—The study of the hydrogen ion dependence of a reaction necessarily involves a change in concentration of hydrogen ion and it is usually replaced by lithium or sodium ions in order to maintain constant ionic strength. Since such a replacement changes the medium, possible changes in the pertinent activity coefficients at constant ionic strength must be considered. According to the Brönsted principle of specific interaction of ions[14] the activity coefficients of the reactant ions, if positively charged, will not be influenced by the concentrations of other positive ions at constant ionic strength. The success of this principle suggests that, at most, such medium effects will be small. This is borne out by the work of Zielen and Sullivan,[15] who studied the effect of substituting Li$^+$ or Na$^+$ for H$^+$ on the formal potentials of some oxidation couples. Essentially no effect was found on the Fe^{+2}–Fe^{+3} couple, a small effect was found on the Hg^0–Hg$_2^{+2}$ couple, and a linear change in potential was found for the Hg$_2^{+2}$–Hg^{+2} and NpO$_2^+$–NpO$_2^{+2}$ couples. It is interesting that for the last couple the effect was about 1/3 as large when Li$^+$ was substituted for H$^+$ as when Na$^+$ was used.

In oxidation–reduction kinetics it has been found that substituting Li$^+$ for Na$^+$ at constant ionic strength has a very small effect on the Pu(IV)–U(IV) reaction[16] and changes the rate by about 8% in the Pu(VI)–V(III) reaction,[4c] by about 16% in the Pu(IV)–Fe(II) reaction,[2] and by about 20% in the Pu(VI)–Fe(II) (present study) and Pu(VI)–U(IV)[3] reactions.

In spite of these variations in the pertinent activity coefficient quotients it is important to note that, with only one or two exceptions, all oxidation–reduction

reactions show an empirical hydrogen ion dependence of the form $k' = k_i(\mathrm{H}^+)^i + k_{i+1}(\mathrm{H}^+)^{i+1} + \ldots$ where k' is the apparent second-order rate constant and i is an integer. Very often only one term in the series appears and only very rarely are more than two terms significant. In the cases of only one term, either the medium effect is very small or there is a fortuitous cancellation of medium effects with those due to an actual path. In the other cases it is necessary that the medium effect on an individual rate constant be given by

$$k_i = k_i^0(1 + a_i[\mathrm{H}^+]) \qquad (7)$$

This expression is the one to be expected if the activity coefficients of all the species involved in the net activation process obey Harned's rule.[17] From this rule we expect $\ln k_i = \ln k_i^0 + a_i[\mathrm{H}^+]$, which for reasonably small values of a_i reduces to (7).

From this discussion we conclude that it is safe to assume that for a reaction among positive ions, the effect of substituting H$^+$ for Na$^+$ or for Li$^+$ at constant ionic strength is given by (7). It also seems reasonable that a_i is probably less than 0.1, at least for Li$^+$.

Mechanism.—The increase in rate with decrease in hydrogen ion concentration suggests that hydrolyzed species such as FeOH$^+$ or PuO$_2$OH$^+$ may be the reactive ions. The extent of hydrolysis in the experimental solutions is small enough, however, so that the stoichiometric concentrations of Pu(VI) and Fe(II) are essentially identical with the concentrations of the unhydrolyzed ions, PuO$_2^{+2}$ and Fe^{+2}.[18] Since the form of a rate law gives the formulas of the activated complexes involved in the reaction, but tells nothing about the actual species which react, we have chosen to formulate mechanisms in terms of net reactions of principal species, one for each distinguishable activated complex. If rapid equilibria are established either before or after the actual rate-determining steps they are included in these net reactions. This procedure avoids the writing of kinetically indistinguishable steps, but requires that the rate of each net reaction be explicitly stated. Such a mechanism is

$$\mathrm{PuO_2^{+2}} + \mathrm{Fe^{+2}} = \mathrm{PuO_2^+} + \mathrm{Fe^{+3}},$$

$$\text{rate} = k_0[\mathrm{PuO_2^{+2}}][\mathrm{Fe^{+2}}] \qquad (8)$$

$$\mathrm{PuO_2^{+2}} + \mathrm{Fe^{+2}} = \mathrm{PuO_2^+} + \mathrm{Fe^{+3}},$$

$$\text{rate} = k_1[\mathrm{PuO_2^{+2}}][\mathrm{Fe^{+2}}]/[\mathrm{H}^+] \qquad (9)$$
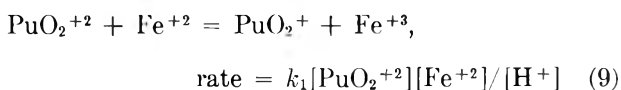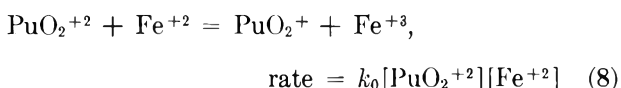
The net reaction in (9) is the same as that in (8) because equilibria which occur before and after the actual rate-determining step effectively cancel. According to this mechanism the apparent second-order rate constant, k', is given by $k' = k_0 + k_1/[\mathrm{H}^+]$. Allowing for pos-

(14) (a) J. N. Brönsted, *J. Am. Chem. Soc.*, **44**, 877 (1922), or (b) R. A. Robinson and R. H. Stokes, "Electrolyte Solutions," Butterworths Scientific Publications, London, 1955, p. 425.

(15) A. J. Zielen and J. C. Sullivan, *J. Phys. Chem.*, **66**, 1065 (1962).

(16) T. W. Newton, *ibid.*, **63**, 1493 (1959).

(17) See, for example, ref. 14b, Chapter 15.

(18) J. Bjerrum, G. Schwarzenbach, and L. G. Sillén, "Stability Constants. Part II: Inorganic Ligands," Special Publication No. 7, The Chemical Society, London, 1958.

sible effects of the medium change as discussed in the previous section gives

$$k' = k_0^0(1 + a_0[H^+]) + k_1^0(1 + a_1[H^+])/[H^+] =$$
$$(k_0^0 + k_1^0 a_1) + k_1^0/[H^+] + k_0^0 a_0[H^+] \quad (10)$$

This equation has the same form as the alternative rate law (6), and if it may be assumed that $a_0 = a_1$ the experimental values of the parameters D, E, and F lead to $k_0^0 = 700\ M^{-1}$ sec.$^{-1}$, $k_1^0 = 28.6$ sec.$^{-1}$, and $a_0 = a_1 = 0.166$, for LiClO$_4$ solutions at $0.1°$. Although this value for a_0 and a_1 is not unreasonable, we believe that the mechanism given by eq. 8, 9, and 10 is unsatisfactory because, as shown in Fig. 1, the associated rate law, (6), fits the experimental data quite poorly. This lack of fit cannot be attributed to a medium effect without the assumption of a severely non-linear one. Another argument for rejecting this rate law is that the temperature dependences of the parameters D, E, and F appear unreasonable. Plots of their logarithms vs. $1/T$ are quite non-linear.

Since rate law (5) does fit the data satisfactorily, a plausible mechanism consistent with it was sought. The form of the rate law suggests the operation of an inhibiting back reaction similar to that which was found in the Pu(VI)–U(IV) reaction.[3] A mechanism in terms of net reactions, as discussed above, which leads to a rate law in agreement with the experimental observations is

$$PuO_2^{+2} + Fe^{+2} = PuO_2^+ + Fe^{+3}$$
$$\text{rate} = k_0[PuO_2^{+2}][Fe^{+2}] \quad (8)$$

$$PuO_2^{+2} + Fe^{+2} \rightleftarrows PuO_2 \cdot Fe^{+4}$$
$$\text{rate} = k_2[PuO_2^{+2}][Fe^{+2}] - k_3[PuO_2 \cdot Fe^{+4}] \quad (11)$$

$$PuO_2 \cdot Fe^{+4} = PuO_2^+ + Fe^{+3}$$
$$\text{rate} = k_4[PuO_2 \cdot Fe^{+4}] \quad (12)$$

$$PuO_2 \cdot Fe^{+4} = PuO_2^+ + Fe^{+3}$$
$$\text{rate} = k_5[PuO_2 \cdot Fe^{+4}]/[H^+] \quad (13)$$
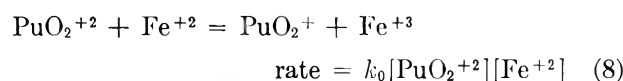
The usual steady-state approximation for the concentration of the intermediate leads to

$$k' = \frac{-d(PuO_2^{+2})/dt}{(PuO_2^{+2})(Fe^{+2})} = k_0 + \frac{k_2k_4 + k_2k_5(H^+)^{-1}}{k_3 + k_4 + k_5(H^+)^{-1}}$$

This expression can be rearranged to give

$$k' = \left[\frac{k_0k_3 + (k_0 + k_2)k_4}{k_3 + k_4}\right] +$$
$$\frac{1}{\left[\frac{k_3 + k_4}{k_2k_3}\right] + \left[\frac{(k_3 + k_4)^2}{k_2k_3k_5}\right](H^+)} \quad (14)$$

which, as long as k_0 and k_4 are not both zero, has the same form as the empirical rate law, eq. 5. If it is assumed that the medium effects on these rate constants are given by (7), the resulting rate law is complicated by the presence of the a_i terms; however, the form of the rate law is unaltered providing certain reasonable conditions are met.

The activated complexes indicated by reactions 8, 11, and 12 all have the same formula: $(PuO_2 \cdot Fe^{+4})^*$. They differ 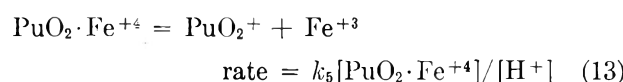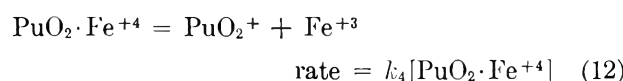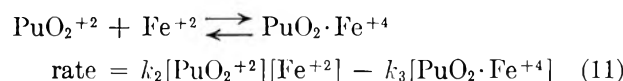from each other in the substances from which they are formed (reactants or intermediate) and the substances to which they go (products or intermediate). Since the form of (14) is unchanged if either k_0 or k_4 is zero, the experimental rate law requires an activated complex of the above formula which decomposes to Fe^{+3} and PuO_2^+, but gives no information as to whether it is formed from PuO_2^{+2} and Fe^{+2} by reaction 8, or whether it is formed from the intermediate by reaction 12, or both. For comparison with other reactions, it is convenient to consider the net processes for the formation of these activated complexes from the original reactants whether they are actually formed in this way or not. Table VI shows the apparent rate constants associated with each of these net activation processes in terms of the experimental parameters under each of the two limiting assumptions: $k_0 = 0$ and $k_4 = 0$. It is seen that the values of the apparent rate constants, and also the thermodynamic quantities of activation, depend on which substances are assumed to form the activated complex.

TABLE VI
EVALUATION OF THE EFFECTIVE RATE CONSTANTS FROM THE EXPERIMENTAL PARAMETERS

Net activation process[a]	Assumption $k_4 = 0$	$k_0 = 0$
(a) $PuO_2^{+2} + Fe^{+2} = [PuO_2Fe^{+4}]_a^*$	$k_0 = A$	$k_2k_4/k_3 = A(1 + AB)$
(b) $PuO_2^{+2} + Fe^{+2} = [PuO_2Fe^{+4}]_b^*$	$k_2 = 1/B$	$k_2 = (1 + AB)/B$
(c) $PuO_2^{+2} + Fe^{+2} + H_2O = (PuO_2-FeOH^{+3}]_c^* + H^+$	$k_2k_5/k_3 = 1/C$	$k_2k_5/k_3 = (1 + AB)^2/C$

[a] Activated complexes (a) and (b) have the same formula but differ in that the former decomposes to the final products, PuO_2^+ and Fe^{+3}, while the latter goes to the intermediate, $PuO_2 \cdot Fe^{+4}$.

This situation differs in an important way from the common one in which the rate law is not affected even though an activated complex with a particular formula can be formed by more than one path from different intermediate species which are in equilibrium with the principal reactants. In such a case, the ΔF^* for the formation of the activated complex from the principal reactants does not depend on which species are assumed actually to form the activated complex.

The postulation of the intermediate, $PuO_2 \cdot Fe^{+4}$, seems quite reasonable to us in view of the evidence recently presented for the similar ions $NpO_2 \cdot Cr^{+4}$[6] and $UO_2 \cdot Cr^{+4}$.[7] Also, reaction 4 can readily be explained as the reaction between $PuO_2 \cdot Fe^{+4}$ and excess Fe(II).

Thermodynamic Quantities of Activation.—The thermodynamic quantities of activation have been calculated under the assumption of the mechanism 8, 11, 12, and 13. The medium effects, which are probably small, have been neglected, as has been done in all previous calculations of the activation parameters for other reactions. The mechanism indicates that the reaction involves at least three different activated complexes which are produced in as many different net activation processes. The values calculated for ΔH^* and ΔS^* for these processes will depend on the relative importance of the k_0 and k_4 paths in the mechanism. Therefore, calculations were made for both the LiClO$_4$ and NaClO$_4$ solutions under the two limiting assumptions, $k_4 = 0$ and $k_0 = 0$.

TABLE VII

THERMODYNAMIC QUANTITIES OF ACTIVATION

Solution	Net act. process[a]	Assumption $k_4 = 0$		Assumption $k_0 = 0$		Average	
		ΔS^*	ΔH^*	ΔS^*	ΔH^*	ΔS^*	ΔH^*
	(a)	−28.34 (0.63)[b]	4.91 (0.18)	−31.60 (0.71)	3.83 (0.20)	−29.97 (1.63)[c]	4.37 (0.54)
LiClO₄	(b)	−10.48 (1.64)	9.31 (0.46)	−14.73 (1.12)	7.95 (0.31)	−12.60 (2.12)	8.63 (0.68)
	(c)	−11.29 (1.69)	10.17 (0.48)	−15.49 (1.82)	8.66 (0.52)	−13.39 (2.10)	9.42 (0.76)
		(2.52)[d]		(2.45)		...	
	(a)	−28.63 (0.88)	4.81 (0.25)	−32.61 (1.02)	3.47 (0.29)	−30.62 (1.99)	4.14 (0.67)
NaClO₄	(b)	−14.41 (2.05)	8.41 (0.57)	−17.91 (1.26)	7.20 (0.35)	−16.16 (1.75)	7.81 (0.60)
	(c)	−5.60 (2.81)	11.72 (0.80)	−10.71 (2.74)	9.94 (0.73)	−8.16 (2.56)	10.83 (0.89)
		(2.72)		(2.60)		...	

[a] The net activation processes and the effective rate constants are listed in Table VI. [b] In the first four columns the quantities in parentheses are the standard deviations. [c] In the last two columns they are the deviations from the mean. [d] These quantities are the r.m.s. % deviations.

Since the rate constants A, $1/B$, $1/C$, etc., cannot be determined independently, their individual temperature coefficients were not used in the calculation of the thermodynamic quantities of activation. Rather, the ΔS^* and ΔH^* values for the three net activation processes were determined simultaneously from the experimental k' values at all three temperatures and all of the hydrogen ion concentrations. The expression, $k_i = (k_B/h)T \exp(\Delta S_i^*/R) \exp(\Delta H_i^*/RT)$, from Eyring's absolute reaction rate theory, was substituted into eq. 14 for k_0, k_2, and $k_2 k_5/k_3$ for the assumption $k_4 = 0$, and for k_2 and $k_2 k_4/k_3$ for the assumption $k_0 = 0$. The data were fit to the resulting function of $[H^+]$ and T using a non-linear least-squares program which minimizes the square of the per cent deviations of the calculated k' values from the observed ones.[11] An important advantage of this procedure, based on all the data simultaneously, is that it provides objective estimates of the precision of the activation parameters, ΔS_i^* and ΔH_i^*. The results of these calculations are summarized in Table VII.

Significantly different values for ΔS^* and ΔH^* were obtained under the two limiting assumptions; however, the actual values probably lie within the ranges. The effect of substituting NaClO₄ for LiClO₄ is seen to be primarily on the ΔS^* values for activation processes (b) and (c).

The ΔH^* for activation process (a) is quite low, very close to that reported[4a] for the analogous reaction between PuO_2^{+2} and Pu^{+3}. The other heats are in the range found for simple electron exchange reactions such as $Pu^{+3}-Pu^{+4}$,[19] $Fe^{+2}-Fe^{+3}$,[20] or $Fe(CN)_6^{-4}-Fe(CN)_6^{-3}$.[21]

The ΔS^* values have been used to estimate the formal ionic entropy of the three activated complexes; these are given in Table VIII. Activated complex (b) is normal in that its entropy is in the range of values found for other complexes with a charge of +4. The entropies for activated complex (c) are somewhat more negative than the values for other +3 activated complexes.[22]

(19) T. K. Keenan, *J. Phys. Chem.*, **61**, 1117 (1957).

(20) J. Silverman and R. W. Dodson, *ibid.*, **56**, 846 (1952).

(21) A. C. Wahl and C. F. Deck, quoted by F. Basolo and R. B. Pearson, "Mechanisms of Inorganic Reactions," John Wiley and Sons, Inc., New York, N. Y., 1958, p. 318.

TABLE VIII

FORMAL IONIC ENTROPIES OF THE ACTIVATED COMPLEXES

Activated complex	$S^*_{comp.}$, e.u. In LiClO₄	In NaClO₄
[PuO₂Fe⁺⁴]ₐ*	−84 ± 2	−85 ± 2
[PuO₂Fe⁺⁴]ᵦ*	−67 ± 2	−70 ± 2
[PuO₂FeOH⁺³]ᵪ*	−50 ± 2	−45 ± 3

For the hypothetical process of changing activated complex (b) into activated complex (a) in NaClO₄, we calculate $\Delta H^* = -3.7 \pm 0.5$ kcal./mole and $\Delta S^* = -14.5 \pm 1$ e.u. In LiClO₄ the corresponding values are -4 kcal./mole and -17.4 e.u. It is interesting to compare these values with those for the conversion of an inner-sphere to an outer-sphere complex. For the process

$$Co(NH_3)_5SO_4^+ + H_2O = Co(NH_3)_5H_2O \cdot SO_4^+ \quad (15)$$
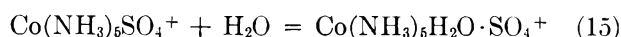
Posey and Taube[23] report $\Delta H = -3.95$ kcal./mole and $\Delta S = -13$ e.u. in 1 M NaClO₄. The similarity between the heat and entropy changes for these two processes strongly suggests that activated complex (a) is outer-sphere, such as $[OPuO \cdot H_2O \cdot Fe^{+4}]^*$, and (b) is inner sphere, perhaps $[OPuOFe^{+4}]^*$.

Chloride Ion Dependence.—The effect of chloride ion on the rate appears to be quite complicated: Table IV shows that a concentration of 0.1 M increases the parameter A, decreases B, and increases C. An approximate explanation of this can be given in terms of reactions 4–8 by assuming that k_0 and k_4 are unaffected by Cl^-, k_1 and k_2 are each increased by about 50% in 0.1 M Cl^-, and that k_3 is zero in the absence of Cl^- but becomes equal to about 1/3 of k_2 in 0.1 M solutions. If, for the chloride solutions, B is taken as its best value plus one standard deviation and C as its best value minus one standard deviation, values of A are calculated which are 23 and 6% high at 0.1 and 9.8°, respectively. The size of these deviations makes it appear likely that an additional reaction path operates in chloride solutions, the rate of which has a hydrogen ion dependence other than 0 or −1.

(22) T. W. Newton and S. W. Rabideau, *J. Phys. Chem.*, **63**, 365 (1959).

(23) F. A. Posey and H. Taube, *J. Am. Chem. Soc.*, **78**, 15 (1956).

DISTRIBUTION EXPERIMENTS IN FUSED SALTS. II. THE DISTRIBUTION OF PbCl₂ BETWEEN KNO₃ AND AgCl, AND PbBr₂ BETWEEN KNO₃ AND AgBr

By John H. Kennedy

University of California, Santa Barbara, Calif.

The distribution of lead chloride in the system KNO₃–AgCl at 480° was found to depend on three equilibria: the distribution constant of PbCl₂ molecules between the two phases and the two dissociation constants of PbCl₂ in KNO₃. The constants for the quadratic equation were determined by the method of least squares from a series of experiments in which potassium chloride was added, and the distribution of lead chloride between AgCl and KNO₃ was measured as a function of the chloride concentration in the KNO₃ phase. The constants were: $K = [PbCl_2]_{KNO_3}/[PbCl_2]_{AgCl} = 0.72$; $k_1 = [PbCl^+][Cl^-]/[PbCl_2] = 0.39$ mole/kg.; $k_2 = [Pb^{++}] \cdot [Cl^-]^2/[PbCl_2] = 0.02$ (mole/kg.)². The distribution of lead bromide between AgBr and KNO₃ at 450° was also studied, and the constants were $K = 0.55$, $k_1 = 0.15$ mole/kg., and $k_2 = 0.02$ (mole/kg.)².

In recent years nearly every technique used to study aqueous solutions has been applied to the study of fused salt solutions. One such technique is solvent extraction using a fused salt as one or both of the liquid phases. Isaac, Fields, and Gruen have studied the distribution of solutes between fused nitrates and tributyl phosphate,[1] while our studies have concentrated on using two immiscible fused salts.[2] Belyaev[3] listed some two phase fused salt systems, and during the present investigation others were found (AgCl/KBF₄–NaBF₄ and PbCl₂/KBF₄–NaBF₄). AgCl/KNO₃, AgBr/KNO₃, AgCl/K₂S₂O₇, AgCl/KHSO₄, AgCl/KBF₄–NaBF₄, and PbCl₂/KBF₄–NaBF₄ were well defined two phase systems with low mutual solubilities (*ca.* 1% by weight), and the distribution of various solutes between the two phases is being studied.

Experimental

A diagram of the apparatus used for the distribution experiments was published previously.[2] Fifty grams of each of the two fused salt solvents were melted, and the temperature was controlled with a Wheelco electronic temperature controller (±3°). A quantity of potassium halide and 200 mg. of lead halide were added and the mixture was stirred for ten minutes. The two phases were allowed to separate. The plug of frozen salt in the capillary outlet was then melted by turning on the auxiliary heater, and the molten mixture flowed out the capillary tube into the sample collector. Several portions of each phase were collected and analyzed.

Lead was determined polarographically in 1 *F* citric acid (pH 3.0) as supporting electrolyte. The silver chloride phases were dissolved in ammonium hydroxide while the silver bromide phases were dissolved in potassium cyanide. After addition of citric acid, the silver halides were precipitated by further acidification leaving lead in solution as the citrate complex.

The concentration of halide in the potassium nitrate phase was determined by dissolving the sample in water, adding 1 *F* silver nitrate until precipitation ceased, filtering, drying, and weighing. This method gave the total concentration of halide. The concentrations of AgX and 2(AgX₂⁻) were subtracted from this value to obtain the concentration of simple halide ion in the molten potassium nitrate.

The solubility of silver halide in molten potassium nitrate was found by drawing samples from the top to avoid collecting droplets of the silver halide phase when the mixture flowed out the capillary outlet and weighing the amount of silver halide present in the drawn-off sample.

Results

Lead Chloride.—During the study of the distribution of thallium chloride between silver chloride and potassium nitrate it was shown that the observed distribution coefficient depended on two equilibria[2]

$$K_0 = K + K/k[Cl^-]_{KNO_3}$$

where K was the true distribution constant and k was the association constant for TiCl in KNO₃. Thus, by plotting K_0 *vs.* $[Cl^-]^{-1}_{KNO_3}$, one could determine K from the intercept and K/k from the slope.

In the present study, it was found that the distribution of lead chloride between AgCl and KNO₃ at 480° was also affected by the addition of KCl. The results are given in Table I, and Fig. 1 shows a plot analogous to the thallium chloride case. At high chloride concentrations the distribution approximated a straight line indicating that the predominant species are

$$PbCl_2 \xrightarrow{k_1} PbCl^+ + Cl^-$$

$$k_1 = [PbCl^+][Cl^-]/[PbCl_2]$$
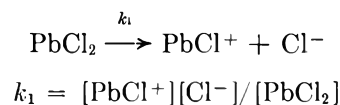
However, at low chloride concentrations, the fraction of lead found in the potassium nitrate phase deviated from the straight line indicating the existence of another lead species, Pb^{++}

$$PbCl_2 \xrightarrow{k_2} Pb^{++} + 2Cl^-$$
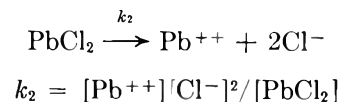
$$k_2 = [Pb^{++}][Cl^-]^2/[PbCl_2]$$

The observed distribution coefficient was

$$K_0 = (PbCl_2 + PbCl^+ + Pb^{++})_{KNO_2}/(PbCl_2)_{AgCl}$$

$$K_0 = K + k_1K[Cl^-]^{-1} + k_2K[Cl^-]^{-2}$$

where K is the distribution constant

$$K = [PbCl_2]_{KNO_3}/[PbCl_2]_{AgCl}$$

The chloride ion concentration was determined from the total chloride found in the potassium nitrate phase and subtracting the concentrations of AgCl and twice AgCl₂⁻ which were present in molten potassium nitrate. These values were calculated from published

(1) N. M. Isaac, P. R. Fields, and D. M. Gruen, *J. Inorg. Nucl. Chem.*, **21**, 152 (1961).

(2) J. H. Kennedy, *J. Phys. Chem.*, **65**, 1030 (1961).

(3) I. N. Belyaev, *Uspekhi Khimii*, **29**, 899 (1960).

TABLE I

DISTRIBUTION OF LEAD CHLORIDE

50 g. KNO₃, 50 g. AgCl, 200 mg. PbCl₂, 480°

Lead concn., mg. PbCl₂/g. soln.				KCl added,	Total Cl,	[Cl⁻].	
KNO₃	AgCl	Total, mg. PbCl₂	K_0	g.	molal	molal	$[Cl^-]^{-1}$
2.22	1.67	206	1.3	6.0	0.830	0.533	1.9
2.24	1.61	203	1.4	5.0	.667	.423	2.4
2.26	1.52	197	1.5	4.5	.556	.349	2.9
2.50	1.37	201	1.8	4.0	.477	.295	3.4
2.75	1.23	205	2.2	3.0	.345	.206	4.8
3.14	0.88	206	3.6	2.5	.257	.147	6.8
3.16	.83	205	3.8	2.5	.239	.135	7.4
3.16	.80	202	3.9	2.0	.210	.115	8.7
3.30	.61	199	5.4	1.5	.189	.101	9.9
3.34	.53	196	6.3	1.2	.162	.083	12.1
3.48	.48	200	7.2	1.0	.141	.068	14.6
3.56	.39	199	9.1	0.5	.130	.061	16.4
3.64[a]	.27	196	13.5	0.2	.109	.047	21.4

[a] This point was not used in the least squares calculation since the uncertainty in both K_0 and $[Cl^-]^{-1}$ was much greater than in the other experiments.

TABLE II

DISTRIBUTION OF LEAD BROMIDE

50 g. KNO₃, 50 g. AgBr, 200 mg. PbBr₂, 450°

Lead concn., mg. PbBr₂/g. soln.				KBr added,	Total Br,		
KNO₃	AgBr	Total, mg. PbBr₂	K_0	g.	molal	[Br⁻]	$[Br^-]^{-1}$
1.75	2.07	203	0.85	6.0	0.461	0.365	2.74
1.78	2.07	202	0.86	5.0	.384	.304	3.29
2.03	1.83	199	1.11	4.0	.316	.250	4.00
2.26	1.64	200	1.38	3.0	.227	.179	5.59
2.47	1.56	205	1.59	2.5	.186	.146	6.85
2.64	1.31	201	2.02	2.0	.167	.131	7.62
2.98	0.94	199	3.16	1.5	.106	.082	12.2
3.27	.70	200	4.68	1.0	.084	.064	15.6
3.71[a]	.28	201	13	0.5	.050	.037	27
				BaBr₂			
3.25	.78	204	4.16	1.0	.075	.057	17.5
2.65	1.19	196	2.23	2.0	.140	.110	9.10
1.94	1.91	200	1.02	4.0	.228	.181	5.52
(100 g.)	(50 g.)						
1.69	0.65	201	2.56	2.0	.115	.090	11.1
(100 g.)	(25 g.)						
1.84	1.09	211	1.69	2.0	.176	.139	7.20
(50 g.)	(100 g.)						
2.74	0.82	217	3.34	2.0	.104	.081	12.4

[a] This point was not used in the least squares calculation since the uncertainty in both K_0 and $[Br^-]^{-1}$ was much greater than in the other experiments.

constants and the solubility of AgCl in these systems (see section on solubility of silver halides).

K, k_1, and k_2 were determined by the method of least squares for the equation type

$$y = a + bx + cx^2$$

and the constants are summarized in Table III.

TABLE III

DISTRIBUTION AND DISSOCIATION CONSTANTS FOR PbCl₂ AND PbBr₂ IN KNO₃

	k_1 (mole/ kg.)	k_2 (mole/ kg.)²	K	k_1/k_2 1st assoc.	$1/k_1$ 2nd assoc.
PbCl₂ (480°)	0.39	0.02	0.72	20	2.6
PbBr₂ (450°)	0.15	0.02	0.55	7.5	6.7

It should be noted that the correction for AgCl and AgCl₂⁻ was large, affecting the calculation of k_1 and especially k_2 markedly. For example, the values of the constants determined from the line drawn through the uncorrected points (curve A in Fig. 1) were $K = 0.63$, $k_1 = 0.73$ mole/kg., and $k_2 = 0.08$ (mole/kg.)². The
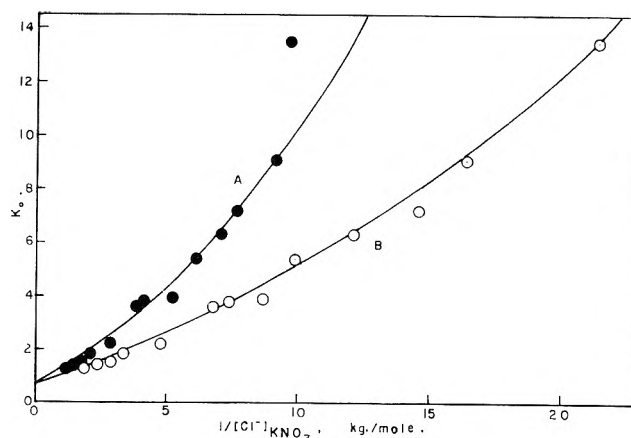
Fig. 1.—Plot of PbCl₂ distribution in KNO₃–AgCl system, 480°: A, (total chloride)⁻¹, ●; B, (chloride ion)⁻¹, O.

distribution constant was affected slightly, k_1 changed by a factor of two, while k_2 changed by a factor of four.

If anion complexes were formed at high chloride concentrations, the distribution coefficient should increase with increasing chloride concentration. No such evidence was found, but certainly anion complexes would be possible at higher chloride concentrations than were studied, and especially in fused chlorides. It has been assumed that PbCl₂ was the predominant species in AgCl although no difference in the results would be observed if only a certain fraction of the lead existed as PbCl₂. The addition of AgBr to AgCl (up to 40 g. of AgBr; 10 g. of AgCl) did not affect the lead chloride distribution appreciably, which supports the idea that the changes in distribution coefficient which were observed were due to changes in the lead species present in potassium nitrate.

Lead Bromide.—The distribution of lead bromide between potassium nitrate and silver bromide at 450° was also studied. The attainment of equilibrium was checked as was done for thallium chloride.[2] In one experiment PbBr₂ was added to molten KNO₃, then AgBr was added; in a second, lead bromide was added to molten AgBr and then KNO₃ was added; while in the third, PbBr₂ was added to the mixture of solvents. The distribution coefficients were 1.98, 1.94, and 2.02, respectively, indicating that equilibrium was achieved.

The same type of an approach was used for PbBr₂ distribution as PbCl₂, using KBr as the added solute instead of KCl. The results are given in Table II and Fig. 2 is analogous to Fig. 1. Table III is a summation of the various constants determined from these experiments including the values for the association constants since these are more often quoted from e.m.f. experiments.

The triangle points in Fig. 2 refer to experiments where the solvent ratio was other than 50–50 g. (i.e., 50/100, 25/100, 100/50 AgBr/KNO₃), and the results show that even though the total lead concentration varied (200 mg. of PbBr₂ and 1 g. of KBr used in all three experiments), the distribution coefficient depended on the bromide ion concentration in the potassium nitrate phase.

The square points in Fig. 2 refer to experiments where barium bromide was substituted for potassium bromide. Although barium resides entirely in the potassium nitrate phase, bromide is transported across the boundary as potassium bromide.
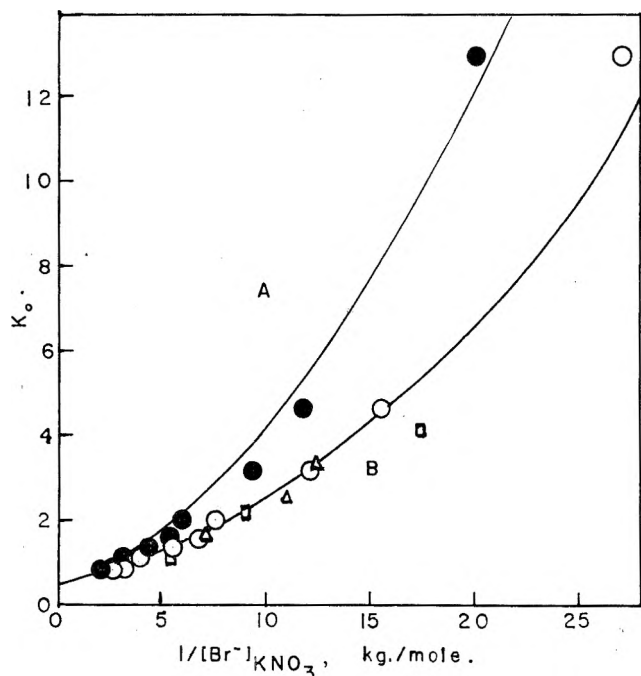
Fig. 2.—Plot of $PbBr_2$ distribution in KNO_3–AgBr system, 450°:
A, (total bromide)$^{-1}$, ●: B, (bromide ion)$^{-1}$, O.

$$(BaBr_2)_{KNO_3} + KNO_3 \longrightarrow$$

$$[Ba(NO_3)_2]_{KNO_3} + (KBr)_{KNO_3} \longrightarrow (KBr)_{AgBr}$$
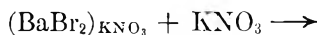
Thus, the systems were not too different from those containing only potassium bromide as the added solute, but the results show that the presence of barium in the potassium nitrate phase has little effect on the lead distribution.

Discussion

Braunstein, Blander, and Lindgren[4] have recalculated and tabulated various association constants which have been reported in nitrate melts determined from e.m.f. studies and other methods. Although no work was done at 480°, the first association constant for lead at 300° was 60 moles of solvent/mole of lead and decreased with increasing temperature
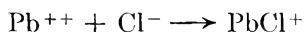
$$Pb^{++} + Cl^- \longrightarrow PbCl^+$$

$$k = [PbCl^+]/[Pb^{++}][Cl^-]$$

Combining k_1 and k_2, one obtains the relation

$$k_1/k_2 = k = 0.39/0.02 = 20 \text{ kg./mole}$$

Since the molecular weight of KNO_3 is 101

$k = 20$ kg./mole $\times$ 10 moles of solvent/kg. =

200 moles of solvent/mole of lead

Thus, the value for the first association constant obtained from these experiments appeared high. The second association constant was reported to be 3 by Duke and Iverson from solubility studies at 300°.[5] The value of 2.6 reported here appears to be in agreement, since Duke and Iverson reported little temperature dependence.

The first association constant for lead bromide was measured by Duke and Garfinkel at temperatures be-

(4) J. Braunstein, M. Blander, and R. M. Lindgren, *J. Am. Chem. Soc.*, **84**, 1529 (1962).

(5) F. R. Duke and M. L. Iverson, *J. Phys. Chem.*, **62**, 417 (1958).

tween 250 and 319° in mixed $NaNO_3$–KNO_3; at 319° it was 11 and decreased with increasing temperature.[6] The second association constant was reported as 6.2. Thus, the constants calculated from distribution coefficients are in fair agreement with the values obtained from other methods.

It should be noted that in these experiments that the second association constant is determined from the first deviation from simple distribution law while in the e.m.f. experiments the first association constant is determined from the first deviation from the Nernst equation. Thus, the two methods are complementary, although both methods can be used to determine both association constants.

Solubility of Silver Halides in KNO_3.—The mutual solubility in any liquid–liquid system is important for theoretical calculations because of possible change in solvent nature and for practical calculations because of possible loss or contamination of solvent. In the fused salt systems studied the solubility of silver halide in KNO_3 was even more important since any extra halide ion in the KNO_3 phase would affect the lead distribution.

The solubility of AgCl and AgBr in KNO_3 was determined in KNO_3 containing various amounts of potassium halide, and the results are shown in Fig. 3.

Only the silver halide which dissociates will increase the halide ion concentration. AgX will not affect the halide ion concentration and AgX_2^- will decrease the halide ion concentration. The total solubility is

$$S = [Ag^+] + [AgX] + [AgX_2^-]$$

In terms of the equilibrium constants

$$K_{sp} = [Ag^+][X^-]$$

$$K_1 = [AgX]/[Ag^+][X^-]$$

$$K_2 = [AgX_2^-]/[AgX][X^-]$$

the solubility is

$$S = \frac{K_{sp}}{[X^-]} + K_1 K_{sp} + K_1 K_2 K_{sp}[X^-] \qquad (1)$$

When no excess halide ion is added to the KNO_3 phase, the concentration of $[AgX_2^-]$ will be small, and the solubility is approximately

$$S \cong K_{sp}^{1/2} + K_1 K_{sp} \qquad (2)$$

In the determination of halide ion concentration, total halide was found by addition of excess silver ion and filtering off the silver halide. From this value must be subtracted the amount of halide complexed as AgX and the amount of halide complexed as AgX_2^- which was present originally.

Although not all the constants have been measured for these systems, approximations can be made from published values for some of the constants and the solubility given here.

Flengas and Rideal give the value of K_{sp} for AgCl at 248° as 4.89×10^{-6} and $\Delta H = 18.3$ kcal.[7]

Extrapolating this to 480°, a value of 1.2×10^{-3} is

(6) F. R. Duke and H. M. Garfinkel, *ibid.*, **65**, 1627 (1961).

(7) S. N. Flengas and K. Rideal, *Proc. Roy. Soc.* (London), **233**, 443 (1955).

obtained. Using this in equation 2 a value of 60 for K_1 was obtained from the solubility of 0.107 m with no added halide ion. This value is high compared to the e.m.f. value of Alvarez-Funes, Braunstein, and Blander (20 on molality basis).[8] Actually, using the value of 20 for K_1 leads to $K_{sp} = 2.7 \times 10^{-3}$, which is not unreasonable considering the 220° extrapolation and change from $NaNO_3$–KNO_3 to KNO_3 solvent. K_2 was estimated by solving eq. 1 and 3 simultaneously for [Cl⁻] and K_2. The values for K_2 ranged between 4 and 9. However, using these constants it can be seen that [AgCl₂⁻] cannot be neglected even when no excess chloride is added. This would mean that K_{sp} was actually smaller than 2.7×10^{-3}. For calculating the chloride ion concentrations the following approximate values were used: $K_{sp} = 2 \times 10^{-3}$, $K_1 = 20$, $K_2 = 6$.

The total chloride concentration (found by analysis) was

$$\text{total} = [\text{Cl}^-] + [\text{AgCl}] + 2[\text{AgCl}_2^-]$$

$$\text{total} = [\text{Cl}^-] + [K_1 K_{sp}] + 2K_1 K_2 K_{sp}[\text{Cl}^-] \quad (3)$$

$$[\text{Cl}^-] = \frac{\text{total} - K_1 K_{sp}}{1 + 2K_1 K_2 K_{sp}} = \frac{\text{total} - 0.040}{1 + 0.48}$$

The final equation was used in calculating the chloride ion concentrations in Table I. Equation 3 neglects complexation with lead, but the lead concentration in KNO_3 never exceeded 0.013 m. In addition, when the halide concentration was so low that 0.013 would be appreciable, the fraction of lead complexed with halide was low.

In the case of AgBr, K_1 has been measured at various temperatures,[8] and at 450° the value is about 73. From the solubility reported here $K_{sp} = 6 \times 10^{-5}$ and $K_2 = 30$. Alvarez-Funes, Braunstein, and Blander report $K_2 = 27$ at 452° which shows good agreement for this constant. Their published value was used for calculating bromide concentrations. The equation used for

(8) A. Alvarez-Funes, J. Braunstein, and M. Blander, *J. Am. Chem. Soc.*, **84**, 1538 (1962).
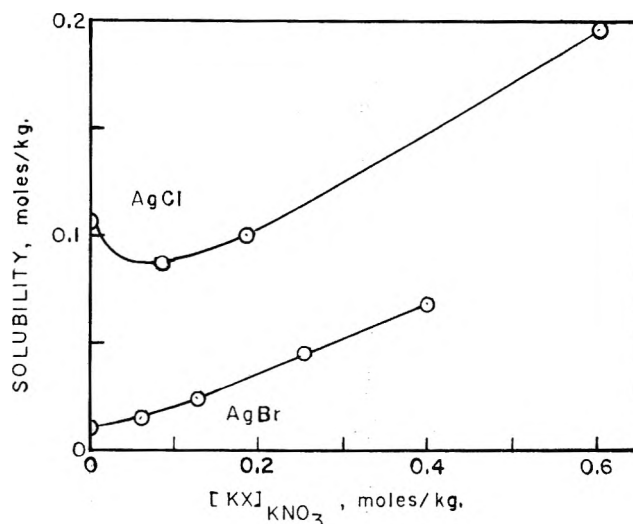
Fig. 3.—Solubility of AgCl and AgBr in KNO_3.

obtaining bromide ion concentrations from the total bromide found by analysis was

$$[\text{Br}^-] = \frac{\text{total} - K_1 K_{sp}}{1 + 2K_1 K_2 K_{sp}} = \frac{\text{total} - 0.004}{1 + 0.24}$$

Thus, the correction for bromide was much less than for the chloride system, and slight errors in the constants would have less effect on the calculation of the lead halide dissociation constants. In fact, the constants for the line drawn through the uncorrected points in Fig. 2 (curve A) were $K = 0.57$, $k_1 = 0.15$, and $k_2 = 0.038$. Only k_2 was changed appreciably by this calculation. Obviously, it would be more satisfying to measure the halide ion activity directly in the molten KNO_3 phase, and hopefully, measurements of this type will be made in the future.

THE THERMODYNAMICS OF THE SOLUTION OF POLAR GASES IN WATER; THE HEAT, FREE ENERGY, AND ENTROPY OF SOLUTION OF HYDRAZOIC ACID

By L. A. D'Orazio and R. H. Wood

Department of Chemistry, University of Delaware, Newark, Delaware

The vapor pressures of hydrazoic acid solutions have been measured from 0 to 50°. The free energies of solution have been determined at 0.0, 24.42, 35.95, and 49.46° and the free energy, enthalpy, and entropy of solution at 25° have been calculated. The free energies and enthalpies of formation and absolute entropies for gaseous hydrazoic acid, aqueous hydrazoic acid, and the aqueous azide ion have also been calculated. The results for hydrazoic acid together with other measurements indicate that the structure of the cavity around strong hydrogen bonding solutes is different from the structure around non-polar solutes and involves hydrogen bonds between the solute and the water molecules.

Introduction

Except for the calorimetric determination of the heat of solution by Gunther, *et al.*,[1] there are no thermo-

(1) P. Gunther, P. Mayer, and F. Muller-Skjold, *Z. physik. Chem.*, **A175**, 154 (1935).

dynamic data on the reaction of gaseous hydrazoic acid with water to form a solution. The thermodynamics of this reaction are of interest for two reasons. First, these measurements, together with certain other known thermodynamic values, allow the calculation of

the free energy and enthalpy of hydrazoic acid gas and the free energy and entropy of aqueous hydrazoic acid and the azide ion. Second, solutions of non-electrolytes in water show some unusual characteristics. In the case of the inert gases the model of Eley[2] seems to predict the behavior fairly well. Frank[3] has shown that the polar gases obey a Barklay–Butler correlation that is quite different from the correlation for the non-polar gases. Powell[4] has shown that the entropies of solution of gaseous non-electrolytes in water are much lower than the entropies of solution in benzene. However, some polar molecules (HF,[5] HCN, H_2S, H_2Se[6]) have entropies which are higher than the predictions of Powell's correlation while other polar molecules (NH_3 and H_2O) obey Powell's correlation. In trying to find an explanation for this anomalous behavior it became evident that more data on the entropies of solution of polar gases in water would be useful.

Experimental

A. Preparation of HN_3 Solution.—A 22% solution of reagent sulfuric acid was slowly added to a boiling 14% reagent sodium azide solution in a 500-cc. flask fitted with a 6-in. Vigreux column. The hydrazoic acid solution coming over was collected in glass and stored in the dark. It was found that preparations of the hydrazoic acid solution[7] without the Vigreux column contained small amounts of sulfuric acid probably due to local distillation or physical entrainment in the distillate vapors.

B. Vapor Pressure Measurements.—The vapor pressure measuring apparatus consisted of a 145.8-ml. flask fitted with a dropping funnel, an outlet for evacuating the flask, and a short oil manometer which was connected by way of a pressure reservoir to the main mercury manometer. All connections were made with ground glass joints. At 0° only the vapor pressure chamber was thermostated, but at all other temperatures the whole vapor-containing system was thermostated. The small oil manometer was used because it allowed the vapor-containing system to be compact and separated from the rest of the system which was, of course, too large to be conveniently thermostated. The pressure of the mercury manometer was kept equal to the pressure in the system by adjusting both arms of the oil manometer to the same height. This was easily done by leaking air into the pressure reservoir through a fine thermometer capillary. The oil levels were adjusted to within 1 mm. of each other. The over-all pressure measurements were accurate to within ±0.2 mm.

A sample of the prepared hydrazoic acid solution was diluted and introduced into the vapor pressure chamber. The sample was degassed by repeated freezing, chamber evacuation, and thawing at reduced pressures. It was found that water could be degassed to less than 0.1 mm. pressure of residual gases by simply freezing at −80°, pumping, thawing under the reduced pressure, refreezing, and pumping down again. On this basis it was decided to repeat this procedure at least three times for each sample of hydrazoic acid solution to ensure degassing to at least the detectable limit of 0.1 mm. pressure.

The vapor pressures were measured at several temperatures after the system reached complete equilibrium. It took about 120 to 150 min. for the pressure readings to reach their final values. In order to ensure complete equilibration the final pressure readings were taken 30 to 60 min. after the pressure stopped changing. The whole procedure generally consumed 3 to 4 hr. Temperatures were measured with a thermometer calibrated at the ice point and the transition point of sodium sulfate decahydrate (32.38°).

(2) D. D. Eley, *Trans. Faraday Soc.*, **35**, 1281 (1939); D. N. Glew, *J. Phys. Chem.*, **66**, 605 (1962).

(3) H. S. Frank and M. W. Evans, *J. Chem. Phys.*, **13**, 507 (1945).

(4) R. E. Powell, *J. Phys. Chem.*, **58**, 528 (1954).

(5) The entropy of solution of HF was calculated from the data of J. C. Brosheer, F. A. Lenfesty, and K. L. Elmore, *Ind. Eng. Chem.*, **39**, 423 (1947).

(6) F. D. Rossini, *et al.*, National Bureau of Standards Circular 500, "Selected Values of Chemical Thermodynamic Properties," U. S. Government Printing Office, Washington, D. C., 1952.

(7) L. F. Audrieth and C. F. Gibbs, *Inorg. Syn.*, **1**, 77 (1939); M. D. Kemp, *J. Chem. Educ.*, **37**, 142 (1960).

C. Analysis of HN_3.—The total hydrazoic acid in the chamber (gas and solution) was analyzed by adding an excess of standard sodium hydroxide solution to the system while under reduced pressure by means of a dropping funnel fitted to the chamber. About 5 min. was allowed for the hydrazoic acid vapor to diffuse back into the solution and be neutralized. The solution was then brought to atmospheric pressure and back titrated with standard sulfuric acid. As a duplicate check the resulting solution was analyzed for azide ion by precipitating and filtering silver azide, dissolving the washed precipitate in ceric ammonium sulfate solution, and precipitating silver chloride. The two results checked to within experimental accuracy which was ±1 mg. of HN_3.

The partial pressure of the hydrazoic acid was calculated by subtracting the water vapor pressure from the total pressure. The water vapor pressure was corrected for the vapor pressure lowering of the solution. The vapor pressure lowering of the solution was quite small and, therefore, any deviation from ideal behavior contributes negligible errors to the calculation. The amount of hydrazoic acid in the gas phase was calculated from the pressure and volume of the vapor. The molality of the solution was calculated from the difference between the total hydrazoic acid and the acid in the gas phase and was corrected for the dissociation of the acid using the ionization constant, $K = 1.91 \times 10^{-5}$, reported by Yui.[8] Other values of the ionization constant have been reported[9] but the accuracy does not seem to be as good.

Results

In Table I, the measured pressures and concentrations are tabulated along with the calculated free energies for the solution reaction. The free energies extrapolated to infinite dilution for each temperature are also shown in Table I. The error limits are a rough estimate of twice the standard deviation. An accurate error analysis was not carried out because of the possibility of systematic errors which are as large as the random errors. The free energies of Table I yielded the equation

$$\log K = -12.6173 + 2.6657 \log T + \frac{2116.050}{T}$$

when using the method of least squares with appropriate weighing factors. The choice of equation is quite arbitrary. This equation was chosen because Valentiner[10] has shown that it represents solubility data very accurately. The data were not sufficiently accurate to evaluate any higher terms which would allow for changes in heat capacity with temperature. The free energy ($\Delta F = -1.47 \pm 0.03$ kcal./mole), enthalpy ($\Delta H = -8.10 \pm 0.3$ kcal./mole), and entropy ($\Delta S = -22.3 \pm 1.1$ cal./mole-deg.) of solution at 25° were calculated from the equation.

The results of the recalculation of the thermodynamic properties of hydrazoic acid and the azide ion are given in Table II. These values were calculated from the heat of formation (65.53 kcal./mole) and heat of neutralization 3.60 kcal./mole) of the aqueous azide ion given by Gray and Waddington,[11] the entropy of gaseous hydrazoic acid (57.083 cal./mole deg.) given by Dows and Pimentel,[12] and the ionization constant of the acid given by Yui.[8]

(8) N. Yui, *Bull. Inst. Phys. Chem. Res.* (Tokyo), **20**, 390 (1941).

(9) A. Hantzsch, *Ber.*, **32**, 3066 (1899); C. A. West, *J. Chem. Soc.*, **77**, 705 (1900); E. Oliveri-Mandala, *Gazzetta*, **46**, 298 (1916); W. S. Hughes, *J. Chem. Soc.*, 491 (1928); H. T. S. Britton and R. A. Robinson, *Trans. Faraday Soc.*, **28**, 531 (1932).

(10) S. Valentiner, *Z. Physik*, **42**, 253 (1927).

(11) P. Gray and T. C. Waddington, *Proc. Roy. Soc.* (London), **A235**, 106 (1956).

(12) D. A. Dows and G. C. Pimentel, *J. Chem. Phys.*, **23**, 1258 (1955).

TABLE I
RESULTS OF SOLUBILITY MEASUREMENTS

Temp., °C.	C_{HN_3}, moles/kg.	P_{HN_3},[a] mm.	$\overline{\Delta F^0}$ (soln.), kcal./mole[b]
0.00	1.807	33.3	-2.02 ± 0.02
	.9473	16.8	$-2.04 \pm .02$
	.3964	7.0	$-2.04 \pm .02$
	.1023	1.8	$-2.04 \pm .07$
	0 (extrapolated)		$-2.05 \pm .05$
24.42	1.651	101.0	-1.490 ± 0.013
	0.9020	55.6	$-1.485 \pm .009$
	.3922	24.5	$-1.479 \pm .007$
	.1019	6.3	$-1.484 \pm .018$
	0 (extrapolated)		$-1.47 \pm .03$
35.95	1.541	153.1	$-1.250 \pm .013$
	0.8675	87.2	$-1.243 \pm .009$
	.3893	40.1	$-1.227 \pm .006$
	.1013	10.9	$-1.203 \pm .015$
	0 (extrapolated)		$-1.20 \pm .02$
49.46	1.397	228.8	$-0.982 \pm .02$
	0.8187	134.8	$-.981 \pm .009$
	.3848	64.9	$-.965 \pm .005$
	.1008	17.7	$-.939 \pm .011$
	0 (extrapolated)		$-.94 \pm .01$

[a] $P_{HN_3} = P_{total} - (p^0 H_2O - \Delta p)$ where Δp is the vapor pressure lowering of water and $p^0 H_2O$ is the vapor pressure of pure water. [b] $\overline{\Delta F^0}$ is the standard partial molal free energy change. The standard states are 1 atm. for the gas and the hypothetical 1 molal concentration for the solution.

TABLE II
HEAT, FREE ENERGY, AND ENTROPY OF FORMATION OF HYDRAZOIC ACID

	ΔF_f^0, kcal./mole	ΔH_f^0, kcal./mole	S, e.u.	ΔS_f^0, e.u.
$HN_3(g)$	78.3	70.0	57.08	-27.17
HN_3 (aq., 1 m)	76.8	61.93	34.8	-49.5
N_3^- (aq., 1 m)	83.2	65.53	25.4	-58.9

Discussion

Gunther's values for the enthalpy of solution[1] varied from -9.73 kcal./mole at a dilution of 0.16 molal to -8.48 kcal./mole at 0.68 molal. These measurements give a heat of dilution of 1.25 kcal./mole from the highest to the lowest concentration. This value is an order of magnitude higher than the usual values for the heat of dilution of a non-electrolyte.[13]

Gray and Waddington estimated the entropy of solution of hydrazoic acid from a knowledge of the entropy of vaporization of liquid hydrazoic acid and an estimate of the entropy of mixing the liquid with water. Their estimate, 25.83 e.u., is close to the present result (22.3 e.u.).

On a Barklay–Butler plot (heat vs. entropy of vaporization) aqueous solutions of the non-polar gases have a much higher entropy of vaporization for a given heat of vaporization than solutions in non-polar solvents.[3] Hydrazoic acid and the other polar gases in water fall fairly close to a straight line which lies between the two extremes for the non-polar gases in water and in non-polar solvents.

A comparison of the change in heat capacities (ΔC_p) for solution of a series of gases is instructive. In Table III the change in heat capacity using Eley's model[2] is given for those cases where the partial molal volume of the solute is known. From Table III it is clear that the change in heat capacity for the non-polar gases is

(13) See, for instance, the heats of dilution of aqueous ammonia, acetic acid. and ethanol. ref. 6

generally smaller but fairly close to the value predicted by Eley. For the polar gases the experimental values are markedly lower than the predicted values, in fact, for those polar gases which form strong hydrogen bonds (e.g., CH_3OH, H_2O, HN_3, HF, HCN), agreement is quite poor and the experimental values are very low. The temperature dependence for the heat of solution calculated according to Eley's model arises from the large change with temperature of the energy required to form a cavity. The results suggest that as the ability to form hydrogen bonds with water increases, the mechanism of solution changes to one which uses hydrogen bonds between the water and solute. This is in contrast to the simple cavity model where the water is restricted to bonding to itself and distorts to form a network surrounding the gas cavity.

TABLE III
CHANGE IN HEAT CAPACITY ON SOLUTION OF SEVERAL GASES IN WATER

Gas	V,[a] ml.	ΔC_p (soln.),[b] cal./mole deg. Eley model	Experimental[e]
A	...	...	$38 \pm 8^{i,l}$
$CH_4{}^c$	35.6	57.8	55 ± 5
CO	36[f]	64	$41 \pm 3^{j,l}$
H_2	26[f]	46	$26 \pm 3^{k,l}$
$C_2H_6{}^d$	51.2[g]	75	$66 \pm 6^{k,l}$
CH_3F	$35.9^h \pm 0.4$	69	35 ± 1^l
CH_3Cl	$46.2^h \pm 0.5$	82	43 ± 1^l
CH_3Br	$53.0^h \pm 0.8$	91	44 ± 1^l
CH_3I	$63.7^h \pm 0.2$	115	86 ± 1^l
CH_3OH	38.9^h	69	28 ± 1^l
N_2O			$33 \pm 5^{m,l}$
H_2Se			0 ± 25^n
H_2S			$36 \pm 10^{o,l}$
H_2O	18	32	10.0^p
HN_3			5 ± 10
HF			0 ± 5^q
HCN			0 ± 15^r

[a] Partial molal volumes. [b] $\Delta C_p = [\Delta H$ soln. (35°) $- \Delta H$ soln. (15°)]/20°. Thus ΔC_p is the average change in heat capacity between 15 and 35°. [c] All methane data from D. N. Glew, J. Phys. Chem., 66, 605 (1962). [d] ΔC_p calculated for the range 20 to 35°. [e] The limits of error are very rough estimates of the accuracy of the determination of ΔC_p. [f] I. Khritchevsky and A. Ilinskaya, Acta Physicochim. URSS, 20, 327 (1945). [g] W. L. Masterson, J. Chem. Phys., 22, 1830 (1954). [h] H. G. Holland and E. A. Moelwyn-Hughes, Trans. Faraday Soc., 52, 297 (1956). [i] T. J. Morrison and N. B. Johnstone, J. Chem. Soc., 3441 (1954). [j] L. W. Winkler, Ber., 34, 1408 (1901). [k] T. J. Morrison and F. Billett, J. Chem. Soc., 3819 (1952). [l] D. N. Glew and E. A. Moelwyn-Hughes, Discussions Faraday Soc., 15, 150 (1953). [m] A. E. Markham and K. E. Kobe, J. Am. Chem. Soc., 63, 449 (1941). [n] A. J. McAmis and W. A. Felsing, ibid., 47, 2633 (1925). [o] R. H. Wright and O. Maass, Can. J. Res., 6, 94 (1932). [p] See ref. 6. [q] J. C. Brosheer, F. A. Lenfesty, and K. L. Elmore, Ind. Eng. Chem., 39, 423 (1947). [r] J. Horuichi and K. Tanabe, J. Res. Inst. Catalysis, U. Hokkaido, 1, 117 (1951).

A similar conclusion was reached by Frank and Wen,[14] who inferred from the entropies of vaporization of ammonia and methanol from aqueous solutions that, "hydrogen bonding solutes, or groups like $-NH_2$ or $-OH$, do not alter the water structure much if at all." In the case of the non-polar substances in water Frank and collaborators[3,14] have shown that a large degree of order (ice-likeness) is induced in the water around a non-polar solute. Claussen and Polglase[15] proposed

(14) H. S. Frank and W. Wen, Discussions Faraday Soc., 24, 133 (1957)

(15) W. F. Claussen and M. F. Polglase, J. Am. Chem. Soc., 74, 4817 (1952).

that the extra order is due to the formation around the solute of cages which are similar to the cages observed in the non-polar gas hydrates.

Another line of evidence that leads to the conclusion that the hydrogen bonding solutes have a different effect on the structure of water is furnished by the fact that the hydrogen halides and ammonia do not form clathrate-type gas hydrates. Instead only the stoichiometric one, two, or three hydrates are formed.[16,17] It is interesting to note that hydrogen sulfide forms a clathrate type hydrate[18] and also has a high change in

heat capacity (Table III). The position of hydrogen selenide is apparently anomalous since it is less polar than hydrogen sulfide, forms a clathrate type gas hydrate,[18] and yet has a very low change in heat capacity between 15 and 35°. This apparent anomaly will probably disappear when more accurate data become available.

In summary, the evidence indicates that for hydrogen bonding solutes only a minimum distortion in the structure of the water occurs and that the solute is hydrogen bonded to the water. However, the non-polar solutes act to promote in the surrounding water a more ordered (ice-like) structure in which the water is hydrogen bonded to itself.

(16) J. H. van der Waals and J. C. Platteeuw, "Advances in Chemical Physics," Vol. II, Interscience Publishers, New York, N. Y., 1959, p. 4.

(17) J. W. Mellor, "A Comprehensive Treatise on Inorganic and Theoretical Chemistry," Longmans, Green and Co., London, 1922.

(18) M. V. Stackelberg and H. R. Muller, Z. Electrochem., 58, 25 (1954).

STUDY OF THE ELECTRON SPIN RESONANCE OF CHROMIUM(III) COMPLEXES IN AQUEOUS SOLUTION

By K. M. Sancier and J. S. Mills

Stanford Research Institute, Menlo Park, California

The electron spin resonance of Cr(III) solutions in nitric and perchloric acids was studied in the range of acid concentration of about 10^{-5} to 22 M. In the pH range of 0 to 3 the spin intensity of the resonance is constant and maximum; its absolute value corresponds to about three spins per Cr(III), and the resonance is attributed to the hexaaquo complex, $Cr(H_2O)_6^{+3}$. At higher pH values the spin intensity decreased to as little as 17% of its maximum value as a result of hydrolysis of the hexaaquo complex and formation of a polynuclear complex. Evidence that a dinuclear species is formed in weak acid solutions is provided by the low spin intensity observed for the dinuclear Cr(III) complex prepared by oxygen oxidation of Cr(II), and also by the similar slow rate of increase of spin intensity resulting from dissociation of the complex when these solutions are made strongly acid. Further evidence is provided by the abrupt decrease of spin intensity which occurs upon addition of concentrated alkali. The spin intensity of Cr(III) in concentrated nitric acid decreased to less than one-half of its maximum value; in concentrated perchloric acid the intensity decreased less. The possibility that inner-coördinated Cr(III) nitrate or perchlorate complexes account for the decrease of spin intensity is ruled out by experiments in which high concentrations of $Mg(ClO_4)_2$ and $Ca(NO_3)_2$ were added. The optical spectra of the strong nitric acid solutions suggest that a dinuclear species is present to account for the decrease of spin intensity. Evidence of outer-sphere complex formation is provided by line width measurements. The relaxation mechanisms which account for the observed line widths are discussed.

Introduction

Electron spin resonance (e.s.r.) measurements of aqueous solutions of chromic ions, Cr(III), have been included as part of studies of transition metal ions in solution.[1-4] The principal emphasis in these studies has been on the dependence of the line width of the resonance on such parameters as type of ligand, concentration, and temperature, and on comparison with the resonance of the solid.

We observed a strong dependence of the observable spin intensity upon the acid concentration of solution of Cr(III) nitrate and perchlorate, and this dependence was studied in terms of various possible complexes.

Experimental

The e.s.r. spectra of various solutions at 15–20° were measured in a 0.5-mm. i.d. quartz capillary with a Varian V-4502 X-band spectrometer with a multipurpose cavity whose Q is approximately 7000, and employing 100-kc. field modulation and a modulation amplitude of about 7 gauss. The e.s.r. spectrum was taken the same day the solution was prepared, except where noted. The

absolute spin intensity of a solution was determined by comparison with a sample of 0.1% pitch in KCl (Varian Associates) of known spin intensity ($\pm 20\%$) with the appropriate filling-factor correction applied.

Solutions of chromic nitrate of various acid concentration were prepared by dissolving $Cr(NO_3)_3 \cdot 9H_2O$ in aqueous solutions of nitric acid of preadjusted concentration of 21.6 to 10^{-3} M, and NaOH was added to obtain less acidic solutions. A set of solutions of chromic perchlorate in $HClO_4$ was prepared in similar fashion. The pH of solutions containing less than 1 M acid was determined with a pH meter, a suitable glass electrode, and a salt bridge for $HClO_4$ solutions. Solutions which are believed to contain Cr(III) predominantly as the hexaaquo complex, $Cr(H_2O)_6^{+3}$, were provided in three ways: (1) by H_2O_2 reduction of CrO_3 in 10 M $HClO_4$;[5] (2) by dissolving in 1 M $HClO_4$ the crystals of $Cr(ClO_4)_3$ crystallized from (1); and (3) the first fraction of chromic perchlorate eluted from a cation-exchange resin.[6]

A solution which contained predominantly the Cr(III) dinuclear species was obtained by zinc reduction of 0.04 M chromic perchlorate in 0.5 M $HClO_4$ or by electrolytic reduction at a mercury cathode, followed by oxidation with oxygen. The absorption spectra of these solutions measured with a Cary spectrophotometer (Model 14) were in agreement with those reported for the dimeric species.[6,7]

$Mg(ClO_4)_2 \cdot 6H_2O$ and $Ca(NO_3)_2 \cdot 6H_2O$ were used for the studies of ionic strength. All chemicals (Baker) were of reagent grade.

(1) R. G. Hayes, Lawrence Radiation Laboratory Report UCRL-9873, Sept. 29, 1961.

(2) B. R. McGarvey, J. Phys. Chem., 61, 1232 (1957).

(3) V. I. Avvakumov, N. S. Garifyanov, B. M. Kozyrev, and P. G. Tishkov, Soviet Phys., JETP, 37, 1110 (1960).

(4) L. S. Singer, J. Chem. Phys., 23, 379 (1955).

(5) A. L. Phipps and R. A. Plane, J. Am. Chem. Soc., 79, 2458 (1957).

(6) J. A. Laswick and R. A. Plane, ibid., 81, 3564 (1959).

(7) M. Ardon and G. Stein, J. Chem. Soc., 2095 (1956).

Results

The results of the dependence of Σ, the spin intensity of the Cr(III) resonance, upon the concentration of HNO_3 and $HClO_4$ and upon the concentration of NaOH solution used to reduce acidity are listed in Table I. The value of the Σ of Cr(III) was calculated mainly by the product $I(\Delta h)^2$—where I is the peak–peak height of the derivative curve and Δh is the line width in gauss between derivative peaks—and also calculated by the first moment of the derivative curves. The results of these methods were consistent within $\pm 10\%$. The values of spin intensity were corrected for the gain setting of the e.s.r. spectrometer and for the Cr(III) concentration, which was in the range of 0.01 to 0.04 M. A solution marked in the table by an asterisk was adjusted successively to the next lower acid concentration with a given solution of NaOH. The maximum observed spin intensity of Cr(III) solutions was arbitrarily set at $\Sigma = 100$; the resonance absorption of such a solution was found in preliminary work to be about three unpaired spins per Cr(III), by comparison of first moments with that of the pitch sample. The experimental error of Σ is within $\pm 10\%$, and that of Δh less than $\pm 5\%$. Within these errors, the sensitivity of the e.s.r. spectrometer was unaffected by the acidity of the solutions in the capillary.

TABLE I

EFFECT OF ACID CONCENTRATION ON SPIN INTENSITY Σ AND LINE WIDTH Δh OF Cr(III)[a]

	Cr(NO$_3$)$_3$ + HNO$_3$				Cr(ClO$_4$)$_3$ + HClO$_4$		
	Σ^c				Σ^c		
$-\log$ [acid][b]	M NaOH[d]			Δh	M NaOH[d]		Δh
	0.05	2	10	(gauss)	0.0	0.5	(gauss)
-1.33	38(2)			310			
-1.20	72(3)			195			
-1.07	78			165			
-1.03					88		
-1.00	79(3)			160	85(3)		115
-0.83	75(2)			165	93		
$-.65$	79			145			
$-.50$	89(2)			140	85(3)		115
$-.35$	83			140	90		
.00	100(3)		*	140	97(2)		130
.25			78	155	100		
.50	97(2)		57	155	100(2)		140
1.00	100(2)	*	45	155	95(2)		140
2.00	100		96 34	155	100(2)	*	145
2.60	97	*		150	97		
3.00	97	100	74 24	155	96	93	150
3.40	95			160			
4.00	76	60		170		66	150
4.50	41	41		155			
4.75	40			170		35	150
4.9	17	17		180			

[a] Concentration in range 0.01 to 0.04 M.   [b] Molar acid concentration, [acid]; pH measured at [acid] $\leq$ 0.   [c] Values of Σ normalized to maximum observed value, arbitrarily set at 100; values in parentheses are number of results averaged (in excess of one).   [d] Concentration of NaOH used to raise pH.

The results for the Cr(III)–HNO$_3$ system—studied in greater detail than Cr(III)–HClO$_4$ because HNO$_3$ could be obtained in higher concentration than HClO$_4$—are plotted in Fig. 1. The solid points represent data obtained for solutions prepared by dissolving Cr(NO$_3$)$_3$ of preadjusted HNO$_3$ concentration; the open points represent data obtained when aqueous NaOH was added to decrease the acidity of a given Cr(III) nitrate
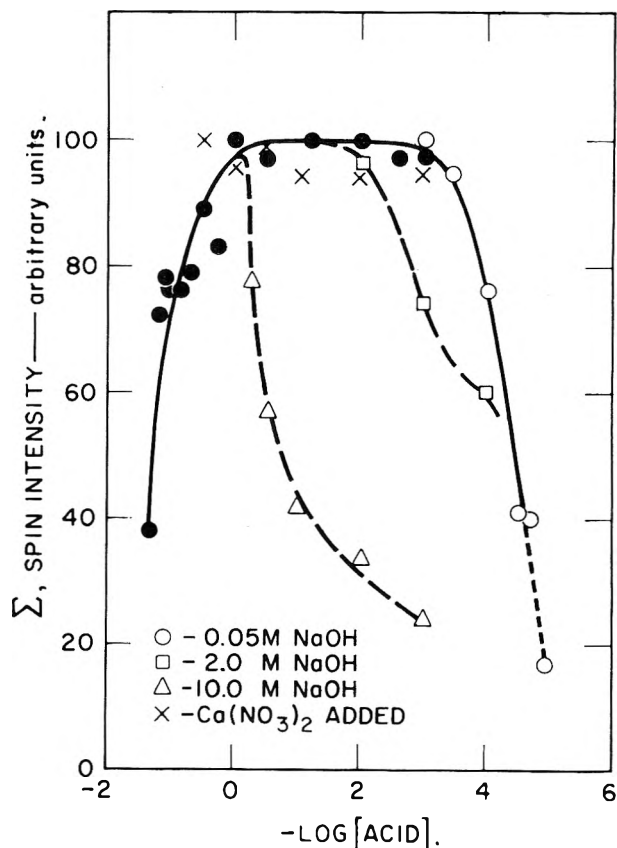
Fig. 1.—Spin intensity, Σ, of 0.04 M Cr(NO$_3$)$_3$ in HNO$_3$ as a function of acid molarity and with Ca(NO$_3$)$_2$ added to make ionic strength 10. Different sets of data are indicated by different symbols, and the open points indicate solutions to which NaOH had been added to raise pH.

solution. The value of spin intensity dropped abruptly when 10 M NaOH was added to reduce acidity (triangular points). The decrease of spin intensity occurred less abruptly when weaker alkali was added to less acidic solutions (square points for 2 M NaOH and circular points for 0.05 M NaOH). Chromic hydroxide precipitated locally when concentrated alkali was added, but the precipitate did not persist. At pH values greater than 4.75, the e.s.r. parameters became dependent upon the history of the solution, and data at pH 4.9 are included in Table I and Fig. 1 to indicate possible values of the parameters.

The decrease of spin intensity resulting from the addition of alkali occurred very rapidly. Even the largest changes occurred within 3 min., the time required to make the measurements. The spin intensity then increased slightly over a period of days as the pH was observed to decrease slightly, presumably as a result of polynucleation. Upon addition of concentrated acid to weak acid solutions the spin intensity increased slowly. For example, when a solution which was originally adjusted to a pH of about 4.8 was acidified with 10 M HNO$_3$ to pH 1, the value of Σ increased in three days from 30 to 48. About the same rate of increase of the spin intensity was observed for the dinuclear species (prepared by oxygen oxidation of Cr(II)) at about pH 1. In order to account for the decrease of spin intensity which occurred when the acid concentration was less than 1 M, two complexes which may contribute to the observed effect were prepared and their e.s.r. spectra measured. In the range 1 to 10^{-3} M acid, the predominant Cr(III) species is
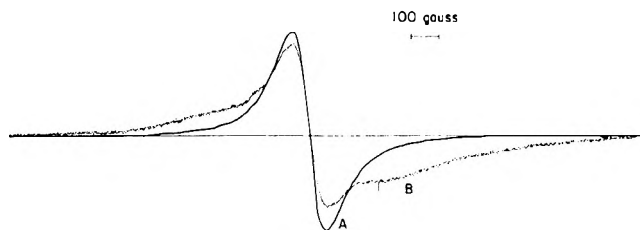
Fig. 2.—First derivative of resonance $Cr(H_2O)_6^{+3}$ (curve A) and dinuclear species (curve B). For the same Cr(III) concentration a factor of 10 greater gain was necessary for curve B.
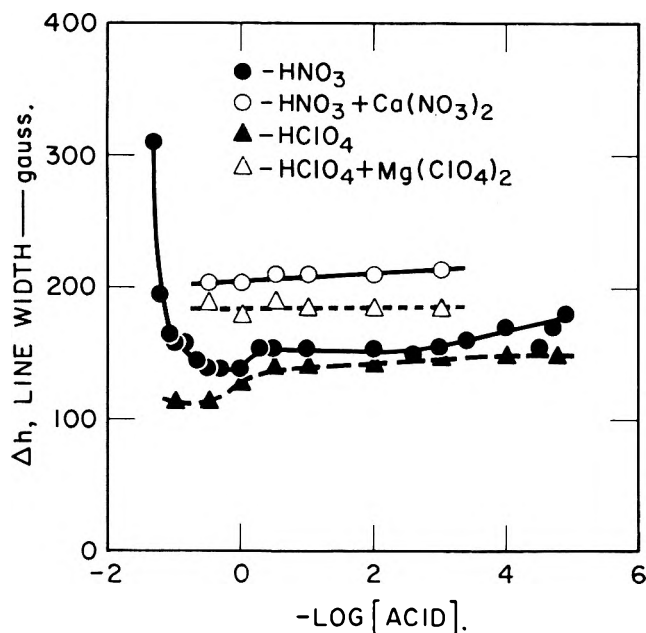
Fig. 3.—Effect of acid concentration and addition of salts on the line width Δh for solutions of $Cr(NO_3)_3$ in HNO_3 with and without $Ca(NO_3)_2$, and of $Cr(ClO_4)_3$ in $HClO_4$ and with and without $Mg(ClO_4)_2$. Salt concentrations were adjusted to maintain ionic strength of solution at 10, assuming complete acid dissociation.

probably the hexaaquo complex ion, $Cr(H_2O)_6^{+3}$. The e.s.r. of each of three solutions in which this complex is believed to predominate (see Experimental) contained a resonance with $\Sigma = 100$ and $\Delta h = 140$ to 150 gauss, which are also the same values as those observed for Cr(III) solutions in the 1 to 10^{-3} M acid range (Table I).

Among the possible hydrolysis products of $Cr(H_2O)_6^{+3}$ is a dinuclear complex. The e.s.r. of a solution containing a dinuclear complex, prepared by reaction of Cr(II) perchlorate with oxygen and measured within 2 hr. of preparation, consisted of two observable resonances: one with $\Delta h = 140$ gauss and $\Sigma = 7$, and the other with $\Delta h \sim 700$ gauss and $\Sigma \sim 8$, both at about the same g-value (2.00). The first derivative curve of this absorption line is compared in Fig. 2 with that of the hexaaquo Cr(III) (different vertical scales). Upon storage of this solution at room temperature, the spin intensity of the 140-gauss line increased while that of the 700-gauss line decreased. After about 20 days the values of Σ and Δh of the resulting resonance resembled those of $Cr(H_2O)_6^{+3}$.

It seemed that the weak resonance (line width of 140–150 gauss), which was observed for the solutions of small acid concentration and for the solution containing the dinuclear species, was due to the presence of a small amount of $Cr(H_2O)_6^{+3}$. However, $Cr(H_2O)_6^{+3}$ could not be recovered from these solutions by cation

exchange (Dowex 50W–12X eluted with 0.1 M lanthanum perchlorate in 1 M $HClO_4$).

A series of measurements was made in order to evaluate whether the decreased spin intensity which occurred when the acid concentration exceeded 1 M was due to increased ionic strength, to complex formation involving nitrate or perchlorate ions, or to undissociated acids. Solutions of 0.04 M chromic nitrate were prepared with $Mg(ClO_4)_2$ in $HClO_4$ and $Ca(NO_3)_2$ in HNO_3 in the acid range 3.3 to 10^{-3} M, so that ionic strength[8] was 10, equivalent to that at 10 M acid assuming complete acid dissociation. The results of the determinations of Σ for $Ca(NO_3)_2$ are presented in Fig. 1 by the "X" points. With the addition of $Ca(NO_3)_2$ to the most concentrated acid solution the $[NO_3^-] = 7.7$ M, assuming complete dissociation of HNO_3. No significant decrease of Σ was produced by addition of these salts. When the nitrate ion concentration was further increased by addition of 10 M $Ca(NO_3)_2$ to a solution of 0.04 M Cr(III) nitrate in 1 M HNO_3 no significant change in spin intensity occurred; the results of line width measurements are plotted in Fig. 3 for the $HClO_4$ and HNO_3 solutions. No change in the e.s.r. properties over a period of three months could be detected for these solutions.

The possibility was considered that the reduction of spin intensity of concentrated nitric acid solutions was due to oxidation of Cr(III). However, no oxidized species were found in these solutions by adding a known amount of ferrous sulfate and titrating with permanganate. The effect of the NO_2 impurity in 15 M HNO_3 on spin intensity was determined by comparison of the e.s.r. of Cr(III) nitrate in colorless nitric acid and in deeply orange nitric acid, and the spin intensities were found not to be significantly different.

The optical absorption spectra of Cr(III) solutions were measured in order to determine whether the species present in concentrated acid solution could be identified. For the two visible bands centered approximately at 4150 and 5800 Å., the data on wave length of the peaks and molar extinction coefficients, ϵ, are listed in Table II for nitric and perchloric acid solutions. The spectral data reported[6] for $Cr(H_2O)_6^{+3}$ and the dinuclear species are also included for comparison.

TABLE II

EFFECT OF ACID CONCENTRATION ON SPECTRUM OF Cr(III) IN $HClO_4$ AND HNO_3 SOLUTIONS

−log [acid]	4100 band λ (Å.)	ϵ (l. cm.$^{-1}$ mole^{-1})	5800 band λ (Å.)	ϵ (l. cm.$^{-1}$ mole^{-1})
$HClO_4$ −1.0	4100	15.5	5800	13.1
0	4070	15.5	5750	12.8
2	4060	15.5	5780	12.8
3	4070	16.8	5780	13.1
4	4120	19.8	5800	14.5
4.75	4150	23	5800	16.8
HNO_3 −1.33	Cut-off		5825	24.7
−1.2	4110	19.5	5760	17.6
0.65	4050	15.1	5730	12.8
Dinuclear[a]	4180	22	5820	18.9
$Cr(H_2O)_6^{+3}$ [a]	4080	15.6	5740	13.4

[a] Reference 6.

Discussion

The hexaaquo chromic complex, $Cr(H_2O)_6^{+3}$, is as-

(8) Ionic strength computed from expression, $\mu = \frac{1}{2}\Sigma C_i n_i^2$.

sumed to be the species in solution in the pH range 0 to 3 which gives rise to the maximum observed spin intensity of $\Sigma = 100$ (Fig. 1). The line width of this resonance, 150 gauss, is in agreement with that reported by Hayes.[1] The value of 210 gauss found by McGarvey[2] for solutions of $KCr(SO_4)_2$ may be higher because he studied higher concentrations of Cr(III). Also, we have found that the line width of Cr(III) is greater for the sulfate than for the nitrate or perchlorate.

The reduction of spin intensity which occurred at pH values greater than 3 when 0.05 M alkali was used to adjust pH suggests an equilibrium with a pK of about 4. This is also the value for the first acid hydrolysis of $Cr(H_2O)_6^{+3}$, and therefore it is reasonable to assume that the reduction of spin intensity results from the hydrolysis. Among the hydrolysis products which may be present are the species $Cr(H_2O)_5OH^{+2}$, $Cr(H_2O)_4(OH)_2^{+1}$, and dinuclear or polynuclear species including olated or oxolated complexes. The complexes $Cr(H_2O)_5OH^{+2}$ and $Cr(H_2O)_4(OH)_2^{+1}$ do not account for the observed decrease in spin intensity because they react rapidly with acid,[9] and the spin intensity increased very slowly when acid was added to a solution at pH 4.75. On the other hand, these complexes may contribute to the observed resonance.

There is strong evidence that a dinuclear or polynuclear species is responsible for the decreased spin intensity observed in weakly acidic solutions or when concentrated alkali was added to Cr(III) solutions. The low spin intensity ($\Sigma = 7$) of solutions containing predominantly dinuclear species, prepared by reaction of oxygen and Cr(II), supports this view. Also the optical spectrum of a Cr(III) perchlorate solution at pH 4.75 strongly resembled that of the dinuclear species (Table II). Furthermore, upon storage at 20° an approximately equal rate of increase of spin intensity of the 140 gauss line was observed for the dinuclear solution (at pH 1) and for the Cr(III) solution at pH 4.75 made acid to pH 1; this rate is very slow as reported for the dissociation of the dinuclear complex.[7] Finally, the abrupt decrease of spin intensity which occurred upon addition of concentrated alkali (Fig. 1) is also attributed to a nucleation process which may be expected to proceed more rapidly at higher values of pH and temperature, conditions which prevail locally upon addition of the alkali. The properties of such solutions have been shown to depend upon the method of addition of alkali.[10]

Several different types of polynuclear Cr(III) species have been postulated,[6,7,9,11] and the e.s.r. results also suggest the existence of more than one type. For example, two such species may be inferred from the e.s.r. of the solution of the dinuclear complex prepared by reaction between O_2 and Cr(II) (Fig. 2). First, the narrow line where $\Delta h = 140$ gauss and $\Sigma = 7$ is probably due to $Cr(H_2O)_6^{+3}$ which was incompletely converted during the oxidation–reduction reaction or which resulted from dissociation upon storage. One polynuclear species is believed responsible for the "missing" spin intensity, $\Sigma \sim 85$, and the missing spin intensity is due either to a very broad (and hence undetectable) resonance or to a complex in which spin

pairing has occurred. Another polynuclear species is probably responsible for the observed broad resonance of $\Delta h = 700$ gauss and $\Sigma \sim 8$.

The e.s.r. measurements further suggest that the type of polynuclear species depends upon their mode of preparation. The species responsible for the low spin intensity upon addition of alkali to a Cr(III) solution evidently forms within minutes at room temperature. In contrast, the polynuclear species previously studied are formed in appreciable amount only after long aging or boiling the solution for at least 10 min. and frequently for many hours.[6,7,9,11] Application of e.s.r. may be useful to identify the various possible types of polynuclear species.

The decreased spin intensity which occurs in the concentrated acid solutions is not due to an ionic strength effect or to an inner complex with nitrate or perchlorate ions, because the addition of large quantities of $Mg(ClO_4)_2$ or $Ca(NO_3)_2$ did not decrease the spin intensity. Furthermore, there is no evidence for the existence of complexes containing coördinated nitrate.[11] It was also shown that the effect was not a result of impurities in nitric acid, or to reduction in the concentration of Cr(III) by nitric acid oxidation. The decrease in spin intensity seems to correlate with the concentration of undissociated acid.

The results of the optical spectra suggest that a dinuclear species is formed in the strong acid solutions (Table II). Polynucleation, which results in formation of a molecule of water and a proton for each ol-type bridge, will occur in solutions of concentrated undissociated acid if the reaction between the undissociated acid and water is favored over the reaction which reverses polynucleation due to sufficiently high activities of protons and water. This explanation, similar to that forwarded by Hall and Eyring[11] to explain the greater facility for oxygen bridge formation of Cr(III) in the presence of ethanol, would account for the greater effect on spin intensity of nitric acid which, at a given concentration, is much less dissociated than perchloric acid.[12] A non-specific solvent effect may contribute to our observed change of extinction coefficient, but probably would not account for the wave length shift since a shift had not been observed previously[13] nor would it explain the pronounced decrease of spin intensity.

To the extent that spin pairing occurs the results of the reduction of spin intensity can be accounted for. In this connection Mulay[14] observed that the magnetic moment of Cr(III) in chromic perchlorate solutions corresponds to the theoretical value (spin-only) up to pH 3 and at higher pH values decreases about 15%, which corresponds to a pairing of less than one spin per Cr(III). However, Mulay reports[15] no significant difference between the magnetic susceptibility of $Cr(H_2O)_6^{+3}$ and the dinuclear species (prepared according to Ardon and Plane[9]), which argues against the presence of this type of dinuclear species in his solutions

(9) M. Ardon and R. A. Plane, J. Am. Chem. Soc., **81**, 3197 (1959).

(10) H. W. Kohlschutter, Angew. Chem., **49**, 865 (1936).

(11) H. T. Hall and H. Eyring, J. Am. Chem. Soc., **72**, 782 (1950).

(12) O. Redlich, E. K. Holt, and J. Bigeleisen, ibid., **66**, 13 (1944): O. Redlich and J. Bigeleisen, ibid., **65**, 1883 (1943); G. C. Hood, O. Redlich, and C. A. Reilly, J. Chem. Phys., **22**, 2067 (1954).

(13) E. L. King, M. J. M. Woods, and H. S. Gates, J. Am. Chem. Soc., **80**, 5015 (1958).

(14) L. N. Mulay, American Chemical Society, 140th National Meeting, September 1961.

(15) L. N. Mulay, in "Advances in the Chemistry of the Coördination Compounds," S. Kirschner, The Macmillan Co., New York, N. Y., 1961, p. 532.

at pH > 3 for which he observed reduction of magnetic moment. There appears to be a discrepancy between Mulay's observations and ours. We observe similar e.s.r. properties for the dinuclear species and for the species present in weakly acidic solutions, e.g., pH 4.75, and differences are attributed principally to dissociation of the latter upon aging. A comparison of the magnetic susceptibility and e.s.r. properties of these solutions, taking into consideration possible changes upon aging, will perhaps clarify the question of whether more than one dinuclear species is involved.

It is unnecessary to postulate spin pairing for some Cr(III) complexes and we have observed no spin resonance for aqueous solutions of Cr(III) acetate, oxalate, and ethylenediaminetetraacetic acid in which spin pairing probably does not occur. Two relaxation processes may contribute to the substantial line broadening and hence to the undetectability of the resonance of the polynuclear Cr(III) complex. The first is due to the anisotropy of the ligand field, resulting in zero-field splitting of the ground state, as discussed by McGarvey.[2] Also, Hayes[1] has attributed the broad resonances in two Cr(III) complexes (unspecified) to distortion of the octahedral configuration. A second relaxation process may arise from orbital interactions between the Cr(III) ions via the oxygen bridge. The latter mechanism has been proposed to explain spin pairing in crystalline basic rhodo complexes.[16,17] The relative contributions of each of the two relaxation processes will depend upon the molecular configuration of the complex, the presence and number of -ol and -oxo bridges affixed to a Cr(III) ion, and the extent of polynucleation.

There is evidence of second coördination interaction from the results of line width. For example, upon increasing the concentration of nitric acid, the line width passed through a minimum of about 140 gauss and then increased to 310 gauss; for perchloric acid solutions the line width decreased in the same acid concentration as nitric acid but remained at a low value of 115 gauss (Table I and Fig. 3). This behavior is interpreted as evidence of a second coördination interaction (outer-sphere) with the hexaaquo ion. The anions NO_3^- or ClO_4^- present in these solutions are believed to orient about the Cr(III) at positions corresponding to the center of the faces of the octahedron. As the anion concentration is increased, the electric field about Cr(III) due to this outer-sphere coördination becomes more symmetrical and results in a

reduction in line width. However, as the nitric acid concentration exceeds 3 M ($-\log [HNO_3] = -0.5$), the line width of the observable resonance increases because protons in solution tend to interact with the outer-sphere coördinated NO_3^- to form undissociated HNO_3. This results in a fluctuation of the electric field about the Cr(III) at a frequency[18] approaching the microwave frequency, and provides a relaxation process adequate to broaden the line to 310 gauss. In perchloric acid solutions the concentration of undissociated $HClO_4$ is not adequate to provide this relaxation process; however, it is adequate to reduce spin intensity slightly, presumably by formation of a polynuclear complex.

The line width also depends upon the type of anion associated with chromium in the salt used to prepare the solutions. With solutions of pH $\geq$ 0.5 and of comparable Cr(III) concentrations, the line width was greater for NO_3^- than ClO_4^- (Table I and Fig. 3), and in preliminary work the line width was even greater for SO_4^{-2} solutions, obtained from $Cr_2(SO_4)_3\cdot16H_2O$. Typical values of line width observed for 0.04 M chromic salt solutions at pH 1 are 140, 155, and 180 gauss for ClO_4^-, NO_3^-, and SO_4^{-2}, respectively. This broadening suggests a second coördination effect which depends upon the electric field about Cr(III) as affected by the charge distribution on the anion.

Evidence of another type of second coördination interaction appears from a preliminary study made of the effect of non-paramagnetic salts on the line width of Cr(III). The results (Fig. 3) show that for a given molar concentration of the two salts, the line width was increased significantly more by $Ca(NO_3)_2$ than by $Mg(ClO_4)_2$. The additional line broadening in the presence of these salts is due principally to the effect of the metal cation, since comparable concentrations of NO_3^- and ClO_4^- provided by the corresponding acids did not provide such broad lines. The mechanism of line broadening here is postulated to be due to ion-pair formation between the cations Ca^{+2} and Mg^{+2} and the anions in the second coördination sphere.

(16) A. Earnshaw and J. Lewis, *J. Chem. Soc.*, 396 (1961).

(17) W. K. Wilmarth, H. Graff, and S. T. Gustin, *J. Am. Chem. Soc.*, **78**, 2683 (1956).

(18) M. Eigen, *Discussions Faraday Soc.*, **17**, 194 (1954).

ELECTRONIC SPECTRA AND STRUCTURE OF α- AND β-NAPHTHOL[1]

BY KICHISUKE NISHIMOTO

Department of Chemistry, Faculty of Science, Osaka City University, Sumiyoshi-ku, Osaka, Japan

Received November 16, 1962

A semi-empirical theory based on ASMO-CI method is applied to the electronic structure of α- and β-naphthol. The calculated results are, on the whole, in satisfactory agreement with the experiment. In spite of the absence of D_{2h} symmetry, the nature of the electronic spectrum of α-naphthol is well correlated with that of naphthalene. The effect of substitution at the α-position of naphthalene causes a substantial red shift in the B_{2u} band, and a rather small shift in the B_{3u}^- band. On the other hand, in β-naphthol the characteristics of the naphthalene spectra are completely destroyed, because the configuration corresponding to naphthalene's B_{2u} band interacts strongly with the configuration corresponding to the B_{3u}^- band. Our calculation can also explain other molecular properties, such as hydrogen bond forming power and dipole moments in the various electronic states.

Introduction

In a previous paper,[2] a semi-empirical theory was applied to the calculation of the electronic spectra and electronic structure of phenol to study the effect of substitution on the parent hydrocarbon. According to the calculation, the polarizations of the excited states of benzene are still preserved by the substitution of a hydroxyl group, accompanied with the considerable change in the intensities and frequencies of the electronic transitions. Our next interest is to study the effect of substitution on the electronic structure of a more complicated molecule, such as naphthalene.

In naphthalene derivatives, the effect of substitution on the electronic spectra of naphthalene depends considerably upon the position where the substituent is attached to the molecule.[3-7] The near-ultraviolet spectra of naphthalene have three absorption maxima.[8] The high frequency band in the region of 45,300 cm.$^{-1}$ has the greatest intensity; the medium intensity band in the 36,400 cm.$^{-1}$ region is assigned to B_{2u}; and the weakest band near 32,200 cm.$^{-1}$, to B_{3-u}. The substitution at the α-position of naphthalene causes a substantial red shift in B_{2u} band and a rather small shift in B_{3u}^- band. On the other hand, the substitution at the β-position leads apparently to slight blue shift in the former band and a rather larger red shift in the latter. The band intensities have a tendency to increase as band shifts to the red.

Recently, a theoretical study has been made by Baba and Suzuki[5] to elucidate this interesting phenomenon. The electronic spectra of α-naphthol were successfully explained by their theory, but those of β-naphthol were still open to question. In this paper, a semi-empirical calculation will be applied to the electronic spectra of naphthols to make clear this problem. In addition, some molecular properties, such as hydrogen bond forming power and dipole moments in the various electronic states, of naphthols will be discussed.

The Calculation

In this paper the following approximations are used: First, differential overlap is neglected.[9,10] Second, the

integrals over atomic orbitals (AO) are estimated by a semi-empirical procedure. Finally, the core structures of the naphthols are assumed as indicated in Fig. 1. All nearest carbon–carbon distances are assumed to be 1.390 Å., and the carbon–oxygen distance to be 1.460 Å. These values of interatomic distances are the same as those used in the study of phenol.[2]

The procedure of calculation is as follows

(1) We set up Hückel MO's, using the same parameters as those of phenol.[2] The Hückel MO's, ψ_i, are expressed in the form

$$\psi_i = \sum_\mu C_{i\mu}\phi_\mu \tag{1}$$

where ϕ_μ is the μ-th $2p\pi$ AO and $C_{i\mu}$ is the coefficient to be determined by variational procedure. A secular equation of the eleventh degree must be solved.

(2) The configurational wave functions, χ_i, are built up as antisymmetrized products of these MO's. The wave function and the corresponding energy for the ground state are denoted by χ_0 and H_0, respectively. The excited configuration which arises from the excitation of an electron from an occupied orbital ψ_i to a vacant orbital $\psi_{k'}$ is written as $^1\chi_{i-k'}$ or $^3\chi_{i-k'}$, where the superscripts 1 and 3 are associated with singlet and triplet, respectively. The configurational energy $H_{i-k'}$ associated with $\chi_{i-k'}$ is calculated by two methods described in our previous papers. One (Method I) is given in ref. 2. Another one (Method II) is found in ref. 11. Electron repulsion integrals are calculated by the methods proposed in our previous papers.[2,12]

(3) The electronic state functions, Ψ_a's, are represented by the linear combinations of configurational wave functions

$$\Psi_a = \sum_i d_{ai}\chi_i \tag{2}$$

where d_{ai} is a coefficient to be determined by the variation principle. In the present calculation, the excited state functions are expressed by the linear combinations of the four lowest singly excited configurations, $\chi_{1-1'}$, $\chi_{2-2'}$, $\chi_{1-2'}$, and $\chi_{2-1'}$. We must therefore solve a secular determinant of fourth degree, in which the matrix elements have the form

$$H_{i-k', j-1'} = \int \chi_{i-k'}H\chi_{j-1'}\, dv \tag{3}$$

where H is the total Hamiltonian for the system.

(1) Presented in part at the Symposium on Electronic States in Molecules held by the Chem. Soc. of Japan, Oct., 1961.

(2) K. Nishimoto and R. Fujishiro, *Bull. Chem. Soc. Japan*, **31**, 1036 (1958).

(3) R. A. Friedel and M. Orchin, "Ultraviolet Spectra of Aromatic Compounds," John Wiley and Sons, New York, N. Y., 1951.

(4) D. M. Hercules and L. B. Rogers, *Spectrochim. Acta*, 393 (1959).

(5) H. Baba and S. Suzuki, *Bull. Chem. Soc. Japan*, **34**, 82 (1961).

(6) C. J. P. Spruit, *Rec. trav. chim.*, **68**, 309 (1949).

(7) C. Daglish, *J. Am. Chem. Soc.*, **72**, 4859 (1950).

(8) American Petroleum Institute Research Project 44, Ultraviolet Spectral Data, Serial No. 640, 654.

(9) R. Pariser and R. G. Parr, *J. Chem. Phys.*, **21**, 466, 767 (1953).

(10) R. Pariser, *ibid.*, **24**, 250 (1956).

(11) K. Nishimoto and R. Fujishiro, *Bull. Chem. Soc. Japan*, **35**, 905 (1962).

(12) K. Nishimoto and N. Mataga, *Z. physik. Chem.* (Frankfurt), **12**, 335 (1957).
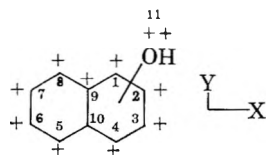
Fig. 1.—Core structure of naphthols.
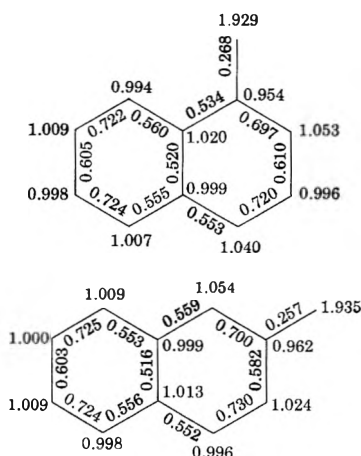
Fig. 2.—Molecular diagrams of naphthols.

In the case of naphthalene, the secular determinant is factorized into two determinants of second degree, owing to the D_{2h} symmetry of the molecule. Moreover, the configurations $\chi_{1-2'}$ and $\chi_{2-1'}$, which both belong to the irreducible representation B_{3u}, are degenerate. The allowed electronic state energies, $E(B_{3u})$, associated with the B_{3u} electronic states can be calculated, therefore, as

$$^1E_{\pm}(B_{3u}) = -1.6180\beta_{cc} + 1.183 \pm 0.810 + H_0 \text{ e.v.}$$
(4)

hence

$$^1H_{1-2'} = {}^1H_{2-1'} = -1.6180\beta_{cc} + 1.183 + H_0 \text{ e.v.}$$

$$^1H_{1-2', 2-1'} = 0.810 \text{ e.v.}$$

where β_{cc} means a core integral associated with the nearest carbon–carbon neighbors. As pointed out by many workers,[13-15] the weakest band of naphthalene near 32,200 cm.$^{-1}$ should be assigned to $^1B_{3u}{}^-$ species. Using this frequency, we obtain the semi-empirically estimated value of β_{cc} as

$$\beta_{cc} = -2.236 \text{ e.v.}$$

Calculated integrals over MO's employing our parameters are collected in the Appendix.

(4) According to the method described by Mulliken and Rieke,[16] the oscillator strength, f, associated with the transition of an electron from Ψ_0 to Ψ_a is calculated, that is

$$f = 1.085 + 10^{11}\hat{\nu}_{0a} (D_{0a})^2$$
(5)

where $\hat{\nu}_{0a}$ is the frequency of the transition in cm.$^{-1}$. D_{0a} is the transition moment vector defined by

$$D_{0a} = \int \Psi_0 \sum_i e_i r_i \Psi_a \, dv$$
(6)

(13) J. A. Pople, Proc. Phys. Soc. (London), **A68**, 81 (1955).

(14) R. Lefebvre and C. Moser, J. Chem. Soc., 1557 (1956).

(15) N. Mataga, K. Nishimoto, and S. Mataga, Bull. Chem. Soc. Japan, **32**, 395 (1959).

(16) R. S. Mulliken and C. A. Rieke, Rep. Progr. Phys., **8**, 231 (1941).

where e_i and r_i are the charge and the position vector of the i-th particle, respectively.

Discussion

(A) **Hückel MO's and Molecular Diagrams.**— Calculated orbital energies and the corresponding MO's are given in the Appendix. As a result of the calculation, eleven orthonormalized MO's for the molecule are obtained. In the ground state of the molecule, the lowest six are doubly occupied by electrons. As pointed out in our previous paper,[17] the molecular diagrams of the aromatic derivatives can be found from their vacant orbital sets, so that the lowest excited states of the molecule can also be established from their set and a few occupied highest orbitals.[11] Calculated molecular diagrams of the naphthols are shown in Fig. 2. In the Appendix, only the orbitals to be used in the present calculation are collected. Referring to the Appendix one finds that the effect of substitution on the naphthalene MO's depends entirely upon the position where the substituent is attached to the molecule. That is, α-substitution exerts the most potential influence upon ψ_1 and $\psi_{1'}$ of naphthalene, whereas ψ_2 and $\psi_{2'}$ are not affected at all. On the other hand, β-substitution has the greatest effect on ψ_1 and $\psi_{1'}$ and on ψ_2 and $\psi_{2'}$ to some extent. This situation may be essentially connected with the various spectral changes caused by the substitution.

(B) **Near-Ultraviolet Absorption Spectra.**—A main purpose of this paper is to elucidate the nature of the two lowest excited states of the naphthols. The nature of the excited state can be characterized by its transition moment vector given by eq. 6, which determines the direction of polarization of the transition. The calculated results for the naphthols are summarized in Tables I and II. For comparison, the results for naphthalene are also shown in the tables. Calculated electronic state functions are summarized in the Appendix. As indicated in Table I, the calculated spectra of the naphthols are in satisfactory agreement with experimental values in general. From the present calculation we can draw the following conclusions:

(1) In spite of the absence of D_{2h} symmetry, the direction of polarization of the electronic transitions in α-naphthol coincides practically with that of naphthalene. That is, substitution at the α-position creates no interaction between the $^1B_{2u}$ and $^1B_{3u}$ bands.

(2) In the case of β-naphthol, the characteristics of the naphthalene spectrum are completely destroyed, because the configuration corresponding to naphthalene's $^1B_{2u}$ species interacts strongly with the configuration corresponding to its $^1B_{3u}{}^-$ species. As indicated in the Appendix, the excited state corresponding to the intensified band in the region of 30,470 cm.$^{-1}$ contains the configuration corresponding to the $^1B_{2u}$ species to the extent of about 30%, and is polarized approximately in the direction perpendicular to the oxygen–carbon bond. The excited state near 36,600 cm.$^{-1}$ includes the configuration corresponding to the $^1B_{3u}{}^-$ species to the extent of about 35%.

(3) The Ψ_2 state of β-naphthol is polarized in nearly the same direction as the Ψ_1 state. Therefore, it will be difficult to assign the excited states of β-naphthol on

(17) K. Nishimoto and R. Fujishiro, Bull. Chem. Soc. Japan, **32**, 699 (1959).

TABLE I

EXCITED STATES OF NAPHTHALENE AND NAPHTHOLS (SINGLET STATES)

Excited state	Excitation energy (e.v.) Calcd.		Obsd.[a]	Oscillator strength (f) Calcd.		Obsd.[a]	Polarization[b] Calcd.	
	Method I	Method II		Method I	Method II		Method I	Method II
				Naphthalene				
Ψ_1	(3.991)		3.99	0		0.002	x	
Ψ_2	4.260		4.51	0.294		0.11	y	
Ψ_3	5.611		5.62	2.097		1.70	x	
Ψ_4	6.165		...	0.810		...	y	
				α-Naphthol				
Ψ_1	3.928	3.881	3.86	0.013	0.019	0.016	x	x
Ψ_2	4.010	3.933	4.29	0.332	0.332	0.102	y	y
Ψ_3	5.490	5.456	5.80	1.949	1.928	0.892	x	x
Ψ_4	6.169	6.165	...	0.802	0.792	...	y	y
				β-Naphthol				
Ψ_1	3.880	3.732	3.78	0.066	0.076	0.0211	116°	126°
Ψ_2	4.233	4.195	4.54	0.195	0.174	0.0811	104°	111°
Ψ_3	5.414	5.310	5.53	2.037	1.945	1.06	190°	195°
Ψ_4	5.896	5.745	...	0.763	0.802	...	76°	115°

[a] Reference 5. [b] Numerical value gives an angle between the transition moment vector and x-axis of the molecule.

TABLE II

CALCULATED EXCITATION ENERGIES OF NAPHTHALENE AND NAPHTHOLS (E.V.) (TRIPLET STATES)

Excited state	Naphthalene	α-Naphthol Method I	Method II	β-Naphthol Method I	Method II
Ψ_1	2.277	2.197	2.117	2.273	2.232
Ψ_2	3.487	3.388	3.327	3.388	3.243
Ψ_3	3.991	3.955	3.928	3.792	3.627
Ψ_4	4.076	4.080	4.084	4.200	4.109

the basis of polarization experiments of the absorption spectra.

Theoretical results (1) and (2) conform to the experiment published by Padhye, et al.[18] They reported that for both α- and β-naphthalene derivatives the longest wave length absorption bands were polarized perpendicular to the direction of the dipole moment vectors of the molecules. Our calculation indicates that both α- and β-naphthol have the dipole moments nearly along their oxygen–carbon bond axes, as shown in Table III.

TABLE III

CALCULATED π-MOMENTS OF NAPHTHOLS IN VARIOUS ELECTRONIC STATES[a] (IN D)

Electronic state	α-Naphthol Method I	Method II	β-Naphthol Method I	Method II
Ψ_0	1.34 (91°)		1.19 (13°)	
Ψ_1	2.71 (21°)	2.75 (22°)	3.75 (21°)	3.83 (20°)
Ψ_2	3.70 (18°)	3.71 (18°)	3.31 (33°)	3.31 (33°)

[a] Numerical value in parentheses gives an angle between the dipole moment vector and the x-axis of molecule.

(C) Dipole Moment.—We usually partition the total dipole moment of a molecule into a σ-moment and a π-moment. Unfortunately, we have no precise information about the σ-moments of the naphthols. At first approximation, it is, however, reasonable to assume the σ-moment of a molecule is independent of the π-electronic states. Here we calculate only the π-moments of the naphthols in the various electronic states. The calculated results at the Franck–Condon states are shown in Table III.

It is interesting to note the π-moments in Ψ_1 states which correspond to the fluorescent states. The π-

(18) M. R. Padhye, N. R. Rao, and K. Venkataraman, Proc. Indian Acad. Sci., **38A**, 297 (1953).

moment of α-naphthol in Ψ_1 state is in a direction nearly perpendicular to that of the ground state, whereas the π-moment of β-naphthol in that state is in a direction approximately parallel to that in the ground state. If we assume that the dipole moments of excited states in the equilibrium configurations are the same as those of the Franck–Condon states, the solvent arrangement around an α-naphthol molecule in the ground state should be inadequate to maximum interaction between the solvent molecules and an α-naphthol molecule in the fluorescent state. Therefore after the excitation, rearrangement of solvent molecules would take place in this case. The excited states of the naphthols are calculated to polar than their ground states. Therefore the polar effect of the solvent[19] leads to the red shifts.

(D) Hydrogen Bond Forming Power.—It is a well known fact that the hydrogen bond forming power of a X–H bond increases with increase in the electronegativity of the X atom.[20,21] The electronegativity of oxygen atom in the naphthols should increase with decrease in π-electron density on the atom. The calculated net charges on the oxygen atoms for various electronic states of the naphthols are given in Table IV.

TABLE IV

CALCULATED NET CHARGE ON SUBSTITUENT (IN UNITS OF e)

Electronic state	α-Naphthol Method I	Method II	β-Naphthol Method I	Method II
Ψ_0	+0.071		+0.065	
Ψ_1	+0.113	+0.116	+0.142	+0.146
Ψ_2	+0.135	+0.135	+0.120	+0.127

Based on this table, we can expect the following consequences: (1) In the ground states, the hydrogen bond forming power of α-naphthol should be almost the same as that of β-naphthol. This expectation agrees with the experiment of Baba and Suzuki.[22] (2) The naphthols should form stronger hydrogen

(19) E. G. McRae, J. Phys. Chem., **61**, 562 (1957).

(20) L. Pauling, "The Nature of Chemical Bond," 2nd Ed., Cornell Univ. Press, Ithaca, New York, 1940.

(21) G. G. Pimentel and A. L. McClellan, "The Hydrogen Bond," W. H. Freeman and Co., San Francisco, Calif., 1960.

(22) H. Baba and S. Suzuki, J. Phys., Chem. **35**, 1118 (1961).

bonds when they are in the fluorescent state than when they are in the ground state. The experiments reported by Weller[23] and Mataga, et al.,[24] support this conclusion. Present calculation indicates that in the fluorescent state β-naphthol forms stronger hydrogen bonds than α-naphthol.

We hope to discuss the reactivity of aromatic hydroxyl derivatives in a separate paper, using various reaction indices.

Acknowledgment.—The author wishes to thank Professor R. Fujishiro and Dr. N. Mataga for valuable discussion.

Appendix. Numerical Results for Naphthalene and Naphthols

TABLE IA[a]
HÜCKEL MO'S FOR α-NAPHTHOL

i	k_i	μ = 1	2	3	4	5	6	7	8	9	10	11
5'	-2.3152	0.3208	-0.2383	0.2307	-0.2959	-0.2959	0.2238	-0.2250	0.2973	-0.4633	0.4544	-0.0589
4'	-1.6302	0.2945	-0.4279	0.4030	-0.2290	0.2835	-0.4325	0.4217	-0.2548	-0.0062	-0.0296	-0.0658
3'	-1.3310	0.4047	-0.1407	-0.2172	0.4300	0.3706	-0.1379	-0.1869	0.3866	-0.3277	-0.3351	-0.1000
2'	-1.0000	0	-0.4083	0.4083	0	0	0.4083	-0.4083	0	0.4083	-0.4083	0
1'	-0.6583	0.4118	-0.2165	-0.2692	0.3938	-0.4393	0.2792	0.2556	-0.4474	0.0390	0.0100	-0.1336
1	0.5265	0.4047	0.3391	-0.2262	-0.4582	0.3725	0.2112	-0.2614	-0.3427	0.0777	-0.0150	-0.2910
2	1.0000	0	0.4083	0.4083	0	0	0.4083	0.4083	0	-0.4083	-0.4083	0

TABLE IIA[a]
HÜCKEL MO'S FOR β-NAPHTHOL

i	k_i	μ = 1	2	3	4	5	6	7	8	9	10	11
5'	-2.3102	0.3064	-0.2496	0.2382	-0.3005	-0.2951	0.2254	-0.2258	0.2961	-0.4583	0.4562	0.0459
4'	-1.6486	0.2665	-0.4579	0.4172	-0.2298	0.2744	-0.4140	0.4081	-0.2589	0.0186	-0.0383	0.1019
3'	-1.3082	0.3856	-0.1793	-0.1823	0.4177	0.3839	-0.1380	-0.2033	0.4040	-0.3252	-0.3642	0.0446
2'	-1.0318	-0.0302	-0.3983	0.3641	0.0227	-0.0523	0.4415	-0.4031	-0.0255	0.4294	-0.3874	0.1101
1'	-0.6324	0.3981	-0.2374	-0.3024	0.4286	-0.4340	0.2431	0.2803	-0.4204	-0.0144	0.0313	0.0776
1	0.5731	0.4789	0.3087	-0.1389	-0.3883	0.3745	0.2982	-0.2036	-0.4149	-0.0342	-0.0836	-0.2330
2	0.8815	0.0288	0.3198	0.5067	0.1268	-0.1805	0.2358	0.3883	0.1066	-0.2944	-0.3947	-0.3622

[a] μ and i label the AO's and the MO's according to eq. 1. Columns 3–13 list the AO coefficient $C_{i\mu}$. The orbital energy, ϵ_i, associated with ψ_i is given by $\epsilon_i = \alpha + k_i\beta$.

TABLE IIIA
CALCULATED INTERCONFIGURATIONAL MATRIX ELEMENTS FOR SINGLET STATES (IN E.V.)

	Naphthalene	α-Naphthol Method I	Method II	β-Naphthol Method I	Method II
$^1H_{1-1',1-1'} - H_0$	4.365	4.109	4.028	4.232	4.180
$^1H_{1-1',2-2'}$	-0.434	-0.451	-0.451	-0.441	-0.441
$^1H_{1-1',1-2'}$	0	0.001	-0.001	0.072	0.068
$^1H_{1-1',2-1'}$	0	0.001	0.001	-0.138	-0.228
$^1H_{2-2',2-2'} - H_0$	6.060	6.070	6.070	5.777	5.608
$^1H_{2-2',1-2'}$	0	0.004	0.004	0.036	-0.054
$^1H_{2-2',2-1'}$	0	0.000	0.000	-0.083	-0.087
$^1H_{1-2',1-2'} - H_0$	4.801	4.575	4.498	4.773	4.715
$^1H_{1-2',2-1'}$	0.810	0.769	0.769	0.703	0.703
$^1H_{2-1',2-1'} - H_0$	4.801	4.843	4.839	4.641	4.478

TABLE IVA
EXCITED STATE WAVE FUNCTIONS FOR NAPHTHALENE AND NAPHTHOLS (SINGLET STATES)

Excitation energy (e.v.)	Excited state wave function

Naphthalene

3.991	$\Psi_1 = 0.7071(\chi_{1-2'} - \chi_{2-1'})$
4.260	$\Psi_2 = 0.9721\chi_{1-2'} + 0.2345\chi_{2-2'}$
5.611	$\Psi_3 = 0.7071(\chi_{1-2'} + \chi_{2-1'})$
6.165	$\Psi_4 = 0.2345\chi_{1-1'} - 0.9721\chi_{2-2'}$

α-Naphthol (Method I)

3.928	$\Psi_1 = 0.7654\chi_{1-2'} - 0.6435\chi_{2-1'}$
4.010	$\Psi_2 = 0.9768\chi_{1-1'} + 0.2140\chi_{2-2'}$
5.490	$\Psi_3 = 0.6435\chi_{1-2'} + 0.7654\chi_{2-1'}$
6.169	$\Psi_4 = 0.2140\chi_{1-1'} - 0.9768\chi_{2-2'}$

α-Naphthol (Method II)

3.881	$\Psi_1 = 0.7799\chi_{1-2'} - 0.6259\chi_{2-1'}$
3.933	$\Psi_2 = 0.9784\chi_{1-1'} + 0.2066\chi_{2-2'}$
5.456	$\Psi_3 = 0.6259\chi_{1-2'} + 0.7799\chi_{2-1'}$
6.165	$\Psi_4 = 0.2066\chi_{1-1'} - 0.9784\chi_{2-2'}$

Excitation energy (e.v.)	Excited state wave function

β-Naphthol (Method I)

3.880	$\Psi_1 = 0.5580\chi_{1-1'} + 0.1667\chi_{2-2'} + 0.6129\chi_{2-1'} - 0.5340\chi_{1-2'}$
4.233	$\Psi_2 = 0.7886\chi_{1-1'} + 0.1936\chi_{2-2'} - 0.4097\chi_{2-1'} + 0.4156\chi_{1-2'}$
5.414	$\Psi_3 = 0.0441\chi_{1-1'} + 0.0275\chi_{2-2'} + 0.6745\chi_{2-1'} + 0.7365\chi_{1-2'}$
5.896	$\Psi_4 = 0.2528\chi_{1-1'} - 0.9662\chi_{2-2'} + 0.0475\chi_{2-1'} + 0.0149\chi_{1-2'}$

β-Naphthol (Method II)

3.732	$\Psi_1 = 0.5510\chi_{1-1'} + 0.1455\chi_{2-2'} + 0.6540\chi_{2-1'} - 0.4976\chi_{1-2'}$
4.195	$\Psi_2 = 0.7808\chi_{1-1'} + 0.2370\chi_{2-2'} - 0.3797\chi_{2-1'} + 0.4359\chi_{1-2'}$
5.310	$\Psi_3 = 0.1346\chi_{1-1'} + 0.1238\chi_{2-2'} + 0.6481\chi_{2-1'} + 0.7392\chi_{1-2'}$
5.745	$\Psi_4 = 0.2604\chi_{1-1'} - 0.9520\chi_{2-2'} + 0.0934\chi_{2-1'} + 0.1310\chi_{1-2'}$

(23) A. Weller, Z. Elektrochem., 56, 662 (1952).
(24) N. Mataga, Y. Kaifu, and M. Koizumi, Bull. Chem. Soc. Japan, 29, 115 (1956).

COÖRDINATION COMPOUNDS. VI. DETERMINATION OF THERMODYNAMIC DATA FOR ACETYLACETONE IN MIXED SOLVENTS

By Philip S. Gentile, Michael Cefola,

Department of Chemistry, Fordham University, Bronx 58, N. Y.

and Alfred V. Celiano

Department of Chemistry, Seton Hall University, South Orange, N. J.

Thermodynamic data for acetylacetone have been determined in mixed solvents by standard methods. On the basis of a mathematical model, functions of the stability constant at constant temperature and constant dielectric constant have been defined and evaluated. The thermodynamic data obtained by both methods are in good agreement.

Introduction

In a previous communication[1] the thermodynamic dissociation constants of acetylacetone in two and three component solvent systems at 25° were reported. It was found that these dissociation constants were related linearly to the reciprocal of the dielectric constant of the solvent and were independent of the nature of the solvent in the dielectric range 80–30. In this paper the dissociation constants of the same ligand in methanol–water and dioxane–water mixtures are reported, as well as a method of evaluating the standard free energy, enthalpy, and entropy of ionization.

It has long been recognized that the effect of temperature on the ionization constants of acids is not only related to the energy required to break the chemical bond and the energy of solvation but is also related to the work done in separating the solvated charged products to their equilibrium distances. The latter electrical work was considered by Born[2] on the basis of elementary electrostatic theory.

Another approach may be found in the Bjerrum–Fuoss ion-pair model.[3,4] Denison and Ramsey[5] have simplified the original concept by assuming that two oppositely charged ions exist either in contact as an associated ion-pair, or at such a large distance apart that the coulombic force between them is negligible.

In evaluating the thermodynamic quantities associated with ionization, both the chemical and electrical factors must be taken into account. Much of the work done up to the present has involved the determination of ionization constants in a single solvent or solvent system. The variation of pK with temperature is then employed to calculate the total ΔF^0, ΔH^0, and ΔS^0 and the electrical parts of these quantities are then calculated on the basis of a theoretical model, more or less complex. Such an approach has been considered invalid by Harned and Owen,[6] primarily because the solvent in a system containing ions is not a uniform medium of unvarying dielectric constant. It is considered in this paper, however, that if the dissociation constants were determined at various temperatures and in mixed solvents of varying dielectric constants, then both the chemical and electrical thermodynamic

quantities might be determined without consideration of a particular model, *i.e.*, on the basis of a purely mathematical separation of these terms.

Such information would be useful for the correlation of data already present in the literature on the stability of chelates, where choice of solvent system so often depends on the solubility of chelating agents, metal salts, and the resulting chelate compound.

The approach outlined above, *i.e.*, the purely mathematical separation of thermodynamic quantities, is based on two assumptions; first, that the change in solvent composition does not appreciably change the basic strength of the mixed solvent employed in this study. This assumption seems warranted when we consider the linear relationship between pK and 1/D at a given temperature. Second, that as solvent mixtures vary there is no preferential solvation by the solvent present in excess. Fuoss[7] considered the same problem in dealing with the purely electrostatic factors affecting ion pair formation and concluded that constancy of solvation appears to be a safe assumption.

Experimental

The experimental procedure and the data obtained at 25° for acetylacetone in various mixed solvents have been described elsewhere.[1] Additional data for the same systems for use in this paper were obtained at 0 and 40°.

Results

The solvents used were methanol–water and dioxane–water mixtures because activity coefficients are given[8] only for these particular mixtures at three different temperatures (0, 25, and 40°).

Representative values of pK for acetylacetone (pK = $-\log K_a$), which will be used in the discussions are listed in Table I, and these plus additional pK values are plotted against 1/D in Fig. 1. The equations for the linear portions of the lines in Fig. 1, *i.e.*, from values of 1/D between 0.01 and 0.03, determined by the method of least squares are

$$\text{p}K = 104.7(1/D) + 7.89 \text{ at } 0° \qquad (1)$$

$$\text{p}K = 77.0(1/D) + 7.99 \text{ at } 25° \qquad (2)$$

$$\text{p}K = 67.9(1/D) + 8.00 \text{ at } 40° \qquad (3)$$

These equations represent the experimental data within ±0.02 log unit. All subsequent discussion is limited to the region of linearity between pK and 1/D. The

(1) P. S. Gentile, M. Cefola, and A. V. Celiano, *J. Phys. Chem.*, **67**, 1083 (1963).

(2) M. Born, *Z. Physik*, **1**, 45 (1920).

(3) J. Bjerrum, *Kgl. Danske Videnskab Selskab.*, **7**, No. 9 (1926).

(4) R. M. Fuoss and C. A. Kraus, *J. Am. Chem. Soc.*, **55**, 1019 (1933).

(5) J. T. Denison and J. B. Ramsey, *ibid.*, **77**, 2615 (1955).

(6) H. S. Harned and B. B. Owen, "The Physical Chemistry of Electrolytic Solutions," Reinhold Publ. Corp., New York, N. Y., 1958.

(7) R. M. Fuoss and C. A. Kraus, *J. Am. Chem. Soc.*, **79**, 3304 (1957).

(8) Reference 6, p. 726 ff.

<div align="center">

Table I

pK of Acetylacetone in Various Solvent Systems

</div>

System no.	Solvent system	Weight, %	0°		25°		40°	
			1/D	pK	1/D	pK	1/D	pK
I	Water	0.00	0.01135	9.07	0.1273	8.97	0.01367	8.90
II	Methanol–Water	35.98	.01440	9.40	.01623	9.22	.01757	9.15
III	Methanol–Water	45.66	.01557	9.51	.01763	9.38	.01904	9.27
IV	Methanol–Water	54.15	.01669	9.62	.01897	9.47	.02061	9.40
V	Methanol–Water	65.82	.01862	9.82	.02118	9.63	.02320	9.57
VI	Dioxane–Water	21.36	.01481	9.41	.01672	9.25	.02631	9.75
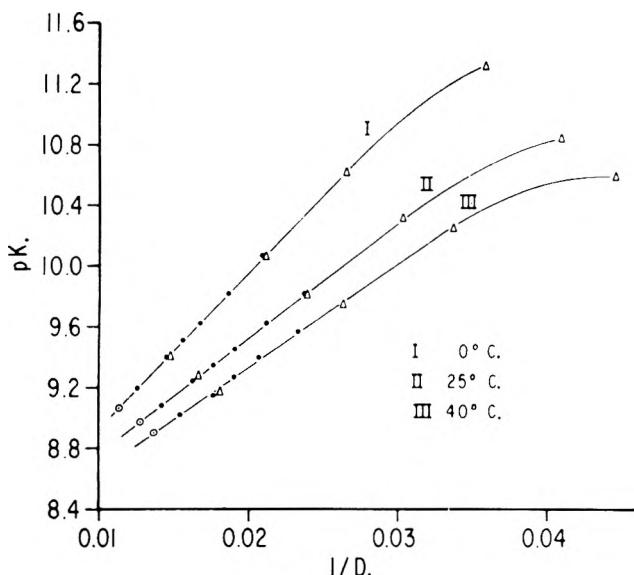
Fig. 1.—pK values plotted against $1/D$: ○, water; ●, methanol–water; △, dioxane–water.

method of least squares was utilized in all calculations. All thermodynamic values are for the process of ionization.

Evaluation of ΔH^0.—A plot of pK vs. $1/T$ for a particular solvent system (I, II, etc.), the classical method for evaluation of ΔH^0, proves to be non-linear between 0 and 40°.

For an exact calculation of ΔH^0, one may employ the treatment of Douglas and Crockford.[9] The resulting equation is

$$\Delta H_T^0 = \frac{RT_1T_2 \ln (K_2/K_1)}{T_2 - T_1} \qquad (4)$$

Walde[10] has developed an equation to include higher powers of T. Thus, it was shown that whether ΔH^0 is a linear, quadratic, cubic, or quartic function of the temperature, equation 4 can still be used to calculate ΔH^0 from the values of K and the two corresponding temperatures.

The data in Table I were treated in this manner. Values of pK at 0 and 40° were employed since any other combination would decrease the accuracy of the calculated ΔH^0. The ΔH_T^0 values calculated from eq. 4 are those for the temperature, $T = 292.3°K.$, and are listed in Table IV. They are reliable only to ±400 cal. mole^{-1}. Since ΔH^0 is only known at this temperature with any degree of accuracy, it is impossible to calculate ΔS^0, since ΔF^0 can only be calculated if the constants in Walde's equation are known. This approach can, therefore, only yield a limited amount of thermodynamic data for an individual solvent system.

(9) T. B. Douglas and H. D. Crockford, J. Am. Chem. Soc., 57, 97 (1935).
(10) A. W. Walde, J. Phys. Chem., 43, 431 (1939).

At first glance one might suspect that ΔH^0 is a function of temperature because ΔC_p is a function of temperature. However, according to Pitzer[11] and Everett and Wynne-Jones[12] ΔC_p is independent of temperature for many acid dissociation reactions. If such be the case for the dissociation of acetylacetone, one might then explain the observed non-linearity of pK vs. $1/T$ solely on the basis of the temperature coefficient of the dielectric constant and its effect on pK. This, however, is equivalent to stating that in the present case pK is a function of temperature and dielectric constant and is independent of the nature of the solvent system. Therefore

$$pK = f(D,T) \qquad (5)$$

$$dpK = \left(\frac{\partial pK}{\partial D}\right)_T dD + \left(\frac{\partial pK}{\partial T}\right)_D dT \qquad (6)$$

Dividing through by dT

$$\frac{dpK}{dT} = \left(\frac{\partial pK}{\partial D}\right)_T \frac{dD}{dT} + \left(\frac{\partial pK}{\partial T}\right)_D \qquad (7)$$

is obtained. But

$$\frac{dpK}{dT} = \frac{-\Delta H^0}{2.303RT^2} \qquad (8)$$

where ΔH^0 is the standard enthalpy change and R is the gas constant. Equation 8 therefore becomes

$$-\Delta H^0 = 2.303RT^2 \left(\frac{\partial pK}{\partial D}\right)_T \frac{dD}{dT} +$$
$$2.303RT^2 \left(\frac{\partial pK}{\partial T}\right)_D \qquad (9)$$

An examination of eq. 9, which results from a purely mathematical treatment and is independent of any theory, reveals that the ΔH^0 of a reaction consists of two heat terms, ΔQ_T^0 and ΔQ_D^0, which we shall define as

$$\Delta Q_T^0 \equiv 2.303RT^2 \left(\frac{\partial pK}{\partial D}\right)_T \frac{dD}{dT} \qquad (10)$$

and

$$\Delta Q_D^0 \equiv 2.303RT^2 \left(\frac{\partial pK}{\partial T}\right)_D \qquad (11)$$

and

$$\Delta H^0 = \Delta Q_T^0 + \Delta Q_D^0 \qquad (12)$$

It is, therefore, possible to evaluate the influence of temperature or dielectric constant alone on the heat of

(11) K. S. Pitzer, J. Am. Chem. Soc., 59, 2365 (1937).
(12) D. H. Everett and W. F. K. Wynne-Jones, Trans. Faraday Soc., 35, 1380 (1939).

reaction, by employing eq. 10 and 11, the sum of which should give the same value for ΔH^0, as that determined by Crockford's method.

Evaluation of ΔQ_T^0.—For a given temperature and given solvent system, D and dD/dT can be obtained from the data of Åkerlöf and Short.[13,14] The expression $(\partial pK/\partial D)_T$ is obtained by differentiation of equations similar to eq. 1, 2, and 3, with respect to D. The derivative will be $-c/D^2$, where c is the appropriate coefficient of $1/D$. ΔQ_T^0 approaches zero as D approaches ∞.

Evaluation of ΔQ_D^0.—Since the term $(\partial pK/\partial T)_D$ in eq. 11 is a function of the dielectric constant, it is necessary to calculate isodielectric pK values of acetylacetone at several different temperatures. This may be done visually by drawing a vertical line at any desired dielectric in Fig. 1 and evaluating pK values from curves I, II, and III. A more accurate method, and the one used in these calculations, is to solve eq. 1, 2, and 3 for the pK value by substituting the same dielectric constants into the three equations. Representative pK values are listed in Table II and are plotted against $1/T$ in Fig. 2. From the calculated slopes of these lines $(\partial pK/\partial T)_D$ may be evaluated and substituted into eq. 11 to give the ΔQ_D^0 values. Since in Fig. 2 pK is linear with respect to $1/T$ for isodielectric solvents, it follows that ΔQ_D^0, the heat of the reaction at a given dielectric constant, is invariant over the temperature range 0 to 40°. This implies that ΔC_p is in fact independent of temperature over the same temperature range, as predicted earlier.

TABLE II

pK VALUES OF ACETYLACETONE AT REPRESENTATIVE DIELECTRIC CONSTANTS

$1/D$	pK (0°)	pK (25°)	pK (40°)
0.01135	9.08	8.87	8.77
.01440	9.40	9.10	8.98
.01557	9.52	9.19	9.06
.01669	9.64	9.28	9.13
.01862	9.84	9.42	9.26
.01481	9.44	9.13	9.01
.02109	10.10	9.62	9.43

ΔQ_D^0 and its Relationship to Dielectric Constant.— Values for ΔQ_D were calculated as described above and are themselves linearly related to $1/D$. The equation for this line which is independent of temperature for 0 to 40° was determined to be

$$\Delta Q_D^0 = 3.684 \times 10^5 \left(\frac{1}{D}\right) - 1155 \text{ cal./mole} \quad (13)$$

The value -1155 cal. per mole is a ΔQ_D^0 extrapolated to infinite dielectric constant and is the value of the standard enthalpy change at infinite dielectric constant, since $\Delta Q_T^0 \to 0$ when $D \to \infty$. This experimental fact supports the assumption of Baughan[15] and Gurney[16] that $(\Delta H^0)_{D = \infty}$ is independent of temperature.

Table III lists the ΔQ_D^0, ΔQ_T^0, and ΔH^0, calculated from eq. 9, for solvent systems I through VI. These values are reliable to ± 100 cal. mole^{-1}.

Reliability of ΔH^0 Values.—In order to determine the reliability of ΔH^0 values calculated by eq. 12 one must

(13) G. Åkerlöf, *J. Am. Chem. Soc.*, **54**, 4125 (1932).
(14) G. Åkerlöf and O. A. Short, *ibid.*, **58**, 1241 (1936).
(15) E. C. Baughan, *J. Chem. Phys.*, **6**, 499 (1938).
(16) R. W. Gurney, *ibid.*, **7**, 951 (1939).
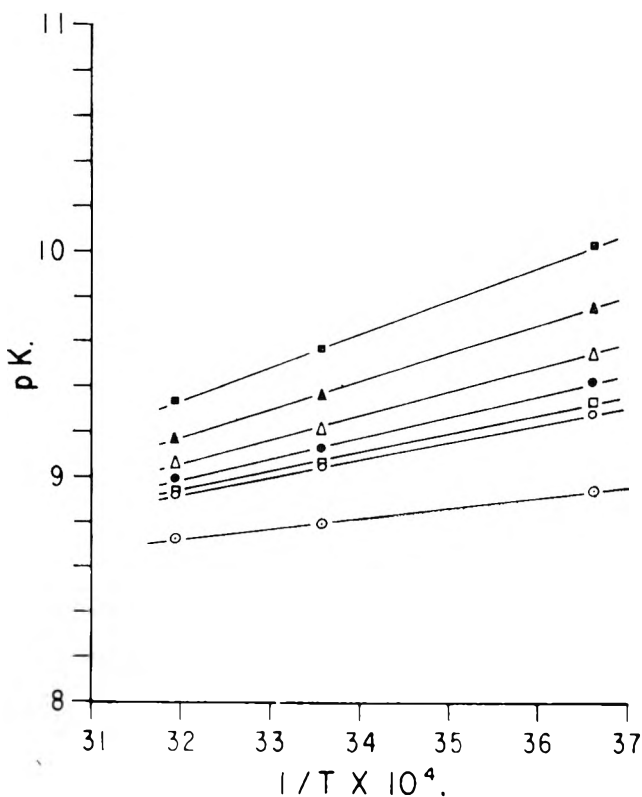
Fig. 2.—Isodielectric pK values plotted against $1/T$ (values given are those for $1/D$): ⊖, 0.01135; ○, 0.01440; ●, 0.01557; △, 0.01669; ▲, 0.01862; □, 0.01481; ■, 0.02109.

compare the values determined by Crockford's method, *i.e.*, ΔH_T^0 at 292.3°K., with those determined by eq. 12. In order to accomplish this, ΔQ_T^0 and ΔQ_D^0 must be evaluated for the solvent systems studied and for the temperature 292.3°K. Since ΔQ_D^0 is independent of temperature, this term may be evaluated directly from eq. 13, using the dielectric constant of solvent systems I–VI at 292.3°K.

Q_T^0 is evaluated by constructing a graph of pK *vs.* $1/D$ for 292.3°K. This curve was not determined experimentally but was evaluated from the isodielectric curves in Fig. 2 at the appropriate temperature. The resulting curve of pK *vs.* $1/D$ is linear, as those in Fig. 1, and obeys the equation

$$pK = 84.7 \left(\frac{1}{D}\right) + 7.96, \text{ at } T = 292.3°K. \quad (14)$$

ΔQ_T^0 was then calculated from eq. 10.

The values of ΔH^0 determined by the two methods are compared in Table IV. The excellent correlation between ΔH^0 values determined by the two methods lends support to the feasibility of separating ΔH^0 into the terms ΔQ_D^0 and ΔQ_T^0.

Evaluation of ΔS^0.—ΔF^0 is related to the pK by the equation

$$\Delta F^0 = 2.303RT \, pK \quad (15)$$

Since it has been shown that pK is linearly related to $1/D$ (eq. 1–3), ΔF^0 is similarly related to $1/D$. The equations for ΔF^0 are

$$\Delta F^0_{273.2} = \left[130.8 \left(\frac{1}{D}\right) + 9.87 \right] \times 10^3 \text{ cal. mole}^{-1}$$

$$\quad (16)$$

TABLE III
Standard Heat of Ionization of Acetylacetone (kcal. mole^{-1})

Solvent system	0°			25°			40°		
	ΔQ_T^0	ΔQ_D^0	ΔH^0	ΔQ_T^0	ΔQ_D^0	ΔH^0	ΔQ_T^0	ΔQ_D^0	ΔH^0
I	−1.9	3.0	1.1	−1.8	3.5	1.7	−1.9	3.9	2.0
II	−2.3	4.2	1.9	−2.5	4.8	2.3	−2.9	5.3	2.4
III	−2.5	4.6	2.1	−2.8	5.3	2.5	−3.2	5.8	2.6
IV	−2.8	5.0	2.2	−3.2	5.8	2.6	−3.7	6.4	2.7
V	−3.3	5.7	2.4	−3.7	6.7	3.0	−4.3	7.4	3.1
VI	−2.4	4.3	1.9	−2.7	5.0	2.3	−3.1	5.5	2.4

TABLE IV
Standard Heat of Ionization, ΔH (kcal. $^{-1}$) of Acetylacetone at 19.1°

Solvent	$1/D$	ΔQ_T^0	ΔQ_D^0	$(\Delta H^0)^a$	$(\Delta H^0)^b$
I	0.01240	−1.9	3.4	1.5	1.5
II	.01575	−2.5	4.6	2.1	2.1
III	.01706	−2.8	5.1	2.3	2.3
IV	.01841	−3.2	5.6	2.4	2.4
V	.02053	−3.7	6.4	2.7	2.5
VI	.01623	−2.7	4.8	2.1	2.1

^{a} Calculated from eq. 9. ^{b} Calculated from Crockford's method.

$$-\Delta S^0 = \frac{d(\Delta F)}{dT} = \left[\frac{\partial(\Delta F^0)}{\partial T}\right]_D + \left[\frac{\partial(\Delta F^0)}{\partial D}\right]_T \frac{dD}{dT}$$
(21)

We define

$$\Delta S_D^0 = -\left[\frac{\partial(\Delta F^0)}{\partial T}\right]_D \tag{22}$$

$$\Delta S_T^0 = -\left[\frac{\partial(\Delta F^0)}{\partial D}\right]_T dD \tag{23}$$

The evaluation of ΔS_D^0 and ΔS_T^0 is completely analogous to that of ΔQ_D^0 and ΔQ_T^0. ΔS_D^0 is independent of

TABLE V
Standard Entropies (cal. mole^{-1} deg.$^{-1}$) of Ionization of Acetylacetone

Solvent system	0°			25°			40°		
	ΔS_T^0	ΔS_D^0	ΔS^0_{total}	ΔS_T^0	ΔS_D^0	ΔS^0_{total}	ΔS_T^0	ΔS_D^0	ΔS^0_{total}
I	− 6.9	−30.4	−37.3	− 6.1	−29.3	−35.4	− 6.1	−28.5	−34.6
II	− 8.3	−27.8	−36.1	− 8.5	−26.3	−34.8	− 9.2	−25.1	−34.3
III	− 9.2	−26.8	−36.0	− 9.5	−25.1	−34.6	−10.2	−23.9	−34.1
IV	−10.4	−25.9	−36.3	−10.8	−23.9	−34.7	−11.8	−22.5	−34.3
V	−11.9	−24.2	−36.1	−12.4	−22.1	−34.5	−13.8	−20.3	−34.1
VI	− 8.8	−27.5	−36.3	− 9.0	−25.9	−34.9	− 9.8	−24.7	−34.5

$$\Delta F^0_{298.2} = \left[105.1\left(\frac{1}{D}\right) + 10.9\right] \times 10^3 \text{ cal. mole}^{-1}$$
(17)

$$\Delta F^0_{313.2} = \left[97.4\left(\frac{1}{D}\right) + 11.5\right] \times 10^3 \text{ cal. mole}^{-1}$$
(18)

ΔS^0 may be calculated from the temperature coefficient of ΔF^0

$$-\Delta S^0 = \frac{d(\Delta F^0)}{dT} \tag{19}$$

Just as ΔH^0 may be separated into two terms, ΔQ_D^0 and ΔQ_T^0, so ΔS^0 may be treated in the same fashion

$$\Delta F^0 = f(T, D) \tag{20}$$

temperature and bears a linear relationship to the reciprocal of the dielectric constant, expressed by the equation

$$\Delta S_D^0 = 851.7\left(\frac{1}{D}\right) - 40.1 \text{ e.u.} \tag{24}$$

It is evident that extrapolation to infinite dielectric constant yields a value of $(\Delta S_D^0)_{\to\infty} = -40.1$ e.u. Table V is a list of ΔS_D^0, ΔS_T^0, and ΔS^0_{total} for the solvent systems studied. ΔS_D^0 and ΔS_T^0 are reliable to ±0.2 e.u., rendering ΔS^0_{total} reliable to ±0.4 e.u.

It is of interest to note that the standard entropy of ionization of acetylacetone is constant at a given temperature being independent of solvent system and dielectric constant.

PREPARATION AND PROPERTIES OF Sr₂FeO₃F

By Francis Galasso and Wilda Darby

United Aircraft Corporation, Research Laboratories, East Hartford, Connecticut

Extension of the study carried out previously on K₂NbO₃F has resulted in the preparation of Sr₂FeO₃F, another oxyfluoride with the K₂NiF₄ structure. Electrical measurements show that it is a p-type semiconductor which exhibits a Seebeck coefficient of 22.7 μv./deg. A comparison of its c/a ratio and anisotropic thermal expansion with some ternary oxides having the K₂NiF₄ structure gives some indication that the fluoride ions may be preferentially located at the apical positions in the anion octahedra surrounding the small cations.

Introduction

Recently the preparation of K₂NbO₃F, an oxyfluoride with the tetragonal K₂NiF₄ structure, was reported by this Laboratory.[1] Unlike ternary oxides and fluorides reported as having this structure, K₂NbO₃F exhibited a larger c/a ratio than the 3.41 value which satisfies the geometrical conditions of touching spheres. A study of the properties of this compound leads to the conclusion that the elongated "c" axis may be caused by the fluoride ions being located preferentially in the apical positions of the octahedra surrounding the small metal ions in the unit cell (Fig. 1).

Continuation of this research has resulted in the preparation of another oxyfluoride Sr₂FeO₃F, with the K₂NiF₄ structure. The purpose of this report is to present the structural data and properties of this new oxyfluoride, in comparison with K₂NiF₄-type strontium ternary oxides and with K₂NbO₃F.

Experimental Investigations

Preparation of Sr₂FeO₃F.—Powder samples of Sr₂FeO₃F were prepared by heating mixtures of strontium oxide or carbonate, strontium fluoride, and ferric oxide in a 3:1:1 molar ratio in a platinum crucible in air. After firing at 1000°, the sample was reground, pressed into a pellet, and sintered at 1200°. The compound dissociated when heated above 1200°.

Chemical Analysis.—Samples of the compound were analyzed by Ledoux and Company of Teaneck, New Jersey, for strontium, iron, and fluorine content. *Anal.* Calcd. for Sr₂FeO₃F: Sr, 58.79; Fe, 18.74; F, 6.37. Found: Sr, 57.60; Fe, 18.80; F, 6.78.

X-Ray Analysis.—Powder X-ray diffraction photographs were taken of the Sr₂FeO₃F samples using a 114.6 mm. diameter Philips powder camera with copper Kα radiation. Since these X-ray patterns were similar to that of K₂NbO₃F, one of them was indexed on the basis of the body-centered tetragonal unit cell with $a = 3.84$ and $c = 12.98$ Å. Atomic positions were adopted from space group I-4/mmm (No. 139), as originally determined for K₂NiF₄; however, the fluoride ions were considered to be randomly distributed only in the $0,0,z_X$, etc., positions: two iron ions at $0,0,0$ and $^1/_2,^1/_2,^1/_2$; four strontium ions at $0,0,z_{Sr}$; $0,0,\bar{z}_{Sr}$; $^1/_2,^1/_2,^1/_2 + z_{Sr}$; $^1/_2,^1/_2,^1/_2 - z_{Sr}$; two fluoride and two oxygen ions at $0,0,z_X$; $0,0,\bar{z}_X$; $^1/_2,^1/_2,^1/_2 + z_X$; $^1/_2,^1/_2,^1/_2 - z_X$; and four oxygen ions at $^1/_2,0,0$; $0,^1/_2,0$; $0,^1/_2,^1/_2$; $^1/_2,0,^1/_2$. The relative intensities of the powder diffraction lines were calculated with $z_{Sr} = 0.352$ and $z_X = 0.151$, neglecting temperature and absorption effects. Table I presents calculated and observed indexing and relative intensity data.

Property Measurements. Thermal Expansion.—High temperature X-ray diffractometer tracings were made between 25 and 1000° using a Norelco diffractometer with an attached Tem-Pres heater. Figure 2 presents the "a" and "c" axes expansion for Sr₂FeO₃F and Sr₂TiO₄. It was found that the thermal coefficient of expansion is nearly the same in the "a" and "c" directions for Sr₂TiO₄ and in the "a" direction for Sr₂FeO₃F, while expansion along "c" in the oxyfluoride is greater. For Sr₂FeO₃F $α_a = 1.45 \times 10^{-5}$, $α_c = 1.93 \times 10^{-5}$, and for Sr₂TiO₄ $α_a = 1.46 \times 10^{-5}$, $α_c = 1.44 \times 10^{-5}$.

Electrical Resistance.—Pellets for resistance measurements were prepared by compacting powdered Sr₂FeO₃F in a 1.59 cm.

die under 710 kg./cm.² followed by sintering at 1000°. The pellets were sanded to flatten the surface and then plated with evaporated gold.

TABLE I
POWDER X-RAY DIFFRACTION DATA FOR Sr₂FeO₃F

hkl	sin² θ (obsd.)	sin² θ (calcd.)	I (obsd.)	I (calcd.)
002	0.0141	0.0141	5	6
101	.0440	.0438	5	4
004	.0566	.0565	5	6
103	.0719	.0720	100	100
110	.0805	.0805	100	90
112	.0944	.0946	<5	2
006	.1280	.1271	25	19
105		.1285		6
114	.1372	.1370	25	22
200	.1611	.1610	40	36
116	.2075	.2076	10ᵃ	19
107	.2131	.2132	5	4
204	.2175	.2175	5	4
008	.2258	.2259	<5	3
213	.2333	.2330	40	36
206	.2885	.2881	20	17
118	.3065	.3064	<5	3
220	.3219	.3220	10	10
217	.3743	.3742	5	4
208	.3863	.3869	5	5
303	.3943	.3940	8	7
310	.4031	.4025	10	10
1, 1, 10	.4353	.4335	5	4
226	.4493	.4491	8	8
314	.4589	.4590	5	5

ᵃ Diffuse.

Direct current resistance *vs.* temperature measurements were obtained using a two-probe method. The sample, which was inserted in a holder consisting of platinum electrodes, platinum lead-in wires, and a thermocouple in contact with one of the electrodes, was placed in a heater. The voltage was monitored using a Kintel microvolt-ammeter, Model 203A-R. Current through the pellet was measured with a Keithley 410 micro-microammeter. A plot of log ρ *vs.* 1/T for two samples (Fig. 3) shows that Sr₂FeO₃F exhibits typical semiconductor behavior over the temperature range of 25 to 319°. While the curves are not superimposable, they are parallel. The difference in the resistivities of the two samples can probably be attributed to slight variances in preparation conditions of the polycrystalline pellets. From an analysis of these curves using the equation $ρ = ρ_0 \exp(E/kT)$, it was found that the conduction activation energy for Sr₂FeO₃F equls 0.18 e.v.

Seebeck E.m.f.—Seebeck e.m.f. *vs.* temperature data were obtained under vacuum on the same pellets as were used for resistance measurements. The sample was placed between copper electrodes surrounded by a radial heater. Holes were drilled through each electrode 0.025 cm. away from the sample face. Thermocouples were threaded through the holes and held in intimate contact with the electrode by a set screw. Quartz tubing was used to insulate the thermocouple wires inside the electrodes. Power was supplied to the heater by a Kahn & Co., Inc., KC-208 variable d.c. power supply. A Leeds & Northrup K3 potentiometer measured the e.m.f. using one arm of each

(1) F. Galasso and W. Darby, *J. Phys. Chem.*, **66**, 1318 (1962).
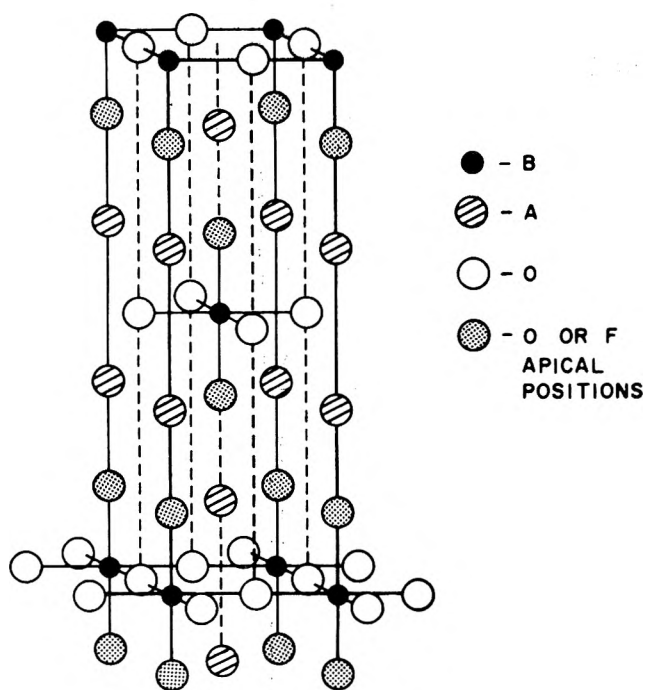
Fig. 1.—K_2NiF_4 structure.

Fig. 2.—Thermal expansion data—Sr_2FeO_3F and Sr_2TiO_4.

Fig. 3.—D.c. resistivity for Sr_2FeO_3F.

Fig. 4.—Seebeck e.m.f. for Sr_2FeO_3F.

thermocouple. Results indicate that Sr_2FeO_3F is a p-type material. A plot of Seebeck e.m.f. vs. ΔT (Fig. 4) shows a linear function and a Seebeck coefficient of 22.7 $\mu v./deg.$

TABLE II

LATTICE CONSTANTS FOR STRONTIUM COMPOUNDS WITH THE K_2NiF_4 STRUCTURE

	a (Å.)	c (Å.)	c/a	Ref.
Sr_2SnO_4	4.04	12.53	3.10	2
Sr_2TiO_4	3.88	12.60	3.25	3, 4
Sr_2MnO_4	3.79	12.43	3.28	5
Sr_2MoO_4	3.92	12.84	3.28	5
Sr_2RuO_4	3.87	12.74	3.29	6
Sr_2IrO_4	3.89	12.92	3.32	7
Sr_3RhO_4	3.85	12.90	3.35	6
Sr_2FeO_3F	3.84	12.98	3.38	

(2) R. Weiss and R. Faivre, Compt. rend., **248**, 106 (1959).

(3) S. N. Ruddlesden and P. Popper, Acta Cryst., **10**, 538 (1957).

(4) K. Lukaszewicz, Roczniki Chem., **33**, 239 (1959).

(5) D. Balz and K. Plieth, Z. Elektrochem., **59**, 6, 545 (1955).

(6) J. J. Randall and R. Ward, J. Am. Chem. Soc., **81**, 2629 (1959).

(7) J. J. Randall, L. Katz, and R. Ward, ibid., **79**, 266 (1957).

Discussion of Results

In Table II are listed the lattice parameters reported for the strontium K_2NiF_4-type compounds. It can be seen that the c/a ratio for Sr_2FeO_3F is largest and therefore approaches the ideal value of 3.41 as determined from the geometrical conditions of touching spheres more nearly than do the oxides. The fact that it does not exceed this value, as was found for K_2Nb-

O_3F, is reflected in its expansion coefficients; the rate of expansion in the "c" direction is only 1.3 times as large as that in the "a" while the K_2NbO_3F expansion in the "c" direction was more than twice that in the "a". However, it should be noted that there is a difference between the strontium titanium oxide and the strontium iron oxyfluoride expansion data. This, when coupled with the fact that Sr_2FeO_3F does exhibit a large c/a ratio, indicates that the fluoride ions may be preferentially located at the apical positions in the anion octahedra surrounding the iron ions.

The results of the electrical measurements show that Sr_2FeO_3F is a p-type semiconductor exhibiting a negative temperature coefficient of resistance from 25 to 319°. It is interesting that K_2NbO_3F also showed a drop in resistance with increasing temperature at low temperatures but at higher temperatures it exhibited a positive coefficient of resistance.[1] This difference in the resistance behavior of the two compounds in ceramic form may be caused by the more marked anisotropic behavior exhibited by K_2NbO_3F.

RARE EARTH OXIDE SYSTEMS. THE HYSTERESIS EFFECTS IN PRASEODYMIUM OXIDE[1]

By Paul A. Faeth[2] and Alan F. Clifford

Department of Chemistry, Purdue University, Lafayette, Indiana

Received November 21, 1962

The composition–pressure diagram of the Pr–O system has been studied between 10^{-5} and 150 mm. oxygen pressure using a quartz beam microbalance. The isotherms between 400 and 500° show hysteresis between $PrO_{1.80}$ and $PrO_{1.83}$ as the pressure varies. At 465° a hysteresis loop extends over the entire pressure range. Everett's theory of hysteresis is compared to the Pr–O isotherms at 465°. The seven theorems proposed by Everett are cited and discussed with reference to the Pr–O data. In general, the agreement between the properties of Everett's theoretical model of a domain system and the properties of the Pr–O system is good. Results of a preliminary study of the region between loop boundaries indicate that more than two domain states are present. The behavior of the praseodymium oxide system is thought to be a result of its being composed of domains of various stable compositions, $PrO_{1.83}$, $PrO_{1.80}$, etc. The domains change composition as a function of the oxygen pressure.

Introduction

During an investigation of the phase diagram of praseodymium oxide,[3] hysteresis effects were observed between adjacent, stable, non-stoichiometric compositions. The stable compositions are essentially the same ones that were observed by Eyring, *et al.*[3b] The hysteresis loops studied appear between 400 and 1000° and 10^{-5} to 150 mm. oxygen pressure. At 465° a rather broad hysteresis loop appears for the Pr–O system between $PrO_{1.80}$ and $PrO_{1.83}$ and exists over most of the pressure region investigated in this study. Other loops were observed at higher and lower temperatures but none was so broad or lent itself to investigation so conveniently as the loop at 465°. Most of the other hysteresis loops observed extended over only a 70–80 mm. pressure range; the loop at 465° extended about 150 mm.

Although several theories of hysteresis have been proposed, they are usually specific for certain processes (adsorption, magnetism, etc.). The subject in general is not well understood. By considering a collection of the different types of stimuli which produce hysteresis effects, Everett[4] arrived at a general theory of hysteresis based on the existence of domains; the domains are postulated to be small groups of atoms which react to certain stimuli (gas pressure, magnetic field, etc.) as a unit and which may exist in one of several different energy states. According to Everett's model[4a] each individual domain will exhibit a square hysteresis loop if the dependent property (composition, magnetization, etc.) is considered as a function of the independent property (gas pressure, magnetic field, etc.). According to Everett (in a simple situation) if a domain exists in an energy state I, and the magnitude of the independent variable (X) is increased, a critical value, X_u, will be approached; the domain will be converted from state I to a state II if X_u is exceeded. Furthermore, if a domain exists in state II and X is decreased, a critical value, X_l, will be approached, at which value the domain will be converted from state II to state I. The condition $X_u > X_l$ prevails.

In a real system it is reasonable to expect the existence of many domains. A typical hysteresis curve which is observed for the stimuli mentioned above is shown in Fig. 1. As a first approximation any point on the curve represents the additive contribution of domains which have the same critical values of X. The sigmoidal curve implies a distribution of values of X_u and X_l for the domains.

In the course of his work, Everett[4c] suggested seven theorems which should apply in general to most systems exhibiting hysteresis effects. The unmodified theory is limited since it stipulates that only two states are available to the domains and that the domains are independent. The case of dependent and independent domains has been treated by Enderby.[5] It is the purpose of this study to show the qualitative similarities

(1) (a) Presented in part at the 138th National Meeting of the American Chemical Society in New York City, N. Y., September, 1960. (b) This research was supported by the United States Air Force through the Air Force Office of Scientific Research of the Air Research and Development Command, under contract No. AF 18(603)-45. Reproduction in whole or in part is permitted for any purpose of the United States Government.

(2) Department of Chemical and Metallurgical Engineering, The University of Michigan, Ann Arbor, Michigan.

(3) (a) J. M. Honig, A. F. Clifford, and P. A. Faeth, *Inorg. Chem.*, in press; (b) R. E. Ferguson, E. D. Guth, and L. Eyring, *J. Am. Chem. Soc.*, **76**, 3890 (1954).

(4) (a) D. H. Everett and W. I. Whitton, *Trans. Faraday Soc.*, **48**, 749 (1952); (b) D. H. Everett and F. W. Smith, *ibid.*, **50**, 187 (1954); (c) D. H. Everett, *ibid.*, **50**, 1077 (1954); (d) *ibid.*, **51**, 1551 (1955).
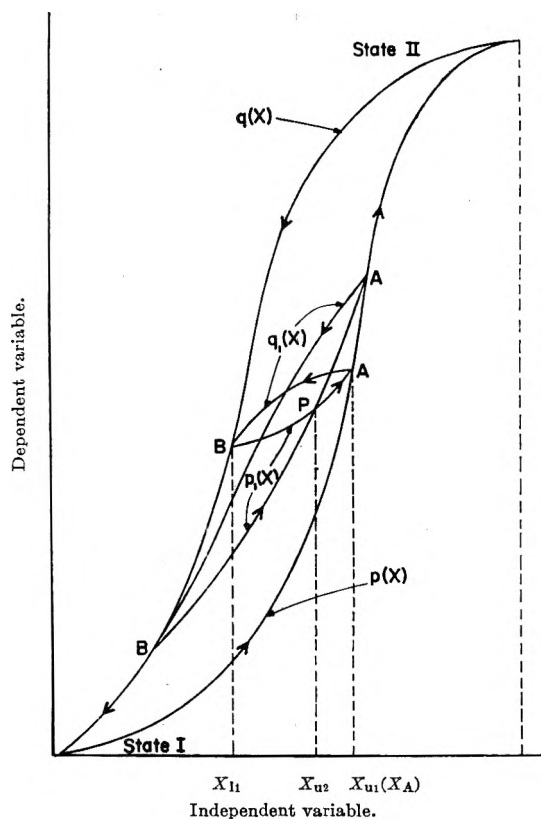
Fig. 1.—A typical hysteresis loop. The symbolism follows that proposed by Everett.
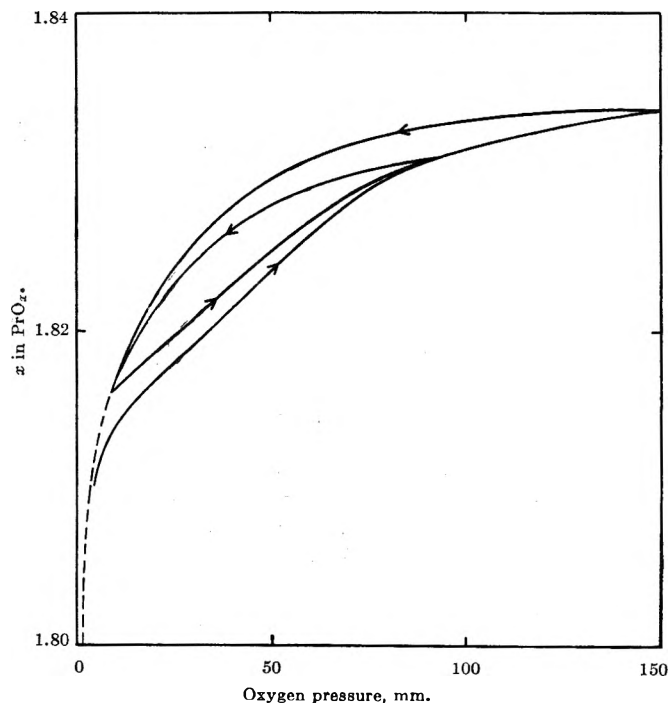
Fig. 2.—A Pr–O isotherm which illustrates theorems I and II.

between the properties of a theoretical system showing hysteresis as proposed by Everett and the experimental properties of the Pr–O system at 465°.

Experimental

The measurement of the changes in stoichiometry of the Pr–O system as a function of oxygen pressure at constant temperature was made using a quartz beam microbalance.[6] The

---

(5) (a) J. A. Enderby, *Trans. Faraday Soc.*, **51**, 835 (1955); (b) *ibid.*, **52**, 106 (1956).

(6) A. W. Czanderna and J. M. Honig, *Anal. Chem.*, **29**, 1206 (1957).

microbalance had a sensitivity of 0.05 μg. and a reproducibility of 0.1 μg. Approximately 50 mg. of praseodymium oxide (Pr_6O_{11}) was suspended from one arm of the balance in a small fused-silica bulb by using quartz fibers; a matching empty bulb was similarly suspended as a counterpoise. The balance was contained in a Pyrex glass envelope fitted with two fused silica extensions which surrounded the sample of praseodymium oxide and its counterweight. Furnaces were fitted around the fused silica extensions and provided a constant temperature. The oxygen pressure was measured and maintained using standard vacuum equipment.

The counterpoise side of the balance was equipped with an Alnico needle which was suspended from the balance into the field of an externally mounted solenoid. Changes in mass were determined by passing a current through the solenoid and observing the amount of current necessary to maintain the balance in a null position. The current passed through a standard resistance, the voltage drop across which was used as a measure of the mass changes. Mass changes of one microgram were considered to be the limit of practical mass resolution. The mass changes are illustrated in the figures as a function of oxygen pressure.

The criterion for equilibrium was established as that value of the mass which remained constant for one hour under the conditions of the experiment. It had been found in earlier, exploratory experiments that equilibrium was established in approximately ten minutes for experimental points which then were essentially unaltered after 15 hours. Plots of mass change *vs.* time were used to establish the equilibrium value of a particular set of conditions; frequently the equilibrium value of the mass oscillated a few micrograms about the mean value.

Praseodymium oxide (99.9%) was obtained from the Lindsay Chemical Company. The oxygen and nitrogen gases used in the experiments were obtained from the thermal decomposition of $KMnO_4$ and NaN_3, respectively.

Results and Discussion

It was decided to make a comparison between the properties of a set of Pr–O isotherms measured in the vicinity of 465° and the general properties of hysteresis systems proposed as theorems by Everett.

Appropriate portions of Everett's theorems will be cited and a comparison made with illustrations which were constructed from the data of an experimental study of the Pr–O system. No rigorous justification will be attempted at this time as to agreement or disagreement between the theorems and the experimental results. The symbolism cited by Everett in the theorems is illustrated in Fig. 1.

Theorem I.—"If the primary descending curves meet the descending boundary curve then the primary ascending curves will meet the ascending boundary curve; this behavior corresponds to a relatively narrow distribution of domain properties."

Theorem II.—"If all the primary descending curves converge on the lower intersection point of the main loop all the ascending curves will converge on the upper intersection point; this behavior corresponds to a wide distribution of domain properties."

Ordinarily one would not expect both of these theorems to hold for a specific example. Since Everett does not discuss a "medium sized" distribution, a corollary which considers the intermediate case may be in order. Figure 2 illustrates a distribution which may be described as being between the limits set by theorems I and II. A preliminary investigation of the internal region (see below) of the hysteresis loop of the Pr–O system at 465° suggests that several distributions are operating in this region. Each contributing member of the total loop may be thought of as a "narrow" distribution (theorem I). The combined effect of several narrow distributions appears to produce a

"wide" distribution of properties (theorem II) although not in the sense necessarily intended by Everett.

Theorem III.—"The slope of any descending scanning curve must always be less than that of the descending boundary curve at the same value of X; similarly that of any ascending scanning curve must be less than that of the ascending boundary curve at the same value of X. The slope of any scanning curve is zero at a reversal point."

Figures 2 and 3 serve to illustrate this theorem. The slopes of the primary curves are less than the respective boundary curves. The slope at the reversal point does not appear to be zero; however, there does appear to be a tendency for the descending primary curve to comply with this point of the theorem. In some instances the slope is negative, a fact which is not understood at this time. The effect has been observed also during a study of the rate of uptake of oxygen by PrO_x, and details will be reported in a later publication.

It should perhaps be mentioned that the theorems presented by Everett are related to the slopes of the curves for which the fraction of domains in state II was plotted vs. the external variable. In these terms the slope of any scanning curve is zero at a reversal point. However, any externally measured quantity (e.g., oxygen content in this case) is subject both to reversible and irreversible changes. The slope of a scanning curve at the reversal point is equal to the reversible part of the change (compare reference 4c, equation 8). This would explain perhaps why the slopes of the experimental curves at the reversal points are not zero.

Theorem IV.—"If the path of the system is reversed at A ($X = X_A$) and X is changed to X_B and back to X_A, then the system will return to A, it follows that any oscillation of X between given limits X_A and X_B will lead to a loop of constant shape and area independent of the position A in the loop."

In general the first part of this theorem applies to the Pr–O system and is illustrated by Fig. 2 and 3. Figure 3 shows that the second part of the theorem is not necessarily applicable. In this case the two sets of scanning curves obtained between the same pressure limits are quite different. The lower set exhibits a measurable loop but the upper set does not. It appears that scanning loop size is dependent upon the region of the main loop under investigation. It is possible, however, that there are regions where the second portion of the theorem would apply, but with the present knowledge of the system, these regions are difficult to isolate. Non-compliance with the theorem is to be expected in a system in which several domain states contribute to the hysteresis. Quinn and McIntosh[7] found the same general result with the adsorption of butane on porous Vycor glass. While Everett's theorem requires an equal area and the same shaped loops, the modification of Enderby[5] requires only equal areas; in any event neither of the proposals fits the Pr–O system under the conditions of the experiment.

Theorem V.—"If when the system returns to A as envisaged in theorem IV, X continues to increase, the system will move along the same curve as that which would have been followed if no loop had been traversed from A."

Theorem V is considered to apply to the Pr–O system

(7) H. W. Quinn and R. McIntosh, *Can. J. Chem.*, **35**, 745 (1957).
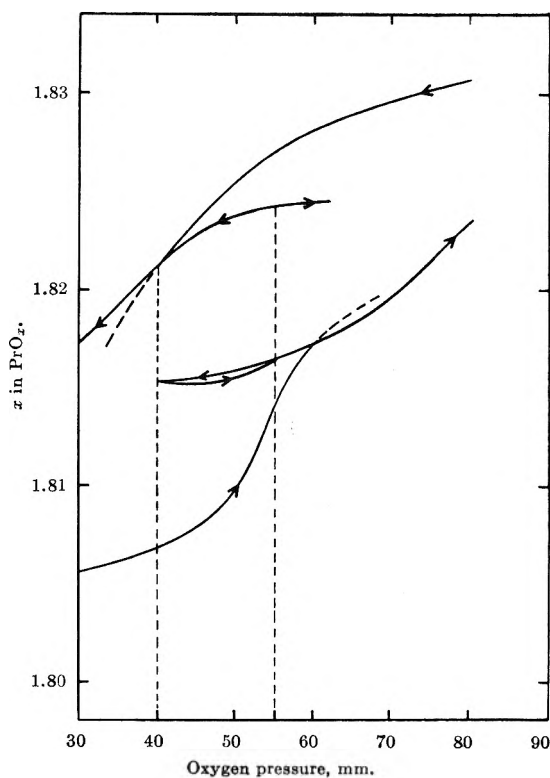
Fig. 3.—A Pr–O isotherm which illustrates theorems III, IV, and V.
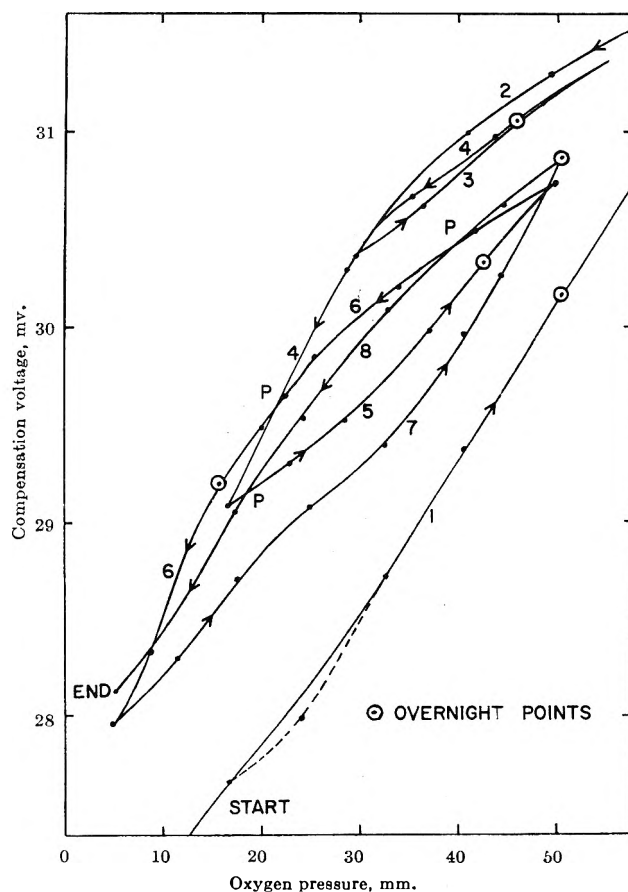
Fig. 4.—A Pr–O isotherm which illustrates theorem VI.

(Fig. 3). As the pressure is increased from A, the plot of the experimental data extends below the ascending boundary curve. The tendency of the curve as it emerges from A is to have a smaller slope than the envelope curve. This suggests that the scanning procedure has caused a change in the system properties.
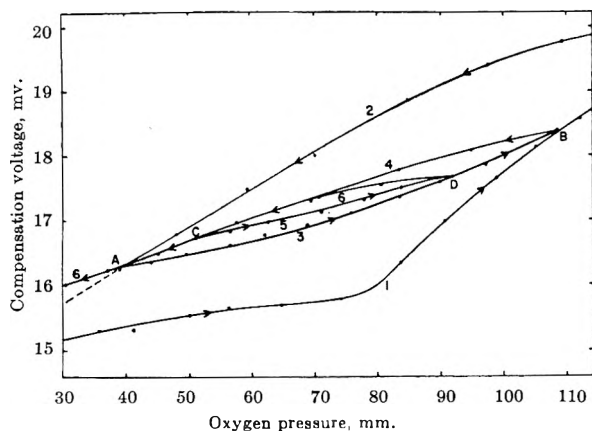
Fig. 5.—A Pr–O isotherm which illustrates theorem VII.
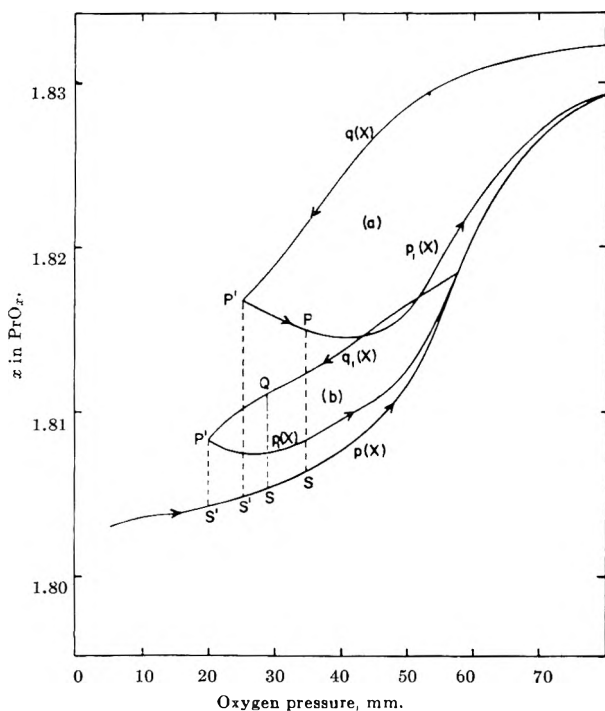
Fig. 6.—Scanning curves for a Pr–O isotherm at 465°.

For example, one may suppose that a specific distribution of properties, which is a result of only two overlapping distributions, is somehow resolved into two separate distributions by the scanning process; a gap between such distributions might cause the deviation from the envelope. This effect is thought to occur in the recent work of Everett and Nordon[8] on the Pd–H system.

Theorem VI.—"Any point P within the hysteresis loop can be reached in a number of ways from lower values of X, some from higher. The system will have definite static macroscopic properties at this point, but its state will not be completely defined since its behavior when it moves away from P depends on the route by which this point was approached."

Figure 4 illustrates an isotherm with many cross overs (P points). The numbers adjacent to the various paths signify the order in which the measurements were made and the arrows indicate increasing or decreasing oxygen pressure. With a little patience we found various paths which led to the same values of the coördinates. No reason is obvious which guarantees that the same macroscopic state is present at an

intersection point when the point is approached via different routes. There are very likely a great many ways to reach the coördinates at P.

High temperature X-ray data obtained under solid-gas equilibrium conditions are likely to show the presence of mixtures of two different crystal structures (state I and state II), the proportions of which may be affected by the atomically ordered and disordered arrangements associated with each defect structure. Thermodynamic properties for such mixtures are likely to vary with respect to these proportions. Eyring and Baenziger[9] have indicated somewhat that mixtures do exist although their work was done on quenched samples.

Theorem VII.—"If a system is taken through a series of oscillations of X of decreasing amplitude, after the nth reversal the system moves toward the point at which the $(n - 1)$th reversal occurred; if the system is carried through this point, it moves toward the $(n - 3)$th reversal point and so on."

Figure 5 is an illustration of theorem VII as it applies to the Pr–O system at about 460°. The path of the experiment may be followed by observing the sequence of numbers adjacent to the paths and the arrows on each path. The system is such that n equals 5 at reversal point D. Point C represents the $(n - 1)$th reversal point, and point A represents the $(n - 3)$th reversal point. The Pr–O system moves from reversal point D through the reversal points C and A as prescribed by theorem VII. It should be noted that the scanning curves close with the boundaries of each of the antecedent loops, i.e., loop ABA closes on the boundary curves 1 and 2· the loop CDC closes on the boundary curves of the loop generated by the scanning curves 3 and 4. This behavior does not necessarily follow the proposed model as postulated by Everett.[4]

The comparison above shows that in general there is a great similarity between Everett's theory and the Pr–O system. Complicating effects such as domain fracture, domain interaction, changing domain property distributions, and overlapping domain states are believed to be present and tend to confuse the comparison.

In section 6 of Everett's paper[4c] a method of calculation of a domain distribution is proposed. Curve a of Fig. 6 represents an isotherm that was measured near 465°. The pressure was increased over Pr_2O_3 from 10^{-6} mm. and the ascending boundary curve $p(X)$ was produced. The pressure was reduced from 150 to 25 mm. along the descending boundary curve $q(X)$ and increased again to 80 mm. where the primary ascending curve $p_1(X)$ closed on the envelope.

A plot of the derivative of the function $P'S' - PS$ (Everett's $g'(X_1,X)$) as a function of the oxygen pressure is shown in Fig. 7 (curve a), in which three peak-regions are obvious. An interpretation of these results is that the peaks represent residues of domain distributions that were converted to a lower (composition) domain state. This was brought about as the pressure was reduced. When the pressure was increased, these domains were transformed again to a higher (composition) domain state. It is difficult to say what the transitions are; however, it may be that peak 1 is caused by domains that remained in the $x = 1.80$ state, peak 2 is caused by domain state stability

(8) D. H. Everett and P. Nordon, *Proc. Roy. Soc.* (London), **A259**, 341 (1960).

(9) L. Eyring and N. C. Baenziger, "Chemical Physics of Nonmetallic Crystals," W. A. Benjamin, Inc., New York,N. Y., 1962, p. 428.

in the $x = 1.83$ state, and peak 3 is related to domains that remained in some state beyond $x = 1.83$ (perhaps $x = 2.0$).

A similar isotherm is represented as b in Fig. 6. However, in this case the descending boundary curve was not traversed. The resulting distribution curve b is shown in Fig. 7. It can be seen that these curves are quite similar, and curve b is displaced from a. In accordance with the theory the curves show that a lesser number of domains were converted from state I to state II in case b than in case a by using this particular scanning procedure. Since $p(X)$ can be reproduced, $p'(X)$ in Fig. 7 has a maximum, the limits of which are reasonably well defined. However, $g'(X_1,X)$ is dependent on X_1, and maxima for these curves will depend on X_1. It is interesting to note that the peaks of Fig. 7 are rather sharply defined and indicate that the interaction between domains in different states is probably small.

The question naturally arises as to the nature of a domain in the Pr–O system. In our opinion, a single domain may be described qualitatively as being composed of a specific number of Pr atoms. The various compositions ($x = 1.83$, 1.80, etc.) are the domain state limits[10] and represent specific crystal structures.[9]

An analogy to a disordered alloy system[11] is perhaps best used to describe the qualitative behavior of the postulated domain of PrO_x. The possible variation of the free energy of a PrO_x domain is illustrated in Fig. 8a. I and II represent the two states available to the domain. Curves CAFBH and GBEAD apply to states I ($x = 1.80$) and II ($x = 1.83$), respectively. Path CAF represents state I plus excess oxygen and path GBE represents oxygen-deficient state II. Points A ($E \rightarrow A$) and B ($F \rightarrow B$) represent phase changes which are dependent on the oxygen concentration and order in the domain. Curves DA or CA and GB or HB could be the same curves. The path for a transformation would be, for increasing pressure

(state I) $C \longrightarrow A \longrightarrow F(F \longrightarrow B) \longrightarrow G(H)$ (state II)

and for decreasing pressure

(state II) $G \longrightarrow B \longrightarrow E(E \longrightarrow A) \longrightarrow C(D)$ (state I)

The paths followed by the system will be those which offer the lowest free energy. The hypothesis that a domain may be oxygen deficient or contain excess oxygen implies that the individual hysteresis loop for a domain does not have to be rectangular.

A projection of the curves of Fig. 8a in the pressure–disorder plane is shown in Fig. 8b. The lines 1–2 and 3–4 are drawn to aid in showing the similarity between the regions about points A and B and the theoretical curves obtained by Anderson[12] and Rees[13] for the general case of a large stoichiometric defect. In both cases it appears that these authors assume the limit of existence of one crystal structure (anion-excess) and

(10) A. F. Clifford and P. A. Faeth, "Rare Earth Research," The Macmillan Co., New York, N. Y., 1961, p. 105.

(11) R. Fowler and E. A. Guggenheim, "Statistical Thermodynamics," Cambridge, 1956, p. 601.

(12) J. S. Anderson, Proc. Roy. Soc. (London), A185, 69 (1946).

(13) A. L. G. Rees, "Chemistry of the Defect Solid State," Methuen, London, 1954, Chap. II.
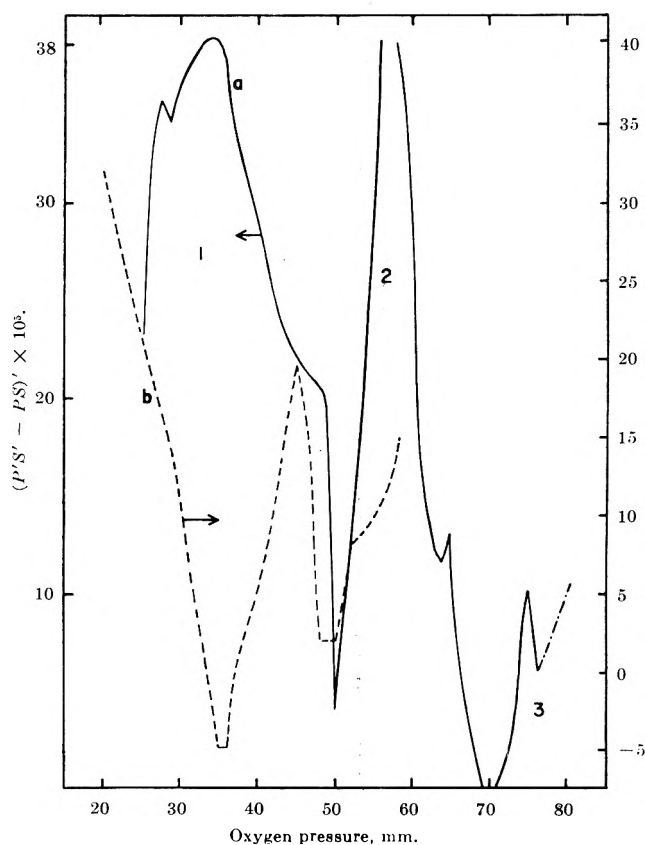
Fig. 7.—Distribution functions for the isotherms of Fig. 6.
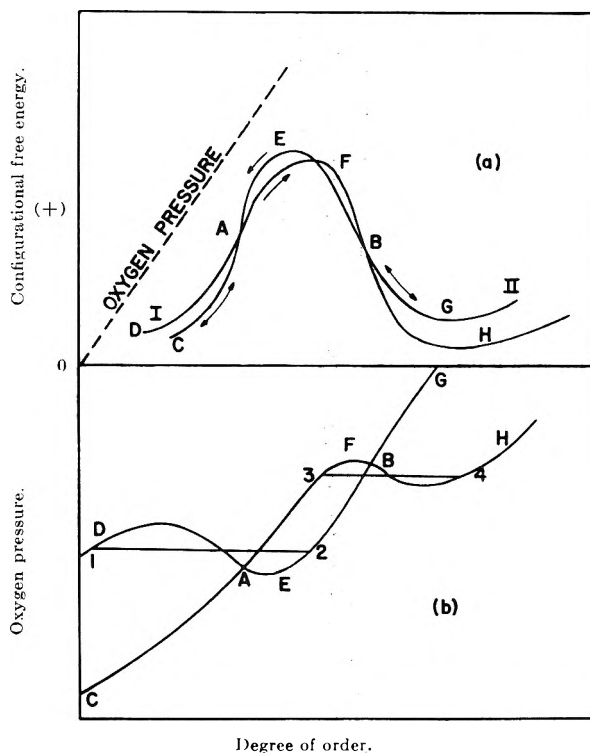
Fig. 8.—(a) Possible variation of the configurational free energy with system order and oxygen pressure. (b) Projection of the variation of configurational free energy in the order–pressure plan.

another (anion-deficient) at constant composition is the same. If the limits are different, hysteresis effects should be expected regardless of the existence of domains. Further work along these lines is continuing.

A CAPACITY FLOW REACTOR FOR DETERMINING THE KINETICS OF HOMOGENEOUS GAS PHASE REACTIONS

BY J. DE GRAAF AND HAROLD KWART[1]

Organisch Chemisch Laboratorium of the Rijksuniversiteit te Leiden, The Netherlands

Received December 3, 1962

A "capacity flow" or "steady state" reactor applicable to study of the kinetics of high temperature homogeneous gas phase reactions has been constructed. The anticipated range of applicability of this apparatus has been discussed. Data obtained in this fashion on the rates of pyrolysis of ethyl acetate have been presented and compared to values measured by other authors by means of tube flow reactors. Some consideration has been given to the sources of error and the reliability of the activation parameters computed from our measurement.

Introduction

The methods and practices commonly applied in studying the kinetics of homogeneous gas phase reactions have recently been reviewed by Walters[2] and Maccoll.[3] These authors have classified existing knowledge in the categories of static and flow methods and have considered various applications in both of these categories together with their respective advantages. Evidently, in both methods two distinct measurements must be made in order to achieve a measure of the rate of reaction; the extent of reaction and the time of reaction, although in the flow methods the time measurements are effected on a space coördinate.

The particular advantages of the flow methods have been realized in tube-flow reactors in which a time invariant concentration gradient is established along the length of a tubular reaction chamber. These circumstances lend themselves very well for measurement of very rapid reaction rates in solution[3] as well as in the gas phase. A type of continuous flow reactor first discussed by Denbigh and co-workers,[4] called the "capacity flow" or "steady state" reactor, has been experimentally elaborated by Hammett and co-workers.[5]

The capacity flow reactor seems to have been applied previously only for homogeneous liquid phase kinetics. It differs in essence from the usual flow reactor[3] in that the reaction space is a well stirred vessel instead of an unstirred tube. As in the tube reactor, the capacity flow reactor also approaches a steady state but here the composition is uniform and invariant throughout the reaction zone.

We have undertaken to develop a capacity flow reactor designed for rate measurements on homogeneous gas phase reactions in the effort to realize one of the inherent advantages of the method, namely, for determination of the instantaneous rate of reaction as a function of *entirely constant* reaction conditions. It has already been pointed out by Young and Hammett[5] that variation of reaction conditions during the course of reaction in a static system or in a tube flow system may lead to

a very real kinetic deviation. Complex reactions are particularly susceptible to this possibility for inherent error in the traditional methods of gas phase kinetic measurements. Furthermore, mathematical analysis of the kinetics of complex reactions, ordinarily quite difficult when applied to static and tube flow reactor data, is carried out (as we shall see) much more simply by means of the capacity flow treatment of gas phase reactions.

It will also be seen that several other factors, which often present difficulties in tube flow reactor measurement of homogeneous gas phase kinetics, are readily overcome in the capacity flow method. Thus, while the effect of change in volume during the reaction and the effect of diffusion must be reckoned with in the tube flow reactor, these variables are readily eliminated in the capacity flow experiment. In addition, due to the conventional difficulties in regulating for perfect temperature uniformity over the full length of the tube reactor,[6] such "end effects" and longitudinal temperature gradients result in significant errors in rate measurements on high activation energy reactions. The stirred reactor condition ensures against such contingencies and renders errors due to irregularities in temperature control easily detectable.

We have discussed below the elements of design of a capacity flow reactor and associated apparatus, which was constructed for measurement of homogeneous gas phase kinetics at temperatures up to 600°. We have indicated how this design may be applied for determination of reaction rates, reaction orders, and other parameters in complex reactions. We have also presented data obtained with this reactor in studies of a relatively simple reaction, the pyrolysis of ethyl acetate, in order to achieve a comparison with results reported in the literature on the same reaction and obtained by means of the conventional tube flow reactors.

Experimental

Design Features of the Homogeneous Gas Phase Capacity Flow Reactor.—The accompanying sketch represents the design of an apparatus which is presently being applied in a kinetic study of the high temperature chlorination of aromatic hydrocarbons. Alternatively, however, provision can be readily made to permit the use of any other liquid substrate than "aromatic" and any other gaseous reagent than the "Cl_2" indicated. This complex reaction is merely used for illustration.

The reactor chamber VII and the various flow control elements are all integrally mounted on a frame, which is readily movable or secured in a desired position on rails mounted in the vertical plane above the center of the thermostated bath. In the condition of measurement the reactor chamber and the premix coils

(1) Author to whom inquiries should be addressed at his permanent address, The University of Delaware, Department of Chemistry, Newark, Delaware. The work reported here was carried out while this author was National Science Foundation Senior Post-doctoral Fellow and Visiting Professor at the University of Leiden, 1960–1961.

(2) W. D. Walters in "Technique of Organic Chemistry," Vol. 8, Interscience Publishers, Inc., New York, N. Y., 1953, p. 231.

(3) A. Maccoll, ref. 2, Vol. 8, part I, 1961, p. 427.

(4) R. Stead, F. M. Page, and K. G. Denbigh, *Discussions Faraday Soc.*, **2**, 263 (1947); K. G. Denbigh and M. Hicks, *Trans. Faraday Soc.*, **44**, 479 (1948).

(5) H. B. Young and L. P. Hammett, *J. Am. Chem. Soc.*, **72**, 280 (1950); J. Saldick and L. P. Hammett, *ibid.*, **72**, 283 (1950); M. J. Rand and L. P. Hammett, *ibid.*, **72**, 287 (1950). See also R. L. Burnett, Dissertation, Columbia University, as reported in *Dissertation Abstr.*, **20**, 4537 (1960).

(6) S. W. Benson, *J. Chem. Phys.*, **22**, 46 (1954).

which lead to the entrance port at its very bottom are immersed in the thermostated bath to the fluid level.

The left arm of the premix coil leads to the reactor from the preheater-evaporator V, by means of which the liquid component (here labeled aromatic) is smoothly volatilized and admixed with the nitrogen carrier gas. About a dozen turns of 5-cm. arbor premix coils, fabricated from 4-mm. bore tubing, were calculated to be of sufficient length when immersed in the bath to bring the gas mixture to bath temperature and convey it directly to the entrance port directly beneath the stirrer. The right arm premix coils were of the same construction and served a similar function in conveying the preheated (in section VI) mixture of the second reaction component (here labeled Cl_2) and the carrier gas to the locus of mixing of the reactive components.

Some attention had to be given to the division of the carrier gas flow leading into the respective arms of the premix coils. This had to be done to assure that the two streams of gases have nearly the same flow velocities at the point of their confluence, and that there shall be little or no tendency for back diffusion of the one stream into the premix coils conducting the other. One of the ways in which this was accomplished is illustrated in Fig. 1. Here the total flow of carrier gas was metered by the flowmeter complex I, which consisted of a rotameter equipped with a choice of by-passing capillaries that permitted altering the range of controllable gas flow. The flow of gas that issued from I was divided between the two arms by a combination of a fixed capillary differential manometer-flowmeter, shown as III, and a variable capillary device shown as IV. The latter consisted of a long hypodermic syringe needle penetrating a neoprene diaphragm seal and closely fitted to the inside diameter of a length of uniform bore glass tubing. The length of needle extending into the glass sleeve was readily adjusted and thus controlled the resistance to gas flow into section VI and hence to the right arm premix coils. Alternatively, when the flow rates required were large enough to produce undesirable pressure upstream of the flowmeter complex I, the differential manometer III had to be replaced by a variable capillary similar to IV. From among the apparently innumerable combinations possible with two such variable capillaries a constant total resistance to gas flow was obtained which permitted a choice in the range 1:5 to 5:1 in the division of carrier gas flow velocities in the two arms. The smooth, oscillation-free flow of carrier gas was assured by placing a 2-l. ballast bulb in the line before I.

A continuous flow of liquid reagent (aromatic) was delivered to the evaporator V by means of a motor-driven syringe pump capable of a very large range of delivery rates; (Unita 1, Braun, Melsungen, Germany). However, the achievement of an oscillation-free flow and constant composition of the mixture of carrier gas and volatilized aromatic required careful adjustment of the temperature of the evaporator. The desired condition of steady flow and composition of the gas stream from V was monitored and judged to be acceptable on the basis of measurements with a Katharometer (thermal conductivity meter), similar to that used as a gas-chromatography detector element. The actual evaporator which fulfilled these rigorous demands is pictured as the upper part of section V in the figure. The (aromatic) liquid from the syringe pump entered the system through the inner (part) of the concentric tubes and discharged onto a saucer shaped hollow under which a variac controlled heater element was mounted. The end of the concentric delivery tube approached to within 1 mm. of the heated saucer. The carrier gas which flowed in the outer annulus of the concentric tubes impinged directly onto the heated surface and rapidly conveyed the volatilized liquid into the surrounding, glass-helix packed void (which was heated by the tube furnace as shown) and thence to the left arm premix coils immersed in the thermostat fluid. The total void volume of V and the premix coils was negligibly small compared to the void volume of the stirred reactor VII. The katharometric monitor showed conclusively that the ideal condition for attaining a steady, constant composition flow lies in the use of an evaporator temperature that is only slightly higher than the boiling temperature of the liquid to be volatilized.

The main reactor chamber VII was fashioned from a spherically shaped Pyrex flask with four shallow, vertical pleats to improve the mixing action imparted by the glass paddle stirrer (shown). The void space in the neck of the flask above the actual reactor volume was reduced to a negligible amount by use of an evacuated length of tube connecting the trubore stirrer shaft to the stirrer paddle. This tube rotated with very small

AROMATIC
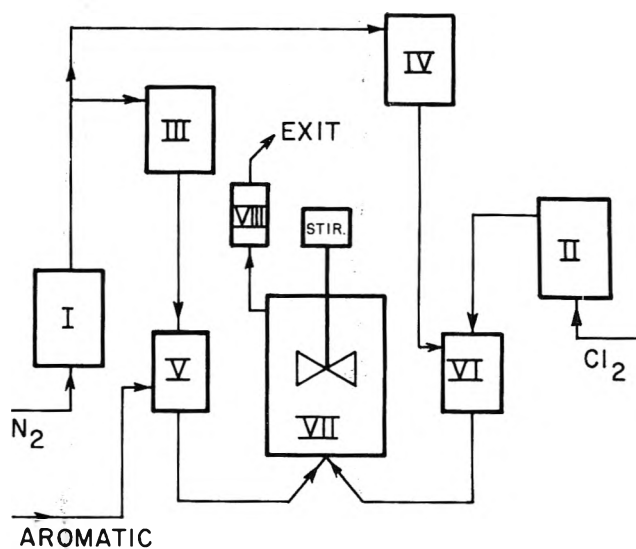
Fig. 1.—Schematic representation of the reactor (see text for legend).

clearance in the neck of the reactor (above the level of the thermostat fluid). The clearance, however, was sufficient to allow unobstructed flow of the (steady state) gas composition into the cold condenser flasks at VIII. In the present instance the neck of the reactor and the connecting exit tube were wrapped with heating elements and maintained at about 200°.

The stirrer seal directly above the neck had to be resistant to hot Cl_2, HCl, and chloroaromatics without permitting metal in contact with the gas stream. A spring-backed Teflon disk attached to the stirrer shaft and rotating tightly against a fluorocarbon-greased, ground surface provided both the necessary sealing action and chemical and thermal inertness. The trubore bearing for the stirrer shaft was silicone grease lubricated and water cooled. The annular space between the removable stirrer bearing and the Teflon disk seal was kept under a slight positive pressure of pure, dry nitrogen bubbling through about 2 cm. of sulfuric acid downstream. This construction effectively prevented water and oxygen from diffusing into the reaction zone through the stirrer seal. The rotation of the stirrer was readily regulated by a variable speed motor also mounted on the rack and driving the shaft through a flexible cable coupling.

Considerable latitude was possible in the design of the traps VIII in which the steady-state reaction product was received and thereafter analyzed. The two trap combination shown in Fig. 1 followed the suggestion of Huyten[7] for breaking up the misting tendency that occurs with rapid cooling of the hot gases. Alternatively, for very difficult cases, we were equipped to use a high voltage Cottrell precipitator.

The thermostated bath consisted of an open top stainless steel tank which was insulated by at least 10 cm. of magnesia–asbestos powder. A removable cover of thick Transite sheet, appropriately slotted to accommodate the immersion heater, thermostat controls, and the stirred reactor, could be put in place over the top of the bath. The thermostat fluid consisted of a mixture of KNO_3 (53%), $NaNO_2$ (40%), and $NaNO_3$ (7%) called Hitec (E. I. du Pont de Nemours) melting at 160° and stable, without fuming, to more than 600°. For control temperatures below 175°, a common heating oil could be used instead of the Hitec. The heating element was a 1500-watt stainless steel immersion type which was regulated by a bimetallic relay (Jumo STE-O-15A, West Germany) controlling 10% of the energy supplied by a 200V–10A Variac. The temperature was sensed by an iron–constantan thermocouple calibrated by an Anschutz thermometer at 360° and the temperature of condensing sulfur vapor at 444.6°. The range of variation from the set temperature of the thermostated bath was always less than 1.0° as measured by a Cambridge potentiometer.

The gas composition of the capacity flow reactor was determined by analysis of the rapidly-cooled effluent gases. Several possible analytical procedures were available. Wherever possible gas–liquid chromatography was applied to obtain a quantitative estimate of the proportions of the various components of the reaction products. Alternatively, titration of a timed sample for

(7) F. H. Huyten, Chem. Weekblad, 57, 209 (1961).

a single component (e.g., acetic acid from the pyrolysis of acetates or unreacted chlorine or the amount of HCl formed as a product of chlorination) was used to obtain the required analytical data on the composition of the product. In practice the incidence of a steady state in the reactor gas composition was detected by the constancy of successive analyses in timed trials of the effluent stream.

Kinetic Calculations: Typical Methods for Computing Reaction Order and Rate Constants from Capacity Flow Reactor Data: Typical Case 1 —The Reaction A + B → C + D.

—An excess of N_2 as carrier gas is used; for example, $ArH + Cl_2 \rightarrow ArCl + HCl$. For this case the rate reaction, R, in moles per second is given by the product of the *constant* volume of the reactor (V) in liters and the specific rate in moles per liter per second (r)

$$R = Vr = kC_A^a C_B^b V \quad (1)$$

where C_I^i, in general, is taken to represent the concentration dependence of any component, I, present in the reactor and, therefore, in the effluent stream at the steady state. It is clear also that

$$\log R = \log kV + b \log C_B + a \log C_A \quad (2)$$

and that in a series of runs employing large excess of component B, (and therefore, at constant concentration C_B), we can expect a linear plot of $\log R$ vs. $\log C_A$ with a slope equal to a (the order with respect to A) and intercept given by $\log kVC_B^b$. It will be seen that a similar series at constant C_A will lead to an estimate of b as well as the value of the rate constant k at the particular temperature of the reactor.

To compute these parameters, then, we require only data on the composition of the effluent stream under given conditions of input flow of the reactants and carrier gas. This is easily realized, for instance, when we can measure the relative concentrations of a reagent and a product in the effluent stream at the steady state by vapor phase chromatographic or titrimetric procedures. Thus, let $Y = N_C/N_A$, where N_{N_2}, N_{A_0}, N_{B_0} are the, respective, flow velocities of each of the influent gases in moles per second and N_A, N_C, and N_D are the corresponding quantities of the components A, C, and D in the effluent stream. Consequently, since

$$N_{A_0} = N_C + N_A$$
$$N_{A_0} = N_C(1 + 1/Y) \quad (3)$$

and, since the rate of reaction is also the rate at which the product (e.g., N_C) flows from the reactor at the steady state, then

$$R = N_C = N_{A_0} \frac{Y}{(Y + 1)} \quad (4)$$

It is also obvious that in our constant volume reactor $Y = C_C/C_A$, and, therefore

$$C_A = \frac{1}{Y} \left[\frac{N_C}{N_{A_0} + N_{B_0} + N_{N_2}} \right] K \quad (5)$$

where

$$K = \frac{\text{pressure in atmospheres}}{\text{(gas constant) (absolute temp.)}}$$

Typical Case 2 —The Reaction A → C + D.

—An excess of N_2 as carrier gas is used; for example $CH_3COOC_2H_5 \rightarrow CH_3COOH + C_2H_4$ the distinctive feature of this reaction is that two moles are formed from one, or

$$2(N_{A_0} - N_A) = N_C + N_D$$

and the total number of moles in the reactor at the steady state is given by

$$\Sigma_N = 2N_{A_0} - N_A + N_{N_2} \quad (6)$$

It is clear, too, that

$$R = kVC_A^a = kV \left[\frac{N_A}{\Sigma_N} \right]^a K^a \quad (7)$$

Again, our analytical data (determined on the effluent stream) gives us $Y = N_C/N_A$, the value of R and N_C by eq. 4. Where the reaction is known to be first order ($a = 1$), on appropriate substitution into eq. 7 and rearranging the resulting expression we arrive at

$$k = \frac{N_C}{KVN_A} \Sigma_N \quad (8)$$

This in turn can be simplified to

$$k = \frac{Y}{KV} [N_{A_0} + N_C + N_{N_2}] \quad (9)$$

Under certain conditions this is susceptible to further reduction, since, when working at low conversions (e.g., $Y = 0.1$) and in high carrier gas dilution (e.g., $N_{N_2}/N_{A_0} = 5$), an approximation is possible which considerably simplified the computation of the rate constant. Under these circumstances, $N_C \ll (N_{N_2} + N_{A_0})$, and we get

$$k = \frac{Y}{KV} [N_{A_0} + N_{N_2}] \quad (10)$$

the proper application of which results in only a negligible error compared to the value of k computed according to eq. 9 (see Table I).

The Pyrolysis of Ethyl Acetate—Testing of the Homogeneous Gas Phase Capacity Flow Reactor.

—In order to establish the validity of our design of the capacity flow reactor, we undertook to determine with our apparatus the rates as a function of temperature and the activation parameters for the pyrolysis of ethyl acetate. These quantities have been previously reported by several independent investigators utilizing variants of the tube flow reactor techniques of measurement. The data in Table I summarize our results expressed in the terms of the computational procedures discussed above (see eq. 9 and 10).

Admittedly, the apparatus shown in the accompanying figure is not the ideal design for a one component, monomolecular system such as ester pyrolysis, since only one-half of the capacity was in use; that is to say, only the premix coils leading from preheater V were needed and those from VI were inactive in these experiments. However, this introduced only a small uncertainty in the actual volume of the reactor, or put another way, in the effective contact time, since the total heater volume from the point of evaporation of the substrate in V to the entrance port of the reactor

TABLE I

DATA ON THE PYROLYSIS OF ETHYL ACETATE TAKEN BY THE CAPACITY FLOW REACTOR AND COMPUTATIONS THEREON

Run no.	N_{A0} (10^6) Flow velocity of ethyl acetate input in moles/sec.	N_{N_2} (10^6) Flow velocity of nitrogen and toluene in moles/sec.	Y $\dfrac{C_{acetic}}{C_{ester}}$ in the effluent	KV (10^3)	k (10^3) Computed from eq. 9	k (10^3) Computed from eq. 10	$\dfrac{1000}{T}$
P16	6.80	77.60	0.0283	6.16	0.389	0.387	1.541
P11	2.17	48.30	.085	6.05	.712	.710	1.512
P18	3.67	54.25	.079	6.00	.766	.763	1.500
P17	2.75	47.55	.234	5.80	2.05	2.03	1.451
P19	1.88	50.53	.504	5.66	4.73	4.67	1.415
P20	1.41	47.89	1.17	5.52	10.6	10.5	1.380
P15	1.67	41.38	1.53	5.48	12.3	12.0	1.371
P24	1.24	122.3	1.69	5.30	39.8	39.4	1.325
P23	1.24	122.3	3.15	5.18	75.6	75.2	1.295
P21	1.24	122.3	10.28	4.97	258.	255.	1.242

was, indeed, only a small fraction of the total reactor volume. Our results, therefore, could be compared with the earlier values reported in the literature.[8-11]

An Arrhenius plot of our data listed in Table I may be compared to analogous plots of data in the literature.[10,11] It will be seen that in the temperature range covered by all three sets of data our points appear to fall very well within the limits of uncertainty delineated both by Blades[10] and by Scheer[11] for their own results. The close coincidence of the respective experimental values can be realized from a comparison of all three reports at a given temperature; for example, the value of k (sec.$^{-1}$) at 489° computed by Scheer from Blades'

TABLE II

ARRHENIUS EQUATION COMPUTATIONS[a]

Temp. range covered (°C.)	$k = B'T \exp(-\Delta E/RT)$ (degrees^{-1} sec.$^{-1}$)	ΔE (kcal.)	Ref.
376–531	1.85×10^8	43.6	This work
434–531	3.9×10^8	44.5	This work
376–414	4.3×10^6	41.0	This work
452–537	1.65×10^9	46.5	Scheer[11]
503–610	4.38×10^9	43.4	Blades[11]

[a] According to ref. 9.

data is 0.079–0.082, from his own data 0.075, and we have calculated 0.071 by interpolation. However, the increased sensitivity, afforded by our capacity flow reactor method of measurement, permits us to determine the rates and activation parameters as well at considerably lower temperatures than investigated by the previous authors.[10,11] Thus, we noted that for the temperature range between 376 and 414° the data depart from the linear relation observed at the higher temperatures and are best approximated by a new line with reduced values of ΔE and B' (see Table II). Although it is not a common occurrence in reactions like ester pyrolysis which have a very simple path, many reasons have been discussed which would contrive to produce departures from linearity in an Arrhenius plot over a large temperature range. For example, the incidence of a heterogeneous catalysis mechanism has been identified as responsible for curvature in the Arrhenius plot of nitric oxide decomposition studied by Wise and Frech.[12] The curvature we observed for ethyl acetate pyrolysis, however, is not likely to originate in this fashion since it is well established that increased (neutral) surface area

in the reactor is without influence on the rate. This must be particularly true of our capacity flow reactor where the surface to volume ratio has been enormously reduced compared to the conventional tube flow reactors previously employed for rate measurements.

Others have suggested[6] that the occurrence of a temperature gradient in a reactor can lead to significant distortion of the Arrhenius plot and the parameters computed therefrom. This criticism, however, cannot be levelled at the well stirred capacity flow reactor which is characterized by almost perfect temperature homogeneity. It is more likely a possibility to be anticipated in some tube flow reactor designs.

From such considerations we have concluded that the causes of curvature in our Arrhenius plot are not to be found in the techniques by which we have measured the pyrolysis rates.[13] Rather we have assumed that certain factors controlled by the mechanism of reaction are operating to produce the observed deviation. Thus, in principle the entropy (ΔS^*) and enthalpy (ΔH^*) of activation are temperature dependent quantities comprising the ΔE term in the Arrhenius plot. The fact that ΔE is most often computed from the slope of a straight line plot implies that ΔS^* and ΔH^* are linearly interdependent. That is to say, in the algebraic relation

$$\Delta H^* = \beta \Delta S^* + \gamma \qquad (11)$$

both β and γ are generally constant or experience only small variation over a relatively wide range of temperatures. The empirical fact of eq. 11 has been discussed by several authors[14-16] who have noted its applicability in a wide variety of reaction series and in both rate and equilibrium processes.

While it is not possible at present to understand fully all the mechanistic details which contribute to the departure from eq. 11 at low temperatures and the consequent shift in the slope and intercept of the Arrhenius line, we have surmised that the ΔS^* term is most strongly implicated. This correlates very well with the Fowler and Guggenheim[17] treatment and the Hinshel-

(8) G. K. Burgess, *J. Res. Natl. Bur. Std.*, **1**, 635 (1923).

(9) R. S. Brokaw and R. N. Pease, *J. Am. Chem. Soc.*, **72**, 3237 (1950).

(10) A. T. Blades and P. W. Gilderson, *Can. J. Chem.*, **38**, 1407 (1960).

(11) J. C. Scheer, Dissertation, University of Amsterdam, 1961.

(12) H. Wise and M. F. Frech, *J. Chem. Phys.*, **20**, 22 (1952).

(13) J. W. Engelsma, E. C. Kooyman, and J. C. van der Bij, *Rec. trav. chim. Pays Bas*, **76**, 325 (1957); J. W. Engelsma and E. C. Kooyman, *Proc. Kon. Akad. Wet.*, **B60**, 321 (1957); *Proc. Chem. Soc.*, 258 (1958). Further studies applying this capacity flow reactor to studying the kinetics of high temperature gas phase aromatic halogenation are presently in progress in the laboratories of Professor Kooyman.

(14) J. E. Leffler, *J. Org. Chem.*, **20**, 1202 (1955).

(15) C. G. Overberger and R. W. Cummins, *J. Am. Chem. Soc.*, **75**, 4250 (1953).

(16) W. K. Wilmarth and N. Schwartz, *ibid.*, **77**, 4543 (1955).

wood–Lindemann[18] theory of unimolecular reactions which give strong consideration to the number of internal degrees of freedom in the configuration of the activated complex. We hope to give this matter more careful scrutiny in further investigations applying the

(17) R. H. Fowler and E. A. Guggenheim, "Statistical Thermodynamics," Cambridge University Press, Cambridge, 1939, pp. 524–527.

(18) C. N. Hinshelwood, "Kinetics of Chemical Change," Oxford University Press, Oxford, 1947, pp. 79–83.

capacity flow reactor to high temperature gas phase reactions.

ENERGY ACCOMMODATION IN EXOTHERMIC HETEROGENEOUS CATALYTIC REACTIONS[1]

By Bernard J. Wood, James S. Mills, and Henry Wise

Stanford Research Institute, Menlo Park, California

The steady-state flux of mass and of energy at a solid catalytic surface due to heterogeneous recombination of hydrogen atoms were evaluated by a combination of e.p.r. and calorimetric techniques. The catalytic surfaces employed were filaments of nickel, platinum, and tungsten. In general, only a fraction of the energy of atom recombination was found to be accommodated by the catalyst. The results suggest an upper limit to the energy flux which a solid can accept. This is interpreted to be governed by the lattice force constant of the catalyst which may be the rate-limiting factor in certain exothermic catalytic processes.

Introduction

Recent observations[2] of the heat flux to metal filaments exposed to a hydrogen discharge of fixed intensity indicated that, of the total energy liberated by the surface-recombining hydrogen atoms, only a fraction was dissipated as heat in the catalyst. The remainder was apparently carried away by desorbing hydrogen molecules formed by heterogeneous atom recombination. Other investigators[3] have reported the appearance of electronically excited nitrogen molecules in the proximity of a catalytic surface exposed to nitrogen atoms.

From this qualitative evidence, it appears likely that the efficiency of energy transfer within the crystal lattice of a catalyst may play a fundamental role in exothermic heterogeneous processes. Indeed, the activity of various solid materials for atom recombination has been correlated[2,4] with the Debye characteristic temperature of the catalyst which, to a first approximation, is a measure of the lattice force constant and hence determines the upper frequency limit at which heat may be transferred through the lattice by spontaneous phonon emission. To investigate this problem further, we have made quantitative measurements of the fraction of available reaction energy imparted to a catalytic surface on which hydrogen atoms are recombining.

Experimental

I. **Method.**—The objective of our experiment was to measure simultaneously the steady-state mass and energy flux at the catalytic surface due to heterogeneous atom recombination. From such data, the reaction energy accommodation coefficient for the surface was computed, *i.e.*, the fraction of available energy transferred to the solid. Atomic hydrogen possesses a net electron magnetic moment; hence, electron paramagnetic resonance (e.p.r.) spectroscopy was selected as a method for evaluating the flux of atoms flowing through a tube toward a catalytic surface.

The power input to the surface attributable to the exothermicity associated with heterogeneous atom recombination was determined calorimetrically.[2]

II. **Apparatus.**—In essence, the experimental apparatus consisted of a tube through which hydrogen gas at a reduced pressure was pumped. At one region in the tube the gas was partially dissociated in a radiofrequency (RF) discharge. Downstream from the discharge an e.p.r. cavity was located, and immediately downstream from the cavity a catalytic filament was situated.

The vacuum system (Fig. 1) was fabricated from Pyrex glass with the exception of a fused quartz section through the e.p.r. cavity. This tube had an outside diameter of 10 mm. and a wall thickness of approximately 0.75 mm. Prior to insertion in the vacuum system, the tube was washed with concentrated nitric acid, followed by thorough rinsing with ethanol and then with distilled water.

Atoms were produced[2] in a 17 mc./sec. electrodeless discharge. Atom concentration was varied by adjusting the RF input to the discharge. The total pressure in the system was controlled by varying the gas input rate through an adjustable leak, a Granville–Phillips valve.

The catalytic filament was located downstream from the e.p.r. cavity, but the physical dimensions of the cavity limited the minimum distance between its center and the filament to 16 tube radii. Hydrogen atom recombination on the walls of the quartz tube[5] causes a loss of atoms between the e.p.r. cavity and the filament, under the flow conditions prevailing in our experiments, which was estimated from a theoretical analysis.[6] In addition, the atom concentration profile within the quartz tube was verified experimentally by positioning the quartz tube so that the e.p.r. cavity and its attendant magnet, mounted on a wheeled carriage, could be moved back and forth horizontally along the tube (Fig. 1). In this manner the longitudinal concentration gradient of atoms in the tube was evaluated (Fig. 2).

III. **Catalysts.**—The catalytic surface, in the form of a coiled filament, was supported on 16 gage glass-insulated copper wires and was attached to a glass-encapsulated iron armature so that its longitudinal position in the quartz tube could be adjusted from outside the tube with a magnet. Details of the measurement of the rate of heat input attributable to atom recombination on the filament surface are given in an earlier publication.[2] Surface areas were calculated from the measured dimensions of the wires. Average surface temperatures were computed from the measured values of filament resistance, the filament dimensions, and values of resistivity reported in the literature for the various metals.[2]

(1) This work was supported by Project Squid, Office of Naval Research, Department of the Navy.

(2) B. J. Wood and H. Wise, *J. Phys. Chem.*, **65**, 1976 (1961).

(3) R. R. Reeves, G. Mannella, and P. Harteck, *J. Chem. Phys.*, **32**, 946 (1960); *Can. J. Chem.*, **38**, 1648 (1960).

(4) H. Wise and W. A. Rosser, "Ninth (International) Symposium on Combustion," Cornell University, Ithaca, N. Y., 1962.

(5) B. J. Wood and H. Wise, *J. Phys. Chem.*, **66**, 1049 (1962).

(6) H. Wise and C. M. Ablow, *J. Chem. Phys.*, **35**, 10 (1961).

IV. **E.p.r. Spectrometry.**—E.p.r. spectrometry has been employed by several investigators[7-11] to measure the concentrations of gaseous atomic species by observing the intensity of their paramagnetic resonance absorption. The principal problem associated with the use of this method for such purposes is the derivation of a relationship between the indicated resonance absorption intensity of the species and the actual number of the species in the e.p.r. cavity. Since the fine structure and the theory of the e.p.r. spectrum of molecular oxygen have been examined and developed in detail,[12] we chose to employ molecular oxygen as a calibration standard. That is, the concentration of atomic species in the cavity was evaluated by comparing the resonance absorption of the atoms with the absorption of a known pressure of oxygen molecules for a fixed set of geometric and instrumental parameters.

In our experiments a Varian Model V4502 e.p.r. spectrometer with a six-inch magnet was employed. This instrument utilizes a 100 kc./sec. field modulation unit with a multipurpose microwave cavity whose Q is approximately 7000. Microwave energy absorption by a species with an unpaired electron is due to transitions between Zeeman energy levels, and occurs when the species is placed in a magnetic field H and an alternating electric field of frequency ν such that $h\nu = gBH$, where g is the spectroscopic splitting factor, h is Planck's constant, and B is the Bohr magneton 0.92732×10^{-20} erg gauss^{-1}. The Varian spectrometer is operated as a fixed frequency instrument ($\nu \cong 9.4$ kMc./sec.) in which the magnetic field is varied to attain the resonance condition. The derivative of the absorption of the paramagnetic species is detected, amplified, and recorded. The recorded signal is proportional to the derivative of the imaginary part of the complex susceptibility with respect to the magnetic field, $d\chi''/dH$. The total number of unpaired electron spins in the cavity is proportional to the integrated intensity $\int\chi''dH$. Using the development of Krongelb and Strandberg[8] we may write expressions for the number density of oxygen molecules and hydrogen atoms in terms of their integrated intensities. Thus

$$N_{O_2} = \frac{4kT}{\hbar\omega\pi} \times \frac{Z}{f_{\pm}g_{eff}B} \times \frac{\int\chi''_{O_2}\,dH}{[4|(JM|\mu_x|J'M')|^2 \exp(-E_{JM}/kT)]} \quad (1)$$

and

$$N_H = \frac{2(2I+1)(6kT)\int\chi''_H dH}{\hbar\omega\pi\,g\,BS(S+1)f_+} \quad (2)$$

where

N_{O_2} and N_H are, respectively, the no. of oxygen molecules and hydrogen atoms per cm.^{3}

$\hbar = h/2\pi$

$\omega = 2\pi\nu$

k is the Boltzmann constant

T is the temperature in °K.

E_{JM} is the energy of a given transition

$f_{\pm}$ and f_+ are the filling factors associated with the respective transitions

Z is the partition sum $_J\Sigma_M \exp(-E_{JM}/kT)$

$g_{eff} = d\nu/dH$

M and J are, respectively, the magnetic and total angular momentum quantum numbers, and

$|(JM|\mu_x|J'M')|^2$ is the absolute square of the matrix element for all transitions such that $\Delta M = \pm 1$, where μ_x is the magnetic field operator that causes spin transitions

I is the spin of the proton

S is the spin quantum number (in the case of H we use this notation which is distinct from J in O_2 matrix elements).

(7) T. M. Shaw, *J. Chem. Phys.*, **30**, 1366 (1959).

(8) S. Krongelb and M. W. P. Strandberg, *ibid.*, **31**, 1788 (1961).

(9) D. S. Hacker, S. A. Marshall, and M. Steinberg, *ibid.*, **35**, 1788 (1961).

(10) C. A. Barth, A. F. Hildebrandt, and M. Patapoff, *Discussions Faraday Soc.*, **33**, (1962).

(11) T. C. Marshall, *Phys. Fluids*, **5**, 743 (1962).

(12) M. Tinkham and M. W. P. Strandberg, *Phys. Rev.*, **97**, 937 (1955).
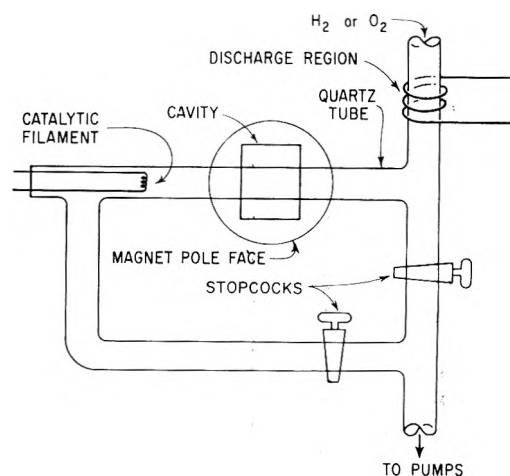
Fig. 1.—Schematic diagram of apparatus.
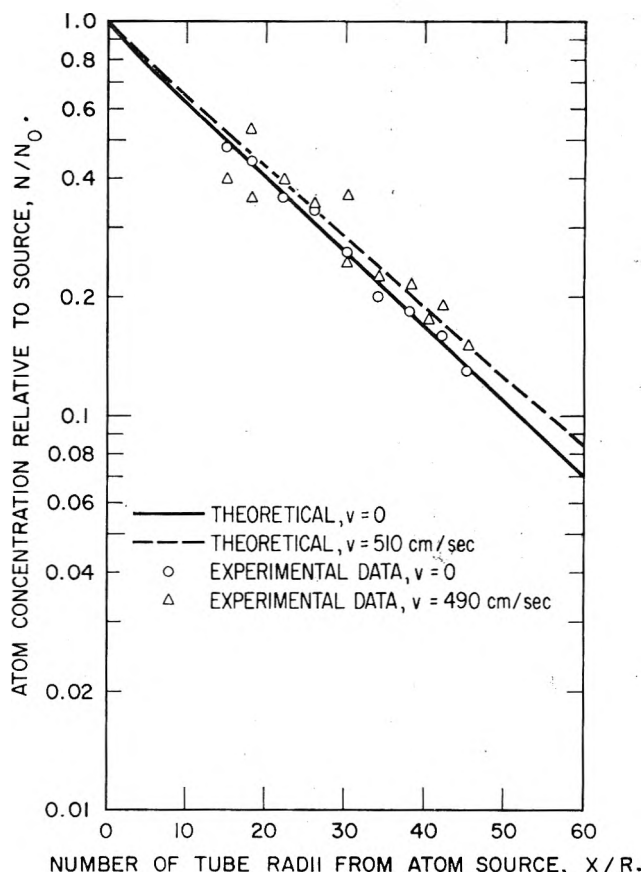
Fig. 2.—Theoretical[6] and experimental hydrogen atom concentration gradients in quartz tube of radius $R = 0.425$ cm., with tungsten filament located at $x/R = 60$, and total pressure $P = 41 \mu$. Theoretical curves calculated on the basis of $\gamma = 2 \times 10^{-3}$ and $\gamma' = 0.05$.

Dividing equation 1 by 2 we obtain

$$\frac{N_H}{N_{O_2}} = \frac{3f_{\pm}g_{eff}(2I+1)}{f_+ gZ} \times \frac{[4|(JM|\mu_x|J'M')|^2 \exp(-E_{JM}/kT)]}{[S(S+1)]} \times \frac{\int\chi''_H dH}{\int\chi''_{O_2} dH} \quad (3)$$

For atomic hydrogen $I = \frac{1}{2}$ and $S = \frac{1}{2}$. The partition sum Z for oxygen may be approximated by its classical value $3kT/2B'$ $= 217$ where B', a conversion constant for molecular oxygen, $= 43102$ Mc./sec. Also, the ratio of filling factors, $f_{\pm}/f_+ = 1$ since the dimensions and geometry of the cavity and quartz tube are the same for both gases. The g-value for hydrogen atoms is

Fig. 3.—Upper paramagnetic resonance absorption line of atomic hydrogen. The integrated intensity of this line indicates an atomic concentration of 3.95×10^{14} atoms/cm.^{3}.

the same as for a free electron, 2.0023. The quantity in brackets in the numerator is termed the "calculated intensity" by Tinkham and Strandberg[12] and has been evaluated by them for a large number of oxygen resonance absorption lines. We chose the line arising from the transition $K = J = 1, \Delta M = -1 \rightarrow 0$ which appears at $H = 5583.8$ gauss and $\nu = 9.47675$ kMc./sec. The calculated intensity[12] for this line is 0.741 and the value of g_{eff} is 1.96.

Inserting the appropriate numerical values of these parameters in eq. 3 we obtain

$$N_H = 2.68 \times 10^{-2} N_{O_2} \frac{\int \chi''_H dH}{\int \chi''_{O_2} dH} \quad (4)$$

or

$$N_H = 8.65 \times 10^{14} P_{O_2} \frac{\int \chi''_H dH}{\int \chi''_{O_2} dH} \quad (5)$$

where P_{O_2} is the pressure of oxygen in mm.

For experiments of the type employed in our study, the integrated intensity of the resonance absorption line, $\int \chi'' dH$, may be evaluated from the experimental data by reducing the function to the form of a first moment of the absorption. The first moment of the derivative function $d\chi''/dH$, as defined, may be integrated by parts to give

$$\int_{-\infty}^{+\infty} H(d\chi''/dH)dH = H\chi'' \Big|_{-\infty}^{+\infty} - \int_{-\infty}^{+\infty} \chi'' dH \quad (6)$$

If $d\chi''/dH$ is of such order that the function is Lorentzian in shape, then the integrated quantity $H\chi'' \Big|_{-\infty}^{+\infty}$ in eq. 6 becomes zero, and the intensity may be readily evaluated by numerical integration

$$\int_{-\infty}^{+\infty} H(d\chi''/dH)dH = \lim_{\Delta H \to 0} \sum_{-\infty}^{+\infty} H(d\chi''/dH)\Delta H \quad (7)$$

The values of integrated intensity obtained by use of eq. 7 are meaningful even though the line shape may be distorted by overmodulation.[13] In our work, however, a fixed modulation amplitude was selected empirically such that the recorded signals were not over-modulated and this value was used for all of our experiments.

To avoid problems associated with microwave power saturation of the observed electron spin transitions, the Varian low power microwave bridge was used. The microwave power incident on the sample in the cavity varied between 2.0 and 20 milliwatts. In practice, the power required to saturate the sample was determined by observing e.p.r. signal intensity as a function of incident power, then reducing the power level below saturated values.

As a rule, measurements were made with fixed settings of incident power and signal amplifier gain. In several experiments, where these parameters were varied, corrections were made by means of an empirical calibration of these respective functions with samples of molecular oxygen at known pressures.

Lines were identified by measuring the magnetic field H at resonance with a proton fluxmeter. The molecular oxygen

(13) K. Halbach, Phys. Rev., 119, 1230 (1960).

resonance line of interest appeared at $H = 5454$ gauss and $\nu = 9.2565$ kMc./sec., which corresponds to the line reported by Tinkham and Strandberg[12] at $H = 5584$ gauss and $\nu = 9.4768$ kMc./sec. The hydrogen atom e.p.r. spectrum[14] consists of two absorption lines of equal intensity separated by 506.8 gauss and centered on either side of $g = 2$ ($H = 3338$ gauss, $\nu = 9.3839$ kMc./sec.). The upper line is shown in Fig. 3.

V. Gases.—Ordinary grade compressed oxygen was employed. The manufacturer's stated purity was 99.5–99.8 volume % O_2.

Matheson pre-purified grade hydrogen was passed through a De-oxo unit to remove traces of O_2. In some experiments the gas was bubbled through water at room temperature prior to its introduction into the vacuum system. (It has been demonstrated that traces of water vapor enhance the quantity of hydrogen atoms in the vicinity of an electrodeless discharge.[15]) The minimum detectable concentration of hydrogen atoms by e.p.r. spectrometry in our apparatus was approximately 1×10^{13} atoms/cm.^{3}.

Results

Considering both convective flow and diffusion, the total flux of atoms to the filament, Φ, is given by

$$\Phi = \Phi_{diff} + \Phi_{conv} \quad (8)$$

For first-order kinetics of heterogeneous atom removal the diffusive term is related to the atom-concentration gradient at the catalytic surface, located at a fixed position $x = L$, by[16]

$$\Phi_{diff} = -D_{12} (\partial N/\partial x)_L = \frac{\gamma' c N}{4 D_{12}[1 - (\gamma'/2)]} \quad (9)$$

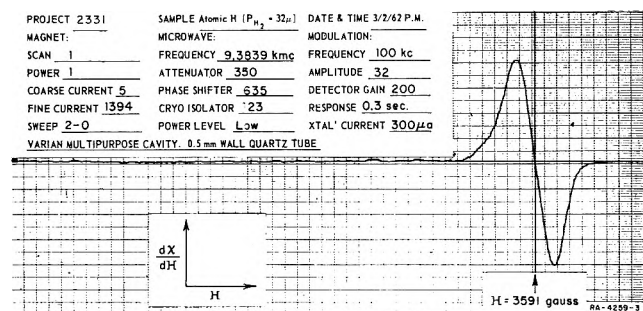where D_{12} is the binary diffusion coefficient of hydrogen atoms through the molecular gas, c, the mean atomic velocity, γ', the recombination coefficient defined as the fraction of incident atoms which recombine, and N, the hydrogen atom density.

The effective contribution of the convective term to atom recombination on the solid is given by

$$\Phi_r = \gamma' \Phi_{conv} = \gamma' v N \quad (10)$$

where v is the linear velocity of the flowing gas. Consequently the effective total flux of recombining atoms is

$$\Phi_s = \gamma' N \left\{ \frac{c}{2(2 - \gamma')} + v \right\} \quad (11)$$

For the case of hydrogen atoms the magnitude of the convective flow term in eq. 11 is of the order of 1% of that of the diffusive flow term at the pumping speeds encountered in our experiments. The contribution of bulk flow to Φ_s was therefore neglected in our calculations. Experimental evaluation of the atom concentration gradients in the tube under conditions or both convective-diffusive flow and diffusive flow only demonstrated that neglect of the convective flow term in eq. 11 was justified (Fig. 2).

The steady-state heterogeneous recombination process may be described in terms of an energy balance

$$w/A = \Phi_s \beta Q \quad (12)$$

where w is the net power input to the filament due to heterogeneous atom recombination, A is the geometric surface area of the filament, Q is the heat of recombination of hydrogen atoms $= 8.5 \times 10^{-20}$ cal./atom, and β the reaction energy accommodation coefficient. Sub-

(14) N. F. Ramsey, "Molecular Beams," Oxford University Press, London, 1956, p. 246.

(15) F. Kaufman and F. P. Del Greco, J. Chem. Phys., 35, 1895 (1961).

(16) H. Motz and H. Wise, ibid., 32, 1893 (1960).

stituting eq. 11 (less the negligible convective flow term) into eq. 12, we obtain

$$\beta = \frac{4w[1 - \gamma'/2]}{NcAQ\gamma'} \qquad (13)$$

The values of β obtained in this way from our experimental data are shown in Table I.

TABLE I

EXPERIMENTAL VALUES OF REACTION ENERGY ACCOMMODATION COEFFICIENTS, β, FOR HYDROGEN ATOM RECOMBINATION ON METALS

(Gas temperature = 300°K.)

Catalytic surface (filament)	Filament temp. (°K.)	Range of atom concn.[b] [(atoms/ cm.³) × 10⁻¹⁴]	Total gas density [(mole- cules/cm.³) × 10⁻¹⁴]	γ'[a]	β (av.)
Nickel	423	0.15–2.4	51.8	0.20	0.60 ± 0.11
Tungsten	443	.34–7.8	48.5	.07	.79 ± .08
	480	.33–2.9	10.4	.07	.81 ± .05
	773	.69–10.4	10.4	.07	.85 ± .13
Platinum	376	.79–2.2	26.0	.040	.49 ± .07
	378	.66–2.1	28.2	.040	.57 ± .07
	588	.30–1.7	28.2	.079	.25 ± .03
	813	.94–5.6	26.0	.10	.19 ± .02

[a] Values of γ' were calculated from data of ref. 2 using most recently reported[17] values of D_{12}. [b] Atom concentrations were evaluated at the e.p.r. cavity and were varied within the indicated range of values at the indicated total gas density by adjusting the RF power input to the discharge.

Discussion

The measured values of β (Table I) seem to strengthen the hypothesis[2] that the relative efficiency with which this energy can be removed from the reacting system is the key to catalytic efficiency for reactions of this type. To some degree the magnitude of β appears to be inversely related to the value of γ'. This is particularly evident in the case of platinum, which exhibits a variation in recombination coefficient with temperature.[2] It is of interest to observe that the product $\beta\gamma'$ is constant over the range of filament temperatures measured. From this observation and from eq. 13, we may con-

clude that there exists an upper limit to the energy flux which the solid can accept.

Such an interpretation finds an analogy in the case of collisional energy transfer between a gaseous species and a solid surface in the absence of chemical reaction. Theoretical considerations[18] based on a classical model lead to the conclusion that the transfer of energy, by spontaneous phonon emission into the crystal lattice from the point of impact, becomes less efficient when the kinetic energy of the incident particle lies above a certain level. In a steady state process, therefore, in which the total rate of energy input to the surface exceeds this level, only a fraction of the liberated energy can be accommodated.

The variation in accommodation coefficients among various solids is a function of the lattice force constant of the crystal; the greater the magnitude of this parameter, the smaller the quantity of energy that can be transferred by phonon emission per collision.[19] This fundamental characteristic of a crystal, however, may be altered by the introduction of foreign atoms or ions into the lattice. The dissolution of hydrogen in certain metals, for example, has been demonstrated to profoundly affect such physical properties as metal atom spacing in the lattice[20] and possibly the electron-energy distribution. Such lattice changes may be expected to influence phonon transfer and may account for the variation in β with temperature in the case of platinum.

It appears that the hydrogen molecules formed in heterogeneous recombinations are not in thermal equilibrium with the catalyst. Hence, these particles must leave the surface with an excess of energy in the form of internal and/or translational modes. A quantitative evaluation of the energy distribution in such desorbed molecules would be of some importance to studies concerned with energy transfer in the presence of exothermic heterogeneous chemical reaction.

Acknowledgment.—We wish to express our thanks to Mr. Dan J. Schott for his assistance in this experimental program.

(17) S. Weissman and E. A. Mason, *J. Chem. Phys.*, **36**, 794 (1962).

(18) N. Cabrera, *Discussions Faraday Soc.*, **28**, 16 (1959).

(19) R. W. Zwanzig, *J. Chem. Phys.*, **32**, 1173 (1960).

(20) D. P. Smith, "Hydrogen in Metals," University of Chicago Press, Chicago, Illinois, 1948.

THE "DIRECT EFFECT" IN THE RADIOLYSIS OF AQUEOUS SODIUM NITRATE SOLUTIONS

By H. A. Mahlman

Chemistry Division, Oak Ridge National Laboratory,[1] Oak Ridge, Tennessee

Received December 26, 1962

Oxygen-18 enriched water was used to determine the source of molecular oxygen formed during the Co-60 γ-radiolysis of aqueous sodium nitrate solutions. Mass spectrographic analyses of the O_2 indicated that the oxygen came from two sources: (1) the joint participation of H_2O and NO_3^- and (2) from the nitrate ions. The oxygen formed by decomposition of the nitrate ion is directly proportional to the dissolved solute. Since nitrite ion is the only major nitrogen-containing radiolysis product, the over-all decomposition is consistent with $NO_3^- \rightsquigarrow NO_2^- + 0.5O_2$. The $G(O_2)$ was measured in the Ce^{+4}–0.4 M H_2SO_4–$NaNO_3$ system and, like the $G(Ce^{+3})$ in this system, increased rapidly as a function of the $NaNO_3$ concentration at low $NaNO_3$ concentrations and at a slower rate, directly proportional to $NaNO_3$ concentration, at high $NaNO_3$ concentrations. The $G(O_2)$ from radiolysis of the NO_3^- in H_2O^{18}–$NaNO_3$ solutions is correlated with the directly proportional regions of the $G(Ce^{+3})$ and the $G(O_2)$ measured in the Ce^{+4}–0.4 M H_2SO_4–$NaNO_3$ system.

Introduction

The radiation chemistry of dilute aqueous solutions has been interpreted on an initial decomposition of solvent into oxidizing and reducing species and their subsequent reactions with each other or with dissolved solutes. The observed chemical reactions are consistent with the identification of these species as the OH radical and the H atom and/or solvated electron. When concentrated aqueous solutions are irradiated, however, some product yields increase and can no longer be explained by the currently accepted radical yields observed in dilute aqueous solutions. These increased yields have been descriptively termed "direct action" and are in general directly proportional to the concentration of the dissolved solute. The purpose of this paper is to present evidence for a directly proportional direct action effect on the nitrate ion in aqueous $NaNO_3$ solutions and to correlate these findings with the previous work of the author. The enhanced cerous yield after corrections have been made for known Ce^{+4} reduction reactions in the Ce^{+4}–0.4 M H_2SO_4–$NaNO_3$ solution[2,3] has been divided into two individual contributions that will be discussed in terms of nitrate decomposition by direct action and by scavenging.

Experimental

Reagent grade Baker and Adamson sodium nitrate and potassium bromide, C.P. sulfuric acid, and G. Frederick Smith analytical reagent ceric acid sulfate were used in the experiments. The sodium nitrate was recrystallized three times from specially distilled water recovering only the middle 50% on each crystallization. The potassium bromide, however, was used without recrystallization. The sulfuric acid was redistilled in the presence of ceric ion using only the middle ⅓ portion for the preparation of a ceric ion stock solution. Water used for the recrystallization of $NaNO_3$ and for the acidic ceric solutions was purified by distilling water from a Barnstead still from acid dichromate solution, a basic permanganate solution, and then in an all-silica system. Storage was in silica vessels.

The acidic ceric solutions were prepared for irradiation from the ceric stock solution to contain 0.0004 M ceric ion, 0.4 M H_2SO_4, and the desired concentration of $NaNO_3$. They were deaerated by repeated freezing, evacuating to 10^{-6} mm. pressure, and thawing and irradiated in a 600-curie cobalt-60 γ-ray source. Quantitative oxygen determinations were made by ignition with hydrogen on a platinum filament.

For the isotopic experiments, oxygen-18 enriched water, containing 1.6% O-18, was obtained from the Operations Division of the Laboratory. This water was purified by distillation from an acidic potassium dichromate solution and then in an all-silica system. Further purification was effected by irradiating the air-saturated water in the cobalt-60 γ-ray source and then photolyzing any peroxide that was formed. After repeating the irradiation-photolysis cycle three times, the water was used to prepare the $NaNO_3$ solutions.

Solutions were prepared to contain 10^{-3} M potassium bromide, to protect the molecular hydrogen formed during irradiation from OH radical attack, and the desired amount of recrystallized sodium nitrate for the concentration range 1.0 to 6.0 molar in sodium nitrate. These solutions were deaerated as previously described. After irradiation the irradiation cells were opened and the permanent gases, hydrogen and oxygen, were recovered and analyzed by the Mass Spectrographic Laboratory. The possible molecular oxygen masses 32, 34, and 36 were monitored. In other similarly prepared samples the quantity of hydrogen and oxygen was determined by ignition on a platinum filament with oxygen and hydrogen, respectively.

The dose rate of the cobalt-60 γ-ray source was determined by the oxidation rate of ferrous ion in an air-saturated 0.4 M H_2SO_4 solution. It was assumed that 15.6 ferrous ions were oxidized per 100 e.v. of absorbed energy.[4] The increase in the ferric ion spectrophotometric absorption was measured on a Cary recording spectrophotometer, using the 25° molar extinction coefficient of 2240 at 3050 Å.[4] Since the solutions contained large amounts of solute, the increase in energy absorption was calculated using γ mass absorption coefficients.[5] The yields, $G(product)$, defined as the number of molecules formed per 100 e.v. of absorbed energy, are reported on the basis of total absorbed energy.

The experimental details and techniques utilized to determine the $G(C^{+3})$ in the Ce^{+4}–0.4 M H_2SO_4–$NaNO_3$ solutions have been reported.[3]

Results and Discussion

Although the exchange of oxygen atoms between H_2O^{18} and NO_3^- takes place in acid solution[6] it should not be a factor at the pH used for these experiments.[7] The presence of the molecular oxygen mass 34 above that predicted from the natural abundance of the oxygen isotopes in nitrate ion indicates that the water has participated in the solution decomposition. In Table I, the per cent of molecular oxygen mass 34 observed is given for the $NaNO_3$ concentrations 1.0 to 6.0 M. Using oxygen mass 34 as the criterion to determine the extent of water participation the balance of the molecular oxygen must come from the only other oxygen-containing molecule or ion in the solution—the nitrate ion. The $G(O_2)$ from the nitrate ion, $G(O_2)_{NO_3^-}$, as calculated from the mass spectrographic data is also given in Table

(1) Operated by Union Carbide Corporation for the Atomic Energy Commission.

(2) T. J. Sworski, *J. Am. Chem. Soc.*, **77**, 4689 (1955).

(3) H. A. Mahlman, *J. Phys. Chem.*, **64**, 1598 (1960).

(4) C. J. Hochanadel and J. A. Ghormley, *J. Chem. Phys.*, **21**, 880 (1953).

(5) H. A. Mahlman and G. K. Schweitzer, *J. Inorg. Nucl. Chem.*, **5**, 213 (1958).

(6) M. Anbar, M. Halmann, and S. Pinchas, *J. Chem. Soc.*, 1242 (1960).

(7) M. Anbar, personal communication.

I and plotted in Fig. 1. An explanation of the positive $G(O_2)_{NO_3}$- intercept equal to 0.05 is not apparent; however, it is readily seen in Fig. 1 that the increase in the $G(O_2)_{NO_3}$- is directly proportional to the $NaNO_3$ concentration in the solution. This change in the $G(O_2)_{NO_3}$- will be utilized in the interpretation and conclusions of this paper.

Fig. 1.—The $G(O_2)_{NO_3}$- as a function of the $NaNO_3$ concentration.

TABLE I

OXYGEN AND HYDROGEN YIELDS AS A FUNCTION OF $NaNO_3$ CONCENTRATION

$NaNO_3$, M	% O_2 mass 34 obsd.	H_2O^{18}–$NaNO_3$ Fraction oxygen mass 34	H_2O^{18}–$NaNO_3$ Total obsd. $G(O_2)$	$G(O_2)_{NO_3}$-	Ce^{+4}– 0.4 M H_2SO_4– $NaNO_3$ $G(H_2)$	Ce^{+4}– 0.4 M H_2SO_4– $NaNO_3$ $G(O_2)$
0	..	..	..	..	0.45	0.80
0.5	..	..	..	..	.154	1.17
1.0	1.84	0.57	0.20	0.09	.098	1.41
2.0	1.39	.43	.31	.18	.066	1.48
	1.30	.41				
3.0	1.37	.43	.42	.25	.055	1.54
	1.28	.40				
4.0	1.29	.40	.50	.30	.045	1.61
5.0	1.12	.35	.56	.36	.041	1.66
6.0	1.02	.31	.63	.43	...	..

Since nitrite ion has been shown to be the only major nitrogen-containing product,[8] stoichiometric amounts of NO_2- and O_2 may reasonably be expected to be formed according to the over-all equation

$$NO_3^- \rightsquigarrow NO_2^- + \frac{1}{2}O_2 \qquad (1)$$
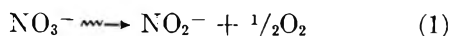
If this reaction or its equivalent takes place it should be easily detected in a Ce^{+4}–0.4 M H_2SO_4–$NaNO_3$ solution, since the Ce^{+4} ion is readily reduced in acid solution by nitrite ion. In Fig. 2, curve A represents the observed reduction of ceric ions in a Ce^{+4}–0.4 M H_2SO_4–$NaNO_3$ solution.[3] There is a rapid initial increase in the $G(Ce^{+3})$ with increasing nitrate concentration. At higher nitrate concentrations the $G(Ce^{+3})$ increases less rapidly and becomes a linear function of the $NaNO_3$ concentration. Let us discuss the Ce^{+4}–0.4 M H_2SO_4–$NaNO_3$ system by first presenting the radiation induced ceric reduction mechanism[9] that takes place in the absence of $NaNO_3$.

$$Ce^{+4} + H \longrightarrow Ce^{+3} + H^+ \qquad (2)$$

$$Ce^{+4} + H_2O_2 \longrightarrow Ce^{+3} + H^+ + HO_2 \qquad (3)$$

$$Ce^{+4} + HO_2 \longrightarrow Ce^{+3} + H^+ + O_2 \qquad (4)$$

$$Ce^{+3} + OH \longrightarrow Ce^{+4} + OH^- \qquad (5)$$
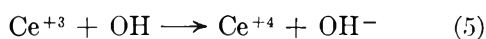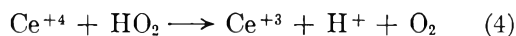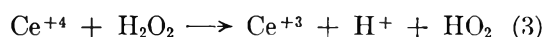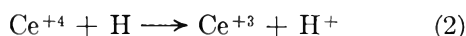
The reaction of Ce^{+4} with H atoms (reaction 2) can successfully compete with the recombination of H atoms to form molecular hydrogen.[10] Thus the $G(Ce^{+3})$ is given by $2G_{H_2O_2} + G_H - G_{OH} + 2[0.45 - G(H_2)]$. Since the G_{OH} has been shown to be constant as the $NaNO_3$ concentration was varied over a wide range,[2,3] it was assumed that the ceric reduction was also constant and equal to the same reduction rate as in 0.4 M H_2SO_4. Thus, the reduction of Ce^{+4} by the radiolysis of solvent is given by curve C in Fig. 2 as $G(Ce^{+3}) = 2.38$.[3]

Fig. 2.—Isolation of the enhanced $G(Ce^{+3})$ in the Ce^{+4}–0.4 M H_2SO_4–$NaNO_3$ system: curve A, observed $G(Ce^{+3})$; curve B, equivalent $G(Ce^{+3})$ due to the suppression of $G(H_2)$; curve C, $G(Ce^{+3})$ observed in the absence of $NaNO_3$ equal to $2G_{H_2O_2} + G_H - G_{OH} + 2[0.45 - G(H_2)]$.

The suppression of the molecular hydrogen yield,[11] $G(H_2)$, indicates that the rate constant for the reaction $NO_3^- + H$ is sufficiently large to successfully compete with $H + H$ to form molecular hydrogen. In Table I the $G(H_2)$ observed in Ce^{+4}–0.4 M H_2SO_4–$NaNO_3$ solutions are given. The decrease in the $G(H_2)$ manifests itself by forming nitrite ion[12] or a precursor which reduces a stoichiometric equivalent amount of ceric ion. In Fig. 2, the difference between curve C and curve B represents the $G(Ce^{+3})$ attributable to the suppression of molecular hydrogen by nitrate ions.

The difference between curve A and curve B is a measurement of the corrected enhanced cerous yield and is plotted in Fig. 3. We see that as the $NaNO_3$ concentration increases there is an initial rapid increase in the ceric reduction yield which then becomes linearly dependent upon the sodium nitrate concentration. If we extrapolate this linear portion, i.e., the cerous yield at $NaNO_3$ concentrations 2 molar and greater back to

(8) H. A. Mahlman, unpublished results, Chemistry Division Information Meeting, Oct., 1961.

(9) A. O. Allen, Radiation Res., 1, 87 (1954).

(10) H. A. Mahlman, J. Am. Chem. Soc., 81, 3203 (1959).

(11) (a) H. A. Mahlman and J. W. Boyle, J. Chem. Phys., 27, 1434 (1957); (b) H. A. Mahlman, ibid., 31, 993 (1959).

(12) N. A. Bakh, Conference of the Academy of Science of the U.S.S.R. on the Peaceful Uses of Atomic Energy, 1955.
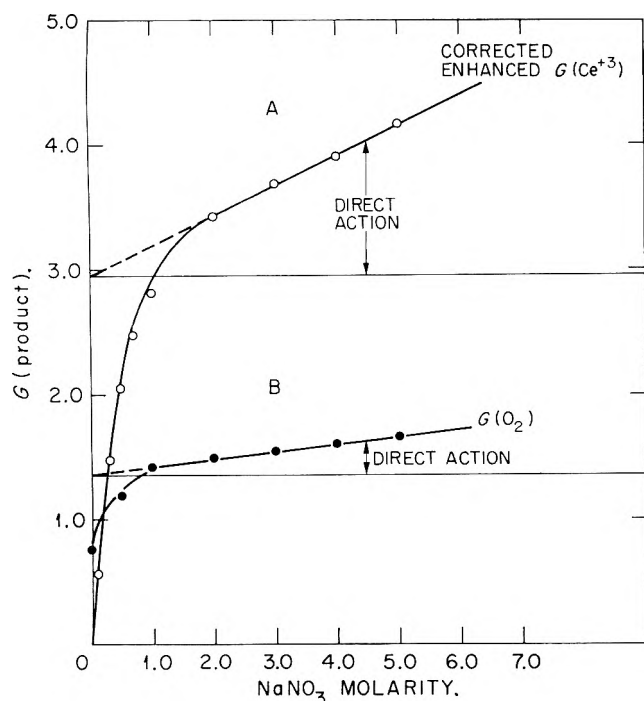
Fig. 3.—Isolation of the direct effect in the Ce^{+4}–0.4 M H$_2$SO$_4$–NaNO$_3$ system: A, ionic data—G(Ce^{+3}). B, molecular data—G(O$_2$).
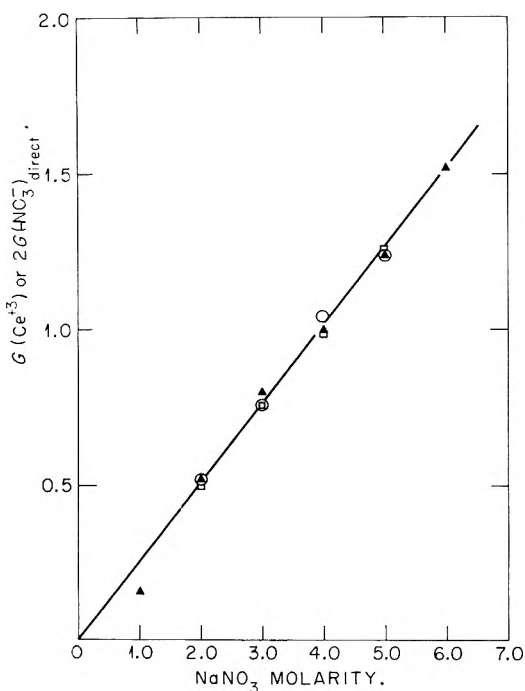
Fig. 4.—Comparison of G(O$_2$)$_{NO_3^-}$ stoichiometric equivalent G(Ce^{+3}) with the G(Ce^{+3}) and the stoichiometrically equivalent G(Ce^{+3}) from G(O$_2$) in the Ce^{+4}–0.4 M H$_2$SO$_4$–NaNO$_3$ system: O, G(Ce^{+3}) equivalent to G(O$_2$) mass 32 originating from NO$_3^-$; ▲, G(Ce^{+3}) equivalent to G(O$_2$) in the Ce^{+4}–0.4 M H$_2$SO$_4$–NaNO$_3$ system; □, isolated G(Ce^{+3}) direct effect in the Ce^{+4}–0.4 M H$_2$SO$_4$–NaNO$_3$ system.

zero NaNO$_3$ molarity, we have divided the corrected enhanced Ce^{+3} yield into two contributions: (1) a contribution directly proportional to NaNO$_3$ concentration (the direct effect) and (2) a contribution that increases with the NaNO$_3$ molarity until a maximum yield is reached and then remains constant.

The directly proportional region may be correlated with the oxygen-18 enriched water–NaNO$_3$ studies. As indicated in Fig. 1, we have a directly proportional rela-

tionship between the molecular oxygen arising from the sodium nitrate and the sodium nitrate concentration. If the over-all reaction given as eq. 1 takes place to form molecular oxygen and nitrite, then we should be able to correlate the directly proportional increase in the ceric reduction with the formation of O$_2$ from nitrate ion. For each molecule of oxygen found two nitrite ions are formed, each of which may reduce two ceric ions. With this stoichiometry, Fig. 4 is used to compare the direct effect from the oxygen-18 enriched water–NaNO$_3$ studies with the direct effect isolated from the Ce^{+4}–0.4 M H$_2$SO$_4$–NaNO$_3$ studies. In Fig. 4 the open circular points (O) represent the equivalent G(Ce^{+3}) as determined from the G(O$_2$) (mass 32) in the oxygen-18 enriched water–NaNO$_3$ system while the open square points (□) are those of the isolated direct action cerous yield, G(Ce^{+3})$_{NO_3^-}$. As readily seen, the agreement between the G(Ce^{+3})$_{NO_3^-}$ measurements and isotopic oxygen measurements is well within experimental error.

The molecular oxygen evolved during the cobalt-60 γ-radiolysis of Ce^{+4}–0.4 M H$_2$SO$_4$–NaNO$_3$ solutions may also be correlated with the G(Ce^{+3}). The G(O$_2$), listed in Table I are presented in Fig. 3. As in the ionic Ce^{+3} analyses there is an initial rapid increase in the G(O$_2$) which then becomes linearly dependent upon the NaNO$_3$ concentration. Extrapolation of this linear portion of the G(O$_2$) to zero NaNO$_3$ molarity separates the region of direct action from the other contributions. If reaction 1 represents the formation of O$_2$ and NO$_2^-$ by direct action, then the ionic cerous yield and the G(O$_2$) in this Ce^{-4} 0.4 M H$_2$SO$_4$–NaNO$_3$ system should be equivalent. The solid triangular points (▲) in Fig. 4 are the equivalent G(Ce^{+3}) calculated as discussed previously from the G(O$_2$). The agreement is equally good.

The other mechanism, a proposed scavenging mechanism for the reduction of Ce^{+4}, has not been deduced. We may, however, delineate some criteria for this mechanism. These are (1) the magnitude of the effect is about G = 2.92, which is essentially the OH radical yield; (2) the non-linear nature of the increased G(Ce^{+3}) suggests a scavenging reaction; and (3) the G_{OH} is constant,[2,3] independent of the sodium nitrate concentration. Thus, we may conclude that if the OH radical is scavenged by nitrate ion, as has been suggested by Challenger and Masters,[13] one of the products of the reaction reacts in the same manner as the OH radical, i.e., by oxidizing Ce^{+3} and Tl$^+$. It is difficult, indeed, to conceive and delineate a mechanism for the initial rapid increase in the cerous yield consistent with the criteria outlined above.

Summary

The use of oxygen-18 enriched water was utilized to ascertain the origin of the molecular oxygen evolved during the irradiation of deaerated aqueous sodium nitrate solutions. The directly proportional relationship of O$_2$ formation from nitrate ions with the sodium nitrate concentration in oxygen-18 labeled water solutions was compared with the O$_2$ formed during the radiolysis of Ce^{+4}–0.4 M H$_2$SO$_4$–NaNO$_3$ solutions. It was also compared with the increased Ce^{+4} reduction in the same system after the appropriate corrections

(13) G. E. Challenger and B. J. Masters, J. Am. Chem. Soc., 77, 1063 (1955).

were made for the known contributions to the ceric reduction. Corrections in the observed $G(Ce^{+3})$ included reduction of ceric ions by molecular and radical radiolysis products, and the reduction of the $G(H_2)$ caused by the scavenging action of the nitrate ion for hydrogen atoms. Isolation of a $G(Ce^{+3})$ directly proportional to the $NaNO_3$ concentration was accomplished after these corrections were made. Excellent correlation was obtained between the isolated $G(Ce^{+3})$ which is directly proportional to the $NaNO_3$ concentration, the stoichiometrically equivalent $G(Ce^{+3})$ as deduced from the $G(O_2)$ measured in Ce^{+4}–0.4 M H_2SO_4–$NaNO_3$ solutions, and the stoichiometrically equivalent $G(Ce^{+3})$

calculated from the $G(O_2)$ originating from the radiation-induced decomposition of nitrate ion in enriched oxygen-18 H_2O–$NaNO_3$ solutions. This correlation supports the over-all decomposition as $NO_3^- \rightsquigarrow \rightarrow NO_2^- + \frac{1}{2}O_2$.

CONVECTIVE MASS TRANSFER IN A DIAPHRAGM DIFFUSION CELL

By John T. Holmes,[1] Charles R. Wilke, and Donald R. Olander

Department of Chemical Engineering, and the Lawrence Radiation Laboratory, University of California, Berkeley, Cal.

Received December 26, 1962

A fundamental assumption implicit in the analysis of a diaphragm diffusion cell is that the sole resistance to transport resides in the porous glass disk, through which the solute moves by molecular diffusion. This paper presents an experimental examination of the resistance to mass transfer in the fluid regions adjacent to either side of the porous disk. The presence of an external mass transfer resistance has been observed by others who have recommended that all diffusion measurements be conducted at stirring speeds greater than an empirically determined value where the cell constant becomes independent of the stirring rate. However, the external mass transfer coefficients depend not only on the stirring speed, but also upon the viscosity and diffusivity of the solute–solvent system as well. There is no justification for assuming that operation above the critical speed found for the calibration fluid will eliminate the external mass transfer resistance in a system of larger viscosity and small diffusivity. Both free- and forced-convection mass transfer characteristics of a vertical diaphragm cell were investigated and the results correlated in terms of stirrer speed and the fluid properties. The data indicate that operation above a critical speed is appropriate for a number of common systems but that significant errors can arise for systems of high viscosity and low diffusivity and that for high reproducibility and accuracy, cells stirred by free convection alone should not be employed.

Introduction

A fundamental simplification implicit in the analysis of a diaphragm diffusion cell is the hypothesis that the sole resistance to transport resides in the porous glass disk, through which the solute moves by molecular diffusion. More precisely, this model involves two independent assumptions: first, that there is no bulk convective flow through the pores of the disk, and second, that the resistance to mass transfer in the fluid regions adjacent to either side of the disk is negligible. This paper presents an experimental examination of the second assumption. Bulk convection through the pores has been observed,[2] but will not be considered here.

The presence of an external convection mass transfer resistance has been observed by Stokes[2a] and Lewis[3] as an increase in the cell constant with the rotational speed of stirring bars in the two compartments. Above a certain speed, the cell constant becomes independent of stirring rate and these workers recommend that all diffusion measurements be conducted at speeds greater than the empirical determined critical value. However, the external mass transfer coefficients depend not only on the stirrer speed, but upon the viscosity and diffusivity of the solute–solvent system as well. There is no justification for assuming that operation above the critical speed found for the calibration fluid (generally 0.1 N KCl in water at 25°) will eliminate the external

mass transfer resistance in a system of larger viscosity and smaller diffusivity, e.g., solute dodecane in tetradecane at 15°. Therefore, the free- and forced-convection mass transfer characteristics of the vertical diaphragm cell, shown in Fig. 1, were investigated and the results correlated in terms of stirrer speed and fluid properties.

Experimental

Apparatus.—Ace Glass E porosity disks were employed in a vertical position. The diaphragms were 5.0 cm. in diameter, 0.5 cm. thick, and with a nominal pore size range between 3 and 8 μ. The cell compartments were each approximately 125 cc. in volume and were stirred with 1-in. long Teflon-covered bar magnets. The cells were calibrated with 0.2 N HCl using the data of Stokes[2a] as reference diffusion coefficients. Densities were measured with a Westphal balance, and were reproducible to ±0.2%. Viscosities were measured with an Oswald viscosimeter calibrated with distilled water and were reproducible to ±0.5%. All data were taken at 25.0 ± 0.1°. The four stirring speeds obtainable with the equipment were measured with a stroboscope. For additional details of the equipment and experimental procedure, see ref. 4.

Effect of Fluid Properties and Stirring Speed.—Solute transfer from one compartment of the cell to the other occurs in the following sequence: (a) convective transfer through the boundary layer on the disk in the compartment containing the concentrated solution; (b) molecular diffusion through the sintered glass disk; (c) convective transfer through the boundary layer on the disk in the compartment containing the dilute solutions. Assuming pseudo steady-state operation, the mass transfer rate is given by eq. 1

(1) Argonne National Laboratory, Argonne, Illinois.

(2) (a) R. H. Stokes, *J. Am. Chem. Soc.*, **72**, 763 (1950); (b) A. Emanuel and D. R. Olander, *J. Chem. Eng. Data*, **8**, 31 (1963).

(3) J. B. Lewis, *J. Appl. Chem.* (London), **5**, 228 (1955).

(4) J. T. Holmes, USAEC Report UCRL-9145 (1960).
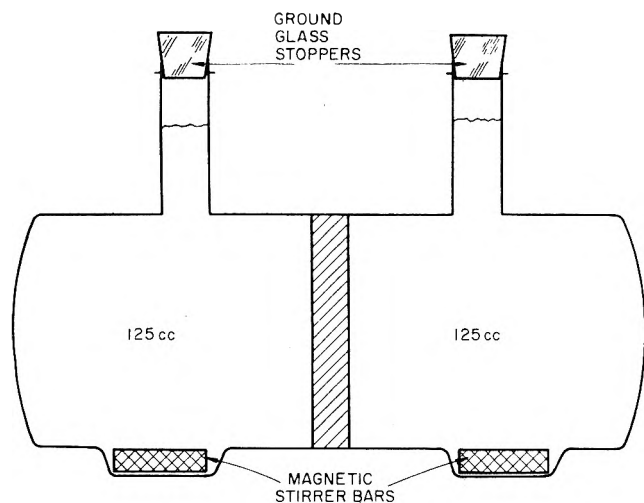
Fig. 1.—The diaphragm cell.
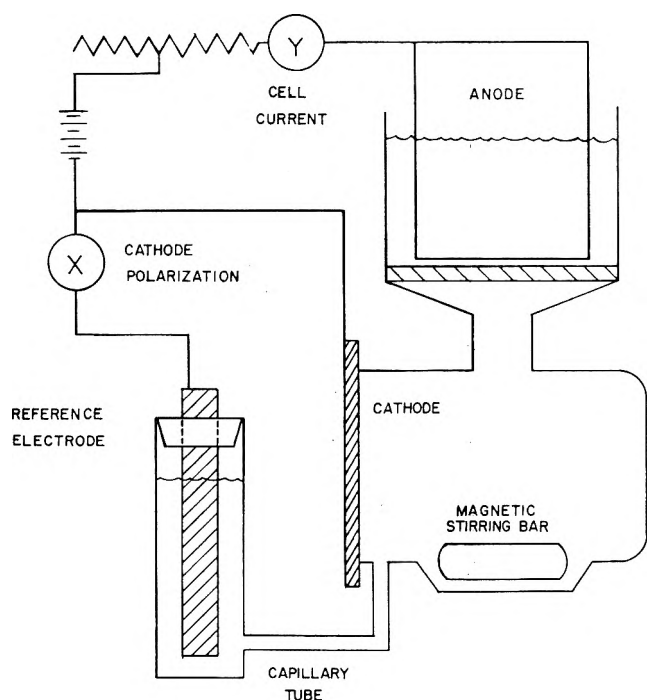
Fig. 2.—Electrochemical half-cell.

$$N = kA(C_1 - C_{1_i}) = DA'/l\,(C_{1_i} - C_{2_i}) = kA(C_2 - C_2) \quad (1)$$

where N is the molar transfer rate of the solute, k the external mass transfer coefficient (assumed the same on both sides of the disk) in cm./sec., A the gross area of the disk, D the diffusion coefficient, and A'/l the effective area-to-length ratio of the pores in the disk. Concentrations involved are: C_1, in the bulk of compartment one; C_{1_i} the edge of the diaphragm in compartment one; C_{2_i} at the edge of the diaphragm in compartment two; C_2 in the bulk of compartment two. A material balance for each compartment yields

$$N = -V_1\frac{dC_1}{dt} = V_2\frac{dC_2}{dt} \quad (2)$$

where V_1 and V_2 are the volumes of the two compartments and t the time. Combining eq. 1 and 2 and integrating

$$\ln\,(\Delta C_0/\Delta C_t) = \beta Dt \quad (3)$$

where

$$\beta = \left(\frac{1}{V_1} + \frac{1}{V_2}\right)\frac{1}{2D/kA + l/A'}, \quad (4)$$

ΔC_0 and ΔC_t are the differences in the concentration between the two compartments initially and at time t, respectively. β is the experimentally determined cell constant. Above the critical stirring speed, $l/A' \gg 2D/kA$, and eq. 4 reduces to the standard expression for the cell constant. The factor $2D/kA$ accounts for the external mass transfer resistance due to the laminar fluid layers on the diaphragm cell.

Evaluation of the Mass Transfer Coefficients.—The mass transfer coefficients required in eq. 4 have been measured by electrochemical limiting-current experiments in a half-cell identical with one side of the apparatus shown in Fig. 1. This system is shown schematically in Fig. 2. Wilke, et al.,[5,6] have shown that limiting current experiments in copper sulfate and silver perchlorate solutions were diffusion controlled, and thus provided direct measure of the mass transfer characteristics of the electrolytic cell. The rate of deposition of copper is given by

$$N = k(C - C_i) = (1 - \tau)\,I/z\mathfrak{F} \quad (5)$$

$C - C_i$ is the concentration difference between the bulk liquid phase and the electrode surface, and for this case is equal to C. τ is the transference number for copper, I the limiting current, z the valence of the cation, and $\mathfrak{F}$ the faraday. Limiting currents were measured in solutions whose viscosity and diffusivity were varied by the addition of glycerol. The mass transfer coefficients computed from equation 5 were correlated by the dimensionless relation

$$Nu = 0.050Re^{0.79}Sc^{0.38} \quad (6)$$

where Nu is the mass transfer Nusselt number, kd/D, Re a modified Reynolds number, nd^2/ν, and Sc the Schmidt group, ν/D. d is the length of the stirrer bar, n the stirrer speed, and ν the kinematic viscosity. The length parameter used in the Nusselt and Reynolds numbers has been arbitrarily taken as the stirrer bar length. Since this is not the only dimension of significance in the system, nor was d varied in this study, its use in forming the dimensionless groups of eq. 6 must be regarded solely as a matter of convenience in correlation. Figure 3 presents a plot of eq. 6 and the data from which it was obtained. Several free convection experiments (no stirring) were performed in the same electrolytic half-cell. The resulting mass transfer coefficients for the three solutions listed in Table I were correlated by

$$Nu' = 0.57\,[Sc{\cdot}Gr]^{1/4} \quad (7)$$

where $Nu = kr/D$ and Gr is the Grashoff number, $[r^3 g(\rho - \rho_i)\rho_{avg}]/\mu^2_{avg}$, r is the radius of the disk, and $\rho - \rho_i$ the density difference between the bulk and the electrode surface. Equation 7 agrees well with the relation proposed by Wilke, et al.,[5,6] for natural convection mass transfer from a free vertical wall, except that their constant was 0.66. The difference can be attributed to the

(5) C. R. Wilke, C. W. Tobias, and M. Eisenberg, *Chem. Eng. Progr.*, **49**, 633 (1953).

(6) C. R. Wilke, M. Eisenberg, and C. W. Tobias, *J. Electrochem. Soc.* **100**, 513 (1953).

use of a circular rather than a square surface, as demonstrated in the Appendix.

<div align="center">

TABLE I

FREE CONVECTION MASS TRANSFER

</div>

Solution	I	II	III
H_2SO_4 concn. (moles/l.)	1.495	0.745	1.143
$CuSO_4$ concn. (moles/l.)	0.259	0.380	0.587
Glycerol concn. (moles/ l.)	0.00	5.90	3.10
Density (g./cc.)	1.124	1.205	1.177
Viscosity (cp.)	1.457	9.310	4.093
$D \times 10^5$ (cm.^{2}/sec.)	0.513	0.122	0.234
Schmidt number (Sc)	2316	62,360	12,800
Grashoff number (Gr)	2.48×10^6	8.67×10^4	7.88×10^5
Nusselt number (Nu)	154	161	182
$Nu'/(Sc\ Gr)^{1/4}$	0.556	0.592	0.574

Effect of the External Mass Transfer on the Cell Constant.—Assuming the mass transfer behavior from a copper surface to be identical with that for the glass disk, eq. 6 and 7 permit the mass transfer coefficient k, and hence the group $2D/kA$, to be evaluated for any solute–solvent system. Although the absolute values of the correction factors are limited to the particular geometry of cell used in this study, the relative magnitudes of $2D/kA$ and l/A' and the variation of $2D/kA$ with fluid properties should be comparable in any diaphragm cell (vertical or horizontal) of this general type.

The magnitudes of $2D/kA$ for a variety of solute–solvent systems and at several stirring speeds are presented in Table II. These figures should be compared to the

<div align="center">

TABLE II

CORRECTION TO CELL CONSTANT DUE TO EXTERNAL MASS TRANSFER RESISTANCE FOR A DIAPHRAGM FOR WHICH $l/A' = 230 \times 10^{-3}$ CM.$^{-1}$

</div>

		Correction $2D/kA$, cm.$^{-1} \times 10^3$		
		$n = 0$ (Free convection)	$n = 220$ r.p.m.	$n = 350$ r.p.m.
Solvent	Solute			
Water	0.1 N KCl	8.8	1.1	0.70
Water	0.2 N HCl	16.0	1.3	.85
Hexane	Toluene	..	1.1	.77
Cyclohexane	Toluene	..	1.2	.76
Decane	Toluene	..	1.4	.80
Tetradecane	Toluene	..	1.5	.91

value of $l/A' = 230 \times 10^{-3}$ cm.$^{-1}$ for a typical diffusion cell (computed from the cell constant at high stirring speeds). Although the forced convection correction factor varied by as much as 40% with the fluid properties, it never amounted to more than 0.5% of l/A' at the stirring speeds considered. Moreover, the sum $2D/kA + l/A'$, which is involved in the assumed constancy of β, varied by less than 0.2% with fluid properties. Since the precision of the experimental method usually does not warrant corrections of this order of magnitude, it can be concluded that provided the critical stirring speed is approached the cell constants obtained from KCl measurements will be applicable to most other solvent–solute systems. For free convection, on the other hand, $2D/kA$ is not negligible compared to l/A'. Table II indicates that there should be 3.8% decrease in the unstirred cell constant for 0.1 N KCl calibration and 6.8% for 0.2 N HCl.

To verify the predicted effect of free and forced convection for HCl, the cell constants for four diaphragms were measured without stirring and with stirring at 350 r.p.m. These results are presented in Table III. The
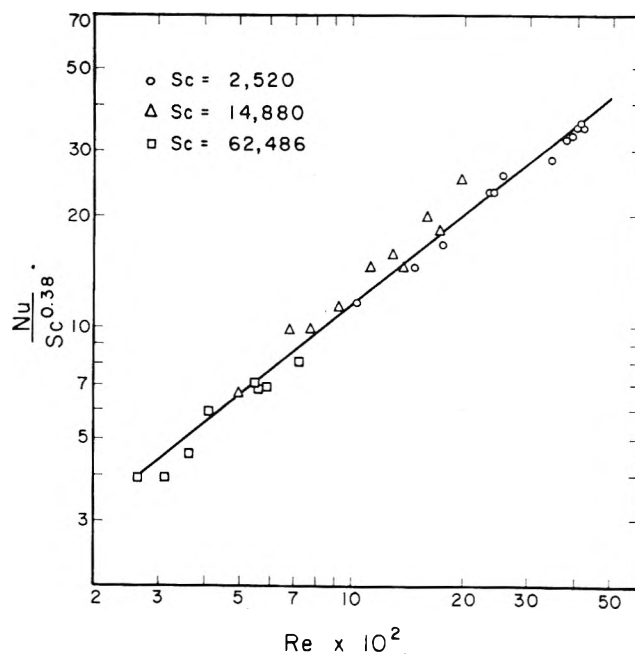
Fig. 3.—Forced convection mass transfer correlation.
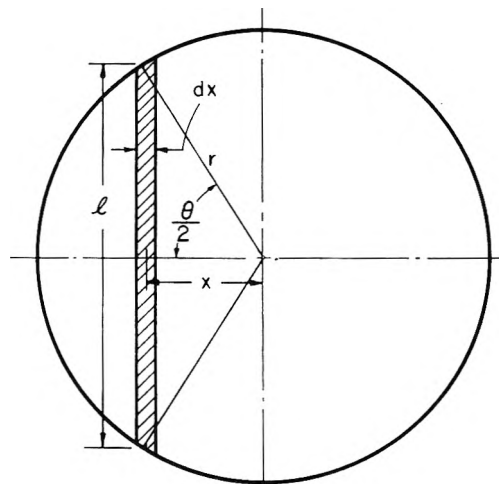
Fig. 4.—Diagram of the conversion of a plate mass transfer coefficient to that from a disk.

average difference (fourth column) is 6.4%, which compares well with the 6.8% decrease predicted from the mass transfer coefficient given by eq. 7. The observed variations from cell to cell are believed to be due to random mechanical vibrations in the apparatus. For comparison, Stokes[2a] found a 6.0% difference between stirred and unstirred cell constants for 0.1 N HCl.

<div align="center">

TABLE III

EFFECT OF STIRRING SPEED UPON THE CELL CONSTANT FOR VARIOUS DIAPHRAGMS

Cell constant, β, cm.$^{-2} \times 10^2$

</div>

	$n = 0$		
Cell no.	(Free convection)	$n = 350$ r.p.m.	% Difference
12	2.21	2.33	5.2
13	2.44	2.66	8.3
14	2.27	2.45	7.3
25	1.85	1.94	4.6

Another study of forced convection effects was recently presented by Peterson and Gregor[7] for an ion-exchange membrane system. Although their data are

(7) M. A. Peterson and H. P. Gregor, J. Electrochem. Soc., 106, 1051 (1959).

in qualitative agreement with the current study, they are not complete enough to be expressed in the general terms of eq. 6 and are therefore limited to the electrolytic solutions they investigated.

Conclusion

The data presented here indicate that cell constants obtained from calibration with dilute KCl or HCl at stirring speeds in the neighborhood of the critical speed will remain constant for most other solute–solvent systems of interest. However, if highly porous diaphragms or fluid systems of high viscosity and low diffusivity are employed, then the external mass transfer resistance may be an appreciable fraction of the resistance of the glass disk. In this case, use of the correction factor $2D/kA$ is required for precise measurements.

For high reproducibility and accuracy, cells stirred by free convection alone should not be employed. However, when somewhat lower accuracy is allowable, it may be convenient experimentally to employ a free convection cell and estimate the mass transfer effects by the methods suggested above.

Appendix

The free convection mass transfer correlation for square plates l cm. on a side is[5,6]

$$Nu = \frac{k_p l}{D} = 0.66 [Gr\, Sc]^{1/4}$$

where k_p is the mass transfer coefficient for a square plate, Sc is the Schmidt number, and the Gr is the Grashoff number. For fixed values of the physical properties and the density riving force, $k_p = C_l^{-1/4}$ where C is the constant

$$C = 0.66D\, \frac{2(\rho - \rho_i)\rho_{avg}Sc^{1/4}}{\mu^2_{avg}}$$

Assume that this relation applies to the local mass transfer coefficient on the segment of the circular plate shown in Fig. 4. This assumption implies that the parameter l is the height of the plate, that the above correlation applies to rectangles as well as squares, and the width of the rectangle is not significant.

The average mass transfer coefficient for a circular disk of radius r is then

$$k = \frac{\int_a k_p dA}{dA} = \frac{C \int_a l^{-1/4} dA}{\pi r^2}$$

From Fig. 4, $l = 2r \sin(\theta/2)$, $x = r \cos(\theta/2)$, and $dA = l\, dx = -r^2 \sin^2(\theta/2)\, d\theta$. Inserting this into the integral

$$k = \left[\frac{2^{1/4}}{\sqrt{\pi}} \frac{\Gamma(11/8)}{\Gamma(15/8)} \right] Cr^{-1/4} = 0.886Cr^{-1/4}$$

when $\Gamma(n)$ denotes the complete γ function of n. Inserting the expression for C, the disk mass transfer coefficient correlation can be written as

$$Nu' = \frac{kr}{D} = (0.886)(0.66) [Gr\, Sc]^{1/4}$$

where Gr is based upon the disk radius r.

Thus, the varying height of the disk surface reduces the average mass transfer coefficient from that which would exist for a plate of uniform height r by a factor of 0.886. The combined constant in the above expression is 0.58, which is very close to that observed (eq. 7).

THE THEORY OF ELECTRON SCATTERING FROM MOLECULES.
I. THEORETICAL DEVELOPMENT[1]

By T. Iijima, R. A. Bonham, and T. Ando

Department of Chemistry, Indiana University, Bloomington, Indiana

Received December 26, 1962

The quantum theory of electron scattering from molecules in the gas phase is developed. Expressions which include the effects of chemical binding are presented and the intensity averages to be expected for various types of experiments are discussed in terms of the theory. The quantum mechanical average over the rotational states of the molecule is shown to be reducible to the classical method of averaging rotational motion except in the case of extremely high energy resolution of the scattered electrons.

The scattering cross section of fast electrons exciting a molecule from an initial state i to a final state f is given by the formula[2]

$$I_{if} = |\vec{k_f}| < \psi^i |L_{if}|\psi^f > < \psi^f |L_{if}^*|\psi^i >/|\vec{k_i}| \quad (1.1)$$

where according to the first Born approximation, L is given as

$$L_{if} = (-\exp[ik_f r]/4\pi r) \int U(\vec{r_1}, \ldots, \vec{r_s}) \times$$
$$\exp[i(\vec{k_i} - \vec{k_f}) \cdot \vec{r_s}]\, d\tau_s \quad (1.2)$$

with the interaction potential $U(\vec{r_1}, \ldots, \vec{r_s})$. The wave function of the initial state of the molecule is ψ^i,

that of the final state is ψ^f, the incident wave vector is $\vec{k_i}$ and $\vec{k_f}$ is the scattered wave vector. The intensity of electrons observed by a diffraction experiment is the sum of I_{if} over all initial and final states of the molecule

$$I = \sum_i W^i \sum_f |\vec{k_f}| < \psi^i |L_{if}|\psi^f > < \psi^f |L_{if}^*| \psi^i >/|\vec{k_i}|$$

$$(1.3)$$

where W^i is the Boltzmann factor of the initial state i.

Using the approximation $|\vec{k_f}| = |\vec{k_i}|$[3] which is valid as long as the energy of the incident electron is large compared with the loss of energy and as long as extremely small scattering angles are not considered, the summation over final states can be carried out simply by

(1) Contribution Number 1109 from the Chemical Laboratories of Indiana University.

(2) L. Schiff, "Quantum Mechanics," McGraw–Hill Book Co., Inc., New York, N. Y., 1955, p. 206.

(3) P. M. Morse, *Physik. Z.*, **33**, 443 (1932).

use of the closure property of the wave functions, leading to the result

$$I = \sum_i W^i < \psi^i | L_{ii} L_{ii}^* | \psi^i > \qquad (1.4)$$

The total wave function, ψ^i, for the molecule may be separated into electronic, vibrational, and rotational parts as[4]

$$\psi^i = \psi_R^{\ i} \psi_V^{\ i} \psi_e \qquad (1.5)$$

and similarly, we have

$$W^i = W_R^{\ i} W_V^{\ i} W_e^{\ i} \qquad (1.6)$$

where the origin is at the center of mass of the system.

Dropping the superscript i, and noting that for most cases W_e is unity, we obtain the result

$$I = \sum_R W_R \sum_V W_V < \psi_R \psi_V \psi_e | L L^* | \psi_e \psi_V \psi_R > \qquad (1.7)$$

where ψ_e is the wave function of the ground electronic state of the molecule, R and V denote a set of quantum numbers specifying a rotational state and a vibrational state, respectively.

If we observe, by means of a velocity analyzer, the intensity of the electrons which have excited the same final electronic state of a molecule and have excited all of the rotational and vibrational states associated with this final electronic state, then the intensity expression, making use of closure arguments, can be written as[5]

$$I' = \sum_R W_R \sum_V W_V < \psi_R \psi_V | | < \psi_e^{\ i} | L | \psi_e^{\ f} > |^2 | \psi_V \psi_R > \qquad (1.8)$$

If the resolving power of the analyzer were increased to the point that individual vibrational energy losses could be resolved, then the intensity for a particular vibrational state, from the same arguments given above, would be given as

$$I'' = \sum_R W_R W_V^{\ i} < \psi_R | | < \psi_V^{\ i} \psi_e^{\ i} | L | \psi_e^{\ f} \psi_V^{\ f} > |^2 | \psi_R > \qquad (1.9)$$

Continuing this line of argument to even higher energy resolution would result finally in the intensity expression for a rotational excitation

$$I''' = W_R^{\ i} W_V^{\ i} | < \psi_R^{\ i} \psi_V^{\ i} \psi_e^{\ i} | L | \psi_e^{\ f} \psi_V^{\ f} \psi_R^{\ f} > |^2 \qquad (1.10)$$

It is interesting to note that if no attempt is made to resolve the various energy losses, then the total intensity is simply the average of an intensity operator LL^*. On the other hand, in the case of extremely high energy resolution, the total intensity is given as the square of the average of an amplitude operator L.

The Electronic Average.—The electronic average in equation 1.7, $< \psi_e | L_{ii} L_{ii}^* | \psi_e >$, can be derived in a more convenient form for a general polyatomic molecule by proceeding as follows.

We let the potential $U(\vec{r}_1, \vec{r}_2, \ldots, \vec{r}_n, \vec{r}_s)$ be given by

$$U(\vec{r}_1, \vec{r}_2, \ldots \vec{r}_n, \vec{r}_s) =$$
$$(-2/a) \left\{ \sum_{n=1}^N \left[Z_n / r_{ns} - \sum_{i=1}^{Z_n} (1/r_{si}) \right] \right\} \qquad (2.0)$$

(4) Cf., Eyring, Walter, and Kimball, "Quantum Chemistry," John Wiley and Sons, Inc., New York, N. Y. 1954.

(5) Cf., J. Karle, J. Chem. Phys., **35**, 963 (1961); D. A. Swick, Rev. Sci. Instr., **31**, 525 (1960).

where a is $\hbar^2/me^2$, m is the mass of the electron, n refers to the nth nuclear center, s to the coördinate of the colliding electron and i to the coördinate of ith electron which is assigned to the nth nucleus for convenience.

By means of the relations

$$\vec{r}_s = \vec{r}_n + \vec{r}_{ns} \qquad (2.1)$$

$$\vec{r}_s = \vec{r}_i + \vec{r}_{is} \qquad (2.2)$$

and

$$\vec{r}_i = \vec{r}_n + \vec{r}_{in} \qquad (2.3)$$

we can write L in the form

$$L = 2 \exp[ikr] \left\{ \sum_{n=1}^N \left(Z_n - \sum_{i=1}^{Z_n} \exp[i\,\vec{s}\cdot\vec{r}_{in}] \right) \right\} \times$$
$$\exp[i\,\vec{s}\cdot\vec{r}_n]/ars^2 \qquad (2.4)$$

where we have integrated over the coördinate, $\vec{r}_s$, and where $\vec{s} = \vec{k}_i - \vec{k}_f$ and $s = |\vec{s}|$.

The intensity operator LL^* can then be written as

$$LL^* = (4/a^2r^2s^4) \sum_{n=1}^N \sum_{m=1}^N \left\{ Z_n Z_m - \right.$$
$$\sum_{i=1}^{Z_n} Z_m \exp[i\,\vec{s}\cdot\vec{r}_{in}] - \sum_{i=1}^{Z_m} Z_n \exp[-i\,\vec{s}\cdot\vec{r}_{jm}] +$$
$$\left. \sum_{i=1}^{Z_n} \sum_{j=1}^{Z_m} \exp[i\,\vec{s}\cdot(\vec{r}_{in} - \vec{r}_{jm})] \right\} \exp[i\,\vec{s}\cdot\vec{r}_{nm}] \qquad (2.5)$$

where

$$\vec{r}_{nm} = \vec{r}_n - \vec{r}_m \qquad (2.6)$$

Accordingly, $< \psi_e | LL^* | \psi_e >$ can be shown to be[6]

$$< \psi_e | LL^* | \psi_e > = (4/a^2r^2s^4) \sum_{n=1}^N \sum_{m=1}^N$$
$$\{ Z_n Z_m - Z_n F_m^* - Z_m F_n + S_{nm} \} \exp[i\,\vec{s}\cdot\vec{r}_{nm}] \qquad (2.7)$$

with

$$F_n = \sum_{i=1}^{Z_n} \int \psi_e^* \psi_e \exp[i\,\vec{s}\cdot\vec{r}_{in}] d\tau \qquad (2.8)$$

and

$$S_{nm} = \sum_{i=1}^{Z_n} \sum_{j=1}^{Z_m} \int \psi_e^* \psi_e \exp[i\,\vec{s}\cdot(\vec{r}_{in} - \vec{r}_{jm})] d\tau \qquad (2.9)$$

where the integrations are over all the electronic coördinates.

Detailed calculations using the above formulas are presently underway for the case of H_2 and will be presented in a later paper. The intensity expression for electrons exciting the same initial and final electronic state can also be formulated in terms of the integrals given in (2.8) and (2.9) by using (1.8) with the potential given by (2.0).

The Rotational Average.—The effect of coupling between vibration and rotation is usually treated as a perturbation to the vibrational wave function, i.e., the perturbation of the centrifugal stretching and that of the Coriolis coupling, if necessary. The perturbed wave function depends not only on the vibrational quantum numbers, but also on the rotational quantum numbers

(6) L. S. Bartell, to be published.

except for one rotational quantum number which specifies the space degeneracy of the rotational states. By introducing the notation, F, for $<\psi_e|LL^*|\psi_e>$, eq. 1.7 can be rewritten as

$$I = \sum_{TM} W_T \sum_V W_V \int\int \psi_{TM}^* \psi_{VT}^* F \psi_{VT} \psi_{TM} \, d\tau_{rot} \, d\tau_{vib}$$

(3.0)

where T denotes the set of rotational quantum numbers without one denoted by M, which specifies the space degeneracy

The summation over M

$$F_T = \sum_{M=1}^{g_T} \psi_{TM}^* \psi_{TM}$$

(3.1)

where g_T is the degree of degeneracy of the state T, can be shown to be a constant independent of the coördinates. In fact, since $\psi_{T1}, \psi_{T2}, \ldots \psi_{T_{g_T}}$ constitutes a basis of a unitary representation of the rotation group,[7] the transform $R\psi_{TM}$ of ψ_{TM} under the rotation R may be written in the form

$$R\psi_{TM} = \sum_{K=1}^{g_T} u_{KM}\psi_{TK}$$

(3.2)

with the unitary matrix (u_{KM}). Consequently

$$RF_T = \sum_M (R\psi_{TM})^* R\psi_{TM}$$

$$= \sum_M \sum_{K,L} u_{KM}^* u_{LM} \psi_{TK}^* \psi_{TL}$$

$$= \sum_{K,L} \left(\sum_M u_{KM}^* u_{LM}\right) \psi_{TK}^* \psi_{TL}$$

$$= \sum_{K,L} \delta_{K,L} \psi_{TK}^* \psi_{TL} = \sum_K \psi_{TK}^* \psi_{TK} = F_T$$

(3.3)

Thus, F_T is invariant under every rotation and this means that it must be a constant. The magnitude of the constant, F_T, can easily be obtained by integrating both sides of eq. 3.1 in the following manner

(7) E. R. Wigner, "Group Theory," Academic Press, New York, N. Y., 1959, p. 102 and 111.

$$\int F_T \, d\tau_{rot} = F_T \int d\tau_{rot} = 4\pi F_T$$ (3.4)

$$= \int \sum_M \psi_{TM}^* \psi_{TM} \, d\tau_{rot} =$$

$$\sum_M \int \psi_{TM}^* \psi_{TM} \, d\tau_{rot} = \sum_M 1 = g_T$$

which results in the expression for F_T[8]

$$F_T = (1/4\pi)g_T$$ (3.5)

The above result can be used to simplify eq. 3.0 to the form

$$I = \sum_T g_T W_T \sum_V W_V \int (d\tau_{rot}/4\pi) \int \psi_{VT}^* F \psi_{VT} \, d\tau_{vib}$$

(3.6)

where only the classical average over rotation[9] and the usual vibrational and electronic averages remain.

Thus, the classical and quantum mechanical rotational averages are shown to give equivalent results in the absence of any perturbing field. A detailed presentation of the vibrational average, including centrifugal effects, for the diatomic case has been presented elsewhere[10]

It is hoped that the theory discussed here will form a basis for future investigations into the effects of bonding on diffraction patterns and the interpretation of the electron diffraction patterns obtained in velocity analyzer experiments.

(8) The treatment presented in equations 3.4 to 3.6 is valid only in the case of linear molecules where the degree of rotational freedom is two. For the case of general polyatomic molecules where there is an internal degree of rotational freedom in addition to two orientational freedoms, we have $F_T = (1/8\pi^2)g_T$ in place of equation 3.5..

(9) P. Debye, *J. Chem. Phys.*, **9**, 55 (1941).

(10) R. A. Bonham and J. L. Peacher, to be published.

THE ELIMINATION OF LIQUID JUNCTION POTENTIALS WITH THE GLASS ELECTRODE[1]

BY A. J. ZIELEN

Chemistry Division, Argonne National Laboratory, Argonne, Illinois

Received December 28, 1962

With proper cancellation of asymmetry potentials and using 0.1 m HCl as a reference point, the hydrogen ion response of Beckman GP glass electrodes at 25° was found ideal in a variety of solutions ranging in extremes from a pH 4.7 acetate buffer to 6 m H_2SO_4. Definite glass electrode errors were observed only in HCl solutions greater than about 0.5 m. This provides the basis for a simple and accurate general procedure for the determination of cell potentials free from liquid junction effects. Activity coefficients of HCl at 25° in the range 0.001 to 4 m were determined with a precision equal to that obtained in the best conventional cell potential work.

Introduction

Liquid junction potentials in galvanic cells are an old and recurrent problem. In practice salt bridges of various types are usually employed to minimize these effects. However, the only certain elimination of junction potentials requires an ingenious though tedious

extrapolation procedure.[2] In recent work we have utilized the glass electrode as an accurate and convenient means of obtaining cell potentials free of liquid junction effects.[3] Since common electrode poisons and oxidizing or reducing agents have no effect on the glass

(1) Based on work performed under the auspices of the U. S. Atomic Energy Commission.

(2) H. S. Harned and B. B. Owen, "The Physical Chemistry of Electrolytic Solutions," Reinhold Publ. Corp., New York, N. Y., 3rd Ed., 1958, pp. 448-451.

electrode,[4] the method should be suitable for a wide variety of cells. To establish definitely the validity of the procedure, two types of experiments are reported here.

First a measure of the absolute accuracy was obtained by determining the standard potential of the silver–silver chloride electrode and activity coefficients of hydrochloric acid and comparing with other highly precise data. In the second and more crucial series, possible differences in the hydrogen ion response of glass electrodes were determined in pairs of solutions differing widely in acidity, ionic strength, and composition. This was a vital point since our method depends on identical glass electrode response in two different (though usually similar) solutions: one for calibrating the glass electrode vs. a standard hydrogen electrode and the other the test solution and electrode of interest.

Experimental

Electrodes.—Thermal-electrolytic silver–silver chloride electrodes were prepared as outlined by Bates.[5] The silver oxide used was washed thirty-five times, the last five with triple distilled water. Electrodes were aged two months in distilled water before use. Sets of four electrodes customarily agreed within 0.01 mv. and never exceeded 0.02 mv. average deviation from a reference pair of electrodes aged for a year.

Two markedly different types of platinized platinum hydrogen electrodes were employed, prepared according to the directions of Bates and Hills and Ives.[6] Excellent performance was obtained with both; however, the minimal platinization of the Hills and Ives type was favored in most experiments. Before each platinization the substrate was cleaned by stripping the old coating with dilute aqua regia followed by treatment with hot concentrated nitric acid and cathodic electrolysis in 0.01 M sulfuric acid. Fresh hydrogen electrodes were prepared for each cell and never used longer than two days.

Four different glass electrodes, designated A through D and all Beckman GP Type 39177, were used. These electrodes were kept wet constantly by storage in distilled water when not in use. New glass electrodes must be conditioned by soaking in water for three days to a week before use. One new electrode was conditioned and stored in 0.1 M HCl, but no marked difference was observed from the simple water treatment.

Reagents.—Electro-grade hydrogen and pre-purified nitrogen were obtained from commercial cylinders. Either or both gases could be passed simultaneously through two independent gas lines that each contained an Ascarite tube and a deoxygenating furnace tube packed with copper turnings held at 500°. A commercial platinum catalyst cartridge was also connected directly to the outlet of the hydrogen cylinder. Before each use of nitrogen the copper turnings of the furnace tube were freshly reduced by a preliminary passage of hydrogen. Initially the gas lines and joints were of all metal and glass construction. Leakage problems forced the use of a few short joints of Tygon tubing but no deleterious effects were observed.[7]

Triple-distilled water was used in the preparation and dilution of all stock solutions. Reagent grade hydrochloric acid was doubly redistilled, retaining each time only the middle third of the distillate. References to the preparation and standardization of the sodium and lithium perchlorate stock solutions have been summarized previously.[8] All other solutions were prepared from reagent grade materials without additional purification and standardized by conventional procedures.

In the work with the silver–silver chloride electrode, great care was necessary in standardizing the hydrochloric acid cell

solutions. A concentration error here of 0.02% corresponds to 0.01 mv. in e.m.f. Direct titration against the acidimetric standard tris-(hydroxymethyl)-aminomethane or THAM (Fisher Scientific Co., Primary Standard, 99.95% assay) was found very useful.[9,10] Using weight burets for the bulk of the titration and a one-ml. ultramicro buret for final adjustment of the potentiometric end point, a routine precision of better than 0.01% was attained. A gravimetric determination of a 0.1 m stock by weighing silver chloride agreed with the THAM value to five significant figures.

Cell solutions 0.1 m or greater were titrated directly at the end of each run. Calculated values based on gravimetric dilutions of a 0.1 m stock were used for cells at lower concentrations. All weighings were corrected to in vacuo conditions, and the molal or moles/kg. of water concentration scale was used throughout.

Apparatus.—As before[3] cell potentials were measured to 0.01 mv. with a precision potentiometer and a Cary Model 31-V vibrating reed electrometer as the null point detector. However, details of our circuit have not been presented. In particular, balancing the potentiometer and checking the electrometer zero point were found to be very awkward operations if the external potentiometer feedback circuit of the Cary instrument was used. A great simplification was gained by direct series opposing connection of the test cell and potentiometer with the potential difference serving as the electrometer input. The potentiometer was modified so that potential constantly appeared at the e.m.f. posts. This was easily done by shorting the e.m.f. terminals of the standard cell-e.m.f. switch. After modification this switch was always kept in the standard cell position. The zero point of the electrometer could be checked and the potentiometer could be balanced in customary fashion at any time without disturbing the cell potential measurements. A polarity reversing switch with center off position between the potentiometer and test cell was found very convenient and served as a safeguard against shorting of the potentiometer.

With due care against ground loops, shielded cable leads were used throughout, and all equipment rested on an equal potential surface (grounded). However, it was not necessary to shield the potentiometer or the test cell or to ground the cell solutions. The high impedance circuit was very sensitive to dial movements of the Leeds and Northrup K-2 potentiometer previously used,[3] but this difficulty was largely removed by replacement with a Rubicon High Precision Type B potentiometer. Generally the potentiometer was set at an even dial division within 0.1 mv. of the null point, and the final figure was obtained from a recorder chart of the electrometer output. The recorder provided the customary benefits of averaging out the combined uncertainties due to noise level and zero drift (ca. 0.01 mv.) and also was very useful in checking the decay of spurious potentials usually generated in switching electrodes and in zero checks of the electrometer.

Two standard cells, calibrated against laboratory standards certified by the National Bureau of Standards, were used to standardize the potentiometer. Daily checks were also run on the complete measuring circuit by substitution of a standard cell in place of the test cell. The standard cells were mounted in an insulated and shielded metal box with a switching circuit that allowed either to be used in these functions. Work did not proceed unless all checks agreed within 0.02 mv. All measurements were carried out in a constant temperature room, 25 ± 1°.

One series of experiments (results in Fig. 1) was run using the test cell previously described.[3a] An all-glass cell of improved design was used in all other runs. Two compartments separated by a spray trap were enclosed in a common jacket through which water thermostated at 25.00 ± 0.01° was pumped. Each compartment contained about 20 ml. of test solution, the first with an inlet tube ending in a fritted disk serving as a gas presaturator and the second housing a glass electrode and either a hydrogen or silver–silver chloride electrode. A distilled water scrubbing tower provided approximate adjustment of the water content of the gas before entering the presaturator compartment. Continuous gas bubbling provided agitation of the cell solutions. The electrode compartment could be flushed and refilled with a fresh solution sample by gas pressure. Mountings for the electrodes and the caps of the compartments were standard taper glass fittings.

(3) (a) J. C. Sullivan, J. C. Hindman, and A. J. Zielen, J. Am. Chem. Soc., 83, 3373 (1961); (b) A. J. Zielen and J. C. Sullivan, J. Phys. Chem., 66, 1065 (1962).

(4) D. J. G. Ives and G. J. Janz, "Reference Electrodes," Academic Press, New York, N. Y., 1961, pp. 231, 239, 240.

(5) R. G. Bates, "Electrometric pH Determinations," John Wiley and Sons, Inc., New York, N. Y., 1954, pp. 204–207.

(6) Reference 4, pp. 107, 108.

(7) Reference 4, p. 94.

(8) J. C. Sullivan, A. J. Zielen, and J. C. Hindman, J. Am. Chem. Soc., 82, 5288 (1960).

(9) J. H. Fossum, P. C. Markunas, and J. A. Riddick, Anal. Chem., 23, 491 (1951).

(10) R. G. Bates and H. B. Hetzer, J. Phys. Chem., 65, 667 (1961).

Generally two such cells were employed simultaneously. Duplicate measurements with two different glass electrodes could thus be obtained with continuous equilibria undisturbed in both cells. An Applied Physics Cary No. 3099050 three-position transfer switch provided multiple glass electrode input connections to the electrometer.

Procedure.—For the determination of the standard potential of the silver–silver chloride electrode and the activity coefficients of hydrochloric acid, the following cell pairs were run simultaneously

$$\text{Pt, H}_2(1 \text{ atm.})|\text{HCl } (m)|\text{glass} \qquad (1)$$

$$\text{Ag, AgCl}|\text{HCl } (m)|\text{glass} \qquad (2)$$
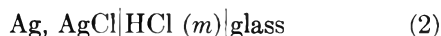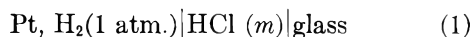
The molal concentration m of hydrochloric acid was identical in each cell pair, and experiments covered a range of 0.001 to 4 m. Cell 2 was run under a continuous atomosphere of nitrogen, with the dissolved air being removed from the solution by gas bubbling before insertion of the Ag–AgCl electrode. All electrodes were thoroughly rinsed with solutions identical with those in the cells before insertion.

After allowing an initial equilibration period of about 2 hr., cell potentials of 1 and 2 were measured at 15 to 20 min. intervals to establish glass electrode drift rates.[3a] The two glass electrodes were then quickly interchanged—in this series without rinsing or drying—and the new drift rates established. Both cells were allowed to stand overnight with continuous gas bubbling, and the entire procedure was repeated the next morning. Then the electrode compartment of cell 2 was flushed and refilled with a fresh solution sample without disturbing the Ag–AgCl electrode, and a third series of measurements was run. The agreement between all six values thus obtained for each acid concentration was very good (mean average deviation = 27 μv.).

The series of experiments testing medium effects on the glass electrode hydrogen ion response required only minor modifications in the above procedure. Here a glass electrode was "standardized" in 0.1 m HCl $vs.$ either a hydrogen or Ag–AgCl electrode and then was transferred to a solution differing markedly in composition and acidity containing a pre-equilibrated hydrogen electrode. In transfer the glass electrode was either rinsed with distilled water and dried with tissue or merely rinsed with a sample of the new solution.

The latter treatment was preferred since steady drift rates usually are established within 5 to 10 min. after transfer while a threefold longer period might be required after the harsher treatment of drying the electrode. However, it has been repeatedly demonstrated that a glass electrode can be subjected to either treatment; and after being returned to the same cell, the extrapolated potentials at the moment of transfer as obtained from the two drift rates will agree within 0.03 to 0.04 mv. Usually an even better check is obtained, the final precision depending on the amount of extrapolation needed and the magnitude of the glass electrode drift rate.

Drifts in glass electrode potentials were followed for a period of about 100 min., and within experimental error they could be taken as linear with time.[11] Using the calculated least squares straight lines for the electrode drifts, unbiased values of the cell potentials were obtained at the moment of glass electrode transfer. This common extrapolation time differs from that previously reported,[3a] but it is theoretically more sound and definitely improves the precision of results when a glass electrode is subjected to gross changes in medium.

Conventional barometric and vapor pressure corrections were applied to reduce all hydrogen electrode results to the standard one atmosphere. The excess hydrostatic pressure correction noted by Hills and Ives[12] was included and amounted to ca. 0.05 mv. in this work. All potentials are given in absolute volts. The signs of cells and relative electrode potentials are in accord with the Stockholm Convention.[13]

Results and Discussion

The potential developed by a glass electrode when placed in a solution can be considered as consisting of at least three components: (1) that due to the internal

reference electrode and assumed reasonably constant; (2) the hydrogen ion response or potential generally attributed to the transfer of hydrogen ions across the glass membrane boundary[14]; (3) the asymmetry potential due to differences in the two surfaces of the glass membrane. Beck and Wynne-Jones[15] consider the asymmetry potential time dependent and the real source of so-called glass electrode errors. This led Covington and Prue[16] to the first truly precise measurements with the glass electrode, utilizing a time extrapolation procedure for the cancellation of asymmetry potentials identical in principle with the method of this work.

In brief the difference (or sum) of two independent cell potentials, each with the same glass electrode, is obtained. If one cell consists of the glass and a hydrogen electrode, complete cancellation of all components of the glass electrode potential is achieved. This will hold for any combination of cells provided the hydrogen ion response of the glass electrode is identical though not necessarily ideal in the two cell solutions. The net result is thermodynamically equivalent to the potential of the second cell alone with a hydrogen electrode replacing the glass electrode.

Activity Coefficients of HCl.—Applying the above to the measurements of cell pairs 1 and 2, potentials were obtained for the equivalent cell

$$\text{Pt, H}_2 \text{ (1 atm.)}|\text{HCl } (m)|\text{AgCl, Ag} \qquad (3)$$
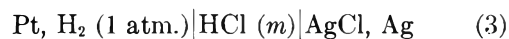
the e.m.f. of which is given by

$$E = E^0 - 2RT/F \ln m\gamma_\pm \qquad (4)$$

where E is the observed cell potential, E^0 is the standard potential of the Ag–AgCl electrode, m and $\gamma_\pm$ are the molal concentration and mean molal activity coefficient of hydrochloric acid, and the other symbols have their usual significance. The data are summarized in Table I with nearly all cell potentials the mean of six determinations. A total of four Ag–AgCl and three glass electrodes (B, C, and D) were used.

TABLE I
DIFFERENCE IN POTENTIAL AT 25° OF CELLS 1 AND 2

m of HCl	E, abs. v.	m of HCl	E, abs. v.	m of HCl	E, abs. v.
0.0010028	0.57893	0.020017	0.43014	1.0049	0.23293
.0020035	.54414	.050103	.38569	1.9880	.18670
.0049975	.49844[a]	.10049	.35211	2.9919	.15200
.009999	.46415[b]	.50842	.27135	3.9994	.12212

[a],[b] Mean of 12 and 3 values, respectively; all others mean of 6 values.

The measurements of Harned and Ehlers[17] and Bates and Bower,[18] hereafter abbreviated as H & E and B & B, are the most thorough studies of cell 3 by conventional methods and classical examples of precision work. To compare these results and the present study, activity coefficients of HCl were calculated independently from each data set using the current best values of the necessary constants. This was done by use of a

(11) Over longer periods, especially with high drift rates, some curvature is usually evident (cf. 4 m HCl results in Fig. 2).

(12) G. J. Hills and D. J. G. Ives, *J. Chem. Soc.*, 305 (1951).

(13) J. A. Christiansen, *J. Am. Chem. Soc.*, **82**, 5517 (1960).

(14) By variations in composition of the glass membrane, response to other cations can be enhanced: reference 4, pp. 234, 244.

(15) W. H. Beck and W. F. K. Wynne-Jones, *J. chim. phys.*, **49**, C97 (1952).

(16) A. K. Covington and J. E. Prue, *J. Chem. Soc.*, 3696, 3701 (1955); 1567, 1930 (1957).

(17) H. S. Harned and R. W. Ehlers, *J. Am. Chem. Soc.*, **54**, 1350 (1932); **55**, 2179 (1933).

(18) R. G. Bates and V. E. Bower, *J. Res. Natl. Bur. Std.*, **53**, 283 (1954).

generalized non-linear least squares program for the IBM 704 computer. Several semiempirical types of Debye–Hückel equations of the general form given by Harned and Owen[19] were tried. Over the entire concentration range to 4 m HCl, the best four parameter fit was found with the equation

$$\log \gamma_\pm = -Ac^{1/2}/(1 + Ba^*c^{1/2}) + \text{Ext.} + Cc + Dc^{3/2} + Ec^2 - \log(1 + 0.03603m) \quad (5)$$

$$c = 0.9972m - 0.01817m^2 \quad (6)$$

where c is the molar concentration, A and B are the familiar constants of the Debye–Hückel theory, and Ext. represents the total contribution of the extended terms of Gronwall, LaMer, and Sandved.[20] The ion-size parameter a^* and the empirical parameters C, D, and E were adjustable. Equation 6 gives the conversion relation of c and m valid to 4 m at 25° and was taken from H & E.[17]

In the computer program equations 5 and 6 were substituted into 4 in order to include E^0 as a parameter in the least squares adjustment. Except for the B & B[18] data where only smooth curve values at rounded molalities were given, the individual data points (not mean values) with equal weight assigned to each E were used. The data of H & E[17] were converted to absolute volts before use. The values of the Debye–Hückel parameters A and B were taken from Robinson and Stokes[21] and R, T, and F were obtained from a recent listing by Hetzer, Robinson, and Bates.[22] Since the contribution of Ext. in equation 5 was very minor, the values calculated by H & E[17] for $a^* = 4.3$ Å. were used regardless of the final value assigned to a^*.

A summary of the least squares treatment is presented in Table II. With these parameter values activity coefficients or cell potentials can be calculated anywhere within the listed concentration range with the full accuracy of the original data. With the exception of E^0 an excess of significant figures has been retained for calculating purposes.

TABLE II

LEAST SQUARES PARAMETERS AT 25° FOR $\gamma_\pm$ OF HCl BY EQUATION 5

	This work	B & B[18] data	H & E[17] data
E^0, abs. v.	0.22235	0.22234	0.22253
a^*, Å.	4.901	4.512	4.766
$10C$	0.9681	1.3496	1.0851
$100D$	2.334	0	1.272
$1000E$	1.427	0	4.221
σ_{fit}, μv.	42	70[a]	60
Concn. range, m	0.001–4.0	0.001–0.1	0.003–4.0

[a] Original data fit given by B & B[18]; smooth curve data actually gave 7 μv.

Note that the shorter concentration range of the B & B[18] data allowed the use of a simpler form of equation 5 with parameters D and E set at zero. Similarly and limited to the same concentration range, the values E^0 = 0.22235 and 0.22257 abs. v., $a^* = 4.732$ and 5.352 Å., and $10C = 1.1853$ and 0.6846 were obtained, respectively, from the present data and that of H & E.[17] The

respective standard deviations of E or σ_{fit} values were 36 and 65 μv.

The various a^* values and the 4.3 Å. results obtained by both H & E[17] and B & B[18] indicate the empirical nature of this parameter and the limited significance to be attached to the "distance of closest approach."[23] However, the E^0 results are in excellent agreement with the values obtained by B & B,[18] who have also summarized other work on cell 3 and discussed the difference in the E^0 obtained from the data of H & E.[17] Taniguchi and Janz[24] have suggested a difference in bias potentials of the thermal-electrolytic Ag–AgCl electrode as the cause of the discrepancy in E^0 values. Fortunately as long as the apparent E^0 remains constant there is no error in the calculation of activity coefficients from the e.m.f. data.

Smoothed cell potentials and activity coefficients were obtained for all three data sets with the parameters of Table II, and representative values are presented in Table III. Addition of the respective Δ quantities to the E and $\gamma_\pm$ values obtained from the present investigation will give the results calculated with the other data sets. With the possible exception of the highest HCl concentration, where the difference is less than 0.2%, the values are seen to be in excellent agreement and amply indicate the reliability of the glass electrode results. Indeed, the standard deviations listed in Table II would suggest a higher precision level was attained with the glass electrode than with the earlier, conventional studies. The agreement is also notably better than that achieved by Covington and Prue[16] in their precision glass electrode work.

TABLE III

SMOOTHED POTENTIALS OF CELL 3 AND $\gamma_\pm$ OF HCl AT 25°

m of HCl	E,[a] abs. v.	$-\Delta E$, mv.		$\gamma_\pm$[a]	$\Delta\gamma_\pm \times 10^3$	
		B & B[18]	H & E[17]		B & B[18]	H & E[17]
0.001	0.57910	−0.01	0.18	0.9652	−0.1	0.0
.002	.54419	− .01	.18	.9521	− .1	.0
.005	.49841	− .01	.18	.9283	− .2	− .1
.01	.46413	.00	.19	.9045	− .3	− .2
.02	.43019	.00	.19	.8755	− .4	− .2
.05	.38579	.00	.20	.8310	− .3	− .3
.1	.35237	− .03	.19	.7963	.2	− .3
.5	.27222	....	.15	.7578	...	.5
1	.23322	....	.12	.8094	...	.9
2	.18626	....	.15	1.0093	...	.6
3	.15172	....	.16	1.3178	...	.6
4	.12211	....	.08	1.759	...	3.0

[a] This investigation.

Medium Effects.—In the experiments of the previous section the glass electrode was interchanged between identical cell solutions. Admittedly this represents an ideal case of limited applicability. The other extreme where the two cell solutions are deliberately made to differ widely in acidity and composition is of more practical interest.

For a given glass electrode and except for asymmetry potential changes, the potential of cell 1 should be independent of the concentration or type of acid employed. That is provided the glass electrode passes the very severe test of an ideal Nernst slope, perfectly cancelling the hydrogen electrode over the hydrogen ion activity range covered. This was tested in experiments using

(19) Reference 2, eq. 11-5-2, p. 467.
(20) T. H. Gronwall, V. K. LaMer, and K. Sandved, *Physik. Z.*, **29**, 358 (1928).
(21) R. A. Robinson and R. H. Stokes, "Electrolyte Solutions," 2nd Ed., Academic Press, Inc., New York, N. Y., 1959, p. 468.
(22) H. B. Hetzer, R. A. Robinson, and R. G. Bates, *J. Phys. Chem.*, **66**, 1423 (1962).
(23) Reference 4, pp. 37, 38; reference 21, pp. 235–238.
(24) H. Taniguchi and G. J. Janz, *J. Electrochem. Soc.*, **104**, 123 (1957).
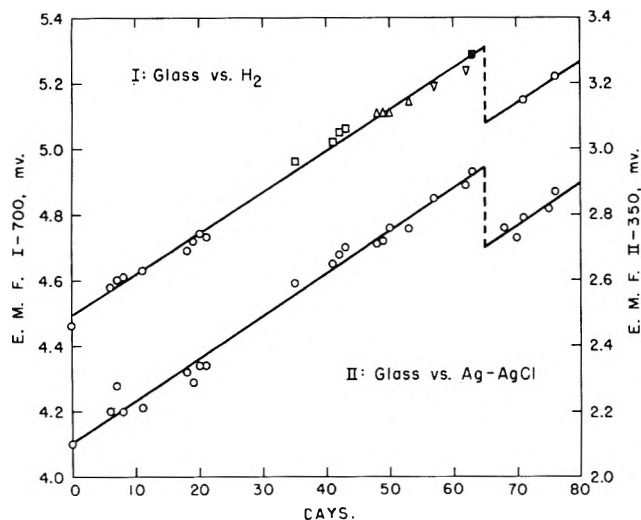
Fig. 1.—Daily record (at moment of transfer) of glass electrode A vs. H_2 and Ag–AgCl electrodes: O, 0.1 m HCl; □, 0.1, 0.5, 1, and 2 m H_2SO_4 in order; △, same as previous series using $HClO_4$; ▽, 1 m $NaClO_4$ + 1 m $HClO_4$; ■, 6 m H_2SO_4.
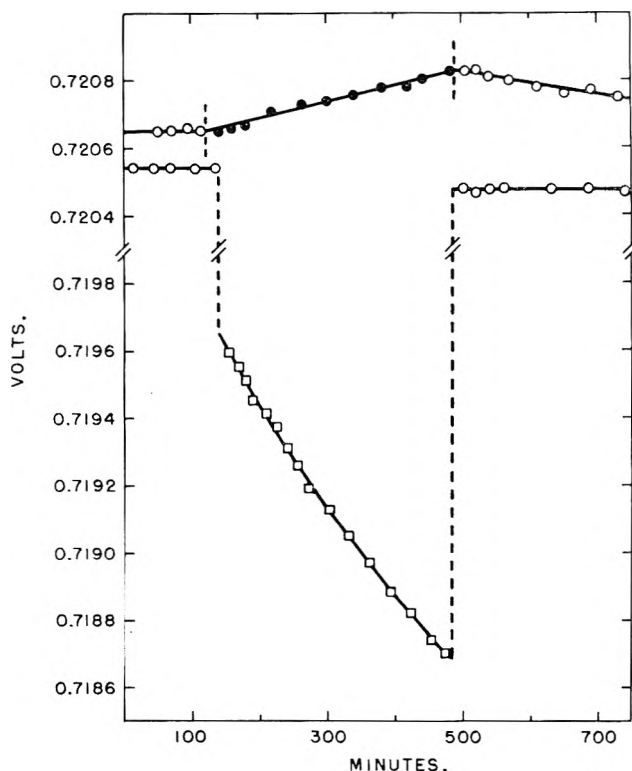
Fig. 2.—Comparison of glass electrode C vs. H_2 electrode in 0.1 m HCl, O, and 4 m solutions of $HClO_4$, ●, or HCl, □. Dashed lines are moment of glass electrode transfer.

cell pairs similar to 1 and 2. In this series a single glass electrode (A) was used, cell 2 always contained 0.1 m HCl, and a variety of perchloric and sulfuric acid solutions were employed in cell 1. The results are presented in Fig. 1.

This figure is merely a day by day record of the two cell potentials (at the moment of glass electrode transfer), and as such it includes the continual drift of the glass electrode. It is probably only a fortuitous convenience that the drift for this particular electrode appears linear. The abrupt breaks in the plot at ca. 65 days represent vexing though typical glass electrode behavior. However, the observed constant difference in the cell potentials is the important point. Twenty-two cell pairs are presented in Fig. 1, eleven with the two

cell solutions identical (0.1 m HCl) and the remaining half with varying degrees of difference in the cell solutions. The mean potential differences and standard deviations of the two sets are, respectively, 352.38 ± 0.03 and 352.36 ± 0.02 abs. mv., in excellent agreement with the 0.1 m value of Table III. The check is also notable in that these data were obtained using completely different apparatus and electrodes.

A second series of tests was run using the cell pairs

$$\text{Pt, } H_2 \text{ (atm.)} | \text{HCl (0.1 } m) | \text{glass} \qquad (7)$$

$$\text{Pt, } H_2 \text{ (1 atm.)} | \text{HX (} m) | \text{glass} \qquad (8)$$
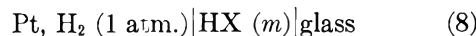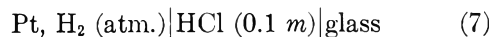
Here the potential difference of cells 7 and 8 should be zero regardless of the nature of HX or the magnitude of m, again provided the glass electrode response is ideal between the two solutions. Table IV summarizes the results with $E_8 - E_7$ representing the observed difference in the above cell potentials at the moment of glass electrode transfer. Multiple entries indicate repeated experiments.

TABLE IV

DIFFERENCE IN POTENTIALS AT 25° OF CELLS 7 AND 8

Cell 8 solution	$E_8 - E_7$, mv.	Glass electrode
0.05 m HAc + 0.05 m NaAc[a]	0.01, 0.00	C
4 m H_2SO_4	−0.03, 0.00	C
4 m $HClO_4$	−0.01, −0.02, −0.01	C
2 m $NaClO_4$ + 2 m $HClO_4$	0.00	C
2 m $LiClO_4$ + 2 m $HClO_4$	−0.04, 0.02, 0.00	C, B, C
0.5 m HCl	−0.06	D
1 m HCl	−0.17	D
2 m HCl	−0.58	D
3 m HCl	−1.36	D
4 m HCl	−2.91	D
4 m HCl	−0.69, −0.89, −1.14	C
3.9 m NaCl + 0.1 m HCl	−0.13, −0.15	B, C

[a] Acetate buffer, ca. pH 4.7.

Clearly any errors in glass electrode response are either negligibly small or at the limit of detection in all solutions studied except the HCl series. The marked behavior difference of the same glass electrode (C) in 4 m solutions of $HClO_4$ and HCl is vividly illustrated in Fig. 2. This figure also indicates that the magnitude of the error in HCl solutions depends on the time of contact. Accordingly all the results of Table IV were obtained with transfer of the glass electrode from 0.1 m HCl to the second cell, i.e., cell 8.

An adequate explanation for the HCl errors cannot be furnished at present. The data of Table IV show the effect to be not very reproducible and to depend on the electrode used. Also the chloride ion alone cannot be the primary cause since the error at high NaCl concentration is sharply reduced though still appreciable. An entirely different possibility is that the hydrogen electrode instead of the glass electrode is at fault. However, this can be eliminated since Pitzer and Brewer[25] have demonstrated that activity coefficients obtained with data from cell 3 in the range 4 to 10 m HCl are in good agreement with the results of vapor pressure measurements. In any event the results of Table III at high HCl concentration definitely indicate accurate values can be obtained with the present procedure even under conditions of errors in the glass electrode response.

(25) G. M. Lewis and M. Randall (reviewed by K. S. Pitzer and L. Brewer), "Thermodynamics," 2nd Ed., McGraw-Hill Book Co., Inc., New York, N. Y., 1961, pp. 312, 317.

A more exhaustive search probably would reveal other examples of definite glass electrode errors. And of course hydrofluoric acid or strongly alkaline solutions where there is a definite chemical attack on the glass membrane represent special cases. However, the essential point is that ideal behavior appears to be more the norm than the exception. This is contrary to much of the reported work on glass electrode behavior, especially the so-called negative or high acid error.[26] In reality there is no contradiction. Other than the special case of zero asymmetry potential, the glass electrode must always be considered in error; but this error can be cancelled revealing the masked ideal hydrogen ion response.

The entire subject of errors in the high acid region remains controversial. For many years Dole's[27] theory of difference in water activity on the two sides of the glass membrane was widely accepted, but in the last decade convincing evidence has been found against it.[15,28] This led Schwabe and Glöckner[29] to a careful study of the time dependence of glass electrode errors—

so important in the present application—and to the development of an entirely new theory based on excessive sorption of protons by the glass membrane gel layer in high acid solutions.

Regardless of the true origin of glass electrode errors, the present work shows clearly that the proper technique produces thermodynamically significant results of the highest precision over a truly remarkable range of solution composition and acidity. In essence the glass electrode is converted into a chemically inert hydrogen electrode, eliminating the need of physically separated electrode compartments joined by a salt bridge. Of course other reference electrodes could be used. However, the hydrogen electrode is by far the most reliable; and by definition it is the reference standard of all relative electrode potentials. There is also the unique practical advantage that the concentration of the calibrating cell solution need not be known accurately when the hydrogen electrode is used.

(26) Reference 4, pp. 244-246.

(27) M. Dole, *J. Am. Chem. Soc.*, **54**, 2120, 3095 (1932).

(28) (a) E. E. Sinclair and A. E. Martell, *J. Chem. Phys.*, **18**, 224, 992 (1950); (b) M. Dole, *ibid.*, **18**, 573, 1411 (1950).

(29) K. Schwabe and G. Glöckner. *Z. Elektrochem.*, **59**, 504 (1955).

DILUTE SOLUTION PROPERTIES OF TACTIC POLY-(METHYL METHACRYLATES). II. ISOTACTIC FRACTIONS IN A THETA SOLVENT

By Sonja Krause and Elizabeth Cohn-Ginsberg

Research Division, Rohm and Haas Company, Bristol, Pa.

Precipitation temperature–concentration measurements on fractions of different molecular weight were used to obtain the theta temperature of isotactic poly-(methyl methacrylate) in acetonitrile, 27.6°. Intrinsic viscosities of a number of fractions were measured at 20, 27.6, 35, and 50°. These measurements were used to calculate the intrinsic viscosity–molecular weight relationship at each temperature and various derived quantities for each molecular weight used.

Introduction

In part I of this series,[1] it was shown that the dilute solution properties of isotactic poly-(methyl methacrylate) differ from those of conventional, free-radically initiated poly-(methyl methacrylate) even in the thermodynamically good solvents, acetone and benzene. The measured intrinsic viscosities and radii of gyration of the isotactic poly-(methyl methacrylate) fractions in acetone solution were used to predict the intrinsic viscosity–molecular weight relationship of the isotactic polymer in a theta solvent. From this, it was further predicted that molecules of the isotactic poly-(methyl methacrylate) should be much more expanded in a theta solvent than molecules of conventional poly-(methyl methacrylate) of the same molecular weight. The work presented here confirms these predictions.

Experimental

The preparation and fractionation of the sample of isotactic poly-(methyl methacrylate) used for this work have been described previously.[1] The polymer had been characterized as isotactic from its infrared spectrum,[2] having a J-value[3] of 33. Samples of isotactic poly-(methyl methacrylate) generally have J-values between 25 and 35,[3] the most isotactic samples having the lowest J-values.

The number average molecular weights of all the fractions used in this work were determined from the intensity of the absorption at 304 mμ of the fluorenyl end-group on each polymer chain.[4] Each fraction was further characterized either by its weight average molecular weight as obtained from light scattering data in acetone solution[1] or by its viscosity average molecular weight as calculated from its intrinsic viscosity in acetone: $[\eta]$ in dl./g.

$$[\eta] = 2.30 \times 10^{-4}M^{0.63} \qquad (1)$$

Equation 1 was previously obtained for these isotactic fractions in acetone solution.[1]

The acetonitrile used for all our work was distilled through a packed column and a center cut of constant boiling point was collected in each distillation. The n^{25}D of these center cuts ranged from 1.34142 to 1.34147.

The thermometers used for precipitation temperature measurements and for the intrinsic viscosities were calibrated against other thermometers which had been calibrated at the National Bureau of Standards.

Intrinsic viscosities were obtained at each temperature using Cannon–Ubbelohde semimicro viscometers with solvent flow times above 90 sec. so that no kinetic energy corrections were necessary. No shear corrections were necessary because of the low values of all the intrinsic viscosities obtained. At least three concentrations were run for each intrinsic viscosity determination.

The solutions for the precipitation temperature–concentration measurements were made up by weight in long test tubes which were shaken continuously (mechanically) while immersed in a water–propylene glycol or water–ethylene glycol mixture whose temperature was changed at a rate not exceeding 0.2°/min.

(1) S. Krause and E. Cohn-Ginsberg, *Polymer*, in press.

(2) U. Baumann, H. Schreiber, and K. Tessmar, *Makromol. Chem.*, **36**, 81 (1959).

(3) W. E. Goode, F. H. Owens, R. P. Fellmann, W. H. Snyder, and J. E. Moore. *J. Polymer Sci.*, **46**, 317 (1960).

(4) D. L. Glusker, E. Stiles, and B. Yoncoskie, *ibid.*, **49**, 297 (1961).
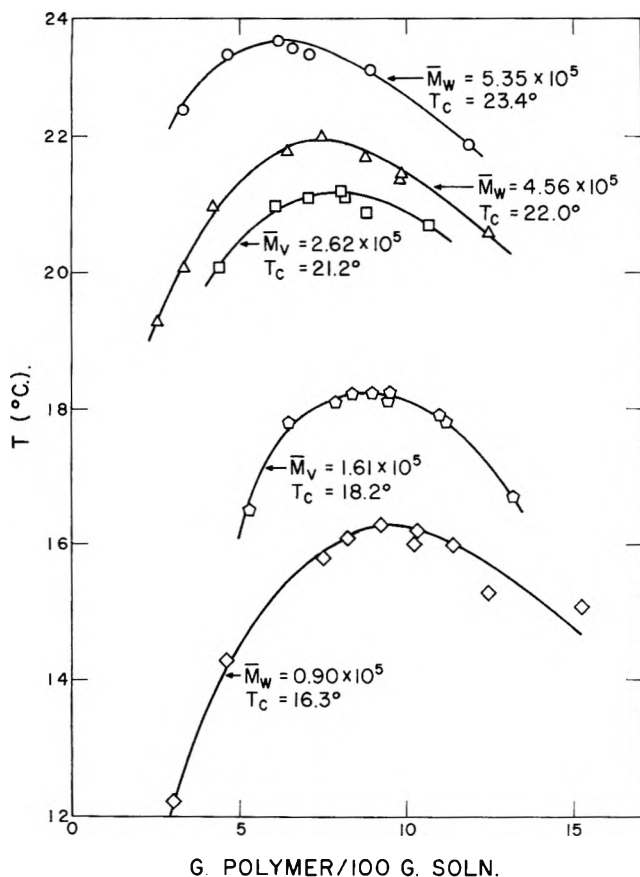
Fig. 1.—Precipitation temperature vs. concentration of fractions of isotactic poly-(methyl methacrylate) in acetonitrile.
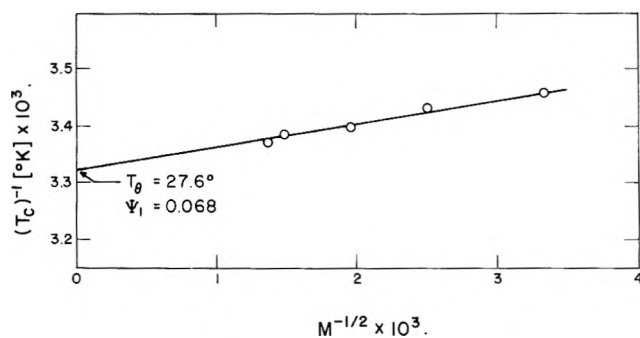
Fig. 2.—$1/T_c$ vs. $1/M^{1/2}$ for fractions of isotactic poly-(methyl methacrylate) in acetonitrile solution.

The temperature at which turbidity first appeared on cooling and the temperature at which the last of the turbidity disappeared on heating were noted in sequence for each solution until a set of four or five consistent readings was obtained. The average of these readings was considered the precipitation temperature of the solution.

Results

The molecular weight data obtained in acetone solution for the fractions used in this work are shown in Table I.

Figure 1 shows the precipitation temperature–concentration data for five of the fractions in acetonitrile.

The theta temperature for the system isotactic poly-(methyl methacrylate)–acetonitrile was obtained from the data shown in Fig. 1 by plotting the reciprocal of the critical temperature (in degrees Kelvin) of each fraction against the reciprocal of the square root of its weight or viscosity average molecular weight ($\bar{M}_w$ was used where both averages were available) according to the equation

$$1/T_c = (1/\theta)(1 + b/M^{1/2}) \tag{2}$$

TABLE I
FRACTIONS OF ISOTACTIC POLY-(METHYL METHACRYLATE) USED FOR THIS WORK

Fraction	$\bar{M}_n \times 10^{-5}$	$[\eta]$ 30° acetone (dl./g.)	$\bar{M}_v \times 10^{-5}$	$\bar{M}_w \times 10^{-5}$	$\bar{M}_w/\bar{M}_n$	$\bar{M}_v/\bar{M}_n$
B5,6A	3.89	0.875	5.2	5.35 ± 0.01	1.4	1.3
A6	2.02	.62	3.00	4.56 ± 0.13	2.3	1.5
B7,8B	1.93	.570	2.62	...	...	1.4
B7,8D	1.46	.483	1.87	...	...	1.3
B9,10A	1.33	.42	1.61	...	...	1.2
B9,10B	1.13	.370	1.23	...	...	1.1
B12	0.77	.295	0.91	0.90 ± 0.03	1.2	1.2
B13	.692	.260	.70	...	...	1.0
B16	.406	.21	.50	...	...	1.2
B19	.284	.147	.284	...	...	1.0

where

$$b = (V_1/v)^{1/2}/\psi_1 \tag{3}$$

where θ stands for the theta temperature in degrees Kelvin, M is the molecular weight of the fraction, V_1 is the molar volume of the solvent, v is the specific volume of the polymer, and ψ_1 is an entropy parameter.[5] This plot, shown in Fig. 2, together with eq. 2 and 3, yields

$$\theta = 27.6 \pm 0.5°$$

$$\psi_1 = 0.068$$

for isotactic poly-(methyl methacrylate). Fox[6] reported a theta temperature of 45.0° and a ψ_1 value of 0.145 for conventional poly-(methyl methacrylate) in acetonitrile.

Table II shows the intrinsic viscosities in acetonitrile solution at various temperatures of five of the fractions of isotactic poly-(methyl methacrylate).

TABLE II
INTRINSIC VISCOSITIES OF ISOTACTIC POLY-(METHYL METHACRYLATE)

Fraction	$\bar{M}_v \times 10^{-5}$ (acetone)	Intrinsic viscosity in acetonitrile 20°	27.5°	35°	50°
B7,8D	1.87	0.297	0.324	0.354	0.394
B9,10B	1.23	.244	.258	.276	.292
B13	0.70	.198	.205	.206	.219
B16	.50	.166	.168	.164	.174
B19	.284	.127	.128	.127	.132

The data in Table II yielded the following intrinsic viscosity–molecular weight relationships using least squares calculations

$$T = 20° \quad [\eta] = 13.0 \times 10^{-4}M^{0.448} \tag{4}$$

$$T = 27.6° \quad [\eta] = 7.55 \times 10^{-4}M^{0.500}$$
$$\text{(if exponent is set at 0.500)} \tag{5}$$

$$T = 35° \quad [\eta] = 4.6 \times 10^{-4}M^{0.546} \tag{6}$$

$$T = 50° \quad [\eta] = 2.62 \times 10^{-4}M^{0.602} \tag{7}$$

Discussion

The value, 7.55×10^{-4}, of the constant in the $[\eta]$–M relationship of isotactic poly-(methyl methacrylate) at its theta temperature in acetonitrile is quite different from the value, 4.8×10^{-4}, obtained by Fox[6] for conventional poly-(methyl methacrylate) in a number of sol-

(5) P. J. Flory, "Principles of Polymer Chemistry," Cornell Univ. Press, Ithaca, N. Y., 1953, Chapters XII and XIII.

(6) T. G Fox, Polymer, 3, 111 (1962).

vents in which the theta temperature varied from about 30 to 70°. It is interesting to note that a value of about 7×10^{-4} was predicted for this constant from the intrinsic viscosity–molecular weight data of these isotactic poly-(methyl methacrylate) fractions in acetone.[1] This constant, K, is related to the unperturbed end-to-end distance of the polymer coils, $(\overline{r_0^2})^{1/2}$, by the equation[7]

$$K = \phi(\overline{r_0^2}/M)^{1/2} \qquad (8)$$

where ϕ is a universal constant used here as 2.1×10^{21}.[5] According to eq. 8, the higher value of K for isotactic poly-(methyl methacrylate) indicates that the isotactic molecules are more expanded in the unperturbed state than are those of conventional poly-(methyl methacrylate). The value of $(\overline{r_0^2}/M)^{1/2}$ obtained for the isotactic molecules in this work is compared with values obtained for conventional poly-(methyl methacrylate) by previous investigators in Table III.

TABLE III
Unperturbed Dimensions of Poly-(methyl methacrylate)

Polymer type	T (°C.)	$K \times 10^4$	$(\overline{r_0^2}/M)^{1/2} \times 10^{11}$
Isotactic	27.6	7.55	720
Conventional[6]	30–70	4.8	612
Conventional[8]	25	5.92	656
Conventional[9]	26.2	5.59	643

In part I of this series, it was shown[1] that the molecules of isotactic poly-(methyl methacrylate) remained more expanded than those of conventional poly-(methyl methacrylate) in acetone, a thermodynamically good solvent for both polymer configurations.

It was rather startling to find that isotactic poly-(methyl methacrylate), a crystallizable polymer (m.p. $\approx 160°$),[10] should fail to crystallize from acetonitrile, a solvent from which it precipitates at a temperature so far below its melting point. One might expect that

rather unique specific interactions between polymer and solvent in this system keep the polymer from crystallizing. However, the polymer behaves as if this were a perfectly normal polymer–solvent system, as can be seen from Fig. 1 and 2, Table II, and equations 4 through 7.

There is one extra item of information that shows something unusual about the acetonitrile–isotactic poly-(methyl methacrylate) system. The parameter, ψ_1, which was obtained from Fig. 2, can also be obtained from the data in Table II, that is, from intrinsic viscosity–temperature data, by plotting $(\alpha^5 - \alpha^3)/M^{1/2}$ vs. $1/T$ according to the equation[5]

$$(\alpha^5 - \alpha^3)/M^{1/2} = 2C_M \psi_1(1 - \theta/T) \qquad (9)$$

where

$$C_M = 1.4 \times 10^{-24} (v^2/V_1)\phi/K \qquad (10)$$

and α is the expansion factor of the polymer coils, calculated from

$$[\eta] = KM^{1/2}\alpha^3 \qquad (11)$$

where the constant K always refers to its observed value at the theta temperature. Such a plot, based only on the data from the two highest molecular weight fractions in Table II (the others showed too small a variation in intrinsic viscosity with temperature to be very useful for this calculation), yielded a value of about 0.05 for ψ_1, in good agreement with the value of 0.068 found from eq. 2. This agreement is very unusual. Krigbaum[11] and Fox[6] have pointed out that the values of ψ_1 obtained by the two methods used here are generally not in agreement. Values obtained from equation 2 are almost always five to ten times greater than those obtained from equation 9, except for some recent data on polyelectrolyte systems, poly-(vinyl sulfate) in aqueous alkali halide solutions.[12]

(7) P. J. Flory and T. G Fox, *J. Am. Chem. Soc.*, **73**, 1904 (1951).

(8) S. N. Chinai and C. W. Bondurant, Jr., *J. Polymer Sci.*, **33**, 471 (1958).

(9) S. N. Chinai and R. J. Valles, *ibid.*, **39**, 363 (1959).

(10) T. G Fox, B. S. Garrett, W. E. Goode, S. Gratch, J. F. Kincaid, A. Spell, and J. D. Stroupe, *J. Am. Chem. Soc.*, **80**, 1768 (1958).

(11) W. R. Krigbaum, *ibid.*, **76**, 3758 (1954).

(12) H. Eisenberg and D. Woodside, *J. Chem. Phys.*, **36**, 1844 (1962).

THE KINETICS OF THE DECARBOXYLATION OF BENZYLMALONIC ACID AND CINNAMALMALONIC ACID

By Louis Watts Clark

Department of Chemistry, Western Carolina College, Cullowhee, N. C.

Kinetic data are reported for the decarboxylation of benzylmalonic acid in n-butyric acid, n-decanoic acid, m-cresol, and p-cresol, and of cinnamalmalonic acid in phenol, m-cresol, and p-cresol. The activation parameters were calculated and the isokinetic temperatures for the two reactions were determined from the slopes of the enthalpy–entropy plots. These were found to be equal to the melting points of the acids. A mathematical analysis was made of the effect of experimental error on the validity of the observed enthalpy–entropy relationship.

A change from one reaction to another in a reaction series taking place in homogeneous solution may involve (a) changes in solvent and/or (b) changes in the species undergoing reaction. Both types of change are capable of providing valuable information on the

mechanism and energetics of a reaction. Theoretically an unlimited degree of change is possible in a given reaction series.

The decarboxylation of malonic acid and its derivatives in solution represents a reaction series which has

been studied for over half a century. One aspect of this study is to investigate the effect of change of solvent on the decarboxylation of the parent substance, malonic acid. The other aspect is to investigate the effect on the reaction produced by modification of the parent substance—in other words, the study of the decarboxylation of derivatives of malonic acid.

The first aspect—kinetic studies on the decarboxylation of malonic acid in various solvents—has been studied extensively, with results which have yielded a wealth of data on the reaction.[1] The second aspect—kinetic studies on the decarboxylation of derivatives of malonic acid—has not been studied as thoroughly as has the first. Bernoulli and Jakubowics[2] studied the decarboxylation of several malonic acid derivatives in aqueous solution between 76 and 110°. Jakubowics[3] studied the rate of decarboxylation of several disubstituted malonic acid derivatives in 0.2 N aqueous solution between 90 and 110°. Muus[4] has studied the decarboxylation of dibromomalonic acid in water, and Gelles[5] that of phenylmalonic acid in water at 45°. The present writer[6] has studied the decarboxylation of cinnamalmalonic acid in several aromatic amines.

The present paper reports results of kinetic studies which have been carried out in this Laboratory on the decarboxylation of cinnamalmalonic acid in phenol, m-cresol, and p-cresol, and of benzylmalonic acid in n-butyric acid, n-decanoic acid, m-cresol, and p-cresol.

Experimental

The cinnamalmalonic acid used in this research was prepared by the condensation of cinnamaldehyde with malonic acid in acetic acid at 95° according to the procedure described in the literature[7] and was purified by recrystallization from absolute ethanol. The melting point was carefully determined a large number of times using a thermometer which was calibrated against another thermometer calibrated by the U. S. Bureau of Standards, and it turned out to be 199° (cor.). This is somewhat lower than the value reported in the temperature (208°).[7] The benzylmalonic acid proved to be 100.0% pure by titration with standard base. It melted at 121° (cor.).

The solvents were reagent grade and were distilled at atmospheric pressure immediately before use.

The apparatus and technique have been described previously.[8] In each experiment a quantity of acid was used which would furnish 40.0 ml. of CO_2 at STP on complete reaction. This amount was calculated on the basis of the actual molar volume of CO_2 at STP, 22,267 ml.[9] These quantities were, for cinnamalmalonic acid, 0.3917 g., and for benzylmalonic acid, 0.3489 g.

Results

The solubility of cinnamalmalonic acid in water at 25° was measured by titration of a saturated filtered solution with standard base. It was found to be 0.138 g. per 100 g. of water.

Smooth first-order kinetics over the greater portion of the reaction were obtained in the decarboxylation of both benzylmalonic acid and cinnamalmalonic acid in the various solvents used. Reactions in each solvent

(1) (a) G. Fraenkel, R. L. Belford, and P. E. Yankwich, J. Am. Chem. Soc., 76, 15 (1954); (b) L. W. Clark, J. Phys. Chem., 66, 125 (1962), and previous papers in this series.

(2) A. L. Bernoulli and H. Jakubowics, Helv. Chim. Acta, 4, 1018 (1921).

(3) H. Jakubowics, Z. anorg. allgem. Chem., 121, 113 (1921).

(4) J. Muus, J. Phys. Chem., 39, 343 (1935).

(5) E. Gelles, J. Am. Chem. Soc., 75, 6199 (1953).

(6) L. W. Clark, J. Phys. Chem., 66, 836 (1962).

(7) L. F. Fieser and M. Fieser, "Introduction to Organic Chemistry," D. C. Heath and Co., Boston, Mass., 1957, p. 443. See also Beilstein, Vol. IX, p. 912.

(8) L. W. Clark, J. Phys. Chem., 60, 1150 (1956).

(9) S. Glasstone and D. Lewis, "Elements of Physical Chemistry," 2nd Ed., D. Van Nostrand Co., Inc., New York, N. Y., 1960, p. 43.

were carried out two or three times at three or four temperatures over a 20° temperature range. The average values of the apparent first-order rate constants for the decarboxylation reaction in the various solvents at the different temperatures studied were obtained in the usual manner from the slopes of the experimental logarithmic plots. These are shown in Table I.

TABLE I

A. APPARENT FIRST-ORDER RATE CONSTANTS FOR THE DECARBOXYLATION OF BENZYLMALONIC ACID IN SEVERAL SOLVENTS

Solvent	Temp., °C. (cor.)	$k \times 10^4$ (sec.$^{-1}$)	Av. dev.
n-Butyric acid	121.63	1.18	0.02
	131.53	2.47	.02
	141.25	4.94	.04
n-Decanoic acid	122.00	1.22	.02
	131.66	2.79	.02
	141.68	6.42	.03
m-Cresol	120.46	2.21	.03
	130.97	5.37	.03
	140.63	11.3	.05
p-Cresol	120.46	2.27	.03
	130.97	5.73	.03
	140.63	12.9	.05

B. APPARENT FIRST-ORDER RATE CONSTANTS FOR THE DECARBOXYLATION OF CINNAMALMALONIC ACID IN SEVERAL SOLVENTS

Solvent			
Phenol	158.30	1.37	0.02
	167.85	2.72	.02
	177.10	5.17	.03
m-Cresol	150.49	1.17	.03
	160.15	2.15	.04
	170.35	3.95	.05
p-Cresol	160.05	1.58	.04
	171.86	3.74	.04
	180.25	6.71	.05

Table II shows the parameters of the absolute reaction rate equation[10] calculated from the data given in

$$k = \frac{\kappa T}{h} e^{\Delta S^*/R} e^{-\Delta H^*/RT}$$

Table I. Corresponding values for the malonic acid reaction are also included for the sake of comparison.

TABLE II

ACTIVATION PARAMETERS FOR THE DECARBOXYLATION OF MALONIC ACID AND DERIVATIVES IN SEVERAL LIQUIDS

(ΔH^* values are in kcal./mole, ΔS^* values are in e.u./mole)

Solvent	Malonic acid ΔH^*	Malonic acid ΔS^*	Benzylmalonic acid ΔH^*	Benzylmalonic acid ΔS^*	Cinnamalmalonic acid ΔH^*	Cinnamalmalonic acid ΔS^*
Melt	35.8	+11.9	29.4	− 2.6		
n-Butyric acid	32.3	+ 2.5	23.0	−18.9		
m-Cresol	32.3	+ 3.2	25.3	−11.6	22.0	−25.2
p-Cresol	29.8	− 2.4	27.6	− 5.7	27.1	−14.2
Phenol	27.3	− 8.9			26.3	−16.0
Decanoic acid	26.6	−11.0	26.9	− 9.0		

Discussion of Results

A comparison of the ΔH^* values in Table II reveals that the electrophilicities of the two derivatives are larger than that of the parent acid. Also, the differences in the ΔS^* values shown in the table are in harmony with the differences in the relative steric effects of the benzyl group and the cinnamal group as compared with hydrogen.

(10) S. Glasstone, K. J. Laidler, and H. Eyring, "The Theory of Rate Processes," McGraw-Hill Book Co., Inc., New York, N. Y., 1941, p. 14.

TABLE III

DECARBOXYLATION STUDIES. MATHEMATICAL ANALYSIS OF THE EFFECT OF ERRORS ON THE ΔH^*-ΔS^* RELATIONSHIP

Compound undergoing decarboxylation	Solvents	2δ (kcal./mole)	Obsd. range of ΔH^* $(d\Delta H^*)$ (kcal./mole)	$\dfrac{d\Delta H^*}{2\delta}$	Isokinetic temp., °C.
I. Cinnamalmalonic acid (m.p. 199°)	Phenols, cresols	2.5	5.1	2.0	198
II. Oxalic acid[a] (m.p. 194°)	Cresols, glycols, amines	3.6	17.9	5.0	194
III. Oxanilic acid[b] (m.p. 150°)	Ethers, tertiary amines	3.6	28.4	7.8	150
IV. Malonic acid[c] (m.p. 134°)	(a) Cresols, acids, nitro compounds	3.7	12.3	3.3	134
	(b) Alcohols	2.1	6.7	3.2	134
V. Benzylmalonic acid (m.p. 121°)	Acids, cresols	3.2	6.4	2.0	121

[a] See ref. 13.   [b] See ref. 14.   [c] See ref. 12.

A plot of the values of ΔH^* vs. ΔS^* shown in Table II are linear for each reacting species. Line I of Fig. 1 is the plot for the cinnamalmalonic acid reaction in phenol and cresols. Line II is the plot for the benzylmalonic acid reaction in the molten state and in the two acids, n-butyric acid and n-decanoic acid. The parameters for the benzylmalonic acid reaction in the cresols are not plotted, but would form a third line, below and parallel to line II. The fact that the parameters for the decarboxylation of each acid in the various solvents all fall on a straight line is indicative of a uniformity of mechanism.[11]

The so-called isokinetic temperature is found from the slope of the ΔH^*-ΔS^* plot. At the isokinetic temperature the free energies of activation, and therefore the rate constants, of all the reactions included in the plot are equal.[11] The slope of line I of Fig. 1 is 471°K. This corresponds to 198°, which is very nearly the melting point of cinnamalmalonic acid. The slope of line II of Fig. 1 is 394°K. This corresponds to 121°, which is the melting point of benzylmalonic acid. It has been shown previously that the isokinetic temperatures for the decarboxylation of malonic acid,[12] oxalic acid,[13] and oxanilic acid,[14] are likewise equal to their melting points.

Petersen, et al.,[15] have discussed the effects of experimental error on the validity of the enthalpy–entropy relationship. It is worthwhile applying their analysis to the results of the present investigation, as well as to those in the three additional cases mentioned above.

They have shown that the maximum possible error in ΔH^* in the positive direction (δ) can be calculated by means of the equation

$$\delta = R\,\frac{T'T}{T' - T}\,\ln\frac{(1 + \alpha)}{(1 - \alpha)}$$

or, if $\alpha < < 1$

$$\delta = 2R\,\frac{T'T}{T' - T}\,\alpha$$

where α is the maximum possible fractional error in k, and T and T' are the temperature limits of the reaction. If the range of ΔH^* values be designated by $d\Delta H^*$,

(11) J. E. Leffler, J. Org. Chem., 20, 1202 (1955).
(12) L. W. Clark, J. Phys. Chem., 67, 526 (1963).
(13) L. W. Clark, ibid., 67, 1355 (1963).
(14) L. W. Clark, ibid., 66, 1543 (1962).
(15) R. C. Petersen, J. H. Markgraf, and S. D. Ross, J. Am. Chem. Soc., 83, 3819 (1961).
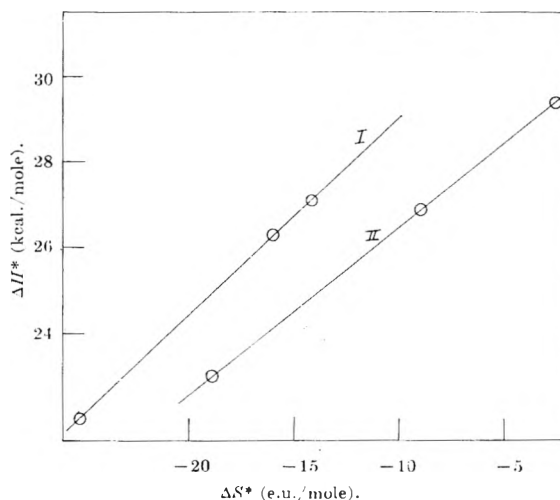
Fig. 1.—Enthalpy–entropy plots for the decarboxylation of malonic acid derivatives in various liquids: I, cinnamalmalonic acid in m-cresol, phenol, and p-cresol; II, benzylmalonic acid in n-butyric acid, n-decanoic acid, and in the molten state.

and the total maximum possible error in ΔH^* by 2δ, then the ratio: $d\Delta H^*/2\delta$, must be at least equal to unity if any validity can be assumed in the observed enthalpy–entropy relationship. Furthermore, this ratio must be much larger than unity if any details of the relationship can be confidently inferred.

The results of the mathematical analysis in the case of the five compounds in question, according to the above discussion, are shown in Table III, the compounds being arranged in the order of decreasing melting points. (The maximum possible fractional error in k has been assumed to be 0.05.)

It will be seen in Table III that the ratio, $d\Delta H^*/2\delta$, for all the reactions shown is greater than unity, and is very much greater than unity in the case of oxalic acid and oxanilic acid. These results indicate that the coincidence between the melting point and the isokinetic temperature is probably not fortuitous, nor the result of experimental error, but is probably a general kinetic relationship in the case of unimolecular reactions.

It is of interest to point out in this connection that, in the case of the isomerization of azobenzene in a series of solvents, the isokinetic temperature has been found to be equal to its melting point, namely 68°.[16]

(16) R. J. W. Le Fevre and J. Northcott, J. Chem. Soc., 867 (1953).

THE REVERSIBLE THERMAL DENATURATION OF CHYMOTRYPSINOGEN.[1]
I. EXPERIMENTAL CHARACTERIZATION

BY JOHN BRANDTS[2] AND RUFUS LUMRY

Laboratory for Biophysical Chemistry, Department of Chemistry, University of Minnesota, Minneapolis, Minnesota

The thermal denaturation of chymotrypsinogen has been studied in the pH range from 2 to 3 by means of viscometry, rotatory dispersion, refractometry, and ultraviolet spectroscopy. Rotatory dispersion indicates a small helix content, if any, which is not altered by denaturation in water. Changes in all parameters are small despite the very large thermodynamic changes. Difference spectra are interpreted to mean that some indole groups come into contact with water on denaturation. Two alternative descriptions of the reaction are given: (1) The denatured protein forms a porous ball of small dimensions. Solvent penetrates to nearly all regions of the polypeptide. The domain of denaturation consists of most of the protein and there is much freedom of rotation about single bonds within this region. (2) Only a single coöperative unit consisting of side chains melts on denaturation; the conformation of the backbone is unchanged. Solvent penetrates the melted region, but in a highly restricted manner such that single water molecules or small aggregates must be formed to comply with space restrictions within this region. Both descriptions emphasize the role of hydrophobic bonds and their control by factors of water structure. The absence of change in the rotation parameter a_0 is attributed to accidental compensation. Studies of organic additives and urea show two kinds of denaturation phenomena: (A) at low additive concentration the native protein is unstabilized in such a way that increased temperature and increased additive concentration work in the same direction; (B) at high organic additive concentrations (but not urea) increasing temperature reverses the effect of additive. At high additive concentrations the measured parameters undergo drastic changes. Rotatory dispersion studies suggest that there is an increase in folding though little increase in the net amount of right or left handed helix content.

Introduction

There exists at present little direct information leading to a quantitative description of the factors determining the stability of folded proteins. Even qualitative statements are often uncertain. For example one may entertain the point of view that hydrogen bonds stabilize or that they unstabilize protein folding in solution as a matter of faith rather than a matter of fact. Estimates of the maximum stabilizing free energy per helix hydrogen bond in an unstrained α-helix obtained from the titration data of Wada for poly-α-glutamic acid place this figure at about 400 cal.,[3] but many consider this value much too high for proteins. The status of hydrogen bonds in non-helix parts of the molecule is even more complicated. One can say with some certainty that the cost of unsatisfied hydrogen-bonding valences in energy coin is too great to make this a common occurrence. However, the logistical problem which nature has had to face in providing correct geometry for all such hydrogen-bonding valences is very great. If she has taken the pains to solve this problem in detail, hydrogen bonds in amorphous regions may be stabilizing. If she has not, such valences may be a positive deterent to stable folding. Since what little evidence there is indicates that water molecules only very infrequently are found to be permanent residents inside proteins, it would appear that the orientation problem involved in making four good hydrogen bonds to each water molecule has thus far in evolution been only occasionally solved. Whether the less complicated problems associated with internal serine and threonine hydrogen bonding, for example, have been solved or not remains an open question. Whether or not such problems require solution in the construction of stably folded proteins depends on the other sources of stabilizing free

energy. Chief among these now appears the "hydrophobic bond,"[4] a conceptually simple structure actually made very complicated by its vital dependence on unknown factors of water structure. The latter are no less complicated today than they have been for many years and it seems probable that a phenomenological approach to the hydrophobic bond will be more useful than one based on analyses of water structure. A phenomenological approach to this problem, to hydrogen bond enthalpies and to the conformational entropy problem as these problems appear in chymotrypsinogen forms the subject of the subsequent paper.[5] In the present paper we shall describe experiments conducted to characterize the reversible thermal denaturation of this protein in the acid region. There has been little detailed work on the reversible thermal denaturation of globular proteins until recently and our understanding of such reactions is remarkably slight. The thermal denaturation of chymotrypsinogen was originally detected by Kunitz and Northrup[6] and in a pioneering paper Eisenberg and Schwert[7] provided much of the fundamental work needed to support more detailed study. They reported a standard enthalpy of denaturation of 100 kcal. and a standard entropy of denaturation of 315 e.u. at pH 2. What makes such a large entropy change of particular interest, however, is Schellman's[8] finding that the denaturation reaction occurs without detectable change in specific rotation. It is a purpose of this paper to provide a more detailed picture of the denaturation reaction.

Results

The Transition in Aqueous Solvents. Thermodynamics.—Eisenberg and Schwert[7] have shown that a true equilibrium exists between native and thermally denatured chymotrypsinogen in solutions of pH 3 or below if the protein concentration is low and the solu-

(1) This work was supported by research grants from the National Institutes of Health and the Louis and Maud Hill Family Foundation. Fellowship support for J. B. was received from the National Science Foundation and the General Electric Corporation.

(2) Taken in part from a thesis presented to the University of Minnesota in partial fulfillment of the requirements for the Ph.D. Degree, August, 1961.

(3) A. Wada, *Mol. Physics*, **3**, 409 (1960).

(4) W. Kauzmann, *Advan. Protein Chem.*, **14**, 1 (1959).

(5) J. Brandts, to be submitted.

(6) M. Kunitz and J. G. Northrup, *J. Gen. Physiol.*, **18**, 433 (1935).

(7) M. A. Eisenberg and G. W. Schwert, *ibid.*, **34**, 583 (1951).

(8) J. A. Schellman, *Compt. rend. trav. lab. Carlsberg, Ser. Chim.*, **30**, 450 (1958).

tion contains no added neutral salt. In all of our studies we have adjusted solution conditions to ensure maximum reversibility. The above authors have assumed, as is fully substantiated by their data and ours, that an equilibrium exists between a single denatured and a single native species, *i.e.*

$$N(\text{native}) \rightleftharpoons D(\text{denatured})$$

$$K = (D)/(N)$$
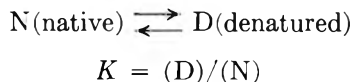
By taking advantage of the insolubility of the denatured protein in a high salt buffer the thermodynamic constants may be obtained from a van't Hoff plot by the usual relations

$$\Delta H^0 = -R \, d(\ln K)/d(1/T)$$

$$\Delta S^0 = \Delta H^0/T_0$$

where T_0 is the temperature at which the standard free energy change is zero and is ordinarily referred to as the transition temperature. We will use T_0 as a measure of the relative stability of native and denatured chymotrypsinogen since, in this instance, it is usually more convenient to use than the free energy differences.

The above authors reported the following values at pH 2.0: $\Delta H^0 = 100$ kcal., $\Delta S^0 = 315$ e.u., and $T_0 = 43°$; and at pH 3.0: $\Delta H^0 = 143$ kcal., $\Delta S^0 = 432$ e.u., and $T_0 = 57°$. They reported that the van't Hoff plots were linear for data at a single pH and concluded that ΔH^0 and ΔS^0 were temperature independent. In the present study we have found a definite curvature in the van't Hoff plots and, although our average values are in close agreement with those previously reported, the precise values of ΔH^0 and ΔS^0 are markedly dependent on temperature. The failure of Eisenberg and Schwert to detect the temperature variations probably resulted from the narrow temperature range, about $5°$, over which their measurements of the equilibrium constant were made. The presentation of our thermodynamic data and its probable significance will be discussed in detail in the subsequent paper.[5]

Ultraviolet Absorption.—The ultraviolet absorption spectrum of chymotrypsinogen in the wave length region above 250 mμ is largely determined by seven tryptophan residues with minor contributions from four tyrosine residues. Chervenka[9] has reported a change in this spectrum accompanying urea denaturation of the protein and our results show a similar shift during thermal denaturation, the difference spectra being characterized by three minima at 293, 286, and 276 mμ, decreasing in size in that order (Fig. 1). These minima arise from blue shifts of about 1 mμ in the absorption peaks during denaturation as well as from a general decrease in extinction coefficients. The appearance of the denatured form can be readily followed by the growth of the largest trough in the difference spectrum as the temperature is increased. An example of this procedure is shown in Fig. 2. The abrupt changes in extinction coefficient illustrate the coöperative nature of the transition and the increased stability of the native protein as the pH is increased is evident from the shift in T_0.

The behavior of the chymotrypsinogen difference spectra fits the picture presented by Yanari and Bovey,[10] who suggested such effects were to be attributed to

(9) C. H. Chervenka, *Biochim. Biophys. Acta*, **31**, 85 (1959).

(10) S. Yanari and F. A. Bovey, *J. Biol. Chem.*, **235**, 2818 (1960).
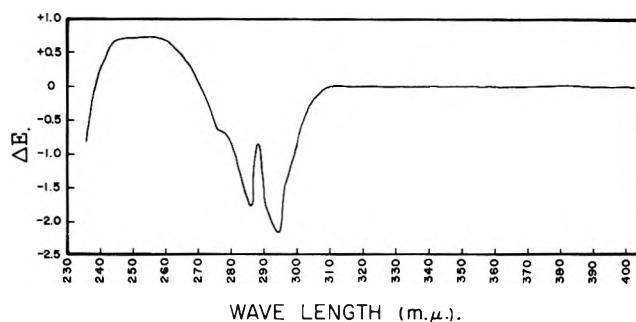
Fig. 1.—The difference spectrum of denatured (50°) and native chymotrypsinogen at pH 2.0.
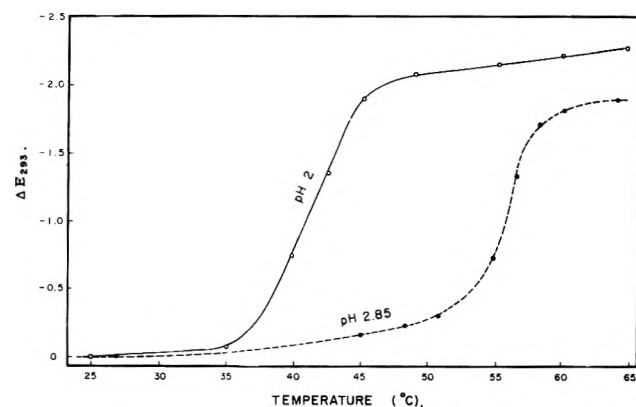
Fig. 2.—The influence of temperature on the extinction coefficient at 293 mμ.

changes in the immediate environment of the absorbing residues. In particular the substitution of an environment of lower polarizability (*e.g.*, water) for one of higher polarizability (*e.g.*, an organic solvent) has been shown to produce difference spectra for the model compound L-tryptophan which are quite similar in appearance to that in Fig. 1.[10,11] The similarity of these spectra lends support to the hypothesis that some tryptophan residues in the native protein are located primarily in local high-polarizability regions but become exposed to water or other low polarizability neighbors on denaturation.

Optical Rotation.—The use of optical rotation as a means of measuring helix content of proteins still rests on a very uncertain foundation and will continue to do so at least until more definitive results are obtained in the ultraviolet region where the active chromophores absorb. Optically active structures other than α-helices may well exist in proteins and their presence can lead to quite erroneous results in interpretation. Recognizing the limitations of the method we will nevertheless attempt to obtain some information on conformational changes during denaturation from rotatory-dispersion data.

The Moffitt equation may be expressed in the form[12]

$$|\alpha| = \frac{100(n^2 + 2)}{M} \left[\frac{a_0\lambda_0^2}{(\lambda^2 - \lambda_0^2)} + \frac{b_0\lambda_0^4}{(\lambda^2 - \lambda_0^2)^2} \right]$$

where M is the average residue weight, n is the solvent refractive index, and $[\alpha]$ the specific rotation at wave length λ. It is customarily assumed that λ_0 has a value of 212 mμ but in the present case it was found that no single value of λ_0 would precisely represent the experimental results over the entire wave length region from

(11) J. Foss, *Biochim. Biophys. Acta*, **47**, 569 (1961).

(12) P. Urnes and P. Doty, *Advan. Protein Chem.*, **16**, 401 (1961).
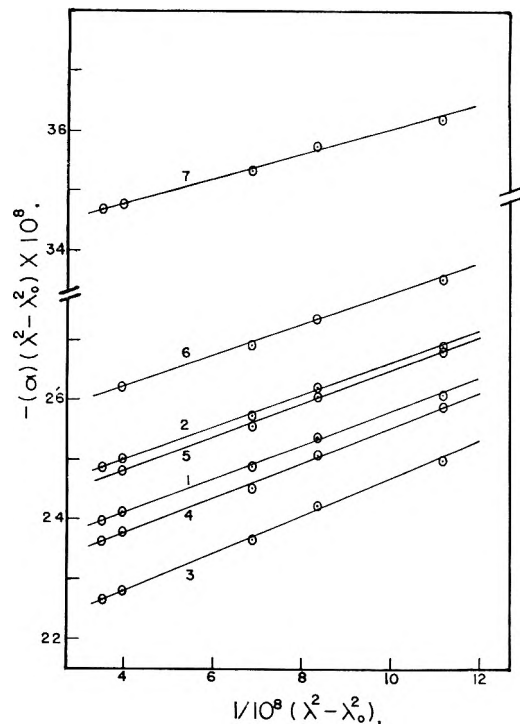
Fig. 3.—Moffitt plots for chymotrypsinogen under various conditions. curve 1, pH 2.0, 38°; curve 2, pH 2.0, 54°; curve 3, pH 2.85, 48°; curve 4, pH 2.85, 64°; curve 5, 1.3 M urea, pH 2.0, 24°; curve 6, 1.3 M urea, pH 2.0, 45°; curve 7, 8 M urea, pH 2.0, 20°.
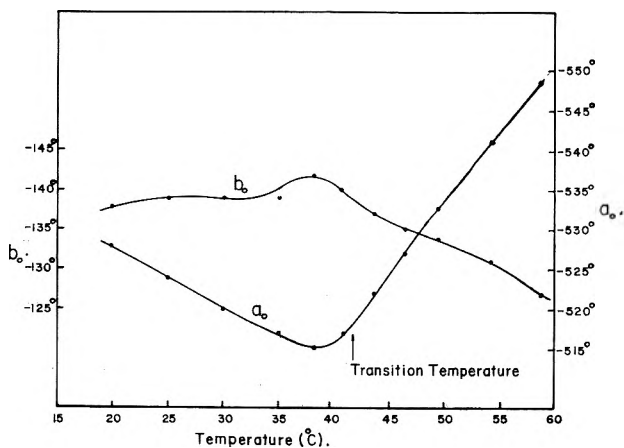
Fig. 4.—The effect of temperature on rotatory dispersion parameters at pH 2.0.

580 to 365 mμ. We have therefore chosen a value of λ_0 of 209 mμ since this value minimizes the deviations of the experimental results from the Moffitt equation.

Some typical results are plotted in terms of the Moffitt equation in Fig. 3. It is apparent that the systematic deviations from linearity are very small, amounting to less than a degree in specific rotation even at the higher wave lengths, but they were found to be reproducible and outside the range of experimental error. The failure of chymotrypsinogen to follow the Moffitt equation more precisely may result from its abnormally high content of amino acids such as threonine, proline, tryptophan, tyrosine, and phenylalanine which have "unusual"[13] rotatory behavior in the visible and near-ultraviolet. Other proteins checked in this Laboratory, with the exception of chymotrypsin, appear to obey the

(13) J. Strem, Y. S. Krisna-Prasad, and J. A. Schellman, *Tetrahedron*, **13**, 176 (1961).

Moffitt equation as well as can be expected from the approximate character of this expression.

Figure 4 shows the dispersion parameters, a_0 and b_0, obtained from the Moffitt plots for chymotrypsinogen in water solutions of pH 2.0 at various temperatures in the region of the thermal denaturation. The transition temperature marked is that obtained from solubility, difference spectra, and other physical properties. The denaturation is not well defined by rotatory-dispersion parameters because the rather large temperature dependence of the dispersion parameters of the denatured protein completely obscures the small differences between the native and denatured forms in the transition region.

The low temperature value of b_0, $-138°$, implies that native chymotrypsinogen has a low helix content. The customary method of estimation, i.e.[12]

$$\% \text{ helix} = (b_0/-650°) \times 100$$

leads to a helix content of about 20% if one assumes that all helix present is of a right-handed twist. In the temperature region from 38 to 48°, where chymotrypsinogen is more than 90% converted from the native to denatured form as measured by other physical properties, b_0 changes by only 5°.

Although the changes in a_0 during denaturation are somewhat larger than those in b_0, they are still small by usual standards. In passing from the native protein (38°) to the denatured protein (48°) a_0 changes by only 13° from -517 to $-530°$. In terms of specific rotation, this corresponds to a change of 1.5° at the sodium-D line. In contrast to the thermally denatured protein it will be seen that urea-denatured chymotrypsinogen has an a_0 which is 200° more levorotatory than the native form. Thus, in terms of optical rotation alone, the thermally denatured protein is very similar to the native form and quite different from the urea-denatured species, suggesting that the urea-denatured protein is probably more extensively unfolded than the thermally-denatured form.

The Moffitt parameters for the denaturation at pH 2.85 are shown in Fig. 5. The shift in T_0 to 56° is immediately apparent. Once again at this higher pH, b_0 is nearly constant throughout the transition region. The change in a_0 is about 25°. This is about twice the change observed at pH 2.0 and probably results from the much greater temperature coefficient of rotation for the denatured form than for the native form, clearly illustrated in Fig. 4.

Viscosity.—Because the very large entropy of denaturation suggested that the structural differences between native and denatured chymotrypsinogen might be large, it was thought that the small changes in rotatory dispersion parameters might not adequately reveal the extent of unfolding during denaturation. For this reason we studied the changes in reduced viscosity during denaturation. This parameter generally is assumed to be sensitive to the size–shape properties of macromolecules in solution.

The results of the viscosity studies at pH 2.0 in 1% ethanol are seen in Fig. 6. The transition in viscosity seems to parallel the changes in ultraviolet absorption, solubility, and optical rotation, although the accuracy of the viscosity data does not permit a close comparison. The reduced viscosity changes from 0.044 to 0.072 in the transition region and, although this is a rather small

change when compared to the five- and tenfold increases common for urea denaturation, it does suggest that significant structural modifications occur during thermal denaturation.

Refractive Increment.—The index of refraction of a solution is related to the specific volume of the solution by the Lorentz–Lorenz equation

$$(n^2 - 1)/(n^2 + 2) = r/V$$

where n is the index of refraction, r the specific refractivity, and V is the specific volume of the solution. Kauzmann[14] has measured the changes in both refractive index and volume which occurred in the urea denaturation of ovalbumin and concluded that the changes in refractive index could be accounted for entirely in terms of the volume change and that the specific refractivity remained constant during denaturation. If this is also true in the thermal denaturation of chymotrypsinogen, as probably is the case, then the volume change during denaturation may be calculated readily from the refractive increments of the native and denatured proteins.

The temperature dependence of the refractive increment of chymotrypsinogen at pH 2.0 is shown in Fig. 7. The transition to the denatured form shows significant changes in the refractive increment and if the extrapolated value of the native protein at 50° is compared with the observed value of the denatured protein at the same temperature by the Lorentz–Lorenz equation, it is found that the transition to denatured chymotrypsinogen occurs with an increase in partial molar volume amounting to 125 ml./mole. This is comparable in magnitude to the volume increases measured dilatometrically by Heymann[15] for the heat denaturation of other proteins. Holcomb and Van Holde[16] have found that the coefficient of expansion of thermally denatured ribonuclease is fourfold greater than that of the native form and, consequently, that denaturation may occur with either positive or negative volume changes depending on the temperature. It is regrettable that experimental difficulties prevented the measurement of the refractive increment of denatured chymotrypsinogen at higher temperatures.

Stauff and Rasper[17] reported that the refractive increment of chymotrypsinogen showed an extremely sharp increase at pH 2.7 and 39° which they attributed to thermal denaturation. They also found a corresponding decrease in partial molar volume measured in a dilatometer. We attempted to repeat their results on several occasions but found the refractive increment exhibited normal behavior characteristic of the native protein below 50° at pH 2.7. The results in this study show that the transition temperature at pH 2.7 occurs at 55° rather than 39°, in good agreement with the results of Eisenberg and Schwert. There appears to be no obvious explanation for these discrepancies in experimental results.

The Influence of Solvent Composition. Organic Solvents.—The stability of the native protein is

(14) W. Kauzmann, in "Influence of Temperature on Biological Systems," F. H. Johnson, Ed., American Physiological Society, Washington, D. C., 1957, p. 9.

(15) E. Heymann, *Biochem. J.*, **30**, 127 (1936).

(16) D. N. Holcomb and K. E. Van Holde, *J. Phys. Chem.*, **66**, 1999 (1962).

(17) Von J. Stauff and J. Rasper. *Kolloid Z.*, **159**, 97 (1958).
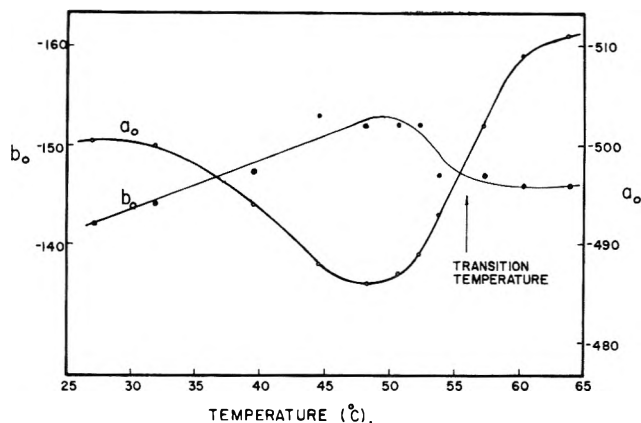
Fig. 5.—The effect of temperature on rotatory dispersion parameters at pH 2.85.
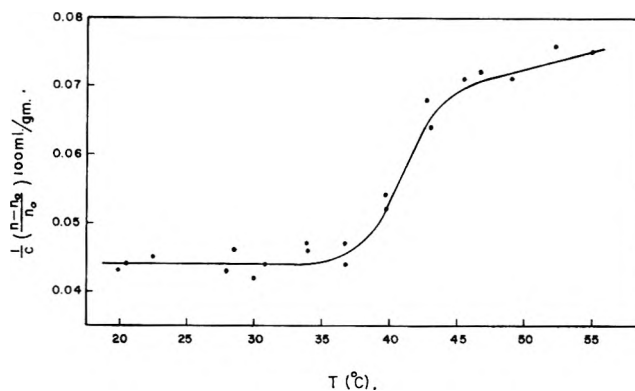
Fig. 6.—Reduced viscosity of chymotrypsinogen at pH 2.0 as a function of temperature (in 1% ethanol).
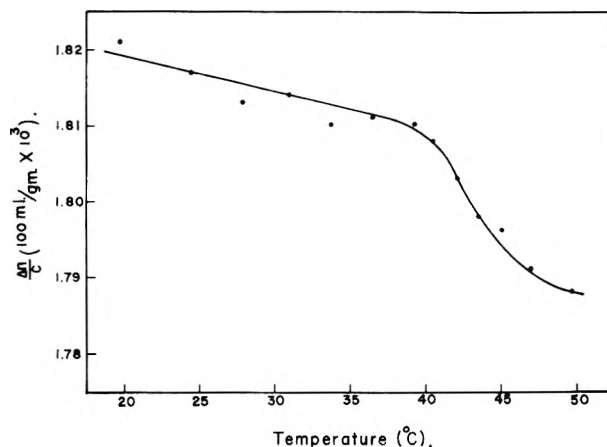
Fig. 7.—The influence of temperature on refractive increment, pH 2.0.

markedly decreased in solutions containing moderate amounts of organic additives such as ethanol and dioxane. Figure 8 summarizes difference-spectra data obtained in solutions containing 6.25 volume % dioxane. The observed transition temperatures, 34° at pH 2 and 50° at pH 3, are 9° and 7°, respectively, below those found for the denaturation in pure water at the same pH values. The same trends in stability were observed in ethanol–water solvents at pH 2.0. Table I shows the decrease in transition temperature as the ethanol concentration is increased. When the ethanol concentration is as high as 19%, the denatured protein has a greater stability at room temperature than the native.

The presence of organic solvents in the reaction mixture does not seem to produce any serious alterations in the character of the transition since the size and shape

Fig. 8.—The effect of temperature on the extinction coefficient in 6.25% dioxane solutions.

TABLE I

THE TRANSITION TEMPERATURE OF THERMAL DENATURATION
IN VARYING ETHANOL CONCENTRATIONS, pH 2.0

Vol. % EtOH	T_0, °C.
0	43
2	40
10	36
15	28
19	Below 25

region as measured by the decrease in transition temperature. This coöperative action of organic solvents with temperature toward the facilitation of thermal denaturation probably is an indication that hydrophobic forces are of some importance in maintaining the integrity of the native protein.

There is yet another effect of organic solvents on the conformation of this protein appearing at higher concentrations of added solvent. Figure 9 shows the behavior of the dispersion parameters as the amount of dioxane in the solvent is changed at pH 2, 20°. The changes in both a_0 and b_0 proceed rather slowly until a concentration of 10–15% dioxane is reached and then more pronounced changes occur as the solution is further enriched in dioxane. It may be significant that 15% is the approximate concentration of dioxane at which the "thermal" denaturation occurs at these conditions of pH and temperature. In 70% dioxane, a_0 has changed from the pure-water value of $-530°$ to $-190°$ while b_0 increases from $-138°$ to $-75°$. The large decrease in the levorotatory value of a_0 is in a direction commonly associated with an increase in folding while a strict interpretation of the b_0 change suggests a small loss in helical folding. We do not want to overemphasize the popular interpretation of b_0 for the small changes observed in the present instance since these changes may be a reflection primarily of the changing solvent composition. Nevertheless, it does seem significant that there is no indication of a large increase in net helix content as the activity of the water is decreased, a phenomenon which has been observed for several other proteins.[18–20]

It is not possible that the large changes in a_0 are entirely the result of solvent effects since the rotation changes did not occur instantaneously upon addition of dioxane but extended over several hours. In addition, the rotational changes appeared to be reversed by increasing the temperature, which implies that conformational changes are at least partially responsible. Thus, as a solution of chymotrypsinogen in 20% dioxane was heated from 20 to 55°, a_0 changed from $-409°$ to $-530°$ while b_0 changed from $-119°$ at the lower temperature to $-146°$. The high temperature values of both a_0 and b_0 are very close to those of the thermally denatured protein in pure water. A mildly aggregated species of chymotrypsinogen is also formed in slow equilibrium in these higher concentrations of dioxane. The appearance of the polymer was followed by taking aliquots from the polarimeter tube and spinning these samples in an ultracentrifuge until the two peaks were separated. Both the monomer and heavy component gave schlieren peaks which were sharp and symmetrical and no intermediate components were indicated. The pro-

Fig. 9.—The effect of dioxane on the rotatory dispersion parameters at pH 2, 20°.

Fig. 10.—Changes in specific rotation and the state of aggregation after addition of 20% dioxane, pH 2.

of the difference spectra in these moderate concentrations of ethanol and dioxane were similar to those observed in pure water. Similarly, the changes in rotation for thermal denaturation in ethanol–water solvents were also very small as will be discussed below. The primary consequence of the presence of these additives in the solvent is to produce instability in the denaturing

(18) C. Tanford, P. K. De, and V. G. Taggart, J. Am. Chem. Soc., 82, 6028 (1960).
(19) R. Weber and C. Tanford, ibid., 81, 3255 (1959).
(20) P. Doty, Rev. Modern Phys., 31, 107 (1959).

portion of heavy component in the dioxane solution was calculated from the relative area under the two peaks and appears also in Fig. 10. The changes in rotation are completely over before 50% of the heavy component has formed which suggests that the optical rotation changes are brought about by monomolecular conformational changes and the formation of the heavy component proceeds somewhat slower and with little or no change in rotation. It is not possible to say precisely what is the molecular weight of the heavy component since no attempt was made to determine its frictional factor. Its sedimentation constant was about three times that of the monomer in 20% dioxane but the precise value was quite dependent on the dioxane concentration.

Identical temperature effects were observed with ethanol solutions as seen in Fig. 11. Once again, there is a definite decrease in levorotation as ethanol is added at room temperature. At high temperature all the curves appear to converge to that of the thermally denatured protein in pure water. The coöperative nature of the transition is well illustrated in the higher ethanol concentrations where the characteristic S-shaped curve is evident. This high temperature transition in higher concentrations of organic additives should not be confused with the ordinary thermal denaturation which, in 19% ethanol, occurs below room temperature and proceeds with only small changes in rotation. The foot of the thermal transition can be recognized as the point where $d[\alpha]/dT$ changes sign and this occurs at increasingly lower temperatures as the ethanol concentration is increased (Fig. 11). We emphasize that temperature and organic solvent work in opposite ways in the second denaturation reaction occurring only at very high concentrations of organic additives.

Effect of Urea.—Most highly folded proteins are sensitive to moderate concentrations of urea, particularly when the folded form has only marginal stability in the absence of urea. This is well illustrated by the rotatory dispersion data of Fig. 12 which show that a rather small concentration of urea, 1.3 M, is quite effective in lowering the transition temperature of the thermal denaturation from the pure water value of 43 to 32°. In addition to this shift in the stability of the two forms, the small concentration of urea slightly alters the character of the transition as indicated by the accentuation in the changes in both a_0 and b_0 during denaturation. The change in b_0 from −140 to −126° suggests a loss in helical folding in 2% of the residues, a modest change but considerably greater than that observed in pure water. The change in a_0, from −530 to −560°, is over twice as large as that observed in pure water at this pH. Another significant difference is that the high temperature slope of a_0 is much smaller in urea. All of these facts suggest that there are additional alterations in protein structure which occur when the denaturation proceeds in urea, possibly the unfolding of a small helical segment. These small changes are superimposed on the more profound structural changes which occur in both pure water and urea solutions; it is the latter changes that are primarily responsible for the large increases in enthalpy and entropy during denaturation although they provide only minor contributions to the optical rotatory properties of the protein at the transition temperature.
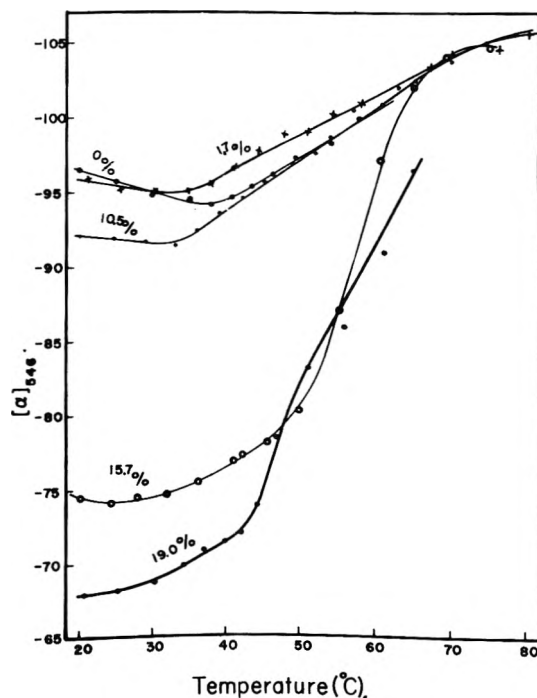
Fig. 11.—The influence of temperature on the specific rotation of chymotrypsinogen in various concentrations of ethanol, pH 2.0. Volume concentrations of ethanol are given.
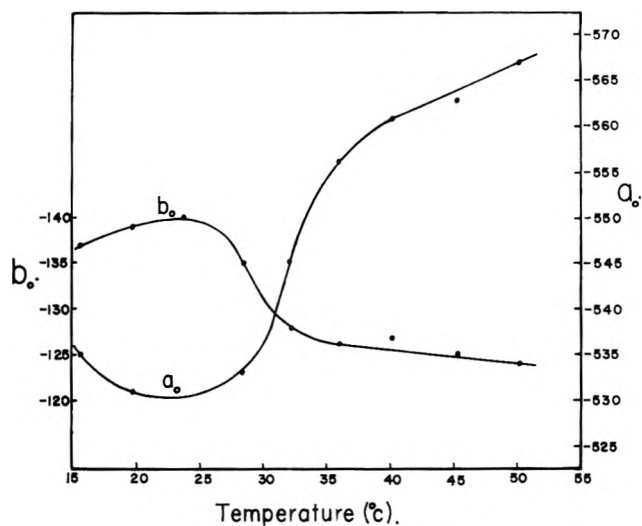
Fig. 12.—The effect of temperature on rotatory dispersion parameters in 1.3 M urea solution, pH 2.0.

Higher concentrations of urea produce more drastic changes in optical rotation. Table II shows the values of the Moffitt parameters obtained in 8 M urea solution, pH 2.0. It is significant that, even in this high concentration of urea, b_0 still has a value of −96° at 20° compared with the value of −138° for the native protein in water at this pH and temperature. The non-zero value of b_0 in 8 M urea remains a puzzle in these studies. If, as most current opinion holds, b_0 is strictly dependent only on ordered sub-structures of the protein, chymotrypsinogen is markedly resistant to total unfolding of such sub-structures. Such a situation might be a consequence of an unusually large stabilizing effect of the five disulfide bonds. There is, however, no particular reason to suppose that these bonds are necessarily stabilizing and there may be other sources of contributions to b_0. Thus it has not yet been excluded that the disulfide bonds themselves play such a role through

nearby asymmetric carbons nor even that the asymmetric carbons in the side chains of the threonine residues contribute to b_0 in the totally unfolded state. Chymotrypsinogen has an abnormally high content (22 residues) of the latter.

TABLE II

THE MOFFITT PARAMETERS FOR NATIVE AND UREA DENATURED CHYMOTRYPSINOGEN, pH 2.0

	a_0	b_0
Native, 20°	−528	−138
8 M urea, 20°	−728	−96
8 M urea, 57°	−645	−126

It should be noted that Imahori[21] reported a b_0 of zero for chymotrypsinogen in 8 M urea at pH 7.7, quite at variance with our results at pH 2. Our results are, however, identical with those of Schellman[22] for the same protein in 8 M urea at pH 6.5 when compared in terms of λ_c and $[\alpha]_D$.

Although high urea concentrations have only small effects on b_0, the increase of 200° in the levorotatory value of a_0 indicates that profound structural changes do take place. As the temperature of the 8 M urea solution is increased to 57°, a_0 becomes much less levorotatory, in keeping with the usual temperature dependence observed for flexible chains.[23]

Discussion

The Question of Reversibility.—Some time ago it was pointed out that,[24] at least in most cases, free energy must be the determinant of protein folding with the consequence that amino-acid sequence will in such cases determine folding. In the present study we conclude that the thermal denaturation of chymotrypsinogen is totally reversible in the pH range 2–3 at temperatures below 70° and it therefore is highly probable that the forms characterized as "native" and "reversibly denatured" are the forms of greatest thermodynamic stability under the particular conditions in which they exist. Accurate measurements of optical rotatory dispersion, ultraviolet difference spectra, solubility, viscosity, sedimentation velocity, and refractive increment indicate total reversibility. In terms of specific rotation the initial native and the denatured protein were identical within 0.05% in repeated experiments despite the fact that the denatured state was maintained for several hours at high temperatures before cooling.

The Influence of Solvent Composition. Hydrogen Ion Concentration.—The data of Eisenberg and Schwert,[7] consistent with our data, show that there is a net uptake of three protons by chymotrypsinogen on denaturation. Eisenberg and Schwert concluded that both ΔS^0 and ΔH^0 were strongly pH dependent, considerably more so in the case of the entropy change than could be expected from any simple dependence on hydrogen ion concentration. It is now apparent, however, that this analysis is incorrect. The effect of decreasing hydrogen ion concentration on denaturation is to shift the temperature range for denaturation to higher temperatures. The thermodynamic quantities are strongly dependent on temperatures as shown by the curvature of the van't Hoff plots. Hence the effect of pH as measured by Eisenberg and Schwert and by us is primarily due to changing temperature.

Ionic Strength.—The ionic strength studies carried out in this investigation served only to confirm the results reported by Eisenberg and Schwert,[7] who found a small apparent shift of the equilibrium constant to the denatured form when neutral salt was added at pH 2. In 0.02 M NaCl the shift amounts to a reduction in T_0 of only 1° but it must be borne in mind that the concentration of protons is 10^{-2} M and the concentration of chloride ions slightly higher since HCl was added for pH adjustment. However, aggregation occurs rather rapidly even if no more than 0.001 M neutral salt is added. Thus the charged groups which prevent aggregation at low ionic strength have already become highly shielded at this low salt concentration which has no apparent effect on the reversible denaturation reaction. This evidence supports the assumption that the electrostatic differences between the native and denatured forms make only minor contributions to their relative stability.

Organic Solvents.—The position of the tryptophan absorption maxima suggest that a large fraction of the many non-polar residues in native chymotrypsinogen are concentrated in hydrophobic regions of the protein and are unavailable to solvent. The changes in absorption maxima further indicate that these groups become more available to solvent in the denatured state. This rupture of hydrophobic interactions appears to be an important part of the structural changes associated with the denaturation and this is verified to a large extent by the downward shift in transition temperature observed when small concentrations of dioxane or ethanol are added. However, one must recognize several potential effects of organic additives on folded proteins in solution. As mentioned, they can reduce the stability of intramolecular hydrophobic bonds either by an indirect effect on water's tendency to form clathrate structures or through the formation of hydrophobic bonds between the added organic species and protein groups. The lowering of the dielectric constant by the addition of organic solvents can alter the electrostatic energy associated with the existing charged groups and it can also produce a change in the net charge by shifting the pK values for the ionizable groups on the protein. In the present case it does not seem probable that the pK values of the three groups which are titrated during denaturation will be altered in a large way by the change in dielectric constant of the solvent since the pK of these groups is abnormally low in the native protein (below 1.5 at 25°) and is probably dependent primarily on local environment in the folded protein rather than the bulk solvent phase. Finally, if the presence of organic additives significantly reduces the activity of water, intramolecular hydrogen bonds should become more stable.

Since low concentrations of dioxane and ethanol decrease T_0 without any apparent qualitative changes in the denaturation reaction, an unstabilizing mechanism must be sought. In view of the lack of any pronounced effect of ionic strength on the reaction, the electrostatic factor cannot be very important. It appears probable that the destabilization of the folded protein in the presence of these additives results primarily from a

(21) K. Imahori, A. Yoshida, and H. Hashisume, *Biochim. Biophys. Acta*, **45**, 380 (1960).

(22) J. A. Schellman, *Compt. rend. trav. lab. Carlsberg, Ser. Chim.*, **30**, 450 (1958).

(23) C. Schellman and J. A. Schellman, *ibid.*, **30**, 463 (1958).

(24) R. Lumry and H. Eyring, *J. Phys. Chem.*, **58**, 110 (1954).

weakening of hydrophobic interactions with a small effect due to shifts in the pK's of the abnormal ionizing groups.

Although not directly concerned with the denaturation reaction, the large rotational changes which were seen to occur in high concentrations of dioxane and ethanol require some discussion. The "thermal" denaturation can be made to occur at room temperature by the addition of approximately 15% ethanol or dioxane at pH 2 and, as mentioned before, this occurs with large changes in thermodynamics but only nominal changes in rotation. As larger amounts of organic solvents are added at room temperature, chymotrypsinogen undergoes a second conformational change characterized by a large decrease in levorotation. These large rotational changes suggest a significant reorientation of the backbone and, since they are in a direction opposite to those seen in unfolding by urea, it is probable that they result not from a further unfolding but from a refolding of the protein as it attempts to satisfy its free-energy requirements as the solvent composition is varied. We must expect in solutions of low water activity that this is primarily accomplished by forming hydrogen bonds. In this case, however, the changes in rotatory dispersion indicate that there is no increase in excess right-handed helical content even when the water concentration is as low as 30%. The data may be consistent with the formation of an intramolecular β-sheet but it seems equally possible that some other ordered or amorphous structure is formed. At high temperatures the enthalpy stabilization of the hydrogen-bonded structure is no longer sufficient to maintain the low entropy structure and it transforms in a coöperative fashion to a structure which, in terms of optical rotation, appears identical with that of the thermally denatured protein in pure water. There is no change in the spectra of the tryptophan residues during this latter transition which may mean that the temperature-labile portion of the molecule is available to solvent in both the low and high temperature forms.

Urea.—The ability of urea to facilitate denaturation has in the past been attributed to its ability to break intramolecular hydrogen bonds. The validity of this interpretation has been questioned recently by studies which indicate that urea may not be a better hydrogen bond former than water.[25-27] On the other hand, it now appears certain that urea does weaken hydrophobic bonds.[4,28] The most direct evidence pertaining to proteins comes from a recent study[29] which shows that the free energy for the transfer of non-polar amino acid side chains from a non-polar solvent to water solutions is reduced by several hundred calories on addition of urea to 8 M concentration. The comparison of these results with the solubilities in aqueous ethanol[5] solutions suggests that 2.5 M urea should be roughly equivalent to 10% ethanol in decreasing the stability of hydrophobic bonds at 25°, but in the present study we have found that it requires only 1 M urea to lower the transition temperature by an amount identical with the lowering produced by 10% ethanol and it would thus appear that

the denaturing action of urea cannot be accounted for entirely by its effects on hydrophobic bonds. A similar conclusion was reached by Tanford[18] for the denaturation of β-lactoglobulin. The results can be best explained in the present case by assuming that urea decreases the stability of both intramolecular hydrogen bonds and hydrophobic bonds with perhaps small contributions from electrostatics.

The Small Viscosity Change.—Viscosity data obtained in water or very weak concentrations of ethanol suggest that unfolding during denaturation is incomplete. The 75% increase we observe at pH 2 appears at first glance to be inconsistent with large changes in folded structure. Such a conclusion may be incorrect. It is quite true that much larger increases in reduced viscosity occur on denaturation by urea. For example, Neurath[30] found a change from 0.04 to 0.16 for chymotrypsinogen on adding urea to a final concentration of 7 M. However Kauzmann has pointed out that water is a much poorer solvent for denatured proteins than urea solutions so that unfolded proteins will approximate random coils only in solvents at least as good as urea solutions. There is a small but important set of facts in the literature which suggests that size and shape changes during thermal denaturation can be characteristically small. Saenko[31] concluded that in the absence of aggregation the intrinsic viscosity of serum albumin does not increase on heat denaturation. Strachitskii and Firfarova[32] found no change in molecular asymmetry for the same process. Holcomb and Van Holde[16] have reported small changes in viscosity, sedimentation coefficient, and molecular asymmetry during thermal denaturation of ribonuclease. They were lead to conclude that the process resulted in only a moderate amount of unfolding, a conclusion which may be challanged. It is quite possible that the thermal denaturation of ribonuclease and chymotrypsinogen is essentially the same as urea denaturation but that the unfolded form in water shows a tendency to be oriented in conformations which favor short-time contacts between hydrophobic groups or considerable intrapeptide hydrogen bonding. Note that Kauzmann[33] observed a fivefold decrease in the viscosity of irreversibly denatured ovalbumin on transfer from 10 M urea to water. The possibility thus exists that extensive unfolding of the native conformation to form a poorly solvated porous ball can occur without any large change in viscosity. Thus viscosity does not yield any positive evidence unfavorable to extensive unfolding. Nor if much unfolding occurs, can viscosity distinguish between extensive unfolding of only a fraction of the peptide chain and a partial unfolding of the whole chain.

The ultraviolet difference spectra indicate a change in solvation state on denaturation though these too provide no distinction as to the amount of protein thus affected. The proton-exchange studies of Wilcox[34] demonstrated that a core of some thirty non-exchangeable protons of the native protein disappeared on thermal denaturation. The fact that all protons are fast-

(25) I. M. Klotz and A. Franzen, J. Am. Chem. Soc., 82, 5241 (1960).
(26) I. M. Klotz, private communication.
(27) M. Levy and J. Magoulas, Abstracts, 139th National Meeting of American Chemical Society, St. Louis, Missouri. March 1961, p. 20C.
(28) W. Bruning and A. Holtzer, J. Am. Chem. Soc., 83, 4865 (1961).
(29) P. L. Whitney and C. Tanford, J. Biol. Chem., 237, PC1735 (1962).

(30) H. Neurath, J. A. Rupley, and W. J. Dreyer, Arch. Biochem. Biophys., 65, 243 (1956).
(31) T. V. Saenko, Ukr. Biokhim. Zh., 24, 196 (1952).
(32) K. I. Strachitskii and K. F. Firfarova, Biokhimiya, 18, 235 (1953).
(33) W. Kauzmann in "The Mechanism of Enzymic Action," W. D. McElroy and B. Glass, Ed., John Hopkins Press. Baltimore, Md., 1954, p. 70.
(34) P. E. Wilcox, Biochim. Biophys. Acta, 34, 602 (1959).

exchanging in the thermally denatured form shows that all parts of the molecule become exposed to water for sufficiently long periods of time to combine with catalytic ions. However this does not prove that the time–average conformation is one of extensive unfolding.

The Problem of the Small Rotation Change.—The best evidence favoring extensive unfolding during thermal denaturation is the large values of ΔS^0 and ΔH^0. These large values as well as a number of our other observations might be consistent with a microscopic first-order phase change of solvent water, perhaps a melting of some extensive and well organized hydration shell about the protein along the line originally suggested by Schwert and Eisenberg[7] or a release of internal water molecules trapped in a protein-bounded hole as suggested by Stauff and Rasper.[17] Interpretations of this sort have the virtue that they provide a simple explanation for the lack of any significant change in rotatory dispersion parameters on denaturation of chymotrypsinogen. They have the positive disadvantage that they are totally inconsistent with our current pictures of protein hydration which emphasize strong hydration about charges and poor hydrophobic interaction at the interface between water and non-polar side chains. They also appear inconsistent with the changes in solvation indicated by difference-spectra and proton-exchange experiments. It is thus necessary to turn to other explanations of the data. The most confusing among the observations is the small rotation change.

It is improbable that an entropy change of 400 e.u. can be explained on the basis of any change in the interaction between protein and water which leaves the conformation of the protein essentially unchanged. This being true, it seems scarcely possible that increased freedom of vicinal groups can occur without changes in a_0 no matter what the size of the coöperative unit for denaturation. It is very unsatisfying to be forced to conclude that the small rotation change is an accidental consequence of a balance of the factors influencing rotation. We may imagine that simultaneous unfolding of equal segments of left- and right-hand helix occur to explain the absence of any change in b_0. However in addition to the improbability of such an occurrence the small value of b_0 implies that native chymotrypsinogen is a protein of low helix content and is stabilized to a large extent by an amorphous folding of the peptide backbone which favors hydrophobic interactions at least as much as hydrogen-bond interactions.[35] Compensatory action seems improbable in such a case. We note also that even in 8 M urea the b_0 value is only slightly different from that of the native protein. It is thus probable that relatively small changes in helix content occur on thermal denaturation.

The absence of change in a_0 is quite another matter but it is possible that the effect on rotation of increased freedom of vicinal groups may be exactly balanced by some other effect, possibly an effect due to change in solvation state or possibly a coincidental aspect of

averaging of the residue rotations in the native protein. Such balancing conditions would appear to be accidental rather than any natural consequence of the properties of the sources of rotation themselves. Proteins such as chymotrypsin,[36] soybean inhibitor,[37] and ribonuclease[38] display significant a_0 changes on thermal denaturation though soybean inhibitor under some pH conditions becomes less levorotatory and ribonuclease more. Foss[11] appears to have found one transition on heating lysozyme which is accompanied by a change in difference spectrum but none in rotation. There is thus in these observations some support for the "accidental" hypothesis as an explanation for the lack of a_0 change in chymotrypsinogen denaturation. In any event this hypothesis is the only one reasonably consistent with our several kinds of observations which has occurred to us up to this time.

There is a further aspect of the rotation results which is puzzling. It is generally believed that the absolute magnitude of the rotation of a random polymer should decrease with increasing temperature[39] as a result of the increase in motion of vicinal groups. Such behavior is observed with most urea-denatured proteins and with some oxidized proteins thought to be in random conformations. Thermally denatured chymotrypsinogen on the other hand shows a large temperature coefficient but of opposite sign. Chymotrypsin[36] demonstrates similar behavior but has a significant change in a_0 on thermal denaturation.

The Alternative Interpretations of the Denaturation Reaction.—Since optical rotation studies show no further coöperative change on heating to 90°; since the optical rotation of the thermally denatured form is much less levorotatory than the urea-denatured species which also has a larger ultraviolet difference spectrum; and since trypsin-treated chymotrypsinogen has an even higher difference in extinction coefficients at the main peak of the difference spectrum than that of the thermally denatured protein,[40] it is probable that there is a part of the chymotrypsinogen molecule which is extremely stable and is unfolded only in high concentrations of urea or other suitable denaturants. This implies the existence of two or more coöperative structural units of different stability perhaps stabilized by different distributions of the various types of secondary forces. Foss[11] has observed that for lysozyme thermal denaturation proceeds in two distinct steps and he has postulated that one step involves the unfolding of regularly ordered regions of the molecule and the second occurs in regions of predominantly amorphous structure. Leonard and Foster[41] have observed stable intermediates in the unfolding of serum albumin. Such results are still fundamentally consistent with the "all-or-none" concept of denaturation if one accepts the possibility that local regions may have local integrity so that more than one coöperatively folded region can exist within a single molecule. This does not seem unreasonable.

Our results suggest that the thermal denaturation of chymotrypsinogen consists of a coöperative unfolding of

(35) Kraut's recent X-ray diffraction structure for chymotrypsinogen allows for the possibility of only a very small amount of helix structure. If his crystalline form is the same as that of the native protein in solution, and this is by no means certain, the possibility of small b_0 change through accidental compensation of contributions from unfolding of left- and right-hand helix segments can be discounted. The occurrence of negligible change in b_0 must then be attributed to no change in helix content. J. Kraut, *Proc. Natl. Acad. Sci. U. S.*, **48**, 1417 (1962).

(36) J. Brandts and R. Lumry, *J. Am. Chem. Soc.*, **83**, 4290 (1961).

(37) J. Brandts, unpublished observations from this Laboratory.

(38) J. G. Foss and J. A. Schellman, *J. Phys. Chem.*, **63**, 2007 (1959).

(39) W. Kauzmann and H. Eyring, *J. Chem. Phys.*, **9**, 41 (1950).

(40) B. Labouesse, communicated by G. Hess.

(41) W. J. Leonard, Jr., and J. P. Foster, *J. Biol. Chem.*, **236**, 2662 (1961).

amorphous structure of the compact native protein. All indications are that the thermally-denatured protein is freely available to solvent. The unfolding process may be extensive in the sense that many or all of the residues are involved but it appears certain that the denatured form does not have the properties of a random coil. There is at present no satisfying explanation for the small change in rotatory dispersion parameters on denaturation and the possibility seems to exist that current interpretations of such data from denaturation reactions may be in error.

Two quite different descriptions of the denaturation reaction are possible.

A. On heating some only moderately stable surface domain undergoes a coöperative general increase in freedom which reduces the interaction between non-polar groups and increases the interaction between these groups and water.[36] The melted groups are, however, held close to each other by the unchanged backbone and the remaining tertiary structure. The conformational entropy of the side chains is increased but this increase is partially offset by the usual loss in water entropy associated with the breaking of hydrophobic bonds. In addition there is a requirement for the production of single molecules of water or small aggregates broken from the general solvent to fill the irregular and frequently changing spatial requirements of the holes which now exist among side chains. In terms of model transfer reactions there is a transfer of non-polar groups from non-polar or weakly polar solvents to water and there is also a transfer of water from liquid water to non-polar solvents. The latter transfer reaction would seem to be required if the denatured protein retains a compact structure. However the transfer of one mole of water from liquid water to liquid hydrocarbons has a large free-energy increase and as a result would appear to be quite unfavorable. In the series heptane to butane the enthalpy increase is 8.5 to 11 kcal.[42] For benzene it is 7 kcal. The unitary entropy increase is in the range of 11–20 e.u. The enthalpy and entropy have the proper sign for denaturation but the net free energy change is so large and positive that the number of such transfer reactions per denatured protein molecule must be seriously limited.

B. The denaturation process of chymotrypsinogen is the same as is generally proposed for thermal denaturation. This process has not yet been established in any case. A large part of the molecule experiences a general loss of folded structure with concomitant increase in conformational entropy partially offset by the negative entropy contributions from oil-to-water transfers of the non-polar chains. This process requires a major decrease in the number of inter-peptide hydrogen bonds.

Alternative B is on the whole more appealing and it has provided a model with which a remarkably self-consistent quantitative description of the process has been made.[5] However if the viscosity data are to be interpreted as meaning that the denatured protein has undergone only a small swelling, water to oil transfers must be of some importance and it is probable that the correct description of the denaturation process will be found to contain elements of both explanations. Although

neither explanation is satisfactory, especially in regard to rotatory dispersion changes, both appear to be superior to other alternatives and both are sufficiently detailed to be susceptible to further theoretical and experimental test.

The large dependence of T_j on hydrogen-ion concentration first observed for chymotrypsinogen by Schwert and Eisenberg is common to all reversible denaturation reactions which have been studied in any detail. In chymotrypsinogen it cannot be due primarily to the increase in electrostatic energy as the system departs farther and farther from the isoelectric point. It must therefore be due to the changed free energy state of ionizable groups which either in the native or the denatured protein are buried in the restrictive internal environment of the folded protein. These groups detectable by their anomalous titration behavior probably make relatively small contributions to the total values of ΔS^0 and ΔH^0 for denaturation but their contributions are nevertheless crucial in determining the balance of entropy and enthalpy and thus the sign of the free energy of denaturation. The small contributions which these groups make to the thermodynamics of denaturation are magnified by the temperature dependence of entropy and enthalpy contributions from hydrophobic bond breaking in a manner which will be discussed in the subsequent paper.[5]

Material and Methods

Preparation of Chymotrypsinogen Solutions.—The α-chymotrypsinogen used in all the experiments was from batch 678-84A, Worthington Biochemicals Corp. (Freehold, N. J.). The purity of the preparation was checked by chromatographing a portion on a column of carboxymethyl cellulose (Carl Scheicher and Schuell Co.). Elution was accomplished by using 0.05 M citrate buffer, pH 4.3, in which the NaCl concentration was varied linearly from zero to 0.5 M. More than 99% of the material emerged as a single symmetrical peak and further purification was not attempted. The preparation showed a residual chymotrypsin activity of 0.4% when assayed using acetyl-L-tyrosine ethyl ester.

Concentrations of solutions were measured by their absorption at 282 mμ. The optical density of 1% solution at pH 2.0 was 20.3, determined from dry weights by heating the samples to 115° until constant weight was attained. In solutions containing dioxane, ethanol, or urea, a 40 l. dilution with water of pH 2 was made before reading the optical density.

The urea used was Merck reagent grade and was recrystallized once from 35% ethanol. Eastman Red Label dioxane was passed through an activated alumina column immediately before using to remove peroxides. U.S.P. 95% ethanol was used directly. All other reagents were of the best grades available and were used without further treatment.

pH Measurements.—The routine measurements of the pH of solutions were made on a Cambridge Research Model pH meter and were reproducible to 0.02 unit. In the case of mixed solvents containing ethanol or dioxane there are small errors in the readings given by the glass electrode. These amount to only 0.1 unit in 60% ethanol at pH 2.[43] In the case of dioxane solutions[44] the error is less than 0.1 when the dioxane concentration is smaller than 20% but becomes appreciably greater in higher concentrations. The readings given in the text are those indicated by the pH meter and have not been corrected.

Difference Spectra.—Ultraviolet difference spectra were measured on the Cary 11 double-beam spectrophotometer using matched 1-cm. quartz cells. For temperature studies two cells were filled with aliquots of the same solution. The temperature of the cell in the sample beam was changed by circulating water through the cell housing and temperature control was found to be better than 0.1°. The reference cell was held at room temperature.

(42) Calculated from the data of C. Block, G. Jaris, and H. S. Taylor, *J. Chem. Phys.*, **16**, 537 (1948).

(43) M. Dole, "The Glass Electrode," John Wiley and Sons, New York, N. Y., p. 142.

(44) H. Edelhoch, *J. Am. Chem. Soc.*, **80**, 6648 (1958).

Solubility.—The procedure used for solubility analysis of denatured and native chymotrypsinogen was identical in all respects with that described by Eisenberg and Schwert.[7]

Optical Rotatory Dispersion.—Optical rotation data were taken on a Rudolph Model 200 photoelectric polarimeter with the rocking prism attachment. The photomultiplier voltage of the photometer was increased to 480 volts to improve the sensitivity without loss in signal to noise ratio.

The same two-decimeter, jacketed cell, which was found to have excellent axial alignment, was used for nearly all experiments. Optically inactive glass end plates were used and the screw caps were put on very lightly to prevent the introduction of strains. In aqueous solvents the end plates were sealed onto the sample cell with a small amount of Apiezon T grease and the screw caps put on just tight enough to prevent the end plates from sliding. In this way, the cells could be made completely inactive optically and, more important, they remained inactive as the temperature of the cell was changed.

A medium-pressure mercury lamp (G.E. Uviarc, UA-3) was used as a light source and the 577.0, 546.1, 435.8 404.7, and 365.0 mμ emission bands were sorted out with a dispersion monochromator. The wave lengths of the transmitted light were checked by measuring the optical rotation of a standard quartz plate at the peak of the transmission bands in question. The transmitted light was found to be accurate (when compared to the literature values for the emission lines of low pressure mercury lamps) and reproducible to 0.05 mμ when the slit width of the monochromator was below 0.04 mm., the maximum value used for nearly all readings.

Adequate temperature control, better than 0.1° at temperatures below 60°, was obtained by circulating water from a constant temperature bath through the jacket of the sample cell and through the cell housing.

Under the conditions employed (symmetrical angle of 0.75°) the average standard deviation in a set of readings was slightly less than 0.001° of absolute rotation. Each data point represents two to six independent readings, depending on the precision. In solutions containing large amounts of dioxane there was a noticeable amount of light scattering and the symmetrical angle and the slit width had to be increased, introducing slightly larger errors in both the measured rotations and the reported wave lengths.

Viscosity.—Modified Ostwald viscometers were used for the measurements of reduced viscosity. These viscometers had flow times of 15 min. at room temperature. To minimize any irreversible aggregation protein concentrations less than 0.4% were used in viscosity studies, as in all other studies. Both the protein solutions and solvents were filtered through a fine sintered glass funnel by applying positive pressure before they were introduced into the viscometers.

For temperature studies two similar viscometers were used, one filled with solvent and the other with solution. The viscometers were immersed in a constant temperature bath, controlled by a thermoregulator to ±0.01. Flow-time ratios were determined at several temperatures and found to have a constant value R. The reduced viscosity could then be calculated at each temperature by the equation $(\eta - \eta_0)/c = (Rt^1 - t_0^2) \cdot \rho/t_0^2 c\rho_0$ where t^1 is the flow time of solution in viscometer 1, t_0^2 the flow time of solvent in viscometer 2 at the same temperature, and R is the flow time ratio t^2/t^1 for the same solvent at the same temperature. The concentration in g./100 ml. is c and ρ is the solution density.

Refractive Increments.—The Rayleigh interference optics on a Spinco Model H electrophoresis and diffusion apparatus were used in the determination of refractive increments of chymotrypsinogen solutions. A medium pressure mercury lamp (G.E. AH-4) was the light source and the 546 mμ band was sorted out with an absorption filter.

The number of fringes intercepted by a line extending parallel to the fringes from the solvent side of the cell to the solution side, ΔJ, was counted by using a traveling microscope. The largest errors (0.1 fringe) were encountered at higher temperatures where the fringes were not perfectly straight but showed a waviness due to small temperature variations in the cell and to pronounced mirror imperfection. The refractive increment, $\Delta n/c$, was calculated from the number of intercepted fringes by the relation $\Delta n/x = \Delta J\lambda/L$, where λ is the wave length, L the length of solution the light passes through, and c is the protein concentration in g./100 ml.

The use of expensive Tiselius cells at temperatures above 50° is not recommended. It was found that cracks may develop at the base of the center section where it is fused to the ground glass plate.

VACUUM ULTRAVIOLET PHOTOCHEMISTRY. VI. PHOTOLYSIS OF CYCLOPROPANE WITH THE XENON RESONANCE LINES

By C. L. CURRIE, S.J., H. OKABE,[1] AND J. R. MCNESBY[1]

National Bureau of Standards, Washington 25, D. C.

The photolysis of cyclopropane has been carried out at 1470 Å. at room temperature. The relative yields of products as well as isotopic analyses of hydrogen, methane, and ethylene resulting from the photolysis of equimolar mixtures of cyclopropane and cyclopropane-d_6 indicate the following primary processes in order of decreasing importance: c-$C_3H_6 \rightarrow CH_2 + C_2H_4$; c-$C_3H_6 \rightarrow H_2 + C_3H_4$; c-$C_3H_6 \rightarrow H + C_3H_5$. Atomic hydrogen probably forms molecular hydrogen by wall recombination. It is suggested that methane and ethane are formed from the methyl radical produced in the reaction: $CH_2 + c$-$C_3H_6 \rightarrow c$-$C_3H_5CH_3^* \rightarrow CH_3 + C_3H_5$. The mechanisms of formation of other products are discussed briefly.

Introduction

In recent years, experimental studies have been carried out on photolyses of some typical alkanes[2-4] and alkenes[2,3] with some very surprising results concerning the nature of the primary processes. A third class of hydrocarbon molecules, the cycloalkanes, has not hitherto been subjected to a direct photochemical investigation. The mercury ($^3P_1$) sensitized reaction

of cyclopropane has been investigated recently.[5] It was concluded that the main primary process at room temperature is the formation of an excited triplet state rather than C–H bond rupture.

The photolysis of the simplest cycloalkane, cyclopropane, has been studied at 1470 Å. in the present work. There are three regions of continuous absorption in the spectrum of cyclopropane[6] with maxima at 1202, 1449, and 1594 Å. The pyrolysis of cyclopropane

(1) Authors to whom requests for reprints should be directed.
(2) (a) H. Okabe and J. R. McNesby, *J. Chem. Phys.*, **34**, 668 (1961); (b) *ibid.*, **36**, 601 (1962).
(3) M. C. Sauer, Jr., and L. M. Dorfman, *ibid.*, **35**, 497 (1961).
(4) H. Okabe and J. R. McNesby, *ibid.*, **37**, 1340 (1962).

(5) D. W. Setser, B. S. Rabinovitch, and E. G. Spittler, *ibid.*, **35**, 1840 (1961).
(6) P. Wagner and A. B. F. Duncan, *ibid.*, **21**, 516 (1953).

has been studied extensively[7] and is certainly the simplest organic reaction known, the only product being propylene.

It is to be expected that the direct photolysis will be quite different from the mercury-sensitized photolysis because of the large difference in energies imparted to the cyclopropane molecule. The large number of reaction products signifies the complexity of the reaction and no attempt has been made to understand all reaction processes. In the present work, isotopic analyses of some important products, hydrogen, methane, and ethylene, were made in an effort to understand the major chemical events in the cyclopropane photolysis.

Experimental

The light source was a conventional xenon resonance lamp[2] with tantalum electrodes. The reaction vessel, 230 cc. in volume, was isolated from the lamp by a lithium fluoride window. The absorption coefficient of cyclopropane was measured either with a McPherson 50 cm. monochromator in conjunction with a sodium salicylate coated photomultiplier or by measuring the photoionization current of triethylamine between two tungsten electrodes placed behind the reaction vessel. In the latter case, a potential of 70 volts (d.c.) was applied between two electrodes and the current arising from the photoionization of 300 μ of triethylamine (i.p. 7.5 e.v.) was measured by a Kiethley 610 electrometer.

The absorption coefficient, k, of cyclopropane, defined as $I = I_0 e^{-kpl}$, where p is the pressure in atmospheres at 25°, and l, the path length in cm., is 260 ± 15 at 1470 Å. The absorption coefficients measured by the latter photoionization technique are $k_\Delta = 254 \pm 30$ and $k_{\Delta-d_6} = 206 \pm 20$, in good agreement with the coefficient measured with a monochromator. In agreement with other saturated hydrocarbons deuterated cyclopropane has a smaller absorption coefficient.

Analyses were carried out by means of gas chromatography, using two Perkin–Elmer D (tetraisobutylene) columns in series at room temperature or a single J (silica gel) column at 92°. All products through C_4 were identified by the use of standard samples of known pure compounds. When ambiguous, this identification was confirmed by trapping the effluent fraction and submitting the sample to mass spectrometric analysis. Estimates of the relative amounts of C_2 through C_4 products were made by comparing the chromatogram of a synthetic mixture with that of the reaction mixture. The non-condensable methane/hydrogen product ratio was measured on a mass spectrometer and their total absolute amount was obtained with a McLeod gage.

In experiments with isotopic mixtures, the isotopic composition of the products hydrogen, methane, and ethylene was determined by mass spectrometry. In order to minimize secondary reactions, conversions were kept below one per cent.

Purification of Cyclopropane.—Cylinder cyclopropane and cyclopropane-d_6 were purified by means of gas chromatography, using a silica gel column. The resulting cyclopropane contained less than 0.02% propylene as the only impurity, and the cyclopropane-d_6 contained less than 0.05% ethylene as the only detectable impurity. The light and heavy materials were distilled through Ascarite and P_2O_5 and stored separately behind metal valves. Repeated mass spectrometric analysis before and after purification and storage showed that some exchange took place when a mixture of the light and heavy cyclopropane was purified together, the silica gel presumably catalyzing the process. Mass spectrometric analysis showed that cyclopropane-d_6 contained 10.4% C_3D_5H. In the analysis of the C_4 fraction, n-butane and $trans$-butene-2 as well as butene-1 and isobutane were indistinguishable and are reported together. Also the C_3 fraction contained a single peak corresponding to C_3H_8 and $CH_3C\equiv CH$ and these are reported together. A few analyses using a silica gel chromatographic column suggests that the latter peak consists roughly of equal amounts of C_3H_8 and $CH_3C\equiv CH$.

(7) A. F. Trotman-Dickenson, "Gas Kinetics," Butterworths, London, 1955 p. 65.

Results and Discussion

A. The Photolysis Products.—The products of the photolysis of cyclopropane at 1470 Å. were found to be methane, hydrogen, acetylene, ethylene, ethane, propylene, propane, propyne, allene, isobutane, $trans$-butene-2, and/or n-butane, methylcyclopropane, cis-butene-2. A complete product analysis is shown in Table I.

TABLE I
PRODUCTS OF THE PHOTOLYSIS OF CYCLOPROPANE AT THE XENON RESONANCE LINES

Time of photolysis, min.	30	30	30	30
Cyclopropane pressure (mm.)	20	7	4.8	4.8
H_2	15[a]	19.2[a]	...	...
CH_4	4.6[a]	5.3[a]	...	...
C_2H_2	14	11	14	19
C_2H_4	100	100	100	100
C_2H_6	20	15	19	14
$CH_3CH=CH_2$	11	11	7	12
$C_3H_8 + CH_3—C\equiv CH$	21	20	13	14
$CH_2=C=CH_2$	31	31	...	19
Butene-1 + isobutene	17	15	19	10
$trans$-Butene-2 + n-butane	3.9	...	...	3
Methylcyclopropane	8.4	...	6	7
cis-Butene-2	14.8	...	8	5
Isobutane	Trace	...	...	...

^{a} Determined in a separate experiment from the $H_2:CH_4:C_2H_4$ composition. Relative amounts of products normalized to ethylene = 100.

It is difficult to attach quantitative significance to the results in Table I since their precisions were severely limited by the analytical method and low conversions. The relative amounts were reliable to only about ±20%.

B. Mechanism of Ethylene Formation.—The following processes (1 and 2) may be postulated for the formation of ethylene

$$c\text{-}C_3H_6 \xrightarrow{h\nu} CH_2 + C_2H_4 \qquad (1)$$

$$CH_2 + c\text{-}C_3H_6 \longrightarrow C_4H_8^* \longrightarrow 2C_2H_4 \qquad (2)$$
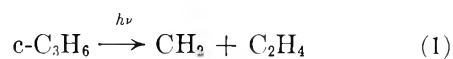
In order to test whether process 2 can be of any importance, an equimolar mixture of c-C_3H_6 + c-C_3D_6 was photolyzed, and the result is given in Table II. If step 2 takes place to an appreciable extent, it is expected that $C_2H_2D_2$ would be found in the product along with C_2H_4 and C_2D_4. The result clearly shows that this is not the case. The presence of only minor amounts of C_2H_3D and C_2D_3H also excludes the possibility that ethylene is formed from the disproportionation of the C_2H_3 radical.

$$2C_2H_3 \longrightarrow C_2H_4 + C_2H_2 \qquad (3)$$

It is concluded that step 1 is the major source of ethylene. The ratio, $\Phi C_2H_4/\Phi C_2D_4 = 1.2$, agrees well with the difference of the absorption coefficient of cyclopropane, $k_\Delta/k_{\Delta-d_6} = 1.2$. The non-radical formation of ethylene was also observed in the radiolysis of cyclopropane[8] and was attributed to an ion–molecule reaction of the hydrogen atom transfer type

$$c\text{-}C_3H_6^+ + c\text{-}C_3H_6 \longrightarrow c\text{-}C_3H_7^+ + c\text{-}C_3H_5 \quad (4)$$
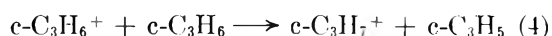
(8) K. Yang, J. Phys. Chem., 65, 42 (1961).

Table II

Photolysis of a Mixture of Cyclopropane and Cyclopropane-d_6 at the Xenon Resonance Lines: Isotopic Analysis of Products

Cyclopropane (mm.)		Hydrogen (%)			Methane (%)					Ethylene (%)				
Δ	Δ-d_6	H₂	HD	D₂	CH₄	CH₃D	CH₂D₂	CD₃H	CD₄	C₂H₄	C₂H₃D	C₂H₂D₂	C₂D₃H	C₂D₄
0	5.0	7.1	7.9	85.0	...	...	...	13.0	87.0	...	...	...	...	...
0	6.0	7.5	6.6	85.9	...	...	...	13.0	87.0	...	...	2.0	10.3	87.7
3.0	3.0	53.2	20.5	26.3	30.7	15.8	15.8	20.4	17.3	48.9	3.3	5.6	5.1	37.1
3.0[a]	3.0	53.2	19.4	27.4	31.6	16.2	16.2	18.2	17.8	51.5	3.5	5.3	0.7	39.0
11.0[a]	9.9	48.4	20.5	31.1	29.0	15.7	16.0	20.4	18.9	45.5	5.6	1.1	0.3	47.5
11.0[a]	9.9	48.5	19.2	32.3	28.0	16.0	18.0	19.5	18.5	47.5	7.7	2.8	0.6	41.4
10.0[a]	10.0	55.4	20.2	24.4	31.6	13.1	19.7	18.1	17.5	...	...	...	...	...

[a] Corrected for hydrogen, methane, and ethylene from Δ-d_6.

Table III

Photolysis of Cyclopropane in the Presence of C₂D₆ and C₂D₄ at Xenon Resonance Lines: Isotopic Analysis of Hydrogen and Methane

	Hydrogen (%)			Methane (%)				
	H₂	HD	D₂	CH₄	CH₃D	CH₂D₂	CD₃H	CD₄
20 mm. Δ + 20 mm. C₂D₆	26.4	3.8	69.7	48	14	6	14	18
7 mm. Δ + 0.54 mm. C₂D₄	86.0	3.9	10.0	81.5	10	3.8	2.5	2.0
9.9 mm. Δ + 9.9 mm. C₂D₄	14.4	2.7	82.9	...	...	...	...	...

$$c\text{-}C_3H_7{}^+ \longrightarrow CH_3{}^+ + C_2H_4 \qquad (5)$$
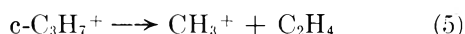
However, a mechanism involving a decomposition of a neutral excited molecule into CH_2 and ethylene is equally probable.

C. Mechanism of Hydrogen and Methane Formation.

—The isotopic composition of hydrogen in the mixture of cyclopropane and cyclopropane-d_6 (Table II) shows a substantial amount of HD (20%). The ratio $(HD)^2/(H_2)(D_2)$ of 0.28, however, is considerably smaller than the equilibrium ratio of about 4 derived from an entirely atomic, recombination mechanism. A large H_2 production in the presence of 7.7% C_2D_4 (Table III) signifies the importance of a molecular process. Thus, although the main process is the formation of molecular hydrogen, the atomic process (reaction

$$c\text{-}C_3H_6 \longrightarrow H + C_3H_5 \qquad (6)$$
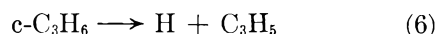
6) contributes to the formation of hydrogen. The presence of 20% HD in the hydrogen fraction in the c-C_3H_6 + c-C_3D_6 photolysis proves that H and D atoms are formed to a significant extent. Of considerable importance is the question of how the H and D atoms eventually form molecular hydrogen. It is generally believed that abstraction reactions are responsible ultimately for hydrogen production.

$$D + c\text{-}C_3H_6 \longrightarrow HD + C_3H_5 \qquad (7)$$

$$D + c\text{-}C_3H_6 \longrightarrow D_2 + C_3D_5 \qquad (8)$$

$$H + c\text{-}C_3H_6 \longrightarrow H_2 + C_3H_5 \qquad (9)$$

$$H + c\text{-}C_3H_6 \longrightarrow HD + C_3D_5 \qquad (10)$$
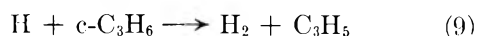
These reactions must compete with the self-scavenging reaction which, in the present case, is mainly reaction 11 and the corresponding reactions of the various isotopic species.

$$H + C_2H_4 \longrightarrow C_2H_5 \qquad (11)$$
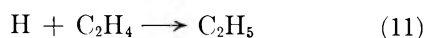
Back[9] has recently obtained the ratio $k_{11}/k_{12} = 25,000$ at room temperature

$$H + C_2H_6 \longrightarrow H_2 + C_2H_5 \qquad (12)$$
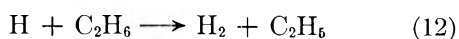
(9) R. A. Back, *Can. J. Chem.*, **37**, 1834 (1959).

Now, it is known[10] that $k_9/k_{12} < 1$ and it follows that $k_{11}/k_9 > 25,000$. Referring to Table I in which reactions proceeded to about 0.5% conversion, the average ratio $[C_2H_4]/[c\text{-}C_3H_6] \sim 0.001$ during reaction can be estimated. The ratio of the rate of the scavenging reaction, R_s, to that of the abstraction, R_a, is given approximately by $R_s/R_a \approx (k_{11}/k_9)([C_2H_4])/([c\text{-}C_3H_6])$

$$R_s/R_a > 25 \qquad (13)$$

On this basis, nearly all H and D atoms should have been self-scavenged and no HD should have been observed in the photolysis of c-C_3H_6 + c-C_3D_6.

In order to explain the appearance of large amounts of HD in the photolysis of this mixture, it seems necessary to invoke a mode of hydrogen production by an atomic mechanism which is faster than the abstraction mechanism. The most probable alternatives seem to be a wall recombination of H atoms or abstraction by hot H atoms. Since absorption is very strong in the vacuum ultraviolet photolysis of hydrocarbons, the reaction volume in which H atoms are present is very small; the self-scavenger diffuses out of this reaction zone thereby becoming unavailable to the H atoms. Thus, the physical situation is favorable for the wall recombination of H atoms.

The values of 13,000[11] and 40,000[12] for the ratio k_{11}/k_{12} were obtained independently and support this postulate. Bradley, Melville, and Robb[13] obtained 2100 for the same ratio but this value appears to be an order of magnitude too low.

The isotopic composition of methane in Table II shows that the ratios $CH_4:CH_3D:CH_2D_2:CD_3H:CD_4$ are approximately 2:1:1.2:1.3:1.2. This indicates that there is little possibility that methane is formed primarily (1) from a molecular detachment process or (2) from the abstraction of hydrogen by methyl radicals or the combination of atomic hydrogen and methyl radical, since process 1 should give CH_4

(10) Reference 7, p. 177.

(11) K. R. Jennings and R. J. Cvetanovic, *J. Chem. Phys.*, **35**, 1233 (1961); B. deB. Darwent and R. Roberts, *Discussions Faraday Soc.*, **14**, 55 (1953).

(12) K. Yang and P. L. Gant, *J. Phys. Chem.*, **65**, 1861 (1961).

(13) J. N. Bradley, H. W. Melville, and J. C. Robb, *Proc. Roy. Soc.* (London), **A236**, 454 (1956).

and CD_4 predominantly and process 2 should give CH_4, CH_3D, CD_3H, and CD_4 but not CH_2D_2. It is proposed that the mechanism of methane formation involves reaction 14

$$CH_2 + c\text{-}C_3H_6 \longrightarrow c\text{-}C_3H_5CH_3{}^* \longrightarrow$$
$$CH_3 + C_3H_5 \quad (14)$$
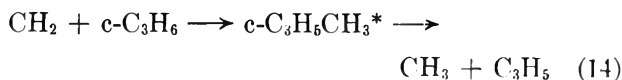
This reaction is analogous to the process[14]

$$CH_2 + CH_4 \longrightarrow C_2H_6{}^* \longrightarrow 2CH_3 \quad (15)$$
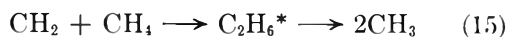
The methane is formed either from the methyl radical abstraction of hydrogen or combination of a hydrogen atom with a methyl radical.

D. Higher Hydrocarbons.—Because of the complexity of the nature of the higher hydrocarbon prod-

(14) J. A. Bell and G. B. Kistiakowsky, *J. Am. Chem. Soc.*, **84**, 3417 (1962).

ucts, the mechanism suggested for their formation are somewhat speculative. (1) Ethane is formed probably by recombination of CH_3 radicals produced in the consecutive reactions 1 and 6. (2) Propylene may be formed in a primary process or by association of H with C_3H_5 radicals formed in reactions 6 and 14. (3) Propane and *n*-butane may be formed by association of CH_3 and C_2H_5, respectively, with C_2H_5 being formed by secondary reaction of H with C_2H_4. (4) Allene and propyne are formed by the primary process

$$c\text{-}C_3H_6 \xrightarrow{h\nu} C_3H_4 + H_2 \quad (16)$$
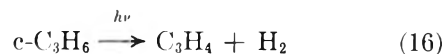
(5) The butenes and methylcyclopropanes are formed by isomerization and collisional stabilizations, respectively, of the excited methylcyclopropane formed in reaction 14.[15]

(15) J. N. Butler and G. B. Kistiakowsky, *ibid.*, **82**, 759 (1960).

THE INFLUENCE OF INCORPORATED RADIOACTIVITY AND EXTERNAL RADIATION ON THE DEHYDRATION OF CYCLOHEXANOL OVER SULFATE CATALYSTS[1]

By N. A. Krohn and Hilton A. Smith

Department of Chemistry, University of Tennessee, Knoxville, Tennessee, and Oak Ridge National Laboratory, Oak Ridge, Tennessee[2]

The vapor phase dehydration of cyclohexanol on magnesium sulfate and magnesium sulfate–sodium sulfate catalysts was studied. The effects of the incorporation of radioactive sulfur into the sulfate radical, of X-irradiation of the catalyst while in use, and of preirradiation with Co^{60} γ-rays were investigated. When compared on a unit surface area basis, the radioactive catalysts were found to be less active than non-radioactive catalysts of similar composition. This effect persisted even after the radioactivity had substantially decayed. Neither preirradiation with Co^{60} γ-rays nor X-irradiation of the catalyst while in use had any effect. It is concluded that the reported enhancements of catalytic activity upon the incorporation of S^{35} are erroneous and that the emission of β-particles from the catalyst during its use is of no consequence. The reports of enhanced catalytic activity may be attributed to the fact that for a given set of preparative conditions the radioactive catalysts had larger surface areas than their non-radioactive counterparts and that apparently this had not been considered.

Introduction

The study of the effects of radiation on solid catalysts is a relatively new but growing field. Recent reviews have been written by Turkevich,[3] Haissinsky,[4] and Taylor.[5,6] Bombardment of catalysts by γ-rays, X-rays, neutrons, protons, electrons, α particles, and argon ions has shown beyond doubt that ionization and displacement effects caused by radiations can affect the catalytic activity of solids, sometimes favorably and sometimes adversely. In most studies, the catalysts were irradiated before use. In a few cases, radiation was externally supplied while the reaction took place.

Balandin, Spitsyn, and co-workers in a novel approach have investigated the effects of incorporating radioisotopes directly into solids. One of the systems

studied was the vapor phase dehydration of cyclohexanol over magnesium sulfate–sodium sulfate catalysts that contained various amounts of sulfur-35.[7] Their results indicated that radiosulfur enhanced the catalytic activity, the percentage increase being proportional to the logarithm of the specific radioactivity of the catalyst, and reaching 171% of the activity of non-radioactive catalyst when the concentration of S^{35} was 105.2 mc. S^{35}/g. The apparent activation energies were found to be 1–2 kcal./mole lower on the radioactive catalysts.

In later studies on the dehydration of *n*-dodecyl alcohol of $MgSO_4$ catalysts, the presence of sulfur-35 was found to decrease the catalytic activity.[8] In this same paper, data were reported on the dehydration of cyclohexanol over $MgSO_4$ which showed the radioactive catalyst to be more active at temperatures above ~330°, but less active at lower temperatures, with the reaction having a much higher apparent activation energy on the radioactive catalyst. In both cases,

(1) This paper is based on a thesis presented to the University of Tennessee by N. A. Krohn in partial fulfillment of the requirements for the Ph.D. degree, June, 1962. The work was carried out at Oak Ridge National Laboratory.

(2) Operated by Union Carbide Nuclear Company for the U. S. Atomic Energy Commission.

(3) J. Turkevich, *Proc. U. N. Conf. Peaceful Uses At. Energy, 2nd, Geneva, 1958*, **29**, 375 (1959).

(4) M. Haissinsky, *Actes congr. intern. catalyse, 2e, Paris, 1960*, **2**, 1429 (1961).

(5) E. H. Taylor, *J. Chem. Educ.*, **36**, 396 (1959).

(6) E. H. Taylor, *Nucleonics*, **20**, No. 1, 53 (1962).

(7) A. A. Balandin, V. I. Spitsyn, N. P. Dobrosel'skaya, I. E. Mikhailenko, I. V. Vereschinskii, and P. Ya. Glazunov, *Actes congr. intern. catalyse, 2e, Paris, 1960*, **2**, 1415 (1961).

(8) V. I. Spitsyn, I. E. Mikhailenko, and G. N. Pirogova, *Dokl. Akad. Nauk SSSR*, **140**, 1090 (1961).

however, the apparent activation energies were lower then previously reported for magnesium sulfate.

In view of these conflicting results, a program was undertaken to study these phenomena more extensively.

Experimental

Cyclohexanol.—Eastman Kodak cyclohexanol was redistilled through a 1 m. vacuum-jacketed column packed with glass helices. The purified product had the following properties: b.p. 161° (760 mm.); m.p. 25.1°; n^{30}D 1.46286.

Catalysts.—The catalysts were prepared by evaporating to dryness mixtures of stock solutions of C.P. $MgSO_4$ and Na_2SO_4. The resultant cake was ground and sieved. The 30–40 mesh particles obtained were further dried in air and *in vacuo* at 400 to 500° prior to use. Bulk densities varied from 0.48 to 0.85 g./ml., depending primarily on batch size.

Radioactivity was added as $MgS^{35}O_4$ obtained by neutralizing $H_2S^{35}O_4$ with MgO. The HCl present with the $H_2S^{35}O_4$ (as obtained from the Oak Ridge National Laboratory Isotopes Division) was removed by evaporating to fuming three times with 0.5 ml. of concentrated H_2SO_4. This procedure was also followed in preparing non-radioactive catalysts in several cases.

In order to make valid comparisons of the catalytic activity of radioactive and non-radioactive catalysts, the surface areas were measured by the B.E.T. method with nitrogen and krypton as adsorbates. The Russian workers did not report surface areas and apparently assumed that similar preparation procedures would produce catalysts of similar specific surface areas. Our results indicate that this is not the case, and that in general, radioactive catalysts prepared side by side with non-radioactive ones have larger specific surfaces, as shown in Table I. It was also found that exposure to moist air must be completely avoided in order to get reproducible surface area measurements on anhydrous $MgSO_4$.

Table I

SURFACE AREAS OF RADIOACTIVE AND NON-RADIOACTIVE CATALYSTS AFTER SIMILAR DRYING TREATMENTS

Catalyst composition	Heat treatment Temp., °C.	Time, hr.	Specific radio-activity, mc./g.	Surface area by N_2 adsorption, m²./g.	X-Ray crystallite size, Å.
$MgSO_4$	500	20	0	4.6	656
			48.0	7.0	508
$MgSO_4 \sim 1\%$ Na	400	16	0	6.0	...
			45.8	13.1	...
$MgSO_4 \sim 1.4\%$ Na	450	16	0	1.8	...
			7.5	9.0	...
$MgSO_4 \sim 1.6\%$ Na	410	16	0	2.2	...
			40.5	3.2	...
$MgSO_4 \sim 2.5\%$ Na	425	4	0	3.3	722
			10.3	4.2	454

Apparatus.—The kinetic measurements were made in an inclined tube flow system heated in a tube furnace. The cyclohexanol was metered in as liquid at 0.314 ml./min. from a syringe operated through a gear train by a 1-r.p.m. Bodine motor. The reaction tubes were made of 8–10-mm. Pyrex glass tubing about 60 cm. long with 50–150 mg. of 30–40 mesh catalyst supported in the middle between two glass wool plugs.

The lower plug was supported on indentations in the tube wall and after insertion was tamped down to give a flat upper surface. The catalyst was then loaded into the tube which was then lightly tapped to settle the catalyst bed. The second glass wool plug was then inserted and gently tamped so that the catalyst bed was held firmly in place. The good reproducibility between data taken on several catalyst beds of several sizes indicated that uniform packing of the catalyst beds was achieved by this technique. The upper half of the tube was filled with glass beads to act as an evaporator for the cyclohexanol. At the outlet the products and unreacted alcohol were condensed and collected in a graduated receiver. Temperature was controlled to ±1° by adjusting the voltage supplied to the tube furnace.

Procedure.—The catalysts lose activity with time in use. Therefore, after determining their initial activity as a function of

temperature, they were aged to steady state conditions by 7 to 12 hr. of reaction time at the highest temperature at which they were subsequently to be used. After this treatment, the temperature dependence of the catalyzed reaction rate was again determined. The extent of reaction was determined by measuring the bromine number of samples collected while the reaction tube was maintained at constant temperature. No measurable dehydration took place in the absence of catalyst. No products other than cyclohexene and water were detected by vapor-phase chromatography or by infrared analysis regardless of the catalyst composition or the presence of radioactivity. Under the experimental conditions used, the extent of reaction rarely exceeded 10%, so the per cent reacted could be plotted against the reciprocal of absolute temperature to obtain apparent activation energies. In preliminary experiments the effect of changing the space velocity was studied by varying the feed rate from 0.125 to 0.314 ml./min. at constant bed size and by varying the bed size from 50 to 150 mg. at constant feed rate. It was found that the fraction of alcohol dehydrated varied inversely with the space velocity indicating that the measurements were not diffusion or equilibrium limited. It was also shown that contamination of the hygroscopic cyclohexanol with as much as 10 mole % of water had no effect other than as a feed diluent.

Results

Initial Rate Studies.—The variations found between the measured surface areas of radioactive and non-radioactive catalysts, even when prepared in the same manner, made it plain that obtaining radioactive and non-radioactive catalysts of the same surface areas and with the same preparation histories for comparison purposes was not practicable. Therefore, a series of experiments was made on non-radioactive magnesium sulfate and magnesium sulfate–sodium sulfate catalysts to determine the effect of variations in the specific surface area and in the preparation procedure on the catalytic activity in the dehydration of cyclohexanol.

One large batch of non-radioactive magnesium sulfate catalyst prepared from the C.P. salt and one large batch prepared by the reaction of magnesium oxide with sulfuric acid were split into several portions and each portion given a different heat treatment. Two other batches, smaller in size in order to duplicate more closely the radioactive preparation procedures, were prepared from C.P. magnesium sulfate. These were not divided and only a single heat treatment was given in each case. Catalyst properties are given in Table II.

The initial catalytic activity for the dehydration of cyclohexanol was determined for each of the catalyst preparations as a function of temperature. The results are shown by the upper line in Fig. 1. All of the experimentally observed numbers were normalized to one square meter of catalyst surface as measured by the B.E.T. method with nitrogen gas as the adsorbate. Actual conversions ranged from 0.6 to 28.8%. For simplification a single line was drawn through all the points from all of the runs to show the over-all behavior. The apparent activation energy is 24.6 ± 0.6 kcal./mole.

When normalized to unit surface area, the catalytic activity of non-radioactive magnesium sulfate was constant to within ±25% regardless of variations in the specific surface area or the method of preparation used.

For comparison, three radioactive magnesium sulfate catalysts were prepared and their initial catalytic activities determined as a function of temperature. When the per cent of cyclohexanol reacted was normalized to one square meter of catalyst surface, as shown in the lower curve of Fig. 1, good agreement was again obtained among the radioactive catalysts, but

TABLE II

PROPERTIES OF CATALYST PREPARATIONS

Surface area,[f] m²/g.

Catalyst	Initial (N₂)	(Kr)	After use (Kr)	S³⁵ activity, mc./g.	Wt. % Na	Bulk density,[f] g./ml.
MRA[a]	12.2			0	0	0.83
MRB[a]	15.2			0	0	.78
MRC[a]	7.7			0	0	.76
MRD[a]	3.6	2.7	2.4	0	0	.85
MRF[a]	7.0	5.5	4.9	0	0	
MOA[b]	10.3			0	0	.72
MOB[b]	8.7			0	0	.76
MOC[b]	2.5			0	0	.73
MOF[b]	4.9			0	0	
IAB[c]	4.5	3.3	3.0	0	0	.48
IAR[c]	8.8			0	0	.49
AA[c]	7.4	5.2	5.0	45.5	0	.48
AB[c]	5.8	4.4		35.6	0	.57
AC[c]	3.3		2.1	32.2	0	.46
MSB[d]	5.7	4.1	2.7	0	1.63	.78
MSC[d]	1.5	1.1		0	1.63	.78
ISA[c]	6.2	4.4	3.9	0	0.98	.57
ISB[c]	3.3	2.2	2.2	0	2.43	.71
IS-2A[c]	3.0			0	1.60	
ASA[c]	5.0	3.9	3.8	10.3	0.93	.55
ASB[c]		2.2	2.0	11.3	2.54	

[a] C.P. MgSO₄ solutions dried under various conditions. [b] MgSO₄ from reaction of MgO with H₂SO₄ dried under various conditions. [c] C.P. MgSO₄ plus indicated Na₂SO₄ and MgS³⁵O₄ mixed in solutions and dried in small batches. [d] Solution of C.P. MgSO₄ and Na₂SO₄ dried under various conditions. [e] Using 16.2 Å.² and 19.5 Å.² for the areas of N₂ and Kr, respectively [f] Measured on 30–40 mesh particles.

Fig. 1.—The temperature dependence of the rate of dehydration of cyclohexanol on fresh magnesium sulfate catalysts.

Fig. 2.—The temperature dependence of the rate of dehydration of cyclohexanol on fresh magnesium sulfate–sodium sulfate catalysts.

they were less than half as active catalytically as the non-radioactive preparations. The specific surface areas varied from 3.3 to 7.4 m.²/g. as measured by the B.E.T. method using nitrogen as the adsorbate, and the sulfur-35 content varied from 32.2 to 45.5 mc./g. at the time of the kinetic measurements. The value of the apparent activation energy from a least squares fit of all of the points was 24.5 ± 1.0 kcal./mole, in good agreement with the values observed for the non-radioactive catalyst.

Similar experiments with sodium sulfate containing catalysts again showed the radioactive materials to be poorer catalysts than the non-radioactive, but in this case an increase in the apparent activation energy was also observed, as shown in Fig. 2. The initial catalytic activity per unit surface was constant within ±30% despite variations in the amount of sodium present, but was somewhat lower than that for pure magnesium sulfate. The large decrease in catalytic activity upon the addition of similar amounts of sodium sulfate reported in the literature apparently was not corrected for differences in specific surface area.[7] Since the presence of sodium sulfate enhances the sintering of magnesium sulfate considerably, catalytic activity compared on a weight basis shows a large effect, its magnitude depending on the time and temperature of drying of the catalysts.

Aging Studies.—The aging of the catalysts under reaction conditions is a complex phenomenon. Typical aging curves are given in Fig. 3. The dashed portions of the curves indicate the time that elapsed during the initial rate measurements as a function of temperature. The second point on each curve represents the activity of the catalyst upon reheating to 402 to 404°.
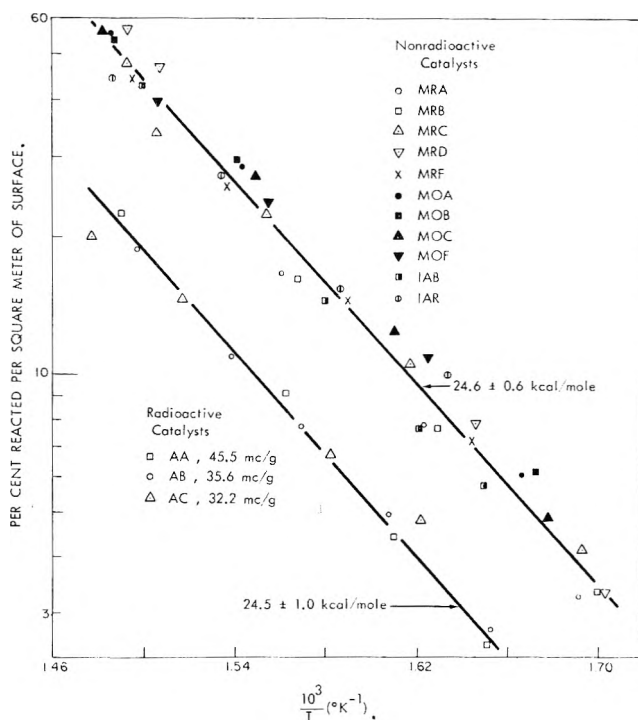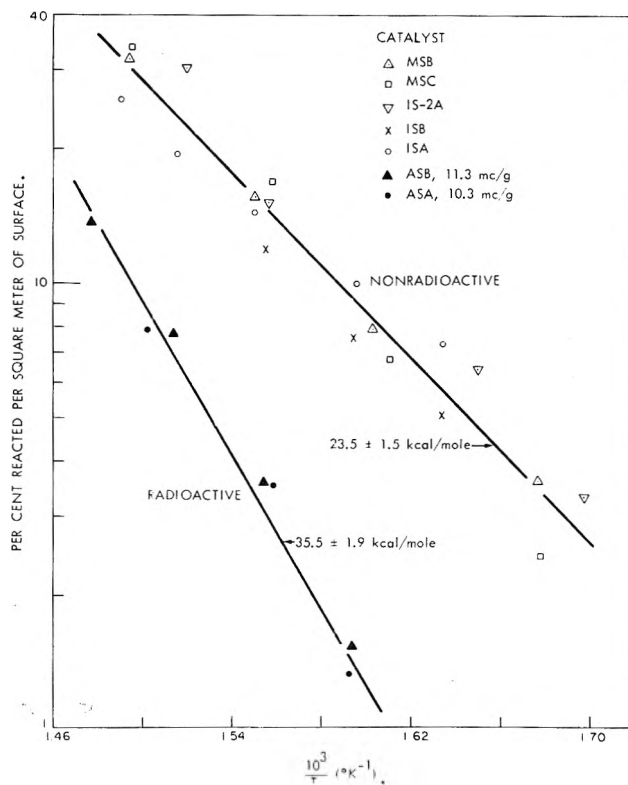
The break in the curve of catalytic activity vs. time is difficult to explain. It is not purely a temperature–time phenomena, but occurs only on use. Balandin reported similar behavior at 270 to 330° on 30-ml. beds of magnesium sulfate after periods of time in use of 70 to 90 hr. and attributed the effect to progressive hydration of the surface.[9] At the temperature of aging

(9) A. A. Balandin, M. B. Turova-Polak, A. E. Agronomev, I. M. Khorlina, and L. S. Konkova, Dokl. Akad. Nauk SSSR, 114, 773 (1957).
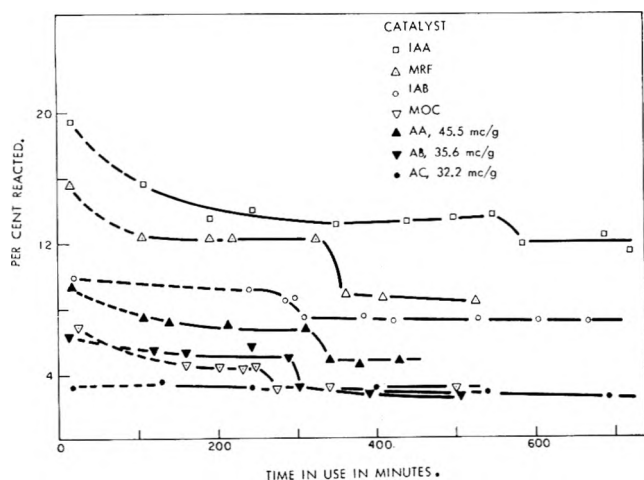
Fig. 3.—The aging of magnesium sulfate catalysts; 50 mg. of catalyst, 402–404°: open symbols, non-radioactive; filled symbols, radioactive catalysts.
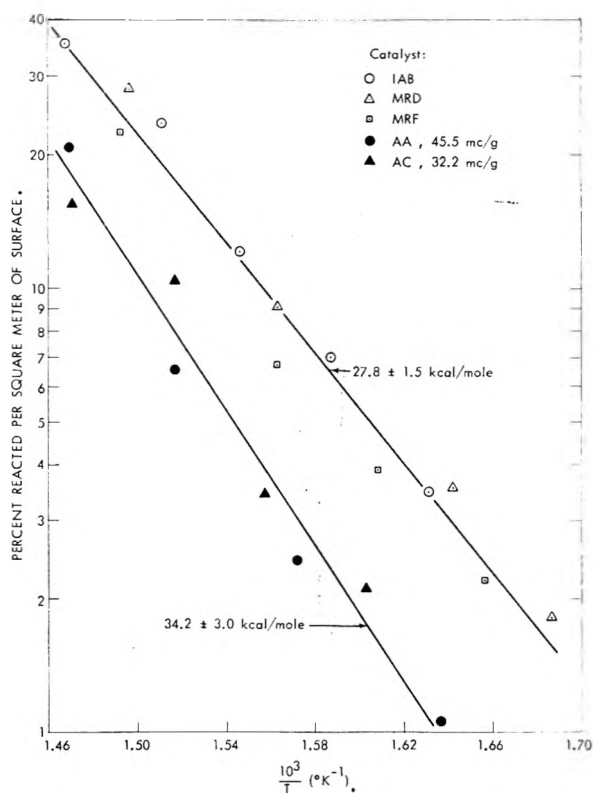
Fig. 4.—The temperature dependence of the rate of dehydration of cyclohexanol on aged magnesium sulfate catalysts.

Fig. 5.—The temperature dependence of the rate of dehydration of cyclohexanol over aged magnesium sulfate–sodium sulfate catalysts.
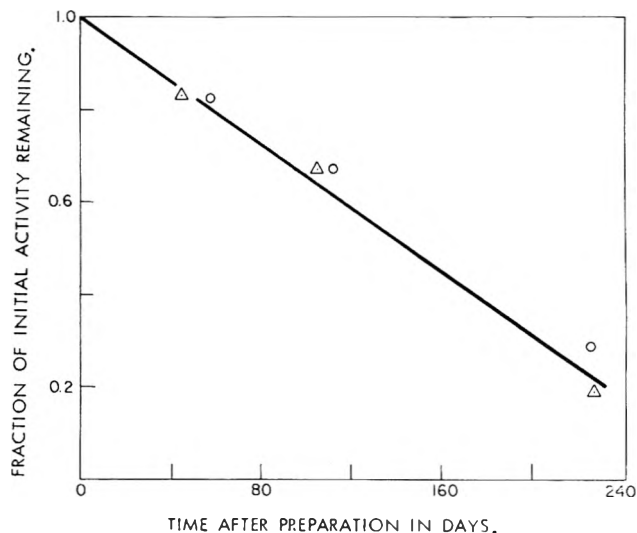
Fig. 6.—The effect of storage time on the activity of magnesium sulfate–sodium sulfate catalysts at 408°: ⊙, radioactive; △, non-radioactive.

used in the present experiments, however, hydration is unlikely. Even in the presence of a 654 mm. pressure of water vapor, magnesium sulfate is in the anhydrous form at temperatures above 370°.[10] Further, if only hydration were involved, the catalytic activity should be regenerated upon redrying of the material, whereas it was shown in our work that such is not the case. Therefore, the phenomenon must be related to a permanent change in the structure of the catalyst surface which requires an induction period in the presence of the reacting vapors.

Steady-State Reaction Rate Studies.—After aging to steady-state activity, the temperature dependence of the reaction rate was again determined for several

(10) J. S. Cho, F. A. Olsen, and M. E. Wadsworth, "Infrared Evidence for Bisulfate Formation in the Dehydration of Magnesium Sulfate," Technical Report No. 1, University of Utah, October 5, 1962.

catalysts. Because of the small size of the catalyst beds, the final surface areas of the catalysts were measured using the B.E.T. method with krypton as the adsorbate. Comparison of results of krypton adsorption with those using nitrogen for ten different catalyst preparations showed the latter to average 1.37 ± 0.07 times as great. Therefore, the results of these experiments, shown in Fig. 4 and 5, were normalized on the basis of a surface area obtained by applying this factor to the measured surface areas, so that direct comparisons can be made between these figures and those presented above when surface areas were measured with nitrogen as adsorbate. It is seen that aging decreases the catalyst activity in all cases and tends to

increase the apparent activation energy. The radio-active catalysts remain inferior.

Miscellaneous Experiments.—One of the most interesting observations reported in the literature of the effect of S^{35} on these catalysts was a decrease of catalytic activity as the radioactivity decayed.[7] This appeared to be powerful evidence that the reported enhancements of catalytic activity depended on the rate of emission of β-particles by the catalyst during use. However, studies were apparently not made of the behavior of the non-radioactive catalysts after similar storage times.

To clarify this point, the catalytic activities of a radioactive and non-radioactive catalyst were redetermined after storage times up to 227 days. It was found that the catalytic activity decreased linearly with time in both cases and that radioactive and non-radioactive catalysts lost the same fraction of their steady-state activity in the same period of time as shown in Fig. 6. Since the effect is linear with time over the period studied, it is obvious from the radioactive decay law that the decrease of the catalytic activity of the radioactive catalyst is also linearly related to the logarithm of the specific radioactivity. However, since the non-radioactive catalyst showed similar behavior, the effect must be a property of the catalyst not dependent on radiation.

In another group of experiments, the problems which arise in trying to duplicate catalyst surfaces for comparative purposes were circumvented by directing X-rays generated at 180 and 300 kv. on the catalyst bed while the dehydration reaction was proceeding.[11] The dose rates of 123 and 113 rad/min., respectively, were comparable to those from the S^{35} in the radioactive catalysts. No effects were found, in agreement with

(11) N. A. Krohn and H. A. Smith, *J. Phys. Chem.*, **65**, 1919 (1961).

previous Russian work utilizing an 800-kev. electron beam.[7] Preirradiation with Co^{60} γ-rays to 10^{11} ergs/g. was also without effect.

Conclusions

From the results of these experiments, it is concluded that the reported enhancements of catalytic activity in the dehydration of cyclohexanol by the addition of radioactive sulfur to the sulfate catalysts are erroneous because comparisons were apparently made on the basis of unit weight rather than unit surface area. When compared on the latter basis, the radioactive materials were found to be less active catalytically than non-radioactive catalysts of the same composition. In general, for a given set of preparative conditions, the radioactive catalysts have larger surface areas than their non-radioactive counterparts, and this was not apparently considered in the previous work.

It is also concluded that since both the non-radioactive and radioactive materials lose catalytic activity with storage time this phenomenon is not related to the decay of the radioactivity, but is a property of the catalyst surface. Thus, the emission of β-particles from the catalyst during the time the dehydration reaction is taking place is of no consequence. This conclusion is supported by the fact that irradiation of the catalyst with X-rays or electrons while the reaction was proceeding had no effect.

ELECTRONEGATIVITY. IV. ORBITAL ELECTRONEGATIVITIES OF THE NEUTRAL ATOMS OF THE PERIODS THREE A AND FOUR A AND OF POSITIVE IONS OF PERIODS ONE AND TWO[1]

By Jürgen Hinze[2] and H. H. Jaffé

Department of Chemistry, University of Cincinnati, Cincinnati 21, Ohio

The orbital electronegativities of the neutral atoms of the A elements of rows three and four and of the monopositive ions of periods one and two are reported and briefly discussed.

Introduction

In the preceding articles of this series,[1] electronegativity has been discussed, based on Mulliken's theoretically well justified[3,4] definition[5]

$$\chi = \frac{I_v + E_v}{2} \qquad (1)$$

This discussion leads to the conclusion that electro-

(1) (a) J. Hinze and H. H. Jaffé, *J. Am. Chem. Soc.*, **84**, 540 (1962); (b) J. Hinze, M. A. Whitehead, and H. H. Jaffé, *ibid.*, **85**, 148 (1963); (c) J. Hinze and H. H. Jaffé, *Can. J. Chem.*, **41**, 1315 (1963).

(2) Department of Chemistry, Rice Univ., Houston 1, Texas.

(3) R. S. Mulliken, *J. Chim. Phys.*, **46**, 497 (1949).

(4) W. Moffitt, *Proc. Roy. Soc.* (London), **A202**, 548 (1950).

(5) R. S. Mulliken, *J. Chem. Phys.*, **2**, 782 (1934).

negativity is the property not of an atom, but of an orbital of an atom in a molecule. The electronegativities computed in the light of these considerations for the elements of the first and second rows of the periodic system[1a] and for the elements of the first transition series[1c] show that such orbital electronegativities are considerably dependent on the character of the orbitals considered, and differences of more than one Pauling unit in electronegativity of the same atom but different hybrid orbitals are no exception. Consequently, it seems of interest to have available orbital electronegativities for different valence states for the heavier elements also.

Furthermore, it has been indicated in the first article[1a] that, on the basis of Mulliken's definition, one has to

TABLE I
VALENCE STATE PROMOTION ENERGIES IN[a] E.v.

Valence state	K	Ca+
s	0.0	0.0
p	1.61	3.13

	K^-b	Ca	Sc+	Ga+
sp	2.43	2.15	1.88	6.59
pp	1.52	4.86	8.21	14.42
didi	1.73	1.91	2.09	5.89
diπ	1.97	3.51	5.04	10.51
trtr	1.82	2.95	4.08	8.89
trπ	1.82	3.96	6.09	11.81
tete	1.80	3.45	5.10	10.33

	Zn^-b	Ga	Ge+	As++	Se+++	Ca^-c
spp	3.64	5.84	8.13	10.35	12.52	2.4
ppp	8.00	12.50	17.27	21.91	26.26	5.3
didiπ	3.28	5.31	7.39	9.45	11.45	2.1
diππ	5.82	9.17	12.70	16.13	19.39	3.8
trtrtr	3.16	5.13	7.14	9.15	11.09	1.9
trtrtrπ	4.93	7.82	10.85	13.80	16.62	3.2
tetete	4.46	7.11	9.86	12.57	15.15	2.8

	Ga^-b	Ge	As+	Se++
sppp	4.10	6.58	8.48	11.24
didiππ	4.24	6.37	8.18	10.47
trtrπ	4.28	6.30	8.08	10.21
tetetete	4.30	6.26	8.03	10.09

	Ge^-b	As	Se+
s²ppp	0.92	0.89	0.86
sp²pp	3.52	7.48	11.45
di²diππ	2.22	4.19	6.15
didiπ²π	3.43	7.14	10.85
tr²trtrπ	2.61	5.13	7.65
trtrtrπ²	3.39	7.02	10.65
te²tetete	2.80	5.58	8.35

	As^-b	Se	Br+	Kr++
s²p²pp	0.21	0.39	0.39	0.65
sp²p²p	4.75	8.22	12.05	15.34
di²di²ππ	0.21	0.39	0.39	0.65
di²diπ²π	2.48	4.30	6.22	8.00
didiπ²π²	4.54	7.75	11.28	14.33
tr²tr²trπ	1.72	3.00	4.28	5.55
tr²trtrπ²	3.14	5.40	7.82	10.00
te²te²tete	2.43	4.18	6.03	7.74

	Se^-b	Br	Kr+	Rb++	Sr+++
s²p²p²p	0.06	0.15	0.22	0.30	0.40
sp²p²p²	8.38	10.95	13.51	16.12	18.66

	Rb	Sr+
s	0.0	0.0
p	1.58	1.83

Valence state	Rb^-	Sr	Y+	In+
sp	0.45	2.04	3.63	6.10
pp	1.22	4.46	7.70	12.51
didi	0.55	1.83	3.11	5.57
diπ	.84	3.25	5.67	9.30
trtr	.75	2.75	4.76	8.00
trπ	.97	3.65	6.34	10.37
tete	.86	3.20	5.53	9.17

	Cd^-b	In	Sn+	Sb++	Te+++	Sr^-c
spp	4.05	5.70	7.41	9.21	10.69	2.4
ppp	8.08	11.70	15.24	18.71	22.44	5.3
didiπ	3.79	5.25	6.80	8.50	9.72	2.1
diππ	6.07	8.69	11.32	13.96	16.56	3.8
trtrtr	3.70	5.11	6.59	8.27	9.40	1.9
trtrtrπ	5.28	7.49	9.75	12.06	14.18	3.2
tetete	4.86	6.86	8.91	11.07	12.90	2.8

	In^-b	Sn	Sb+	Te++
s²pp	0.07	0.40	0.40	1.11
sp²p	5.38	7.47	9.66	11.69
p²pp	8.87	11.71	16.78	18.49
didiπ²	5.05	7.08	8.91	11.04
diπ²π	7.13	9.59	13.22	15.09
di²ππ	5.07	6.82	10.09	11.09
di²diπ	2.66	3.93	5.03	6.40
tr²trtr	3.15	4.94	6.24	7.88
tr²trπ	5.02	6.87	9.17	11.00
trtrπ²	6.40	8.71	11.70	13.67
te²tete	4.98	6.86	9.31	10.91
sppp	4.56	6.42	7.91	9.95
didiππ	4.23	6.04	7.16	9.30
trtrtrπ	4.12	5.91	6.90	9.09
tetetete	4.06	5.84	6.78	8.98

	Sn^-b	Sb	Te+
s²ppp	−0.30	0.29	0.89
sp²pp	2.09	6.63	11.17
di²diππ	0.89	3.46	6.02
didiπ²π	2.04	6.30	10.55
tr²trtrπ	1.27	4.37	7.47
trtrtrπ²	2.02	6.19	10.35
te²tetete	1.45	4.79	8.14

	Sb^-b	Te	I+	Xe++
s²p²pp	0.21	0.44	0.69	0.91
sp²p²p	4.10	6.95	10.70	13.10
di²di²ππ	0.21	0.44	0.69	0.91
di²diπ²π	2.15	3.70	5.70	7.01
didiπ²π²	3.88	6.55	10.05	12.31
tr²tr²trπ	1.51	2.61	4.03	4.98
tr²trtrπ²	2.70	4.60	7.08	8.69
te²te²tete	2.10	3.59	5.53	6.81

	Te^-b	I	Xe+	Cs++	Ba+++
s²p²p²p	0.16	0.31	0.44	0.57	0.74
sp²p²p²	6.32	10.17	11.26	15.84	18.96

[a] Calculations also have been made for valence states of the same elements with lower valence; such values are contained in J. Hinze, Ph.D. Dissertation, University of Cincinnati, 1962. [b] Extrapolated values. [c] Roughly estimated values.

expect considerably different electronegativity values for ions. To demonstrate this and to make available orbital electronegativities of some positive ions we have computed such values for the elements of the first two rows of periodic table.

Procedure.—The evaluation of the orbital electronegativities with Mulliken's definition has been described in detail in the first article of this series,[1a] and only a short outline will be given here. The essential part is the computation of the valence state ionization potentials, I_v, and electron affinities, E_v, or in the case of positive ions, the first and second valence state ionization potentials, $I_v(1)$ and $I_v(2)$, respectively.

(a) Orbital Electronegativities of the Neutral Elements of Rows Three and Four.—The valence state ionization potentials required are obtained from the ground state potentials, I_g, and the corresponding promotion of energies of the positive ion and atom, P^+ and P^0, respectively, according to

$$I_v = I_g + P^+ - P^0 \qquad (2)$$

and analogously the valence state electron affinities are calculated from the ground state electron affinities, E_g,

and the promotion energies of atom and negative ion, following

$$E_v = E_g + P^0 - P^- \qquad (3)$$

Here the valence state promotion energies represent the energies required to elevate an atom or ion to the valence state, which, as defined by van Vleck,[6] is the hypothetical "state" of an atom, chosen so that the interactions of the electrons of the atom are as nearly as possible the same as they would be if the atom is part of a molecule. The detailed description of the computation of such valence state promotion energies, following Mulliken's[5] and van Vleck's[6] method, has been given previously.[1a]

The Slater–Condon parameters used here for the computation of the promotion energies are those obtained and reported earlier.[7] It is again necessary to use the parameters determined from several configurations simultaneously, implying that equivalent parameters have the same value for the configurations. Although it is known that the assumption of the configuration independence of Slater–Condon parameters is questionable, it has been shown[7] that this assumption is acceptable on the level of the approximations inherent in the Slater–Condon treatment.

The promotion energies of the negative ions, which cannot be computed directly, are obtained as described in the first article[1a] from a linear extrapolation of the corresponding promotion energies of successive states of ionization in an isoelectronic sequence. Such an extrapolation, however, is not possible for the promotion energies of Ca^- and Sr^-, since the necessary spectral information is not available for the isoelectronic positive ions. Consequently the promotion energies of Ca^- and Sr^- are estimated roughly, guided by the corresponding energies for Mg^- and Be^-, which are known.[1a] All the promotion energies computed and used for the evaluation of valence state ionization potentials and electron affinities are given in Table I.

Ground state ionization potentials, experimentally determined from spectral data, are accurately known. The values used here are chosen from Moore's tables.[8] Unfortunately, the ground state electron affinities are not so readily obtainable, and only the values for Br and I have been determined experimentally.[9] The values used for the other elements are those extrapolated by Ginsberg and Miller.[10] The ground state ionization potentials and the electron affinities used are listed in Table II.

With the entries of Tables I and II, the valence state ionization potentials, valence state electron affinities, and the orbital electronegativities are readily obtained using eq. 1, 2, and 3. The results are listed in Table III, where the last column gives the electronegativities in Pauling units, more familiar to the chemist. The transformation used is[1a]

$$\chi_p = 0.336(\chi_m - 0.615) \qquad (4)$$

(b) Orbital Electronegativities of the Positive Ions

(6) J. H. van Vleck, J. Chem. Phys. **2**, 20 (1934).

(7) J. Hinze and H. H. Jaffé, ibid., **38**, 1834 (1963).

(8) C. E. Moore, "Atomic Energy Levels," National Bureau of Standards Circular No. 467, Vol. I–III, and private communication.

(9) T. L. Bailey, J. Chem. Phys., **28**, 792 (1958).

(10) A. P. Ginsberg and J. M. Miller, J. Inorg. Nucl. Chem., **7**, 351 (1958).

TABLE II
GROUND STATE IONIZATION POTENTIALS AND ELECTRON AFFINITIES IN (E.V.)

	E_g	I_g
K	0.00	4.34
Ca	.11	6.11
Ga	.18	6.00
Ge	1.20	7.88
As	0.65	9.81
Se	2.20	9.75
Br	3.55	11.84
Rb	0.00	4.18
Sr	0.10	5.69
In	0.20	5.78
Sn	1.00	7.34
Sb	1.10	8.64
Te	2.30	9.01
I	3.21	10.45

of the Elements of Rows One and Two.—The evaluation of the orbital electronegativities for the positive ions of rows one and two of the periodic system is essentially the same as described above. However, it is much simplified, since the promotion energies required, of atoms and singly and doubly positive ions, have already been computed,[1a] and the ground state first and second ionization potential can be taken from Moore's tables.[8] Thus, it is merely necessary to combine all these data analogously to eq. 2, 3, and 1 to evaluate the valence state ionization potentials and orbital electronegativities of the positive ions. The results obtained are listed in Table IV, where again the last column gives the electronegativities in Pauling units, converted using eq. 4.

Discussion

The Mulliken definition of electronegativity is the only non-empirical one available, and has received wide acclaim and acceptance[11,12]; it is the only readily available scheme for distinguishing between different hybrids and different types of orbitals. However, in considering the problems of evaluation of electronegativity it *frequently* has been pointed out that the Mulliken electronegativity is difficult to compute because electron affinity data are required which *frequently* are not available. This apparent limitation of the Mulliken definition, however, is not at all serious. Generally the electron affinity can, by purely empirical guesswork, be estimated to within 1 e.v., and the resulting uncertainty in electronegativity is only of the order of 0.16 Pauling unit. Thus, any uncertainties in the electron affinity obtained in the present work have very little effect on the resulting electronegativities.

The electronegativities obtained in the present work and listed in Table III for the neutral atoms of rows three and four, and in Table IV for the positive ions of rows one and two of the periodic system, show the considerable dependence on valence states that would be expected from the similar behavior of the electronegativities of the neutral atoms of rows one and two reported previously.[1a] Again, as already reported for the first two groups, the valence state electronegativities are linear functions of the hybridization parameter.

It seems of particular interest to compare the electronegativities obtained in this work with values for group

(11) C. A. Coulson, "Valence," Clarendon Press, London, 1952.

(12) H. O. Pritchard and H. A. Skinner, Chem. Rev., **55**, 745 (1955).

TABLE III

VALENCE STATE IONIZATION POTENTIALS, ELECTRON AFFINITIES, AND ORBITAL ELECTRONEGATIVITIES OF ELEMENTS OF ROW 3 AND 4[a]

Atom	Configuration	Orbital	I_v	E_v	x_p
K(V₁)	s	s	4.34	1.46	0.77
		p	2.73	0.77	0.38
Ca(V₂)	sp	s	7.09	2.26	1.36
		p	3.96	−0.24	0.42
	pp	p	4.38	−0.53	.65
	didi	σ	5.76	1.02	.93
	diπ	σ	5.73	0.42	.83
		π	4.16	− .38	.43
	trtr	σ	5.25	.06	.68
	trπ	σ	5.28	− .13	.66
		π	4.25	− .33	.45
	tete	σ	5.01	− .04	.63
Ga(V₃)	spp	s	14.58	5.57	3.18
		p	6.75	1.78	1.22
	ppp	p	7.92	8.40	2.54
	didiπ	σ	11.19	3.15	2.20
		π	6.58	1.10	1.09
	di$\pi\pi$	σ	11.25	7.25	2.90
		π	7.33	5.09	1.88
	trtrtr	σ	9.76	2.28	1.82
	trtrπ	σ	9.99	5.13	2.33
		π	7.07	3.69	1.60
	tetete	σ	9.22	4.02	2.02
Ge(V₄)	sppp	s	18.57	6.86	4.06
		p	9.43	4.26	2.09
	didi$\pi\pi$	σ	14.21	5.35	3.08
		π	8.89	4.14	1.98
	trtrtrπ	σ	12.43	4.89	2.70
		π	8.72	4.11	1.95
	tetetete	σ	11.48	4.66	2.50
As(V₃)	s^2ppp	p	9.36	1.33	1.59
	sp^2pp	s	16.22	7.92	3.84
		p	12.16	3.38	2.40
	di^2di$\pi\pi$	σ	13.39	4.63	2.82
		π	10.75	2.26	1.99
	didi$\pi^2\pi$	σ	14.53	5.31	3.13
		π	12.19	3.25	2.39
	tr^2trtrπ	σ	13.00	4.06	2.66
		π	11.24	2.64	2.12
	trtrtrπ^2	σ	13.84	4.53	2.88
	te^2tetete	σ	12.80	3.81	2.58
Se(V₂)	s^2p^2pp	p	11.68	2.52	2.18
	sp^2p^2p	s	20.49	10.36	4.97
		p	14.44	2.04	2.56
	$di^2di^2\pi\pi$	π	11.68	2.52	2.18
	di^2di$\pi^2\pi$	σ	17.29	6.44	3.78
		π	13.06	2.28	2.37
	didi$\pi^2\pi^2$	σ	17.94	5.73	3.77
	tr^2tr^2trπ	σ	15.68	5.14	3.29
		π	12.59	2.37	2.31
	tr^2trtrπ^2	σ	16.28	4.77	3.33
	te^2te^2tete	σ	15.29	4.24	3.07
Br(V₁)	$s^2p^2p^2$p	p	13.10	3.70	2.62
	$sp^2p^2p^2$	s	22.07	14.50	5.94
Rb(V₁)	s	s	4.18	0	0.50
		p	2.60	1.84	0.54
Sr(V₂)	sp	s	6.62	2.14	1.26
		p	3.65	−0.36	0.34
	pp	p	4.20	− .94	.34
	didi	σ	5.34	.93	.85
	diπ	σ	5.41	.15	.73
		π	3.92	− .65	.34

Atom	Configuration	Orbital	I_v	E_v	x_p
Sr(V₂)	trtr	σ	4.92	− .15	.59
	trπ	σ	5.01	− .46	.56
		π	4.02	− .65	.36
	tete	σ	4.72	− .30	.54
In(V₃)	spp	s	12.60	5.83	2.88
		p	6.19	0.52	0.92
	ppp	p	6.62	3.01	1.41
	didiπ	σ	9.84	2.79	1.91
		π	6.11	0.40	0.88
	di$\pi\pi$	σ	9.61	3.82	2.04
		π	6.40	1.76	1.16
	trtrtr	σ	8.68	1.89	1.57
	trtrπ	σ	8.67	2.67	1.70
		π	6.30	1.29	1.07
	tetete	σ	8.10	2.08	1.50
Sn(V₂)	s^2pp	p	6.94	0.87	1.10
	sp^2p	s	16.34	7.94	3.87
		p	8.51	5.54	2.15
	p^2pp	p	12.10	10.11	3.52
	didiπ^2	σ	12.81	6.35	3.01
	di$\pi^2\pi$	σ	14.22	8.92	3.68
		π	10.30	7.82	2.84
	$di^2\pi\pi$	π	10.15	6.15	2.53
	di^2diπ	σ	13.04	4.40	2.72
		π	7.90	3.20	1.66
	tr^2trtr	σ	11.43	4.61	2.49
	tr^2trπ	σ	12.65	6.55	3.02
		π	9.50	5.80	2.36
	trtrπ^2	σ	12.49	7.64	3.17
	te^2tete	σ	11.57	6.16	2.77
Sn(V₄)	sppp	s	16.16	7.72	3.80
		p	8.32	5.33	2.08
	didi$\pi\pi$	σ	12.64	6.15	2.94
		π	8.10	5.00	1.99
	trtrtrπ	σ	11.17	5.64	2.62
		π	8.02	4.89	1.96
	tetetete	σ	10.40	5.39	2.44
Sb(V₃)	s^2ppp	p	8.75	1.18	1.46
	sp^2pp	s	18.80	7.51	4.22
		p	11.68	3.62	2.36
	di^2di$\pi\pi$	σ	15.27	4.35	3.09
		π	10.21	2.41	1.91
	didi$\pi^2\pi$	σ	15.56	5.25	3.29
		π	11.25	3.52	2.27
	tr^2trtrπ	σ	13.89	3.97	2.79
		π	10.51	2.77	2.02
	trtrtrπ^2	σ	14.16	4.58	2.94
	te^2tetete	σ	13.16	3.79	2.64
Te(V₂)	s^2p^2pp	p	11.04	2.58	2.08
	sp^2p^2p	s	20.78	9.09	4.81
		p	14.80	2.93	2.77
	$di^2di^2\pi\pi$	π	11.04	2.58	2.08
	di^2di$\pi^2\pi$	σ	17.12	5.84	3.65
		π	12.91	2.76	2.43
	didi$\pi^2\pi^2$	σ	18.19	5.61	3.79
	tr^2tr^2trπ	σ	15.36	4.75	3.17
		π	12.29	2.70	2.31
	tr^2trtrπ^2	σ	16.26	4.69	3.31
	te^2te^2tete	σ	15.11	4.20	3.04
I(V₁)	$s^2p^2p^2$p	p	12.67	3.52	2.52
	$sp^2p^2p^2$	s	18.00	13.38	5.06

[a] See footnote a, Table I.

IV elements obtained empirically by other workers.[13] Our values for tetrahedral Ge and Sn are seen to be con- sistently somewhat higher than the empirical values (Ge 2.0, 1.8–1.9; Sn^{IV} 1.9, 1.8). This fact may, most likely, be ascribed to some hybridization with d-orbitals in the heavy elements; the d-orbitals have low ioniza-

(13) R. S. Drago, J. Inorg. Nucl. Chem., 15. 237 (1960); A. L. Allred and E. G. Rochow, ibid., 5, 269 (1958).

TABLE IV

Electronegativity and Ionization Potentials of Positive Ions

Ion	Configuration	Orbital	I_v	E_v	χ_p	Ion	Configuration	Orbital	I_v	E_v	χ_p
Be+	s	s	18.21	9.32	6.10	Mg+	s	s	15.03	7.64	3.60
	p	p	14.25	5.32	3.08		p	p	10.60	4.67	2.36
B+	sp	s	25.40	14.05	6.42	Al+	sp	s	20.15	11.32	5.08
		p	19.40	7.38	4.29			p	13.48	5.99	3.07
	pp	p	18.91	7.37	4.21		pp	p	14.34	6.03	3.21
	didi	σ	23.48	9.64	5.36		didi	σ	17.47	8.00	4.07
	diπ	σ	22.16	8.94	5.02		diπ	σ	17.25	7.59	3.97
		π	19.16	7.37	4.25			π	13.92	6.00	3.14
	trtr	σ	21.72	8.33	4.84		trtr	σ	16.28	7.01	3.70
	trπ	σ	21.08	8.02	6.36		trπ	σ	16.28	6.74	3.68
		π	19.08	7.37	4.23			π	14.06	5.92	3.17
	tete	σ	20.93	7.88	4.63		tete	σ	15.75	6.64	3.56
C+	spp	s	33.03	19.42	8.60	Si+	spp	s	24.68	14.93	6.45
		p	23.93	9.91	5.48			p	16.56	8.61	4.02
	ppp	p	23.29	11.65	5.66		ppp	p	16.56	11.42	4.49
	didiπ	σ	29.85	13.29	7.04		didiπ	σ	21.43	10.95	5.23
		π	23.86	9.83	5.45			π	16.50	8.60	4.01
	di$\pi\pi$	σ	28.16	12.96	6.70		di$\pi\pi$	σ	20.62	11.56	5.20
		π	23.61	10.78	5.57			π	16.55	10.02	4.26
	trtrtr	σ	28.14	11.83	6.50		trtrtr	σ	19.96	9.99	4.83
	trtrπ	σ	27.36	11.91	6.39		trtrπ	σ	19.62	10.57	4.87
		π	23.68	10.45	5.52			π	16.53	9.54	4.17
	tetete	σ	26.71	11.37	6.19		tetete	σ	18.97	10.08	4.67
N+	sppp	s	41.84	25.59	11.12	P+	sppp	s	31.24	18.61	8.17
		p	28.69	12.48	6.69			p	20.72	11.55	5.22
	didi$\pi\pi$	σ	37.00	17.24	8.90		didi$\pi\pi$	σ	27.01	14.05	6.69
		π	28.70	12.06	6.64			π	20.69	10.96	5.11
	trtrtrπ	σ	34.62	15.09	8.15		trtrtrπ	σ	25.14	12.72	6.15
		π	28.71	11.96	6.63			π	20.68	10.76	5.08
	tetetete	σ	33.29	14.14	7.76		tetetete	σ	24.10	12.09	5.88
O+	s^{2}ppp	p	34.15	14.61	7.98	S+	s^{2}ppp	p	22.91	11.05	5.50
	sp^{2}pp	s	51.41	32.29	13.86		sp^{2}pp	s	35.18	21.13	9.26
		p	34.22	15.86	8.21			p	24.49	11.98	5.92
	di^{2}di$\pi\pi$	σ	46.80	23.45	11.59		di^{2}di$\pi\pi$	σ	31.57	16.09	7.80
		π	34.19	15.24	8.10			π	23.70	11.51	5.71
	didi$\pi^2\pi$	σ	44.56	22.34	11.03		didi$\pi^2\pi$	σ	30.61	15.78	7.59
		π	33.95	15.53	8.11			π	24.00	11.92	5.83
	tr^{2}trtrπ	σ	42.49	20.15	10.32		te^{2}teteπ	σ	28.99	14.38	7.08
		π	34.08	15.30	8.09			π	23.74	11.65	5.74
	trtrtrπ^2	σ	41.39	19.64	10.05		trtrtrπ^2	σ	28.51	14.33	6.99
	te^{2}tetete	σ	40.31	18.70	9.70		te^{3}tetete	σ	27.65	13.64	6.73

tion potentials and electron affinities, and hence must have low orbital electronegativities. Even a relatively small contribution of such orbitals would consequently be expected to significantly depress the electronegativity. Unfortunately, a calculation of d-orbital electronegativity by the Mulliken method is not feasible, because the necessary spectroscopic data are not available. Finally, the sensitivity of the electronegativity of the heavy elements to d-orbital hybridization[1c] indicates that their electronegativities need to be considered as especially variable, since this hybridization itself is a sensitive function of many factors, e.g., the formal charge.[14]

The electronegativities calculated for the positive ions are, as might have been expected, considerably higher than for the neutral atoms. The magnitude of the difference may seem somewhat surprising, ranging from about a factor of 3 for the early members in a period to a factor of 2 in the late members. It must, however, be realized that these values refer to integral positive charges not compensated by inductive effects or ionic character, and are calculated from data appli-

cable to the gaseous state, whereas the electronegativities are to be used generally for molecules in solution. Obviously, effects such as stabilization by solvation with polarization (charge shift) of solvent molecules may appreciably affect these values.

It may further be worth noting that the ion commonly encountered as an intermediate in organic chemistry, say C(tr,tr,tr). An electronegativity can also be obtained for an "ion" in which the charge is accumulated on the central atom by inductive charge transfer,[1b] say C(tr$^{2/3}$tr$^{2/3}$tr$^{2/3}$$\pi$). The electronegativity of an "ion" formed in this way tends to be slightly lower than for the more normal one; thus, as a comparison

$$\chi[\text{C}^+(\text{tetete})] = 6.19; \quad \chi[\text{C}^+(\text{te}^{2/3}\text{te}^{2/3}\text{te})] = 6.11$$

(14) H. H. Jaffé, J. Phys. Chem., 58, 185 (1954); D. P. Craig and C. Zauli, J. Chem. Phys., 37, 601, 609 (1962).

versity of Cincinnati Computing Center and Grant G-19281 from the National Science Foundation in carrying

out the extensive computations necessary is also gratefully acknowledged.

THE ENTHALPIES OF FORMATION OF ZIRCONIUM DIHYDRIDE AND ZIRCONIUM DIDEUTERIDE[1]

By Donald R. Fredrickson, Ralph L. Nuttall, Howard E. Flotow, and Ward N. Hubbard

Argonne National Laboratory, Argonne, Illinois

Received January 11, 1963

The standard energies of combustion of ZrH_2 and ZrD_2 were determined by precision oxygen bomb calorimetry. The values found for ΔE_c^0 were -290.03 ± 0.24 kcal. mole^{-1} of ZrH_2 and -290.80 ± 0.18 kcal. mole^{-1} of ZrD_2. At 298.15°K. the enthalpy of formation, ΔH_f^0, and the Gibbs energy of formation, ΔG_f^0, were calculated to be -38.90 ± 0.31 kcal. mole^{-1} and -29.32 ± 0.31 kcal. mole^{-1}, respectively, for ZrH_2, and -40.22 ± 0.27 kcal. mole^{-1} and -29.86 ± 0.27 kcal. mole^{-1}, respectively, for ZrD_2.

Introduction

The heat of combustion of $ZrH_{1.92}$ was measured at 18° by Sieverts, Gotta, and Halberstadt.[2] They reported an energy of combustion of -282.0 kcal. mole^{-1} for this material. They also measured the energy of combustion of zirconium using the same source material as was used to make their hydride. The energy of combustion of this zirconium was -255.5 kcal. mole^{-1}. Using the above values for zirconium and ZrH_2 and a value of -67.57 kcal. mole^{-1} for the energy of formation of water, they calculated enthalpy of formation values of -38.9 kcal. mole^{-1} of $ZrH_{1.92}$ and -40.5 kcal. mole^{-1} of ZrH_2. No calorimetric data leading to the enthalpy of formation of ZrD_2 have been published.

Equilibrium hydrogen pressures at various H/Zr atomic ratios in the temperature range 600 to 1200°K. have been measured by a number of investigators.[3] These data can be used to obtain partial molal enthalpies of solution of hydrogen in the hydride phases. These partial molal enthalpies of solution can be integrated over the composition range to give the enthalpy of formation of a particular hydride. Martin and Rees[3c] reported a value of -41.4 kcal. mole^{-1} for the enthalpy of formation of ZrH_2. Morton and Stark[4] have measured equilibrium dissociation pressures for deuterides with D/Zr atomic ratios between 0.02 and 1.80. They report partial molal enthalpies of solution of deuterium over this composition range. On the basis of their data, we estimate the enthalpy of formation of ZrD_2 to be about -42 kcal. mole^{-1}.

Because of uncertainties due to sample impurities, experimental errors, and approximations, all of the above values of ΔH_f^0 are believed to be uncertain by at least ± 3 kcal. mole^{-1}. It therefore seemed worthwhile to determine these enthalpies more accurately by using purer samples and precision bomb calorimetry.

This paper describes measurements of the energies of reaction represented by the equations

$$ZrH_2(s) + {}^3/_2O_2(g) = ZrO_2(s) + H_2O(l) \quad (1)$$

and

$$ZrD_2(s) + {}^3/_2O_2(g) = ZrO_2(s) + D_2O(l) \quad (2)$$

at 298.15°K. These data were combined with other appropriate thermodynamic quantities to calculate enthalpies of formation, ΔH_f^0, at 298.15°K. and at 0°K. and the Gibbs energy of formation, ΔG_f^0, at 298.15°K. of ZrH_2 and ZrD_2. The uncertainty in the value of ΔH_f^0 for ZrH_2 reported in this paper is about an order of magnitude less than the values reported previously. The difference between the ΔH_f^0 of ZrH_2 and that of ZrD_2 at 298.15°K. calculated from these results agree with the difference calculated[5] from heat capacity data.

Experimental

Samples.—The ZrH_2 and ZrD_2 samples which were used for the heat of combustion measurements reported in this paper were previously used at this Laboratory for heat capacity determinations.[5] It was found[5] by analyses that the impurities in each sample amounted to less than 0.1%. The compounds as originally prepared were in the form of irregular pieces which varied in size from about 0.1 to 3 mm. on an edge. Preliminary attempts to burn this material in the combustion bomb were unsatisfactory because some of the hydride pieces exploded and the scattered fragments did not burn completely. This difficulty was eliminated by burning powdered samples of particle size 100 μ or less. The powdered material with its concomitant large surface area was found to oxidize at a measurable rate in air. The samples were therefore prepared, weighed, and sealed in plastic bags in a helium-filled drybox where the combined oxygen and water concentration was less than 0.1%. ZrH_2 is hard and brittle and it was found convenient to prepare powdered samples in the drybox by crushing the ZrH_2 and ZrD_2 with a hardened steel pestle on a hardened steel plate. Particles which would pass through a 240 mesh brass screen but which were retained on a 400 mesh brass screen were used for the calorimetric measurements.

Spectrographic analyses of the powdered ZrH_2 and ZrD_2 samples showed that both samples contained, within the error of the analyses, the same impurity levels. The elements detected were present in amounts equal to the following in parts per million: Mg, 3; Cu, 40; Fe, 200; and Pb, 40. Other elements looked for, but not detected, are given with the lower limits of detection in reference 5. Chemical analysis of the ZrH_2 showed 564, 19, and 170 parts per million of oxygen, nitrogen, and carbon, respectively. For ZrD_2 the results of the chemical analyses for
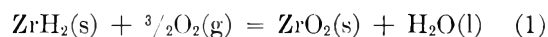
(1) This work was performed under the auspices of the U. S. Atomic Energy Commission.

(2) A. Sieverts, A. Gotta, and S. Halberstadt, *Z. anorg. allgem. Chem.*, **187**, 159 (1930).
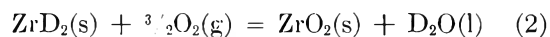
(3) (a) A. Sieverts and E. Roell, *ibid.*, **153**, 289 (1926); (b) M. N. A. Hall, S. L. H. Martin, and A. L. G. Rees, *Trans. Faraday Soc.*, **41**, 306 (1945); (c) S. L. H. Martin and A. L. G. Rees, *ibid.*, **50**, 343 (1954); (d) R. K. Edwards, P. Levesque, and P. Cubicciotti, *J. Am. Chem. Soc.*, **77**, 1307 (1955); (e) E. A. Gulbransen and K. F. Andrew, *J. Metals*, **7**, 136 (1955); (f) C. E. Ells and A. D. McQuillan, *J. Inst. Metals*, **85**, 89 (1956–57); (g) M. W. Mallett and W. M. Albrecht, *J. Electrochem. Soc.*, **104**, 142 (1957); (h) L. D. LaGrange, L. J. Dykstra, J. M. Dixon, and U. Merten, *J. Phys. Chem.*, **63**, 2035 (1959); (i) G. G. Libowitz, *J. Nucl. Mater.*, **5**, 2 (1962).

(4) J. R. Morton and D. S. Stark, *Trans. Faraday Soc.*, **56**, 351 (1960).

(5) H. E. Flotow and D. W. Osborne, *J. Chem. Phys.*, **34**, 1418 (1961).

oxygen, nitrogen, and carbon were 562, 19, and 170 parts per million, respectively.

The amounts of hydrogen and deuterium in the powdered ZrH_2 and ZrD_2 samples, respectively, were determined by measuring the volumes of H_2 and D_2 evolved at 1300°. For the ZrH_2 sample, the volume of pure H_2 obtained per gram of hydride was 239.8 ± 0.2 cc. (STP) and for ZrD_2 the volume of D_2 and HD obtained per gram of deuteride was 235.1 ± 0.2 cc. (STP). The volumes calculated for pure ZrH_2 and ZrD_2 are 240.40 cc. (STP) and 235.35 cc. (STP), respectively. The gas obtained from the ZrD_2 contained 99.65 atom % D and 0.35 atom % H. The fact that the experimentally obtained volumes are a little less than the theoretical ones can be accounted for by the impurities. It therefore seems reasonable to assume that the hydrogen and deuterium are combined with zirconium to form the compounds $ZrH_{2.000}$ ± 0.004 and $ZrD_{2.000}$ ± 0.004, respectively.

Apparatus.—The calorimetric system consisted of a rotating bomb calorimeter[6] and a platinum-lined combustion bomb. This is a stainless steel bomb lined with 0.01 in. thick platinum. The electrodes and internal fittings are fabricated from platinum. The energy equivalent of the calorimetric system, E(calorimeter), was determined by combustion of benzoic acid (National Bureau of Standards, sample 39 h) in oxygen at 30 atm. pressure. A series of seven combustions gave a value of 3578.99 ± 0.22 cal. deg.$^{-1}$ for E(calorimeter); the uncertainty given is the standard deviation of the mean.
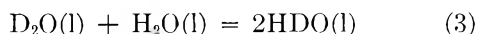
Combustion Techniques.—The powdered samples were sealed in Mylar polyester plastic bags by a procedure adapted from one used by Good and co-workers.[7]

Figure 1 shows the sample support arrangement. A 0.050 in. thick platinum plate attached with posts to the bomb head supports the sample dish and shield. The Mylar bag containing the sample lies on a 0.187-in. layer of ZrO_2 pressed into a platinum dish. This layer of ZrO_2 prevents the platinum from melting. A platinum shield around the dish prevents any particles from spattering onto the bomb walls. The bomb was filled with oxygen at 15 atm. pressure and also contained 1 ml. of H_2O The addition of water is a standard calorimetric practice to minimize the correction for the heat of vaporization where water is one of the products of the combustion. Ignition was accomplished by a cotton fuse attached to a platinum wire which was electrically heated.

Because combustion of the Mylar used to encapsulate the samples contributes about 7% of the total heat evolved, an accurate value of the energy of combustion of Mylar was determined. The Mylar samples were equilibrated and weighed in a drybox to eliminate a correction for absorbed moisture. Approximately 0.5-g. samples were burned in oxygen at 20 atm. pressure using the same arrangement as was used for the benzoic acid calibration experiments.

Reaction Products.—ZrH_2 burns in oxygen in accordance with eq. 1 and ZrD_2 in accordance with eq. 2. In each case the solid product was examined by X-ray diffraction analysis and found to be a single phase of monoclinic ZrO_2. No appreciable change in weight of this ZrO_2 occurred when it was heated in air at 1000° for 1 hr. Analysis of the gas evolved when this ZrO_2 was heated *in vacuo* at 1300° showed negligible amounts of hydrogen or deuterium.

The D_2O formed by the combustion of ZrD_2 equilibrated with the H_2O present in the bomb according to the equation

$$D_2O(l) + H_2O(l) = 2HDO(l) \qquad (3)$$

The enthalpy change for this reaction has been measured by Skripov and Povyshev.[8] They correlated their data by using the equilibrium constant[9] for eq. 3

$$K = \frac{[HDO]^2}{[D_2O][H_2O]} = 3.80 \text{ at } 298.15°K.$$

and obtained a value of $\Delta H = 15.5 ± 0.5$ cal. mole^{-1} of HDO formed. The heat absorbed by reaction 3 is included in item 6 of Table II.

Fig. 1.—Sample support arrangement for the combustion of ZrH_2 and ZrD_2: A, platinum lining; B, enclosed sample; C, ZrO_2 layer; D, platinum plate; E, capsule with 1 ml. of H_2O; F, cotton fuse; G, platinum ignition wire; H, platinum spatter shield; I, platinum dish; J, electrode for ignition wire.

Results

Experimental Results.—Tables I and II give the combustion data and the calculated standard energy of combustion for ZrH_2 and ZrD_2, respectively. The energy values are expressed in terms of a calorie defined as exactly equal to 4.1840 absolute joules. The molecular weights of ZrH_2 and ZrD_2 were taken as 93.24 and 95.24, respectively. The corrections to standard states were applied in the manner described by Hubbard, Scott, and Waddington.[10] The symbols employed in Tables I and II are explained in ref. 10. The meaning of the symbols used in Tables I and II are as follows: (1) m', the mass of material burned corrected to the weight *in vacuo*; (2) Δt_c, the observed temperature increase of the calorimeter corrected for heat exchange between the calorimeter and its surroundings; (3) $\mathcal{E}$(calor.)$(-\Delta t_c)$, the energy equivalent of the calorimetric system multiplied by the corrected temperature increase; (4) $\Delta E_{contents}$, the energy absorbed by the contents of the bomb during the hypothetical isothermal process at 298.15°K.; (5) $\Delta E_{ignition}$, the measured energy input for ignition of the fuse; (6) ΔE_{cor}, the sum of several minor corrections to the measured energy[10]; (7) ΔE_{Mylar}, the energy associated with the combustion of the Mylar bag, based on a value of $-5477.19 ± 1.03$

(6) W. N. Hubbard, C. Katz, and G. Waddington, *J. Phys. Chem.*, **58**, 142 (1954).

(7) W. D. Good, *et al.*, *ibid.*, **63**, 1133 (1959).

(8) V. P. Skripov and L. V. Povyshev, *Zh. Fiz. Khim.*, **36**, 325 (1962).

(9) I. Kirshenbaum, "Physical Properties and Analysis of Heavy Water," McGraw-Hill Book Co., Inc., New York, N. Y., 1951, p. 54.
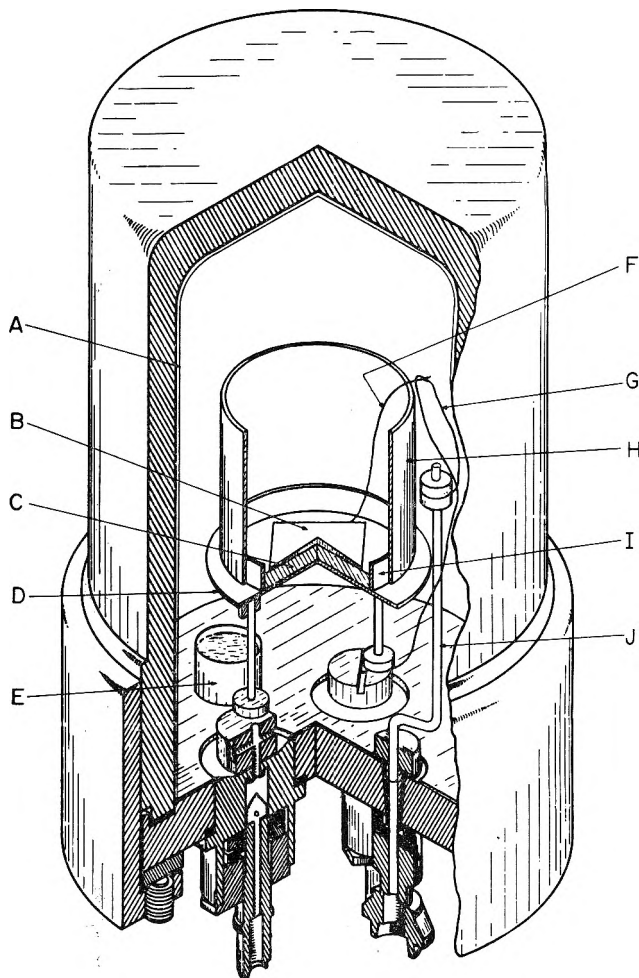
(10) W. N. Hubbard, D. W. Scott, and G. Waddington, Chapter 5 of "Experimental Thermochemistry," Vol. 1, F. D. Rossini, Editor, Interscience Publishers, Inc., New York, N. Y., 1956, pp. 75–128.

<div align="center">

Table I

Results of ZrH_2 Combustion Experiments
</div>

1.	m', g.	1.0878	1.0914	1.1004	1.0972	1.0935
2.	Δt_c, degrees	1.01495	1.01454	1.02613	1.02168	1.01841
3.	$\varepsilon(calor.)(-\Delta t_c)$, cal.	−3632.50	−3631.03	−3672.51	−3656.58	−3644.88
4.	$\Delta E_{contents}$, cal.	−7.08	−7.08	−7.16	−6.93	−6.91
5.	$\Delta E_{ignition}$, cal.	2.90	2.83	2.83	2.83	2.83
6.	ΔE_{cor}, cal.	−2.03	−2.11	−1.01	−0.70	−0.70
7.	ΔE_{Mylar}, cal.	249.76	247.02	253.05	256.33	257.43
8.	ΔE_{cotton}, cal.	5.75	5.79	5.67	5.43	5.67
9.	$\Delta E_c^0/M$, cal. g.$^{-1}$	−3110.13	−3101.14	−3107.17	−3098.45	−3096.99

10. Av. $\Delta E_c^0/M$ = −3102.77 ± 2.53 cal. g.$^{-1}$
11. Energy cor. for impurities = −7.77 ± 0.67 cal. g.$^{-1}$
12. $\Delta E_c^0/M$ (ZrH_2) = −3110.54 ± 2.62 cal. g.$^{-1}$
13. ΔE_c^0 (ZrH_2) = −290.03 ± 0.24 kcal. mole^{-1}

<div align="center">

Table II

Results of ZrD_2 Combustion Experiments
</div>

1.	m', g.	1.0839	1.1147	1.1058	1.1043
2.	Δt_c, deg.	0.99121	1.01975	1.00978	1.00910
3.	$\varepsilon(calor.)(-\Delta t_c)$, cal.	−3547.53	−3649.68	−3613.99	−3611.56
4.	$\Delta E_{contents}$, cal.	−6.72	−6.92	−6.85	−6.84
5.	$\Delta E_{ignition}$, cal.	2.83	2.83	2.82	2.83
6.	ΔE_{cor}, cal.	−1.78	−1.01	−1.71	−2.65
7.	ΔE_{Mylar}, cal.	245.38	248.66	248.66	251.95
8.	ΔE_{cotton}, cal.	5.87	5.55	5.75	5.99
9.	$\Delta E_c^0/M$, cal. g.$^{-1}$	−3046.36	−3050.66	−3043.34	−3042.91

10. Av. $\Delta E_c^0/M$, = −3045.82 ± 1.79 cal. g.$^{-1}$
11. Energy cor. for impurities = −7.49 ± 0.66 cal. g.$^{-1}$
12. $\Delta E_c^0/M$ (ZrD_2) = −3053.31 ± 1.91 cal. g.$^{-1}$
13. ΔE_c^0 (ZrD_2) = −290.80 ± 0.18 kcal. mole^{-1}

cal. g.$^{-1}$ of Mylar (this value was obtained from five combustion experiments and compares with the value of −5476.1 cal. g.$^{-1}$ of Mylar obtained by Good and co-workers[7]); (8) ΔE_{cotton}, the energy associated with the combustion of the cotton fuse, based on a value of −4050 cal. g.$^{-1}$ of cotton obtained in this Laboratory; (9) $\Delta E_c^0/M$, the standard energy of combustion per gram of sample when reacted according to eq. 1 or 2 ($\Delta E_c^0/M$ is the sum of items 3 through 8 divided by the mass of the sample); (10) Av. $\Delta E_c^0/M$, the average standard energy of combustion per gram of sample; (11) the energy correction per gram of sample for impurities described in the next paragraph; (12) $\Delta E_c^0/M(ZrH_2)$ and $\Delta E_c^0/M(ZrD_2)$, the standard energy of combustion per gram for pure ZrH_2 or ZrD_2; (13) $\Delta E_c^0(ZrH_2)$ and ΔE_c^0 (ZrD_2), the standard energy of combustion per mole of ZrH_2 and ZrD_2. The uncertainties given with items 10–13 are expressed as standard deviations.

The thermal corrections for impurities in the samples were made by assuming the impurities to be present as follows: Magnesium as MgO; copper, iron, and lead as elements; nitrogen as ZrN; carbon as ZrC; hydrogen in ZrD_2 as ZrH_2; and oxygen as ZrO_2. Oxygen is the major impurity. It requires the addition of a 0.22% correction to the heat evolved in a combustion. The assumption that the oxygen is present as ZrO_2 is consistent with the results of some combustion experiments made by us using samples of considerably higher oxygen content than the samples used in the presently reported series. This assumption is also in accord with the discussion of Martin and Rees[3c] on the zirconium–hydrogen system. The amount of ZrO_2 present in our samples is too small to be detected by X-ray analysis. The correction for all the other impurities amounts to 0.03% of the heat evolved.

Derived Results.—The values of some thermodynamic functions which were derived from available data are presented in Table III.

<div align="center">

Table III

Derived Thermodynamic Functions
</div>

	T, °K.	ZrH_2	ZrD_2
ΔH_c^0, kcal. mole^{-1}	298.15	−290.92 ± 0.24	−291.69 ± 0.18
ΔH_f^0, kcal. mole^{-1}	298.15	−38.90 ± .31	−40.22 ± .27
ΔS_f^0, cal. deg.$^{-1}$ mole^{-1}	298.15	−32.13 ± .04	−34.75 ± .04
ΔG_f^0, kcal. mole^{-1}	298.15	−29.32 ± .31	−29.86 ± .27
ΔH_f^0, kcal. mole^{-1}	0	−36.85 ± .31	−38.33 ± .27

The relationship $\Delta H_c^0 = \Delta E_c^0 + \Delta nRT$ is used to change from a constant volume process to a constant pressure process. The value of the term ΔnRT amounted to −0.89 kcal. mole^{-1} for the combustion of either ZrH_2 or ZrD_2. The value −261.5 ± 0.2 kcal. mole^{-1} was used for the enthalpy of formation of ZrO_2.[11] The enthalpy of formation of H_2O[12] and D_2O[12] were taken as −68.3174 kcal. mole^{-1} and −70.4133 kcal. mole^{-1}, respectively. ΔS_f^0 is the entropy of formation. The entropies, S^0 at 298.15°K. of Zr,[13] H_2,[14] ZrH_2,[5] D_2,[14] and ZrD_2[5] were taken as 9.292, 31.209, 8.374, 34.622, and 9.168 cal. deg.$^{-1}$ mole^{-1}, respectively. The data given in ref. 5, 13, and 14 were used to calculate the enthalpies of formation at 0°K.

The difference, ΔH_f^0 (ZrH_2) − ΔH_f^0 (ZrD_2), at 298.15°K. has been reported by Flotow and Osborne[5] to be 1.01 ± 0.08 kcal. mole^{-1}. This difference cal-

(11) G. L. Humphrey, J. Am. Chem. Soc., **76**, 978 (1954).

(12) "Selected Values of Chemical Thermodynamic Properties," National Bureau of Standards Circular 500, U. S. Government Printing Office, Washington, D. C., 1952.

(13) G. B. Skinner and H. L. Johnston, J. Am. Chem. Soc., **73**, 4549 (1951).

(14) H. W. Woolley, R. B. Scott, and F. G. Brickwedde, J. Res. Natl. Bur. Std., **41**, 379 (1948).

culated from Table III is 1.32 ± 0.29 kcal. mole^{-1}; the limit of error is the standard deviation based upon the scatter of the experimental data given in Tables I and II as item 10. The two values agree within the limits of the errors.

THE SURFACE CHEMISTRY OF CONDENSATION NUCLEI. I. THE SINTERING OF SILVER IODIDE

By M. L. CORRIN AND NANCY S. STORM

Department of Chemistry, University of Arizona, Tucson, Arizona

Several methods for the preparation of finely divided reasonably pure silver iodide were investigated. The most satisfactory involved the solution of precipitated AgI in liquid ammonia and the removal of the ammonia under anhydrous conditions. Specific surface areas on the order of 0.6 m.^{2}/g. thus were obtained. The surface area was found to decrease slowly with time at room temperature. The area was reduced by a factor of 30 on gentle grinding. All samples investigated were contaminated to some extent with ammonium nitrate. The rate of change of surface area with time at 77, 100, and 125° was determined. The rate data could be fitted to a second-order rate equation if it were assumed that only 62% of the surface was involved in the sintering process. Activation energy for the sintering process was on the order of 16 kcal./mole. The extreme lability of the AgI surface is pointed out.

Introduction

For some time silver iodide has been the focus of considerable attention as an efficient nucleating material for the formation of ice from supercooled water vapor. Although silver iodide was originally selected on the basis of an epitactic argument,[1] *i.e.*, the close similarity of its lattice parameters to those of ice, there is presently considerable question regarding the actual mechanism by which silver iodide, or other solid nucleant, acts. Presumably the surface properties of the nucleant must be of major importance since it is the interaction between the surface of the nucleant and the surrounding vapor which leads eventually to the formation of the new phase.[2-4]

We have begun a systematic study of the surface properties of those solids which serve as ice nucleants and of the interaction between the surface of the nucleant and water vapor. The items reported in this investigation deal with the preparation of finely divided silver iodide and with the stability of the silver iodide surfaces thus prepared. The stability has been measured in terms of the specific surface area and its variation with time and temperature.

Experimental

Preparation of AgI. Precipitation from Dilute Aqueous Solution.—The optimum ion concentration for the coagulation of a silver iodide hydrosol has been shown to be 0.142 molar.[5] In accordance with this value, silver iodide was prepared by the dropwise addition of a 0.284 M solution of potassium iodide to a 0.284 M solution of silver nitrate to the stoichiometric end point. The rate of addition was about 20 ml./min.; the mixture was maintained at the boiling point and stirred vigorously during the addition. The resulting precipitate was washed with hot water until the washings were free of nitrate ion; all manipulations were carried out under a red safelight. The specific surface area of the material thus prepared as determined by the application

of the BET relation to the adsorption of krypton at liquid nitrogen temperature was 0.5 m.^{2}/g.

Decomposition of Silver Iodate.—Attempts to prepare silver iodide of large specific surface area by the thermal decomposition of silver iodate were unsuccessful.

Precipitation from Concentrated Aqueous Solution.—It has been reported by Birstein[6] that silver iodide with a specific surface area of 12.5 m.^{2}/g. was prepared by precipitation from concentrated aqueous solution. Birstein's procedure was essentially duplicated by rapidly pouring together a solution containing 59.6 g. of NH$_4$I in 200 ml. of water and a solution containing 67.8 g. of AgNO$_3$ in 200 ml. of water. The precipitate was washed at room temperature until the wash water was free of nitrate ion. The specific surface area was found to be 0.9 m.^{2}/g. It was suspected that the prolonged exposure of the solid to water vapor during washing and drying may have led to particle growth and hence the relatively low surface area. The Birstein procedure was repeated with the addition of two washes with absolute ethanol and one wash with anhydrous diethyl ether. The solid was dried *in vacuo*. The surface area was again about 0.9 m.^{2}/g. Six batches of AgI on the order of 120 g. each were prepared in this manner. The specific surface areas ranged from 0.1 to 1.2 m.^{2}/g. The initial colors were varying shades of pale yellow. On exposure to light the resulting colors ranged from orange to black. It is obvious that these supposedly similar solids were quite different in surface properties.

Precipitation from a Nucleated Solution.—This method was essentially that described by Jaycock and Parfitt.[7] A nucleating solution was prepared by adding sufficient ethyl iodide to 200 ml. of AgNO$_3$ in ethanol to produce a solution initially one millimolar in silver and iodide ions. After aging this solution should contain about 10^{10} AgI nuclei per ml. The solution was allowed to stand for 20 min.; aqueous solutions of AgNO$_3$ and NH$_4$I then were added. The solid cake obtained on filtration was difficult to break up and the resulting low specific surface area of 0.1 m.^{2}/g. determined for the solid may have been due to the excessive manipulation of the solid rather than to the method of preparation.

The preparation of monodisperse AgI sols by precipitation from aqueous solutions under conditions of controlled nucleation has been discussed by Ottewill and Woodbridge[8] and by Edwards, Evans, and LaMer.[9] The latter workers also investigated the ice nucleating properties of their preparations. These methods, however, involve the use of fairly dilute systems and are not reasonably applicable to the preparation of finely divided AgI in the large quantity required for adsorption studies.

(1) B. Vonnegut, *Appl. Phys.*, **18**, 593 (1947).

(2) B. J. Mason, "The Physics of Clouds," The Clarendon Press, Oxford, 1957.

(3) A. C. Zettlemoyer, N. Tcheurekdjiian, and J. J. Chessick, *Nature*, **192**, 653 (1961).

(4) P. G. Hall and F. C. Tompkins, *Trans. Faraday Soc.*, **58**, 1734 (1962).

(5) H. A. Laitinen, "Chemical Analysis," McGraw-Hill Book Co., New York. N. Y., 1960.

(6) S. J. Birstein, *J. Meteorol.*, **12**, 324 (1955).

(7) M. J. Jaycock and G. D. Parfitt, *Trans. Faraday Soc.*, **57**, 791 (1961).

(8) R. H. Ottewill and R. F. Woodbridge, *J. Colloid Sci.*, **16**, 581 (1961).

(9) G. R. Edwards, L. F. Evans, and V. K. LaMer, *ibid.*, **17**, 749 (1962).
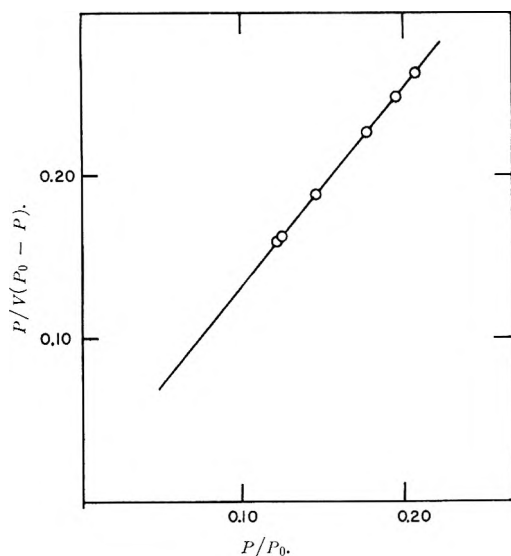
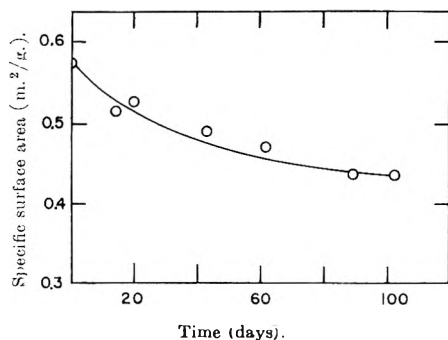Fig. 1.—BET plot for the adsorption of krypton on standard anatase at 76.9°K.

Fig. 2.—The specific surface area of AgI as a function of time of storage at room temperature.

Precipitation from Liquid Ammonia.—It has been shown by Coulter and Candela[10] that AgI may be obtained in relatively finely divided form by decomposition of the complex formed by AgI in liquid ammonia. We have found that if the complex is decomposed by removal of the liquid ammonia in the absence of water vapor, a finely divided solid is obtained directly. In the presence of water vapor (e.g., the use of a water aspirator to remove the ammonia) a lump of solid is obtained. Two hundred grams of AgI prepared by precipitation from aqueous solution was dissolved in 150 ml. of liquid ammonia previously dried over metallic sodium. The ammonia was removed by distillation into a bath held at liquid nitrogen temperature. The solid was brought to room temperature under fore-pump vacuum. When the white complex had completely decomposed, the yellow AgI was obtained largely in the form of a fine powder. Two hundred grams of AgI prepared in this manner were used for the sintering studies described below.

It has been shown by Biltz and Stollenwerk[11] that the equilibrium pressure of ammonia over the most stable AgI ammonia complex (AgI·0.5NH$_3$) is on the order of 30 mm. at 20°. Since the samples of AgI which we employed in our adsorption studies maintained a pressure of less than 1×10^{-4} mm. for at least 3 hr. after pump-out, it is quite obvious we were not dealing with the complex. X-Ray diffraction studies indicated the material prepared from liquid ammonia solution was silver iodide with a complex fault structure. These X-ray diffraction results will be discussed elsewhere.

Effect of Grinding on Surface Area.—The material used was prepared by precipitation from aqueous solution. The sample used as control had a specific surface area of approximately 1 m.^{2}/g. A second sample was placed on a watch glass and a second watch glass placed over the first was rotated gently. This second sample possessed a specific surface area after such gentle grinding of less than 0.03 m.^{2}/g.

Contamination.—When AgI prepared by precipitation from aqueous solution was heated to temperatures exceeding 50° in vacuo on the order of 1×10^{-5} mm., a white sublimate collected in the cold portion of the system. This material was identified by spot tests as ammonium nitrate. The amount of sublimate varied from sample to sample and was observed with material prepared by means of the liquid ammonia treatment. Thus even though the wash water in the AgI preparation was free of nitrate ion, the precipitated AgI contained this ion as a contaminant. Some doubt thus arises as to the validity of measurements made of the adsorption of water vapor on AgI prepared by precipitation from aqueous solution. The existence of a hygroscopic impurity in their material was suspected by Coulter and Candela.[10]

Determination of Surface Area.—Specific surface areas were calculated by the method of Brunauer, Emmett, and Teller[12] from krypton adsorption data determined at liquid nitrogen temperature. The adsorption system employed was conventional; samples were metered out with a doser and pressures measured with a McLeod gage and a cathetometer. At the pressures involved thermal transpiration corrections are negligible. Krypton and helium used for dead space determinations were obtained in sealed glass bulbs. The adsorption bulb was wrapped in black plastic tape to minimize the effect of light on the AgI.

There has been some question in the literature with regard to the proper saturation pressure and area per molecule in the monolayer to be used with krypton.[13-17] Consequently we calibrated the krypton technic by determining adsorption isotherms on a sample of anatase of known area.[18]

The vapor pressure of solid krypton in the liquid nitrogen bath was measured as 1.62 mm. This, according to Freeman and Halsey,[19] corresponds to a temperature of 76.9°K. (The atmospheric pressure over the liquid nitrogen bath was on the order of 710 mm.) From the equations of Freeman and Halsey the vapor pressure of supercooled liquid krypton at 76.9°K. may be calculated as 3.09 mm. A krypton adsorption isotherm at 76.9°K. was measured on the Harkins and Jura standard anatase (specific surface area of 13.8 m.^{2}/g.); the BET plot for this isotherm is given in Fig. 1 with $p_0 = 3.08$ mm. From the BET monolayer capacity, the area occupied per krypton molecule in the monolayer was calculated as 18.2 Å.^{2}. This value was employed in all further calculations.

Treatment of Samples.—The adsorption bulb employed was cylindrical in form. In all temperature runs a zero time isotherm and surface area were measured. The various samples were heated in a 1-l. silicone oil bath controlled to ±2° by a thermoregulator; magnetic stirring was employed. Temperatures were measured with a mercury in glass thermometer checked at the ice point. Time intervals were measured from the time the bath was placed about the sample tube and the time the bath was removed. The bulb was allowed to cool in air.

In one run the AgI was exposed during heating to water vapor supplied from a reservoir of the liquid maintained at 0°. The sample was then dried for at least 48 hr. at room temperature and in vacuo before the isotherm leading to the surface area was measured.

Results and Discussion

It was found impossible to prepare samples of reproducible surface properties by the precipitation of AgI from aqueous solution. The maximum surface area obtained by such precipitation was 2 m.^{2}/g. The surface areas of the various preparations differed widely. The use of liquid ammonia as a solvent allowed the reproducible preparation of AgI samples with surface areas of approximately 0.6 m.^{2}/g. All samples prepared from AgNO$_3$ and NH$_4$I were contaminated with NH$_4$NO$_3$.

The finely divided AgI proved very sensitive to han-

(10) L. V. Coulter and G. A. Candela, *Z. Elektrochem.*, **56**, 449 (1952).

(11) W. Biltz and W. Stollenwerk, *Z. anorg. allgem. Chem.*, **114**, 174 (1920).

(12) S. Brunauer, P. H. Emmett, and E. Teller, *J. Am. Chem. Soc.*, **60**, 309 (1938).

(13) R. A. Beebe, J. B. Beckwith, and J. M. Honig, *ibid.*, **67**, 1554 (1945).

(14) P. J. Malden and J. D. F. Marsh, *J. Phys. Chem.*, **63**, 1309 (1959).

(15) G. L. Gaines, Jr., and P. Cannon, *ibid.*, **64**, 997 (1960).

(16) P. Cannon and G. L. Gaines, Jr., *Nature*, **190**, 340 (1961).

(17) J. M. Haynes, *J. Phys. Chem.*, **66**, 182 (1962).

(18) W. D. Harkins and G. Jura, *J. Am. Chem. Soc.*, **66**, 1362 (1944).

(19) M. P. Freeman and G. D. Halsey, *J. Phys. Chem.*, **60**, 1121 (1956).

dling in terms of its surface area. Simple grinding between two watch glasses resulted in a loss in surface area from 1.0 to 0.03 m.^{2}/g. This effect is not due to pressure alone. When a sample of AgI was stored for 26 days under a weight equivalent to a pressure of 0.1 atmospheres the surface area decreased by only 11%.

The specific surface area was found to decrease slightly with time during storage. Over a period of ninety days the area decreased from 0.57$_6$ to 0.43$_7$ m.^{2}/g. A plot of specific surface area vs. time of storage is given in Fig. 2. This is another measure of the instability of the AgI surface.

The change in specific surface area with respect to time at 55, 77, 100, and 125° is illustrated in Fig. 3. The reproducibility of sintering runs as well as the effect of water vapor during the run is indicated in Fig. 4 for 100°. Heating in the presence of 4.58 mm. of water vapor at 100° does not affect the sintering rate of AgI.

Our results may be tentatively explained on the following basis. It is obvious that the plots of specific surface area vs. time level off and do not approach zero surface area at infinite time. Therefore we assume that only a portion of the surface is involved in the sintering process while the remainder is inactive; we designate that portion which sinters as the active portion of the surface. Thus $S_a = S(1 - b)$ in which b represents the inactive fraction of the surface area. The specific surface areas at the various temperatures as a function of time of heating are given within ±2% by a relation of the form

$$dS_a/dt = -kS_a{}^2$$

i.e., in effect a second-order rate equation in active surface area. The best fit of this equation to the observed data is obtained if b is set equal to 0.38 for runs at 125, 100, and 77°. No attempt was made to fit the data obtained at 55° since the change in surface area with time was small. The following rate constants were obtained

Temp. (°C.)	K, specific rate constant, g. hr./m.^{2}
77	0.12$_5$
100	0.54$_0$
125	2.0$_9$

The activation energy for the sintering process calculated from the values of k at 125 and 100° is 16.$_0$ kcal. while that calculated from the constants at 100 and 77°
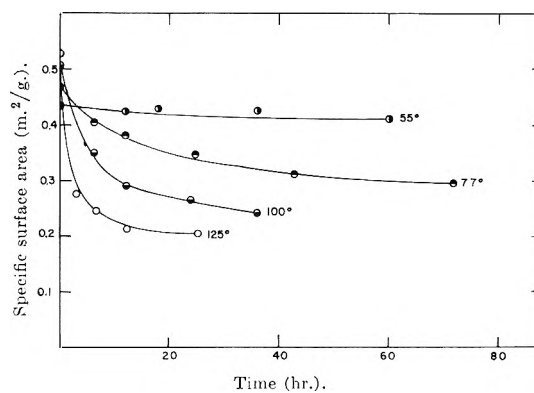

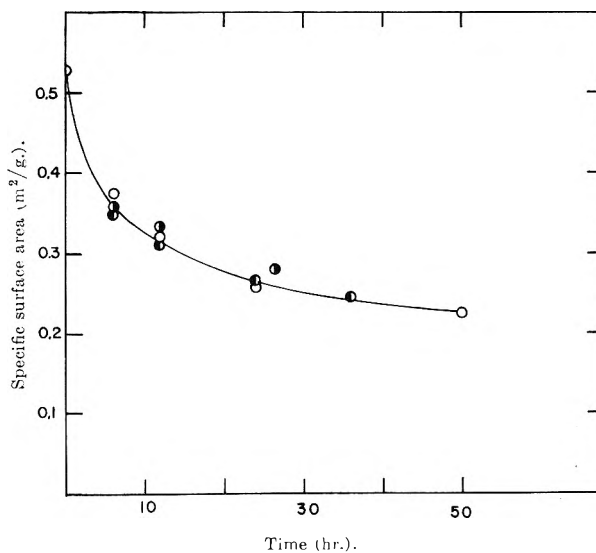Fig. 3.—The specific surface area of AgI as a function of time of heating at 55, 77, 100, and 125°.

Fig. 4.—The effect of water vapor on the sintering of AgI at 100°: O, 4.58 mm. of H$_2$O.

is 16.$_6$ kcal. This activation energy is quite small for processes involving solid phase reactions and serves, in some sense, to explain the great lability of the AgI surface. The second-order rate equation also indicates that the sintering occurs by the fusion of particles rather than by particle growth

THE SEPARATION OF HYDROGEN, HYDROGEN DEUTERIDE, TRITIUM HYDRIDE, DEUTERIUM, TRITIUM DEUTERIDE, AND TRITIUM MIXTURES BY GAS CHROMATOGRAPHY

By Edward H. Carter, Jr., and Hilton A. Smith

Department of Chemistry, The University of Tennessee, Knoxville, Tennessee

The resolution and analysis of the components in hydrogen–deuterium–tritium mixtures have been accomplished by gas chromatography at 77°K. Tritium was incorporated into the sample mixtures in tracer quantities ($N_{T_2} = 10^{-4}$, 2×10^{-1} mc. per standard ml.). Helium, hydrogen, and neon were employed as carrier gases with several columns containing activated alumina and ferric oxide on alumina. Varying degrees of isotope separation were observed with different carriers, adsorbents, and conditions of column activation. Separation factors for the hydrogen isotopes and isomers on various columns at 77°K. were calculated. Flow-modified ionization chambers and a Cary Model 31 vibrating reed electrometer equipped with a 10^{10} (or 10^{11}) ohm leak resistor were employed in series with thermistor-equipped katharometers for the detection of radioactive and non-radioactive hydrogen isotopes. Outputs from the electrometer and the katharometer were recorded simultaneously on two synchronized Brown electronic recorders. Simultaneous ionization chamber and katharometer detection of para-hydrogen, ortho-hydrogen, hydrogen deuteride, and deuterium has been observed.

In recent years various degrees of separation and analysis of hydrogen isotopes and isomers by gas chromatography have been reported.[1-11] These investigations, in general, have concentrated on the resolution of para-hydrogen, ortho-hydrogen, hydrogen deuteride, para-deuterium, and ortho-deuterium, or normal hydrogen, hydrogen deuteride, and normal deuterium without the inclusion of the radioactive hydrogen isotopes in the gas mixtures.

Gant and Yang[12] have reported the resolution of hydrogen, tritium hydride, and tritium in gas mixtures containing approximately 1 atom per cent tritium on a molecular-sieve column at $-161°$ with helium carrier. Smith and Carter[13] have extended the resolution and analysis to mixtures containing tritium in tracer quantities (mole fraction $T_2 = 10^{-4}$) on several columns with helium and hydrogen carriers at 77°K.

With some modifications in previous techniques[13] and equipment, the resolution and analysis of gas samples containing all of the various hydrogen isotopes and isomers, where tritium-containing components were present at tracer levels, have been effected.

Experimental

Apparatus and Materials.—The essential features of the chromatographic and detector systems employed were as follows: The carrier gas from a tank was passed through a sampling system as shown in Fig. 1, thence through the chromatographic column followed immediately by a thermostated (25°) katharometer, similar to that described by Thomas,[14] and a 50-ml. Borkowski ionization chamber, or interchangeable 5-ml. brass chamber, attached to a Cary Model 31 vibrating reed electrometer obtained from the Applied Physics Corporation, Monrovia,

(1) C. O. Thomas and H. A. Smith, *J. Phys. Chem.*, **63**, 427 (1959).

(2) H. A. Smith and P. P. Hunt, *ibid.*, **64**, 383 (1960).

(3) P. P. Hunt and H. A. Smith, *ibid.*, **65**, 87 (1961).

(4) W. R. Moore and H. R. Ward, *J. Am. Chem. Soc.*, **80**, 2909 (1958).

(5) W. A. Van Hook and P. H. Emmett, *J. Phys. Chem.*, **64**, 673 (1960).

(6) S. Ohkoshi, Y. Fujita, and T. Kwan, *Bull. Chem. Soc. Japan*, **31**, 770 (1958); S. Ohkoshi, S. Tenma, Y. Fujita, and T. Kwan, *ibid.*, **31**, 772 (1958); S. Ohkoshi, S. Tenma, Y. Fujita, and T. Kwan, *ibid.*, **31**, 773 (1958).

(7) W. R. Moore and H. R. Ward, *J. Phys. Chem.*, **64**, 832 (1960).

(8) T. Kwan, *J. Res. Inst. Catalysis Japan*, **8**, 18 (1960).

(9) S. Furuyama and T. Kwan, *J. Phys. Chem.*, **65**, 190 (1961).

(10) F. Botter, G. Perriere, and S. Tistchenko, *Comm. Energie At.* (France), *Rappt.*, CEA No. 1962 (1961).

(11) L. Bachmann, E. Bechtold, and E. Cremer, *J. Catalysis*, **1**, 113 (1962).

(12) P. L. Gant and K. Yang, *Science*, **129**, 1548 (1959).

(13) H. A. Smith and E. H. Carter, Jr., "Proceedings of the International Atomic Energy Agency Symposium on the Use of Tritium in the Physical and Biological Sciences," Vol. I, Vienna, Austria, 1962, pp. 121–133.

(14) C. O. Thomas, *J. Chem. Educ.*, **36**, 527 (1959).

California; thence through a flowmeter followed by an oxidizing unit to convert any hydrogen to water vapor and finally through a trap containing Linde Molecular Sieves (size 5A) at Dry Ice–acetone temperature. The katharometer and electrometer outputs were connected to synchronized Brown recording potentiometers. A leak resistor of 10^{10} (or 10^{11}) ohms was installed in the electrometer head between the input terminal and the feedback line, thus allowing the use of a flow system for continuous monitoring of tritium activity emerging from the column.

The reservoirs attached to the sample by-pass cell, as shown in Fig. 1, were used for the preparation of equilibrating or equilibrated mixtures of hydrogen–deuterium–hydrogen deuteride, hydrogen–tritium–tritium hydride, and deuterium–tritium–tritium deuteride. They consisted of 100-ml. glass bulbs carrying two tungsten leads which were brazed to coiled nichrome wire heating elements for isotope exchange equilibration. Various sample mixtures from these reservoirs were injected, at known pressure and volume, into the chromatographic column by diversion of the carrier gas stream through the sample by-pass cell.

The tritium content of one-curie ampoules[13] of tritium containing 0.89 ml. of tritium at 475 mm. pressure was expanded into evacuated metal cylinders of known volume and diluted with hydrogen, deuterium, helium, or neon to the desired tritium activity per standard ml. of gas (0.20–0.25 mc.) for use in the chromatographic experiments. The original mole ratios of tritium to diluent in these gas mixtures were in the range 1.0–1.3×10^{-4}. However, since slow exchange of tritium–hydrogen and tritium–deuterium occurred in the metal reserve tanks, this figure, when corrected for radioactive decay, actually represented one-half the tritium hydride or tritium deuteride mole fraction plus the tritium mole fraction present at any time.

The following procedure, similar to that of Moore and Ward,[7] was used to prepare the ferric oxide on alumina columns: An 80–100 mesh cut of Grade F-20 activated alumina, obtained from the Aluminum Company of America, weighing 250 g. was covered with 400 ml. of a 2 M solution of ferric chloride in a 1-l. erlenmeyer flask. Stirring was carried out intermittently to allow adequate penetration of the alumina by the ferric chloride solution. After a 15-min. stirring period, 3 M aqueous ammonia was added to the slurry until ferric hydroxide precipitation was complete. Stirring was continued during this precipitation. The suspended material was then stirred thoroughly over a 1-hr. period and filtered. The ferric hydroxide precipitate adhered to, or coated, the alumina in this process. The filtered material was then washed several times with distilled water, transferred to an evaporating dish, and placed in a preheated oven at 120° for 24 hr. The dried material was then crushed, rescreened to 80–100 mesh, and used to pack several 7-mm. diameter Pyrex-coiled columns of various lengths for use in the chromatography experiments. These columns were equipped with small standard-taper ball and socket joints for attachment to the apparatus.

The uncoated activated alumina columns were prepared by packing various lengths of 7-mm. diameter Pyrex coils with 80–100 mesh, Grade F-20, activated alumina.

Each column, after installation into the chromatography

apparatus, was cooled to liquid nitrogen temperature ($77 \pm 1\,°K.$) in a 2-l. or 1-l. dewar flask for the elution experiments.

Helium, hydrogen, and neon were employed as carrier gases. Helium, hydrogen, and deuterium have only slightly different thermal conductivities. This property necessitated operation of the katharometer circuit at very high sensitivity for adequate detection of these gases in the presence of excess helium, or preliminary sample oxidation to water vapor prior to detection in the katharometer. For samples containing tritium activity, preliminary oxidation resulted in considerable loss in ionization chamber sensitivity to this activity, in comparison with unoxidized gas-phase detection, and produced considerable elution peak tailing for radioactive tritium components. Therefore unoxidized gas-phase detection of the isotopes was employed and adequate sensitivity to non-radioactive isotopes obtained by high-sensitivity operation of the katharometer circuit.

Helium in a high state of purity was obtained from the Medical Gas Division of Welding Gas Products Company, Knoxville, Tennessee, and was used with and without purification with no resultant change in characteristic hydrogen and deuterium chromatograms. Purification was attempted by passage of the helium through a Linde Molecular Sieve (5A) trap cooled to $77\,°K.$

Neon produces greater sensitivity to hydrogen and deuterium detection by change in thermal conductivity than does helium and can be employed as a carrier gas at liquid nitrogen temperature. Research grade neon was obtained in a high state of purity from the Matheson Company, East Rutherford, New Jersey, and was used without further purification.

Hydrogen was also used as a carrier gas. The hydrogen employed was obtained from Welding Gas Products Company, Knoxville, Tennessee, and was used with and without purification with no resultant change in characteristic deuterium chromatograms. Purification was identical to that employed with helium. Deuterium reported to be 99.5% pure was obtained from General Dynamics Corporation, San Carlos, California.

Experimental Results and Conclusions

Activated Alumina Columns.—With an 8-ft. activated alumina column varying degrees of column activity (dehydration) had a marked effect on the retention times and resolution of hydrogen isotopes. This effect is shown in Fig. 2 for the resolution of the radioactive hydrogen isotopes. As can be seen from an examination of the figure, a progressive increase in activation or dehydration produced an increase in the isotope separation. The method of column activation was unimportant but the final state of activation (extent of water removal) was extremely important and exhibited an upper limit beyond which isotope retention times became prolonged and considerable band broadening was observed even with marked increase in carrier flow rate. Similar degrees of column activity to that given for part C of Fig. 2 were obtained by column activation at $370°$ for a period of 8 hr. under a low helium flow rate.

Under the latter conditions of column activation, the alumina column was found to be effective in the resolution of hydrogen, tritium hydride, deuterium, tritium deuteride, and tritium, as shown in Fig. 3, with only partial equilibration of para-hydrogen and ortho-hydrogen observed at the high column activity. The partial $p\text{-}H_2 \rightleftarrows o\text{-}H_2$ interconversion was evidenced on alumina columns which had been extensively dehydrated. This phenomenon has been reported previously by Moore and Ward[7] and good agreement was found here.

An interesting feature of the electrometer recorder traces for samples similar to that shown in Fig. 3 was evidenced upon conversion from the small-volume (5-ml.) ion chamber to the larger-volume (50-ml.) Borkowski chamber. A somewhat elevated background ion current was exhibited by this chamber partly due to
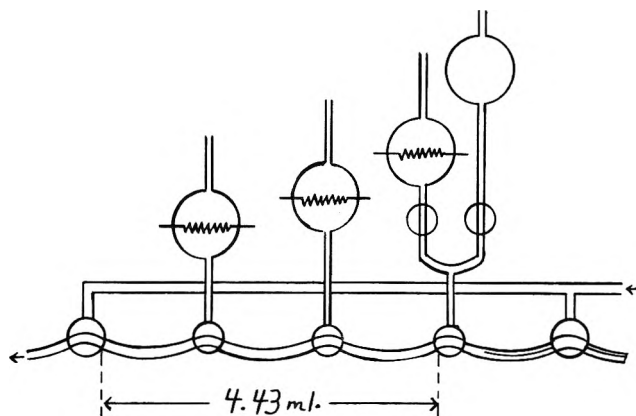

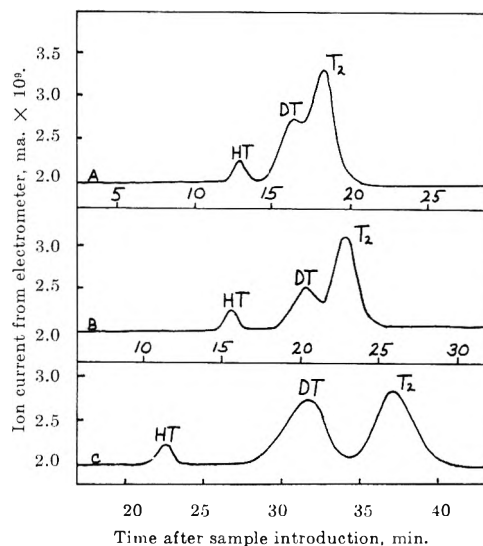
Fig. 1.—Chromatographic sample by-pass cell.

Fig. 2.—Typical electrometer recorder traces for $H_2 + T_2 \rightleftarrows 2HT$ and $D_2 + T_2 \rightleftarrows 2DT$ samples showing the effect of varying degrees of column activation on retention times and resolution of active components on the 8-ft. alumina column with helium carrier at $77\,°K.$ Ion chamber, 5 ml., polarizing potential, -135 v. Column activation prior to samples: (A) heated column in air to $138°$ for 48 hr. after complete deactivation with H_2O, then heated at $200°$ for 3 hr. under vacuum; (B) part A, then heated in a gas–air flame under vacuum for 5 min.; (C) parts A and B, then heated in gas–air flame under vacuum for 10 min.
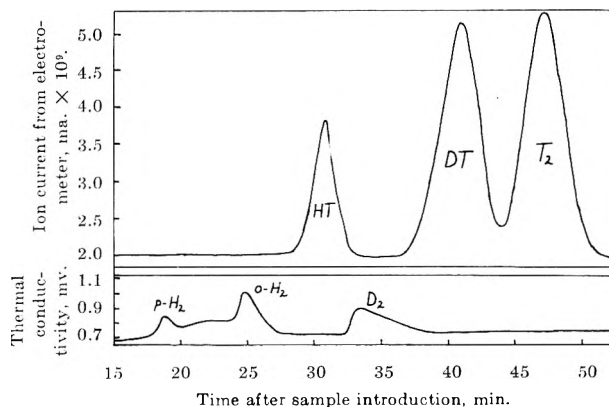

Fig. 3.—Typical synchronized electrometer and katharometer recorder traces for $H_2 + T_2 \rightleftarrows 2HT$ (0.68 std. ml.) and $D_2 + T_2 \rightleftarrows 2DT$ (0.83 std. ml.) sample mixtures with neon carrier at a flow rate of 65 ml. per min. through 8-ft. activated alumina column at $77\,°K.$ Ion chamber, 5 ml., polarizing potential, -135 v. Column activation prior to sample—part C of Fig. 2.

its inherently greater sensitivity to small residual ion currents and also to a pretreatment procedure with a neon–tritium sample having an activity of 2.45×10^{-1}
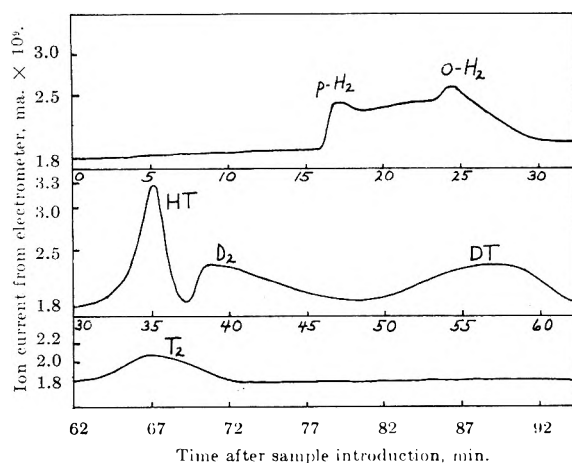
Fig. 4.—Typical electrometer recorder trace for H₂–HT–D₂–DT–T₂ sample mixture (5.23 std. ml.) with helium carrier at a flow rate of 100 ml./min. through an 8-ft. activated (370°, 8 hr.) alumina column at 77°K. Ion chamber, 50 ml., polarizing potential, −135 v.

mc. per standard ml. Under these conditions resolution of hydrogen, tritium hydride, deuterium, tritium deuteride, and tritium was evidenced and adequate detection of both radioactive and non-radioactive hydrogen isotopes was observed with the ion chamber and electrometer as shown in Fig. 4. The small-volume chamber did not exhibit this property.

Hydrogen and deuterium detection sensitivity on the electrometer has been investigated and seems to be a function of the background activity level in the ion chamber. The higher the background ion current, up to a maximum of about 1×10^{-11} amp., the greater was this detection sensitivity. However, no appreciable difference in hydrogen and deuterium detection was observed for equivalent samples eluted at various background levels in the range 10^{-12} to 10^{-11} amp. At backgrounds below 10^{-12} or 10^{-13} amp. this sensitivity decreased. These measurements, of course, were observed at a fixed electrometer sensitivity. At higher electrometer sensitivities adequate detection of hydrogen and/or deuterium elution was obtained even at residual ion current levels as low as 10^{-13} amp. For a given electrometer setting this detection characteristic was reduced considerably by prolonged evacuation and heating of the ion chamber. This procedure, applied over a 24-hr. period, reduced the residual ion current in the chamber to about 10^{-15} amp. With the small-volume chamber this detection did not occur appreciably, though it could be induced slightly with high background activities (200–400 μc. C¹⁴ in the form of labeled nonadecanoic acid deposited on a copper plate attached to the inner wall of the chamber) and high ion-current sensitivities on the electrometer.

With hydrogen as the carrier gas, no detection of deuterium and/or hydrogen deuteride was observed on the electrometer. With neon carrier, ion-chamber elution of hydrogen and deuterium was indicated but at considerably decreased sensitivity to that observed with helium carrier. Adequate detection sensitivity to non-radioactive isotope elution by the 50-ml. chamber with helium carrier occurred in every instance where the residual ion current was $\geq 10^{-12}$ or $\leq 10^{-11}$ amp. Residual ion currents greater than 10^{-11} amp. were impractical since high electrometer sensitivities were necessitated for adequate detection of the tritium concentra-

tions employed, and conversely low electrometer sensitivities were necessary for maintenance of a sufficient electrometer bias range at high background currents. These conditions, therefore, limited the residual ion-current elevation.

No relationship between polarizing potential applied to the chamber and electrometer sensitivity to hydrogen and deuterium detection was observed, as long as this potential was maintained in the ionization chamber region (0–500 v.).

A direct quantitative relationship between hydrogen and deuterium pressure, at fixed volume, and electrometer response with the high-background 50-ml. chamber was also observed; that is, the magnitude of the shift in the charge rate ⇌ leak rate equilibrium position was found to be directly proportional to the hydrogen or deuterium concentration in the helium carrier.

To eliminate the possibility of a memory effect, a separate alumina column was prepared and pure hydrogen, deuterium, and hydrogen–deuterium chromatograms were obtained, identical to the hydrogen and deuterium bands shown in Fig. 4, prior to the exposure to any tritium activity.

There was a striking similarity between the properties of the 50-ml. ion chamber plus low specific background activity in conjunction with the vibrating reed electrometer and beta-ionization detectors of low volume plus high specific background activity employing helium as the carrier gas.[15,16] These beta-ionization detectors were of much lower volume (∼1 ml.) and employed a fixed beta source (Sr-90) of much higher specific activity than the tritium employed in the work. Less-sensitive electrometers were employed for ion-current amplification since residual ion currents were much greater. The Sr-90 beta source in these detectors provides beta particles of sufficient energy to excite carrier gas molecules to a metastable energy state, which upon collision with sample molecules release this energy through ion-pair formation. Commercial helium generally contains sufficient neon, as an impurity, to make it unsuitable for a carrier gas in such detectors, since transferal of energy by metastable helium to neon occurs thereby decreasing the probability of occurrence of energy transfer through ion-pair formation. This difficulty was partially overcome by decreasing the neon content of the helium carrier by passage through a trap containing silica gel at liquid nitrogen temperature prior to the detector. A similar purification occurred in this work since neon was more strongly adsorbed on the alumina columns at liquid nitrogen temperature than was helium. The 50-ml. ion chamber could thus have functioned as a beta detector with helium carrier through the presence of residually adsorbed tritium in the chamber.

With a 12-ft. alumina column, activated at 340° for 53 hr. under a low helium flow rate, helium failed to elute adequately the hydrogen isotopes at 77°K. With hydrogen carrier, however, adequate resolution of hydrogen deuteride, tritium hydride, deuterium, and tritium was observed as shown in Fig. 5. The addition of tritium deuteride to similar sample mixtures resulted in considerable overlap of the deuterium, tritium deuteride, and tritium bands as shown in Fig. 6. These results in-

(15) R. V. Parish and W. H. Parsons, Chem. Ind. (London), 1951 (1961).
(16) J. Serpinet, Anal. Chim. Acta. 25, 505 (1961).

dicated that longer and more highly activated alumina columns were adequate for the resolution of isotope mixtures with hydrogen carrier which did not contain tritium deuteride. In such instances where complete resolution of isotopes is not necessary, adequate detection of the five remaining isotopes of hydrogen can be observed. Increased column length and similar conditions of activation were found to improve the tritium deuteride–tritium resolution. However, pronounced improvement was not evidenced for appreciable increases in column length.

Ferric Oxide on Alumina Columns.—With three ferric oxide on alumina columns containing 20% by weight ferric oxide in series and having a total length of 19 ft., adequate resolution of all the hydrogen isotopes was observed with helium carrier at 77°K. A typical synchronized electrometer and katharometer recorder trace for a sample mixture of the hydrogen isotopes is shown in Fig. 7.

Preliminary deactivation and partial reactivation of the column was necessary in order to obtain optimum isotope resolution. This procedure consisted of column deactivation by filling with distilled water followed by reactivation at 145° for a period of 8–12 hr. under a low helium flow rate. An alternative procedure for water removal, which proved equally effective, was to heat the column to 250° after deactivation for a period of 3 hr. under vacuum. The resolution of hydrogen isotopes under these conditions was such that fractional oxidation and collection of sample components could be effected. With these columns hydrogen was detected in a single band as normal hydrogen since the columns effectively catalyzed the interconversion of spin isomers. This column series also proved effective in the resolution and analysis of isotopes involved in separate equilibrating mixtures of H_2–T_2–HT, D_2–T_2–DT, and H_2–D_2–HD.

Activated Alumina–Ferric Oxide on Alumina Column Series.—Of concern in the resolution of hydrogen, hydrogen deuteride, and deuterium on alumina columns[5] and molecular sieve columns[8–10] has been the ever-existent overlap of the ortho-hydrogen and hydrogen deuteride bands. This overlap is, of course, eliminated by the presence of a paramagnetic material on the column[3,5] which rapidly catalyzes the interconversion of nuclear spin isomers and hence is not important in terms of resolution and analysis of hydrogen–hydrogen deuteride–deuterium mixtures. It would be of interest, however, to resolve para-hydrogen, ortho-hydrogen, hydrogen deuteride, and deuterium on a single chromatogram.

Recently, Furuyama and Kwan[9] suggested that this could be accomplished by the use of an alumina column and a paramagnetic-supported alumina column in series at 77°K. with helium carrier. Their reasoning was that leading para-hydrogen eluted from the alumina column should undergo rapid para $\rightleftarrows$ ortho interconversion during passage through the paramagnetic column and thus present a single band, and that trailing ortho-hydrogen from the alumina column should undergo a similar interconversion and also present a single band. Hence, if the first column was effective in the resolution of para-hydrogen, ortho-hydrogen plus hydrogen deuteride, and deuterium, and the second effective in the resolution of normal hydrogen, hydrogen deuteride, and deuterium, the column series
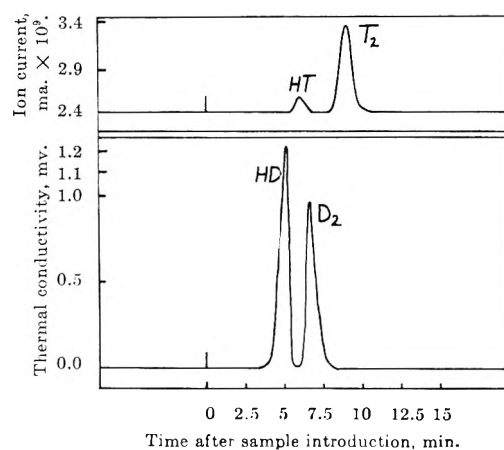

Fig. 5.—Typical synchronized electrometer and katharometer recorder traces for $H_2 + T_2 \rightleftarrows 2HT$ (0.28 std. ml.) and $H_2 + D_2 \rightleftarrows 2HD$ (1.84 std. ml.) sample mixtures with hydrogen carrier at a flow rate of 75 ml./min. through a 12-ft. activated (340°, 53 hr.) alumina column at 77°K. Ion chamber, 5 ml., polarizing potential, –135 v.
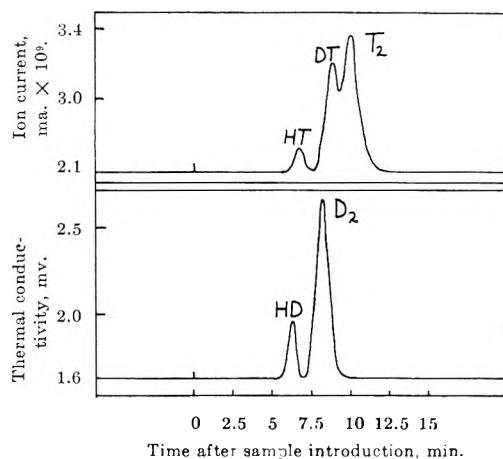

Fig. 6.—Typical synchronized electrometer and katharometer recorder traces for $H_2 + D_2 \rightleftarrows 2HD$ (3.38 std. ml.), $H_2 + T_2 \rightleftarrows 2HT$ (0.84 std. ml.), and $D_2 + T_2 \rightleftarrows 2DT$ (0.43 std. ml.) sample mixtures with hydrogen carrier at a flow rate of 65 ml. per minute through a 12-ft. activated (340°, 53 hr.) alumina column at 77°K. Ion chamber, 5 ml., polarizing potential, –135 v., 100 mv. full-scale sensitivity.

should resolve para-hydrogen, ortho-hydrogen, hydrogen deuteride, and deuterium. These investigators, however, failed to show a chromatogram for such a resolution.

Recent investigations in this Laboratory, as shown in Fig. 8, with a similar column series at 77°K., have shown that the resolution of para-hydrogen, ortho-hydrogen, hydrogen deuteride, and deuterium by this technique was difficult and incomplete due to the remaining overlap of the ortho-hydrogen and hydrogen deuteride bands. Even though the inclusion of hydrogen deuteride in the sample mixtures thus necessitates, at present, the use of paramagnetic-supported alumina for adequate resolution of hydrogen and hydrogen deuteride, further work was indicated with longer columns, since the reasoning about the feasibility of such columns in series for such a separation seems to be correct. Two bands (ortho-hydrogen and hydrogen deuteride) were definitely in evidence, as shown in Fig. 8, whereas with pure alumina only a single band occurs.

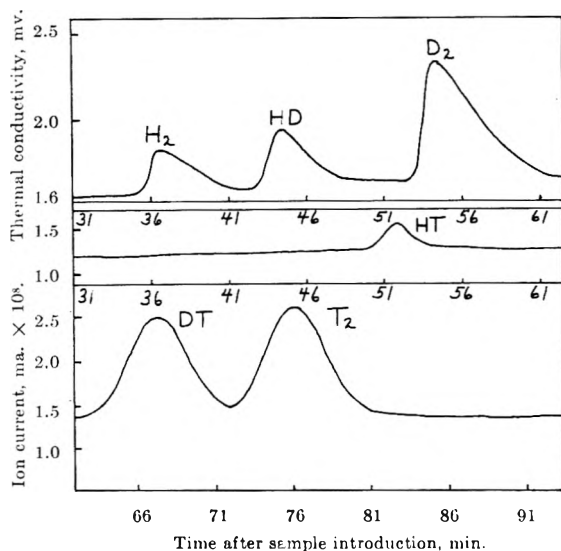**Separation Factors.**—Separation factors for various hydrogen isotopes and isomers on various columns at

Fig. 7.—Typical synchronized electrometer and katharometer recorder traces for $H_2 + D_2 \rightleftarrows 2HD$ (1.48 std. ml.), $H_2 + T_2 \rightleftarrows 2HT$ (1.20 std. ml.), and $D_2 + Y_2 \rightleftarrows 2DT$ (0.69 std. ml.) sample mixtures with helium carrier at a flow rate of 75 ml./min. through a series of partially deactivated ferric oxide on alumina columns, 19 ft. in length, at 77°K. Ion chamber, 50 ml., polarizing potential, -135 v., 1-v. full-scale sensitivity.
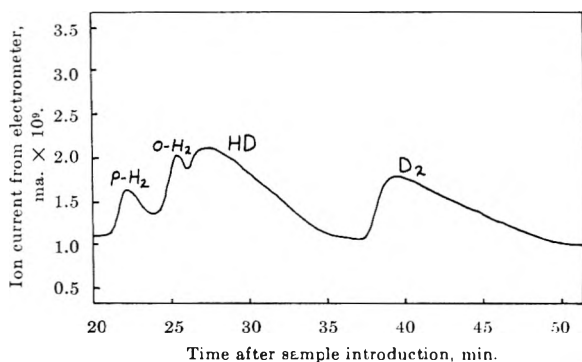

Fig. 8.—Typical electrometer recorder trace for $H_2 + D_2 \rightleftarrows 2HD$ sample (1.91 std. ml.) with helium carrier at a flow rate of 150 ml./min. through a 6-ft. activated (370°, 8 hr.) alumina column in series with an 8-ft. partially deactivated (water, 140°) ferric oxide on alumina column at 77°K. Ion chamber, 50 ml., polarizing potential, -135 v., 100-mv. full-scale sensitivity.

77°K. were calculated from sample chromatograms using the relationship[17]

$$\alpha_{1,2} = \frac{t_2 - t_0}{t_1 - t_0} \qquad (1)$$

where t_1 and t_2 are the retention times for the individual components, and t_0 is the retention time of a marker not adsorbed on the column.

Since both the electrometer and katharometer recorders had synchronized chart speeds, each chart could be marked simultaneously and reproducibly with recorder polarity reversal switches upon introduction of the chromatographic sample to the column. The resulting fiducial marks were taken to be zero time, and all component retention times were referred to these zero-time reference marks. Equation 1 thus simplifies to

(17) V. J. Coates, H. J. Noebels, and I. S. Fagerson, "Gas Chromatography," Academic Press, New York, N. Y., 1958, p. 315.

$$\alpha_{1,2} = \frac{t_2 C}{t_1 C} \qquad (2)$$

where C represents the synchronized chart speed in in./min. Equation 2 further simplifies to

$$\alpha_{1,2} = \frac{d_2}{d_1} \qquad (3)$$

where d_2 and d_1 represent the distances (in. or cm.) from the zero-time reference to the respective component peak maxima in the chromatograms. Some relative separation factors calculated in this manner are given in Table I.

TABLE I

SEPARATION FACTORS FOR VARIOUS HYDROGEN ISOTOPES AND ISOMERS ON VARIOUS COLUMNS AT 77°K.

α^b	Chromatographic column[a]			α^b	Chromatographic column[a]		
	I	II	III		I	II	III
HD, H_2		1.22		DT, HT	1.60	1.30	1.34
D_2, H_2		1.49		T_2, HT	1.93	1.47	1.46
HT, H_2		1.42		T_2, DT	1.20	1.13	1.13
DT, H_2		1.85		o-H_2, p-H_2	1.37		
T_2, H_2		2.08		HT, p-H_2	2.01		
D_2, HD		1.22	1.32	D_2, p-H_2	2.25		
HT, HD		1.17	1.10	DT, p-H_2	3.30		
DT, HD		1.52	1.48	T_2, p-H_2	3.86		
T_2, HD		1.71	1.70	HT, o-H_2	1.46		
D_2, HT	1.12	1.05	1.20	D_2, o-H_2	1.64		
DT, D_2	1.43	1.24	1.11	DT, o-H_2	2.33		
T_2, D_2	1.72	1.40	1.28	T_2, o-H_2	2.81		

[a] Column I, 8-ft. activated alumina (Grade F-20, 80–100 mesh), helium carrier; II, 19-ft. ferric oxide (20%) on alumina, helium carrier; III, 12-ft. activated alumina (Grade F-20, 80–100 mesh), hydrogen carrier. [b] These are average values obtained from separation factors calculated from a series of chromatograms. The average deviation from the mean for the calculated factors was ± 0.01.

It should be emphasized that differing degrees of alumina dehydration for the 8-ft. and 12-ft. alumina columns and the reactivation conditions for the ferric oxide on alumina columns markedly affected the magnitude of the separation factors, and hence component resolution, for various hydrogen isomers and isotopes. In particular, those isotopes showing the largest separation factors were affected more by varying degrees of column activity than were those showing small separation factors. The values given in Table I are thus values which were obtained after column activations which would produce optimum resolution for a maximum number of hydrogen isotopes with reasonably short retention times for the various components.

Factors ranging from 1.00 (no resolution) up to the optimum (not necessarily maximum) resolution values given were observed on all three of the columns reported and were dependent upon the degree of column activity during the sample run. The column activity was determined directly by the column pretreatment conditions, temperature, and time of activation and was empirically measured as a function of the observed magnitude of the tritium–tritium hydride separation factor.

FURTHER STUDIES ON THE MASS SPECTRA OF BUTANOLS. 3-MONODEUTERIO-1-BUTANOL AND 4-MONODEUTERIO-1-BUTANOL

By W. H. McFadden, D. R. Black, and J. W. Corse

Western Regional Research Laboratory,[1] Albany 10, California

Received January 16, 1963

The mass spectra of 1-butanols labeled in the 3- and 4-positions have been obtained in order to extend the existing knowledge of the fragmentation characteristics of alcohols. It is shown that transfer of a hydrogen leading to the rearrangement in which H_2O is lost and the $C_4H_8{}^+$ ion is formed is specific to the hydrogens on position 4. The rearrangement ion $CH_3OH_2{}^+$ is apparently formed by statistically selecting two hydrogens from those on carbons 2, 3, and 4. The hydrogens present on carbon 1 show only a modest tendency to exchange with the others.

Introduction

In prior publications[2,3] the mass spectra of 1,1-dideuterio-1-butanol, 1-monodeuterio-1-butanol, and 2-monodeuterio-1-butanol were reported. The data permitted conclusions with respect to many of the important reactions of 1-butanol under electron impact. The selectivity of alcohols to break at the positions β to the hydroxyl in forming simple bond break ions was shown in accordance with prior studies on alcohol fragmentation.[4-7] Some selectivity was indicated for the abundant ion $C_4H_8{}^+$ formed by loss of H_2O but without data from compounds labeled in positions 3 and 4 a fuller understanding of this rearrangement could not be obtained. Similarly, no information on the formation of the interesting rearrangement ion at mass 33, $CH_3OH_2{}^+$, was possible. In view of continued interest in the field of mass spectral fragmentation, this study was made to clarify uncertain features not determined in the prior works.

Experimental

Sample Preparation. 3-Deuterio-1-butanol.—A solution of 2.40 g. of 3-chloro-1-butanol prepared either from 1,3-butanediol sulfate[8] or from 1,3-butanediol[9] and hydrochloric acid, in 10 ml. of anhydrous ether was added to a cooled, stirred solution of 1.66 g. of lithium aluminum deuteride in 25 ml. of ether. Stirring was continued for 24 hr., and the reaction mixture was slowly hydrolyzed with cold water. Cold dilute hydrochloric acid then was added to neutrality and the ether layer was separated. The aqueous layer was extracted twice with 15-ml. portions of ether which were combined with the original ether layer. This was washed with a small amount of water, dried over magnesium sulfate, and the ether removed by fractional distillation. The residue was purified by gas chromatography on a Carbowax-20M column, 7 ft. long × 1 in. diameter at 120°. The 3-deuterio-1-butanol was collected and re-run for further purification. Vacuum transfer yielded 3-deuterio-1-butanol (as shown by proton magnetic resonance spectrum) in about 15% yield.

4-Deuterio-1-butanol.—A solution of 6.0 g. of 4-chloro-1-butyl benzoate[10] dissolved in 20 ml. of ether was added to a solution of 1.6 g. of lithium aluminum deuteride in 50 ml. of ether with stirring, as described above. After 24 hr. the reaction product was worked up in the manner previously described. In addition to 4-deuterio-1-butanol, the α,α-dideuteriobenzyl alcohol formed from the benzoyl moiety of the starting material was also separated in much higher yield. The low yields of butanols are obviously due to procedural difficulties in their extraction and trapping after gas chromatography.

Isotopic Purity.—The two deuterated 1-butanols were examined by n.m.r. spectrometry to determine isotopic purity. Both samples were shown to be completely monodeuterated within the limits of the method ($\pm 1\%$). However, actual location of the deuterium is less certain. The similarity of the environment of the various hydrogens (particularly the important ones on carbons 3 and 4) makes quantitative interpretation of the integrated n.m.r. curve difficult. The assignment of proton signal to a particular carbon depended upon a partly arbitrary selection of a point on a line whose slope was not zero. The results, although not as favorable as would be desired, are presented in Table I and in the Discussion the mass spectra are interpreted with proper consideration. For the most part, the two spectra are sufficiently similar that any corrections would not alter the conclusions. A detailed discussion of possible corrections is given in the section dealing with loss of H_2O.

TABLE I
DISTRIBUTION OF HYDROGENS AS FOUND BY N.M.R. SPECTROMETRY

	OH	C-1	C-2	C-3	C-4	Σ
3-D-1-butanol	1.06	1.96	2.00	1.19	2.79	9.00
4-D-1-butanol	1.05	1.96	2.00	1.78	2.17	8.96

The n.m.r. spectra also indicated about 1% chemical impurity (due to unexplained methylene hydrogens) in 3-D-1-butanol but this could not be detected in the mass spectrum. The high value for the hydroxyl hydrogen may be due to a trace of water in the samples.

Mass Spectrometer.—The mass spectra were obtained with a Bendix time-of-flight mass spectrometer. The electron accelerating voltage was 70 e.v. and the ionization current was 0.2 μa. Temperature was not measured in the ionization chamber but the source end of the mass spectrometer was 100 $\pm$ 5°. Background pressure was less than 8 × 10^{-8} torr and pressure during introduction of a sample was 2-3 × 10^{-7} torr. The spectra were recorded on a Minneapolis-Honeywell Visacorder at a scan rate of m/e 12 to m/e 100 in 2 min.

Experimental Results

The mass spectra obtained for the two deuterated butanols are presented in Table II along with the spectrum of the undeuterated alcohol. (An abbreviation is used such that -3-D refers to 3-monodeuterio-1-butanol and this convenience will be utilized where desirable.) The ion abundances are the averages of two separate runs and are reported as the percentage of the total measured ionization (m/e 12 to 80). Unless it seemed pertinent to the discussion or general understanding, ions less than 0.2% of the total ionization were omitted.

Background corrections were made in the usual way. No corrections were made for isotopic impurity that may have been indicated by the n.m.r. data. The spectra are not corrected for natural isotopic abundances.

(1) A Laboratory of the Western Utilization Research and Development Division, Agricultural Research Service, U. S. Department of Agriculture.

(2) W. H. McFadden, M. Lounsbury, and A. L. Wahrhaftig, *Can. J. Chem.*, **36**, 990 (1958).

(3) E. L. Eliel and T. J. Prosser, *J. Am. Chem. Soc.*, **78**, 4045 (1956).

(4) J. G. Burr, Jr., *ibid.*, **79**, 751 (1957).

(5) F. E. Condon, H. L. McMurry, and V. Thornton, *J. Chem. Phys.*, **19**, 1010 (1951).

(6) L. Friedman and J. Turkevich, *J. Am. Chem. Soc.*, **74**, 1666 (1952).

(7) C. S. Cummings, II, and W. Bleakney, *Phys. Rev.*, **58**, 787 (1940).

(8) J. Lichtenberger and R. L. Lichtenberger, *Bull. Soc. Chim. France*, 1002 (1948).

(9) J. Verhulst, *Bull. Soc. Chim. Belges*, **40**, 85 (1931).

(10) *Org. Synthesis*, **29**, 30 (1949).

TABLE II

MASS SPECTRA OF DEUTERATED 1-BUTANOLS

m/e	D_0	$-3-D_1$	$-4-D_1$	m/e	D_0	$-3-D_1$	$-4-D_1$
14	0.25	0.26	0.18	37	0.25	0.16	0.21
15	1.44	1.16	.93	38	0.56	0.35	0.43
16	0.09	0.33	.56	39	3.47	2.00	2.08
17	.08	.18	.16	40	0.85	1.73	1.78
18	.16	.60	.51	41	10.83	4.51	4.34
19	.58	.52	.54	42	7.17	8.55	8.14
20	...	.07	.07	43	10.96	6.16	6.51
26	1.21	0.75	0.92	44	1.20	9.09	10.51
				45	1.38	1.79	1.76
27	8.87	5.43	5.83	46	0.15	0.30	0.30
28	3.41	5.25	5.23	47	...	0.06	0.06
29	5.57	4.20	4.10				
30	0.44	3.11	2.63	53	0.26	0.12	0.13
31	14.69	14.34	14.40	54	0.12	0.17	0.16
32	0.38	1.20	0.62	55	2.61	0.60	0.84
33	1.62	1.17	1.23	56	18.18	4.38	7.16
34	...	0.51	0.53	57	1.66	17.58	13.85
				58	0.07	1.49	0.95
				59	.08	0.10	0.08
				73	.35	.07	.07
				74	.52p	.39	.40
				75	...	.55p	.52p

Discussion

Loss of OH or H_2O.—From previous work it had not been possible to determine the mechanism for the formation of the prominent ion $C_4H_8^+$ by loss of H_2O. It was apparent that neither the hydrogens on carbon 1 or those on 2 were involved in forming the H_2O fragment. From the work presented here it is possible to show that the hydrogens on carbon 4 are considerably favored in formation of this complex.

The data confirming this event are summarized in Table III. The abundance of the ions due to loss of masses 17 to 20 are tabulated for 1-butanol and the two deuterated alcohols investigated in this work. Similar data are given for the alcohols reported in ref. 1 and 2 but in this table those data have been made about 10% larger, as a group, so that the total ionization due to loss of masses 17 to 21 appears to be the same and thus gives a better comparison.

TABLE III

IONIZATION OBSERVED DUE TO LOSS OF MASSES 17 TO 21

Mass lost from parent	$-D_0$	$-3-D_1$	$-1-D_1$	$-1-D_1$ ref. 2	$-2-D_1$ ref. 2	$-1-D_2$ ref. 1
					renormalized	
17	1.66	1.49	0.95	1.20	1.28	1.22
18	18.2	17.6	13.8	17.6	18.2	17.6
19	2.6	4.4	7.16	2.96	2.16	2.08
20	0.12	0.60	0.84	0.78	0.37	1.26
21						0.39

It can be seen that location of deuterium at positions 1, 2, or 3 causes only a modest influence in the ionization due to loss of mass 18 or 19. When one of the three hydrogens on position 4 is substituted with deuterium there is a noticeable reduction in the ionization due to loss of mass 18 and a corresponding increase in that due to loss of mass 19. To estimate the percentage of hydrogen that is transferred from carbon 4 in this intramolecular reaction, it is necessary to assume that the percentage of ionization due to each mode of breakdown (*i.e.*, loss of OH, loss of H_2O, etc.) is the same for the substituted molecules. When account is taken of the increased ionization due to loss of 20 mass units

(H_2DO) so that the contribution due to loss of H_3O and HDO can be estimated, then it is apparent that in the rearrangement which subsequently leads to loss of water, more than 80% of the hydrogen that is transferred to the hydroxyl must come from carbon 4. This confirms the previously suggested six-membered cyclical intermediate[2]
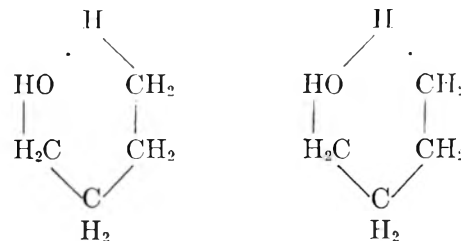
and is in agreement with much recent evidence for cyclical intermediates in esters[11,12] and hydrocarbons.[13,14] It is contradictory to the frequent suggestion that formation of an olefinic structure by transfer of an adjacent hydrogen contributes to the stability of the system. If such occurs, it apparently does so after decomposition of the parent ion.

Table III also indicates that H–D exchange prior to loss of a hydroxyl favors the 4-position. Because the mass spectrometers used in ref. 1 and 2 yield a different percentage of ionization due to loss of OH, direct comparison of the data given of the first row in Table III cannot be made. However, reference to the data for the undeuterated butanol of the original work shows that H–D exchange between the hydroxyl hydrogen and deuterium on positions 1, 2, or 3 occurs only about 10% (per deuterium) but, as is indicated in Table II, occurs about 45% when substituted in position 4.

The compound 1-butanol-3-D_1 appears to yield significantly more ionization due to loss of mass 19 than would be expected considering that there is only a slight reduction in that due to loss of mass 18. This may be due to any of the following causes: (1) loss of DHO, (2) loss of H_3O, (3) presence of the isotopic impurity -4-D_1 as indicated by Table I. It does not seem reasonable at this time to speculate on this observation.

The possibility of considerable amounts of -3-D_1 in 1-butanol-4-D_1 and of -4-D_1 in 1-butanol-3-D_1 must be considered. Table I indicates that these may be present in amounts of about 10 to 20%. The n.m.r. data are unfortunately not certain enough to rely on for correction calculations but they definitely establish an upper limit. It must now be noted that if such calculations were performed on the basis of the n.m.r. results, then the conclusions stated with respect to the loss of H_2O would be more firmly established. In Table III the data for loss of 18 would be greater for -3-D_1 and less for -4-D_1 and that for loss of 19 would be less for -3-D_1 and greater for -4-D_1.

Formation of the Ion $CH_3OH_2^+$.—The rearrangement ion $CH_3OH_2^+$ observed at mass 33 had been shown to retain deuterium substituted on carbon 1. Presumably this ion is formed by transfer of two hydrogens from car-

(11) Ng. Dinh-Nguyen, R. Ryhage, and S. Stallberg-Stenhagen, *Arkiv Kemi*, **18**, 393 (1961).

(12) H. O. Colomb, Jr., B. D. Fulks, and V. A. Yarborough, 10th Annual Meeting, A.S.T.M. Committee E-14, New Orleans, La., 1962.

(13) J. H. Beynon, R. A. Saunders, A. Topham, and A. E. Williams, *J. Phys. Chem.*, **65**, 114 (1961).

(14) M. V. Gur'ev, M. V. Tikhomirou, and N. N. Tunitskii, *Zh. Fiz. Khim.*, **32**, 2847 (1958).

bons 2, 3, or 4 to the CH_2OH group. From the present data, and that of Eliel's, it is seen that the transfer of the two hydrogens (deuterium) occurs from any of these three positions in a ratio that is close to that expected if the hydrogens from these positions are randomly selected.

The per cent ionizations observed at masses 32 to 35 for the various deuterated 1-butanols are presented in Table IV. Where a sizable contribution occurs at masses 32 or 33 from deuterated CH_2OH^+, the data have been omitted. For the same reason it was not considered practical to renormalize the data of ref. 1 and 2 as was done for Table II so that they appear about 15 to 20% lower than those of the present work.

TABLE IV

IONIZATION DUE TO CH_2OH^+, $CH_3OH_2^+$, OR DEUTERATED EQUIVALENT STRUCTURES

Mass	D_0	-3-D_1	-4-D_1	-1-D_1 (ref. 3)	-2-D_1 (ref. 3)	-1-D_2 (ref. 2)
32	0.38	..	..	..	..	..
33	1.62	1.17	1.23	0.51	1.17	..
34	..	0.51	0.53	1.40	0.34	0.36
35	..	.	..	..	..	1.32

As was previously noted, the deuterium in position 1 is retained with very little exchange in formation of the ion $CH_3OH_2^+$. With deuterium in positions 2, 3, or 4 there is in all cases a noticeable contribution from the ion $(CH_3OH)D^+$ corresponding to the amount expected from a statistical selection of the various hydrogen or deuterium. This point is to be particularly noted because it is not consistent with an observation made from deuterated isobutyl alcohols. Eliel[3] has shown that for isobutyl alcohol there is no contribution to the $CH_3OH_2^+$ ion from the hydrogen on carbon 2 and the transfer of both hydrogens is apparently from either or both of the methyl groups which in this case are carbon 3. These

scattered and inconsistent results on the formation of this uncommon ion indicate a need for further investigations.

Other Ions.—For the most part no conclusions can be made regarding the formation of the other ions except to confirm those of earlier work. These are briefly summarized in the following.

In accordance with previous data, $C_3H_7^+$ is shown to occur by simple bond break with very little exchange of hydrogen and deuterium.

The ion $C_2H_4OH^+$ occurring at mass 45 had been shown to retain the hydrogens (deuterium) on carbons 1 and 2. Possible exchange of deuterium from those carbons could not be determined. The present data show that the hydrogens on carbon 3 and 4 will exchange with those of the C_2H_4OH to the extent of about 15% for one deuterium.

The ions observed at mass 29 in the spectrum of 1-butanol-D_0 have been shown by high resolution mass spectrometry to consist of about 25% CHO^+ and 75% $C_2H_5^+$.[15] When one deuterium was placed on any of positions 1, 2, 3, or 4, the ionization observed at mass 30 is greater than could be attributed to CDO^+ so that apparently some $C_2H_4D^+$ is formed regardless of the original position of the deuterium. Further speculation would require high resolution data on the deuterated species.

The ions $C_3H_5^+$, $C_3H_3^+$, etc., all contain deuterium regardless of the original labeled position indicating that they occur as secondary daughter ions in which considerable H–D exchange is possible.[16]

Acknowledgment.—We wish to thank Dr. R. E. Lundin for performing the necessary n.m.r. analysis.

(15) J. H. Beynon, private communication.
(16) W. H. McFadden and M. Lounsbury, Can. J. Chem., 40, 1965 (1962).

THE FRACTIONATION OF CARBON ISOTOPES BY ION EXCHANGE EMPLOYING A FORMIC ACID SYSTEM[1]

By CHARLES N. DAVIDSON, CHARLES K. MANN, AND RAYMOND K. SHELINE

Department of Chemistry, Florida State University, Tallahassee, Florida

The fractionation of carbon isotopes has been achieved by ion-exchange displacement chromatography with a CH_3COO^-–$HCOOH$–HCl system on strongly basic Dowex 2 resin. Experiments utilizing C^{14}-labeled formic acid solutions indicated the lighter C^{12} to be enriched in the resin phase. The separation factor, $K = (C^{12}/C^{14})_r/(C^{12}/C^{14})_s$, was measured as a function of temperature and found to increase from 1.0032 at 35.4° to 1.0062 at 6.0°. From the temperature-dependence of K, ΔH^0 for the equilibrium $HC^{12}OOH_s + HC^{14}OO^-_r \rightleftharpoons HC^{14}OOH_s + HC^{12}OO^-_r$, was calculated to be -4.3 cal./mole, and ΔS^0 was found to be -6.3×10^{-3} cal./mole-degree at 25°. K varied from 1.0028 for resin with 2% DVB content to 1.0059 for Dowex 2×10. The subsequent decrease to 1.0055 for resin with 24% DVB was explained by dehydration effects. An extended run utilizing multiple-column operation resulted in enrichment of C^{14} by a factor of almost two in the leading fractions.

Introduction

An efficient, rapid process for the fractionation of the isotopes of carbon is of significant value for several reasons. A large increase in the C^{14}/C^{12} ratio of a sample would permit extension of the presently available range of carbon-dating experiments. High purity C^{12} would have a variety of uses in nuclear physics.

For example, its use in the preparation of carbon-backed targets would reduce the number of impurity reactions occurring during a bombardment. Synthesis of compounds highly enriched in C^{13} would permit increased utilization of nuclear magnetic resonance measurements.

In this experimental study, the feasibility of using ion-exchange displacement chromatography to effect resolution of C^{12}–C^{14} mixtures was investigated using

an $CH_3COO^--HCOOH-HCl$ system on Dowex 2 resin in which association occurs in the solution phase. Several experiments of a similar nature have been described[2-6] and are summarized in Table I. The subscripts r and s indicate the resin and solution phases, respectively. No separation factor was determined for the cyanide system[5] due to the loss of HCN which occurred in the presence of Dowex 2 resin during an experiment of even moderate length.

TABLE I

SUMMARY OF ION-EXCHANGE ISOTOPE SEPARATIONS IN WHICH COMPOUND IS ASSOCIATED IN THE SOLUTION PHASE

Isotopes	Ref.	System	Separation factor K	Heavier isotope concd. in
$B^{10}-B^{11}$	4	$B(OH)_3-B(OH)_4^-$	1.010	$(B(OH)_3)_s$
$C^{12}-C^{14}$	5	$HCN-CN^-$	>1	$(HCN)_s$
$N^{14}-N^{15}$	2	$NH_4OH-NH_4^+$	1.026	$(NH_4^+)_r$
$N^{14}-N^{15}$	6	$NH_4OH-NH_4^+$	1.027	$(NH_4^+)_r$
$S^{32}-S^{34}$	3	$H_2SO_3-HSO_3^-$	1.010	$(HSO_3^-)_r$

Statistical equations have been developed[7,8] which explain the direction and degree of isotopic enrichment in certain gaseous and gas-liquid exchange reactions. However, these expressions are rigorous only for the case of no interaction between molecules and when the molecule is considered to be rotating rigidly and vibrating harmonically with no rotation-vibration interaction. In condensed media involving ion exchangers, intermolecular forces cannot be ignored, but the possibility exists that these effects may be to a large extent self-canceling. Employing the isotopic vibrational frequencies for ammonia and the ammonium ion[7] in conjunction with experimental results[9] involving exchange in a gas-liquid NH_3-NH_4OH system, a K-value of 1.029 is calculated for the nitrogen separation at 25°, N^{15} enriching in the ammonium ion phase. This is in striking agreement (although possibly somewhat fortuitously so in view of the assumptions made) with the experimentally determined K-values.[2,6] Data by Stranks and Harris[10] for HCN and CN^- indicate K = 1.070 at 20° (C^{14} enriching in the HCN phase), in qualitative agreement with experiments.[5]

A rough approximation can be made in the $B(OH)_3-$ $B(OH)_4^-$ case. The Q_{11}/Q_{10} partition function ratio for $B(OH)_3$ can be calculated, assuming the OH's to act as mass units, from the spectroscopic data of Servoss and Clark.[11] Skeletal vibrations of $B^{11}(OH)_4^-$ are known from experiment[12] and the corresponding vibrations for the B^{10}-species can be calculated using the Urey-Bradley potential[13] for a tetrahedral molecule.

In light of these considerations, an approximate value for the separation factor at 25° can be determined.

$$K = \left(\frac{Q_{11}}{Q_{10}}\right)B(OH)_3 \bigg/ \left(\frac{Q_{11}}{Q_{10}}\right)B(OH)_4^- \approx 1.08 \quad (1)$$

The deviation of the calculated K-value from that experimentally determined (K = 1.01) is so large, however, that the correct prediction of the direction of enrichment may be fortuitous.

Sufficient isotopic frequencies are not available for predicting the separation factor observed in the H_2SO_3- HSO_3^- system.[3]

Several preliminary experiments were undertaken with the formate system to demonstrate the sharpness of the chemical boundaries. Employing C^{14}-labeled HCOOH solution, the separation factor, K, was determined as a function of temperature and resin divinylbenzene content. An extended run was made, displacing formate with chloride and utilizing multiple-column operation, to obtain a high specific separation.

Experimental

Resin and Reagents.—Bio-Rad AG 2×8 (100–200 dry mesh) resin was used as received for all experiments described here except those in which cross-linkage was varied. Commercial grade Dowex 2 resins with 2, 10, and 24% divinylbenzene content were provided for these latter runs by the Dow Chemical Co. Particle sizes were 50–100, 100–200, and 200–400 dry mesh, respectively. These resins were physically conditioned by repeated flotation, discarding the fines. Chemical conditioning was effected by twice cycling the resins through the acetate and chloride forms before converting to the acetate form in preparation for a run. Reagent grade chemicals were utilized and made to proper concentration with de-ionized water. Labeled HCOOH solutions were prepared with C^{14}-sodium formate such that the C^{14} mole fraction was in the 10^{-6}–10^{-5} range.

Columns.—A column of 2.27 cm.^{2} cross-sectional area and about 8.1–8.2 cm. in resin height (Cl$^-$ form) was used for all preliminary runs in which the flow rate was varied to test sharpness of the chemical boundaries. The bed was supported by a glass frit and protected from disturbances at the top by a movable polystyrene plug floating on the liquid surface. The column used in the temperature and cross-linkage experiments was 2.83 cm.^{2} in cross-sectional area and about 26 cm. in resin height (Cl$^-$ form). Water of controlled temperature was circulated in a jacket around this column in the temperature experiments. A distance of several cm. was left free of resin at the column top, allowing the solution to attain the desired temperature before reaching the resin. Experiments were performed at 6.0, 14.9, 25.5, and 35.4°, and the temperature was maintained within ±0.1° of these values except in the case of the 6.0° run, in which the deviation was ±0.2°. Runs were not made above 35.4°, because of the thermal instability of Dowex 2 resin. All other experiments were performed at room temperature. The columns employed in the large-scale extended experiment consisted of 1-ft. long sections of flanged Pyrex glass pipe (1-in. i.d.) terminated at each end by a glass neck-down. Dead space was reduced by packing with Pyrex beads. The particulars of this multiple-column system and the details of cycling a band continuously through a small number of columns are similar to those previously described for the nitrogen isotope separation.[2] A pair of platinum foil electrodes (1 cm.^{2} in area) was sealed into the bottom neck-down of each column which, in conjunction with an adjustable microammeter, allowed detection of the invisible $CH_3COO^--HCOO^-$ and $HCOO^--Cl^-$ boundaries.[14]

Analyses.—Total formate in the effluent fractions was determined by standard methods. Aqueous C^{14}-formate was counted at −4° in a Model 314A Packard Tri-Carb liquid scintillation spectrometer using an ethanol–toluene solvent system and employing 2,5-diphenyloxazole (PPO) and 1,4-bis-2-(5-phenyloxazolyl)-benzene (POPOP) as scintillators. Efficiency varied from 10 to 16%. Resin bed capacity was determined by the neutralization method and/or by a direct determination of the formate

(2) F. H. Spedding, J. E. Powell, and H. J. Svec, *J. Am. Chem. Soc.*, **77**, 6125 (1955).

(3) S. Forberg, W. Barnevik, I. Fogelstrom-Fineman, T. Westermark, and H. v. Ubisch, "Proceedings of the International Symposium on Isotope Separation," North-Holland Publishing Co., Amsterdam, Netherlands, 1958, p. 243.

(4) Y. Yoneda, T. Uchijima, and S. Makishima, *J. Phys. Chem.*, **63**, 2057 (1959).

(5) C. N. Davidson, C. K. Mann, and R. K. Sheline, *J. Am. Chem. Soc.*, **83**, 2389 (1961).

(6) M. U. Comas, T. B. Rodriguez, F. C. Castillo, and R. F. Cellini, *Anales Real Soc. Espan. Fis. Quim.* (Madrid), **B57**, 587 (1961).

(7) H. C. Urey, *J. Chem. Soc.*, 562 (1947).

(8) J. Bigeleisen and M. G. Mayer, *J. Chem. Phys.*, **15**, 261 (1947).

(9) H. G. Thode, R. L. Graham, and J. A. Ziegler, *Can. J. Res.*, **23B**, 40 (1945).

(10) D. R. Stranks and G. M. Harris, *J. Am. Chem. Soc.*, **75**, 2015 (1953).

(11) R. R. Servoss and H. M. Clark, *J. Chem. Phys.*, **26**, 1175 (1957).

(12) J. O. Edwards, G. C. Morrison, V. F. Ross, and J. W. Schultz, *J. Am. Chem. Soc.*, **77**, 266 (1955).

(13) H. C. Urey and C. A. Bradley, *Phys. Rev.*, **38**, 1969 (1931).

(14) J. A. McCloskey, *Anal. Chem.*, **33**, 1842 (1961).

displaced from the bed by chloride. In cases where both methods were utilized, results agreed within 1%.

Procedure.—The appropriate resin was slurried into the column, converted to acetate form, and back-washed. Formic acid solution was then loaded and allowed to pass down the column. Solution concentration and specific capacities of the resins were such that the formate band moved at about one-tenth the linear flow speed employed. The same resin bed and feed solutions from the same C14-labeled HCOOH stock solution were employed throughout the temperature runs. In the preliminary experiments and extended run, formate was displaced with hydrochloric acid. Three-ml. fractions were collected from just before breakthrough until the C14/C12 ratio returned to that of the feed solution in the temperature and cross-linkage runs. In the extended experiment, the entire formate band (about 14 in. in length) was collected in 5-ml. fractions after passing through the equivalent of thirty columns.

Results and Discussion

Preliminary Band Contours.—Formate band contours resulting from several runs are illustrated in Fig. 1. It is seen that chemical equilibria of the CH_3COO^-–$HCOOH$–HCl system can be maintained on Dowex 2×8 resin at flow speeds up to at least 1.63 cm./min. Despite these results, flow rates were always maintained as slow as practical in C14-labeled runs to ensure that isotopic equilibrium was achieved within a relatively small column distance.

The resin volume shrank $\sim 3\%$ when changing from CH_3COO^- to $HCOO^-$ form, and an additional 11% shrinkage occurred going from $HCOO^-$ to Cl^- form.

Influence of Temperature.—Results of the temperature runs are graphically illustrated in Fig. 2. The change in C14 mole fraction from that of the feed solution is plotted against the summation of mmoles formic acid found in the effluent. The separation factor, defined as

$$K = \frac{[HC^{14}OOH]_s}{[HC^{12}OOH]_s} \bigg/ \frac{[HC^{14}OO^-]_r}{[HC^{12}OO^-]_r} = \left(\frac{C^{12}}{C^{14}}\right)_r \bigg/ \left(\frac{C^{12}}{C^{14}}\right)_s \quad (2)$$

for each run was calculated from the area under the curve, the total exchange capacity of the resin bed (95.96 mequiv.), and the C14 mole fraction of the feed solution using the formula

$$\epsilon = K - 1 = \frac{\sum_{i=1}^{m} V_i C_i (N_i^* - N_0^*)}{N_0 \left[N_0^* Q - \sum_{i=1}^{m} V_i C_i (N_i^* - N_0^*) \right]} \quad (3)$$

developed by Spedding, et al.[2] Here, V_i is the volume of the ith fraction in ml., C_i is the total HCOOH concentration in mequiv./ml. in the ith fraction, N_i^* and N_0 are the mole fraction of C14 in the ith fraction and the feed solution, respectively, N_0 is the mole fraction of C12 in the feed solution (approximately unity), m is the fraction at which N_i^* first equals N_0^*, and Q is the total exchange capacity of the resin bed in mequiv. Pertinent data and the separation factors are presented in Table II. Values determined for $\epsilon = K - 1$ are estimated to be in error by less than 6%.

It is known that for temperatures less than 300–400°K., isotopic exchange equilibrium constants usually increase with decreasing temperature.[15-17] This

(15) D. A. Lee, *J. Phys. Chem.*, **64**, 187 (1960).

(16) R. H. Betts, W. E. Harris, and M. D. Stevenson, *Can. J. Chem.*, **34**, 65 (1956).
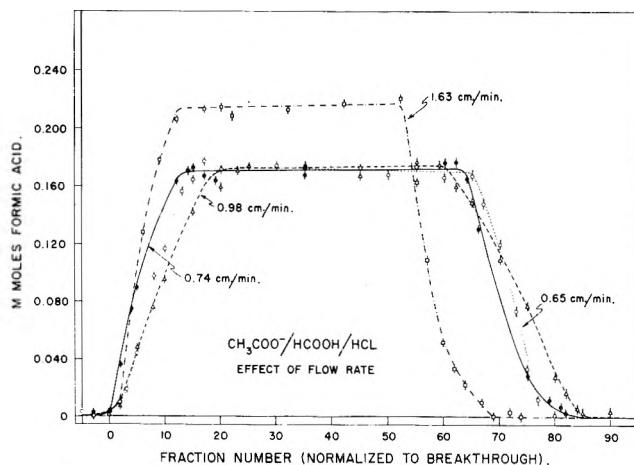
(17) G. M. Murphy, *J. Chem. Phys.*, **5**, 637 (1937).

Fig. 1.—Effect of flow rate on the CH_3COO–$HCOOH$–HCl band contour. Displacement was effected with 0.156 M HCl in the 1.63 cm./min. experiment and 0.125 M HCl in the others. The formate band was slightly tilted in the run at 0.98 cm./min.
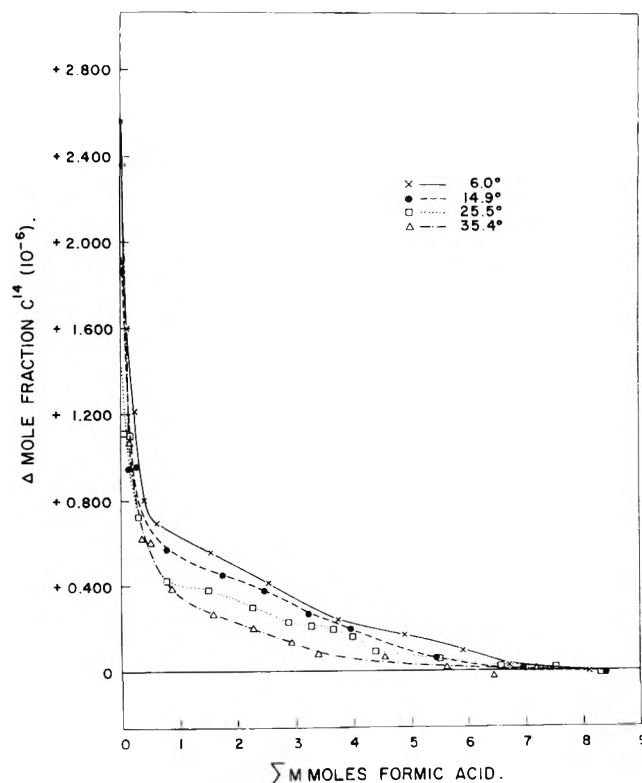

Fig. 2.—Change in C14 mole fraction as a function of HCOOH in the effluent for different temperatures. N_0^* and Q were identical for all runs.

TABLE II

VARIATION OF K WITH TEMPERATURE

Temp., °C.	Av. flow rate, cm./min.	K
6.0	0.25	1.0062
14.9	.25	1.0050
25.5	.27	1.0041
35.4	.24	1.0032

is predicted, not only by statistical calculations of K, but also by the classical Gibbs–Helmholz equation

$$\left[\frac{\partial \ln K}{\partial T} \right] = \frac{\Delta H^0}{RT^2} \quad (4)$$

If the assumption is made that the heat of exchange is independent of temperature or varies only very slowly with temperature in the range considered, this equation
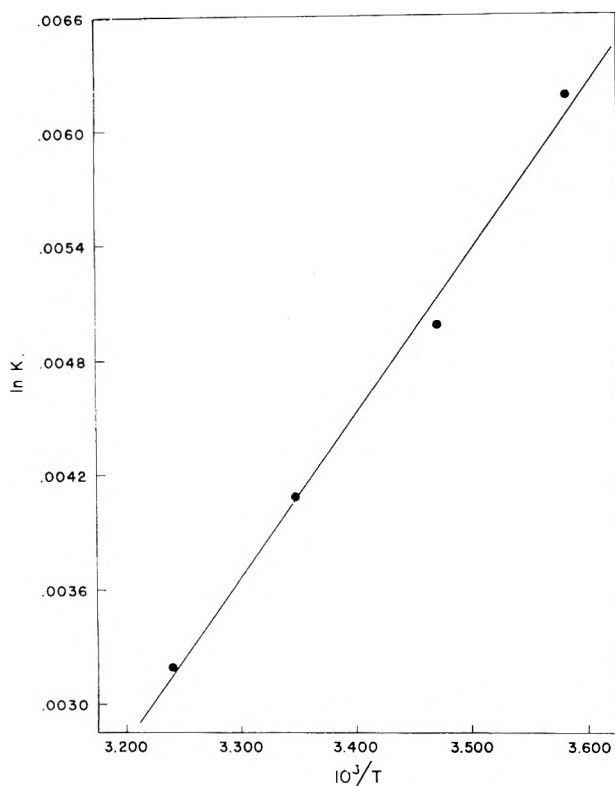
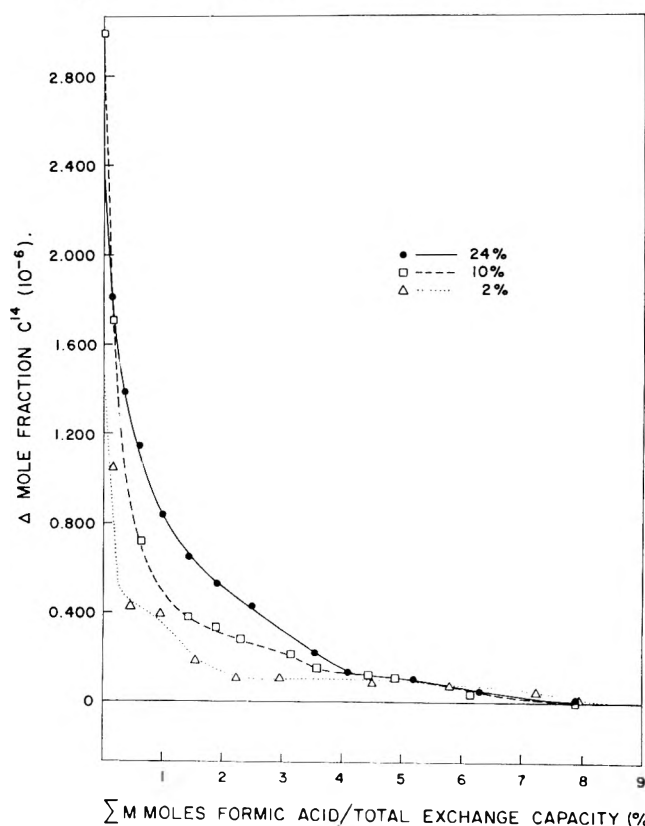Fig. 3.—Natural log of K as a function of $10^3/T$.

Fig. 4.—Change in C^{14} mole fraction as a function of HCOOH in the effluent for different resin divinylbenzene contents. Although the area under the curve in the 24% experiment is greater than in the 10% run, a larger N_0^* value resulted in a slightly smaller value for K.

may be integrated with respect to temperature considering ΔH^0 constant. A plot of ln K against $1/T$ should give a straight line with a slope of $-\Delta H^0/R$ if this assumption is valid. Thus, the heat of exchange is readily obtainable from the temperature dependence

of the separation factor, and the entropy of isotopic exchange at any temperature may be calculated from the formula

$$\Delta F^0 = -RT(\ln K) = \Delta H^0 - T\Delta S^0 \qquad (5)$$

The heat of isotopic exchange in ion-exchange systems has not been previously determined for cases in which the isotope-containing compound is associated in the solution phase. However, in the case of the straightforward ion-exchange separation of Li^6 and Li^7, Lee[15] found the exothermic heat of exchange to be 2.26 cal./mole, and Glueckauf[18] determined $-\Delta H^0$ to be 0.41 cal./mole using the data of Betts, Harris, and Stevenson[16] for the fractionation of strong electrolyte solutions containing Na^{22} and Na^{24}.

In the formate experiments described here, the enrichment of C^{14} increased with decreasing temperature as expected. In Fig. 3. ln K is plotted as a function of $1/T$ indicating the straight line relationship. A least squares linear fit of the data gave a slope indicating $-\Delta H^0$, the heat of isotopic exchange, to be 4.3 cal./mole. ΔS^0 for the isotopic exchange was calculated to be -6.3×10^{-3} cal./mole-degree at 25°.

As can be seen from Fig. 2, C^{14}-formate was enriched at the front of the band, indicating that the heavier isotope was thermodynamically favored in the HCOOH solution phase. It would be interesting to compare statistical predictions with the experimentally determined separation factors, but insufficient data on the fundamental vibrations are available.

Influence of Cross-Linkage.—Results of the cross-linkage (DVB) runs are illustrated in Fig. 4. The change in C^{14} mole fraction from that of the feed solution is plotted as a function of the summation of mmoles formic acid found in the effluent expressed as a percentage of the total exchange capacity of the resin bed. The separation factor for each run was calculated from (3) and is presented in Table III. The separation factor for 8% cross-linked resin was interpolated from results of the temperature dependence of K, by calculating ln K from the least squares equation fitting the data

$$\ln K = -0.02471 + 8.598(1/T) \qquad (6)$$

employing 22° (average room temperature) as the temperature.

TABLE III
VARIATION OF K WITH RESIN CROSS-LINKAGE

% Cross-linkage	mequiv. of resin	Av. flow rate, cm./min.	K
2	54.94	0.35	1.0028
8	95.96	.25	1.0044
10	94.84	.31	1.0059
24	79.08	.31	1.0055

This observation of a maximum in the cross-linkage dependence of K is somewhat analogous to that observed by Ohtaki, et al.,[19] in the fractionation of sodium isotopes, although in the work reported here the lighter isotope is concentrated in the resin. No such maximum was observed in the work of Lee and Begun.[20]

Although an over-all K-value measured in this work

(18) E. Glueckauf, Trans. Faraday Soc., **54**, 1203 (1958).

(19) H. Ohtaki, H. Kakihana, and K. Yamasaki, Z. physik. Chem. (Frankfurt), **21**, 224 (1959).

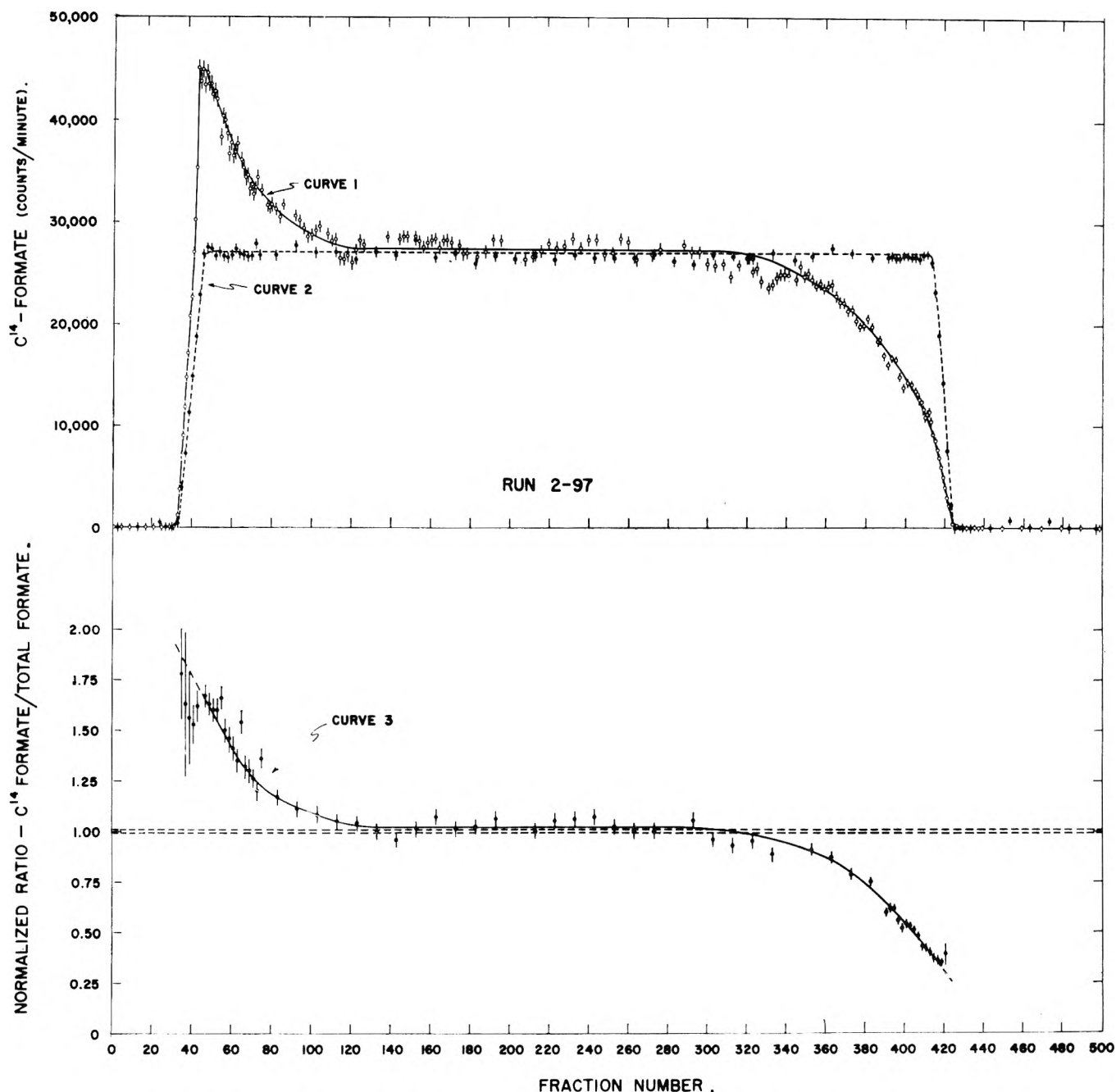(20) D. A. Lee and G. M. Begun, J. Am. Chem. Soc., **81**, 2332 (1959).

Fig. 5.—Results of the extended C^{14}-labeled experiment. Curve 1 indicates C^{14} after the run. Curve 2, given by the product of total formate and the initial specific activity of the HCOOH feed solution, represents C^{14} before the run. Curve 3 illustrates the C^{14}/C^{12} ratio after the experiment with the pre-run ratio normalized to 1.00.

is the product of the equilibrium constant for the association–dissociation, dimerization, and straightforward ion-exchange equilibria, it seems likely that changes in resin cross-linkage will influence mainly the last-mentioned one. Glueckauf[21,22] has shown $\epsilon_{ion\ ex}$ (= $K_{ion\ ex}$ − 1) to be a direct function of the exchanger molality and the difference in hydrated molar volume of the isotopic ions. For highly cross-linked resins such as Dowex 2×24, the dehydrating effect of the resin (directly proportional to the original extent of hydration) on the ions may offset the increase in exchanger molality, resulting in a net decrease in $\epsilon_{ion\ ex}$.

Extended Run.—Quantitative results were obtained in the radioactive, large-scale experiment. Within experimental error, the amount of HCOOH collected after passing the band through thirty columns (5611.3

mequiv. of resin bed) equaled to 231.9 mequiv. loaded at the beginning of the run. Displacement was effected with 0.123 M HCl. The experimental results are shown in Fig. 5 and are to be compared with the cyanide results previously described.[6] Curve 1 represents C^{14}-formate after the run, error bars indicating pipetting error. Curve 2 represents the specific activity originally in the HCOOH solution multiplied by the amount of total formate in each fraction aliquot after the run. This indicates the total formate band contour and represents C^{14}-formate to be expected if isotope separation had not occurred. Errors shown are those in titration. Curve 3 illustrates the ratio of curve 1 to curve 2 (C^{14} after, to C^{14} before) and is identical with the C^{14}/C^{12} ratio after the experiment with the pre-run ratio normalized to 1.00. As can be seen from the figure, C^{14}-formate was enriched at the front of the band by a factor of almost two.

(21) E. Glueckauf, *Trans. Faraday Soc.*, **51**, 1235 (1955).

(22) E. Glueckauf, *J. Am. Chem. Soc.*, **81**, 5262 (1959).

A limited comparison between this system and the cyanide system is warranted and evolves three significant items. (1) The chemical boundaries of the formate system on Dowex 2 resin are sharper than those of the cyanide system, indicating greater suitability of the former system for extended column operation. (2) Since, under similar experimental conditions, twice the C^{14} enrichment was obtained in less than one-third the resin bed length for the HCN as compared with the HCOOH system, it is likely that ϵ ($= K - 1$) for the cyanide system is at least six times as great as the 4.4 $\times$ 10^{-3} room temperature value found for the formate system. (3) From the standpoint of practicality, the quantitative aspects of the formate system make it the superior of the two.

The economical feasibility of producing C^{12} and C^{13} of relatively high purity cannot be accurately determined without resort to pilot plant operations. Although the separation factor for the formate system is smaller than that in some C^{12}–C^{13} gas–liquid exchanges,[23] the combination of a relatively small plate-height and inherent ease of operation could conceivably

outweigh this. Withdrawal of depleted product and addition of more HCOOH feed solution at strategic intervals would enhance the specific separation. The time factor, determined by the rate of approach to isotopic equilibrium, and the durability of the resin must also be considered. Both chloride and excess acetate are recoverable in the regenerative step as a mixture of their ammonium salts. During column operation, displaced acetate is recoverable as its acid.

It is logical to assume that the formate system may be successfully applied to carbon-dating experiments in the laboratory. If enough starting material is available (as would be the case for age determinations of peat beds), the C^{14} content could be concentrated in the leading fractions by a factor of 10–20 after a month or two, using multiple-column operation with much larger columns than those employed here.

(23) C. A. Hutchison, D. W. Stewart, and H. C. Urey, *J. Chem. Phys.*, **8**, 532 (1940).

THE THERMODYNAMICS OF THE TERNARY SYSTEM: UREA–SODIUM CHLORIDE–WATER AT 25°

By V. E. BOWER AND R. A. ROBINSON

Solution Chemistry Section, National Bureau of Standards, Washington, D. C.

Isopiestic vapor pressure measurements have been made on this system at 25°; the activity coefficients of urea in sodium chloride solution and of sodium chloride in urea solution have been evaluated and the extent to which solubilities of one solute in a solution of the other can be calculated is discussed.

Introduction

Previous work has dealt with aqueous solutions of two co-solutes, of which one was mannitol.[1] That solute was chosen because it was one component of some ternary systems in which diffusion measurements were being made. Mannitol has, however, limited solubility in water (1.185 M at 25°) and, in order to obtain measurements over a much greater concentration range, the system urea–sodium chloride–water has now been investigated.

Experimental

Isopiestic measurements were made on this system by the method described previously[1a]; some improvement was made in the device for closing the lids of the isopiestic dishes with the desiccator under vacuum, by drilling a small hole in the center of the copper block; a spike on the lower part of the rotating device fitted into the hole and gave a smoother rotation when closing the lids.

Sodium chloride (Fisher Certified) was recrystallized once from water and dried at 300°. Urea (Fisher Certified) was recrystallized twice from methanol and dried *in vacuo* at room temperature. Calcium chloride (Baker and Adamson, A.C.S. reagent) was recrystallized twice from very slightly acidulated water. A stock solution was prepared and analyzed for chloride content; the analysis was confirmed by allowing solutions of

(1) (a) R. A. Robinson and R. H. Stokes, *J. Phys. Chem.*, **65**, 1954 (1961); (b) F. J. Kelly, R. A. Robinson, and R. H. Stokes, *ibid.*, **65**, 1958 (1961); (c) R. A. Robinson and R. H. Stokes, *ibid.*, **66**, 504 (1962).

TABLE I[a]

ISOPIESTIC SOLUTIONS OF UREA AND SODIUM CHLORIDE[a]

m_B	m_C	m_B	m_C	m_B	m_C
1.0257	0.5329	6.9657	2.8575	14.008	4.7792
1.0395	.5384	8.1817	3.2362	14.306	4.8323
1.6247	.8251	10.427	3.8430	17.826	5.6440
3.6345	1.6876	11.058	4.0304	18.401	5.7660
3.7667	1.7391	11.184	4.0580		

[a] B = urea; C = NaCl.

TABLE II

OSMOTIC AND ACTIVITY COEFFICIENTS OF UREA

m	φ	γ	m	φ	γ	m	φ	γ
0.1	0.996	0.992	2.0	0.931	0.864	9.0	0.827	0.653
.2	.992	.983	2.5	.919	.839	9.5	.824	.644
.3	.987	.975	3.0	.908	.817	10.0	.820	.636
.4	.983	.967	3.5	.899	.798	11.0	.814	.621
.5	.979	.955	4.0	.891	.780	12.0	.809	.608
.6	.975	.951	4.5	.882	.763	13.0	.804	.596
.7	.970	.942	5.0	.874	.747	14.0	.799	.584
.8	.966	.934	5.5	.867	.733	15.0	.794	.573
.9	.962	.927	6.0	.860	.719	16.0	.789	.563
1.0	.958	.921	6.5	.853	.706	17.0	.786	.554
1.2	.952	.908	7.0	.847	.694	18.0	.782	.545
1.4	.947	.896	7.5	.841	.683	19.0	.779	.537
1.6	.942	.885	8.0	.836	.672	20.0	.777	.530
1.8	.936	.874	8.5	.831	.662			

TABLE III[a]

THE SYSTEM: UREA–SODIUM CHLORIDE–WATER

$m_{ref.}$	m_B	m_C	$\dfrac{-\Delta}{m_B m_C}$	%[b]	$m_{ref.}$	m_B	m_C	$\dfrac{-\Delta}{m_B m_C}$	%[b]
0.8251	0.9497	0.3437	0.0334	+0.11	3.0369	3.6315	5.3725	.0015	+ .18
	1.3933	.1175	.0232	− .08		5.5480	4.9085	.0032	+ .15
						8.1565	4.2555	.0034	+ .26
1.6876	0.6992	1.3657	.0115	+ .07	3.1667	15.833	2.5562	.0040	+ .22
	1.9058	0.8129	.0183	− .04					
	2.7444	.4229	.0214	− .05	3.3061	12.944	4.0138	.0095	− .11
						16.047	3.1609	.0091	− .32
2.8575	1.6410	2.2042	.0027	+ .07		18.107	2.5183	.0085	− .25
	3.3504	1.5257	.0049	+ .13					
	5.6181	0.5908	.0092	+ .02	3.3066	5.9585	5.6617	.0097	− .14
						7.5353	5.3145	.0095	+ .02
3.2735	1.1875	2.8232	.0007	− .02		9.2642	4.9271	.0099	+ .01
	2.8039	2.2196	.0025	− .01		11.097	4.4907	.0099	− .05
	4.6672	1.5129	.0052	− .09					
	6.4725	0.7941	.0066	− .04	3.5831	15.002	4.6521	.01566	− .14
						18.697	3.6828	.01426	− .15
4.0304	5.3875	2.1870	.0013	− .11		21.176	2.9449	.01438	− .14
	7.4397	1.4450	.0006	+ .08					
	9.3321	0.7123	.0005	+ .12	3.6420	8.8029	6.2085	.01866	− .26
						10.902	5.7980	.01829	− .11
4.0580	1.3681	3.5868	− .0011	− .07		13.146	5.3200	.01759	− .05
	2.5894	3.1775	.0003	− .13					
	3.9752	2.7050	.0002	− .05	3.7085	10.660	6.0841	.01950	0
						14.069	5.3722	.01818	+0.20
4.7089	6.8252	2.5671	− .0004	− .02		17.432	4.5849	.01686	+ .13
	8.2784	2.0828	.0002	− .09		21.729	3.3889	.01518	+ .26
	9.9866	1.4792	.0006	− .11					
	11.822	0.7897	.0027	− .22	3.8600	14.077	6.0165	.02274	+ .03
						15.994	5.6170	.02163	+ .09
4.7792	2.5380	3.9813	− .0023	+ .02		18.074	5.1455	.02040	+ .11
	6.0157	2.9078	− .0007	+ .02		20.009	4.6360	.01921	+ .13
	11.146	1.1409	− .0015	+ .14					
					3.9293	16.416	5.8467	.02357	− .07
4.8323	1.3415	4.4082	− .0023	− .05		17.982	5.5005	.02246	− .04
	4.4403	3.4657	− .0001	− .11		19.642	5.1060	.02142	− .04
	8.7605	2.0790	− .0011	− .10		21.442	4.6450	.02051	− .02
5.6440	1.6963	5.1551	− .0024	+ .06	4.1372	19.749	6.1820	.02714	....
	5.6620	4.0765	.0006	+ .08					
	11.262	2.4182	− .0001	+ .11	4.3435	20.775	6.9942	(03271)	....
						23.648	6.4167	(03139)	....
5.7660	3.7400	4.7425	.0013	− .06					
	8.7785	3.3588	.0008	+ .17	4.4443	21.340	7.3814	(03445)	....
	15.188	1.2597	− .0007	+ .16		22.988	7.0751	(03365)	....
						24.463	6.7849	(03313)	....
3.0130	9.7975	3.7410	.0034	+ .15		24.759	7.2269	(03308)	....
	12.967	2.8263	.0037	− .13					
	18.009	1.1117	.0023	+ .05					

[a] B = urea; C = NaCl. In the first eleven sets, sodium chloride was the reference electrolyte; in the remainder, calcium chloride. [b] The difference is positive if Δ calculated by eq. 1 is greater than the experimental.

sodium chloride and of calcium chloride to equilibrate in the isopiestic apparatus; the equilibrium concentrations agreed with those reported previously.[2]

Results

A few equilibrations were made between solutions of sodium chloride and of urea (Table I); a large scale plot of the isopiestic ratio against the urea molality showed excellent agreement with the data of Scatchard, Hamer, and Wood.[3] However, the interpretation of any isopiestic measurement depends on the values assigned to the osmotic coefficients of the reference salt, in this case sodium chloride, and the values used by Scatchard, Hamer, and Wood differ slightly from those used[4] in previous work in this series.[1] In order to maintain consistency with the mannitol work, osmotic and activity coefficients of urea have been calculated (Table II) on the same basis.

(2) R. H. Stokes, *Trans. Faraday Soc.*, **41**, 637 (1945).

(3) G. Scatchard, W. J. Hamer, and S. E. Wood, *J. Am. Chem. Soc.*, **60**, 3061 (1938).

(4) R. A. Robinson and R. H. Stokes, "Electrolyte Solutions," Second Edition, Butterworths Scientific Publications, London, 1959, Appendix 8.3.

Isopiestic measurements were made with solutions of urea and sodium chloride equilibrated with either sodium chloride or calcium chloride solutions as references. The results are given in Table III; the first column gives the molality of the reference salt, which was sodium chloride in the first eleven sets and calcium chloride in the remainder. The second and third columns give the molalities of the mixed solutions which were in equilibrium with the solutions whose molalities are given in the first column.

In the analysis of these results we use the function Δ, defined by $\Delta/55.51 = \ln a_{w(B)} + \ln a_{w(C)} - \ln a_{w(M)}$ where $a_{w(M)}$ is the water activity of a solution containing m_B moles of urea and m_C moles of sodium chloride in 1 kg. of water; $a_{w(B)}$ that of a solution of m_B moles of urea only in 1 kg. of water; $a_{w(C)}$ that of a solution of m_C moles of sodium chloride only in 1 kg. of water.

$RT\Delta$ is therefore the free energy change of water when a solution of m_B moles of urea in a kg. of water is mixed isothermally with a solution of m_C moles of
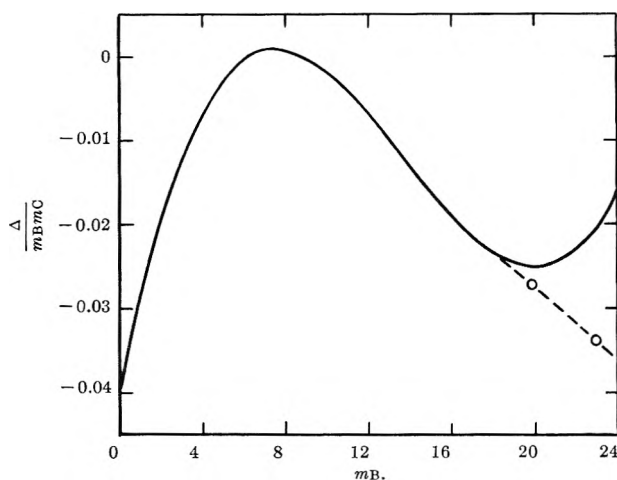
Fig. 1.—The function given by eq. 1; two of the experimental points are shown.

sodium chloride in a kg. of water and a kg. of water is then separated by means of an osmotic membrane.

The quantity $- \Delta/(m_B m_C)$ is given in the fourth column of Table III. The last six entries are enclosed in parentheses because binary systems of urea–water with the molality given in the second column and of sodium chloride–water with the molality given in the third column would have been considerably supersaturated. The Δ function, therefore, had to be calculated using values for the water activity of urea solutions and of sodium chloride solutions extrapolated into the supersaturated regions; for this reason, the last six entries may be unreliable.

Before turning to a discussion of the results, it is worthwhile looking at the magnitude of these effects. In dilute solutions, $\Delta/(m_B m_C)$ is comparatively large and negative, as was found in the systems mannitol–NaCl–water[1b] and mannitol–KCl–water.[1c] Thus, at $m_B = 0.9497$, $m_C = 0.3437$, $55.51 \ln a_{w(M)} = -1.5340$. $55.51 \ln a_{w(B)} = -0.9119$, and $55.51 \ln a_{w(C)} = -0.6330$, so that the mixture effect, as measured by Δ, is -0.0109 and $\Delta/(m_B m_C) = -0.0334$. In more concentrated solutions, Δ becomes less negative and at $m_B = 11.262$, $m_C = 2.4182$, Δ is almost zero. A three-dimensional plot of $\Delta/(m_B m_C)$ against m_B and m_C shows a region where Δ has small but positive values but in concentrated solutions Δ again becomes negative and large. For example, at $m_B = 14.077$, $m_C = 6.0165$, the three $55.51 \ln a_w$ terms are -24.615, -15.305, and -11.236 for the mixture, the urea solution, and the sodium chloride solution, respectively. Consequently, Δ is -1.926 and $\Delta/(m_B m_C)$ is -0.02274.

Discussion

In order to evaluate the activity coefficients of urea and of sodium chloride in these mixed solutions, we seek, as in earlier work,[1a] an analytical expression for $\Delta/(m_B m_C)$ in terms of m_B and m_C where m_B and m_C denote molalities, i.e., moles of urea and moles of sodium chloride, respectively, per kilogram of water. Even after eliminating the last six entries of Table III, for reasons already given, we found that a ten-parameter equation

$$\Delta/(m_B m_C) = A + B m_B + C m_C + D m_B{}^2 + E m_C{}^2 +$$
$$F m_B m_C + G m_B{}^3 + H m_C{}^3 + I m_B{}^2 m_C + J m_B m_C{}^2 \quad (1)$$

was needed. Even with ten parameters, however, the

fit with the experimental values of $\Delta/(m_B m_C)$ was not as good as we desired. After a considerable amount of computation, we found that, if we eliminated the point at $m_B = 19.749$, $m_C = 6.1820$, the remaining data gave, by the method of least squares: $A = -3.9556 \times 10^{-2}$; $B = 5.2731 \times 10^{-3}$; $C = 2.1319 \times 10^{-2}$; $D = -1.934 \times 10^{-4}$; $E = -3.059 \times 10^{-3}$; $F = -1.854 \times 10^{-3}$; $G = 9.1 \times 10^{-7}$; $H = 1.14 \times 10^{-4}$; $I = 3.97 \times 10^{-5}$; $J = 8.96 \times 10^{-5}$; and we got more satisfactory agreement with the experimental data. The extent of the agreement can be assessed in terms of the experimental quantities by reversing the calculation so as to compute the molalities of the reference solutions which would have given the values of $\Delta/(m_B m_C)$ as calculated by eq. 1. The difference between these calculated molalities and the experimental, expressed as a percentage, is given in the last column of Table III.

The difficulty in fitting the point at $m_B = 19.749$, $m_C = 6.1820$ to an equation can be appreciated if a three-dimensional model of the surface represented by eq. 1 is constructed. Figure 1 is a cross-section of this surface for $m_C = 0.32 m_B$. It will be seen that, at low m_B, $\Delta/(m_B m_C)$ increases with increasing m_B to a maximum at about $m_B = 8$ and then decreases to a minimum at about $m_B = 20$, after which it rises rapidly. Up to about $m_B = 19$, the curve can represent the experimental data very well but, at higher concentrations, the equation gives too high values of the function. Clearly, the experimental point in question cannot be fitted to a curve of this type. The point may be experimentally erroneous but we do not think this is so, because the downward trend of $\Delta/(m_B m_C)$ is confirmed by the last six entries in Table III. We have pointed out that these six data were obtained with some extrapolation from the experimental region, but we do not believe that the points are so much in doubt as to bring them onto the calculated curve in Fig. 1. Equation 1, therefore, gives a satisfactory representation of the experimental data except at high values of m_B and m_C. It might, however, be dangerous to use the equation beyond the region of experiment, e.g., for $m_B = 22$, $m_C = 1$, or $m_B = 1 = m_C = 7$.

Activity Coefficients.—It has been shown[1a] that if $\Delta/(m_B m_C) = f'(m_B) + F'(m_C)$ where f' is a function of m_B only and F' of m_C only, then

$$\left(\frac{\partial \ln \gamma_B}{\partial m_C}\right)_{m_B} = \left(\frac{\partial \ln \gamma_C}{\partial m_B}\right)_{m_C} = f'(m_B) + F'(m_C)$$

Equation 1 is not of this form, for it contains cross-products of m_B and m_C. However, by following the procedure used in the earlier paper,[1a] it can be shown that eq. 1 leads to the equations

$$\ln \gamma_B = \ln \gamma_B{}^0 + m_C[A + B m_B + {}^1/_2 C m_C +$$
$$D m_B{}^2 + {}^1/_3 E m_C{}^2 + {}^2/_3 F m_B m_C + G m_B{}^2 + {}^1/_4 H m_B{}^3 +$$
$${}^3/_4 I m_B{}^2 m_C + {}^1/_2 J m_B m_C{}^2]$$

$$2 \ln \gamma_C = 2 \ln \gamma_C{}^0 + m_B[A + {}^1/_2 B m_B + C m_C +$$
$${}^1/_3 D m_B{}^2 + E m_C{}^2 + {}^2/_3 F m_B m_C + {}^1/_4 G m_B{}^3 +$$
$$H m_C{}^3 + {}^1/_2 I m_B{}^2 m_C + {}^3/_4 J m_B m_C{}^2]$$

These equations give the values of $-\log \gamma_B$ and $-\log \gamma_C$ recorded in Tables IV and V. Considering the high solute concentrations that can be reached in this sys-

tem, the change in activity coefficient is not large. The limiting activity coefficient of sodium chloride at $m_C = 0$ and $m_B = 1$ is 0.9804; in 1 M mannitol it is 0.986; even in 20 M urea, the activity coefficient has fallen only to 0.898.

TABLE IV[a]
ACTIVITY COEFFICIENT OF UREA IN SODIUM CHLORIDE SOLUTION

m_B	m_C 0	1	2	3	4	5	6
0	0	0.0130	0.0192	0.0208	0.0198	0.0178	0.0160
1	0.0355	.0468	.0522	.0539	.0526	.0529	.0530
2	.0637	.0734	.0782	.0800	.0804	.0809	.0826
5	.1266	.1324	.1357	.1379	.1404	.1442	.1502
10	.1963	.1983	.2004	.2039	.2093	.2171	.2276
15	.2418	.2429	.2456	.2506	.2580	.2677	.2791
20	.2760	.2788	.2836	.2902	.2984	.3073	.3159

[a] The negative logarithm of the activity coefficient is tabulated.

TABLE V[a]
ACTIVITY COEFFICIENT OF SODIUM CHLORIDE IN UREA SOLUTIONS

m_C	m_B 0	1	2	5	10	15	20
0	0	0.0086	0.0150	0.0299	0.0421	0.0449	0.0468
1	0.1825	.1868	.1905	.1986	.2058	.2100	.2165
2	.1755	.1772	.1787	.1828	.1889	.1969	.2087
3	.1465	.1466	.1473	.1491	.1573	.1701	.1879
4	.1061	.1055	.1054	.1080	.1203	.1397	.1617
5	.0585	.0579	.0580	.0622	.0805	.1059	.1312
6	.0060	.0059	.0067	.0143	.0387	.0694	.0960
ΔG, cal. mole^{-1}	-2.2	1.1	20.5	81.3	161	237	

[a] The negative logarithm of the activity coefficient is tabulated.

The largest effect is found with 6 M NaCl; alone in water at this concentration, sodium chloride has an activity coefficient, $\gamma = 0.986$; in 20 M urea, it is 0.802.

Similarly, the activity coefficient of urea in 1 M solution, 0.921, is lowered to 0.885 by the addition of 6 M NaCl; for 20 M urea, the change is from 0.530 to 0.483 on the addition of a similar amount of sodium chloride.

It will be seen from Table V that, while the effect of urea on the activity coefficient of sodium chloride is generally one of "salting-in," there is a region (approximately $m_C \geq 4$, $m_B \leq 2$) where a very small "salting-out" effect is found.

The quantity $\Delta G = 2RT \ln f_C$ at $m_C = 0$, which can be calculated from the data in the second row of Table V, is the increment in chemical potential when a mole of sodium chloride is transferred from a given mole fraction in water to the same mole fraction in urea–water mixtures in the limit when $m_C = 0$, i.e., it is a measure of the medium effect. Values of ΔG are given in the last row of Table V. That of -2.2 cal. mole^{-1} in 1 M urea can be compared with $+13.6$ cal. mole^{-1} already calculated[1c] for sodium chloride in 1 M mannitol; that of 237 cal. mole^{-1} in 20 M urea (54.8%) with 242 cal. mole^{-1} for hydrochloric acid in 20% dioxane.

Solubility Measurements.—As was shown in earlier papers,[1a,1b] a knowledge of the Δ function over a range of m_B and m_C, along with solubility data for each solute in water, enables the solubility of B in solutions of C to be calculated and vice versa. The calculated solubilities of urea in sodium chloride solutions and of sodium chloride in urea solutions are shown in Fig. 2. Some direct solubility measurements were made. The solubility of sodium chloride in a 10.31 M urea solution was determined by saturating the urea solution with the salt and analyzing an aliquot for chloride; the
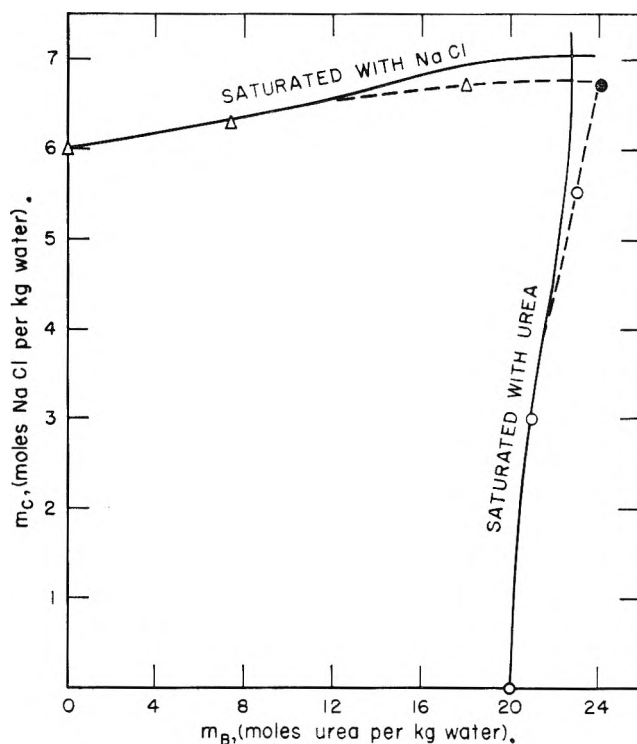

Fig. 2.—Solubility relations: ——, calculated solubility curves; – – –, drawn through the experimental points; △, solubility of NaCl in urea solutions; ⊙, solubility of urea in NaCl solutions; ●, point of mutual saturation.

solubility was found to be 6.465 M, the calculated value being 6.475 M. In 18.00 M urea we found a solubility of 6.722 M whereas the calculated value is 6.927 M.

Similarly, the solubility of urea in a 3.018 M sodium chloride solution was determined by evaporating to dryness in vacuo an aliquot of the saturated solution; from the amount of total solids and the known amount of sodium chloride in the aliquot, the solubility of urea could be determined: found, 21.20 M; calcd., 21.00 M. In 5.520 M NaCl solution, we found a solubility of 23.06 M urea compared with the calculated value of 22.48 M.

Finally, the point of mutual saturation was determined by evaporating to dryness an aliquot of the solution saturated to both urea and sodium chloride; the amount of total solid and an analysis of the chloride content gave solubilities of 24.16 M urea and 6.712 M NaCl. The calculated values are 22.70 M urea and 7.036 M NaCl.

We see, therefore, that we get reasonably good agreement when either the urea concentration (10.31 M) or the sodium chloride concentration (3.018 M) is not too high. If either is high, then solubilities predicted by eq. 1 do not agree with those found experimentally; in particular, eq. 1 does not predict the point of mutual saturation. This might have been expected, for the parameters of eq. 1 were derived with the full knowledge that they were not of much use at high values of m_B and m_C (specifically, $m_B = 19.749$, $m_C = 6.1820$); still less would we expect them to predict the even higher concentrations at the point of mutual saturation.

AUTOMATIC AND COULOMETRIC TITRATIONS IN STUDIES OF CHEMICAL KINETICS. I. COMPLEX FORMATION

By RICHARD E. COVER[1] AND LOUIS MEITES

Department of Chemistry of the Polytechnic Institute of Brooklyn, Brooklyn, N. Y.

When a pseudo-first-order process (such as ligand exchange) is displaced by producing or destroying a reactant at a constant rate, as by automatic or coulometric titration, the rate and equilibrium constants of that process may be deduced from the titration curve obtained by any of the common techniques of end-point detection. Three different chemical systems are considered.

Introduction

In the calculation of titration curves it has always been assumed that chemical equilibrium is attained at every point. When zero-current potentiometry is used for end-point location it has also traditionally been assumed that each of the couples involved is reversible and that electrochemical equilibrium is attained at every point.

Several recent developments have contributed to an enhanced understanding of potentiometric titration curves. These include the realization[2] that an expression similar to the Nernst equation may be written even when the potential-determining couple is not ideally reversible, the demonstration[3,4] of the relationship between the potentiometric titration curve and the voltammetric characteristics of the couples involved, and the recognition[5] of the influence of the nature of the electrode surface on the potentiometric titration curve.

The present paper deals with complications caused by the occurrence of slow chemical reactions in the solution phase, so that chemical equilibrium is not attained at the instant of measurement. The procedure followed has been to conceive of a number of hypothetical models for titration systems and to establish and integrate the corresponding kinetic equations. The integrated equations, relating the concentrations of various species to time, describe titration curves that are characteristic of such end-point detection techniques as amperometry and spectrophotometry. Through these equations, the zero-current potential may also be related to time. Analysis of the results gives rise to various procedures for the extraction of rate and equilibrium constants from titration-curve data.

Throughout this work it has been assumed that the reaction is isothermal, that mixing is instantaneous, and that the volume change during titration is negligible. Generally these requirements can be closely approximated in practice. It has also been assumed that the rate of addition of titrant is constant. This is the case in coulometric titrations, in which the reagent is electrogenerated by the flow of a constant current (that, contrary to conventional practice, is not interrupted while measurements are made), as well as in automatic titrations, in which the reagent is continuously added by means of a constant-rate buret or

equivalent device. The equations that follow are written for the latter case. They may be converted to the form appropriate for coulometric titrations by using the relation

$$i/F = NV' = nv\rho \quad (1)$$

where i is the constant electrolysis current (amp.), F is the faraday (96491.2 coulombs/equivalent), N is the oxidation–reduction normality of the titrant (equivalents/cm.^{3}), V' is the constant volume rate of addition of titrant (cm.^{3}/sec.), n is the number of electrons involved in the oxidation or reduction of each molecule or ion of the species being titrated, v is the volume of the solution titrated (cm.^{3}), and ρ is the constant stoichiometric rate of addition of titrant (mole-cm.$^{-3}$ sec.$^{-1}$).

All of the systems considered below are formulated in the following way. It is assumed that a species A is titrated with a species T', and that the reaction between these may be written

$$A + T' \underset{k_A}{\overset{k_{-A}}{\rightleftarrows}} A' + T \quad (2)$$
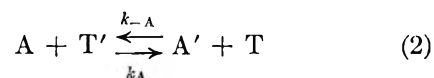
where A and T are the oxidized and A' and T' the reduced forms of the couples, and k_A and k_{-A} are second-order or pseudo-second-order rate constants (mole^{-1} cm.^{3} sec.$^{-1}$). It is further assumed that the forward reaction is very fast and that the equilibrium lies far to the right—in effect, that $k_{-A} = 0$ and $k_A = \infty$. Then the rate equations for the system are

$$\text{when } C_A > 0, C_{T'} = 0 \text{ and } dC_A/dt = -\rho \quad (3)$$

$$\text{when } C_{T'} > 0, C_A = 0 \text{ and } dC_{T'}/dt = \rho \quad (4)$$

where t is the elapsed titration time (sec.), C_X is the concentration of species X (moles/cm.^{3}), and ρ is defined by eq. 1. If the A–A' couple is potential-determining, then the Nernst expression becomes simply (at 25°)

$$E = E^{0'} - \frac{0.0591}{n_A} \log \frac{t}{t^* - t} \quad (5)$$

where E is the zero-current potential at time t, $E^{0'}$ is the formal potential of the A–A' couple, n_A is the number of electrons involved in the rate-determining step of the electroreduction of A to A', and t^* is the value of t at the equivalence point. E and $E^{0'}$ are, of course, referred to the same reference electrode.

This mode of formulation is simple and easily manipulated. The assumptions made will be closely satisfied by many chemical systems, particularly when the rate of titrant addition is low. Moreover, this formulation permits the potential–time function to be evaluated

(1) This paper is based on the dissertation submitted by Richard E. Cover to the Faculty of the Polytechnic Institute of Brooklyn in partial fulfillment of the requirements for the degree of Doctor of Philosophy in June, 1962.

(2) S. Glasstone, K. J. Laidler, and H. Eyring, "The Theory of Rate Processes," McGraw-Hill Book Co., Inc., New York, N. Y., 1941, pp. 575–577.

(3) J. Coursier, *Anal. Chim. Acta*, **7**, 77 (1952).

(4) I. M. Kolthoff, *Anal. Chem.*, **26**, 1685 (1954).

(5) J. W. Ross and I. Shain, *ibid.*, **28**, 548 (1956).

even when both of the reacting couples are electroactive, since it eliminates the necessity of considering the titrant couple before the end point.

An equation can be derived which, in principle, permits the calculation of the zero-current potential from information on the composition of the solution even if the cathodic process is not the reverse of the anodic one. It is[6]

$$E = E^{\dagger} - \frac{0.0591}{\gamma n_{\mathrm{D}} - \beta' n_{\mathrm{B}}'} \log \frac{C_{\mathrm{B}}'}{C_{\mathrm{D}}} \qquad (6)$$

where γ and β' are effective transfer coefficients for the reduction of species D and the oxidation of species B', respectively, n_{D} and n_{B}' are the numbers of electrons involved in the rate-determining steps of these processes, and $E^{\dagger}$ is obtainable from free-energy considerations. The parameters γ and β' are assumed to be constant in the derivation of this expression; where it has been used in this work, it has been assumed that $(\gamma n_{\mathrm{D}} - \beta' n_{\mathrm{B}}') = 1$.

The procedure recommended below for the treatment of potentiometric data is a simple one that provides a sensitive diagnostic technique for the identification of the various kinetic complications that may occur. As was shown above, for the straightforward reduction of a single species the potential before the equivalence point is described by eq. 5; consequently a plot of E or $(E - E^{0'})$ vs. $\log t/(t^* - t)$ should be linear and have a slope of $-0.0591/n_{\mathrm{A}}$ v. This is not so when a slow side reaction also occurs. Plotting experimental data in this way will then give non-linear curves whose comparison with the theoretical ones should provide much insight into the nature of the system.

It is arbitrarily assumed here that the titrant is a reducing agent. Cases like those below in which the titrant is an oxidizing agent will be described by equations identical with those given here except for the sign of the change of potential with time.

Results and Discussion

System 1.—This system may be represented by the scheme

$$B \underset{k_1}{\overset{k_{-1}}{\rightleftarrows}} A \xrightarrow{\mathrm{T}'} A'$$
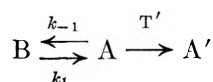
That is, species A, which on reaction with the titrant T' undergoes reduction to A', is in slow equilibrium with another species, B, in the same oxidation state. The first-order or pseudo-first-order rate constants k_1 and k_{-1} are expressed in sec.$^{-1}$.

This system is described by the equations

$$dC_{\mathrm{A}}/dt = -k_{\mathrm{A}}C_{\mathrm{A}}C_{\mathrm{T}'} - k_{-1}C_{\mathrm{A}} + k_1 C_{\mathrm{B}} \qquad (7)$$

$$dC_{\mathrm{B}}/dt = k_{-1}C_{\mathrm{A}} - k_1 C_{\mathrm{B}} \qquad (8)$$

$$dC_{\mathrm{T}'}/dt = \rho - k_{\mathrm{A}}C_{\mathrm{A}}C_{\mathrm{T}'} \qquad (9)$$

$$dC_{\mathrm{A}'}/dt = dC_{\mathrm{T}}/dt = k_{\mathrm{A}}C_{\mathrm{A}}C_{\mathrm{T}'} \qquad (10)$$

It is convenient to define a time τ such that $C_{\mathrm{A}} \rightarrow 0$ as $t \rightarrow \tau$. Then, with the aid of eq. 3 and 4, the solutions of the rate equations become, for $t \leq \tau$

(6) R. E. Cover, Ph.D. Dissertation, Polytechnic Institute of Brooklyn, 1962.

$$C_{\mathrm{A}} = \frac{\rho}{G_1} [k_1(t^* - t) - k_{-1}/G_1] + e^{-G_1 t} \left[C_{\mathrm{A}}^0 - \frac{\rho}{G_1} (k_1 t^* - k_{-1}/G_1) \right] \qquad (11)$$

$$C_{\mathrm{B}} = \frac{k_{-1}\rho}{G_1} \left[t^* - t + \frac{1}{G_1} \right] + e^{-G_1 t} \left[C_{\mathrm{B}}^0 - \frac{k_{-1}\rho}{G_1} \left(t^* + \frac{1}{G_1} \right) \right] \qquad (12)$$

where $G_1 = (k_1 + k_{-1})$ and C_{X}^0 is the value of C_{X} at $t = 0$.

If species A and B are assumed to be in equilibrium at $t = 0$, eq. 11 and 12 may be further simplified to

$$C_{\mathrm{A}} = \frac{\rho}{G_1^2} [k_1 G_1(t^* - t) - k_{-1} + k_{-1}e^{-G_1 t}] \qquad (13)$$

$$C_{\mathrm{B}} = \frac{\rho}{G_1^2} [k_{-1}G_1(t^* - t) + k_{-1} - k_{-1}e^{-G_1 t}] \qquad (14)$$

The exponential terms in eq. 11–14 may be made negligible by increasing the sample size or decreasing ρ. Then C_{A} and C_{B} will decrease linearly with time. If meither can be followed during the titration (by amperometry, spectrophotometry, or another technique), the rate constants can be evaluated from data on the linear portions of the concentration–time curves. One has

$$k_1 = \frac{S_{\mathrm{A}}}{(I_{\mathrm{A}} + t^* S_{\mathrm{A}})(K_1 + 1)} \qquad (15)$$

$$k_{-1} = \frac{-S_{\mathrm{B}}}{(I_{\mathrm{B}} + t^* S_{\mathrm{B}})(K_1 + 1)} \qquad (16)$$

where I_{X} and S_{X} are the intercept and slope, respectively, of the linear portion of the plot of C_{X} vs. t, and $K_1 = k_1/k_{-1}$.

In applying eq. 15 and 16, the equivalence-point time t^* would, of course, be calculated a priori from the concentrations of the solutions, the rate of addition of titrant, and the stoichiometry of the reaction. Equilibrium measurements are not necessary for the evaluation of K_1, which is more conveniently obtained from these equations as

$$K_1 = -S_{\mathrm{A}}(I_{\mathrm{B}} + t^* S_{\mathrm{B}})/S_{\mathrm{B}}(I_{\mathrm{A}} + t^* S_{\mathrm{A}}) \qquad (17)$$

Obviously it is unnecessary to know the actual concentrations of A and B (i.e., the constant of proportionality relating these concentrations to the measured diffusion current, absorbance, etc.). Finally, the calculation can still be performed even if only one of these substances can be followed, since

$$C_{\mathrm{A}} + C_{\mathrm{B}} = \rho(t^* - t) \qquad (18)$$

which, of course, is valid only for $t \leq \tau$. The value of τ in any experiment may be estimated by considering its properties: (1) $0 \leq \tau \leq t^*$, (2) $C_{\mathrm{A}} = 0$ for $t \geq \tau$, and (3) only if $t \leq \tau$ can C_{B} vary linearly with time.

When $t \geq \tau$ (so that $C_{\mathrm{A}} = 0$), the assumptions that A and B are in equilibrium at $t = 0$ and that the exponential terms in eq. 13 and 14 are negligible at $t = \tau$ lead to the following solutions of the rate equations.
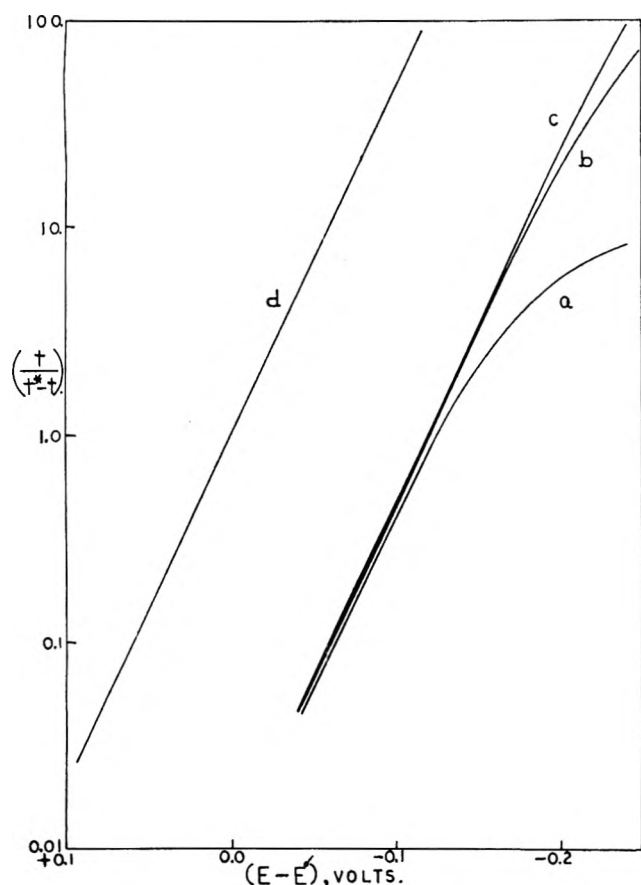
Fig. 1.—Plots of $(E - E^{0\prime})$ vs. log $t/(t^* - t)$ for system 1. The A–A' couple is assumed to be potential-determining; $n_A = 1$, $k_{-1} = 100k_1 = 1.67$ sec.$^{-1}$, $t^* = $ (a) 600, (b) 6000, and (c) 60,000 sec. Curve (d) represents the simple equilibrium case in which the side reaction B $\rightleftharpoons$ A does not occur.

Fig. 2.—Plots of $(E - E^{0\prime})$ vs. log $t/(t^* - t)$ for system 1. The B–A' couple is assumed to be potential-determining; $n_A = 1$, $k_{-1} = 100k_1 = 1.67$ sec.$^{-1}$, $t^* = $ (a) 60, (b) 600, and (c) 6000 sec.

$$C_B = \frac{\rho k_{-1}}{k_1 G_1} \exp\left[k_1(t^* - t) - \frac{k_{-1}}{G_1} \right] \quad (19)$$

$$C_T = C_A' = \rho \left\{ t^* - \frac{k_{-1}}{k_1 G_1} \exp\left[k_1(t^* - t) - \frac{k_{-1}}{G_1} \right] \right\} \quad (20)$$

$$C_T' = \rho \left\{ t - t^* + \frac{k_{-1}}{k_1 G_1} \exp\left[k_1(t^* - t) - \frac{k_{-1}}{G_1} \right] \right\} \quad (21)$$

It is clear from eq. 19 that a plot of ln C_B vs. t in this interval will be linear and will have a slope equal to $-k_1$. Consequently, if C_B is followed throughout the titration, k_1 can be evaluated. Then

$$k_{-1} = \frac{kC_B^0}{\rho t^* - C_B^0} \quad (22)$$

The value of k_1 may also be determined by following C_A' or C_T in this interval, since, from eq. 20, a plot of either ln $(\rho t^* - C_A')$ or ln $(\rho t^* - C_T)$ vs. t will be linear and will have a slope equal to $-k_1$.

The rate constants can also be evaluated from potentiometric data if the potential in the interval $t \leq \tau$ is controlled by the A–A' couple and if the value of C_A is known at some time during this interval. If, in addition, the exponential term in eq. 11 is negligible for an appreciable portion of this interval, then since
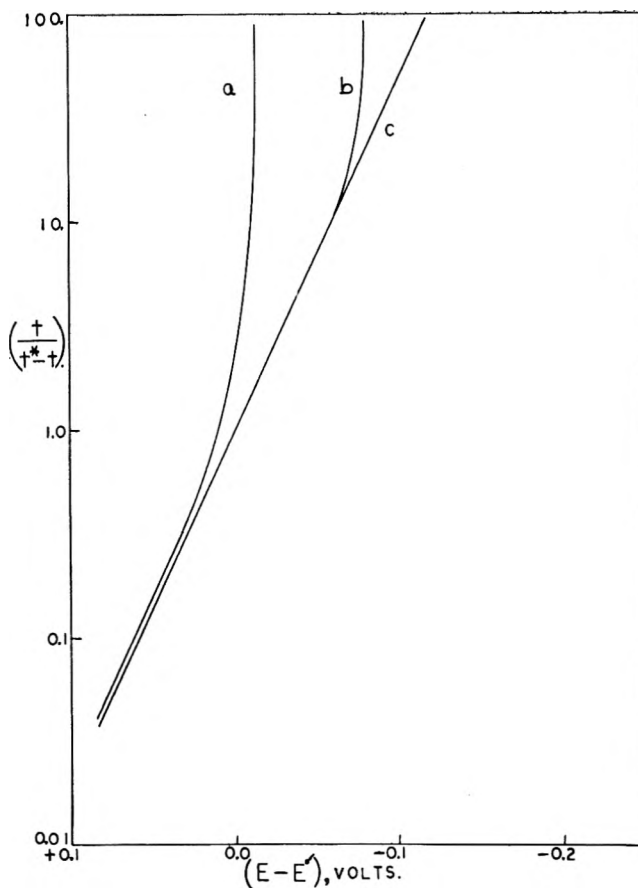
$$C_A' = \rho t \quad (23)$$

throughout this interval, one can use the value of C_A' together with the measured potential and the Nernst equation to calculate the change in C_A relative to some known value of C_A during the titration. At any pair of times t_1 and t_2 one has

$$E_2 - E_1 + \frac{0.0591}{n_A} \log \frac{t_2}{t_1} = \frac{0.0591}{n_A} \log \frac{C_{A_2}}{C_{A_1}} \quad (24)$$

This permits the evaluation of the function R_t, which is defined as the ratio C_A/C_{A_1}, at varous times during the titration. When the exponential term in eq. 11 becomes negligible, R_t becomes a linear function of time. Data obtained in the time interval in which this is so may be used for the evaluation of the rate constants in the following manner.

Let R_M and R_N be two values of R_t at the corresponding times t_M and t_N on the linear portion of a plot of R_t vs. t, and let $R_1' = R_M/R_N$. Then it can be shown[6] that

$$k_1 G_1 = k_{-1} Q_1 \quad (25)$$

where

$$Q_1 = \frac{R_1' - 1}{t^*(R_1' - 1) - R_1' t_N + t_M} \quad (26)$$

If C_A^0 (the value of C_A at $t = 0$) is known, and if the system was in equilibrium at $t = 0$, then k_1 is given by

$$k_1 = Q_1 \left[1 - \frac{C_A^0}{\rho t^*} \right] \quad (27)$$

and

$$k_{-1} = \frac{k_1{}^2}{Q_1 - k_1} \quad (28)$$

If the value of C_A is known at t_M but not at $t = 0$, one may evaluate C_A at t_N (from the relation $C_{AN} = C_{AM}/R_1'$) and then calculate k_1 from

$$C_{AM} - C_{AN} = \rho(t_N - t_M)(Q_1 - k_1)/Q_1 \quad (29)$$

and k_{-1} from eq. 28.

In a titration of this system, the end point precedes the equivalence point if C_A is followed or if the A–A′ couple controls the potential before the end point. This is because $C_A \rightarrow 0$ as $t \rightarrow \tau$, while τ is given by

$$\tau = t^* - \frac{1}{K_1 G_1} \quad (30)$$

Since $k_1 G_1 > 0$, clearly $\tau < t^*$. The absolute error, $t^* - \tau$, is constant and equal to $1/K_1 G_1$, but the relative error, $(\tau/t^*) - 1$, approaches zero with increasing t^*. The end point also precedes the equivalence point if it is the variation of C_A', C_B, C_T, or C_T' that is followed. Increasing t^*, either by increasing the sample size or by decreasing ρ, tends to decrease the error in all of these cases.

Figures 1 and 2 show plots of the potential function $(E - E^{0\prime})$ vs. $\log t/(t^* - t)$ and illustrate the behavior that will be observed in this system on varying t^*. For a simple reversible system, of course, such a plot should be a straight line with a slope of $-0.0591/n$ v. and an intercept [at $t/(t^* - t) = 1$] of 0. If the A–A′ couple is potential-determining, however, the curve is not linear (Fig. 1) and the end point precedes the equivalence point. If the B–A′ couple is potential-determining (Fig. 2), a non-linear curve is again obtained but the curvature is in the opposite direction and the end point follows the equivalence point.

In either case the curves approach linearity as t^* increases and the end point error decreases. For the case in which the A–A′ couple is potential-determining the limiting expression as $t^* \rightarrow \infty$ is

$$E = E^{0\prime} - \frac{0.0591}{n_A} \log \frac{1 + K_1}{K_1} - \frac{0.0591}{n_A} \log \frac{t}{t^* - t} \quad (31)$$

System 2.—This system may be represented by the scheme

$$A \xrightarrow{T'} A' \underset{k_2}{\overset{k_{-2}}{\rightleftarrows}} B'$$
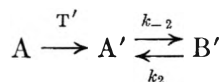
That is, species A is reduced to A′ by the titrant T′, and A′ is in slow equilibrium with another species, B′, which is in the same (reduced) oxidation state. The first-order or pseudo-first-order rate constants k_2 and k_{-2} are expressed in sec.$^{-1}$.

This system is described by the equations

$$dC_A/dt = -k_A C_A C_T' \quad (32)$$

$$dC_A'/dt = k_A C_A C_T' + k_2 C_B' - k_{-2} C_A' \quad (33)$$

$$dC_B/dt = k_{-2} C_A' - k_2 C_B' \quad (34)$$

With the aid of eq. 3 and 4, the solutions of the rate equations for the interval $t \leq t^*$ are found to be

$$C_A = \rho(t^* - t) \quad (35)$$

$$C_A' = \frac{\rho}{G_2{}^2}[k_2 G_2 t + k_{-2} - k_{-2} e^{-G_2 t}] \quad (36)$$

$$C_B' = \frac{\rho}{G_2{}^2}[k_{-2} G_2 t - k_{-2} + k_{-2} e^{-G_2 t}] \quad (37)$$

where $G_2 = k_2 + k_{-2}$. For the interval $t \geq t^*$ the solutions are

$$C_A' = \frac{\rho}{G_2{}^2}\{k_2 G_2 t^* - k_{-2} \exp[G_2(t^* - t)]\} \quad (38)$$

$$C_B' = \frac{\rho}{G_2{}^2}\{k_{-2} G_2 t^* - k_{-2} \exp[G_2(* - t)]\} \quad (39)$$

assuming that the exponential terms in eq. 36 and 37 are negligible at $t = t^*$, a condition that will be satisfied if t^* is sufficiently large or if ρ is sufficiently small.

When, in the interval $t \leq t^*$, the exponential terms in eq. 36 and 37 are negligible, C_A' and C_B' will increase linearly with time. If either can be followed during the titration, the rate constants can be evaluated from data on the linear portions of the concentration–time curves. One has

$$k_2 = S_A'/I_A'(K_2 + 1) \quad (40)$$

$$k_{-2} = -S_B'/I_B'(K_2 + 1) \quad (41)$$

where I_X and S_X were defined above (cf. eq. 15 and 16) and $K_2 = k_2/k_{-2}$. Analogously to eq. 17

$$K_2 = -S_A'I_B'/S_B'I_A' \quad (42)$$

If only one of these two concentrations can be followed, the other can be calculated from the relation

$$C_A' + C_B' = \rho t \quad (43)$$

The rate constants can thus be evaluated in a manner similar to that outlined for system 1 in the discussion of eq. 15–18.

They may also be evaluated from potentiometric data if the A–A′ couple is potential-determining in the interval $t \leq t^*$, if either K_2 or the value of C_A' at some instant during the titration is known, and if the exponential term in eq. 36 is negligible for an appreciable time in this interval. Then the value of C_A given by eq. 35 can be used, together with the measured potential and the Nernst equation, to calculate the change in C_A' relative to some arbitrarily chosen value of C_A' during the titration. The function R_t', defined as the ratio C_A'/C_{A_1}', can then be evaluated at various times during the titration (cf. eq. 24 and the accompanying discussion). When the exponential term in eq. 36 becomes negligible, R_t' becomes a linear function of time. As in the discussion of eq. 25–29, let R_M' and R_N' be two values of R_t' on the linear portion of a plot of R_t' vs. t, and let $R_2' = R_M'/R_N'$. Then

$$k_2 G_2 = k_{-2} Q_2 \quad (44)$$

where

$$Q_2 = (1 - R_2')/(R_2' t_N' - t_M') \quad (45)$$

If K_2 is known, k_2 and k_{-2} can be calculated from the equations

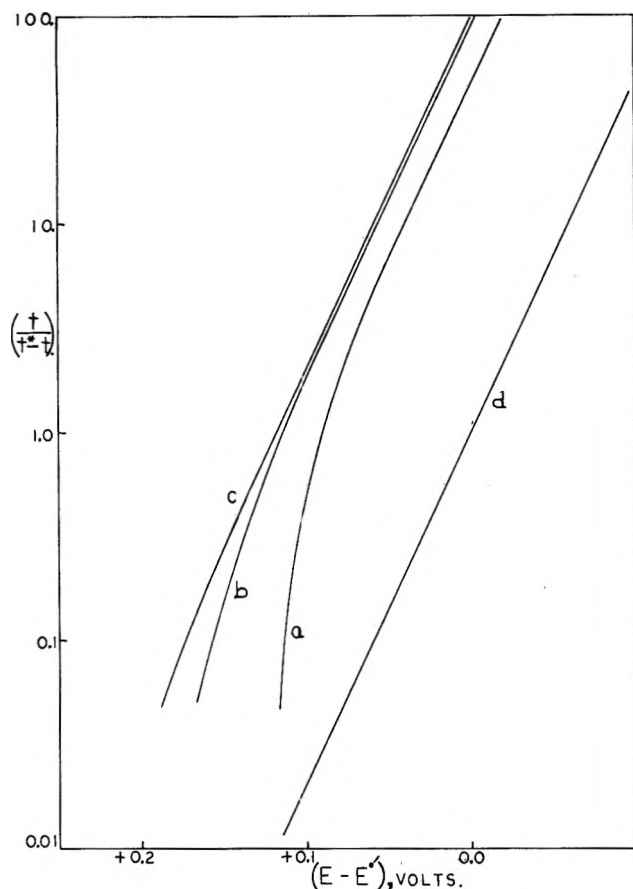$$K_2 = (Q_2 - k_2)/k_2 \quad (46)$$

Fig. 3.—Plots of $(E - E^{0'})$ vs. $\log t/(t^* - t)$ for system 2. The A–A' couple is assumed to be potential-determining; $n_A = 1$, $k_{-2} = 100k_2 = 1.67$ sec.$^{-1}$, $t^* = $ (a) 60, (b) 600, and (c) 6000 sec. Curve (d) represents the simple equilibrium case in which the side reaction A' $\rightleftharpoons$ B' does not occur.

and

$$k_{-2} = k_2^2/(Q_2 - k_2) \qquad (47)$$

If, on the other hand, K_2 is not known but the value of $C_{A'}$ is known at some time $t^\dagger$, k_2 may be calculated from the expression

$$k_2 = Q_2 - \frac{Q_2{}^2 C_{A',t\dagger}}{\rho(Q_2 t^\dagger + 1)} \qquad (48)$$

and k_{-2} may then be calculated from eq. 47.

Figure 3 shows plots of the potential function $(E - E^{0'})$ vs. $\log t/(t^* - t)$ and illustrates the behavior that will be observed in this system on varying t^*; it is assumed that the A–A' couple is potential-determining. The shapes of these curves are characteristic of the system, as is also the case for those shown in Fig. 1 and 2. They approach linearity as t^* increases, and the limiting expression as $t^* \rightarrow \infty$ is

$$E = E^{0'} - \frac{0.0591}{n_A} \log \frac{K_2}{1 + K_2} - \frac{0.0591}{n_A} \log \frac{t}{t^* - t} \qquad (49)$$

The use of amperometry, spectrophotometry, or a similar technique for locating the end point in a titration of this system may give rise to very large errors, as is shown by Fig. 4, which was calculated with the same values of the different parameters as were used to obtain Fig. 3. Similar curves for the other systems considered here and in a subsequent paper may be found in the junior author's dissertation.[6]
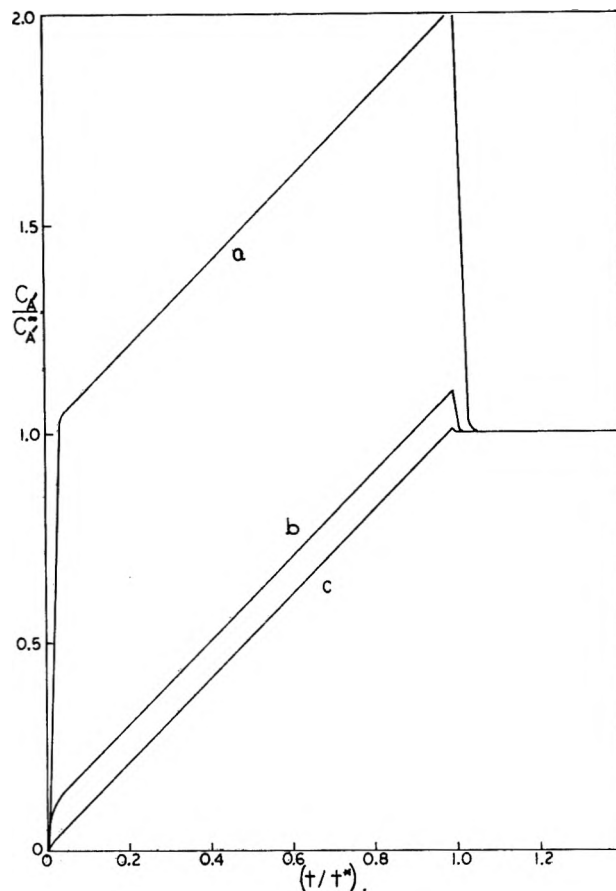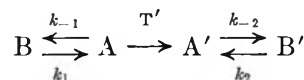

Fig. 4.—Plots of $C_{A'}/C_{A'}{}^{\infty}$ vs. t/t^* for system 2. All parameters are identical with those for the similarly labeled curves in Fig. 3.

System 3.—This system may be represented by the scheme

$$B \underset{k_1}{\overset{k_{-1}}{\rightleftharpoons}} A \overset{T'}{\longrightarrow} A' \underset{k_2}{\overset{k_{-2}}{\rightleftharpoons}} B'$$

That is, species A is in slow equilibrium with another species, B, in the same oxidation state; on reaction with the titrant, T', species A is reduced to A', which in turn is in slow equilibrium with another species, B', in the same (reduced) oxidation state. The titration of osmium(IV) with chromium(II) in hydrochloric acid solutions has been found[6] to exemplify this system under certain conditions, and will be described in detail in a later paper.

System 3 clearly combines the processes represented by systems 1 and 2; as would be expected, many of the equations valid for the latter systems are valid for system 3 as well. This system is described by rate equations identical with eq. 7, 8, 9, 33, and 34.

If a time τ is again defined such that $C_A \rightarrow 0$ as $t \rightarrow \tau$, these rate equations can be integrated as before. For $t \leq \tau$, the variations of C_A and C_B are described by eq. 11–14, derived above for system 1; and the variations of $C_{A'}$ and $C_{B'}$ are described by eq. 36 and 37, derived above for system 2. For $t \geq \tau$, the variations of C_A, C_B, C_T, and $C_{T'}$ are described by eq. 19–21 derived above for system 1; the variations of $C_{A'}$ and $C_{B'}$ in this interval, however, obey equations that are unique to system 3. These are rather complex and ill-suited to the evaluation of the rate constants, and therefore are not presented here; they may be found in the junior author's dissertation as eq. 213 and 214.
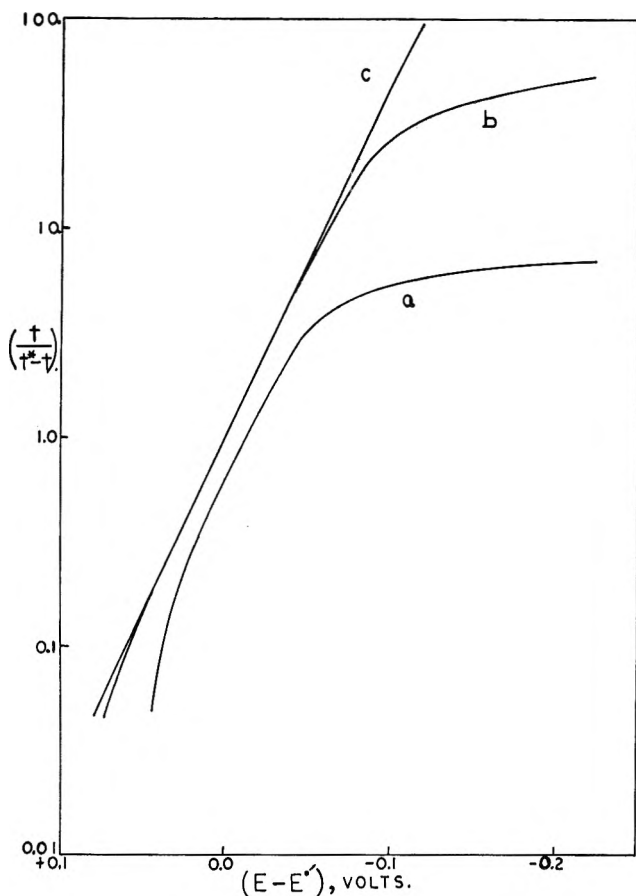
Fig. 5.—Plots of $(E - E^{0\prime})$ vs. log $t/(t^* - t)$ for system 3. The A–A' couple is assumed to be potential-determining; $n_A = 1$, $k_{-1} = k_{-2} = 100k_1 = 100k_2 = 1.67$ sec.$^{-1}$, $t^* =$ (a) 600, (b) 6000, and (c) 60,000 sec.
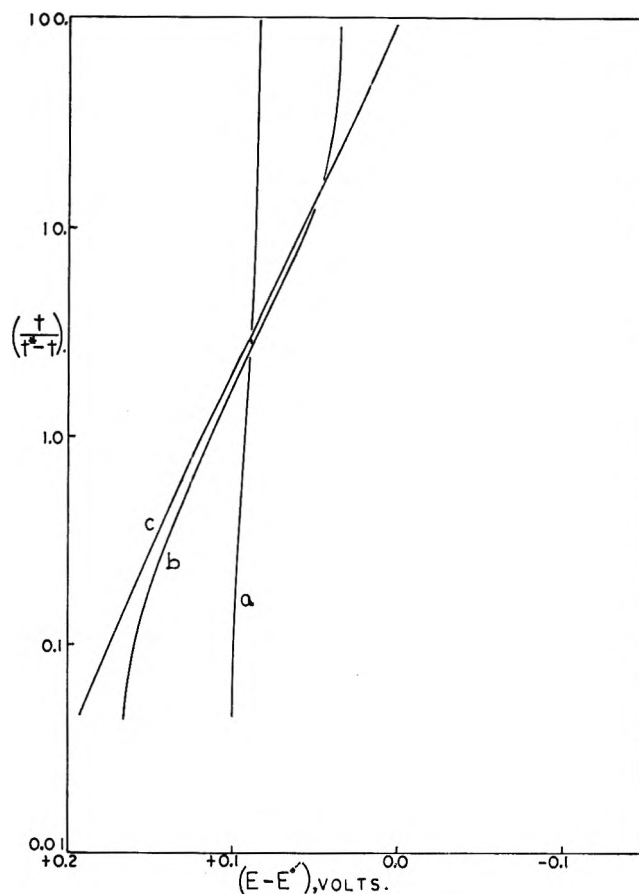

Fig. 6.—Plots of $(E - E^{0\prime})$ vs. log $t/(t^* - t)$ for system 3. The B–A' couple is assumed to be potential-determining; $n_A = 1$, $k_{-1} = k_{-2} = 100k_1 = 100k_2 = 1.67$ sec.$^{-1}$, $t^* =$ (a) 60, (b) 600, and (c) 6000 sec.

If C_A, C_B, C_A', C_B', or C_T is followed during the titration by amperometry, spectrophotometry, or a similar technique, the rate constants k_1, k_{-1}, k_2, and k_{-2} can be evaluated by the procedures described above. They can also be evaluated from potentiometric data if the A–A' couple is potential-determining in the interval $t \leq \tau$ and if the exponential terms in eq. 11 and 36 are negligible for an appreciable time in this interval. Under these conditions the Nernst equation becomes

$$E = E^{0\prime} - \frac{0.0591}{n_A} \log \ [G_1^2(k_2 G_2 t + k_{-2})]/$$

$$\{G_2^2[k_1 G_1(t^* - t) - k_{-1}]\} \quad (50)$$

Clearly the methods outlined for such calculations in systems 1 and 2 are not applicable here, where neither C_A nor C_A' can be evaluated without prior knowledge of the rate constants. In principle, however, there is another viable approach to the problem; it can be shown that

$$\left(\frac{\partial E}{\partial t^*}\right)_t = \frac{0.0257}{n_A[t^* - t - (1/K_1 G_1)]} \quad (51)$$

This would permit the evaluation of $K_1 G_1$ from data obtained in a series of titrations in which the sample size or the value of ρ was changed so as to vary t^*. Plots of E vs. t^* for various arbitrarily selected values of t should

yield a family of straight lines having slopes equal to each other and to the right-hand side of eq. 51. By analogy with the above treatment of system 1, the rate constants k_1 and k_{-1} could then be evaluated if either K_1 or C_A^0 is known; then C_A could be evaluated at any time smaller than or equal to τ by means of eq. 11; and finally the procedure outlined above for system 2 could be used to evaluate k_2 and k_{-2}.

Figures 5 and 6 show plots of the potential function $(E - E^{0\prime})$ vs. log $t/(t^* - t)$, calculated by assuming that either the A–A' couple (in Fig. 5) or the B–B' couple (in Fig. 6) is potential-determining. As in the other systems, the shapes of these curves and the manners in which they are affected by varying t^* are characteristic of both the system and the couple that is assumed to be potential-determining. When the A–A' couple is potential-determining, the limiting expression as $t^* \rightarrow \infty$ is

$$E = E^{0\prime} - \frac{0.0591}{n_A} \log \frac{K_2(1 + K_1)}{K_1(1 + K_2)} -$$

$$\frac{0.0591}{n_A} \log \frac{t}{t^* - t} \quad (52)$$

THE BEHAVIOR OF MONOLAYERS OF PROGRESSIVELY FLUORINATED FATTY ACIDS ADSORBED ON WATER[1]

By Marianne K. Bernett and W. A. Zisman

U. S. Naval Research Laboratory, Washington 25, D. C.

A study has been made on the force–area, surface potential–area and surface moment–area relations of monolayers of two series of progressively fluorinated fatty acids spread on water at various pH values. The series were n-heptadecanoic acids with substitutions in the 17-position of perfluoromethyl, perfluoropropyl, perfluoropentyl, and perfluoroheptyl groups, and n-undecanoic acids with substitutions in the 11-position of perfluoroheptyl, perfluorooctyl, and perfluorodecyl groups. In both series the stability of the monolayers at all pH values falls off rapidly with progressively shorter perfluoro segments. The compressed films of all stable acids are in the liquid-condensed state, indicating limiting areas per molecule of 36 to 38 Å.². The change in surface potentials of all films is larger than those of any aliphatic acid and shows that the dipole is oriented in the opposite direction. By use of the Helmholtz equation the vertical components of the apparent dipole moment were ascertained from the potentials and it was possible to compute, under a given set of conditions, the values of the vertical component of the partially fluorinated chain only. The results are discussed in terms of orientation and packing of the adsorbed molecules, steric hindrance due to the bulky perfluoro segments, and electrostatic repulsion.

Introduction

Previous investigations[2,3] at this Laboratory have been concerned with the surface-chemical properties of adsorbed monolayers of molecules comprising a single linear chain of 16 –CH₂– groups terminated on one end by a –CF₃ group and on the other end by a carboxylic acid or an amino group. Shafrin and Zisman[2] suggested the presence of a strong dipole in the –CH₂–CF₃ linkage in order to explain the small effect of fluorinating the ω-carbon atom on the wettability of the condensed monolayer adsorbed on polished glass or metal substrates. Fox[3] proposed that the same dipole through weakening of the cohesive forces also caused a film expansion in the insoluble monolayers spread on water. More recently Shafrin and Zisman[4] investigated the wettability of monolayers adsorbed on metals using a series of ω-(n-perfluoroalkyl)-heptadecanoic acids and found that the effect on liquid adhesion of the uncompensated dipole at the –CH₂–CF₂– linkage became negligible only when it was located at least 6 carbon atoms below the ω-carbon atom. The present study reports the mechanical and electrical properties of insoluble monolayers on water using the same family of progressively fluorinated fatty acids (the 17-heptadecanoic acids) as well as an analogous family, the perfluoroalkyl substituted 11-undecanoic acids.

Experimental Materials and Procedures

The organic acids studied were highly purified, white, crystalline solids. The ω-trifluorostearic acid had been received from Dr. Gavlin of the Armour Research Foundation[5]; all other fluorinated acids had been prepared by Dr. Brace[6] and were a gift of the Organic Chemicals Department of the du Pont Company. As in the study reported earlier,[4] these compounds were pure enough to be used as received. The stearic acid used for purposes of comparison was Eastman White Label grade (m.p. 69.5°). Table I lists the compounds studied, the number (n) of carbon atoms in the fluorinated chain, the melting point, and a conveniently abbreviated code name which will be used hereafter in this report.

The solvent used to spread the acid on water was n-hexane which had previously been purified by repeated percolation through an adsorption column packed with activated silica gel

TABLE I
Molecular Formulas and Code Designation of the Fluorinated Fatty Acids

Name of compound	n	M.p., °C.	Code
$F(CF_2)_n-(CH_2)_{16}COOH$			
17-(Perfluoroheptyl)-heptadecanoic acid	7	91–92	7F-16H acid
17-(Perfluoropentyl)-heptadecanoic acid	5	77–79	5F-16H acid
17-(Perfluoropropyl)-heptadecanoic acid	3	73–74.5	3F-16H acid
17-(Perfluoromethyl)-heptadecanoic acid	1	70.0–70.5	1F-16H acid
Stearic acid	..	69.5	17H acid
$F(CF_2)_n-(CH_2)_{10}COOH$			
11-(Perfluorodecyl)-undecanoic acid	10	111–112	10F-10H acid
11-(Perfluorooctyl)-undecanoic acid	8	89–90	8F-10H acid
11-(Perfluoroheptyl)-undecanoic acid	7	82–83	7F-10H acid

and alumina. Concentrations of the fluorinated acids in hexane ranged from 1.0×10^{-4} to 6.1×10^{-4} g./ml. of solvent. Each solution was delivered dropwise to the clean water surface of the film balance with a calibrated, self-adjusting, micropipet in a volume selected to give a condensed film occupying from 200 to 240 cm.². The modified Langmuir–Adam film balance used was made of a single piece of Pyrex glass sandblasted[7] to form a trough 0.2 cm. deep, 73 cm. long, and 12 cm. wide. Before the experiments the trough and the movable Pyrex barriers were cleaned with a hot, concentrated, nitric–sulfuric acid solution, rinsed thoroughly with distilled water, and dried in a dust-free atmosphere. A coating of white paraffin wax (melting range 65–70°) was applied while molten to the tray rim and barriers to render them hydrophobic. Film pressures were measured with a Cenco du Nouy torsion head equipped with a piano steel torsion wire (torsion constant 0.3578 degree per dyne/cm.), a lightly paraffined mica float, and two end loops of thin polyethylene ribbon.

The surface potential change (ΔV) due to the adsorption of the monolayer on the water was measured by the vibrating condenser method[8] using an aged stainless steel electrode, 3.7 cm. in diameter, which was held close to the surface of the water in the trough and driven at 200 cycles/sec. by being attached to the diaphragm of an earphone connected to an a.c. generator. Because of the contact potential difference between the electrode and the water, an a.c. signal was generated by the vibrating condenser which was passed through a 200 cycle, band-pass, General Radio high-gain amplifier (Model 1231-B) and then was detected

(1) Presented at the Southwest Regional Meeting of the American Chemical Society in Dallas, Texas, on December 8, 1962.
(2) E. G. Shafrin and W. A. Zisman, *J. Phys. Chem.*, **61**, 1046 (1957).
(3) H. W. Fox, *ibid.*, **61**, 1058 (1957).
(4) E. G. Shafrin and W. A. Zisman, *ibid.*, **66**, 740 (1962).
(5) G. Gavlin and R. G. Maguire, *J. Org. Chem.*, **21**, 1342 (1956).
(6) N. O. Brace, *ibid.*, **27**, 4491 (1962).

(7) As manufactured to order by Fred S. Hickey Corp., Chicago, Illinois.
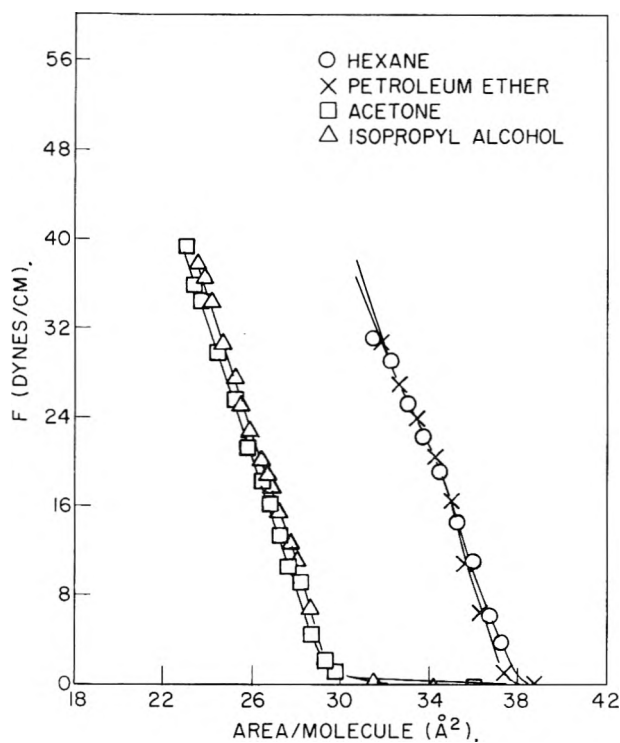(8) W. A. Zisman, *Rev. Sci. Instr.*, **3**, 367 (1932).

Fig. 1.—Effect of spreading solvents on monolayers of 7F-16H acid on substrate of pH 2.2.

by an RCA high-sensitivity, vacuum-tube, voltmeter (Model WV-74A). The contact potential difference was measured by applying an equal and oppositely directed potential difference to the two electrodes with a Rubicon potentiometer so as to give a null in the a.c. signal. This system had a sensitivity of ±2 mv. even when using the convenient condenser air gap of 2 mm.

Aqueous substrates were prepared from water distilled once through a tin-lined still and then twice through an all-quartz still. The water obtained, when in equilibrium with CO_2 of the air, had a pH of 5.8. Appropriate additions of C.P. grade H_2SO_4 or KOH were made in order to obtain various pH values of the aqueous substrate. Film balance experiments were all carried out at 20 ± 0.2°. The more highly fluorinated acids were so slightly soluble in hexane that they had to be stored at 25° or above to keep them from precipitating. At time of delivery to the water surface, however, all of these solutions were at a temperature of 20°.

Results and Discussion

Choice of Spreading Solvent.—A search for a suitable spreading solvent showed that most of the conventional solvents were unable to dissolve the partially fluorinated acids, especially the higher homologs. Previous investigations by Archer, Robbins, and La Mer[9] and others[10,11] have established that the nature of the spreading solvent can exercise a considerable influence on the properties of an adsorbed monolayer. For example, benzene was found to remain in the monolayer even under film pressure, and it caused an increased expansion in the low pressure regions before the formation of liquid-condensed films. Hexane or petroleum ether were found more suitable as spreading solvents; a short-chain alcohol also was satisfactory despite its high water solubility. In view of these findings, a brief study was made of the effect of varying the spreading solvent on the film pressure (F) vs. area per adsorbed molecule (A) of these fluorinated acids.

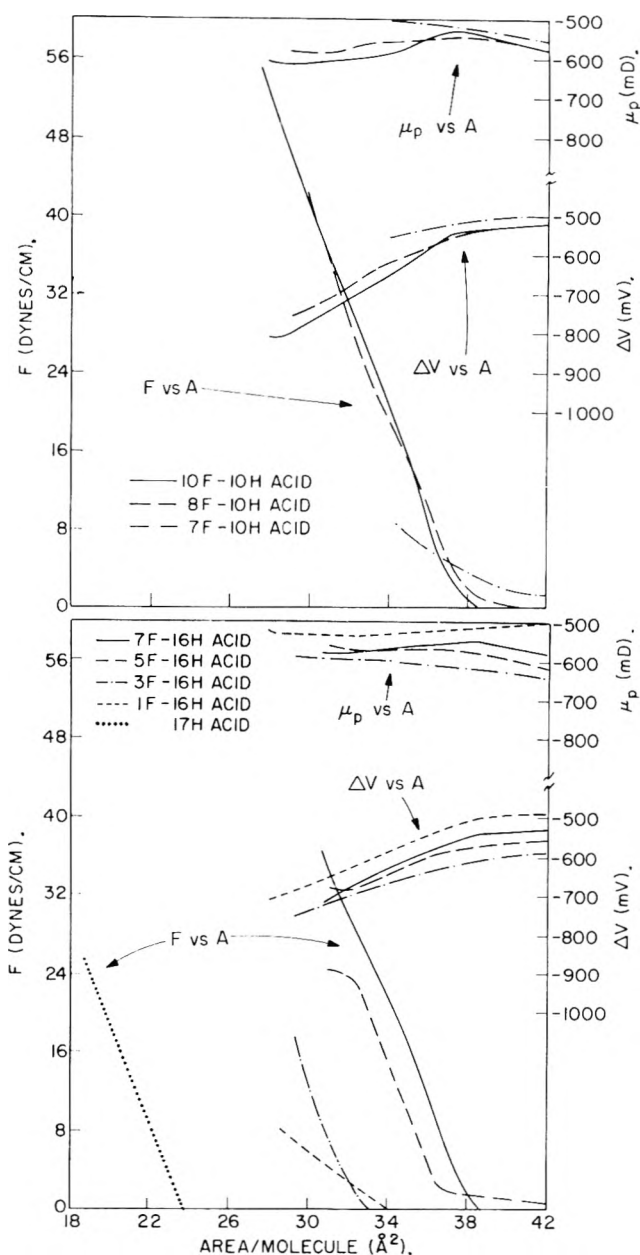Figure 1 graphs the results obtained when the 7F-16H acid was spread on water at pH 2.2 from each of four

(9) (a) R. J. Archer and V. K. LaMer, *J. Phys. Chem.*, **59**, 200 (1955); (b) V. K. LaMer and M. L. Robbins, *ibid.*, **62**, 1291 (1958).

(10) H. D. Cook and H. C. Ries, *ibid.*, **60**, 1533 (1956).

(11) J. P. Miller and L. Nanis, *J. Colloid Sci.*, **17**, 699 (1962).
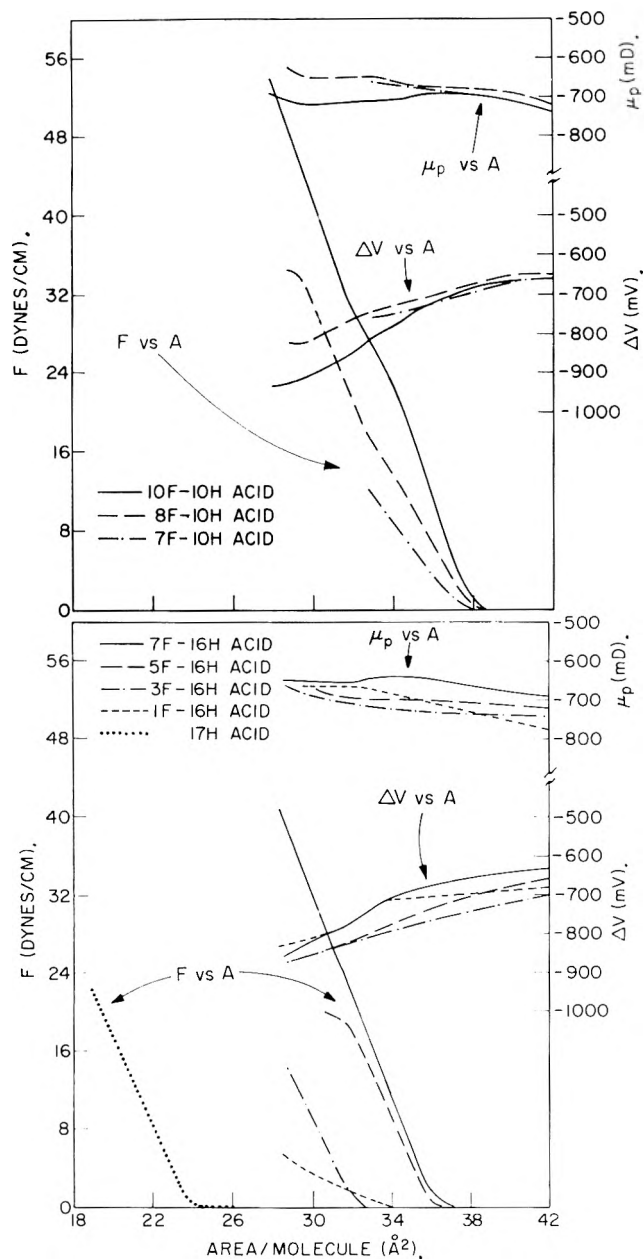
Fig. 2.—Properties of monolayers spread on substrate of pH 2.2 of: (a) (top) nF-10H acids; (b) (bottom) nF-16H acids.

solvents; similar graphs were obtained with the other fluorinated acids studied. Two sets of curves are seen; one set was obtained when the spreading solvents were hexane or petroleum ether and the other set when they were acetone or isopropyl alcohol. The two sets of curves are roughly parallel except that the latter set exhibits an extended gaseous region and is displaced by about 8 Å.² to the left of the former, indicating smaller limiting areas per molecule. Because of the water solubility of the acetone and isopropyl alcohol, it was suspected that these solvents might have carried the organic acid into the aqueous substrate. This suspicion was verified when it was found that the clean hydrophilic platinum foil, employed as an electrode for measuring the surface potential and fully submerged in the film trough, became hydrophobic after several runs with acetone or isopropyl alcohol as the spreading solvent, but remained hydrophilic when hexane or petroleum ether was used instead. Therefore, hexane was chosen as the most suitable spreading solvent for this investigation, in spite of its lower solvent power for the more

Fig. 3.—Properties of monolayers spread on substrate of pH 5.8 of: (a) (top) nF-10H acids; (b) (bottom) nF-16H acids.

Fig. 4.—Properties of monolayers spread on substrate of pH 8.6 of: (a) (top) nF-10H acids; (b) (bottom) nF-16H acids.

highly fluorinated acids. Hence, only the right hand set of curves in Fig. 1 will be used hereafter.

Film Pressure vs. **Area per Molecule.**—In Fig. 2a and 2b are F vs. A graphs for each of the seven fluorinated acids when spread on an aqueous substrate at pH 2.2. In the undecanoic acid series (Fig. 2a), the compound with the largest number of –CF$_2$–groups (10F-10H acid) supported the highest film pressure, 55 dynes/cm.; the next lower member (8F-10H acid) collapsed at 43 dynes/cm.; and the lowest member (7F-10H acid) collapsed at only 9 dynes/cm. Each curve was reversible at all film pressures except close to the collapse value. Any member of this series of acids containing fewer than seven –CF$_2$–groups could not be studied with the film balance because its collapse pressure was too low. An analogous decrease in film stability occurred in the family of substituted heptadecanoic acids (Fig. 2b); the highest collapse pressure (37 dynes/cm.) was exhibited by the 7F-16H acid, which has the largest number of –CF$_2$– groups, and the lowest collapse pressure (6 dynes/cm.) was encountered with the lowest
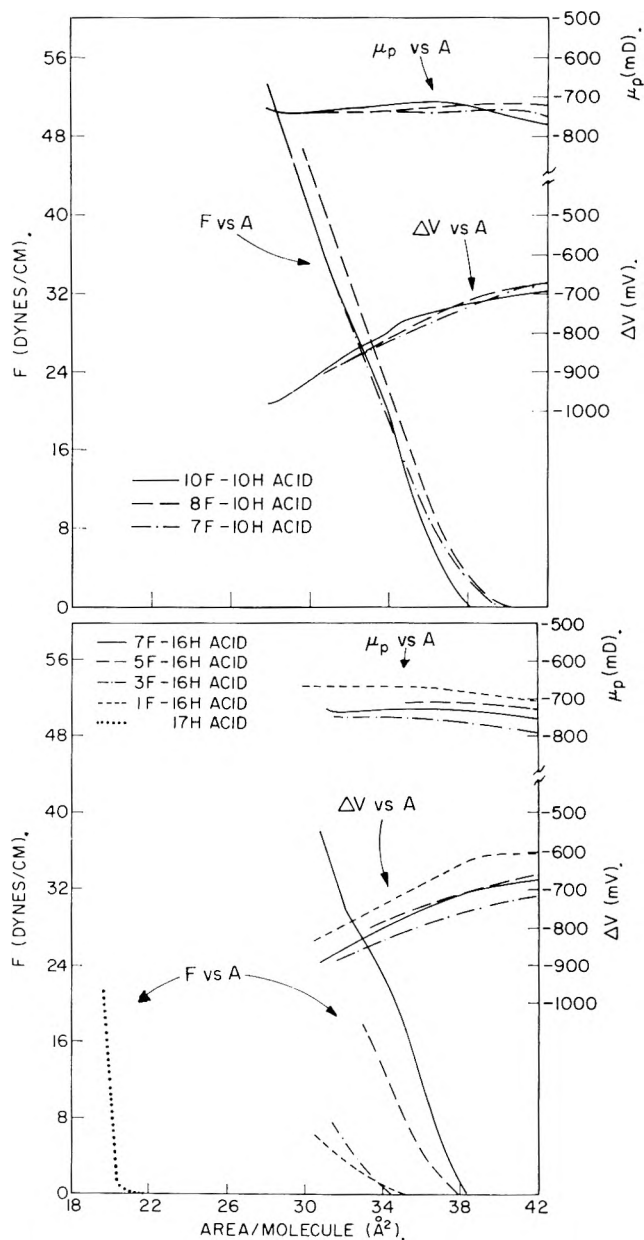
member (1F-16H acid). Again the F vs. A curves were reversible over the entire range of film pressures except close to the collapse point. Data obtained under the same conditions using a monolayer of stearic acid, 17H acid, are also graphed in Fig. 2b for comparison.

Figures 3a and 3b show the F vs. A curves of these two homologous families of insoluble compounds when spread on water at pH 5.8 and Fig. 4a and 4b show the results obtained at pH 8.6. With the exception of the two shortest members of each family of acids, all curves obtained at one pH are roughly parallel and close to one another especially at the higher pressures. The minor effect of varying the pH on the shape and position of the F vs. A curves is exemplified by the behavior of the 10F-10H acid shown in Fig. 5. Thus, regardless of the length of the fluorinated segment or of the hydrocarbon segment and of the value of substrate pH, the limiting area (A_0) observed with the more stable films varies between 36 and 38 Å.^{2} per molecule (Table II). However, values of A as well as of F at the collapse point show larger variations. The smallest value of A

for all films (27.5 Å.^{2}) was observed with 10F-10H acid at pH 2.2; this is close to the cross-sectional area of 25.1 Å.^{2} of a perfluoroalkane chain as measured on a Stuart–Briegleb molecular model.

From the slopes of the F vs. A curves of the more condensed monolayers, it was found that the compressibility $[(-1/A)(\partial A/\partial F)]$ of the 10F-10H acid film ranges from 0.0054 to 0.0062, and is of the same magnitude for the other longer-chain acids. This falls within the range of compressibilities of the liquid-condensed monolayers of fatty acid reported by Harkins,[12] and hence it would appear that these fluorinated monolayers are all liquid-condensed up to the collapse pressure. This inference was proved correct by some simple spreading experiments on these monolayers, using a film trough covered with a duplex film of oxidized "indicator oil"[13] in order to be able to see the boundary of the spread monolayer of fluorinated acid. Even at the maximum pressures obtained with the indicator oil (20–25 dynes/cm.), no solid-condensed monolayers of
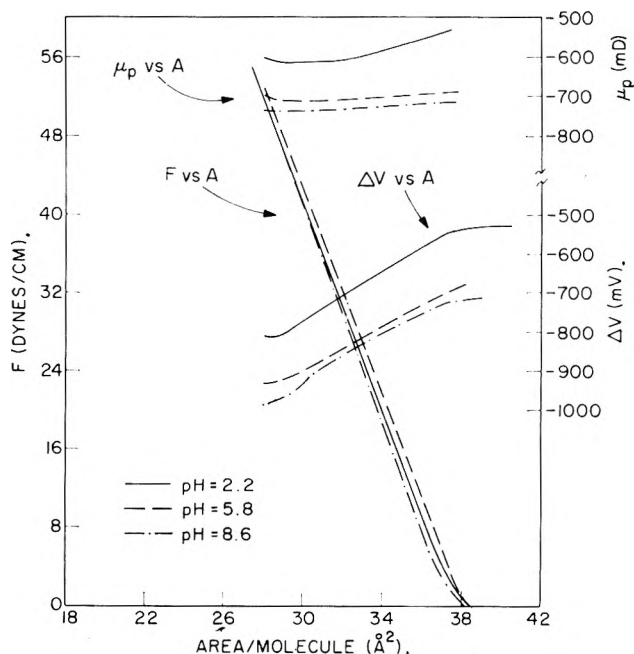

Fig. 5.—Effect of substrate pH on properties of spread 10F-10H acid monolayer.

At pH5.8 only the higher homologs (7F-16H and 10F-10H acids) became rigid, and at pH 2.2 none became rigid. These experiments prove that in the absence of polyvalent metallic ions monolayers of these fluorinated acids are liquid-condensed rather than solid films. All can be transformed at pH 5.8 or higher into solid-condensed films by reaction with appropriate metallic ions in the aqueous substrate, the condensing effect being greater the greater the number of –CF$_2$– groups in the molecule.

The reason why none of these fluorinated acids is able to form solid films on acid water, despite the large number of carbon atoms per molecule, can be found by stereochemical considerations. The portion of the molecule attached to the polar head consists of a hydrocarbon chain having a cross-sectional area of 18.5 Å.^{2}, whereas the fluorinated portion at the other end of the molecule has an area of 25.1 Å.^{2}, or roughly 35% greater. Consequently, the adjacent hydrocarbon chains are hindered from cohering to form a close-packed array. Since the intermolecular forces between adjacent perfluoro alkane chains are weaker than those of alkane chains, complete cohesion and adlineation of the perfluoro alkane chains to produce solid films cannot occur until some number larger than 10 –CF$_2$– groups is present in the chain. Possible models of configuration and packing of condensed monolayers of such molecules have been discussed by Shafrin and Zisman[4] in explaining the effect of such adsorbed monolayers on the wettability of solid surfaces.

Large variations found in the collapse pressures for the various acids (Table II) can be readily understood since increasing the fluorocarbon chain length always increases the intermolecular cohesion, and hence raises the film stability and collapse pressure in both homologous series of acids. On comparing the two series (Table II) it becomes evident that the 16H series of acids forms condensed monolayers, stable enough under moderate pressures, even when the fluorocarbon segment contains only one carbon atom, whereas the 10H series forms stable condensed monolayers only when

TABLE II
LIMITING PROPERTIES OF MONOLAYERS SPREAD ON WATER

Compound	Lim. area A_0 (Å.^{2}/molecule)	Area at collapse A (Å.^{2}/molecule)	Press. at collapse F (dynes/cm.)	Surface potential difference at collapse pressure ΔV(mv.)	Vertical component of dipole moment at collapse pressure μ_p (D.)
			pH 2.2		
10F-10H acid	37.5	27.5	55	−815	−0.615
8F-10H acid	37.0	29.9	43	−755	− .580
7F-10H acid	..	34.5	9 (unstable)	−575	− .535
7F-16H acid	37.8	30.7	37	−720	− .580
5F-16H acid	36.7	32.5	23	−680	− .580
3F-16H acid	32.2	29.3	18 (unstable)	−715	− .590
1F-16H acid	34.0	28.0	8 (unstable)	−710	− .530
17H acid	23.8	19.0	25	+375	+ .185
			pH 5.8		
10F-10H acid	37.5	28.0	53	−930	−0.715
8F-10H acid	36.8	29.0	35	−820	− .650
7F-10H acid	37.2	33.0	12 (unstable)	−760	− .665
7F-16H acid	36.0	28.4	41	−850	− .650
5F-16H acid	36.1	31.7	19	−850	− .675
3F-16H acid	32.1	28.6	14 (unstable)	−875	− .665
1F-16H acid	34.0	28.0	6 (unstable)	−830	− .665
17H acid	23.5	18.5	25	+270	+ .135
			pH 8.6		
10F-10H acid	37.2	28.0	53	−970	−0.740
8F-10H acid	37.5	30.0	46	−905	− .740
7F-10H acid	37.0	31.0	35	−895	− .740
7F-16H acid	37.4	30.8	38	−895	− .730
5F-16H acid	36.9	33.1	17	−825	− .710
3F-16H acid	34.0	31.5	7	−880	− .740
1F-16H acid	36.0	30.5	6	−830	− .670
17H acid	20.4	19.7	23	+220	+ .123

these fluorinated acids was formed on water at pH 2.2, 5.8, or 8.6. The 10F-10H and 7F-16H acids formed somewhat more viscous films at pH 8.6 than did the other acids, and the 1F-16H acid slowly dissolved in the water at all pH values. However, when thorium nitrate (10^{-4} molal) was introduced into the aqueous substrate under the previously spread monolayer of each fluorinated acid, the film promptly became rigid at pH 8.6.

(12) W. D. Harkins, "The Physical Chemistry of Surface Films," Reinhold Publ. Corp., New York, N. Y., 1952, p. 135.

(13) I. Langmuir and V. Schaefer, J. Am. Chem. Soc., 59, 2400 (1937).

the fluorocarbon segment contains seven or more carbon atoms. This would indicate that the hydrocarbon segment must contain over 10 carbon atoms for sufficient chain adlineation to occur in order to compensate for the steric hindrance caused by the larger cross-sectional area of the perfluoro group. The shortest total chain length in each series consistent with obtaining film stability is 18 carbon atoms (1F-16H or 7F-10H acid). Thus, although an 18-carbon, straight-chain, hydrocarbon acid (stearic acid) forms stable solid-condensed monolayers, the progressively fluorinated acids just begin to support pressure at that chain length, and the higher members compress to form only liquid-expanded or, at best, liquid-condensed films.

The F vs. A curve of the highest homolog in each series, and to a lesser extent the next lower acid, evidenced a slight change in slope when F ranged between 12 and 26 dynes/cm., regardless of the pH. The change is significant enough to suggest a shift in molecular packing, especially since every change in the F vs. A curve is also reflected in a corresponding dip in the ΔV vs. A curve.

Because the F vs. A results reported by Fox on the 1F-16H acid[3] were not reasonably related to the other members of the nF-16H family of acids, a sample of the identical acid was also studied with results recorded in Fig. 2b, 3b, and 4b. The results follow logically those obtained with the other members of this homologous series. Several possible causes are suggested why Fox's results are not consistent with the present ones. Fox used a wax-coated brass film trough which, despite the coating of wax, could readily have caused contamination of the aqueous substrate by polyvalent metal ions, especially at higher pH values. Film pressures were measured by the Wilhelmy plate method in which it is essential that the contact angle on the dipping platinum plate always remain zero; these fluorinated acids adsorb very readily on clean platinum and thus may have affected the contact angle. The solvent used by Fox to spread the monolayers was benzene. Benzene has since been shown by LaMer and co-workers[9] to be able to cause a large expansion in the low pressure region of the F vs. A curve. Because 1F-16H acid monolayers can be compressed only through the expanded portion of the isotherm and collapse shortly after becoming condensed, the nature of the spreading solvent used plays an important role. Hence, the use of benzene by Fox may be responsible for his more highly expanded films than the present ones.

Jarvis, Timmons, and Zisman[14] employing the same equipment and methods as used in the present study have observed monolayers of ω-bromostearic acid spread from solutions in n-hexane on an aqueous substrate of pH 2.2. Their F vs. A curve is similar to that of 1F-16H acid in the present investigation with respect to the limiting area (A_0), the compressibility, and the pressure at the collapse point; however, their area per molecule at the collapse pressure is 23 Å.[2] which is smaller than the value of 28 Å.[2] obtained for the 1F-16H acid. This difference in A is reasonable since the radius of the terminal bromine atom is slightly smaller than that of the $-CF_3$ group.

Electrical Properties.—In the Helmholtz equation

$\Delta V = 4\pi\nu\mu_p$, ΔV is the difference in the electrostatic surface potential between the clean water surface and the surface covered by the monolayer of adsorbed organic molecules, μ_p is the component perpendicular to the water surface of the electrostatic dipole moment per adsorbed molecule, and ν is the number of polar organic molecules adsorbed per unit area. When adsorbed in close packing on the surface of water, the fatty acid dipole has its positive end farthest away from the surface. The progressively fluorinated acids discussed here are adsorbed in close packing with the large dipole arising from the fluorinated group pointed in the opposite direction. If ΔV and μ_p for the fatty acids are given positive values, then for the fluorinated acids discussed here ΔV and μ_p will be shown to be strongly negative.

Quite like the F vs. A curves, the ΔV vs. A and μ_p vs. A curves for each series of fluorinated acids at any one substrate pH fall within a narrow band (Fig. 2, 3, and 4). The curves also show that the number of carbon atoms in the perfluorocarbon portion of the molecule has only a minor influence on the values of ΔV and μ_p when A at the collapse pressure reaches 30 Å.[2]. As usual ΔV varies nearly linearly with A once the film has become condensed, and it approaches a minimum value as the film approaches the solid state. Table II (fifth column) compares these values of ΔV of the various films close to the collapse pressure.

As usual in experiments with ionizable hydrophilic groups, varying the pH of the aqueous substrate caused a variation in ΔV for each polar compound. Many years ago Schulman and Hughes[15] reported that the ionization of the carboxylic group at alkaline pH caused a double layer to form with its moment oppositely directed to that of the undissociated COOH group. More recently Sanders and Spink[16] have studied ionization in fatty acid monolayers on very pure water and have found that in the absence of multivalent ions ΔV decreases linearly with increasing pH. They demonstrated that by itself ionization in the monolayer has a much smaller effect on the surface potential than previously supposed. The graph in Fig. 6 of ΔV vs. pH for our stearic acid, observed at the state of packing when A is 21 Å.[2], is in close agreement with these results of Sanders and Spink. Figure 6 also shows the variation of ΔV with pH for the 7F-16H and 10F-10H acids as representatives for the fluorinated acids. Because of the ionization effect, there is a change in ΔV with pH (as seen in Table II) and accompanying it there must be a change in the dipole contribution by the COOH group as a function of pH.

The value of ΔV obtained here involves the resultant of the moment contributed by the carboxylic acid group and those contributed by the carbon–fluorine bonds. The latter must have a resultant located in or adjacent to the fluorocarbon group and so must be well removed from the aqueous substrate. Since the contribution due to the COOH group diminishes as the pH rises, the net value of ΔV becomes more dominated at higher pH values by the resultant of the dipole contribution due to the C–F bonds. Since the latter is a large negative quantity, it is obvious why ΔV ranges from -700 to -970 mv. for the fluorinated acids. Of

(14) N. L. Jarvis, C. O. Timmons, and W. A. Zisman in "Retardation of Evaporation by Monolayers," edited by V. K. LaMer, Academic Press, New York, N. Y., 1962, p. 41.

(15) J. Schulman and A. H. Hughes, *Proc. Roy. Soc.* (London), **A138**, 430 (1936).

(16) J. V. Sanders and J. A. Spink, *Nature*, **175**, 644 (1955).

course, ΔV for films collapsing at low pressures cannot reach such very negative values, as is evident in Fig. 2, 3, and 4. The behavior of graphs of ΔV vs. A and μ_p vs. A at several values of the pH, as shown in Fig. 5 for the 10F-10H acid, is representative of the results obtained with all of the more stable monolayers of these fluorinated acids.

In the last column of Table II are the values of μ_p in Debyes computed from the Helmholtz equation at values of A close to the collapse pressure. Some differences in μ_p are evident among the seven fluorinated acids on any one substrate. However, if one ignores the 1F-16H and 7F-10H acids (because the collapse pressure is too low for these compounds to have fully erected the dipoles) it will be found that μ_p is then independent of the number of carbon atoms in the fluorocarbon chain.

It is now possible to compute the contribution of μ_p arising solely from dipoles in the fluorinated carbon chain. The value of μ_p deduced from the observed values of ΔV for a condensed stearic acid monolayer on water is the vectorial sum of the contribution of vertical components from the COOH group and the hydrogen bonded water molecules attached to it, $\mu_{(COOH)aq}$, and the contribution from the aliphatic chain, $\mu_{C_nH_{2m+1}}$; i.e.

$$\mu_p = \mu_{(COOH)aq} + \mu_{C_mH_{2m+1}}$$

Assuming, as is usual, that only the terminal CH_3-group determines the value of μ_p in a paraffin chain,[17] $\mu_{C_mH_{2m+1}}$ becomes equal to μ_{CH_3}. Hence

$$\mu_p = \mu_{(COOH)aq} + \mu_{CH_3}$$

Although uncertainties remain in the literature about the correct value of the vertical component μ_{CH_3}, a value of 0.3 Debye,[18,19] where the positive direction is pointed from the hydrogen to the carbon atom, has been chosen by many investigators and will be used here. If this vertical moment contribution is subtracted from μ_p, computed from the Helmholtz equation by using the value of ΔV observed for stearic acid when the molecule is vertically oriented on water (i.e., at an area per molecule of 21 Å.²) at the respective pH, the resulting vertical component of the moment $\mu_{(COOH)aq}$ directed with negative end to water is listed in the top line of Table III. Subtracting this value of $\mu_{(COOH)aq}$ of the carboxylic acid group from the μ_p for each of the fluorinated acids as obtained at a packing of 32 Å.² per molecule for each pH (Fig. 2, 3, and 4), the resulting vertical component of the moment is that contributed solely by the segmented chain $F(CF_2)_n(CH_2)_m$ and will be denoted as μ_Φ. Hence

$$\mu_p = \mu_{(COOH)aq} = \mu_\Phi$$

Table III gives the values of μ_p and μ_Φ thus obtained for each substrate pH. The resulting μ_Φ is directed with the negative pole up and away from the water.

It can be seen that all values of μ_Φ are nearly constant at each pH regardless of length of fluorocarbon chain segment or hydrocarbon segment. Hence, any

(17) C. P. Smyth in "Physical Techniques in Organic Chemistry," Vol. II, edited by A. Weissberger, Interscience Press, New York, N. Y., 1946, p. 991.

(18) A. Eucken and L. Meyer, *Phys. Z.*, **30**, 397 (1929).

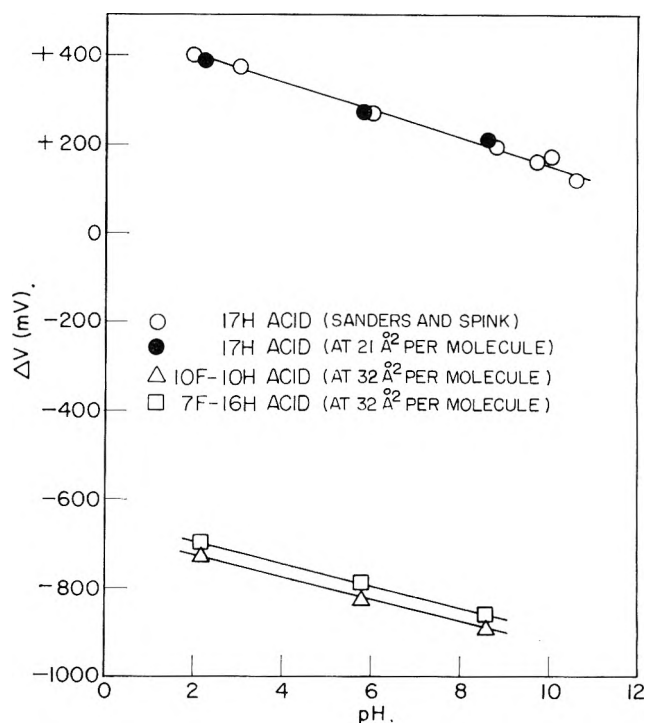(19) J. W. Smith, "Electric Dipole Moments," Butterworths, London, 1955, p. 94.

Fig. 6.—Dependence of surface potentials on pH for compressed monolayers of fatty acids and partially fluorinated acids.

TABLE III

μ_p AND μ_Φ OF PARTIALLY FLUORINATED CHAINS AT AREA PER MOLECULE OF 32 Å.²

$$\mu_p - \mu_{(COOH)aq}{}^a = \mu_\Phi$$

| | pH 2.2 | | pH 5.8 | | pH 8.6 | |
| | ($\mu_{(COOH)aq}$ = 0.090 D.) | | ($\mu_{(COOH)aq}$ = 0.160 D.) | | ($\mu_{(COOH)aq}$ = 0.180 D.) | |
Fluorinated compound	μ_p (D.)	μ_Φ (D.)	μ_p (D.)	μ_Φ (D.)	μ_p (D.)	μ_Φ (D.)
10F-10H acid	0.610	0.520	0.700	0.540	0.730	0.550
8F-10H acid	.580	.490	.650	.490	.730	.550
7F-10H acid	...	...	...	...	.730	.550
7F-16H acid	.570	.480	.650	.490	.730	.550
5F-16H acid	.570	.480	.690	.530	...	...
3F-16H acid	.590	.500	.680	.520	.740	.560
1F-16H acid	.540	.450	.660	.500	.680	.500

a Area per molecule of 21 Å.² for stearic acid.

contributions to μ_Φ arising from any effect due to the polarization of the water dipoles must be minor; and this would be expected because the fluorocarbon chain segment is about 10–20 Å. from the water surface. The maximum 10% variation in μ_Φ with pH, as shown in Table III, may be a result of a slight change with pH of the orientation of the molecular axis at maximum compression. For vertically oriented molecules in the solid-condensed state, such as stearic acid, ΔV is independent of compression, whereas the fluorine-substituted acids manifest an increase in ΔV with increasing compression.

The value of μ_{CF_3} most accepted in the literature for the vertical component of the $-CF_3$ dipole moment, based on dielectric constant studies of appropriate compounds in the gaseous state, is 1.9 D.[20] The values computed here from the properties of the various condensed monolayers on water are all approximately 0.5 D., or only one-fourth as great. These smaller values of the CF_3 group moment may be the result of several effects. There may be induced polarization between adjacent fluorocarbon dipoles at the close packing prev-

(20) R. G. Shulman, B. P. Dailey, and C. H. Townes, *Phys. Rev.*, **78**, 145 (1950).

alent in a liquid-condensed monolayer. There may also be dipole contributions from water molecules which have penetrated between the aliphatic chains in the monolayer. It had been shown repeatedly by many investigators that only highly condensed or solid monolayers can appreciably retard evaporation from the surface of the aqueous substrate. Since a single bromine atom substitution on the ω-carbon atom of stearic acid makes it unable to retard water evaporation[14] whatever the film pressure, the liquid-condensed films of these progressively fluorinated acids will also be unable to prevent evaporation and thus molecularly dispersed water will be present throughout the monolayer. The polarization of such water molecules, especially those nearest the C–F bonds of the fluorinated chain segment, would be expected to decrease μ_Φ.

Only recently Bewig and Zisman[21] have reported

(21) K. W. Bewig and W. A. Zisman, J. Phys. Chem., 67, 130 (1963).

values for μ_D of long-chain amines adsorbed on metals which were about half of the reported values obtained from the same compounds in the gaseous state. They explained the smaller values as resulting from the proximity of the polar end groups to the metal surface and the resulting possibility of induced polarization, as well as from another contribution arising from any oriented water dipoles present on the surface of the metal as one or more adsorbed monolayers. The even smaller values obtained in the present investigation are believed to arise in major part from the dipole contribution from water molecules present in the spaces between the oriented aliphatic chains. From the results of the film balance experiments reported here, such water contributions cannot be eliminated even at the collapse pressures of those monolayers because of steric hindrances to molecular adlineation which prevent formation of a solid film.

ISOPIESTIC VAPOR PRESSURE MEASUREMENTS OF THE TERNARY SYSTEM: SORBITOL–SODIUM CHLORIDE–WATER AT 25°

By V. E. Bower and R. A. Robinson

Solution Chemistry Section, National Bureau of Standards, Washington, D. C.

Isopiestic vapor pressure measurements have been made with solutions of sorbitol and sodium chloride. Each of the diastereoisomers, sorbitol and mannitol, has a "salting-in" effect on sodium chloride, but the effect is larger with sorbitol.

It has been shown[1] that aqueous solutions of D- and DL-tartaric acid have identical vapor pressures within the limits of accuracy of the isopiestic method. This has also been demonstrated[1,2] for D-, L-, and DL-alanine. It may well be asked if this would be true if the two solutions contained, not optical stereoisomers, but diastereoisomers such as D-sorbitol and D-mannitol, especially as it has been shown recently[3] that the standard potential of the $H_2/HCl/AgCl$, Ag cell is not the same with 5% aqueous mannitol and 5% aqueous sorbitol[4] as solvent. Moreover, sorbitol is much more soluble in water than is mannitol; sorbitol has a semihydrate, whereas mannitol crystallizes in the anhydrous form. We have now made isopiestic vapor pressure measurements on aqueous solutions of sorbitol and of sorbitol + sodium chloride which parallel recent measurements[5] on the system: mannitol–sodium chloride–water.

Experimental

D-Sorbitol was obtained from Atlas Chemical Industries, Inc. We used it without further treatment, except that we dried it *in vacuo* over P_2O_5 at room temperature, when it lost 0.058% in weight. We call this Sample A.[6]

(1) R. A. Robinson, P. K. Smith, and E. R. B. Smith, *Trans. Faraday Soc.*, 38, 63 (1942).

(2) R. A. Robinson, *J. Biol. Chem.*, 199, 11 (1952).

(3) R. Gary and R. A. Robinson, to be published.

(4) H. D. Crockford, B. J. Alley, and C. S. Patterson, *J. Elisha Mitchell Sci. Soc.*, 73, 284 (1957).

(5) F. J. Kelly, R. A. Robinson, and R. H. Stokes, *J. Phys. Chem.*, 65, 1958 (1961).

(6) We were informed by Dr. J. D. Brandner of Atlas Chemical Industries, Inc., that this was an aliquot of a sample prepared in their laboratory for reference purposes. It had been separated from other hexitols by formation of the pyridine complex. The sorbitol was regenerated and crystallized several times from alcoholic solution. Impurities were thought to be only a few tenths of one per cent of mannitol, a few hundredths of one per cent of sugars, and a few thousandths of one per cent of ash.

We were also fortunate in obtaining from Dr. Horace S. Isbell a sample of sorbitol used in his previous work.[7] This we call Sample B.

A few measurements were made on solutions of sorbitol alone, using the ordinary Atlas product. This, which we call Sample C, was stated to contain, at the most, 0.65% total sugars and 0.14% of reducing sugars.

Table I gives the molalities of isopiestic solutions of sodium chloride and of sorbitol, the derived osmotic coefficient of sorbitol. and also that of mannitol at the same concentration.[8] Table II records data for solutions containing both sodium chloride and sorbitol; it parallels Table II of ref. 5.

TABLE I[a]

ISOPIESTIC SOLUTIONS OF SODIUM CHLORIDE AND SORBITOL. OSMOTIC COEFFICIENTS OF SORBITOL

m_{NaCl}	m_B	φ_B	φ_D (ref. 8)
0.4998	0.9134	1.0078	1.0066
.6963	1.2725	1.0131	1.0111
.7156	1.3071	1.0142	1.0116
1.0397	1.8990	1.026	....
1.2956	2.3661	1.037	....
1.4089	2.5744	1.042	....
1.6998	3.1113	1.056	....
2.0307	3.7247	1.074	....

[a] B = sorbitol, D = mannitol. Sample A was used in the first two runs, Sample B in the third, and Sample C in the remainder.

Discussion

The first three entries in Table I show that, on the average, sorbitol has an osmotic coefficient 0.002 higher than that of mannitol at the same concentration. This, it is believed, is beyond experimental error.

(7) H. S. Isbell, J. F. Brewster, N. B. Holt, and H. L. Frush, *J. Res. Natl. Bur. Std.*, 40, 129 (1948).

(8) R. A. Robinson and R. H. Stokes, *J. Phys. Chem.*, 65, 1954 (1961).

Table II[a]

The System: Sorbitol–Sodium Chloride–Water

$m_{ref.}$	m_B	m_C	Δ $-m_Bm_C$	% Diff. (1)	% Diff. (11)
0.6963	0.3237	0.5280	0.0486	+0.01	0.46
	.6368	.3583	.0456	+ .02	.55
	.9279	.1958	.0402	0	.40
2.2501	.2553	2.1487	.0510	−0.05	.33
	.5283	2.0357	.0483	− .05	.64
	.8052	1.9156	.0451	− .03	.85
	1.1055	1.7789	.0417	+ .02	1.00
4.0137	0.2227	3.9597	.0811	+ .04	0.34
	.4497	3.8990	.0742	+ .03	.54
	.6980	3.8306	.0713	+ .09	.79
	.9501	3.7575	.0689	+ .20	1.06
5.2807	.2755	5.2367	.0925	− .09	0.23
	.5284	5.1946	.0917	− .09	.45
	.7685	5.1496	.0884	− .14	.63
	1.1349	5.0802	.0870	+ .07	.95
5.9070	0.3229	5.8819	.1246	+ .12	.42
	.5174	5.8579	.1153	+ .07	.56
	.7941	5.8120	.1020	− .14	.60
	1.1079	5.7672	.0999	− .07	.82

[a] The reference solute, whose molality is given in the first column, was NaCl. B = sorbitol, C = NaCl. The fifth column gives the percentage difference in the molality of the reference solution necessary to account for the difference between the observed Δ value and that calculated by eq. 1; a positive difference is quoted if Δ(obsd.) is less than Δ(calcd.). The last column gives the percentage increase in the molality of the reference solution which would occur if sorbitol were replaced by an equivalent amount of mannitol.

More convincing, however, are the results with sorbitol–sodium chloride mixtures. Significant differences between these and the data for mannitol–sodium chloride mixtures can be demonstrated in two ways. The second and third columns of Table II give the molalities of sorbitol and sodium chloride, respectively, in a mixed solution in isopiestic equilibrium with a solution of sodium chloride alone, whose molality is given in the first column. From the data obtained in a previous investigation,[5] it is possible to calculate the molality of sodium chloride in equilibrium with each of these mixed solutions if they had contained mannitol in place of sorbitol. For example, the last mixture of

1.1079 M sorbitol + 5.7672 M NaCl was in equilibrium with 5.9070 M NaCl. A solution of 1.1079 M mannitol + 5.7672 M NaCl would have been in equilibrium with 5.9552 M NaCl. Thus, the two reference solutions of sodium chloride differ by 0.0482 M or 0.82%. This is well beyond experimental error and demonstrates a significant difference between sorbitol and mannitol. The last column of Table II gives these % differences for all the solutions measured.

We can also calculate, for the sorbitol–sodium chloride mixtures, the $\Delta/(m_Bm_C)$ function, which is a measure of the change in free energy of the solvent when the mixed solution is formed from the component solutions.[8] Values of this function are given in the fourth column of Table II. It was found, by the method of least squares, that these could be represented by the equation

$$\frac{\Delta}{m_Bm_C} = -0.05326 + 0.00261m_C -$$

$$0.00235m_C^2 + 0.0134m_B \quad (1)$$

where B = sorbitol, C = NaCl. The fifth column of Table II gives the percentage error in the molality of the reference solution necessary to account for the difference between the observed and calculated Δ values.

For the sorbitol–sodium chloride system at $m_B = m_C = 1$, $\Delta = -0.0396$; from the data also recorded,[5] we calculate for the mannitol–sodium chloride system of the same composition, $\Delta = -0.0133$. At $m_B = 1$, $m_C = 5$, we get $\Delta = -0.428$ for the sorbitol–sodium chloride system and -0.286 for the mannitol–sodium chloride system. This demonstrates, in another way, the difference between sorbitol and mannitol.

We conclude, therefore, that the two diastereoisomers, mannitol and sorbitol, exhibit a real and distinguishable difference in their properties in aqueous solution. Each has a "salting-in" effect on sodium chloride but the effect is larger with sorbitol.

A MASS SPECTROMETRIC STUDY OF HOMONUCLEAR AND HETERONUCLEAR RARE GAS MOLECULE IONS[1]

By M. S. B. Munson, J. L. Franklin, and F. H. Field

Research and Development, Humble Oil & Refining Company, Baytown, Texas

The homonuclear and heteronuclear diatomic ions of all the rare gases except radon have been studied by mass spectrometry. Appearance potentials of all except the HeXe[+] have been measured at pressures where three-body processes could be neglected. All are found to result from chemi-ionization reactions, and our appearance potentials agree well with those of other workers where they are available. Most of the heteronuclear ions have appearance potentials in the ionization continuum of the partner of lower ionization potential. Thus most of the heteronuclear ions exist at energies above one of their dissociation asymptotes, and presumably this is possible because of the non-crossing of potential energy curves. The appearance potentials of HeAr[+], 17.9 e.v., and NeXe[+], 16.0 e.v., occur below the lowest excited state of He and Ne, respectively, and can only be understood as resulting from reaction of a long-lived discrete excited state of argon or xenon existing in their respective ionization continua.

Introduction

The appearance potentials of the homonuclear rare gas molecule ions were measured several years ago, but the limits of precision were quite broad.[2] Previously in this Laboratory we have studied gas phase reactions of rare gas ions and excited atoms, including the kinetics of rare gas molecule ion formation,[3,4] and we felt that a complement to our work would be a redetermination of the appearance potentials with equipment capable of a higher degree of precision than that previously used. During the course of this work new measurements of these appearance potentials were reported,[5] and good agreement exists between the values reported here and the earlier values.

The existence of several of the heteronuclear rare gas molecule ions has been commented on in the literature. Oskam suggested the formation of HeNe[+] by a three-body ion–molecule reaction in He–Ne mixtures subjected to an electric discharge.[6] Although he studied other rare gas mixtures as well, he made no mention of any other heteronuclear rare gas molecule ions. Pahl and Weimer actually observed a second-order HeNe[+] ion mass spectrometrically from the positive column of a glow discharge.[7,8] They argued that the energy of formation of HeNe[+] must be less than 21.56 e.v. because they assumed that excited helium with energy higher than 21.56 e.v. would react by the Penning process

$$He^* + Ne = He + Ne^+ + e \qquad (1)$$

rather than by a process yielding HeNe[+]. By contrast with the He–Ne system, for mixtures of He and Ar and Ne and Ar these workers did not find either the HeAr[+] or NeAr[+] ions.[8] This apparent non-existence of HeAr[+] and NeAr[+] was explained on the basis of the non-overlapping of energies of excited states of Ar with those of He or Ne. Similar reasoning led Biondi

and Holstein to predict that HeAr[+] and NeAr[+] would not be stable.[9]

Fuchs and Kaul, however, observed NeAr[+] mass spectrometrically and obtained a value for the appearance potential of 16.5 e.v.[10]; they also observed the ArKr[+] ion which was discussed in somewhat more detail by Kaul, Lauterbach, and Fuchs.[11] Kaul and Taubert also observed ArXe[+] and KrXe[+] and gave values for the appearance potentials of these ions indicating that they were formed from excited states of the rare gas atoms.[5] Morris, however, was unable to find the KrXe[+] ion in gaseous discharge through a mixture of Kr and Xe with a mass spectrometer probe.[12]

We have made a study of all the binary mixtures of rare gases, except Rn, and have observed mass spectrometrically all of the heteronuclear molecule ions. We have obtained the appearance potentials of all except HeXe[+] and have studied the dependence of certain of them upon pressure.

Experimental

The instrument is a 60° deflection, sector field type mass spectrometer designed for high pressure operation.[13] The appearance potentials were measured with the long source, in which the length of the electron path is 20 mm., because the short source, perhaps because of potential penetrations, never gave satisfactory operation for energy measurements. The short source (7 mm. electron path) proved quite adequate for the pressure studies, however.

Many experiments were made to determine the adequacy of the instrument for the measurement of appearance potentials at high pressures (up to $P_s = 100$–$150\ \mu$). While adequate techniques for appearance potential measurements at analytical pressures ($P_s < 0.1\ \mu$) are well known, the possibility that difficulties would be encountered in operating at very much higher pressures had to be investigated. Most effort was devoted to determining the known differences in appearance potentials of rare gases under different instrumental conditions. The results were satisfactory, for at low source pressures ($P_s < 1\ \mu$) known differences were reproduced with an average error of ± 0.08 e.v., whereas at pressures as high as $150\ \mu$ the average error was ± 0.2 e.v. In addition the appearance potential of Ar_2^+ was independent of source pressure from 10–150 μ. Measurements made with a Faraday cup as an ion collector at a high source pressure and with an electron multiplier at a lower source pressure gave the same results. Furthermore, as long as the intensity of the ion under investigation was maintained at a reasonable value, the appearance potential was independent of the repeller field strength, electron draw-out and electron collector potentials, electron current, magnetic

(1) Supported in part by Project Squid under Contract No. Nonr-3623(S-18).

(2) J. A. Hornbeck and J. P. Molnar, *Phys. Rev.*, **84**, 621 (1951).

(3) F. H. Field, H. N. Head, and J. L. Franklin, *J. Am. Chem. Soc.*, **84**, 1118 (1962).

(4) (a) J. S Dahler, J. L. Franklin, M. S. B. Munson, and F. H. Field, *J. Chem. Phys*, **36**, 3332 (1962); (b) M. S. B. Munson, F. H. Field, and J. L. Franklin, *ibid.*, **37**, 1790 (1962).

(5) W. Kaul and R. Taubert, *Z. Naturforsch.*, **17a**, 88 (1962).

(6) H. J. Oskam, *Philips Res. Rept.*, **13**, 401 (1958).

(7) M. Pahl and U. Weimer, *Naturwiss.*, **44**, 487 (1957).

(8) M. Pahl and U. Weimer, *Z. Naturforsch.*, **12a**, 926 (1957).

(9) M. A. Biondi and T. Holstein, *Phys. Rev.*, **82**, 962 (1951).

(10) R. Fuchs and W. Kaul, *Z. Naturforsch.*, **15a**, 108 (1960).

(11) W. Kaul, U. Lauterbach, and R. Fuchs, *Naturwiss.*, **47**, 353 (1960).

(12) D. Morris, *Proc. Phys. Soc.*, **68**, 11 (1955).

(13) F. H. Field, *J. Am. Chem. Soc.*, **83**, 1523 (1961).

field collimating the electron beam, and the mass or appearance potential of the calibrating ions.

The appearance potentials were determined by the vanishing current technique in which the slopes of the ionization efficiency curves of the calibrating ion and the ion in question were made equal over a 1–2-volt range just above the onset potential by appropriately adjusting the ion intensities. Since the ionization efficiency curves for the molecule ions and the primary calibrating ions have very different shapes, the best method of calibrating the electron energy scale is a matter of some concern. However, in view of the satisfactory results with knowns referred to in the preceding paragraph, we feel that the procedure chosen is reliable.

For the appearance potentials reported in this paper the instrument was fitted with an electron multiplier, which sufficiently increased the sensitivity so that the pressures for all of the measurements were <40 μ. A double square wave generator was connected to the electron draw out and repeller electrodes to give ionization in field free space according to the technique developed by Fox, et al., in their retarding potential difference method of determining ionization potentials.[14] That the ions were formed in an essentially field free space is indicated by the fact that the correction applied to the vanishing current potential of the calibrating gases was generally less than half a volt with the square wave generator in operation; this is to be compared with a correction of several volts for operation without it.

The appearance potentials reported in this paper represent the average of four to six determinations done under slightly different experimental conditions (different repeller voltages, electron currents, etc.) with at least two calibrating ions. The indicated precision represents the average deviation from the mean. Under these conditions, known differences in ionization potential were measured with an average error of ±0.1 e.v.

The rare gases used in these experiments were spectroscopically pure grade from the Air Reduction Company and were purified by passing through charcoal at liquid nitrogen temperatures for He and Ne and fractional volatilization for the others. A particular effort was made to determine the presence of impurities at mass numbers involved in the appearance potential determinations. The check for impurities which would interfere with the homonuclear rare gas ions was done at pressures low enough so that molecule ion formation was negligible, but with other experimental conditions designed for extreme sensitivity of detection. There was in the neon an impurity of mass 40 (presumably $^{40}Ar^+$) of less than 2 div./10^5 div. of $^{20}Ne^+$. No impurities were detected which would have interfered with the measurements of appearance potentials of the other homonuclear rare gas ions.

For the studies on the heteronuclear rare gas molecule ions, each gas was checked separately at a pressure higher than its partial pressure in the mixture. The only interference found was at mass 44 in He–Ar mixtures. In this case a correction was made for the small amount of 44 impurity by subtracting at each voltage the sum of the 44 intensity in pure He and the 44 intensity in pure Ar from the total intensity of mass 44 in the mixture of He + Ar. The intensity of the impurity was very low, but it would have given an appreciably lower appearance potential.

The pressure studies were made by putting a known amount of one rare gas into the short source from one reservoir and obtaining the mass spectrum, then adding various amounts of a second rare gas from another reservoir and determining the mass spectrum after each addition. The pressures were read from a McLeod gage which had been calibrated against source pressure.

The McLeod vs. source pressure calibration was obtained after modifications of the source had been made so that a thermistor could be placed within a chamber connected to the source, but through which no gas flowed. The thermistor voltages were determined as a function of pressure (corrected for temperature variations) with a static pressure in the source. From the thermistor voltages a calibration of McLeod pressure against source pressure could be determined for the flowing system with a precision of about $\pm5\%$. There are indications that the addition of gas from one reservoir increases the partial pressure in the source of the gas from the other reservoir, but these changes are only of the order of 5–10% at the highest pressures involved.

Data and Results

Homonuclear Molecule Ions.—Figure 1 shows a typical ionization efficiency curve, for He_2^+, which

(14) R. E. Fox, W. M. Hickam, D. J. Grove, and T. Kjeldaas, Jr., *Rev. Sci. Instr.*, **26**, 1101 (1955).
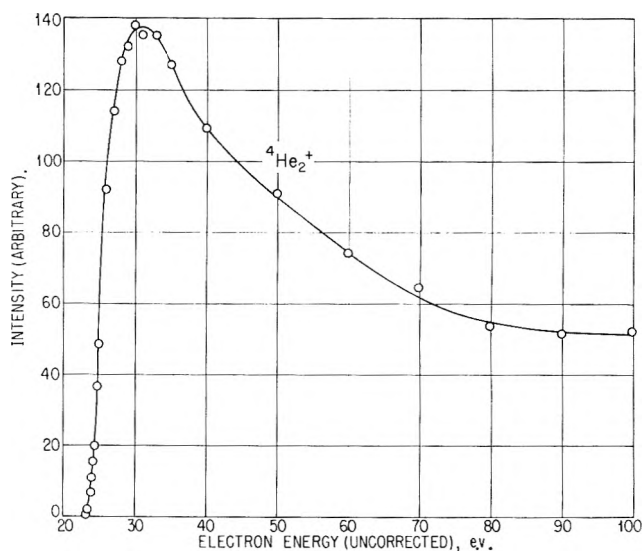

Fig. 1.—Ionization efficiency curve for He_2^+ from He.

exhibits the pronounced maximum characteristic of ions formed from excited states. Very similar curves have been published for Xe_2^+,[15] Kr_2^+,[2] and N_4^+[4] under similar conditions in a mass spectrometer. The exact shape of the curves varies somewhat with experimental conditions; specifically in our equipment the maximum was much sharper with a high field strength of the electron collimating magnet than with a low field strength. Even at low magnet field strength (as was the case in Fig. 1) the maximum for all the molecule ions is sufficient to differentiate between these ions and ions formed by direct ionization or ionic reactions.

Figure 2 shows typical data from which the values of the appearance potentials are obtained. In this case the experimental difference between the ionization potentials of He and Xe (both present in very small amounts in a much higher pressure of Kr) is 12.35 e.v. compared to a difference of 12.45 e.v. calculated from spectroscopic data. This gives us reasonable confidence in the absolute value of our measurements. The lines have a slight curvature just above the threshold, but this is an instrumental effect which is not reproducible. The precision of our measurements is not sufficient to allow, for example, the unambiguous assignment of a break corresponding to the upper limit of the doublet ionization potential for Ar, Kr, and Xe. In some cases, however, a break is present with sufficient reproducibility and clarity to be measured, as in the case of $^{40}Ar^+$ as a very weak interference with $^{20}Ne_2^+$.

Table I shows the values of the appearance potentials of the homonuclear rare gas molecule ions from our data together with literature values. These values supersede the previous value of the appearance potential of Xe_2^+ reported from this Laboratory—11.6 e.v.[15] which is also cited by Kaul and Taubert from another source[16]—and are substantially the same as the values reported by Munson, Field, and Franklin[4] for Ar_2^+ and Kr_2^+, 14.5 ± 0.2 and 13.0 ± 0.1 e.v., respectively. The agreement of the data is gratifying, though two of our values are somewhat lower than the literature values by an amount which is outside our indicated limits of precision. We consider that our values should be

(15) F. H. Field and J. L. Franklin, *J. Am. Chem. Soc.*, **83**, 4509 (1961).

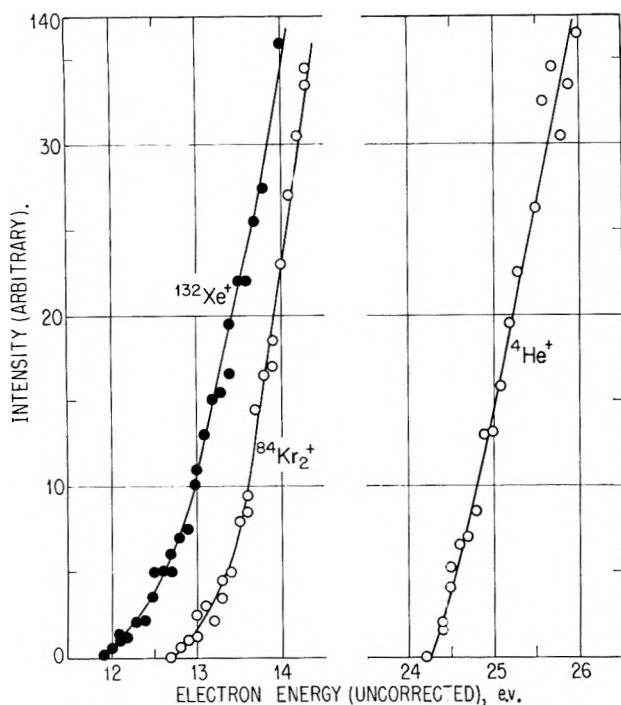(16) F. H. Field and J. L. Franklin, "Symposium on Mass Spectrometry," Oxford, 1961.

Fig. 2.—Representative plots of appearance potential data.

more reliable than the earlier values of Hornbeck and Molnar, but not necessarily more precise than the values of Kaul and co-workers.

TABLE I

APPEARANCE POTENTIALS OF HOMONUCLEAR RARE GAS MOLECULE IONS

R_2^+	These data	$AP(R_2^+)$, e.v. Lit.
He_2^+	23.3 ± 0.1	$23.4,^a\ 23.2^c$
Ne_2^+	$20.9 = .2$	20.9^c
Ar_2^-	$14.7 \pm .1$	$15.1,^b\ 15.1^c$
Kr_2^+	$13.0 \pm .1$	$13.2,^a\ 13.2^c$
Xe_2^+	$11.2 \pm .1$	11.6^a

^{a} Reference 5. ^{b} W. Kaul and R. Fuchs, Z. Naturforsch., 15a, 326 (1960). ^{c} Reference 1.

Table II shows values for the dissociation energy of He_2^+ from various sources, including several calculated values. The mass spectrometric value represents the difference between the ionization potential of He and the appearance potential of He_2^+. The value listed by Herzberg is considered as uncertain, and Pauling cites the other spectroscopic value in his early paper. The two values from the scattering of He^+ by He were obtained from the data of Cramer and Simons. Biondi and Holstein[9] observed in the spectra of helium after a discharge, presumably resulting from He^* produced by the recombination of He_2^+ with electrons, no states of energy less than ca. 23.1 e.v. This observation may be construed as giving about 1.5 e.v. for the dissociation energy of He_2^+.

The other experimental data do not appear to be sufficiently well established to be of concern; it is only the recent calculation of Reagan, Browne, and Matsen, which sets a lower limit for $D_e(He_2^+)$ greater than our value, that is disquieting. The zero point vibrational energy is unlikely to be greater than 0.2 e.v., which is not sufficient to account for the discrepancy. Subtracting about 0.2 e.v. from their value of 2.14 will correspond to an excited state of He of 22.6 e.v. for the lowest energy state which could be involved in

TABLE II

DISSOCIATION ENERGY OF He_2^+

Experimental

Mass spectrometric	$\geqslant 1.3$ e.v.
Spectroscopic	3.1^a
	2.5^b
Scattering	2.16^c
	3.9^d

Calculated

Pauling	0.05^h
Weinbaum	$.7^c$
Moiseiwitsch	$.76^f$
Csavinszky	$.84^g$
Reagan, Browne, and Matsen	2.14^h

^{a} G. Herzberg, "Spectra of Diatomic Molecules," in "Molecular Spectra and Molecular Structure," D. Van Nostrand Co., Inc., New York, N. Y., 1950, p. 536. ^{b} See L. Pauling, J. Chem. Phys., 1, 56 (1933). ^{c} E. A. Mason and J. T. Vanderslice, ibid., 29, 361 (1958). ^{d} W. H. Cramer and J. H. Simons, ibid., 26, 1272 (1957). ^{e} S. Weinbaum, ibid., 3, 547 (1935). ^{f} B. L. Moisewitsch, Proc. Phys. Soc., A69, 653 (1956). ^{g} P. Csavinszky, J. Chem. Phys., 31, 178 (1959). ^{h} P. N. Reagan, J. C. Browne, and F. A. Matsen, J. Am. Chem. Soc., 84, 2650 (1962).

the formation of He_2^+, which is close to the 3^3S level at 22.7 e.v. Our value of 23.3 e.v. for D_0 is nearest the 3^1P level at 23.1 e.v., the highest level for principal quantum number 3. However, one should perhaps not expect the 3^1P or any ^1P level to be the major source of He_2^+ since, according to Fig. 1, He_2^+ has a maximum at about 30–35 e.v., but Gabriel and Heddle report for all ^1P states a maximum in excitation cross section at about 100 e.v.[17]

If we assume that at these pressures the radiation to the ground state is completely trapped then the lifetime of the 3^1P state is 7.4×10^{-8} sec. The lifetimes of the other states of principal quantum number 3, all of lower energy than the 3^1P, are ^3S, 3.6×10^{-8} sec.; ^1S, 8.4×10^{-8} sec.; ^3P, 9.7×10^{-8} sec.; ^3D, 1.4×10^{-8} sec.; and ^1D, 1.5×10^{-8} sec. These values were calculated by Gabriel and Heddle[17] and agree with the less complete set of experimental values of Heron, McWhirter, and Rhoderick.[18] The lifetimes of the different states do not appear to be sufficiently different that one would not expect reaction from all. Excitation cross sections do not appear to be available below about 30 e.v. but extrapolation of the data of Gabriel and Heddle suggests that the cross sections for all of these states should be comparable in magnitude. Since we observe no variation of the appearance potential of He_2^+ with pressure, we do not think that there will be a contribution of lower energy states to the He_2^+ intensity which we are not observing at present because of low intensity. We have no explanation for the discrepancy between our value for $D_0(He_2^+)$ and the calculated one. One may assume that perhaps the 3^1P atomic state forms He_2^+ in an excited level, but there is still no explanation of why the lower states do not react.

Table III shows the dissociation energies of the other homonuclear rare gas ions. For Ne_2^+ there is an indication that $D_0(Ne_2^+) \cong 0.85$ e.v. from the spectral lines observed by Biondi and Holstein.[9] Mason and Vanderslice estimate $D_e(Ne_2^+)$ as between 0.33 and 0.71 e.v.

(17) A. H. Gabriel and D. W. O. Heddle, Proc. Roy. Soc. (London), A258, 124 (1960).
(18) S. Heron, R. W. P. McWhirter, and E. H. Rhoderick, ibid., A234, 565 (1956).

from scattering data of Ne^+ by Ne.[19] There is also a value of 0.0035 e.v. calculated for $D_e(Ar_2^+)$ from ion scattering data,[20] which is much too low.

TABLE III

DISSOCIATION ENERGIES

X	$D(X_2)$, kcal.[a]	$D(X_2^+)$, kcal.	$D(X_2^+) -$ $D(X_2)$, kcal.	MO configuration[d] $X_2 \rightarrow X_2^+$
He	...	30 (1.30 e.v.)	+30	$(\sigma_u{}^*1s)^2 \rightarrow (\sigma_u{}^*1s)$
Ne	...	16 (0.69 e.v.)	16	$(\sigma_u{}^*2p)^2 \rightarrow (\sigma_u{}^*2p)$
Ar	...	25 (1.08 e.v.)	25	
Kr	...	23 (1.00 e.v.)	23	
Xe	...	21 (0.91 e.v.)	21	
F	37	76[b]	39	$(\pi_g{}^*2p)^4 \rightarrow (\pi_g{}^*2p)^3$
Cl	58	97[c]	39	
Br	46	64[c]	18	
I	36	54[c]	18	
O	117	149[c]	31	$(\pi_g{}^*2p)^2 \rightarrow (\pi_g{}^*2p)$
H	104	61[c]	-43	$(\sigma_g1s)^2 \rightarrow (\sigma_g1s)$

[a] Taken from the compilation in S. W. Benson, "Foundations of Chemical Kinetics," McGraw-Hill Book Co., New York, N. Y., 1960, p. 662. [b] R. P. Iczkowski and J. L. Margrave, J. Chem. Phys., 30, 403 (1959). [c] Calculated from AP data in F. H. Field and J. L. Franklin, "Electron Impact Phenomena," Academic Press, New York, N. Y., 1957. [d] From W. Kauzmann, "Quantum Chemistry," Academic Press, New York, N. Y., 1957.

Table III also contains dissociation energies of other compounds for comparison with the dissociation energies of the rare gas molecule ions. It may be seen that the rare gas ion dissociation energies are about half those of the halogen molecules and may be considered as showing the same trend as the halogens, although the variation from Ne_2^+ to Xe_2^+ is about the same as the experimental error. In the examples listed, except H_2, the molecule ion has a larger dissociation energy than the molecule. These are cases for which, according to the simple MO treatment, the molecule ions have one less occupied antibonding molecular orbital than the molecules. From these data we obtain an average increase of 26 kcal. in bond strength caused by removing an antibonding electron, which may be compared with a decrease of 43 kcal. in going from H_2 to H_2^+, removing a bonding electron.

If we note that F_2^- is isoelectronic with Ne_2^+ with similar comparisons for the other halogen molecule negative ions, and assume that $D(R_2^+) \cong D(X_2^-)$ for isoelectronic pairs, then from

$$EA(X_2) = D(X_2^-) - \Delta H_f(X^-) - \Delta H_f(X)$$

we can obtain estimates of the electron affinities of the halogen molecules. From our data we find 63 kcal./mole for the electron affinity of F_2, which compares favorably with a recent estimate of 69 kcal./mole.[21] Similarly for Cl_2 we obtain 55 kcal./mole which may be compared with the tentative value of 39 kcal./mole given by Pritchard.[22] We estimate $EA(Br_2) = 51$ and $EA(I_2) = 45$ kcal./mole, but we know of no data for comparison.

Heteronuclear Molecule Ions.—Figure 3 shows representative ionization efficiency curves for two heteronuclear rare gas molecule ions. Relative intensities are used so that both may easily be plotted on the same

(19) E. A. Mason and J. T. Vanderslice, J. Chem. Phys., 30, 599 (1959).
(20) R. D. Cloney, E. A. Mason, and J. T. Vanderslice, ibid., 36, 1103 (1962).
(21) R. M. Reese, V. H. Dibeler, and J. L. Franklin, ibid., 29, 880 (1958).
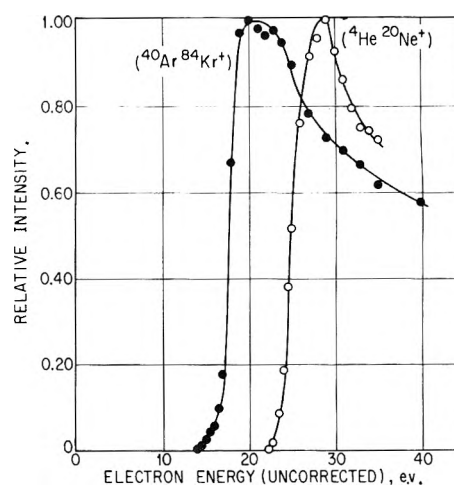(22) H. O. Pritchard, Chem. Rev., 52, 529 (1953).

Fig. 3.—Ionization efficiency curves for heteronuclear rare gas molecule ions.

scale, and each shows the maximum that is characteristic of products of reactions of electronically excited atoms and molecules. Ionization efficiency curves similar to these two were observed for all of the heteronuclear rare gas molecule ions.

We were able to obtain appearance potentials for all of the heteronuclear ions except $HeXe^+$, but the existence of the ion itself was observed. The intensity of $HeXe^+$ was too low and there was too much interference from the high mass wing of the Xe^+ peaks at high pressures to permit a reliable measurement of the appearance potential. The appearance potentials are listed in Table IV with the available literature data. For three of the four previously reported ions the agreement is good. However, for $HeNe^+$ our value is higher than that of Kaul and Taubert by an amount greater than the experimental uncertainty. Our value of 23.4 e.v. is essentially the same as that for He_2^+ so that the lowest states involved in He_2^+ formation also appear to react to form $HeNe^+$. A careful search was made for a lower energy process for the formation of $HeNe^+$, particularly around 20 e.v., but none was observed.

TABLE IV

APPEARANCE POTENTIALS OF HETERONUCLEAR RARE GAS
MOLECULE IONS

Ion	AP (e.v.) — These data	AP (e.v.) — Lit.
$HeNe^+$	23.4 ± 0.1	22.6[5]
$HeAr^+$	17.9 ± .3	
$HeKr^+$	19.9 ± .1	
$NeAr^+$	16.8 ± .1	16.5[10]
$NeKr^+$	16.6 ± .1	
$NeXe^+$	16.0 ± .3	
$ArKr^+$	14.0 ± .1	
$ArXe^+$	13.5 ± .1	13.5[5]
$KrXe^+$	12.3 ± .1	12.2[5]

The heteronuclear ions, with the possible exception of $ArKr^+$, $KrXe^+$, and $HeAr^+$, appear to be formed primarily from excited states of the gas of higher ionization potential which lie above the ionization potential of the other rare gas. For $ArKr^+$ and perhaps $KrXe^+$ the values of the appearance potentials are sufficiently close to the lower ionization potential that it is possible that these ions may be formed from states of either rare gas immediately below the ionization potentials of Kr and Xe, respectively, as well as from states of Ar and Kr above the ionization limits of Kr and Xe.
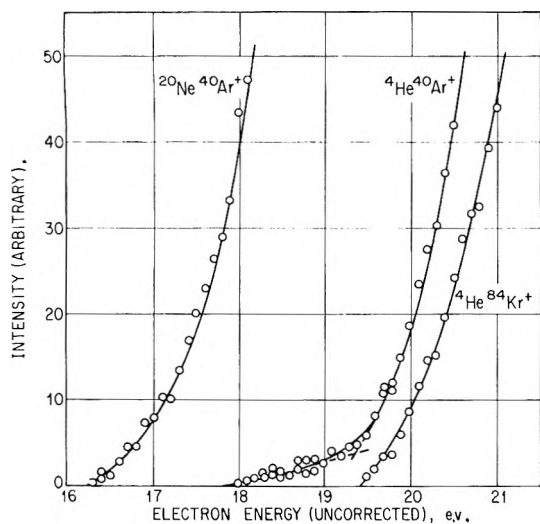
Fig. 4.—Ionization efficiency curves for heteronuclear molecule ions.
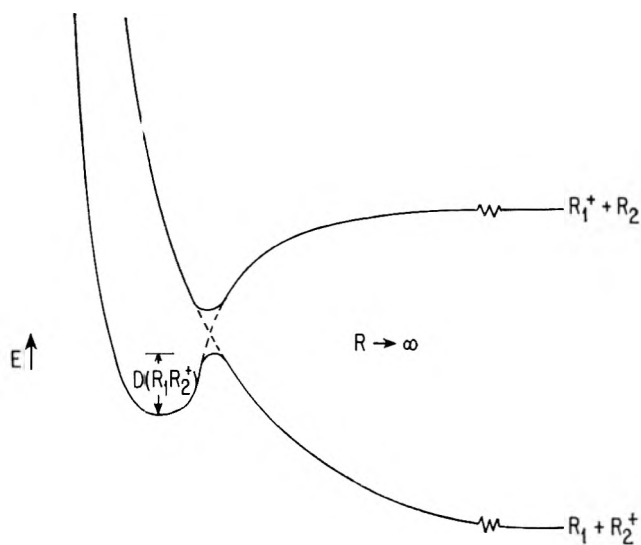

Fig. 5.—Schematic representation for non-crossing rule for states of $R_1R_2^+$.

The 17.9 e.v. value for $AP(HeAr^+)$ cannot be the result of a reaction of an excited state of He, since there is no known state at that energy. The ionization efficiency curve for $HeAr^+$ is somewhat different from the others, in that there is a low voltage tail, giving the appearance potential of 17.9 e.v., but there is a relatively well defined break at about 20 e.v., corresponding in energy to the metastable helium states. Figure 4 shows the ionization efficiency curves for $HeAr^+$, $HeKr^+$, and $NeAr^+$ for a short range above the threshold, indicating this difference. From the relative slopes of these two sections of the curve one is inclined to think that most of the $HeAr^+$ was formed by states of He above 19.9 e.v.

There is some recent evidence for the existence of states of Ar of energy as high as 18 e.v.[23] In other atoms for which states above the ionization limit have been observed, both sharp and broad spectral lines emanating from these states have been noted.[24] The broad lines are associated with states for which auto-ionization may occur, and may have lifetimes as short

as 10^{-13} sec. Normal radiative lifetimes may be associated with the sharp lines, which are perhaps long enough for chemi-ionization reactions to occur. Thus it is possible that states of Ar above the ionization limit can produce the $HeAr^+$ ion.

$HeKr^+$ has an appearance potential corresponding to the helium metastable levels, and $NeAr^+$, $NeKr^+$, and $NeXe^+$ have appearance potentials which correspond well to the neon metastable levels. The $NeXe^+$ appearance potential is below the value of the Ne metastable levels by an amount greater than the expected precision and may perhaps have contributions from at present unknown states of Xe in the ionization continuum in a manner analogous to $HeAr^+$.

The stability of these ions, which is at first surprising since dissociation to the ion of lower ionization potential is strongly exothermic, is probably the result of the non-crossing (or pseudo-crossing) of attractive and repulsive curves.[25] Essentially the same treatment is given for some dipositive diatomic ions in treatments by Bates and Carson for N_2^{++} and O_2^{++} [26] and by Fraga and Ransil for He_2^{++}.[27] The shape of the potential energy curves is indicated in Fig. 5 and shows the activation energy for dissociation to the more stable products. We assume that our appearance potential corresponds to atomic states near the potential minimum for the lower curve, but it is not possible to obtain a value for this dissociation energy from our appearance potential measurements. One would also expect some higher energy atomic states of the gas of higher ionization potential to contribute to heteronuclear molecule ion formation according to the upper curve. No attractive curve results from the lower state of R_1^+ and R_2, for if this were the case the appearance potential of the heteronuclear molecule ion would be lower than the lower of the two ionization potentials.

From the pressure studies there was no noticeable charge exchange between He^+ and Ne or Ar or between Ar^+ and Kr since the quantities $(Ne^+)(He)/(He^+)(Ne)$, $(Ar^+)(He)/(He^+)(Ar)$, and $(Kr^+)(Ar)/(Ar^+)(Kr)$, which represent the ratios of ionization cross sections, were independent of pressure to within $\pm 10\%$. The data of Stedeford and Hasted on charge exchange give $Q(He^+, Ne) = 2 \times 10^{-17}$ cm.^{2} at 100 e.v. and $Q(He^+, Ar) = 1 \times 10^{-16}$ cm.^{2} at about 250 e.v.[28] Cross sections at the lower energies of our mass spectrometer source will be even smaller so that the contribution from charge exchange should be less than our experimental error. The formation of Ar^+, Kr^+, or Ne^+ by the Penning process, reaction 1, is negligible compared to the formation of the ions by direct ionization through electron impact.

The relative intensity of the homonuclear rare gas molecule ion of higher appearance potential was always decreased by the addition of the gas of lower ionization potential as the result of the Penning process and heteronuclear molecule ion formation. There was a small apparent decrease in the ratios $(Ne_2^+)/(Ne^+)$ and $(Ar_2^+)/(Ar^+)$ with the addition of helium which was probably of instrumental origin. A larger decrease

(23) F. J. Cornes and W. Lessman, Z. Naturforsch., 16a, 1396 (1961), who also list earlier references.

(24) H. E. White, "Introduction to Atomic Spectra," McGraw-Hill Book Co., New York, N. Y., 1934, pp. 394–398.

(25) See, for example, C. A. Coulson, "Valence," Clarendon Press, Oxford, 1952, p. 65.

(26) D. R. Bates and T. R. Carson, Proc. Phys. Soc. (London), A68, 1199 (1955).

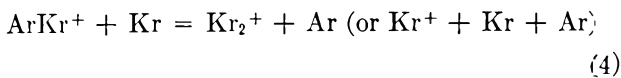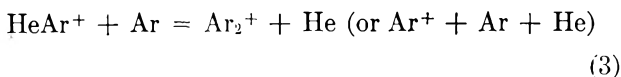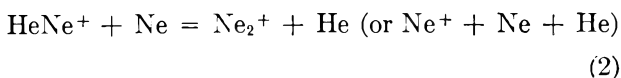(27) S. Fraga and B. J. Ransil, J. Chem. Phys., 37, 1112 (1962).

(28) J. B. H. Stedeford and J. B. Hasted, Proc. Roy. Soc. (London), A227, 466 (1955).

in $(Kr_2^+)/(Kr^+)$ was observed with the addition of Ar which may be instrumental or which may indicate that some of the higher excited states of Kr are reacting to form $ArKr^+$.

As an idea of the relative intensities of the ions found in the systems, for $(He)/(Ne) = 1$ at about 27 e.v. and $P \cong 120\,\mu$, $(^4He^+) = 1.3 \times 10^5$, $(^4He_2^+) = 1.5 \times 10^3$, $(^{20}Ne^+) = 8.9 \times 10^5$, $(^4He^{20}Ne^+) = 1.9 \times 10^3$, and $(^{20}Ne_2^+) = 3.7 \times 10^3$, all ion intensities in the same arbitrary units. For $(He)/(Ar) = 1$ at 26 e.v. and $P \cong 100\,\mu$, $(^4He^+) = 3.5 \times 10^4$, $(^4He_2^+) = 1.4 \times 10^2$, $(^{40}Ar^+) = 1.9 \times 10^6$, $(^4He^{40}Ar^+) = 8.4 \times 10^2$, and $(^{40}Ar_2^+) = 9.3 \times 10^3$. For $(Ar)/(Kr) = 1$ at $P \cong 100\,\mu$ and 20 e.v., $(^{40}Ar^+) = 8.7 \times 10^5$, $(^{40}Ar_2^+) = 2.3 \times 10^3$, $(^{84}Kr^+) = 7.0 \times 10^5$, $(^{40}Ar^{84}Kr^+) = 2.3 \times 10^3$, and $(^{84}Kr_2^+) = 2.1 \times 10^3$. The intensities of heteronuclear molecule ions are less than those of the homonuclear ions which can be made from the components, but the difference is usually less than the order of magnitude indicated by Pahl and Weimer for $HeNe^+$.[3]

Rough pressure studies on all of the heteronuclear rare gas molecule ions indicated an approximately first-order dependence on each gas. More careful studies on He–Ne, He–Ar, and Ar–Kr mixtures gave a good first-order dependence on each rare gas at low pressures. No third-order processes were detected. Although all three reactions

$$HeNe^+ + Ne = Ne_2^+ + He \ (or\ Ne^+ + Ne + He) \quad (2)$$

$$HeAr^+ + Ar = Ar_2^+ + He \ (or\ Ar^+ + Ar + He) \quad (3)$$

$$ArKr^+ + Kr = Kr_2^+ + Ar \ (or\ Kr^+ + Kr + Ar) \quad (4)$$

are exothermic, evidence for reaction 3 only was found. The ratios $(HeNe^+)/(He_2^+)$ and $(ArKr^+)/(Ar_2^+)$ are first order in Ne and Kr pressure, respectively, and inversely proportional to He and Ar pressure, respectively. The ratio $(HeAr^+)/(He_2^+)$ is inversely proportional to He pressure, but is proportional to Ar pressure only at very low pressures. These data are shown in Fig. 6 and indicate a reaction of Ar removing $HeAr^+$ from the system.

From studies of the field strength dependence of the heteronuclear rare gas molecule ions we find that the ions have only excited atom reactants, in agreement with the observations of Kaul and Taubert.[5]

In a manner analogous to that of our two previous studies on excited state reactions of rare gases[3,4] we postulate the following mechanism, in which R_1 is the rare gas of higher ionization potential
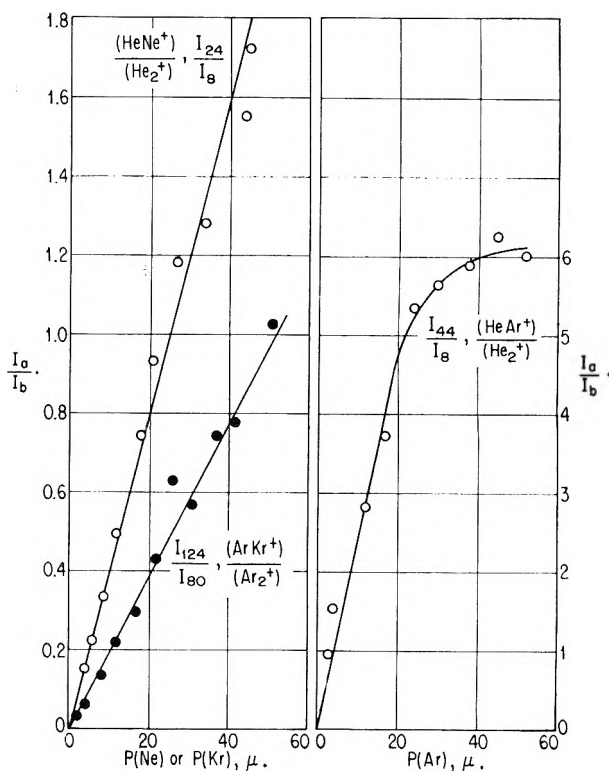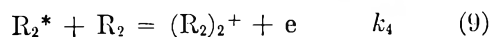
$$R_1 + e = \begin{matrix} R_1^+ + 2e & k_i \\ R_1^* + e & k_e \end{matrix} \quad (5)$$

$$R_2 + e = \begin{matrix} R_2^* + e & k_e' \\ R_2^+ + 2e & k_i' \end{matrix} \quad (6)$$

$$R_1^* + R_2 = \begin{matrix} R_1R_2^+ + e & k_1 \\ R_2^+ + R_1 + e & k_2 \end{matrix} \quad (7)$$

$$R_1^* + R_1 = (R_1)_2^+ + e \qquad k_3 \quad (8)$$
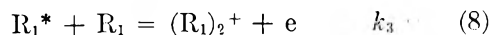
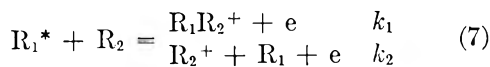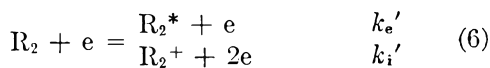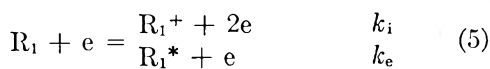$$R_2^* + R_2 = (R_2)_2^+ + e \qquad k_4 \quad (9)$$

Fig. 6.—Ratios of heteronuclear and homonuclear molecule ions as a function of pressure.

$$R_2^* = R_2 + h\nu \qquad k_5 \quad (10)$$

$$R_1^* = R_1 + h\nu \qquad k_6 \quad (11)$$

Making the usual steady-state approximation on R^*, we obtain for low pressures

$$(R_1)_2^+ = k_e k_3 (R_1)^2 t_1 I_e \quad (12)$$

$$(R_1R_2)^+ = k_e k_1 (R_1)(R_2) t_1 I_e \quad (13)$$

$$(R_2)_2^+ = k_e' k_4 (R_2)^2 t_2 I_e \quad (14)$$

in which t_1 and t_2 are the average lifetimes of the excited species R_1 and R_2, respectively, and I_e is the electron current.

Since the lifetimes of the states involved are not

Table V

Relative Rate Constants for Molecule Ions

R_1	R_2	k_1/k_3	$\dfrac{\alpha(R_2)^a}{\alpha(R_1)}$	$\dfrac{k_e'k_4t_2}{k_ek_3t_1}$	$\dfrac{\alpha^2(R_2)^a}{\alpha^2(R_1)}$
He	Ne	1.80		4.0	
		1.37		2.5	
		1.52		3.0	
		1.52		3.1	
		1.62	1.85	3.1	3.4
He	Ar	4.0			
		7.1		63	
		12.2		98	
		7.8	7.67	80	59
Ar	Kr	1.82		3.1	
		1.61		2.2	
		1.7	1.51	2.6	2.3

^{a} Values of polarizability, α, taken from H. H. Landolt and R. Börnstein, "Zahlenwerte und Functionen," Part 3, "Atom und Molecularphysik," Springer-Verlag, Berlin, 1950, 6th Ed., p. 514.

known, we cannot calculate absolute values for the rate constants. Our data are not accurate enough for anything other than a rough estimate of the ratio k_2/k_1, the ratio of ionization by the excited species to heteronuclear molecule ion formation, but for these cases the ratio is of the order of 2–10. The ratios are obtained from the experimental data using a steady state treatment of reactions 5 to 10.

From (12), (13), and (14) we obtain

$$\frac{(R_1R_2)^+}{(R_1)_2{}^+} = \frac{k_1(R_2)}{k_3(R_1)} \tag{15}$$

$$\frac{(R_2)_2{}^+}{(R_1)_2{}^+} = \frac{k_e'k_4(R_2)^2t_2}{k_ek_3(R_1)^2t_1} \tag{16}$$

From (15) we can readily compute the ratio k_1/k_3. The results are given in Table V and, for comparison, the ratios of the polarizabilities of the unexcited atoms, R_2 and R_1, are included. The ratios of rate constants and polarizabilities are surprisingly similar, although we cannot present a reason for the agreement. Similarly, from (16) we obtain the ratio

$$\frac{k_e'k_4t_2}{k_ek_3t_1}$$

Since chemi-ionization reactions are involved, we might expect

$$\frac{k_4}{k_3} \cong \frac{\alpha(R_2)}{\alpha(R_1)}$$

Lampe, Franklin, and Field[29] have shown cross sections for ionization by 70 volt electrons to be proportional to polarizability. If we assume a similar relation for excitation cross section and if we further assume $t_2 \cong t_1$, then we would have for homonuclear chemi-ionization

$$\frac{k_e'k_4t_2}{k_ek_3t_1} \cong \frac{\alpha(R_2)^2}{\alpha(R_1)^2}$$

Again, Table V shows approximate agreement.

Acknowledgments.—We wish to acknowledge the very able assistance of Mr. W. C. Gieger, who performed these experiments with his accustomed competence.

(29) F. W. Lampe, J. L. Franklin, and F. H. Field, *J. Am. Chem. Soc.*, **79**, 6129 (1957).

THE INTERFACIAL SURFACE PRESSURE OF SOLUBLE ALCOHOL MONOLAYERS AT THE WATER–OCTANE INTERFACE

By Joseph J. Jasper and Barton L. Houseman

Department of Chemistry, Wayne State University, Detroit, Michigan

The differential method, furnished by a vertical-pull filmometer, was used to measure the interfacial surface pressures produced by soluble monolayers of five normal alcohols (C_8 to C_{12}) which formed spontaneously at the interface between water and n-octane as the result of positive adsorption. The pressures were varied by changing both the temperature of the two-phase liquid systems and the concentrations of the alcohols in the octane phase. A table is presented which gives the interfacial surface pressures as functions of the concentration and the temperature.

A considerable body of knowledge is now available concerning the properties and states of a large variety of insoluble monolayers on aqueous substrates. This is the result of the extensive studies of Adam,[1] Harkins,[2] Langmuir,[3] and others, whose data have been expressed as functions of various intensive and extensive properties. The interpretation of these relations has led to important generalizations concerning the nature of monolayers, which have proved to be very useful in various aspects of theoretical and applied surface chemistry. Present knowledge concerning monolayers at the interface between two mutually immiscible liquids, however, is not nearly as extensive. A review of the literature reveals that relatively few studies of such monolayers have ever been reported. The apparent neglect of this important and interesting phase of surface chemistry is a probable consequence of the experimental difficulties attending such measurements generally. These difficulties become quite pronounced when the experimental procedure involves the horizontal barrier-float filmometer.

Although this apparatus was designed originally to measure the surface pressure of insoluble monolayers at the surface of aqueous substrates, certain modifications have enabled its limited application to the study of insoluble monolayers at the interface between two immiscible liquids. Typical of such studies were those of Askew and Danielli[4] with protein monolayers at the water–bromobenzene interface.

Although few data are presently available concerning either soluble or insoluble monolayers at the dineric interface, a more complete knowledge of their properties are essential to a better understanding of certain biochemical processes, detergency, lubrication, emulsification, and other phenomena which are dependent on the properties of the interfacial region.

Since the vertical-pull filmometer is applicable both to soluble and insoluble monolayers and measures the film pressure directly,[5] this type of apparatus was adopted for the present study of soluble monolayers at the water–octane interface. A preliminary study[6] clearly demonstrated the practicability and precision of this apparatus.

Soluble monolayers are established at the dineric interface as the result of positive adsorption from one or both of the liquid phases. In order to obtain a pure

(1) N. K. Adam, "The Physics and Chemistry of Surfaces," 3rd Ed., Oxford Univ. Press, London, 1941, Chapter 2.

(2) W. D. Harkins, "The Physical Chemistry of Surface Films," Reinhold Publ. Corp., New York, N. Y., 1952, Chapter 2.

(3) I. Langmuir, *J. Am. Chem. Soc.*, **39**, 1848 (1917).

(4) F. A. Askew and J. F. Danielli, *Proc. Roy. Soc.* (London), **A155**, 695 (1936); *Trans. Faraday Soc.*, **36**, 785 (1940).

(5) W. D. Harkins and T. F. Anderson, *J. Am. Chem. Soc.*, **59**, 2189 (1957).

(6) J. J. Jasper and T. D. Wood, *J. Phys. Chem.*, **60**, 1625 (1956).

phenomenon uncomplicated by reciprocal solubility factors, two liquids were selected which remained practically mutually immiscible over the predetermined temperature range. To establish the most favorable conditions possible, water and n-octane were selected as the liquid components of the system, and a series of long-chain alcohols, soluble only in the organic phase, constituted the monolayer components. The present study was concerned with the measurement of the interfacial surface pressures of these soluble alcohol monolayers over an appreciable temperature and concentration range.

Experimental

Purification of the Compounds.—The alcohols selected for the monolayer component of the system were 1-octanol, 1-nonanol, 1-decanol, 1-undecanol, and 1-dodecanol. This range in molecular weights was determined by the fact that 1-octanol represents the upper limit in the permitted potential solubility in the aqueous phase, and 1-dodecanol the highest homolog that is liquid at ambient temperatures. The best quality of Matheson, Coleman, and Bell alcohols was obtained and further purified by vacuum fractionation. In each case the middle third of the distillate was reserved for the next stage of the experimental procedure. Refractive index values of this fraction were found to differ from those of the "International Critical Tables" by less than two parts in the fourth decimal. Vapor phase chromatographic analysis indicated the following: 1-octanol, no perceptible impurity; 1-nonanol, 3% impurity; 1-decanol, less than 1% impurity; 1-undecanol, 1% impurity; 1-dodecanol, 3% impurity. An examination of the v.p.c. curves led to the conclusion that the contaminants were isomeric alcohols, and this was confirmed by infrared analysis.

Pure grade n-octane (99 mole %) was obtained from Phillips Petroleum Company, and this was treated with lithium aluminum hydride, then distilled. The distillate was passed through a column containing Fisher chromatographic quality adsorption alumina and silica gel, then again distilled. This distillate was examined by infrared spectroscopy, v.p.c., and by refractive index. No impurity was detected.

To obtain water of the highest purity possible, doubly distilled water was first passed through a Barnstead block tin conductivity still, and then distilled in an all-quartz double chamber Heraeus–Quarzschmelze still. The water produced had a conductivity of 10^{-6} mho and was remarkably free of organic impurities.

Description of Apparatus.—The essential parts of the vertical-pull filmometer used in this investigation consisted of a pendant slide suspended through the interfacial region; a glass cell which enclosed the two-phase liquid system; and a sensitive chainomatic balance. The pendant slide is probably the most critical part of the apparatus and is the most difficult to procure and prepare for operation. For the present investigation, it was necessary that the slide material not only be chemically inert and insoluble but also form a very small contact angle with the organic phase and a large one with water. A large number of materials were tested but Du Pont Teflon (TFE) proved to be the most satisfactory in meeting the above prerequisites. A slide was constructed of this material with dimensions 0.1524 cm. in thickness, 1.524 cm. in width, and 2.54 cm. in length. This slide was polished with great care on a metallographic polishing wheel, first with ferric oxide powder on a felt wheel, then with dry chamois, and finally with chamois saturated with water. The resulting mirror-smooth surface appeared to be completely wetted by n-octane but apparently not at all by water. It should be emphasized at this point, however, that it is essential that the surface of the Teflon slide be very clean, smooth, and non-porous if a small contact angle with n-octane is required. Studies by Fox and Zisman[7] have shown that this contact angle is 26° at the air–octane interface. A small hole was drilled close to one end of the slide and through this a fine chromel wire was inserted to form a hook. This enabled the attachment of the slide to the end of a fine gold chain suspended from the left arm of the chainomatic balance through an opening in the floor of the balance case.

The cell designed for the measurements was constructed of Pyrex and had the shape of an oblate spheroid with a diameter of 8.5 cm. and a depth of 5 cm. A 45/50 female standard taper

(7) H. W. Fox and W. A. Zisman, J. Colloid Sci., 5, 514 (1950).

joint was sealed in the center of the upper flattened surface and in the lower surface a hemispherical bubble was blown of sufficient diameter to freely accommodate the pendant slide. The effect was to deepen the cell without greatly increasing the total volume. A smaller tube, terminating in a 14/35 female joint, was sealed adjacent to the larger one to permit introduction of the alcohols into the organic phase of the liquid system within the cell. The male portion of the larger standard joint was tapered to 10 mm. in diameter about 5 cm. above the ground surface and a 10-mm. glass tube, 30 cm. in length, was sealed to this opening. When in operating position, the tube extended along the axis of the joint to within a few centimeters below the opening in the floor of the balance case. The function of this tube was to enclose the gold chain and to guide it into the cell. When the ground glass joints were connected, the cell was effectively closed to the surrounding water of the bath in which it was immersed and the chain to stray air currents which might disturb the freely hanging slide. Special care was taken to prevent the gold chain from making contact with the walls of the tube during the experimental procedure. This was accomplished by careful leveling.

In the operation of the vertical-pull filmometer described above, the pendant slide was suspended through the dineric interface, and the surface tension acting vertically along the horizontal peripheral length of this slide was measured directly by an analytical balance. It is essential that one of the liquids only wet the slide, and this requirement constitutes a major difficulty since materials which are readily wet by one of the liquid components and not the other are not readily available. Any variation in the surface properties of the wetting liquid is immediately signalized by a change in the balance reading which measures either a vertical pull or push, depending upon whether the wetting liquid has the greater or lesser density of the two. It was desired to make interfacial film pressure readings to ±0.05 dyne per cm., and, since 0.03 dyne per cm. was equivalent to a change of about 10^{-4} g. with the pendant slide used, a balance had to be selected which could guarantee this accuracy. The buoyancy difference of the slide in the octane and in the water creates an appreciable damping effect. Thus, as the slide rises, a larger portion of it enters the octane (sp. gr. 0.70) and it becomes heavier; as it drops, more of it enters the water and it becomes lighter. This damping effect decreases the sensitivity by a factor of about ten. Therefore, to achieve an accuracy of 0.0002 g., a balance about ten times more sensitive was required. An Ainsworth TCY semimicro keyboard balance was accordingly selected for use in the measurements. Since the Teflon slide was wet by the less dense octane only, the following equation was used to convert differences in balance readings to dynes per cm.

$$\Delta \gamma_i = \frac{g(-\Delta W)}{2(w + t)}$$

in which γ_i represents the interfacial tension, g the gravitational factor, W the balance reading in grams, w and t, respectively, the width and thickness of the slide. Preliminary trials demonstrated that corrections for buoyancy changes attending the additions of alcohols to the octane phase were negligible, and these accordingly were neglected.

The thermostatic water bath in which the cell was immersed consisted of a 7.5-gal. Pyrex cylinder encased in a large plywood box and insulated with expanded mica. Viewing windows were cut in the box, which permitted inspection of the apparatus from positions diametrically opposite. The windows were covered with plexiglass to reduce thermal radiation. The top was fitted with a plywood cover. A multiple-position, Beckman-type mercury-filled thermoregulator, in conjunction with an amplifier and mercury solenoid, was used to control a 500-watt heat bulb. With this temperature regulation, together with an efficient stirrer, it was possible to maintain the bath temperature constant to ±0.002° at all temperatures above ambient. Temperatures below ambient were attained by circulating cold water through coils in the bath with the heater operating intermittently. Under these conditions the temperature could be maintained constant to ±0.005°. The water bath was mounted on a steel base and the balance on a steel shelf supported by steel framework welded to the base. To ensure minimum vibration, the entire apparatus was placed on steel-to-rubber vibration-damping mountings.

Experimental Procedure.—All glassware that came in contact with the liquids involved in this study was cleaned first with hot chromic acid cleaning solution, then with distilled water rinse,

<div align="center">Table I</div>

<div align="center">Interfacial Surface Pressures of the Alcohols C₈ to C₁₂ (Dynes Cm.⁻¹)</div>

m, volume molal	1-Octanol					1-Nonanol			1-Decanol					1-Undecanol			1-Dodecanol		
	25°	35°	45°	55°	65°	25°	35°	45°	25°	35°	45°	55°	65°	25°	35°	45°	25°	35°	45°
0.01	9.5	7.4	6.0	5.0	4.2	9.6	7.7	6.3	9.5	7.6	6.0	4.8	3.8	9.7	7.5	5.7	9.6	7.8	6.3
.02	14.2	12.0	10.2	8.6	7.1	14.4	12.1	10.0	14.2	12.0	8.9	8.0	6.3	14.1	11.7	9.6	14.0	11.8	9.9
.03	17.3	14.9	13.0	11.1	9.3	17.4	15.0	12.8	16.9	14.6	12.5	10.4	8.4	16.8	14.4	12.2	16.9	14.6	12.4
.04	19.4	17.1	15.0	13.0	11.2	19.4	17.1	14.8	19.1	16.8	14.6	12.4	10.1	19.0	16.5	14.3	18.7	16.6	14.3
.05	21.0	18.6	16.4	14.5	12.6	20.8	18.7	16.4	20.4	18.2	16.0	13.7	11.5	20.3	18.1	15.9	20.2	18.3	16.4
.07	23.0	21.1	19.2	17.2	15.2	22.9	20.9	19.0	22.4	20.4	18.4	16.3	13.9	22.1	20.1	18.1	22.0	20.1	18.2
.10	24.8	23.2	21.7	20.1	18.0	24.6	23.0	21.4	24.2	22.5	20.8	19.0	16.6	23.8	22.1	20.3	23.6	22.0	20.3
.15	26.4	25.2	24.0	22.6	20.7	26.0	24.8	23.6	25.6	24.3	23.0	21.5	19.4	25.4	23.9	22.4	25.1	23.7	22.3
.20	27.5	26.4	25.4	24.4	22.6	27.0	25.9	24.8	26.5	25.4	24.2	22.8	20.9	26.3	25.0	23.7	26.0	24.7	23.4
.30	28.7	27.9	27.1	26.2	24.8	28.3	27.4	26.4	27.7	26.7	25.6	24.4	22.9	27.3	26.2	25.0	27.0	25.9	24.7

and finally with steam. This final step served to remove the last traces of any organic film remaining on the glass and to rapidly dry the glass.

The two-phase liquid systems were prepared by mixing 70 ml. of n-octane and 90 ml. of water in a Pyrex bottle which was fitted with a Teflon seal. The bottle with contents was suspended in the constant temperature bath for at least 5 hr. prior to use to ensure mutual saturation of the liquid phases and to allow any remaining surface active impurities to diffuse to and become adsorbed at the interface.

The initial procedure was to carefully remove the bottle from the bath while using every precaution to avoid disturbing the interface. The cell was next clamped in position within the water bath and allowed to reach thermal equilibrium with the surroundings. Exactly 50 ml. of the octane and 75 ml. of water were carefully pipetted from the center of their respective phases within the bottle and placed in the cell. Since it is highly essential that the Teflon slide be free from contaminants, it was cleaned thoroughly. To accomplish this, the slide was immersed for some time in a hot sulfuric–nitric acid bath, then thoroughly rinsed with distilled water, and finally dried with lens paper. To ensure a zero contact angle with octane, the slide was rubbed with lens paper which had been wetted with that compound. The slide was then attached to the gold chain and suspended through the dineric interface. To exclude any possibility of water from the bath leaking into the cell, elastic rubber seals were stretched over the junction of the two taper joints.

Before the first balance reading was made, the slide was lifted from the interface and lowered several times to dislodge air bubbles. After this, the gold chain was lifted and dropped several times to unkink and untwist the chain links. Balance readings were made on the pure interface during the first half-hour to test for constancy of the initial weight. Addition of alcohols was accomplished with the use of a Starrett micrometer syringe which was calibrated to deliver liquid volumes up to 0.25 ml. with a precision of 0.0001 ml. The syringe fitted through the 14/35 taper joint on the cell in such a way that, when it was inserted as far as possible, the tip of the syringe needle was immersed in the octane about 7 mm. from the dineric interface.

The operation consisted of introducing measured quantities of the alcohols from the micrometer syringe into the octane layer just above the interface. After each addition, weighings were made every few minutes until it was certain that equilibrium had been attained. The time involved in making the additions for each alcohol at a given temperature over the complete concentration range was from 2 to 4 hr. After each addition, it was observed that the more dense alcohol settled to the interface and spread across this region almost instantly. This was further evidenced by the sudden increase in the interfacial surface pressures followed by a slow return to equilibrium values as the alcohol diffused into the octane to become molecularly dispersed.

Rigorous tests indicate that there are several sources of determinate errors attending the experimental procedure. The more important of these are as follows: (a) Contamination from the cell walls brings about a slow decrease in the interfacial tension of the pure interface which may continue for as long as 24 hr. (b) The presence of solids, such as dust, results in irregular and irreproducible readings of the pure interface. Such particles are generally attracted to the break in the interface at the point where the slide penetrates this region. The particle usually becomes attached to the slide and changes the contact angle. (c) A value greater than zero for the slide–octane contact angle produces

symptoms readily detected by the experienced operator. According to the experience of the authors, a contact angle other than zero is labile and shows appreciable hysteresis in the upward and downward motion of the pendant slide. This hysteresis is always reflected in the behavior of the balance pointer. Thus, a marked decrease in the balance sensitivity and a shortening of both the period and average arc of the balance pointer is observed. Detection of any of these irregularities immediately disqualified the experiment. The apparatus was then disassembled and recleaned.

Results

A number of preliminary tests proved that the alcohols were positively adsorbed from the organic phase. Since they are insoluble in the aqueous phase but possess a strongly hydrophilic group, it seems quite reasonable to assume that the molecules must orient at the liquid interface with the hydroxyl groups anchored to the aqueous phase. The positively adsorbed layer possesses properties which are similar to those of insoluble monolayers and, therefore, can be treated similarly. Although the interfacial concentration cannot be varied by lateral compression, this variation can be accomplished spontaneously by increasing the concentration of the surface active alcohols in the organic phase and by varying the temperature.

If it is assumed that the two-dimensional surface pressure equation[8] can be applied to the interfacial region, it may be written as

$$P_i^s = \gamma_i - \gamma_f \qquad (1)$$

where P_i^s represents the lateral pressure exerted by the interfacial monolayer, γ_i the interfacial free surface energy, and γ_f the interfacial free surface energy with the monolayer present. Since $(\gamma_i - \gamma_f)$ may be regarded as the decrease in the interfacial free surface energy attending the positive adsorption of the alcohols at the interface, then

$$P_i^s = -\Delta\gamma_i = -\Delta F_{ad} \qquad (2)$$

The interfacial surface pressures of the five alcohols are tabulated as functions of the volume-molal concentration m and of the temperature (centigrade) in the accompanying table. These data were found to be reproducible to ± 0.08 dyne cm.⁻¹ although the precision of a single reading was ca. ± 0.02 dyne cm.⁻¹. When the interfacial surface pressures corresponding to a given alcohol concentration are plotted as functions of the temperature, a series of isopleths (not shown) are obtained which are convex to the temperature abscissa at the two lower concentrations.

(8) Reference 2, p. 121.

The 1-nonanol, 1-undecanol, and 1-dodecanol isopleths become increasingly linear with increasing concentrations. The 1-octanol and 1-decanol, however, approach linearity and then become concave to the temperature axis as the concentration is increased.

The thermodynamic equation of Clapeyron was modified by Lord Kelvin for application to two-dimensional liquid surfaces. Since this equation is equally applicable to the interfacial region between two-phase liquid systems, it can be written in the form

$$- (d\gamma_i/dT) = L^s/T \qquad (3)$$

With the aid of this equation various thermodynamic quantities relating to the interface can be calculated. By reference to eq. 1 it is to be noted that the pressure P^s of the interfacial monolayer is the difference in the magnitude of two interfacial free surface energies. The larger of these involves the interface between two pure liquid phases, and the lesser the same interface occupied by oriented dipoles which constitute the interfacial monolayer. This is indicated by eq. 2. Substitution of the pressure P^s in eq. 3 gives

$$(dP^s/dT) = L^s/T = \Delta S^s \qquad (4)$$

Therefore, from the temperature differential of P^s, the latent heat of adsorption L^s and the entropy of adsorption ΔS^s can be determined. Likewise, the two-dimensional analog of the well known free energy equation can be written

$$\Delta H^s = P_i{}^s + T(dP^s/dT) \qquad (5)$$

and this enables the calculation of the enthalpy of adsorption. However, since the interfacial tension is a monotonically decreasing function with concavity directed toward the temperature axis, their values must be known over the experimental temperature ranges before the various thermodynamic quantities of eq. 4 and 5 can be calculated. These will be presented in another report.

When the interfacial surface pressures are plotted as functions of the volume-molal concentrations, smooth curves are obtained (not shown in this paper) which closely resemble and, in effect, are adsorption isotherms. For each of the alcohols studied, P^s increased very rapidly with increasing concentration and appears to be approaching a limiting value which is quite probably determined by the structure of the monolayer. As might be expected, P^s decreases with increasing temperature, a characteristic behavior of adsorption phenomena. Thus, for a given alcohol, a series of isotherms is obtained whose initial slopes are decreasingly positive and, consequently, become flatter with increasing temperature. From reference to the table, it is evident that for P^s values up to ca. 0.02 m, a single isotherm would very closely represent all of the alcohols between 25 and 50°. At higher concentrations, the P^s values exhibit an orderly trend with the values decreasing with increasing chain length. At higher concentrations, the P^s values of the shorter chain alcohols are greater throughout this part of the concentration range. It is to be recalled that P^s is related to the water–solution interfacial tension, as shown by eq. 1. From reference to the table, it is of interest to note that the values of γ_f increase with the temperature at the lower concentrations, are approximately constant at ca 0.04 to 0.06 m, and at higher concentrations decrease..

THE IONIZATION POTENTIALS OF MONOSUBSTITUTED PYRIDINES BY ELECTRON IMPACT

By Michael R. Basila and Donald J. Clancy

Gulf Research & Development Company, Pittsburgh, Pennsylvania

The electron impact ionization potentials of a number of monosubstituted pyridines were determined by the same technique and on the identical instrument used by previous workers for mono- and disubstituted benzenes. The combined sets of data provide a self-consistent set for the comparison of substituent effects. Linear relationships are shown to exist between the ionization potentials of the 4-substituted pyridines and the monosubstituted benzenes or *para*-substituted toluenes. Consideration of these linear relationships leads to the suggestion that the electron impact ionization potentials primarily correspond to the removal of a π-electron, and that the substituent effects upon the pyridine π-electrons parallel those upon the benzene or toluene π-electrons, with the heterocyclic nitrogen atom introducing an almost constant perturbation.

Introduction

The recent ionization potential compilation of Kiser[1] contains values for a number of substituted aromatic molecules. However, because of the variety of experimental techniques used in these determinations, *viz.*, photoionization, electron impact, and the spectroscopic technique, these data cannot be used with confidence to examine the effect of substituents on the ionization potentials. For instance, it is well known that for polyatomic molecules, electron impact values are generally several tenths of a volt higher than the corresponding spectroscopic or photoionization values.[2] Furthermore, as Nicholson has indicated,[3] there are at least eight methods for extracting ionization potentials from electron impact data and these sometimes give rise to widely different values. Thus for a study of substituent effects it is desirable to use values which have been determined by the same technique. Relatively few systematic studies of substituent effects on the ionization potentials of aromatic molecules have been made.[4-9] Of these, the most extensive, as well

(1) R. W. Kiser, "Tables of Ionization Potentials," United States Atomic Energy Commission Report TID-6142.

(2) F. H. Field and J. L. Franklin, "Electron Impact Phenomena," Academic Press, Inc., New York, N. Y., 1957.

(3) A. J. C. Nicholson, *J. Chem. Phys.*, **29**, 1312 (1958).

as the most recent, has been that of Crable and Kearns.[9] These authors examined a series of mono- and disubstituted benzenes. They found the substituent effects to be qualitatively consistent with the electrostatic polarization model of Coggeshall,[10] and they demonstrated a correlation between the ionization potential and the σ^+ substituent constants of Brown and Okamoto.[11]

The purpose of this work was to determine electron impact ionization potentials for a series of monosubstituted pyridines in order to compare the substituent effects with those observed in the substituted benzenes.

Experimental

The ionization potentials were determined with the same Consolidated Electrodynamics Corporation Model 21-103 mass spectrometer as was used by Crable and Kearns.[9] The method of extracting the ionization potential from the data was essentially identical with that employed by Crable and Kearns,[9] so that the values obtained are directly comparable with their values. As a check, the ionization potentials of several monosubstituted benzenes were determined and were found in good agreement with their values. The method for calculating the ionization potentials involves first obtaining ionization efficiency curves for the compound of interest and a standard (argon). The data are corrected so that the slopes of the linear portions of the curves are equal and semilogarithmic plots of the exponential part of the corrected data are made. Voltage differences in the threshold region between the unknown and the standard are applied to the standard to obtain the ionization potential of the unknown. The only respect in which the present technique differs from that of Crable and Kearns is in our use of an anode potential of +200 v. as compared to their +40 v. Gas pressures used in this work were low enough to eliminate the tailing effect caused by ions produced near the anode.[12] Several ionization potentials were measured at both anode potentials and no significant differences were noted.

The chemicals used were of the highest purity commercially available. The mass spectrum of each was examined for the presence of higher molecular weight impurities which could give rise to fragments having the same m/z value as the parent ion of interest. No evidence for higher molecular weight impurities was found. The nature of possible interfering substances is thus confined to isomers, which are probably present only in small amounts, if at all.

Results

The ionization potentials determined in this work are given, along with the values of other workers, in Table I. The reproducibility of these measurements is approximately 0.05 v.; however, no estimate of the accuracy can be made. Since the same instrumentation and technique for extracting the ionization potential from the experimental data were used in this work and in that of Crable and Kearns,[9] the combined sets of values form a self-consistent set for the study of substituent effects.

Initially, only the data on the 4-substituted pyridines will be considered since they are more complete, and should be directly comparable to the monosubstituted benzenes and para-substituted toluenes. In Table II the ionization potentials of these three series of compounds are compared. It is immediately apparent that the values for the pyridines are higher than the

(4) J. D. Morrison and A. J. C. Nicholson, J. Chem. Phys., 20, 1021 (1952).

(5) H. Baba, I. Omura, and K. Higasi, Bull. Chem. Soc. Japan, 29, 521 (1956).

(6) I. Omura, H. Baba, K. Higasi, and Y. Kanaoka, ibid., 30, 633 (1957).

(7) K. Watanabe, J. Chem. Phys., 26, 542 (1957).

(8) W. C. Price, R. Bralsford, P. V. Harris, and R. G. Ridley, Spectrochim. Acta, 14, 45 (1959).

(9) G. F. Crable and G. L. Kearns, J. Phys. Chem., 66, 436 (1962).

(10) N. D. Coggeshall, J. Chem. Phys., 32, 1265 (1960).

(11) H. C. Brown and Y. Okamoto, J. Am. Chem. Soc., 80, 4979 (1958).

(12) G. F. Crable and G. L. Kearns, J. Chem. Phys., 36, 558 (1962).

TABLE I
IONIZATION POTENTIALS OF MONOSUBSTITUTED PYRIDINE DERIVATIVES

Compound	This work (e.v.)	Other — Electron impact (e.v.)	Other — Photo-ionization (e.v.)
Pyridine	9.85	9.76[a,b] 9.8[d]	9.23[c,e]
4-Methylpyridine	9.67	9.56[a]	9.01[e]
4-Hydroxypyridine	9.70		
4-Aminopyridine	8.97		
4-Chloropyridine	10.15		
4-Bromopyridine	9.94		
4-Pyridinecarboxaldehyde	10.12		
2-Chloropyridine	9.91		
2-Bromopyridine	9.65		
2-Methylpyridine	9.56	9.66[a]	
2-Pyridinecarboxaldehyde	9.75		

[a] See ref. 5.   [b] See ref. 6.   [c] See ref. 7.   [d] See ref. 13.   [e] See ref. 14.

benzenes and toluenes, and that the substituent effects are qualitatively the same. To further demonstrate these relationships, the pyridine ionization potentials were expressed as a linear function of those of the benzenes and the toluenes and the following equations were determined.

$$I_p = 0.827 I_b + 2.08 \tag{1}$$

$$I_p = 0.827 I_t + 2.29 \tag{2}$$

The subscripts p, b, and t indicate pyridine, benzene, and toluene, respectively. The values of I_p calculated using (1) and (2) are given in Table II. The standard deviation from the experimental values is 0.06 e.v., which closely approximates the experimental reproducibility quoted previously.

TABLE II
IONIZATION POTENTIALS OF 4-SUBSTITUTED PYRIDINES, para-SUBSTITUTED TOLUENES, AND MONOSUBSTITUTED BENZENES

Substituent	Benzene[a] (e.v.)	Toluene[a] (e.v.)	Pyridine — Exptl. (e.v.)	Pyridine — Calcd. (e.v.) Eq. 1	Pyridine — Calcd. (e.v.) Eq. 2
H	9.56	9.18	9.85	9.99	9.88
CH₃	9.18	8.99	9.67	9.67	9.72
OH	9.16	8.97	9.70	9.66	9.71
NH₂	8.32	8.14	8.97	8.96	9.02
Cl	9.60	9.21	10.15	10.02	9.91
Br	9.52	9.22	9.94	9.95	9.91
CHO	9.70	..	10.12	10.10	..

[a] These ionization potentials were taken from the work of Crable and Kearns,[9] with the exception of benzaldehyde, which was measured in this work.

Discussion

The ionization potentials of the benzenes and toluenes obviously correspond to the removal of a π-electron. However, in the case of the pyridines an uncertainty arises pertaining to the type of molecular orbital from which the electron is removed. The electronic spectra of the pyridines are known to exhibit two bands in the near-ultraviolet region due to the $\pi \rightarrow \pi^*$ and $n \rightarrow \pi^*$ transitions.[15,16] Of these, the $n \rightarrow \pi^*$ transition occurs at the longer wave length; for example,

(13) A. Hustrulid, P. Kusch, and J. T. Tate, Phys. Rev., 54, 1037 (1938).

(14) L. D. Isaacs, W. C. Price, and R. G. Ridley, "Vacuum Ultraviolet Spectra and Molecular Ionization Potentials," in "The Threshold of Space," edited by M. Zelikoff, Pergamon Press Ltd., London, 1957, pp. 143–151.

(15) S. F. Mason, Quart. Rev. (London), 15, 287 (1961).

(16) J. H. Rush and H. Sponer, J. Chem. Phys., 20, 1847 (1952).

in pyridine the $\pi \rightarrow \pi^*$ ($^1B_1 \leftarrow {}^1A_1$) and n $\rightarrow \pi^*$ ($^1B_2 \leftarrow$ $^1A_1$) transitions occur at 251 and 270 mμ. respectively.[15,16] The relative magnitudes of the ionization potentials of the n- and π-electrons in pyridine (or the 4-substituted pyridines) cannot be predicted from the electronic spectrum since the upper states are different in the two transitions; however they are thought to be almost equal.[17] Baba, et al.,[5,6] utilizing their electron impact measurements of pyridine, 2-, 3-, and 4-methylpyridine, and the diazines have suggested that the n-electrons have the lowest ionization potential. This conclusion rests strongly on the relative magnitudes of the methyl substituent effect in the 2-, 3-, and 4-positions. Our results on the relative magnitudes of the 2- and the 4-methyl substituent effects are the opposite of theirs. In this respect, it is noteworthy that the ionization potentials of the 2-substituted pyridines which we have measured are all lower than those of the corresponding 4-substituted pyridines.

In the previous section it was shown that within experimental error a linear relationship exists between I_p and I_b or I_t. These relationships have the same slopes and different intercepts. The intercept difference reflects the almost constant substituent effect of the methyl group in the toluenes as compared to the benzenes which has been noted previously.[9] It is indicated by these linear relationships that the apparent substituent effects on the ionization potentials of the pyridine are essentially the same as those observed in the benzenes or toluenes. In the 4-substituted pyridines, it is expected that substituent effects on the n-electrons would be quite subdued as compared to those on the π-electrons, since the mode of interaction is essentially restricted to inductive effects. Thus, the linear relationships (1) and (2) suggest that the electron impact ionization potentials of the 4-substituted pyridines primarily correspond to the removal of a π-electron.

Theoretical calculations have shown that the wave length shift of the lowest frequency $\pi \rightarrow \pi^*$ band (α-band) of the monocyclic azines from that of benzene can be explained as a perturbation of the benzene energy states by the nitrogen atoms.[18-20] Thus it is reasonable that the substituent effects on the benzene and pyridine π-electrons would be linearly related.

The suggestion that the electron impact ionization potentials of the pyridines primarily correspond to the removal of a π-electron does not necessarily mean that the π-electrons have a lower ionization potential than the n-electrons. Recently Fox and Hickam[21] using the RPD method have shown that in the case of benzene, where a number of excited states of the ion occur near the threshold, the extrapolation of the ionization efficiency curve above the break corresponding to an excited state of large cross section (relative to the lower energy states near the threshold) gave a value in good agreement with the conventional electron impact ionization potential. On the other hand the threshold was in excellent agreement with the spectroscopic ionization potential.[21] Thus in the case of the

pyridines if the ionization cross section of the n-electrons were small compared to the π-electrons, it is quite possible[22] that the influence of the n-electrons upon the conventional electron impact ionization potential would be small even if they had the lowest ionization potential. Therefore based on the above considerations, it can be tentatively concluded that the substituent effects on the π-electrons of the nitrogen heterocyclic aromatic ring parallel those on the π-electrons of a normal aromatic ring. It is also of interest to note that the slopes of (1) and (2) are only slightly different from unity, indicating that the perturbation of the π-electrons by the heterocyclic nitrogen atom is almost constant.

Crable and Kearns[9] demonstrated a correlation between the ionization potentials of the monosubstituted benzenes or para-substituted toluenes and the σ^+ substituent constants of Brown and Okamoto.[11] In view of the linear eq. 1 and 2 it is expected that a similar relationship should exist for the 4-substituted pyridines. Crable and Kearns[9] also showed the electrostatic polarization model of Coggeshall[10] could be extended to groups having appreciable dipole moments and they were able to account qualitatively for the observed substituent effects. This model relates the change in ionization potential to the work which must be done in bringing the substituent group from infinity to the positively charged aromatic ring. The two main contributions are the interactions of the positive charge (taken to be in the center of the aromatic ring) with the induced dipole and the permanent dipole moments in the substituent group. The interaction with the induced dipole moment will always lead to a lowering of the ionization potential; however, the interaction with the permanent dipole moment can result in either a higher or lower ionization potential depending upon the moment orientation. The pyridines offer an additional opportunity to test this model, since the center of positive charge will be displaced toward the nitrogen atom (presuming that the molecular orbitals do not change drastically upon ionization).[22] Inspection of Table I shows the 2-substituted pyridines have lower I_p than the 4-substituted; the values for 4-Cl, 4-Br, and 4-CHO are higher than pyridine, and the other 4-substituents are lower; the value for 2-Cl is higher than pyridine and all the other 2-substituents are lower. The electrostatic polarization model applied to the pyridines requires that (1) the interaction energy between the positive charge and the induced dipole and permanent dipole moments be greater in the 2-position than in the 4-position and (2) the interaction energy fall off more rapidly with distance for the induced dipole moment (which varies as r^{-4}) than for the permanent dipole moment (which varies as r^{-2}). The application of these two requirements leads to a satisfactory qualitative account of the above observations. For example, the values for the 2-substituents are expected to be lower than the corresponding 4-substituent except in cases where the permanent dipole moment of the

(17) C. Reid and R. S. Mulliken, J. Am. Chem. Soc., **76**, 3869 (1954).

(18) R. McWeeny and T. E. Peacock, Proc. Phys. Soc. (London), **A70**, 41 (1957).

(19) N. Mataga and K. Nishimoto, Z. physik. Chem., **13**, 140 (1957).

(20) J. N. Murrell, Mol. Phys., **1**, 384 (1958).

(21) R. E. Fox and W. M. Hickam, J. Chem. Phys., **22**, 2059 (1954).

(22) This expectation is based on the theoretical calculations of McWeeny and Peacock[18] on the monocyclic azines which indicate a higher π-electron density near the nitrogen atom. Recent quadrupole resonance measurements[23] support these theoretical results.

(23) E. A. C. Lucken, Trans. Faraday Soc., **57**, 729 (1961).

substituent is large and directed away from the ring. Unfortunately, because of the uncertainties involved,[9] detailed calculations of the change in ionization potentials are not practical. It is evident, however, that there are no gross inconsistencies between the predictions of the model and the observed ionization potential variations.

SINGLE ION ACTIVITIES AND ION-SOLVENT INTERACTION IN DILUTE AQUEOUS SOLUTIONS

By Henry S. Frank

Department of Chemistry, University of Pittsburgh, Pittsburgh 13, Pennsylvania

Received March 11, 1963

A return is proposed to the ascription of physical significance to single ion activities in electrolyte solutions and illustrations are given of two cases where this seems to lead to meaningful results. In 0.1 M HCl γ_{H^+} seems to be about 5% greater than γ_{Cl^-}, in rough agreement with predictions from the previously postulated difference in degree of hydration of H^+ and Cl^-. In dilute solutions of tetraalkylammonium iodides f_{I^-} appears to be larger, and sometimes much larger, than $f_{R_4N^+}$. It is suggested that this is a real phenomenon, and an explanation is offered in terms of the structure-promoting influence of R_4N^+ cations and the structure-breaking effect of I^-. For the convenient tabulation of numerical data relating to single ion activities a new property of ionic solutions is proposed, to be called the mean ionic activity deviation, denoted by $\delta_\pm$, and defined as $\delta_\pm = (f_+{}^\nu{}^+/f_-{}^{\nu-})^{1/\nu}$. When used with the mean ionic activity coefficient, $f_\pm$, this makes accessible the single ion activity coefficients through the identities $f_+ = (f_\pm\delta_\pm)^{\nu/2\nu+}$ and $f_- = (f_\pm/\delta_\pm)^{\nu/2\nu-}$.

Introduction

Although it is now over 30 years since single ion activities were shown[1] to be inaccessible to exact thermodynamics, it has never quite been possible to do without these quantities, and an uneasy compromise has been struck in their regard. That is, it has been agreed not to call any given quantity a single ion activity at the same time that the idea of such an activity has still been used freely in various kinds of derivations,[2] and elaborate procedures have been worked out for getting refined values of pH[3]—*i.e.*, of an effective a_{H^+}. This is not a very satisfactory situation, and one of the purposes of the present essay is to propose that single ion activities and activity coefficients be reinstated as acceptable working quantities. Special care will be necessary to ensure adequate recognition of the inherent uncertainty of any numerical value assigned, but the advantages to be gained seem considerable in the reopening of avenues of investigation, and of interpretation, of ionic solution phenomena. One such avenue has recently been followed[4] in the use of a_{Cl^-} in studying the binding of counterions in polyelectrolyte solutions and several others are explored below.

That there is no difficulty in defining a single-ion activity coefficient in terms of a thought process may be illustrated, among other possibilities, by the fact that this is what is done when the Güntelberg charging process is employed in deriving the equations of the Debye–Hückel theory. The problem has thus been one of accessibility only, and this, in turn, reduces to

that posed by the impossibility of the exact evaluation, by thermodynamic methods, of liquid-junction potentials.[2a] The last-named fact has an interesting implication, namely, that to assert that nothing can be known about single-ion activities is equivalent to stating that nothing can be known about liquid-junction potentials. Since the latter statement is very far from being true, it is both possible and legitimate to make, and to act upon, the converse statement that anything that can be known or guessed about a liquid-junction potential can be made to provide a piece of information, or an estimate, about a single-ion activity.

This is the principle which has been employed in obtaining pH values[3] and in the evaluation, referred to above,[4] of the activity of chloride ion in certain electrolyte solutions. In these applications, experiments are devised in which the potential difference across a liquid junction is imagined (a) to be negligible, (b) to be calculable, or (c) not to change (or to change only trivially) as the test solution is altered in certain ways (for instance, is made to run from high dilution, where the single-ion activity coefficient must be near unity, to the finite concentration of interest). If the errors in such assumptions were zero, one would have exact values of the single-ion activities, or activity ratios, involved. Correspondingly, any estimate of the numerical error the assumptions contain is, when translated, an estimate of the error-limit to be ascribed to the single-ion activity measurement. This in turn makes it possible, by standard thermodynamic means, to evaluate, within the corresponding (estimated) limits of error, a variety of other "non-thermodynamic" quantities of interest.

Single-Ion Activities in 0.1 M HCl.—An an example of what can be done, take the carefully considered values of 1.085 and 1.092 assigned, respectively, by Hitchcock and Taylor[5] and Bates, Pinching, and Smith[6]

(1) E. A. Guggenheim, *J. Phys. Chem.*, **33**, 842 (1929); **34**, 1540 (1930).

(2) See, for example, (a) D. A. MacInnes, "The Principles of Electrochemistry," Dover, New York, N.Y., 1961, Chapter 13; (b) J. G. Kirkwood and I. Oppenheim, "Chemical Thermodynamics," McGraw-Hill Book Co., New York, N. Y., 1961, Chapters 12 and 13.

(3) See, for example, H. S. Harned and B. B. Owen, "The Physical Chemistry of Electrolytic Solutions," 3rd. Ed., Reinhold Publ. Corp., New York, N. Y., 1958, Chapter 10.

(4) S. Lapanje, J. Haebig, H. T. Davis, and S. A. Rice, *J. Am. Chem. Soc.*, **83**, 1590 (1961).

for the pH of 0.1 M HCl. The latter is on a molality basis, and the former becomes 1.086 when corrected to the same basis. These make log $\gamma_{H^+} = -0.086$ or -0.092; but $\gamma_{\pm}$ for this solution is reported as 0.7964,[7] giving for log $\gamma_{\pm}$, that is for $^1/_2(\log \gamma_{H^+} + \log \gamma_{Cl^-})$ the value -0.099, corresponding to log $\gamma_{Cl^-} = -0.112$ or -0.106. Thus log $(\gamma_{H^+}/\gamma_{Cl^-})$ equals 0.026 or 0.014, and $\gamma_{H^+}/\gamma_{Cl^-}$ equals 1.062 or 1.033.

How greatly these numbers are in error is, of course, a question. It seems likely, however, that they are more than qualitatively correct, and that, in 0.1 M HCl at 25°, the single-ion activity coefficient of H$^+$ is in fact about 5% higher than that of Cl$^-$. In support of this conclusion it may be noted that Robinson and Stokes,[8] in their discussion of the influence of hydration on stoichiometric activity coefficients, have ascribed a hydration number of about 8 to HCl, and consider that this is almost entirely cation hydration. A simple extension, however, of their derivation (in fact, a return to the form given earlier by Bjerrum[9]) supplies expressions for the influence of single-ion hydrations upon single-ion activity coefficients. The result for a 1–1 solute, correct to first-order terms in m, is

$$\ln \gamma_+^h = \frac{3h_+ + h_- - 2}{55.51}m$$

$$\ln \gamma_-^h = \frac{3h_- + h_+ - 2}{55.51}m \qquad (1)$$

where h_+ is the cation hydration number, i.e., the number of molecules of water which a cation removes from its solvent function, and h_- the hydration number of the anion. Using eq. 1 one obtains

$$\ln \gamma_{\pm}^h = \frac{2(h_+ + h_-) - 2}{55.51}m$$

the standard result for the contribution which hydration makes to the stoichiometric mean ionic activity coefficient on a molality basis. But eq. 1 also give

$$\ln (\gamma_+/\gamma_-)^h = \frac{2(h_+ - h_-)}{55.51}m \qquad (2)$$

for the spread which differential hydration should produce between ln γ_+ and ln γ_-. Taking $h_+ = 8$ and $h_- = 0$, this predicts 0.013 for log γ_+/γ_- in 0.1 M HCl, somewhat less than the "experimental" values obtained above. Since other influences may also be at work, the agreement seems good enough to lend support to the thesis that the ratio γ_+/γ_- can be meaningfully studied and has, in this solution, a magnitude of about 1.05, as inferred for it from the literature pH values.

Tetraalkylammonium Iodides.—The usefulness of this type of reasoning in opening new fields for study may be illustrated by applying it to the experimental results obtained by Devanathan and Fernando[10] with the cell

Ag, AgI, R$_4$NI(c), KCl(sat), KI(c), AgI, Ag   (3)
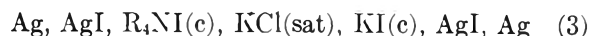
Here R$_4$NI is a tetraalkylammonium iodide, R being methyl, ethyl, n-propyl, or n-butyl. c, which was kept the same on both sides of the cell, was varied from some thousandths to some tenths of a mole/l., and the corresponding e.m.f. values were measured at 25°. Several of these are quoted in column 3 of Table I. Since the single ion conductances of all of the relevant ions are known the liquid junction potentials may be estimated by use of the Henderson equation.[2a] When this is done, they come out to be near 2 mv. in every case, and the difference between the estimated potential for the junction R$_4$NI(c), KCl(sat) and that for the junction KI(c), KCl(sat) which is bucked against it is never more than about 0.2 mv. Since, therefore, the Henderson equation, in spite of the approximations it contains, can hardly give results of the wrong order of magnitude (this is the crux—i.e., the weak point or the strong point—of the argument), it seems justifiable to proceed on the assumption that junction potentials contribute only negligibly to the measured e.m.f. values. This is operationally equivalent to, and therefore constitutes an operational justification for, the assumption made by Devanathan and Fernando that the junction potentials are themselves equal to zero.

Their other assumption, however, is not acceptable, namely, that a measured e.m.f. for cell (3) is equal to $(RT/F) \ln (f_{\pm R_4NI}/f_{\pm KI})$. The analogy of this cell to two pH cells bucked against each other makes clear that what is in question is, instead, the ratio of the single-ion activities of the iodide ion in the two half-cells. Therefore, since the half-cells are always matched by making c the same on both sides, we may write

$$E = \frac{RT}{F} \ln r_I = 0.0592 \log r_I \text{ volts} \qquad (4)$$

where r_I is $f_{I^-(R_4NI)}/f_{I^-(KI)}$, the ratio of the single ion activity coefficient (concentration basis) of I$^-$ in R$_4$NI at the relevant concentration to that in KI at the same concentration.

The values of r_I corresponding to the e.m.f. values quoted in Table I are shown in column 4, and their numerical values are striking. That is, it would probably not have been expected that the single ion activity coefficient of I$^-$ in 0.03 M (C$_4$H$_9$)$_4$NI, for example, would be 8.65 times that of the same ion in a KI solution. Also interesting are the consequences to which one is led if the r_I values are taken seriously. These are displayed in columns 5–9 of Table I. Column 5 gives values of $f_{\pm}$ for R$_4$NI, estimated from the freezing point measurements of Lange.[11] They all fall below the limiting law values, itself a rather remarkable fact. Column 6 gives the corresponding values of $f_{\pm}$ for KI. These were computed from constants for the Hückel equation given by Harned and Owen[12] and are probably not greatly in error (the value for 0.10 M matches that given by Robinson and Stokes).[13] From the $f_{\pm}$ values for the separate salts, $r_{\pm}$ is computed in column 7, namely $f_{\pm R_4NI}/f_{\pm KI}$. But

(5) D. I. Hitchcock and A. C. Taylor, *J. Am. Chem. Soc.*, **59**, 1812 (1937); see also ref. 3.

(6) R. G. Bates, G. D. Pinching, and E. R. Smith, *J. Res. Natl. Bur. Std.*, **45**, 418 (1950).

(7) Reference 3, p. 466.

(8) R. A. Robinson and R. H. Stokes, "Electrolyte Solutions," Butterworths, London, 2nd Ed., 1959, pp. 238–250.

(9) N. Bjerrum, *Z. anorg. allgem. Chem.*, **109**, 275 (1920).

(10) M. A. V. Devanathan and M. J. Fernando, *Trans. Faraday Soc.*, **58**, 784 (1962).

(11) J. Lange, *Z. physik. Chem.*, **A168**, 147 (1934).

(12) Reference 3, p. 510. The distinction between $f_{\pm}$ and $\gamma_{\pm}$ has been neglected here.

(13) Reference 8, p. 494.

Table I

Data and Derived Quantities from Measurements on the Cell

Ag, AgI, R₄NI(c), KCl(sat), KI(c), AgI, Ag

R	c, moles/l.	E, mv.[a]	r_I[b]	$f_{\pm R_4NI}$[c]	$f_{\pm KI}$[d]	$r_\pm$[b]	r_{cat}[b]	$\dfrac{\delta_\pm{}^2 R_4 NI}{\delta_\pm{}^2 KI}$[b]
CH₃	0.03	12.0	1.60	0.812	0.851	0.954	0.570	0.358
C₂H₅	.003	7.8	1.355	.937	.943	.994	.728	.537
	.01	20.5	2.22	.886	.903	.982	.434	.196
	.03	27.3	2.89	.807	.851	.948	.311	.108
	.10	48.1	6.49	.666	.778	.856	.113	.017
	.30	69.1	14.7	.467	.710	.658	.030	.002
C₃H₇	.03	26.7	2.83	.788	.851	.926	.303	.107
C₄H₉	.03	55.5	8.65	.751	.851	.882	.0900	.0104

[a] Ref. 10. [b] See text. [c] Ref. 11. [d] Ref. 12.

$$r_\pm{}^2 = \frac{(f_{R_4N^+} f_{I^-})_{R_4NI}}{(f_{K^+} f_{I^-})_{KI}} = \frac{f_{R_4N^+ (R_4NI)}}{f_{K^+(KI)}} \times r_I = r_{cat} \times r_I \tag{5}$$

This makes accessible the ratio called r_{cat}, which is tabulated in column 8, and is, in words, the ratio of the single ion activity coefficient of R_4N^+ in R_4NI to that of K^+ in a KI solution of equal concentration.

Finally, the ratio of r_{cat} to r_I for the same solution-pair is easily shown to equal

$$\frac{r_{cat}}{r_I} = \frac{(f_{R_4N^+}/f_{I^-})_{R_4NI}}{(f_{K^+}/f_{I^-})_{KI}} = \frac{\delta_\pm{}^2 R_4NI}{\delta_\pm{}^2 KI} \tag{6}$$

Here a new quantity, $\delta_\pm$, has been introduced, of which more will be said below. For the present it suffices to note that it is a property of an individual solution, as $f_\pm$ is, and that it is so defined that for these 1–1 solutes $\delta_\pm{}^2$ is the ratio of the cation activity to the anion activity in the solution under discussion. Thus the ratio 1.05 derived above for f_{H^+}/f_{Cl^-} in 0.1 M HCl is $\delta_\pm{}^2$ for that solution. Column 9 of Table I contains values of $\delta_\pm{}^2 R_4NI/\delta_\pm{}^2 KI$ obtained, according to eq. 6, by dividing the values of column 8 by those of column 4. They show how R₄NI solutions compare with the equivalent KI solutions in respect of the cation/anion activity ratio, and if, provisionally, it may be imagined that $\delta_\pm{}^2 KI$ is, like the value for 0.1 M HCl, not greatly different from unity, then the values in column 9 are approximately equal to $f_{R_4N^+}/f_{I^-}$ in the various solutions to which they correspond.

The physical import of these values is as follows. They say, for instance, that in 0.03 M solutions, f_+ is only some 35% as large as f_- in (CH₃)₄NI, about 10% in (C₂H₅)₄NI and (C₃H₇)₄NI, and about 1% in (C₄H₉)₄I. It may be noted that the accuracy of the values used for $f_\pm$ for R₄NI and for KI does not greatly affect these qualitative conclusions, since $r_{cat}/r_I = r_\pm{}^2/(r_I)^2$, so that even if all of the mean activity coefficients were taken to be unity $\delta^2_{\pm R_4NI}$ would still be 39, 11.9, 12.5, and 1.35%, respectively, for the cases named. One must therefore conclude (a) that the data are seriously inaccurate, (b) that the Henderson equation is inapplicable in such junctions, or (c) that there is something about the system tetraalkylammonium ion–iodide ion–water that makes the relative activity of iodide ion larger—and sometimes very much larger—than that of the tetraalkylammonium ion in these salt solutions.

The position taken here is that while it is too early to set accurate limits to the errors which might enter through alternatives (a)[14] and (b), alternative (c) prob-

ably states something real about what is going on in the solutions. One reason for this judgment is that the falling below the limiting law values of $f_\pm$ in R₄NI solutions already suggests that these are anomalous. Moreover, a qualitative explanation of the anomaly in $\delta_\pm{}^2$ can be offered in terms of existing structural ideas. Taking as an example the comparison of (C₄H₉)₄NI with KI solutions, the interpretation proceeds as follows.

Interpretation and Conclusions

All the evidence that we have[15] indicates that the iodide ion is a strong structure-breaker, that the tetrabutylammonium ion is an even stronger structure-maker, and that the potassium ion has a net effect which is not strong in either sense, though probably slightly structure-breaking. The effect of these structure influences on activity may be approached by imagining a two-stage solution process. If, for example, the structure-shift evoked by addition of I⁻ to the solution could be imagined at first to be inhibited, and the ion considered to be dissolved, initially, in water which retained its previous structure, then a lifting of the inhibition would be followed by a structure shift, and this would necessarily be accompanied by a lowering of the free energy of the system, the amount of this lowering depending on, among other factors, how much work had to be done to break the water structure. Now, in the presence of tetrabutylammonium ions, the water is more structured than it would be if they were not there and therefore, presumably, harder to bring into the random state appropriate to the neighborhood of an iodide ion. The introduction of the latter under these circumstances will therefore be expected to be accompanied by a free energy change which is less negative, partly because extra work must be done on the water and partly because the final state of the water near the I⁻ will presumably be less "favorable" than in pure water. The free energy of hydration of I⁻ in the presence of (C₄H₉)₄N⁺ ions should therefore be less negative than in their absence, and this should produce an increase in escaping tendency—i.e., a raising of activity—over and above the effects produced by other influences which are at work.

In the corresponding KI solution the activity of I⁻ will likewise be subjected to an influence arising from the effect of K⁺ upon the structuredness of the water. Here, however, the influence will be much weaker,

(14) J. C. Rasaiah has set up cells of the type (3) in this Laboratory and has confirmed that large e.m.f.'s are in fact observed.

(15) H. S. Frank and W. Y. Wen, Discussions Faraday Soc., 24, 133 (1957), and references there cited.

since K^+ is much less effective than $(C_4H_9)_4N^+$ in altering structure. $f_{I^-[(C_4H_9)_4NI]}$ will therefore lie higher than $f_{I^-[KI]}$, i.e., r_I is predicted to be greater than unity, in agreement with experiment.

It will be noted that from the point of view of, and to the order of approximation involved in, this discussion the structural effect of $(C_4H_9)_4N^+$ upon f_{I^-} is not a direct ion–ion interaction, since it arises solely from a change which the presence of $(C_4H_9)_4N^+$ produces in the free energy of hydration of I^-. It is in this respect exactly similar to the salting-out effect discussed by Hückel,[16] and may, indeed, be thought of as a supplement to that effect. It thus seems appropriate to speak of structural salting-out and salting-in, and to paraphrase the above discussion by saying that r_I is greater than unity because I^- is more strongly salted-out by $(C_4H_9)_4N^+$ than by K^+.

Before leaving r_I it is necessary to dispose of another effect which, while important in principle, happens in this case not to enter into the final result. This is the structural salting-in influence which, in the model here under discussion, all ionic species must exert upon themselves. Because this effect must always be present, an I^- in $(C_4H_9)_4NI$ will not only be salted-out by $(C_4H_9)_4N^+$ but will also be salted-in by the other I^- ions, and $f_{I^-[(C_4H_9)_4NI]}$ will be the resultant of these two effects (as well as of all of the non-structural ones which are also present). To the first order, however, the structural contributions to $\ln f_{I^-}$ should be additive, and, to the extent that this is true, the self-stabilization of I^- will be the same in $(C_4H_9)_4NI$ as in KI. The contributions on this score to $f_{I^-[(C_4H_9)_4NI]}$ and to $f_{I^-[KI]}$ will therefore cancel when the quotient r_I is formed, and the earlier inferences about this quantity can still be accepted as they stand.

Turning now to the cations, $(C_4H_9)_4N^+$ will be expected to be salted-in by itself and salted-out by I^-. Since we have reason to consider $(C_4H_9)_4N^+$ stronger in its intrinsic structure-altering tendency than is I^-, the former effect should preponderate, and the resultant $f_{(C_4H_9)_4N^+[(C_4H_9)_4NI]}$ should be lower than it would have been if no structural influences had existed. K^+ will also salt itself in, and be salted either in or out (probably somewhat "in") by I^-. Here again, however, the relatively feeble structure-altering tendency of K^+ will make the net effect on f_{K^+} smaller than that on $f_{(C_4H_9)_4N^+}$. We therefore predict, again in agreement with experiment, that r_{cat} should be less than unity.

The salt $(C_4H_9)_4NI$, therefore, forms aqueous solutions in which, on this interpretation, the striking effects which are observed result from three facts: (a) both anion and cation have marked influences on water structure, (b) these are opposite in sense, and (c) one of them has a larger intrinsic magnitude than the other. These lead to the result that the "weaker" ion (here I^-) suffers a net salting-out, and the "stronger" [here $(C_4H_9)_4N^+$] a net salting-in. The quantity we have called $\delta_\pm^2$ is therefore less than unity, and to an extent which far exceeds the corresponding effect in KI, where, indeed, the effect is predicted to be in the opposite direction ($\delta_\pm^2 > 1$; the salting-in effect of iodide on itself should be greater than what it does to K^+).

This is so far, of course, a largely qualitative interpretation, with only such semiquantitative corollaries as that the larger the R group in R_4NI the larger should be the ratio $\delta_\pm^2{}_{R_4NI}/\delta_\pm^2{}_{KI}$. Even this conclusion is only partially borne out in Table I, however, as there seems to be an inversion in order between the tetraethyl and tetrapropyl salts. It is also not clear whether the fact that $f_\pm$ for R_4NI falls below the limiting law line can be accounted for by the extent to which the salting-in of the cation exceeds the salting-out of the anion, or whether some additional factor must be invoked.

The fact that such questions can be raised, however, suggests that we have here an area of inquiry which will repay further study. If there is any meaning at all in the foregoing discussion it is that statements about $f_\pm$ alone (or about the derived quantities $\bar{L}_2$, $\bar{J}_2$, etc.) will not suffice to give a complete account of the thermodynamics of aqueous electrolytes, but that, on the contrary, ways must be sought to obtain, tabulate, and interpret thermodynamic information about individual ions and their behavior in different combinations.

For obtaining such information, renewed attention to liquid junction phenomena seems an obvious line of attack. In addition to the re-examination, from the point of view here taken, of the very considerable body of data already in existence, this would include new experimental work and a wider testing of such additivity relations as those discovered by MacInnes and Yeh.[17] It has also been pointed out[18] that the possibility exists in principle of measuring single electrode potentials by non-thermodynamic (e.g., electrostatic) means, and ways may be discoverable of using such measurements to evaluate single-ion activities.

Assuming that meaningful results can be obtained from such studies, the quantity introduced above as $\delta_\pm$ seems to offer an appropriate way of recording them. It has the desirable attribute of being a property of a neutral species, so that it can be tabulated alongside of $f_\pm$, to which it is, indeed, defined to be a complementary quantity. The definition is

$$\delta_\pm = [f_+^{\nu_+}/f_-^{\nu_-}]^{1/\nu} \text{ or}$$

$$\ln \delta_\pm = \frac{1}{\nu}[\nu_+ \ln f_+ - \nu_- \ln f_-] \qquad (7)$$

It thus follows that

$$f_+ = (f_\pm \delta_\pm)^{\nu/2\nu_+} \text{ and } f_- = (f_\pm/\delta_\pm)^{\nu/2\nu_-}$$

or

$$\ln f_+ = \frac{\nu}{2\nu_+}[\ln f_\pm + \ln \delta_\pm] \text{ and}$$

$$\ln f_- = \frac{\nu}{2\nu_-}[\ln f_\pm - \ln \delta_\pm] \qquad (8)$$

and, since for solutes of symmetrical charge-type $\nu = 2\nu_+ = 2\nu_-$, $\ln f_+$ and $\ln f_-$ are obtained for such sub-

(16) (a) E. Hückel, *Physik. Z.*, **26**, 93 (1925); (b) G. Scatchard, *Chem. Rev.*, **13**, 7 (1933); (c) ref. 3, p. 508.

(17) Ref. 2a; D. A. MacInnes and Y. L. Yeh, *J. Am. Chem. Soc.*, **43**, 2563 (1921). The "Characteristic Potentials" found by these workers for the cells Ag, AgCl, M^ICl (0.1 M), M^{II}Cl (0.1 M), AgCl, Ag combined (a) with the assumption that the Lewis and Sargent expression for the liquid junction potentials is exact (or nearly enough so), (b) with accepted values of $f_\pm$, and (c) with the pH of 0.1 M HCl discussed in the text, lead, by straightforward methods, to the following values of $\delta_\pm$, applicable at 25° and in 0.1 M solutions: HCl, 1.025; LiCl, 0.997; NaCl, 0.990; KCl, 0.926.
(18) Ref. 2b, p. 211.

stances by simple addition or subtraction of $\ln f_\pm$ and $\ln \delta_\pm$. In this case, in plots against $c^{1/2}$, say, the curve for $\ln f_\pm$ lies midway between those for $\ln f_+$ and $\ln f_-$, and $\ln \delta_-$ is the distance separating it from either of them. Corresponding, if less simple, relationships subsist for solutes of more complicated type, and seem to justify the proposal to call $\delta_\pm$ the mean ionic activity deviation. It may be noted also that changing from one scale to another for expressing activity coefficients— i.e., mole fraction, molality, and concentration scales— does not change $\delta_\pm$, since the conversion factors divide out when the ratio is taken. This makes possible the use of the same symbol in all systems.

So far as concerns interpretation, it should be pointed out that structural effects of the sort just discussed, and differential hydration, mentioned earlier, are by no means the only influences that can be imagined to cause f_+ and f_- to differ. In principle, anything that can contribute to non-ideality of the solution could make a contribution here, provided it acted, in the first instance, on the individual ions separately—e.g., heats of hydration. Interionic attractions and repulsions will, on the other hand, probably be symmetrical in their influences on anion and cation, except where charge-type differences produce the sort of formal dissymmetry which appears, say, in the limiting law expressions for the ions of $MgCl_2$. Interionic effects will thus be expected to show up in $f_\pm$, and not in $\delta_\pm$ even if, as may be the case in the tetraalkylammonium iodides, water structure changes were able to alter the shape of the ion cloud in such a way as to require modification of predictions made on purely electrostatic grounds.

NOTES

ELECTRONEGATIVITY OF THE DIFLUORAMINO GROUP

By Raymond Ettinger

Rohm and Haas Company, Redstone Arsenal Research Division, Huntsville, Alabama

Three empirical or semi-empirical methods have been employed in estimating the electronegativity of the difluoramino group ($-NF_2$). The agreement between the three independent methods is remarkably good, indicating that the electronegativity is about 3.3. When this estimate is combined with recent "orbital electronegativity" calculations, one obtains a reasonable picture of the hybridized bonding orbitals of nitrogen in difluoramino compounds.

The first method involves the extension by Wilmshurst[1] of Gordy's[2] relation between an atom's electronegativity and the effective nuclear charge at its covalent boundary. According to Wilmshurst, the group electronegativity of the radical $-AB$ (i.e., the electronegativity of the bonding atom A, perturbed by the other atoms B) can be written

$$\chi_{-AB} = 0.31(n^* + 1)/r + 0.50 \quad (1)$$

where r is the covalent radius of atom A in the AB bond and n^* is the effective number of valence electrons on atom A. The latter quantity was evaluated in the manner outlined by Wilmshurst, assuming the electronegativities of nitrogen and fluorine given in his paper[1]: $\chi_N = 3.01$ and $\chi_F = 3.94$. For the covalent radius of nitrogen in $-NF_2$, we have considered the single bond radii suggested by Pauling[3] ($r_N = 0.70$ Å.) and by Schomaker and Stevenson[4] ($r_N = 0.74$ Å.). Equation 1 gives $\chi_{NF_2} = 3.42$ and 3.26, respectively.

The latter value is preferred because the Schomaker–Stevenson radii for N and F, combined with their interatomic distance correlation, predict 1.38 Å. for the NF bond distance, while the Pauling radii predict 1.34 Å. The experimental NF bond length found in NF_3 is 1.37 Å.

Wilmshurst[5] has further suggested that for polyatomic hydrides HX, where X is a group, the square root of the stretching force constant k_{HX} should be taken as a measure of the electronegativity of X. He gives the following empirical equation for χ_X which is linear in the sensitive vibrational frequency ν_{HX}

$$\chi_X = 1.104 \times 10^{-3}(1 + M_H/M_X)^{-1/2}\nu_{HX} \; (\text{cm.}^{-1}) - 0.24 \quad (2)$$

Although weakly absorbing, the hydrogen stretch frequency in difluoramine[6] has been observed[7] in the gas phase at 3193 cm.$^{-1}$. With this frequency, eq. 2 yields $\chi_{NF_2} = 3.25$.

Yet another method is available for estimating the electron withdrawal power of the difluoramino radical. Dailey and Shoolery[8] have studied the relation between the difference in methyl and methylene proton magnetic resonance shifts and the electronegativity of the substituent in monosubstituted ethanes. A linear expression was found for the ethyl halides which applies moderately well to other substituents.[8]

$$\chi_X = 0.695(\delta_{CH_3} - \delta_{CH_2}) + 1.71 \; (\delta \text{ in p.p.m.}) \quad (3)$$

(In constructing (3), Dailey and Shoolery employed halogen electronegativities which differ slightly from those used by Wilmshurst.[1,5]) The H^1 and F^{19} n.m.r.

(1) J. K. Wilmshurst, J. Chem. Phys., **27**, 1129 (1957).

(2) W. Gordy, Phys. Rev., **69**, 604 (1946).

(3) L. Pauling, "The Nature of the Chemical Bond," 3rd. Ed., Cornell University Press, Ithaca, N. Y., 1960.

(4) V. Schomaker and D. P. Stevenson, J. Am. Chem. Soc., **63**, 37 (1941).

(5) J. K. Wilmshurst, J. Chem. Phys., **28**, 733 (1958).

(6) J. P. Freeman, A. Kennedy, and C. B. Colburn, J. Am. Chem. Soc., **82**, 5304 (1960).

(7) J. J. Comeford, D. E. Mann, L. J. Schoen, and D. R. Lide, Jr., National Bureau of Standards Report 7554.

(8) B. P. Dailey and J. N. Shoolery, J. Am. Chem. Soc., **77**, 3977 (1955). See also P. T. Narasimhan and M. T. Rogers, ibid., **82**, 5983 (1960).

spectra of difluoraminoethane[9] have been obtained. The F^{19} spectrum exhibits a single broad band 129 p.p.m. downfield from trifluoroacetic acid and is otherwise uninformative. The methyl resonance displays a typical 1:2:1 triplet due to coupling (7 c./sec.) with the methylene protons, and its center is 5.9 p.p.m. to the high field side of external benzene (no bulk-susceptibility corrections). The latter shift compares well with the methyl shift in a host of related ethane derivatives[8] and supports the assumption that the electron withdrawal power of substituent groups is almost completely attenuated by the C–C bond. The methylene portion of the $C_2H_5NF_2$ spectrum contains twelve peaks: a triplet arising from coupling (28 c./sec.) to the two fluorines, each component of which is further split into a 1:3:3:1 quartet by the methyl protons. The measured value of $\delta_{CH_3} - \delta_{CH_2}$ was 2.25 p.p.m., which, according to (3), corresponds to $\chi_{NF_2} = 3.27$.

It is tempting to associate the group electronegativity of $-NF_2$ derived herewith the "orbital electronegativity" of nitrogen, for a three bonding valence state, as calculated by Hinze and Jaffé.[10] (The calculations were for neutral atoms, so it is important to note that we are neglecting the effect of partial charges on the atoms.) These authors found that the orbital electronegativity for σ orbitals was linearly related to the amount of s character. Thus, the electronegativities of intermediately hybridized orbitals, such as occur in nitrogen compounds, become available by interpolation. From the data of Hinze and Jaffé,[10] an N orbital electronegativity of 3.3 (Pauling scale) corresponds to a bonding σ orbital of 84% p character. Mashima[11] attempted to explain the observed dipole moment of NF_3 in terms of the hybridization of lone pair and bonding wave functions. He concluded that the hybrids of the N atom could be related simply to the observed bond angle, and the latter predicts 83% p character. In a more general treatment of the same problem, including the contribution of the polarity of the NF bond, La Paglia and Duncan[12] calculated a bonding wave function for NF_3 which was about 80% p in the N part.

(9) J. W. Frazer, J. Inorg. Nucl. Chem., 16, 63 (1960).

(10) J. Hinze and H. H. Jaffé, J. Am. Chem. Soc., 84, 540 (1962).

(11) M. Mashima, J. Chem. Phys., 24, 489 (1956).

(12) S. R. La Paglia and A. B. F. Duncan, ibid., 34, 1003 (1961).

RADIOCARBON-LABELED COMPOUNDS PRODUCED BY THE NEUTRON IRRADIATION OF GUANIDINE HYDROCHLORIDE[1]

By Thomas W. Lapp and Robert W. Kiser

Department of Chemistry, Kansas State University, Manhattan, Kansas

The formation of carbon-14-labeled products resulting from the neutron irradiation of crystalline cyanoguanidine was studied by Lapp and Kiser,[2] and they

indicated that the cyanamide radical, produced by the carbon-14 atom and/or by the accompanying γ-radiation, might play an important role in the formation of the radiocarbon-labeled products observed in solution.

In an effort to obtain a better understanding of the actual processes occurring during the recombination period, we have extended these studies to the neutron irradiation of crystalline guanidine hydrochloride and subsequently studied the various carbon-14-containing compounds present when the target material was dissolved in water. It was anticipated that if the recoil carbon-14 atom or the associated γ-radiation produced the cyanamide radical, it would be possible to explain the production of the various carbon-14-containing compounds observed in the neutron-irradiated sample as arising from reactions of the radio-labeled cyanamide radicals. Specifically, if the cyanamide radical is involved in the cases of both cyanoguanidine and guanidine HCl, we expect to observe very similar radiolabeled products. If these results were realized, it would then suggest that the formation of "simple compounds" from the reaction of carbon-14-containing radicals with the solvent may be relegated to a position of minor importance (at least where a large γ-flux is associated with the neutron flux). The formation of "simple compounds" has been discussed in the studies of acetamide[3] and α-cyanoacetamide.[4] We present in this paper our experimental approaches and findings. We utilize these results in the discussion of the possible reactions producing the radio-labeled species observed in aqueous solution.

Experimental

Sample Preparation and Irradiation.—Guanidine hydrochloride (Eastman Yellow Label) was purified by multiple recrystallizations from methanol and subsequently dried for two hours at 100°; 4.8 g. of the sample was placed in a quartz ampoule which was then attached to a vacuum system. The ampoule and contents were repeatedly flushed with argon and evacuated to less than one micron to rigorously exclude any oxygen, not trapped or dissolved in the solid, from the sample. The quartz ampoule was sealed off under vacuum while the contents of the ampoule were maintained at liquid nitrogen temperature. The irradiations were carried out at Oak Ridge National Laboratories in the graphite reactor. Pertinent data are as follows: neutron flux of approximately 5×10^{11} cm.$^{-2}$ sec.$^{-1}$; irradiation time of 670 hours; γ-ray flux of 4.9×10^5 r. hr.$^{-1}$; maximum sample temperature of 80°. The sample was stored for 39 months following irradiation to allow for the decay of the S^{35} activity, which was also produced during the irradiation as a result of the $Cl^{35}(n,p)S^{35}$ reaction. The ampoule was opened and the tan colored contents were transferred to a Pyrex storage bottle. The sample was maintained in a desiccator over $CaCl_2$ during the course of the experimental study.

Preliminary Experiments.—Each carrier, or its derivative, isolated from the aqueous solution of a portion of the irradiated guanidine hydrochloride was dissolved either directly or by means of a suitable solvent into the scintillator solution. All carbon-14 radioactivity measurements were made using a Packard Tri-Carb liquid scintillation spectrometer. The counting efficiencies and the scintillator solution used in this study have already been described.[2] The total carbon-14 activity present in the irradiated guanidine hydrochloride was determined by dissolution of known portions of the irradiated sample in water. Aliquots were taken and the total activity determined by liquid scintillation counting. An average value for three determinations was 16.1 ± 0.8 μcuries for the 4.8-g. sample; i.e., 3.38 ± 0.2 μcuries/g.

In order to establish the distribution of the carbon-14 activity among the various species likely to result from the neutron irra-

(2) T. W. Lapp and R. W. Kiser, J. Phys. Chem., 66, 152 (1962).

(3) T. W. Lapp and R. W. Kiser, ibid., 66, 1730 (1962).

(4) T. W. Lapp and R. W. Kiser, ibid., 67, 612 (1963).

diation and subsequent dissolution of the sample in water, solutions of the irradiated guanidine hydrochloride were subjected to analyses for the chemical species listed in Table I.

TABLE I

CARBON-14 DISTRIBUTION AMONG VARIOUS COMPOUNDS RESULTING FROM NEUTRON IRRADIATION OF GUANIDINE HYDROCHLORIDE

Fraction	% of total activity	
	Average	Values obtained
$NH_2C(NH)NH_2$ (guanidine)	6.4	6.5, 6.0, 6.8
$CH_3C(NH)NH_2$ (acetamidine)	11.1	11.1, 10.7, 11.4
$NCNHC(NH)NH_2$ (cyanoguani-dine)	12.1	13.8, 10.8, 11.6
$NH_2C(NH)NHC(NH)NH_2$ (biguanide)	16.3	15.4, 15.7, 17.7
$NHN=C(NH_2)N=CH$ (3-amino-1,2,4-triazole)	4.1	4.2, 4.6, 3.4
$NH_2C=NC(NH_2)=NC(NH_2)=N$ (melamine)	21.8	22.3, 19.9, 23.2

Chemical Separations.—Analyses were usually made for one or two carriers in each solution of the target material. The principal problem encountered in the procedures employed in this study was the separation of the various activities free from contamination. Therefore, in an attempt to achieve radiochemical purity, all carriers or their derivatives were isolated and purified to constant specific activity by repeated recrystallizations or distillations.

Separation techniques for essentially all of the chemical species listed in Table I have been previously described.[2,3] We note briefly here only those analytical procedures which are new to this study.

Oxamidine.—Oxamidine was separated utilizing two different procedures. The first procedure consisted of the addition of a carrier amount of oxamide to an aqueous solution of the irradiated sample. The oxamide was recrystallized and acid hydrolyzed to oxalic acid with concentrated hydrochloric acid. Addition of guanidine resulted in the formation of guanidine oxalate, which was treated in the same manner as described previously.[2] This procedure assumes that oxamidine behaves in the same manner as acetamidine when placed in water. The second procedure consisted of an acid hydrolysis of an aqueous solution of the irradiated sample without carrier addition. Following the hydrolysis, a carrier amount of oxalic acid was added and separated as described above. These two procedures gave essentially identical results.

Biguanide (Guanylguanidine).—Biguanide was separated as biguanide sulfate by a modification of the procedure described by Ray.[5] The derivative was recrystallized from an ethanol–water mixture. Dissolution into the scintillator solution was accomplished by adding an aqueous solution of the biguanide sulfate to the scintillator solution.

Melamine.—Melamine was separated by multiple recrystallizations from water. A portion of the recrystallized melamine was dissolved in a known quantity of dilute hydrochloric acid and an aliquot of the dilute acid solution added to the scintillator solution.

3-Amino-1,2,4-triazole.—The triazole was purified by multiple passes through a neutral alumina chromatography column using 95% ethanol. Evaporation of the ethanol solution to a small volume, followed by cooling, resulted in the precipitation of the triazole. A portion of the recrystallized 3-amino-1,2,4-triazole was dissolved in distilled water and an aliquot of the aqueous solution added to the scintillator solution.

Evolved Gases.—Upon opening the quartz ampoule containing the target material, the gaseous products, produced by the neutron irradiation and/or the associated γ-radiation, were collected and analyzed by mass spectrometric techniques. The only product present in detectable quantities was hydrogen.

Results of Analysis.—The results obtained by the procedures described above are given in Table I. In all cases, the data presented are based on specific activity measurements and the percentage activity is based on the total activity of aliquots of

(5) A. K. Ray, Z. Anal. Chem., 155, 18 (1957).

aqueous solutions of the original irradiated guanidine hydrochloride sample.

The total activity isolated in this study was 73.3 ± 4.7% of the total carbon-14 activity induced in the guanidine hydrochloride sample by neutron irradiation. Nearly 84% of the total activity isolated in this study occurred in four compounds: cyanoguanidine, acetamidine, biguanide, and melamine.

Less than 1% of the total activity was found in eight additional chemical species. These eight chemical species are given below with the average value for each compound. The individual values obtained in each determination are given in parentheses. Formaldehyde: 0.2% (0.2, 0.1, 0.3); formic acid: 0.1 (0.1, 0.1, 0.0); acetonitrile: 0.2% (0.2, 0.2, 0.2); methanol: 0.1% (0.1, 0.1, 0.2); methylamine: 0.7% (0.8, 0.5, 0.8); acetone: 0.1% (0.1, 0.1, 0.1); urea: 0.0% (0.0, 0.1, 0.0); oxamidine: 0.1% (0.0, 0.0, 0.3).

Discussion

The recoil carbon-14 atom in guanidine hydrochloride does not appear to be stabilized within the solid matrix in the form of "simple" compounds or in the form of a chemical species which could undergo reaction, such as decomposition or rearrangement, in the presence of water to produce "simple" compounds. Similar observations have also been noted in the investigations of the chemical compounds, containing the recoil carbon-14 atom, produced during the neutron irradiation of crystalline acetamide[3] and α-cyanoacetamide.[4] This small degree of carbon-14 labeling produced in the "simple" compounds suggests that the radiocarbon labeling process occurs primarily as a result of replacement reactions within the solid matrix in which the recoil carbon-14 atom replaces the carbon atom in the unlabeled molecule of guanidine hydrochloride. As a result of this replacement reaction, a fragmentation of the molecule occurs in which only one or two chemical bonds are broken and the multiple rupture of bonds to produce small fragments containing only a single carbon atom does not occur to any significant extent.

The results of this study indicate that the cyanamide radical plays an important role in the production of the final chemical species incorporating the recoil carbon-14 atom. This indication is supported by the results observed in the neutron irradiation of crystalline cyanoguanidine.[2] The production of the cyanamide radical may occur by a replacement reaction of the carbon-14 atom with a guanidine molecule within the solid matrix, after the recoil atom has been slowed down to the point where it is stable toward recombinations. This replacement reaction results in the rupture of a $C-NH_2$ bond. This leads to the formation of the radiocarbon labeled cyanamide radical, which may then undergo reactions with other molecules of the matrix to produce the final chemical compounds observed.

There appears to be no significant interaction of the solvent with the irradiated target material. This can be observed by a comparison of the percentage activity found in urea and in the target material, guanidine. If the solvent reacted significantly with the various matrix-stabilized species, we would expect that the radiocarbon activity in the urea would have been greater than that observed experimentally.

Significant amounts of activity were found in four chemical compounds: cyanoguanidine (12%), acetamidine (11%), guanylguanidine (biguanide) (16%), and melamine (22%). The formations of cyanoguanidine, acetamidine and melamine are suggested to occur in a manner similar to that previously postulated in the study of the neutron irradiation of crystalline cyano-

guanidine.[2] A possible method for the formation of biguanide may be postulated to occur by equation 1.

$$NH_2C^{14}NH + NH_2C(NH)NH_2 \longrightarrow$$

$$NH_2C^{14}(NH)NHC(NH)NH_2 \quad (1)$$
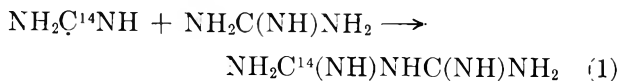
Certainly, alternate possibilities for the formation of biguanide-C^{14} could be written.

Degradation studies of cyanoguanidine, melamine, acetamidine, and biguanide, which would indicate the percentage of the carbon-14 labeling at each carbon position, were not performed, so we are unable to indicate specifically the degree of labeling of the carbon-14 positions in the product molecules.

The neutron irradiation of crystalline guanidine hydrochloride does not cause incorporation of carbon-14 into the "simple" molecules. We would suggest that the incorporation of the recoil carbon-14 atom into the more complex chemical species occurs via replacement reactions of the recoil carbon-14 atom with the guanidine molecule of the matrix to produce the cyanamide radical. This radical then further reacts with other species present in the matrix to produce the final products observed. The study of the radiocarbon-labeled compounds produced by the neutron irradiation of cyanoguanidine[2] and the results of this study appear to occur by the same process, i.e., the intermediate formation of the radiocarbon-labeled cyanamide radical. Certainly the final products observed in solution in both of these studies are readily explained in terms of similar reactions.

PREPARATION AND STUDY OF ORDERING IN A(B'$_{0.33}$Nb$_{0.67}$)O$_3$ PEROVSKITE-TYPE COMPOUNDS

BY FRANCIS GALASSO AND JANE PYLE

United Aircraft Corporation, Research Laboratories, East Hartford, Connecticut

The perovskite structure adopted by many ABO$_3$-type compounds can be described by a cubic unit cell with a large A ion at the center, smaller B ions situated at the corners, and oxygen ions on the edges. When ions of more than one element are present in the B position, the possibility of these ions being ordered exists. A study of Ba(B'$_{0.5}$Nb$_{0.5}$)O$_3$-type compounds demonstrated that size and charge difference of the B position ions had an important effect on their ordering.[1] In a more recent investigation of A(B'$_{0.33}$Ta$_{0.67}$)O$_3$-type compounds, where A is a barium or strontium ion and B' is a smaller divalent ion, these results not only were substantiated but it also was found that the degree of long-range ordering in the B position ions decreased as the difference in the size of these ions became smaller.[2] In order to test the generality of these results for other perovskite-type compounds with two different ions in the B position, a study of ordering was undertaken in an
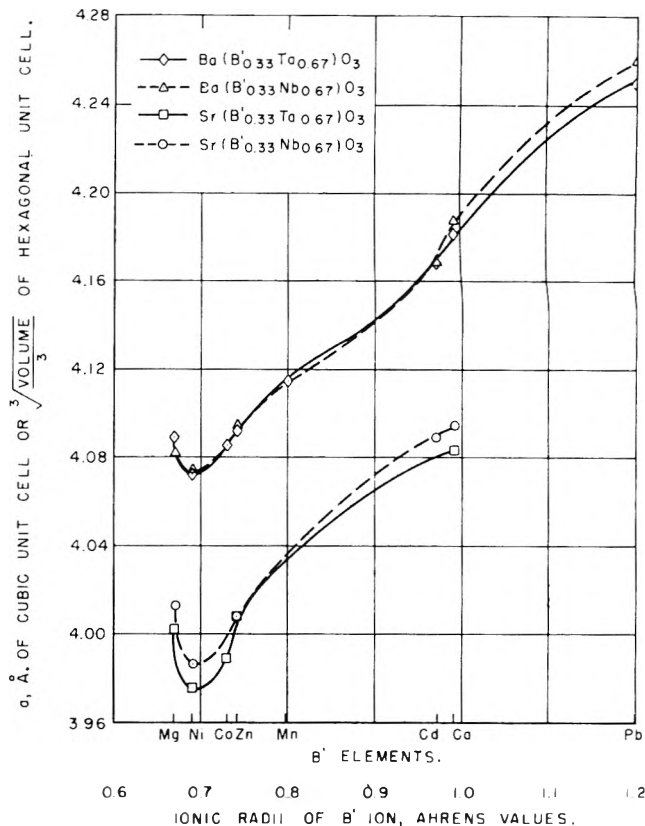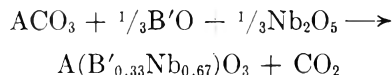

Fig. 1.—Ionic radii of B' ions *vs.* cell size for A(B'$_{0.33}$B''$_{0.67}$)O$_3$-type compounds.

analogous series produced by substituting niobium for tantalum in the A(B'$_{0.33}$Ta$_{0.67}$)O$_3$ compounds. The results of this study are presented in this note.

Experimental

Most of the compounds were mixed according to the equation

$$ACO_3 + \frac{1}{3}B'O + \frac{1}{3}Nb_2O_5 \longrightarrow$$

$$A(B'_{0.33}Nb_{0.67})O_3 + CO_2$$

where A is a strontium or barium ion and B' is a divalent metal ion. The mixtures were heated at 1000° for 10 hr., reground, and reheated at 1400° for 4 hr. Powder X-ray photographs then were taken of the compounds using a Philips 57.3-mm. radius camera with Cu Kα radiation and settings of 40 kv., 30 ma. for 4 hr. For compounds in which B' was cadmium or lead, the X-ray photographs used for indexing were taken using the powders prepared at 1000° because the perovskite phase was found to decompose at higher temperatures and either a Ba$_5$Nb$_4$O$_{15}$ or Sr$_5$Nb$_4$O$_{15}$ phase became predominant.[3]

When the B' ion was iron, strontium or barium oxide was used in place of the carbonates and the compounds were mixed in proportions dictated by the equation

$$AO + \frac{1}{9}Fe + \frac{1}{9}Fe_2O_3 + \frac{1}{3}Nb_2O_5 \longrightarrow$$

$$A(Fe^{II}_{0.33}Nb^{V}_{0.67})O_3$$
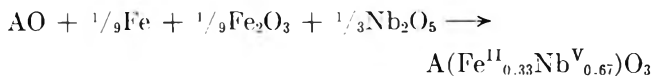
These samples were made into pellets, sealed under vacuum in silica capsules, and heated for approximately 10 hr. at a maximum temperature of 1100° because they melted through the silica at higher temperatures The procedure of heating the compounds to approximately 1400°, when possible, before taking X-ray powder diffraction photographs at room temperature was adopted from a similar study of A(B'$_{0.33}$Ta$_{0.67}$)O$_3$-type compounds for the following reason.[2] When the samples in that study were prepared at 1000° or lower, their X-ray pattern showed ordering lines which were often weak and diffuse and sometimes not even visible. However, if the samples could be heated several hundred degrees higher, presumably the size of the ordering domains was increased which in turn caused the reflections due to ordering to become much sharper. Since similar behavior was observed

(1) F. Galasso and W. Darby, *J. Phys. Chem.*, **66**, 131 (1962).
(2) F. Galasso and J. Pyle, *Inorg. Chem.*, **2**, 482 (1963).
(3) F. Galasso and L. Katz, *Acta Cryst.*, **14**, 647 (1961).

for many of the compounds in this study, it could not be positively concluded that compounds containing iron, cadmium, or lead as the B' ion, which could not be heated above the 1000–1100° temperature range, were not ordered even though no ordering lines were visible in their X-ray patterns. However, for the purpose of this study compounds containing cadmium, lead, or iron were indexed on the basis of an ~4 Å. cubic perovskite unit cell with the exception of $Sr(Fe_{0.33}Nb_{0.67})O_3$ which was indexed on a small tetragonal unit cell. All other compounds, except $Ba(Zn_{0.33}Nb_{0.67})O_3$ and $Ba(Ni_{0.33}Nb_{0.67})O_3$, gave X-ray patterns similar to that of the ordered perovskite $Ba(Sr_{0.33}Ta_{0.67})O_3$ and, therefore, were indexed on the basis of hexagonal unit cells.[4]

Discussion and Results

In a previous study it was observed that any of the $A(B'_{0.33}Ta_{0.67})O_3$ compounds which could be heated to approximately 1400° showed evidence of having the $Ba(Sr_{0.33}Ta_{0.67})O_3$ ordered perovskite-type structure, and also that the degree of ordering in the B position decreased as the size of the B ions decreased.[2] If the compounds which could not be heated higher than 1100° are not considered, the results of this study on analogous niobium compounds with the general formula $A(B'_{0.33}Nb_{0.67})O_3$ are quite similar (see Table I). The most interesting difference found between the $A(B'_{0.33}Nb_{0.67})O_3$ and $A(B'_{0.33}Ta_{0.67})O_3$ compounds lies in the fact that the B ions were ordered in $Ba(Zn_{0.33}Ta_{0.67})O_3$ and $Ba(Ni_{0.33}Ta_{0.67})O_3$, but no evidence of ordering was found in the $Ba(Zn_{0.33}Nb_{0.67})O_3$ and $Ba(Ni_{0.33}Nb_{0.67})O_3$ X-ray patterns even though the size and charge of the tantalum and niobium ions are similar. For the series of $Ba(B'_{0.33}Nb_{0.67})O_3$ compounds listed in Table I, it seemed most reasonable that $Ba(B'_{0.33}Nb_{0.67})O_3$, along with Ba-

TABLE I

STRUCTURE DATA FOR $A(B'_{0.33}Nb_{0.67})O_3$ COMPOUNDS

Compound	Cell[d] size, Å.	Ionic radii of B' ion, Å.[a]	Difference in ionic radii of B position ions, Å.	Unit cell
$Ba(Mg_{0.33}Nb_{0.67})O_3$[c]	$a = 5.77$ $c = 7.08$	0.67	0.02	Hexagonal
$Ba(Ni_{0.33}Nb_{0.67})O_3$[b]	$a = 4.074$	.69	.00	Cubic
$Ba(Zn_{0.33}Nb_{0.67})O_3$[c]	$a = 4.094$	.74	.05	Cubic
$Ba(Fe_{0.33}Nb_{0.67})O_3$	$a = 4.085$	.74	.05	Cubic
$Ba(Cd_{0.33}Nb_{0.67})O_3$	$a = 4.168$	.97	.28	Cubic
$Ba(Ca_{0.33}Nb_{0.67})O_3$	$a = 5.92$ $c = 7.25$	.99	.30	Hexagonal
$Ba(Pb_{0.33}Nb_{0.67})O_3$	$a = 4.26$	1.20	.51	Cubic
$Sr(Mg_{0.33}Nb_{0.67})O_3$	$a = 5.66$ $c = 6.98$	0.67	.02	Hexagonal
$Sr(Ni_{0.33}Nb_{0.67})O_3$	$a = 5.64$ $c = 6.90$	.69	.00	Hexagonal
$Sr(Zn_{0.33}Nb_{0.67})O_3$[c]	$a = 5.66$ $c = 6.95$	.74	.05	Hexagonal
$Sr(Fe_{0.33}Nb_{0.67})O_3$	$a = 3.997$ $c = 4.018$	.74	.05	Tetragonal
$Sr(Cd_{0.33}Nb_{0.67})O_3$	$a = 4.089$	.94	.28	Cubic
$Sr(Ca_{0.33}Nb_{0.67})O_3$	$a = 5.76$ $c = 7.16$	.99	.30	Hexagonal

[a] Ahrens ionic radii values used.[5] [b] Reported by R. Roy, indexed on cubic cell.[6] [c] Reported by F. Galasso, L. Katz, and R. Ward, indexed on cubic cell.[7] [d] Estimated error of ±0.001 Å. for values given to three places, ±0.005 Å. for values given to two places.

$(Mg_{0.33}Nb_{0.67})O_3$ and $Ba(Zn_{0.33}Nb_{0.67})O_3$, would not have an ordered structure because of the small differences in the ionic radii of their B ions. It was surprising to find that $Ba(Mg_{0.33}Nb_{0.67})O_3$, which has a much smaller difference in the radii of its B ions than the zinc compound, adopts the ordered structure. Figure 1 shows, however, that the magnesium ion appears to be much larger in these compounds than Ahrens' value[5] for the radius indicates. If this is the case, the difference in size between the magnesium and niobium ions would be somewhat greater than is indicated in Table I, but still not large enough to be the only cause of ordering in this compound.

Since $Sr(Ni_{0.33}Nb_{0.67})O_3$ and $Sr(Zn_{0.33}Nb_{0.67})O_3$ have the ordered structure while the analogous compounds with barium in the A position do not, it appears that the small size of the A ion also may be a factor contributing to ordering. It must be noted, however, that the size and charge difference of the B ions appear to be the most important causes of their ordering in these compounds, and it is only when their effect is minimized that other factors become most influential in producing an ordered arrangement of B ions.

INTENSITY OF THE 9 kK. BAND AND MOLECULAR ASSOCIATION IN VANADIUM TETRACHLORIDE[1]

BY EUGENE L. GRUBB, F. A. BLANKENSHIP, AND R. LINN BELFORD[2]

Noyes Chemical Laboratory, University of Illinois, Urbana, Illinois

The absolute intensity of a ligand field transition of a simple molecule such as VCl_4 provides a very useful test for molecular calculations. Since the only previous experimental studies[3–5] of the VCl_4 ligand-field bands (~9 kK.) did not provide a reliable oscillator strength we undertook to properly measure it over a small temperature and pressure range. The possibility that strong intermolecular forces are important in VCl_4 in condensed phases has been suggested. The question is crucial in interpretation of optical and magnetic properties. To test this, we also studied band shape and intensity of the 9 kK. band of VCl_4 in condensed phases. In so doing, we obtained some vapor pressure data which substantiate VCl_4 as being a "normal" (i.e., unassociated) liquid at and above room temperature.

Experimental

Four series of measurements were carried out.

Series I.—An apparatus explained and diagrammed in ref. 6 was used. The arrangement allowed the temperature and pressure of the vapor sample to be varied independently. The highly purified sample was sealed into an all-glass apparatus having a glass-sickle null pressure indicator. Since the 9 kK. band shape varies very little over the 25–70° range, the integrated intensity is proportional to peak intensity to ±3%[4,5]; the estimated absolute error from all causes being possibly as large as 17%[5] and the mean absolute deviation ±3% for individual measurements, we fol-

(1) Supported in part by grants from the National Science Foundation, and by NSF and University of Illinois predoctoral fellowships held by F. A. B.

(2) Alfred P. Sloan Research Fellow.

(3) A. G. Whittaker and D. M. Yost, J. Chem. Phys., 17, 188 (1949).

(4) F. A. Blankenship and R. L. Belford, ibid., 36, 633 (1962).

(5) F. A. Blankenship, Doctoral Thesis, University of Illinois, June, 1962.

(6) E. L. Grubb, F. A. Blankenship, and R. L. Belford, Group on Binding and Structure of Metal Complexes Research Report No. 14, Department of Chemistry, University of Illinois.

(4) F. Galasso, J. R. Barrante, and L. Katz, J. Am. Chem. Soc., 83, 2830 (1961).

(5) L. H. Ahrens, "Use of Ionization Potentials: 1, Ionic Radii of the Elements," Geochim. et Cosmochim, Acta, 2, 155 (1952).

(6) R. Roy, J. Am. Ceramic Soc., 37, 581 (1954).

(7) F. Galasso, L. Katz, and R. Ward, J. Am. Chem. Soc., 81, 820 (1959).

lowed in detail the temperature and pressure behavior of only the peak intensity.

Series II.—With 10-cm. fused-quartz cells in a Cary 14 spectrophotometer at room temperature, spectra of N_2 containing VCl_4 vapor at its equilibrium pressure over the liquid were obtained. To calculate concentrations we employed the equilibrium vapor pressure data found in series I and that of Tchukarev, et al.[7]

Series III.—Pure liquid VCl_4 (obtained from the Vanadium Corporation of America) was put into thin cells constructed from optically flat Pyrex plates, gold foil spacers, and epoxy resin. The cell thickness was measured interferometrically. The spectra were determined at room temperature. All manipulations were carried out in the dry N_2 atmosphere.

Series IV.—Utilizing the cells of series III or fused silica cells, we measured spectra of 0.05 to 50% solutions of VCl_4 in well dried CCl_4. For all series, extreme precautions against contamination and decomposition were observed. All results of series II, III, and IV were taken from complete frequency sweeps.

Calculations and Results

The data from runs at the elevated temperatures were processed with the equation $\epsilon = \alpha RT/Pl$, where α ($\equiv \log(I_0/I)$) is the decadic optical density, P the partial pressure of absorbing species, l the cell length, R the ideal gas constant, and T the absolute temperature. The experimental intensity is expressed as oscillator strength, f

$$f \equiv \left(\frac{mc^2}{\pi e^2 N}\right) \int \epsilon \, d\bar{\nu} = 4.33 \times$$

$$10^{-6} \int \epsilon \, d\nu/kK \text{ l. mole}^{-1} \text{ cm.}^{-1}$$

I_0 is the incident intensity of monochromatic light of wave number $\bar{\nu}$, I is the intensity after passage through the absorbing system, m the electronic mass, c the velocity of light, N Avogadro's number, and e the electronic charge. The integration is extended over the complete absorption band. The pressures, P, of VCl_4 at the recorded temperatures were taken directly from the sickle gage of the apparatus after corrections were applied for a small pressure of Cl_2 (originating from slight decomposition of VCl_4). Results are summarized in Table I.

Table I

Intensities of the 9 kK. VCl_4 Absorption Band

	Series I vapor			Series II vapor	Series III liquid	Series IV CCl_4 soln.	
	25°	54°	69°				
Path (mm.)	200	200	200	100	0.019	0.0264	10.0
ϵ_{max}/(l./ mole cm.)	150	142.4	141.3	147	123	122	123
1000f	2.2	2.2	2.2	2.16	2.16	2.09	2.22

All runs in series I and II (vapor) give $\epsilon_{max} = 146 \pm 4$ l./mole cm. The oscillator strength is independent of temperature and pressure over the 25–70° range, and is independent of physical state. (The condensed phases show *slightly* lower, broader bands with the same integrated intensity as the vapor.) These observations add weight to other observations[8-10] that the molecular species present in all three states (vapor, liquid, solution) is in all probability the same—monomer—as one would expect the ligand field band intensity to depend drastically upon molecular symmetry,[5] which should change markedly with polymerization. Mass spectrometric and vapor density measurements[9]

(7) S. A. Tchukarev, M. A. Oranskaya, T. A. Tolmetcheva, and A. K. Yakhkind, Zh. Neorgan. Khim., 1, 30 (1956).

(8) H. E. Roscoe, Ann. Chem. Liebigs, 7, 70 (1869).

(9) J. R. Marquart, unpublished.

(10) W. N. Lipscomb and A. G. Whittaker, J. Am. Chem. Soc., 67, 2019 (1945).

indicate an upper limit of dimer:monomer $< 1:4000$.

The vapor pressure was observed to be 16.85 ± 0.10 torr at 320°K. A good linear plot of log P_{vap} vs. $1/T$ (25 to 150°) shows the enthalpy of vaporization to be 10.0 kcal./mole, which supports the latest[7] of the two previous measurements.[3,7] It is instructive to compare these data for VCl_4 and $TiCl_4$:

	B.p., °K.	ΔS(vap) at b.p., e.u.	ΔH(vap), kcal./mole
$TiCl_4$	411.5	23.8	9.8
VCl_4	422	23.7	10.0

The similarity of these properties suggests that VCl_4 and $TiCl_4$ are very similar, particularly in the strength of their intermolecular cohesive forces. Presumably, $TiCl_4$ is not appreciably associated in liquid or vapor; the above similarity would suggest that VCl_4 also is not dimerized in either state. The Trouton constant (ΔS(vap) at the normal boiling point) has almost the normal value; it is nearly the same for the two molecules $TiCl_4$ and VCl_4. This is further evidence against strong molecular association. The studies of Whittaker and Yost[3] led them to speculate that VCl_4 is a "normal" liquid, not associated; our studies support their view.

SEMICONDUCTIVITY AND PHOTOCONDUCTIVITY OF PURINES AND PYRIMIDINES

By Sadhan Basu and Walter J. Moore

Chemical Laboratory, Indiana University, Bloomington, Indiana

Since the original suggestion of Szent-Györgyi[1] there has been a continuous interest in the possibility that electronic semiconductivity and photoconductivity might play a part in biochemical mechanisms.[2] For example, some unusual effects of radiation on the nucleic acids have been observed. A quantum yield $\phi = 1$ was found for the inactivation of a transforming principle (DNA) by soft X-rays[3] and $\phi = 0.1$ to 1 was reported for various phage preparations.[4] Such high quantum yields in macromolecules suggested that an exciton might travel freely through the molecule until it is trapped at a site at which the elementary reaction of deactivation can occur. Such exciton mechanisms are closely related to the phenomenon of photoconductivity. If, during the course of its motion, the exciton encounters a strong donor or acceptor entity (*i.e.*, a trapping center), then either the positive hole or the negative electron will be trapped, leaving its counterpart mobile. The trapping effect, therefore, leads to the generation of charge carriers which can carry electric current through a conduction band.

Experimental Procedures

In order to obtain further information on such transfer processes in nucleic acids, we decided to measure the conductivity and the photoconductivity of their constituent purines and pyrimidines.

(1) A. Szent-Györgyi, Nature, 148, 157 (1941).

(2) D. D. Eley, "Biological Semiconductivity," in "Horizons in Biochemistry," ed. by M. Kasha and B. Pullman, Academic Press, New York, N. Y., 1962, provides a complete review.

(3) R. Latarjet, H. Ephrussi-Taylor, and N. Rebeyrotte, Rad. Res., Suppl. 1, 417 (1959).

(4) H. Ephrussi-Taylor and R. Latarjet, Biochim. Biophys. Acta, 16, 183 (1955); G. Stent and R. Fuerst, J. Gen. Physiol., 38, 441 (1955).

TABLE I
PHOTOCONDUCTIVITY AND SEMICONDUCTIVITY OF PURINES AND PYRIMIDINES

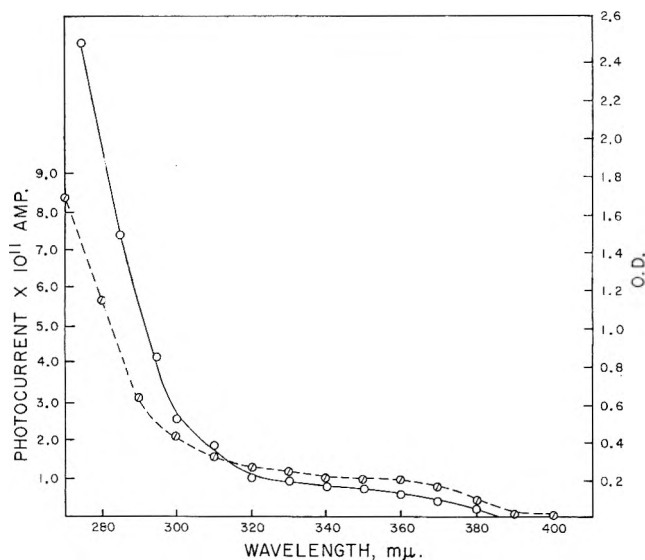| Compound	Dark current $\times$ 10^{11}, amp.	Photocurrent (Δi) $\times$ 10^{11}				E, e.v.	
		290 mμ		360 mμ			
		air	vac.	air	vac.	air	vac.
Adenine	0.26	2.88	1.24	0.71	0	0.56	0.90
Uracil	.50	5.75	4.10	.10	0	.55	1.38
Thymine	.55	4.45	3.20	.70	0	.55	1.09
Cytosine	.50	4.25	2.80	.70	0	.60	1.40
Guanine	.22	2.74	1.09	.60	0	.47	1.10
Hypoxanthine	.25	5.75	3.50	2.24	0	.55	1.10

Fig. 1.—Comparison of absorption spectrum of 0.02 M solution of adenine in water (solid line) and photoconductive action spectrum of adenine powder in air (dashed line).

Ideally these measurements should be made on single crystals but we have not been able to grow suitable crystals of these quite insoluble compounds. Therefore we used thin films of finely powdered samples. The bases were chromatographically purified preparations from the Pabst Laboratories; repeated recrystallizations did not alter their spectral characteristics. The electrodes were quartz plates (Corning Glass Works) rendered conductive by an adherent stannic oxide layer. Blank measurements on sucrose showed essentially zero conductance and photoconductance, indicating that the preparation of the films did not abrade conductive material from the plates. The plates showed a transmission of only 15% at 260 mμ rising sharply to 100% from 320 mμ. In drawing the action curve, the photocurrent was corrected for the transmission characteristics of the quartz and the spectral intensity of the light. The electrical measurements were made by the standard d.c. technique[5] for such "sandwich cells" with the use of a vibrating-reed electrometer. Monochromatic light was isolated from a hydrogen or mercury arc lamp by means of a Bausch and Lomb 250 mm. grating monochromator. Intensity of light was measured with an IP28 phototube calibrated against an oxalic acid dosimeter. Absolute intensity data have little significance since much of the incident light is lost by scattering from the powdered sample, and from 270 to 400 mμ no light passes completely through the conductivity cell. The sample thickness was set by Teflon spacers at 0.0086 cm. The incident light intensity at 290 mμ was 120 μw./cm.[2]; at 360 mμ, 265 μw./cm.[2]. Measurements of dark conduction were made in the temperature range 30 to 70°. The dark conduction was the same in air and *in vacuo* of 10^{-6} torr, but the photocurrent was markedly dependent on the ambient atmosphere. The electric field across the electrodes was 2500 volts/cm. Ohm's law was followed over the range 600 to 9000 volts/cm.

Results and Comments

The experimental results are summarized in Table I. The reproducibility of current measurements on duplicate samples was about 10%. The photoconduc-

(5) B. Rosenberg, *J. Chem. Phys.*, **31**, 238 (1959).

tive action spectrum followed the absorption spectrum of a concentrated water solution of the base. An example is shown in Fig. 1. This correlation is evidence that the measured photoconductivity is a molecular property of the crystals and is not simply a surface effect in the powdered samples.

On the other hand, the importance of surface effects is emphasized by the markedly higher photocurrents in the samples exposed to air. In air, appreciable photocurrent was detected in the range 320 to 380 mμ, but this was practically absent *in vacuo*.

In air, the photocurrent was higher when the sample was illuminated through the positive electrode than when it was illuminated through the negative electrode. *In vacuo*, the photocurrent was independent of the direction of illumination.

The last two columns in Table I give the activation energy E for the semiconduction, computed from $\sigma = \sigma_0 \exp(-E/kT)$. The activation energies were markedly lower in air, although the dark currents at 30° were about the same. Since the band gap for the onset of the photoconduction process is about 3.5 e.v., it is likely that it is not related to the semiconductivity observed from 30 to 70°.

The higher photocurrent in air when the sample is illuminated through the positive electrode is in accord with a mechanism in which the predominant current carriers are positive holes. It is possible that adsorbed oxygen molecules at the crystallite surfaces are then acting as trapping centers for electrons. However, the question of the detailed mechanism of conduction in these materials is likely to be solved only by an exhaustive study of monocrystalline specimens of ultra-high purity, in which surface effects and trapping by impurity centers can be more readily isolated. The present results are at least consistent with exciton mechanisms in irradiated nucleic acids and suggest that adsorption of electron acceptors may influence the electronic properties.

A LANGMUIR MEASUREMENT OF THE SUBLIMATION PRESSURE OF MANGANESE(II) FLUORIDE

BY RENATO G. BAUTISTA AND JOHN L. MARGRAVE*

Department of Chemistry, University of Wisconsin, Madison, Wisconsin

Received February 16, 1963

The sublimation pressure of a single crystal of MnF$_2$ has been measured by the Langmuir free-evaporation technique. Until this work was carried out, no other

* Rice University, Houston, Texas.

experimental data on the sublimation rate of MnF_2 had been reported in the literature. Brewer, Somayajulu, and Brackett[1] have estimated the heat of sublimation to be equal to 75 kcal./mole.

Experimental Apparatus and Techniques

The experiment was carried out with a microbalance built inside a vacuum system. The apparatus has been previously described in detail.[2] It consists basically of a resistance furnace, a beam balance, and an electrical control circuit for the balance to measure the change of voltage with the change in weight. The MnF_2 single crystal was suspended from a holder made of tungsten wire inside a glass envelope contained in the furnace. The temperature was measured by means of a calibrated chromel-alumel thermocouple placed inside the glass envelope.

Several readings were taken of the rate of weight loss of the sample at a given temperature and the time-weighted average of all of the weight loss readings was calculated and reported as one pressure point. These data were used to derive a $\log P$ vs. $1/T$ equation with a Fortran program on a Control Data-1604 digital computer.

Discussion of Results

$MnF_2(g)$ was considered the only important vapor species. The free energy functions for both solid and gaseous MnF_2 were taken from the data compiled by Brewer, Somayajulu, and Brackett.[1]

The experimental results are summarized in Table I. A third law calculation from these data gives $\Delta H^0{}_{298} = 76.4 \pm 1$ kcal./mole for the heat of sublimation while the second law least-square plot of $\log P$ vs. $1/T$ gives $\Delta H^0 = 73.5 \pm 0.5$ kcal./mole at $T_{avg} = 939\ 0°K$. When corrected to $298°K$. using the heat content values compiled by Mah[3] and the molecular constants estimated by Brewer, Somayajulu, and Brackett,[?] the second law approach gives $\Delta H^0{}_{298} = 76.0 \pm 1.0$ kcal./mole.

TABLE I
VAPOR PRESSURE DATA ON MnF₂

T, °K.	P	$\Delta H^0{}_{298}$, kcal./mole
924.1	2.49×10^{-9}	76.46
939.0	4.73×10^{-9}	76.45
952.3	8.54×10^{-9}	76.38
963.8	1.35×10^{-8}	76.39
969.9	1.69×10^{-8}	76.43
982.9	2.78×10^{-8}	76.44
964.3	1.40×10^{-8}	76.36
951.7	8.34×10^{-9}	76.38
887.1	4.94×10^{-10}	76.34
		76.40 ± 0.5 kcal./mole

Using the above sublimation and other available thermochemical data,[4] one calculates the atomization energy of $MnF_2(g)$ to be 217 kcal./mole, which is in good agreement with the 220 kcal./mole estimate of Brewer, et al.[1] This indicates 108.5 kcal./mole for the average bond energy in MnF_2 while Gaydon[5] has estimated $D^0(MnF)$ as 81 kcal./mole from molecular spectra via a linear Birge–Spooner extrapolation.

(1) L. Brewer, G. Somayajulu, and E. Brackett, University of California Radiation Laboratory Report No. 9840, September, 1961; *Chem. Rev.*, **63**, 111 (1963).

(2) L. H. Dreger and J. L. Margrave, *J. Phys. Chem.*, **64**, 1323 (1960); R. C. Paule, Ph.D. Thesis, University of Wisconsin, 1962.

(3) A. D. Mah, U. S. Bureau of Mines, Report of Investigation 5600 (1960).

(4) D. R. Stull and G. C. Sinke, "Thermodynamic Properties of the Elements," Advan. in Chem. Series, ACS, 1956; F. D. Rossini, D. D. Wagman, W. H. Evans, S. Levine, and I. Jaffe, National Bureau of Standards Circular 500 (1952); JANAF Interim Thermochemical Tables, edited by D. R. Stull, The Dow Chemical Company, Midland, Michigan, 1960.

(5) A. G. Gaydon, "Dissociation Energies," Chapman and Hall, Ltd., 1953.
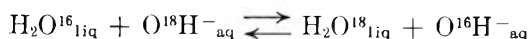
ISOTOPIC FRACTIONATION IN THE $OH^- - H_2O$ EXCHANGE REACTION

BY MICHAEL GREEN AND HENRY TAUBE[1]

George Herbert Jones Laboratory, The University of Chicago, Chicago, Illinois

Received March 15, 1963

It is important to know with some certainty the equilibrium constant in the system

$$H_2O^{16}{}_{liq} + O^{18}H^-{}_{aq} \rightleftharpoons H_2O^{18}{}_{liq} + O^{16}H^-{}_{aq}$$

in order to interpret the fractionation of oxygen isotopes during the hydrolysis of certain complex ions. Values of this constant, K, at 25° have been calculated. Hunt and Taube[2] have obtained a result of 1.035, from vibrational frequencies of H_2O vapor and of OH^- in 10 M solution. More recently Thornton[3] has refined the value to 1.0385 by using the parameters of liquid H_2O and including librations. In both calculations approximate methods were employed in deriving the frequencies for H_2O^{18}. We have therefore performed a direct experiment to measure this quantity, which we find to be 1.045 ± 0.003 at 15°. When an allowance is made for temperature, the agreement with calculated values is quite good.

The actual numerical value of K is an essential feature in arguments about the mechanisms of hydrolysis which we have developed elsewhere.[4]

Experimental

The isotopic composition of a stock quantity of redistilled water was determined by equilibration with carbon dioxide.[5] Freshly cut sodium was held under this water to make a solution approximately 3 M in sodium hydroxide. This solution was held at approximately 15°. A measured volume of liquid was drawn off at a rate of 2–4 ml./hr. under reduced pressure as vapor which was condensed and equilibrated with carbon dioxide. The volume and molarity of the remaining solution were measured. The vapor was drawn off slowly and was therefore assumed to be in isotopic equilibrium with the solution. A value of 1.009 was taken from the graph of Dostrovsky and Raviv[6] for α, the distillation separation factor of H_2O^{16} relative to H_2O^{18}. The relative fugacities of H_2O^{16} and H_2O^{18} are unaffected by Na^+ ions.[7] Values of 1.044 ± 0.004 and 1.046 ± 0.004 were obtained for K in two experiments where the respective mean concentrations of sodium hydroxide were 4.8 and 4.3 M.

The method of Hunt and Taube[3] gives a value of 1.044 for K at 0°, which leads to 1.039 at 15° by interpolation. However their procedure really refers to an equilibrium between aqueous OH^- and H_2O vapor. When an allowance is made for this by multiplying by α, K becomes 1.048 at 15°. Inclusion of the libration of OH^- reduces this quantity to 1.046, which agrees well with the values observed. If it is assumed that Thornton's value[3] has the same temperature depend-

(1) Department of Chemistry, Stanford University, Stanford, California.

(2) H. R. Hunt and H. Taube, *J. Phys. Chem.*, **63**, 124 (1959).

(3) E. R. Thornton, *J. Am. Chem. Soc.*, **84**, 2474 (1962).

(4) M. Green and H. Taube, submitted for publication in *Inorg. Chem.*

(5) C. A. Mills and H. C. Urey, *J. Am. Chem. Soc.*, **62**, 1019 (1940).

(6) "Proc. of International Symposium on Isotope Separation," North-Holland Publ. Co., Amsterdam, 1958, p. 337, ed. by J. Kistemaker, J. Bigeleisen, and A. O. C. Nier.

(7) H. M. Feder and H. Taube, *J. Chem. Phys.*, **20**, 1335 (1952).

ence as that of Hunt and Taube, his method would give a value of 1.0425 at 15°. A value of 1.045 ± 0.003 at 15° seems to be compatible with both experimental and theoretical data. A similar sort of argument points to a value of 1.040 ± 0.003 at 25°.

COMMUNICATIONS TO THE EDITOR

CATIONIC MOBILITIES IN FUSED CESIUM NITRATE AND THALLOUS NITRATE

Sir:

In the course of the past few years many papers dealing with the determination of transport numbers of ions in pure ionic melts have been published. Most of the experiments were made with porous plug cells[1]–[4] in which the plugs act as reference frames for the ionic velocities.

In our present work we used the experimental technique of electrophoresis on thin layers for the determination of single ionic mobilities in molten salts. The layer consisted of fine alumina powder sprayed on a sintered non-porous alumina support strip (30 cm. × 1.5 cm. × 2 mm. thick). The thickness of the layer was about 10 mg./cm.². It was impregnated with the pure salt under test and doped at one end with a small amount of radioactive cations. The cell terminals consisted of two platinum electrodes immersed in the melt contained in crucibles. The electric connection between the crucibles and the strip was achieved by asbestos paper bridges. The potential gradient along the alumina strip during the experiments was measured by two auxiliary platinum wire electrodes in contact with the strip at both ends. The mobility data reported are referred to this potential gradient.

Under normal experimental conditions the field strength was 3–6 v./cm. and the running time was 1–2 hr. The current was 10–45 ma., which corresponds to a maximum Joule heat of 0.2 w./cm.². This value is small enough to avoid temperature differences along the strip.

When the experiment was completed, the strip was cooled to room temperature and the activity distribution scanned by a G.M. window counter in which the aperture was 0.5 mm. In Table I we compare a few results obtained for alkali nitrate melts with those obtained by other authors who determined the porous plug transport numbers in the same systems. We also give original results for cesium nitrate at 450° and thallous nitrate at 250°.

The mobilities in the third column are the results of runs carried out at different potential gradients.

(1) B. B. Owens and F. R. Duke, Ames Laboratory, Iowa State College, Unclassified Report USAEC ISC-992.

(2) R. W. Laity and F. R. Duke, *J. Electrochem. Soc.*, **205**, 197 (1958); "Metals Reference Book," Butterworths Scientific Publications, London, 1955, pp. 614–627.

(3) A. Klemm, *Discussions Faraday Soc.*, **32**, 203 (1961).

(4) E. D. Wolf and F. R. Duke, Ames Laboratory, Iowa State University, Unclassified Report USAEC 19-334.

TABLE I
CATIONIC MOBILITIES OF PURE FUSED SALTS

Salt	T, °C.	$u \times 10^4$, cm.² v.$^{-1}$ sec.$^{-1}$	Av.	Previous work
CsNO$_3$	450	1.56 1.69 1.64	1.63 ± 0.07	...
TlNO$_3$	250	1.08 0.99 1.04 1.11	1.05 ± 0.06	...
NaNO$_3$	350	3.86 3.90 3.84	3.87 ± 0.07	3.86 ± 0.05[a]
KNO$_3$	350	2.04 2.08 2.12	2.08 ± 0.06	2.21 ± 0.11[a]
AgNO$_3$	250	2.57 2.68 2.47	2.57 ± 0.11	2.87 ± 0.19[b]

[a] Reference 1.   [b] Reference 2.

We feel that electrophoresis on thin layers in fused salts is an accurate and useful method for determining electrical transport properties of ionic melts.

DIPARTIMENTO MATERIALI   S. FORCHERI
CHIMICA ALTE TEMPERATURE   C. MONFRINI
C. C. R. EURATOM
ISPRA-VARESE, ITALY

PHOTOCHEMICAL REACTION OF HYDROGEN BROMIDE WITH OLEFINS AT LOW TEMPERATURE

Sir:

A recent electron spin resonance study of the interaction between ultraviolet irradiated hydrogen bromide and various olefins[1] has been interpreted in terms of radicals formed by addition of a bromine atom to the double bond in such a manner that bonding is effectively symmetrical.[1] The alternative reaction considered was hydrogen atom addition, but this was excluded on the grounds that the spectra were not those expected for alkyl radicals, and, for reaction with cyclopentene and 2-butene, spectra were identical when deuterium bromide was used instead of hydrogen bromide.

(1) P. I. Abell and L. H. Piette, *J. Am. Chem. Soc.*, **84**, 916 (1962).

These clear-cut results, which appear to constitute an important advance in our understanding of the mechanism, have been widely accepted and quoted.[2] However, examination of the spectra reported has suggested an interpretation not considered originally,[1] which, if correct, invalidates the conclusions outlined above.

Accepting that photolysis results in the formation of hydrogen and bromine atoms in close contact with olefin molecules, there seems to be a variety of possible products which might remain trapped. Hydrogen atoms were detected in some instances, but in very low relative concentration. Addition of hydrogen has been eliminated, at least in two instances, but attack on allylic hydrogen to give the corresponding allyl radicals is a possibility which was not considered. Bromine atoms, if trapped as such, would not contribute to the observed spectrum. Unsymmetrical "sigma" addition would give radicals whose spin resonance spectra are not expected to resemble those detected. Symmetrical addition will be discussed below. Certainly it would be most surprising if hydrogen atoms were unable to react with the olefins, but that relatively stable bromine atoms reacted very rapidly. It should be stressed that the fate of the photolytic hydrogen atom is a trivial matter for the reaction in fluid solution, since a chain mechanism is involved,[3] but that it is probably of equal importance to that of the bromine atom in a solid at $77°K$.

It is postulated that the radicals detected by Abell and Piette[1] were allylic. This would explain the results of experiments with deuterium bromide, and since these experiments were confined to 2-butene and cyclopentene, the spectra of radicals obtained from these olefins will be discussed in detail.

The spectrum reported for 2-butene radicals consists of seven poorly resolved lines having roughly a binomial distribution of intensities and a separation of between 10.8 and 12.6 gauss. This spectrum is in reasonable accord with expectation for the radical $\dot{C}H_2CH=CHCH_3$. Thus, to a first approximation, the unpaired electron will be distributed equally on C_1 and C_3, so that hyperfine coupling to three α-protons and three β-protons should be observed. Their isotropic coupling constants will be approximately equal in magnitude and about half those normally observed—that is, about 12 gauss.

The spectrum reported for the radical derived from cyclopentene consists of eleven lines of alternating intensities, separated by about 9.4 gauss, the more prominent set of five lines having approximately a binomial distribution of intensities. This result is in good accord with expectation for the cyclopentenyl radical, I. Here there are two equivalent α-protons
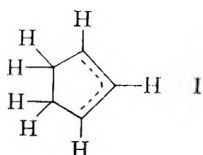
and four equivalent β-protons which should couple more strongly than usual because of their favorable orienta-

tion relative to the plane of the radical. Coupling to the "central" allylic proton should be small and hence simply contributes to the line widths. The coupling constant of 9.4 gauss is assigned to the α-protons, and that of 18.8 gauss to the β-protons. The latter constant should be related to the maximum value $Q_{\beta H}$ of about 50 gauss by the relationship $a_{\beta H} = Q_{\beta H} \cos^2 \theta$, θ being the angle between the radical plane and the plane

H
/
through the relevant C–C unit. Hence a value of about 17 gauss is predicted, if the small negative spin-density on the "central" carbon is ignored. The apparently low value of the α-proton coupling then can be understood in terms of this large delocalization onto the β-protons. However, this theory leaves open the problem of the marked line-width alternation. A simple explanation would be that the α-proton coupling constant is not 9.4 gauss, but slightly greater, say about 11 gauss. This would have the effect of replacing the odd numbered lines by closely spaced doublets, without affecting those with even numbers. As the line widths are too great for resolution of these doublets, the effect on the derivative spectrum would be to reduce drastically the apparent intensities of the odd numbered lines, as is found experimentally. These deductions are reinforced by comparing the results with those of Fessenden[4] for the cyclopentyl radical. The α- and β-proton coupling constants of 21.6 and 35.3 gauss[4] are very close to twice the values now assigned to the cyclopentenyl radical.

Results for some of the other compounds studied can also be understood adequately in terms of the present theory, but these spectra were generally less well resolved and since no studies were made with deuterium bromide addition of hydrogen cannot be ruled out.

The major drawback of the bridging bromine atom concept is that there is no indication, in the spectra discussed above, of any anisotropy in the g-values. Appreciable anisotropy would be expected for the bromine atom adducts, together with a shift in g_{av} to values somewhat greater than that of the free-spin. Unfortunately, g-values are not reported, but judging from one spectrum which displays also the doublet due to trapped hydrogen atoms, the g-values are very close to 2.0023, as expected for simple alkyl or allyl radicals. Furthermore, there is no indication of the expected characteristic hyperfine coupling to bromine.

Thus, despite the fact that there is good evidence from other sources that the chain addition of hydrogen bromide to olefins proceeds via a bridged bromine-olefin intermediate, it is concluded that the electron spin resonance results for radicals trapped during the first stages of the photolysis in the solid phase cannot be taken as evidence in support of this mechanism. Indeed, if the present postulate is correct, they are the result of a minor side process.

(2) See, for example, M. Szwarc, *Chem. Soc.* (London) *Spec. Publ.*, **16**, 103 (1962).

(3) D. H. Hey and W. A. Waters, *Chem. Rev.*, **21**, 169 (1937).

(4) R. W. Fessenden, Mellon Institute Quarterly Report, No. 6041 (1961).

DEPARTMENT OF CHEMISTRY   M. C. R. SYMONS
LEICESTER UNIVERSITY
LEICESTER, ENGLAND

THE MAGNETIC SUSCEPTIBILITY OF PROMETHIUM-147 OXIDE[1]

Sir:

At 25° promethium-147 oxide, whose color resembles that of erbium oxide, was found by the Gouy technique to have specific susceptibility of 15.5×10^{-6} c.g.s. unit. After making an allowance for the diamagnetic contribution in the compound Pm_2O_3, the molar susceptibility was calculated to be 2660×10^{-6} c.g.s. unit. Assuming that the ground state of Pm^{3+} is $^5I_4$ and that the multiplet intervals are large compared to kT, a molar susceptibility of 2960×10^{-6} c.g.s. unit was calculated using the familiar equation.[2] These values are in reasonable agreement.

The promethium-147 used in these experiments was obtained from a Hanford-type waste solution. It was separated from the other fission products by a "displacement-chromatographic" technique[3] in which the diamagnetic Y^{3+} ion was used as a barrier ion. The eluent used was 0.015 M ethylenediaminetetraacetic acid solution, adjusted to a pH of 8.7 with ammonium hydroxide.

The elution sequence[4] under these conditions is such that large separation factors are obtained from the strongly paramagnetic heavy rare earth elements and possible sources of ferromagnetic impurities such as Fe^{3+}, Co^{2+}, and Ni^{2+}. The estimated separation factors for the latter are of the order of 10^9. Since the initial Fe^{3+} concentration of the feed solution was found by spectrographic analysis to be less than 30 p.p.m., the final concentration must be much lower. Spectrographic analysis of the eluate indicated the iron concentration to be considerably less than 10 p.p.m., the limit of this particular measurement. Another indication of the purity of this material is that Am-241 and Eu-154,155 could not be detected, indicating separation factors greater than 10^6.

Promethium from a fraction in the middle of the promethium band was then precipitated as the oxalate. Under these conditions a further separation is obtained from possible sources of ferromagnetic impurities such as Fe^{3+} and Co^{2+}. The oxalate then was ignited at 800° to form the oxide, Pm_2O_3. After the magnetic experiment the sample was dissolved in perchloric acid and ultraviolet, visible, and near-infrared spectra were taken. Only those peaks[5] characteristic of Pm^{+3} were observed.

The Pyrex sample tube (3 mm. i.d. $\times$ 10 cm.) used in the experiment was calibrated using reagent grade ferrous ammonium sulfate ($\chi_g = 31.6 \times 10^{-6}$ c.g.s. unit at 25°).[6]

As a check on the calibration, the susceptibilities of $HgCo(SCN)_4$ and $CuSO_4 \cdot 5H_2O$ were determined, and respective values of 16.4×10^{-6} and 6.08×10^{-6} c.g.s. unit at 25° were obtained which are in agreement with those found by Figgis and Nyholm.[7] A further check
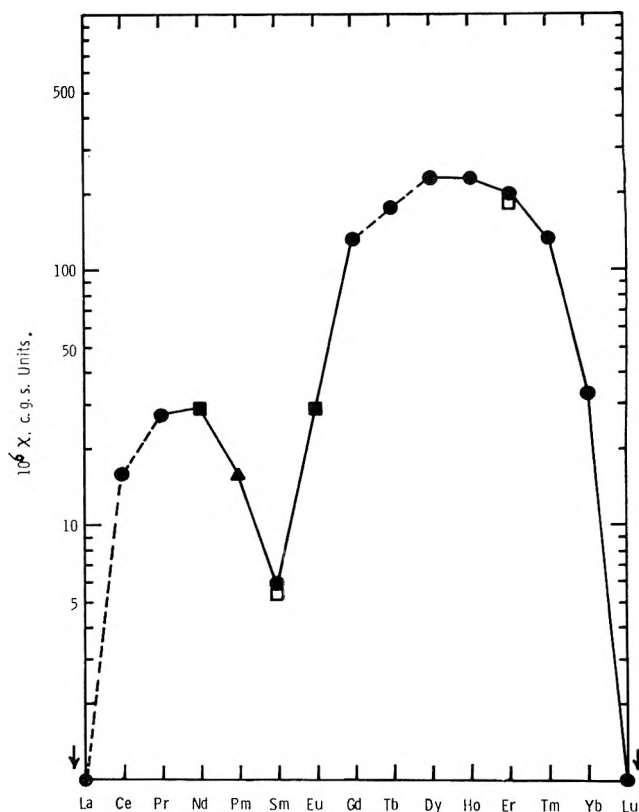

Fig. 1.—The gram-magnetic susceptibilities of the rare earth oxides at 25°. The triangle is the susceptibility of promethium-147 oxide. The solid circles are values taken form Selwood.[8] The solid and open squares are, respectively, values in agreement with and low compared to those reported by Selwood.[8]

involved the determination of the susceptibilities of several other rare earth oxides. These results are shown with that of promethium oxide and those reported by Selwood[8] in Fig. 1.

The sample tube was loaded with the promethium oxide using remote manipulators which were necessitated by the high radiation levels. The sample then was suspended between the poles (1-in. gap) of a Varian 4-in. electromagnet from a semimicro balance by means of a fine copper wire. From the force exerted on a 0.1591-g. sample of promethium oxide at 1.0, 1.2, and 1.4 amp. of magnet current, and after a small correction ($\sim$0.7 mg.) for the paramagnetism associated with the sample tube, respective values of 16.9, 15.5, and 15.5×10^{-6} c.g.s. unit were obtained at 25°.

The fact that the low field value is high compared to the other two measurements suggests the possibility that the sample contains a trace of ferromagnetic impurity, but this seems very unlikely in view of the separation scheme used. Since the two high field measurements are the same within the experimental error of this method, which is estimated to be about 2%, it is suggested that the low field value may be in error. Assuming that the low field susceptibility is in error, a best value of 15.5×10^{-6} c.g.s. unit is obtained using the two high field values. A mean value of 16.0×10^{-6} c.g.s. unit is the result if all values determined are used. If the possibility of ferromagnetic contamination is accepted, an extrapolation to infinite field strength yields a value of about 13×10^{-6} c.g.s. unit.

Self-heating of the sample and development of a

(1) Work performed under Contract No. AT(45-1)-1350 for the U. S. Atomic Energy Commission.

(2) J. H. Van Vleck, "The Theory of Electric and Magnetic Susceptibilities," Oxford University Press, Oxford, 1932, p. 233.

(3) F. H. Spedding and J. E. Powell, *Chem. Eng. Prog., Symp. Series*, **50**, 7 (1954).

(4) D. B. James, J. E. Powell, and F. H. Spedding, *J. Inorg. Nucl. Chem.*, **19**, 133 (1961).

(5) J. B. Gruber and J. G. Conway, *ibid.*, **14**, 303 (1960).

(6) L. C. Jackson, *Phil. Trans. Roy. Soc.* (London), **A224**, 1 (1923).

(7) B. N. Figgis and R. S. Nyholm, *J. Chem. Soc.*, 331 (1959).

(8) P. W. Selwood, "Magnetochemistry," Interscience Publishers, Inc., New York, N. Y., 1956, p. 149.

static charge on the sample tube due to the very intense radiation field ($\sim 3 \times 10^{14}$ disintegrations/min.), non-uniform packing, and, of course, possible ferromagnetic contamination of the sample are possible experimental errors. Since promethium oxide may not be magnetically dilute, there may be an appreciable Weiss constant which makes the observed value lower than that calculated.

Hᴀɴꜰᴏʀᴅ Lᴀʙᴏʀᴀᴛᴏʀɪᴇꜱ   J. C. Sʜᴇᴘᴘᴀʀᴅ
Gᴇɴᴇʀᴀʟ Eʟᴇᴄᴛʀɪᴄ Cᴏᴍᴘᴀɴʏ   E. J. Wʜᴇᴇʟᴡʀɪɢʜᴛ
Rɪᴄʜʟᴀɴᴅ, Wᴀꜱʜɪɴɢᴛᴏɴ   F. P. Rᴏʙᴇʀᴛꜱ

ISOSBESTIC POINTS IN ABSORBANCE SPECTRA

Sir:

With reference to my recent article on the occurrence of isosbestic points[1] it has been kindly drawn to my attention by Dr. K. Buijs that isosbestic points can conceivably occur in closed systems consisting of three variable absorbing species. It was argued in the paper that the occurrence of more than two absorbing species was highly unlikely since the equation

$$\sum_{i=j}^{n} [\epsilon_i(\lambda_c) - \epsilon_j(\lambda_c)] \frac{dC_i}{dC_j} = 0 \qquad (1)$$

must hold at each isosbestic point, requiring in general that all molar absorptivities be equal. Systems which provide constant values of dC_i/dC_j, or derivatives all of which show the same dependence on the variable j, were overlooked. Under these conditions closed systems containing not only three but several absorbing species may give rise to isosbestic points, providing the species can be grouped into not more than two groups wherein the ratios of concentrations of the species within the group are constant. Such systems fall into the category described by Cohen and Fischer[2] wherein the deDonder–Van Rysselberghe parameter can be successfully defined as a system parameter (linearly related systems).

My original conclusions that occurrence of isosbestic points in closed, temperature dependent systems indicates only one absorbing species are still valid, even for linearly related systems. This is directly shown by development of Cohen's and Fischer's equation in extended version with consideration of time, concentration of a jth species, and temperature as independent variables. The equation is given as follows. The reader is referred to the papers cited for definition of symbols.

$$A(\lambda,t,T,nj) = \sum_{i=1}^{n} \frac{\epsilon_i(\lambda,T)[n_i^0 + \nu_i \zeta(T,t,nj)]}{V^0(nj)[1 + \alpha(nj)\Delta T]}$$

In a closed system with equilibrium at each temperature, this equation is reduced to

$$A(\lambda,T) = \sum_{i=1}^{n} \frac{\epsilon_i(\lambda,T)[n_i^0 + \nu_i \zeta(T)]}{V^0[1 + \alpha \Delta T]}$$

For a system of n absorbing species to produce spectra with S wave lengths (λ_{ck}) of temperature invariant absorbance, two conditions must be obeyed, namely

(1) J. R. Morrey, *J. Phys. Chem.*, **66**, 2169 (1962).
(2) M. D. Cohen and E. Fischer, *J. Chem. Soc.*, 3044 (1962).

$$\sum_{i=1}^{n} \frac{\epsilon_i(\lambda_{ck},T)}{(1 + \alpha \Delta T)} = \text{constant}$$

and

$$\sum_{i=1}^{n} \frac{\nu_i \epsilon_i(\lambda_{ck},T)}{1 + \alpha \Delta T} = 0$$

The first equation specifies that the molar absorptivities of all absorbing species in the solution must have the same temperature dependence as the volume of the solution at all S isosbestic points. The probability of such an occurrence for $n > 1$ and $S > 1$ is nil.

Hᴀɴꜰᴏʀᴅ Lᴀʙᴏʀᴀᴛᴏʀɪᴇꜱ   J. R. Mᴏʀʀᴇʏ
Gᴇɴᴇʀᴀʟ Eʟᴇᴄᴛʀɪᴄ Cᴏᴍᴘᴀɴʏ
Rɪᴄʜʟᴀɴᴅ, Wᴀꜱʜɪɴɢᴛᴏɴ

THE CRYSTAL STRUCTURE OF THE MOLECULAR ADDITION COMPOUND XENON DIFLUORIDE–XENON TETRAFLUORIDE

Sir:

The existence of the crystalline phase whose structure is reported here was noted in the earliest examinations[1,2] of the xenon fluorides. Because it could be crystallized from vapor having primarily the infrared spectrum of XeF_4, the substance was reported[3] to be a polymorph of XeF_4. From this assumed composition and the crystallographic data,[3] $a = 6.64$ Å., $b = 7.33$ Å., $c = 6.40$ Å., $\beta = 92° 40'$, $Z = 4$, it was deduced that the density was 10% higher than that of the other form; hence it has been referred to in the literature as "the high-density form of XeF_4." We have shown, by crystal structure analysis, that it is in reality a distinct compound with the composition $XeF_2 \cdot XeF_4$. The true X-ray density is 4.02 g. cm.$^{-3}$.

The preparation of this compound from the elements was described previously,[3] but it should be added that the results of the crystal structure analysis indicate that some XeF_2 must have been present in the predominantly XeF_4 preparation, either by incomplete reaction[4] or by decomposition of XeF_4. Further work is being carried out to prepare larger quantities of $XeF_2 \cdot XeF_4$ by combining the components.

The diffraction intensities from a single crystal of $XeF_2 \cdot XeF_4$ were measured by use of Mo Kα X-rays, a goniostat, and a scintillation counter detector. A total of 574 independent reflections was recorded, which included virtually all having detectable intensity. The specimen grew in size during the data collection, and a normalization factor, derived from repeated measurements of a reference reflection, was applied. The approximate shape of the crystal was determined, making it possible to calculate an absorption correction for each reflection.[5] The mean diameter of the crystal was about 0.015 cm.; the value of the absorption coefficient used was 119.5 cm.$^{-1}$.

(1) C. L. Chernick, *et al.*, *Science*, **138**, 136 (1962).
(2) S. Siegel and E. Gebert, *J. Am. Chem. Soc.*, **85**, 240 (1963).
(3) J. H. Burns, *J. Phys. Chem.*, **67**, 536 (1963).
(4) D. F. Smith, *J. Chem. Phys.*, **38**, 270 (1963).
(5) D. J. Wehe, W. R. Busing, and H. A. Levy, "ORABS, A Fortran Program for Calculating Single Crystal Absorption Corrections," ORNL TM-229, 1962.

A trial structure (and the formula) was determined by the Fourier synthesis method. Previous work[3] gave the space group, $P2_1/c$, and showed that the Xe atoms are in a face-centered arrangement. Xenon atoms in these sites dominate the scattering and determine the signs of all structure factors, $F(hkl)$, for which h, k, l are unmixed (all odd or all even). Electron density maps computed with unmixed-index reflections only should show the structure, but with false symmetry. Such maps were made, but no reasonable assignment of fluorine positions was deduced from them. However, the inclusion in the Fourier series of five of the strongest mixed-index reflections, with signs determined by Sayre's squaring method,[6] yielded an interpretable map. A pair of centrosymmetrically equivalent fluorine atoms was found to be bonded to each Xe atom in positions $2(a)$: $0, 0, 0$; $0, 1/2, 1/2$; and two pairs of fluorine atoms were found to be bonded to each Xe atom in positions $2(d)$: $1/2, 0, 1/2$; $1/2, 1/2, 0$. Attempts to interpret a Fourier map with Xe atoms in positions $4(e)$ with $x = z = 1/4$, $y = 0$, which also gives a face-centered arrangement, did not prove fruitful.

Structure-factor calculations indicated the correctness of the model. It was refined by iterative least-squares procedures using a full-matrix program for the IBM 7090.[7] As the refinement proceeded, it became apparent that the 35 strongest reflections were affected by extinction; consequently they were omitted from the refinement. The agreement factor

$$R = \Sigma \left| F^2{}_{\text{obsd}} - F^2{}_{\text{calcd}} \right| / \Sigma\, F^2{}_{\text{obsd}}$$

reached 0.050. The Xe positions are given above, and the F atoms are in three sets of equivalent positions, $4(e)$: $\pm (x, y, z;\ x, 1/2 - y, 1/2 + z)$, with the following parameters. Least-squares standard errors of the above

	x	y	z
F(1)	0.168	−0.187	0.153
F(2)	.505	.079	.212
F(3)	.240	.109	.516

parameters are all 0.001. Anisotropic temperature factors were determined and will be given in a more detailed discussion later.

The structures of the XeF_2 and XeF_4 molecules in

their respective pure phases were determined previously by neutron diffraction[8] and by X-ray diffraction studies.[2,9] In XeF_2 the Xe–F bond lengths, corrected[10] for thermal motion on the assumption that the fluorine atoms "ride" on xenon, are 2.00 Å.; in XeF_4 the square planar molecule has Xe–F bond lengths, corrected for thermal motion, of 1.95 Å. and the F–Xe–F angle is 90.0°. The corresponding molecular parameters found in this study of the $XeF_2 \cdot XeF_4$ crystal are 2.01 ($\sigma = 0.01$) Å. for the XeF_2 moiety and two values, 1.94 Å. and 1.965 Å. (each with $\sigma = 0.01$), for the XeF_4 moiety with an F(2)–Xe–F(3) angle of 89.0° ($\sigma = 0.4°$). (The distances before thermal correction are 2.00, 1.91, and 1.935.) The errors quoted are least squares measures of precision. We estimate the corresponding measures of accuracy to be about twice as large. The hypothesis that the XeF_4 molecule is square-planar is thus easily consistent with this study, and the individual molecular geometries are retained in this compound with very little change.

In crystalline XeF_2, the closest intermolecular fluorine-to-xenon approach is 3.41 Å., and in XeF_4 there are two such contacts at 3.22 and 3.25 Å. The $XeF_2 \cdot XeF_4$ crystal has close intermolecular fluorine-to-xenon distances of 3.28, 3.35, 3.35, 3.37, and 3.42 Å.; i.e., at about the same average separations as in the two components. The minimum intermolecular fluorine-to-fluorine contact is a little shorter (2.87 Å.) in $XeF_2 \cdot XeF_4$ but this distance is not unusual for non-bonded fluorine atoms. Hence there is no structural evidence for the formation of any strong bonds between molecules, and this phase appears to be appropriately described as a molecular addition compound.

(6) D. Sayre, *Acta Cryst.*, **5**, 60 (1952).

(7) W. R. Busing, K. O. Martin, and H. A. Levy, "ORFLS, A Fortran Crystallographic Least-Squares Program, ORNL TM-305, 1962.

(8) H. A. Levy and P. A. Agron, *J. Am. Chem. Soc.*, **85**, 241 (1963); J. H. Burns, P. A. Agron, and H. A. Levy, *Science*, **139**, 1208 (1963).

(9) J. A. Ibers and W. C. Hamilton, *ibid.*, **139**, 106 (1963); D. H. Templeton, *et al.*, *J. Am. Chem. Soc.*, **85**, 242 (1963).

(10) W. R. Busing and H. A. Levy, paper submitted to *Acta Cryst.*; W. R. Busing and H. A. Levy, "A Crystallographic Function and Error Program for the IBM 704," Rept. No. 59-12-3, Oak Ridge National Laboratory (1959); see also D. W. J. Cruickshank, *Acta Cryst.*, **9**, 757 (1956).

(11) Operated for the Atomic Energy Commission by Union Carbide Corporation.

Reactor Chemistry and   J. H. Burns
   Chemistry Divisions   R. D. Ellison
Oak Ridge National Laboratory[11]   H. A. Levy
Oak Ridge, Tennessee